

6401393

SUBJ  
GTHM  
SPM

UNIVERSITY OF UTAH  
RESEARCH INSTITUTE  
EARTH SCIENCE LAB.

The Self-Potential Method in Geothermal Exploration

Robert F. Corwin

Engineering Geoscience, University of California, Berkeley, CA

Donald B. Hoover

U.S. Geological Survey, Denver, Colorado

May, 1978

Table of Contents

Abstract	1
Introduction	3
Possible mechanisms of self-potential generation by geothermal activity	3
1. Thermoelectric coupling	3
2. Electrokinetic coupling	7
Noise sources and data quality	11
1. Telluric currents	11
2. Streaming potentials	12
3. Conductive mineral deposits	13
4. Cultural activity	14
5. Resistivity variations and uneven topography	15
6. Electrochemical effects	16
a) Electrochemical concentration cells	16
b) Soil moisture and watering of electrodes	18
c) Electrode polarization and drift	20
7. Field procedure	21
Previously reported self-potential surveys in geothermal areas	23
Results of recent surveys	24
1. Leach Hot Springs area, Grass Valley, Nevada	24
2. Cerro Prieto geothermal field, Baja California, Mexico	27
3. Paoha Island, Mono Lake, California	28
4. Roosevelt Hot Springs KGRA, Utah	29
5. Steamboat Springs, Nevada	31

Conclusions	33
Acknowledgments	36
References	37
List of Figures	43
Figures	45

ABSTRACT

Laboratory measurements and field data indicate that self-potential anomalies comparable to those observed in many areas of geothermal activity may be generated by thermoelectric or electrokinetic coupling processes. A study using an analytical technique based on concepts of irreversible thermodynamics indicates that, for a simple spherical source model, potentials generated by electrokinetic coupling may be of greater amplitude than those developed by thermoelectric coupling. Before any more quantitative interpretations of potentials generated by geothermal activity can be made, analytical solutions for more realistic geometries must be developed, and values of in situ coupling coefficients must be obtained.

If the measuring electrodes are not watered, and if telluric currents and changes in electrode polarization are monitored and corrections made for their effects, most self-potential measurements are reproducible within about  $\pm 5$  mV. Reproducible short-wavelength geologic noise of as much as  $\pm 10$  mV, primarily caused by variation in soil properties, is common in arid areas, with lower values in areas of uniform, moist soil. Because self-potential variations may be produced by conductive mineral deposits, stray currents from cultural activity, and changes in geologic or geochemical conditions, self-potential data must be analyzed carefully before a geothermal origin is assigned to observed anomalies.

Self-potential surveys conducted in a variety of geothermal areas show anomalies ranging from about 50 mV to over 2 V in amplitude over



distances of about 100 m to 10 km. The polarity and waveform of the observed anomalies vary, with positive, negative, bipolar, and multipolar anomalies having been reported from different areas. Steep potential gradients often are seen over faults which are thought to act as conduits for thermal fluids. In some areas, anomalies several kilometers wide correlate with regions of known elevated thermal gradient or heat flow.

## Introduction

Self-potential anomalies that appear to be related to geothermal activity have been reported from a considerable number of geothermal areas. In this paper we discuss some possible source mechanisms for these anomalies, and give examples of noise and data reproducibility problems that often are encountered in self-potential work, and are more severe in large-scale geothermal surveys than in the relatively small-scale surveys conducted for mineral exploration. We then briefly summarize previously reported self-potential surveys conducted in geothermal areas and present recent results from five additional areas: Grass Valley, Nevada; Cerro Prieto, Baja California, Mexico; Mono Lake, California; Roosevelt Hot Springs, Utah; and Steamboat Springs, Nevada.

### Possible mechanisms of self-potential generation by geothermal activity

Although the observed self-potential anomalies described later in this paper appear to be related to geothermal activity, the mechanism by which these anomalies are generated is not well understood at this time. However, there is evidence that both the elevated temperature and the circulation of subsurface fluids which are characteristic of geothermal systems are capable of generating surface potential fields comparable in wavelength and amplitude to the self-potential anomalies observed in geothermal areas. The mechanisms by which elevated temperature and the flow of subsurface fluids may generate such anomalies are discussed below.

#### 1. Thermoelectric Coupling

If a temperature gradient is maintained across a sample of rock, a corresponding voltage gradient will appear across the sample. This phe-

nomenon is known as thermoelectric coupling, and may be caused by differential thermal diffusion of ions in the pore fluid and of electrons and donor ions in the rock matrix; a process known as the Soret effect (Heikes and Ure, 1961). The ratio of the voltage to the temperature difference,  $\Delta V/\Delta T$ , is called the thermoelectric coupling coefficient.

Data presented by Nourbecht (1963) for a variety of rock types give thermoelectric coupling coefficients ranging from  $-0.09$  to  $+1.36$  mV/ $^{\circ}$ C, with an average value of about  $0.27$  mV/ $^{\circ}$ C. Dorfman et. al. (1977) obtained coefficients ranging from about  $0.3$  to  $1.5$  mV/ $^{\circ}$ C for a variety of sandstone, limestone and serpentinite samples. In a related experiment by Dorfman et. al. (1977), a point heat source of  $49^{\circ}$ C inserted near the center of a limestone block measuring about  $2 \times 1 \times 1$  m was seen to immediately generate a surface potential field of about  $+20$  mV amplitude centered over the heat source. In an experiment using powdered and crystalline pyrite samples, Yamashita (1961) measured a coupling coefficient of about  $-0.25$  mV/ $^{\circ}$ C.

A technique based on the concepts of irreversible thermodynamics to yield surface self-potential fields generated by subsurface thermoelectric coupling is described by Nourbecht (1963). This approach requires the presence of a boundary that separates regions of differing thermoelectric coupling coefficients and is intersected by a body of elevated temperature relative to its surroundings.

Curves showing the thermoelectric potential generated by a sphere of uniform elevated temperature are given by Nourbecht (1963). As a first approximation to a geothermal model, we consider a buried sphere centered

at a depth equal to its diameter and intersected through its center by a horizontal boundary separating an upper layer of conductivity  $\sigma_1$  from an infinitely deep lower layer of conductivity  $3\sigma_1$  (Fig. 1). For this case, the maximum surface potential is about  $0.15 [(C_1 - C_2)\Delta T]$  mV, where  $C_1$  and  $C_2$  are the thermoelectric coupling coefficients of the upper and lower layers, respectively, and  $\Delta T$  is the temperature difference between the sphere and its surroundings.

For a large value of  $(C_1 - C_2)$  of  $1 \text{ mV}/^\circ\text{C}$  and a  $\Delta T$  of  $100^\circ\text{C}$  the maximum potential is about 15 mV, and for a more realistic value of  $(C_1 - C_2)$  of  $0.2 \text{ mV}/^\circ\text{C}$  the maximum potential is about 3 mV. The polarity of the anomaly depends on the sign of  $(C_1 - C_2)$ . This is an important point, as it indicates that thermoelectric anomalies may be of either positive or negative polarity.

Anomalies generated by this model are of smaller amplitude than usually seen in geothermal areas, and they would be difficult to distinguish from typical background noise (discussed later in this paper). More concentrated areas of high temperature at shallow depth, such as thermal fluids in a fault zone, could result in anomalies of shorter wavelength and greater amplitude, which would be more readily detectable. If the relatively long-wavelength (several km), large-amplitude (50 mV or more) anomalies seen in some geothermal areas are generated by thermoelectric coupling, either the in situ thermoelectric coupling coefficients are larger than those measured in the laboratory, or the sources are of different geometry than the sphere model considered above. More quantitative interpretation of possible thermoelectric effects awaits the measurement of

in situ thermoelectric coupling coefficients in geothermal areas, and the development of analytical methods to calculate the surface self-potential expression for more realistic geothermal models.

Several field examples seem to indicate that measurable self-potentials may be generated by elevated subsurface temperatures. A series of measurements made by Dorfman et al. (1977) over steam and fire flood wells used for secondary recovery of petroleum at depths of about 200 m showed positive self-potentials which correlated with the location of the steam or fire front as determined from temperatures at the heads of recovery wells. In this case, the steep gradients of the surface potential field implied that some sort of vertical structure may have influenced the surface expression of the potential field generated at depth. Electrokinetic coupling (discussed later in this paper) also may have contributed to the anomaly. The boundaries of the self-potential anomalies measured at Leach Hot Springs, Nevada (Figs. 6 and 7), Mono Lake, California (Fig. 10), and Roosevelt Hot Springs, Utah (Fig. 11) appear to correlate with the limits of areas of known anomalously high heat flow, allowing the possibility that at least a portion of these anomalies was generated by thermoelectric coupling.

Self-potential surveys conducted over shallow coal burns provide additional examples of possible thermoelectric coupling in the earth. On the assumption that a shallow coal mine fire might be a good model of a miniature geothermal system, surveys were made of two shallow burns. A survey at Marshall, Colorado (Fig. 2) shows a well-defined negative anomaly of 140 mV peak amplitude centered over what appeared to be the

burning region as evidenced by smoke and steam issuing from some vents. The coal seam is at a depth of about 10 m and is capped to the surface by sandstone.

A survey of a coal burn at Acme, Wyoming gave similar results. In one area the burn was at most 3 m below the surface and rocks glowing red 30 cm below the surface could be seen in slump cracks. A positive anomaly of about 30 mV maximum amplitude was associated with this extreme thermal gradient. Larger anomalies were noted where the overburden was thicker, possibly indicating that electrokinetic effects were augmenting the thermoelectric component.

## 2. Electrokinetic coupling

The flow of a fluid through a porous medium may generate an electric potential gradient (called the electrokinetic or streaming potential) along the flow path by the interaction of the moving pore fluid with the Helmholtz double layer at the pore surface, a process known as electrokinetic coupling (MacInnes, 1961). The streaming potential,  $E$ , generated by the flow of fluid through a capillary tube is given by

$$E = \frac{\rho \epsilon \zeta}{4\pi\eta} \Delta P, \quad (1)$$

where  $\rho$ ,  $\epsilon$ , and  $\eta$  are, respectively, the electrical resistivity, dielectric constant, and viscosity of the pore fluid;  $\Delta P$  is the pressure drop along the flow path (related through Darcy's law to the fluid viscosity and flowrate and permeability of the medium); and  $\zeta$ , the zeta potential, is the voltage across the Helmholtz double layer. Not enough is presently known about the behavior of  $\rho$ ,  $\zeta$ , and  $\eta$  in the pores of rocks and soil to allow direct

calculation of the electrokinetic coupling coefficient  $E/\Delta P$ . As  $\zeta$  may be either positive or negative (Dakhnov, 1962),  $E$  may either increase or decrease along the flow path.

Measured values of the streaming potential coupling coefficient  $E/\Delta P$  in a variety of rocks listed by Nourbehecht (1963) range from -12 to +31 mV/atm in sandstones with distilled water used as the pore fluid. Tuman (1963) obtained  $E/\Delta P$  values of about 150 to 390 mV/atm using 500 ohm-m distilled water in porous sandstones, and about 15 mV/atm using 4.4 ohm-m water. Ahmad (1964) obtained  $E/\Delta P$  values in quartz sands ranging from 50 mV/atm for 24 ohm-m pore fluid to about 2400 mV/atm for 2700 ohm-m pore fluid, and similar results were obtained by Ogilvy et al. (1969). The measurements in quartz sands also revealed that  $E/\Delta P$  is affected by the permeability and grain size of the matrix, factors that do not appear explicitly in (1). The flow of steam in pipes has been seen to generate very large potentials (Klinkenberg and van der Minne, 1958) so it is possible that electrokinetic coupling coefficients for subsurface steam flow may be greater than those listed above for fluid flow.

Self-potential fields produced by the flow of subsurface water have been observed by Ogilvy et al. (1969), who measured variations of as much as 50 mV over zones of water leakage through fissures in the rock floor of a reservoir; and by Bogoslovsky and Ogilvy (1973), who obtained a positive anomaly of 55 mV amplitude that mirrored the groundwater depression cone surrounding a well pumping from a depth of 16 m. Streaming potentials are thought to be the most reasonable explanation for the self-potential anomalies described by Zablocki (1976), Combs and Wilt (1976),

Zohdy et al. (1973), and Anderson and Johnson (1976). As discussed later in this paper, the self-potential contours at Leach Hot Springs, Nevada strongly resemble the pattern of near-surface water flow. Onodera (1974) observed that the self-potential measured across a stationary dipole near a production well in the Otake field, Japan (the length, location and orientation of the dipole are not specified) varied by 28 mV as the flow of the well was turned off and on, the variation being attributed to streaming potentials.

A technique for calculating self-potential fields generated by electrokinetic coupling is given by Nourbehecht (1963). This technique uses the concepts of irreversible thermodynamics to describe the coupling of pressure and potential gradients, and requires that a component of the pressure gradient be parallel to a boundary separating regions of differing electrokinetic coupling coefficients in order for a surface self-potential field to be developed by subsurface fluid flow.

The only electrokinetic model described explicitly by Nourbehecht is a buried spherical pressure source (or sink) in a horizontally layered medium. Although a spherical source probably is not representative of the driving force for fluid flow in a geothermal system, it is instructive to compare surface potential fields generated by this model with those obtained from the thermoelectric case discussed earlier. For the same geometry and resistivity distribution used for the thermoelectric case (Fig. 1), the maximum surface potential above the center of the sphere is about  $0.6 [(C_1 - C_2)\Delta P]$  mV, where  $C_1$  and  $C_2$  are the electrokinetic coupling coefficients in mV/atm of the upper and lower layers respectively



and  $\Delta P$  is the pressure difference across the boundary of the sphere in atmospheres.

For a reasonable value of  $(C_1 - C_2)$  of 10 mV/atm and a pressure difference of 5 atm the maximum potential over the center of the sphere is about 30 mV, about an order of magnitude greater than for the reasonable thermoelectric case discussed previously. The polarity of the anomaly depends on the sign of  $(C_1 - C_2)$  and the direction of the pressure gradient, so anomalies may be of either polarity. Thus, for similar geometry, self-potential anomalies generated by electrokinetic coupling might be expected to be larger in amplitude than those generated by thermoelectric coupling.

An important point of this discussion is that the magnitude and polarity of self-potential anomalies generated by thermoelectric and electrokinetic coupling depend not only on source parameters such as temperature, pressure, and geometry, but also on the magnitudes and differences of the coupling coefficients. Thus even if substantial subsurface temperature and pressure gradients exist in an area, a measurable self-potential anomaly will not be generated unless the coupling coefficients and their differences across boundaries are sufficiently large. Also, even though both driving forces (temperature and pressure) may be present, the contribution of each to the total anomaly will depend on the relative magnitude of the coupling coefficients and their differences. These magnitudes may vary not only from one geothermal area to another, but also from point to point within the same area. Therefore, knowledge of in situ coupling coefficients is necessary before any quantitative comparison between thermoelectric and electrokinetic contributions to a given self-potential anomaly may be made.

### Noise sources and data quality

Self-potential surveys made for conductive mineral exploration often are plagued by high noise levels and poor data reproducibility, problems which have cast the method into some disrepute. These problems are compounded in geothermal surveys, where the wavelength of the anomalies tends to be much longer, and their amplitude smaller than typical for shallow conductive mineral deposits. The long survey lines needed for profiling in geothermal areas increase errors caused by telluric current variations and electrode drift, and the typical geologic background noise level of  $\pm 5$  to  $\pm 10$  mV may interfere with the detection of anomalies of the same magnitude. Survey procedures, such as stepwise advancement of a short measuring dipole ("leapfrog" technique) or the watering of electrodes to improve ground contact, which are adequate for the detection of the short-wavelength, high-amplitude anomalies that are typical of shallow conductive mineral deposits (Sato and Moonéy, 1960) have lead to serious cumulative errors when used over long survey lines. As the necessary precautions for obtaining reliable data in large-scale self-potential surveys are not treated in detail in the standard references on the method (e.g., Parasnis, 1966 ; Broughton Edge and Laby, 1931 ), the sources of noise and error for such surveys are discussed briefly in the following sections.

#### 1. Telluric currents

Long-period telluric currents generated by temporal variations in the earth's magnetic field may be much as several hundred mV/km over resistive terrain (Keller and Frischknecht, 1966). Much of this telluric activity

is between 10 and 40 seconds in period, but there is also considerable energy at longer periods. If significant variations of 10 to 40 second periods occur while a self-potential measurement is being made, several successive peaks and troughs may be averaged to give a reasonable approximation to the true "DC" value. Variations with periods greater than about one minute, however, are much more difficult to recognize during a typical measurement period of less than one minute, and may be erroneously assumed to be spatial variations. An estimate of the level of long-period telluric activity may be gained by recording telluric variations across a stationary dipole in the survey area, but quantitative corrections to the data may be made only if the apparent resistivity of the earth beneath both the stationary dipole and the survey point is known for a period equal to that of a recorded variation.

Telluric variations generally are not as serious a problem in relatively conductive valleys as in mountainous areas, where resistivities usually are higher, lateral resistivity variations are more prominent, and the direction of the currents may vary considerably. Even under ideal geologic conditions, self-potential measurements taken during magnetic storms may exhibit very high noise levels.

## 2. Streaming potentials

As discussed above, electrokinetic coupling may be one of the mechanisms by which geothermal activity generates self-potential anomalies. Such potentials generated by the flow of non-thermal subsurface water would constitute a noise source in geothermal prospecting, and may be a major cause of variations related to topographic effects that are sometimes

observed in self-potential data (Williams et al., 1976; Poldini, 1939).

An extreme example of a topographic effect possibly related to streaming potentials was noted in a survey on Adak Island in the Aleutian chain of Alaska, where self-potential measurements were made in conjunction with other electrical studies to assess the geothermal potential around Adagdak volcano. A strong correlation between a self-potential profile and elevation is seen in Figure 3. The topographic peak of Adagdak, at an elevation of 645 m, was 2693 mV negative with respect to a reference at 15 m above sea level. Because of the large amount of rain on Adak, a streaming potential mechanism provides a reasonable explanation for the observed correlation of self-potential with elevation. Adagdak is normally covered with rain clouds above the 300 m elevation, and snow fields were present in August when the work was done, so an abundant supply of water was available. Assuming that a hydrostatic head due to a water table elevation difference is the driving mechanism, an electrokinetic coupling coefficient of about 100 mV/atm is indicated for the upper slope of Adagdak. This is a reasonable value considering that the ground water is low in dissolved solids and therefore has relatively high resistivity. In this area, the topographically related potential completely overshadowed any possible anomaly caused by geothermal activity. The lack of detailed knowledge of the surface hydrology and of in situ electrokinetic coupling coefficients make it difficult to correct quantitatively for this large potential.

### 3. Conductive mineral deposits

Deposits containing conducting sulfides such as pyrite, phrrhotite, chalcopyrite, chalcocite and covellite, as well as deposits of magnetite, covellite, and graphite are known to generate self-potential anomalies

which almost invariably are negative in polarity over the top of the deposit. The anomalies may be as much as 100 mV in amplitude and seldom exceed a few hundred meters in width (Sato and Mooney, 1960). Sato and Mooney (1960) propose a mechanism for these anomalies in which the conductive mineral deposit serves as a path for electrons to travel upward through the deposit, from the reducing environment at depth to the oxidizing environment at the upper end of the deposit. The corresponding flow of groundwater ions in the earth surrounding the deposit generates the observed anomaly. As conductive minerals, unrelated to present-day geothermal activity, often occur in geothermal areas, their anomalies could present a noise source in geothermal surveys. An example of such an anomaly is shown in Figure 4. The large scale of the anomaly and its onset coincident with Kyle Hot Springs appeared to be of geothermal interest, but test holes at locations KY-1 and KY-3 showed an extensive zone of conductive graphite (with pyrite in KY-3) beginning at a depth of about 40 m (Goldstein, et al., 1976). As heat flow values in the holes were normal for the area, it seems reasonable to infer that the anomaly was caused by the conductive mineralization, operating through the mechanism described above.

#### 4. Cultural activity

Stray currents generated by cultural activity are a major problem in populated (and some unpopulated) areas. Such currents may be generated by power lines, electrical ground, corrosion of pipelines or buried metallic junk, the action of pipeline corrosion protection systems, well casings, and other geophysical activities in the survey area. The currents may be steady, or may take the form of individual spikes or pulses, series of

sinusoidal or square waves, or irregular variations, and may attain amplitudes of tens or hundreds of mV/km at distances greater than 5 km from the source (Hoogervorst, 1975). The use of a telluric monitoring dipole, as mentioned previously, along with careful observations for possible sources of stray currents, is essential to avoid interpreting voltages generated by such currents as natural self-potentials.

#### 5. Resistivity variations and uneven topography

The thermoelectric and electrokinetic processes described previously act essentially as underground current sources. The surface potential fields generated by these sources will be influenced by the subsurface resistivity distribution, and the self-potential field generated by a geothermal source may be distorted by resistivity changes across faults or contacts which are not thermally active. In some cases these self-potential variations may be useful for structural mapping, but care must be taken not to confuse them with anomalies generated by actual thermal activity. As discussed previously, currents produced by telluric activity also are influenced by the resistivity distribution, causing variations in the surface potential field. An example of distortion of a geothermally generated self-potential field caused by a change in resistivity across a contact is seen in the Cerro Prieto data (Fig. 8), discussed later in this paper. Near-surface resistivity variations also may be responsible for some of the large-amplitude, short-wavelength noise often superimposed on longer wavelength self-potential anomalies in the vicinity of a geothermal source.

Uneven topography may affect surface potential fields by distorting

current flow patterns (Grant and West, 1965). As near-surface resistivity also may vary considerably from point to point in areas of uneven topography, it may be difficult to separate the topographic and resistivity effects (non-geothermal streaming potentials also may be generated in such areas). A possible example of these combined effects is seen in the eastern portion of the self-potential profile from Roosevelt Hot Springs (Fig. 11), where the noise level increased considerably in an area of extremely uneven topography.

#### 6. Electrochemical effects

Variations in soil chemistry, temperature, or moisture content probably account for much of the background noise seen in self-potential data. The profile along line A-A' in Grass Valley, Nevada (Fig. 6) shows typical background noise of as much as  $\pm 10$  mV in desert areas. This noise may have wavelengths as short as a few cm, and its amplitude usually is less in areas of moist or more uniform soil. These environmental variations affect the "non-polarizing" electrodes used for field measurements and may result in irreproducible polarization and drift. Preliminary laboratory and field data indicate that different electrode types (e.g., copper-copper sulfate, silver-silver chloride, calomel) may respond differently to changes in soil chemistry, moisture content, and temperature, so it is desirable that the electrode type used for a given survey be specified along with the survey results.

##### a) Electrochemical concentration cells

The potentials generated by chemical concentration cells may reach several hundred mV (MacInnes, 1961), but these values usually will be

seen only across bare metallic electrodes, as the liquid junctions of "non-polarizing" electrodes produce counter potentials and limit the overall cell potential to several tens of mV (Corwin, 1976a). Nourbehecht (1963) estimated that about 20 mV might be the maximum expected value for most geochemical concentration cells. Semenov (1974) reported maximum anomalies of about -30 mV across salt marsh areas, and a survey run across a desert salt flat in Buffalo Valley, Nevada showed no apparent effect of the change in soil chemistry between the salt flat area and the surrounding soil. Positive anomalies of 20 to 40 mV over pegmatite veins, and smaller anomalies over silicified zones, have been attributed to electrochemical effects (Semenov, 1974). As the boundary of the anomaly at Leach Hot Springs, Nevada (Figs. 6 and 7) corresponds to that of a silicified area, it is possible that electrochemical effects contribute to the observed self-potential anomaly.

Alunite may be present in areas of hydrothermal alteration. Very large self-potential anomalies of -1800 mV (Gay, 1967) and -700 mV (Kruger and Lacy, 1949) have been attributed to a concentration cell effect caused by the weathering of alunite to sulfuric acid. The presence of alunite in geothermal areas such as the Dome Fault zone of the Roosevelt Hot Springs KGRA (Parry et al., 1976), then, lends additional uncertainty to the interpretation of self-potential anomalies. The pH difference of about 3.3 between the alunite-bearing and background areas described by Gay (1967) would generate only about 200 mV across a hydrogen ion-reference electrode pair, and preliminary laboratory measurements indicate that pH cells generate even smaller potentials across copper-copper sulfate or other non-polarizing electrode pairs. Thus, it remains unclear whether measured



self-potentials exceeding a few hundred mV could be generated by hydrogen-ion concentration cells produced by the weathering of alunite. Self-potential surveys conducted by one of us (DBH) across alunite deposits in the Wah Wah mountains, Utah, and at the Randsburgh, California KGRA showed no significant anomalies, so alunite may be present without accompanying self-potential activity.

Even though most electrochemical potentials may be limited to a few tens of millivolts, they tend to obscure small, long-wavelength anomalies which may be of geothermal interest. Their effect may be minimized by careful selection of electrode sites for uniform soil conditions, by filtering the field data to reduce short-wavelength variations, or possibly by measuring soil chemical properties at each electrode site for future data correction. Improved electrode design, such as the use of a double electrolyte chamber to further chemically isolate the electrode element from the soil, also may help to reduce electrochemical effects.

b) Soil moisture and watering of electrodes

Variations in soil moisture content often give rise to self-potential variations, with the electrode in the wetter soil usually becoming more positive (Poldini, 1939). Similar variations are caused by the common practice of watering electrodes to improve electrical contact with the ground. Potential variations caused by watering of electrodes generally do not adversely affect commutated resistivity readings, but may seriously degrade self-potential data.

Figure 5 shows the effect of watering copper-copper sulfate electrodes. The electrodes were placed in an acid clay soil and allowed to stabilize for about 15 min (during this period the potential changed by 3 mV). Then,

about 250 ml of water was poured around one electrode, which caused a jump of 14 mV positive with respect to the unwatered electrode. During the 25 min required for absorption of the water into the soil, the potential of the watered electrode dropped, possibly because of a streaming potential generated by the flow of the water into the soil. When the absorption was complete, the potential rose to a maximum of 22 mV over a period of about 1 hour. The positive potential associated with the watered electrode has been attributed by one of us (DBH) to electrode contact potentials related to a capillary effect (Kruyt, 1952).

When large diameter (>2 cm) non-polarizing electrodes are used in the field, contact resistances rarely exceed 20 k ohm (1 to 10 ohms is typical) if care is taken to insert the electrodes firmly into small pits that penetrate through the dry surface soil layer (usually no more than 10-20 cm deep, even in desert soils). Inexpensive voltmeters of  $10^6$  ohm input impedance will not draw appreciable current from the electrodes under these conditions, and there is no need to water the electrodes to reduce contact resistance. When using very small diameter (<5 mm) electrodes, contact resistance seldom exceeds 500 k ohms, and voltmeters having  $10^9$  ohm input impedance have proven satisfactory.

Electrode watering, therefore, may cause persistent electrode potential changes, and elimination of this practice results in improved consistency and reproducibility of self-potential readings. This is particularly true in "leapfrog" surveys, which are subject to positive cumulative error in the traverse direction, caused by the fresher watering of the leading electrode. Natural variations of soil moisture must be carefully noted in the field, with the realization that they may be the cause of self-

potential variations of as much as a few tens of millivolts.

c) Electrode polarization and drift

A spurious potential (polarization) will be measured across an electrode pair if the electrolyte or porous junction of the measuring electrode become contaminated with chemical species not ordinarily present in the electrolyte, or if the electrolyte temperature or porous junction moisture contents differ. Polarization may appear suddenly, for example, after contact of the measuring electrode with a highly concentrated groundwater solution or it may be manifested as drift, as when the porous junction of a base station electrode dries or absorbs groundwater ions over a period of time. Drift may also be observed during the course of a single reading, as the temperature, moisture, and chemical content of the electrode adjust to the values in the soil. Minimizing the amount of time an electrode remains in the ground reduces the chance for contamination. Therefore, readings should be made as quickly as possible, consistent with the level of telluric noise activity. Usually, only a few seconds are needed for the electrode to "settle in", with any drift after this period being a response to environmental conditions. Along with telluric variations and time-varying stray currents, polarization and drift constitute the major source of non-reproducibility in most self-potential measurements.

If the electrolyte temperature of the measuring electrode differs from that of the reference, a potential will appear across the electrode pair. The temperature coefficient for saturated copper-copper sulfate electrodes is about  $0.5 \text{ mV}/^{\circ}\text{C}$  (Ewing, 1939; Poldini, 1939); for silver-

silver chloride electrodes it is somewhat less than half of this value (Corwin and Conti, 1973). The combined polarization and drift caused by these temperature differences, by electrolyte or porous junction contamination, or by drying of the porous junction may be determined during the survey by periodically measuring the voltage between the working electrodes and a reference electrode maintained in a bath of electrolyte solution. The reference electrode maintains a relatively constant potential if its temperature is held constant. This procedure allows polarization and drift corrections to be made to the data. As these corrections may at times amount to some 20 mV, neglecting them may lead to significant errors. An example of data improvement resulting from this procedure is discussed later in this paper, in the description of survey results from Leach Hot Springs, Nevada.

#### 7. Field procedure

It is apparent that much care must be taken to obtain reproducible and meaningful self-potential data. We have found that potential readings are affected by the quality of the electrode contact with the soil, and that this effect is greater than would be predicted from a simple change in circuit resistance relative to the impedance of the measuring instrument. For example, reseating an electrode to reduce the measured circuit resistance from 20 k ohms to 5 k ohms may change the measured potential by 5 or 10 mV, representing a variation of at least several percent for a typical total reading of less than a few hundred mV. For a voltmeter with  $10^6$  ohm input impedance, a source resistance change of 15 k ohms would cause the indicated voltage to change by only a few tenths of a

percent; an amount considerably less than the observed variation. Therefore, electrode contact resistance should be checked at each station, and an effort made to ensure good ground contact and to keep the circuit resistance as uniform as possible from station to station. As the resistance measurement polarizes the electrodes by driving current through them, it should be made after completing the self-potential reading, for as short a time as possible.

Potentials generated by telluric currents should be monitored to assure that they are not misinterpreted as spatial anomalies. Frequent checks of electrode polarization and drift are essential, especially when a "gradient" or "leapfrog" survey configuration (in which a dipole of fixed length is stepped along the survey line, and successive voltages added to obtain the total field) is used. When many such additions are performed, small errors may accumulate to large values. Running such surveys in a closed loop does not provide an absolute check on possible cumulative error, as the polarization of an electrode pair may change magnitude and polarity from reading to reading. Alternating the leading and following electrodes ("leapfrogging") in this type of survey will help to reduce cumulative error caused by electrode polarization. Polarization errors also will affect data for a "total field" survey (in which a fixed base electrode is used for the entire survey) but, as successive readings are not additive as with the "gradient" method, the error of each reading is limited to the maximum value of the polarization. If field measurements are made carefully and the effects of polarization, drift, tellurics, and stray currents are accounted for, most self-potential measurements (if made at identical locations) are repro-

ducible within about  $\pm 5$  mV, even if taken many years apart (Parasnis, 1970).

Reproducible data, of course, are not necessarily meaningful in terms of geothermal activity. The possibility that the measurements have been affected by non-thermal subsurface water flow, conductive mineral deposits, stray currents (and other cultural effects such as plowed fields, cultivation, irrigation, or agricultural chemicals), or soil moisture or chemistry variations must be carefully considered. These effects may be minimized by judicious selection of survey lines and electrode sites, and careful observation and recording of soil type and condition, local geology, vegetation, topography, and cultural manifestations.

#### Previously reported self-potential surveys in geothermal areas

Self-potential anomalies of widely varying amplitude, polarity, and spatial extent have been reported from several geothermal areas. Examples from the United States include positive anomalies of as much as 2300 mV in amplitude and about 1 km in width measured on Kilauea volcano, Hawaii by Zablocki (1976); a negative anomaly of about 200 mV amplitude and about 1 km in width at the northwest edge of the Dunes thermal area, California (Combs and Wilt, 1976); a steep-sided positive anomaly of about 30 mV amplitude and 2 km in width over the Mud Volcano area of Yellowstone National Park, Wyoming (Zohdy et al., 1973); a dipolar anomaly covering about 15 km and of about 900 mV peak-to-peak amplitude over a postulated resurgent dome in Long Valley, California (Anderson and Johnson, 1976); narrow dipolar anomalies of about 60 mV maximum amplitude in areas of known near-surface hot water in the Raft River Valley, Idaho (Williams

et al., 1976 ; Mabey et al., this volume); and a negative anomaly of about 60 mV amplitude and 3 km in width centered over the Leach Hot Springs area of Grass Valley, Nevada (Corwin, 1976a) (an updated version of this survey is discussed below).

Examples from outside the United States include positive anomalies a few hundred meters wide and as much as 400 mV amplitude measured in the Manikaran section of the Parbati Valley geothermal zone, India (Jangi et al., 1976); potential gradients of more than 10 mV/m over electrode spacings of 20 to 50 m in the Aeolian Islands and near Naples, Italy (Rapolla, 1974); and negative anomalies of about 100 mV amplitude and several hundred meters wide extending along fault lines of previously known geothermal activity in the Otake geothermal field, Kyushu, Japan (Onodera, 1974). This last example is especially interesting, as similar self-potential indications in an area of the field where geothermal activity had not been previously observed apparently helped locate test wells which proved productive enough to lead to the construction of a power plant.

#### Results of recent surveys

##### 1. Leach Hot Springs area, Grass Valley, Nevada

The results of a self-potential survey made in August 1974 over the Leach Hot Springs area of Grass Valley, Nevada were described by Corwin (1976a). Data taken along line A-A' are shown in Figure 6, and the location of the line is shown in Figure 7. As the wire reel used for this survey held only 500 m, a new base station was established every kilometer, intermediate readings made every 50 or 100 m to the north and south of the base, and the readings tied to those made from the previous base at the 500 m stations. Polarization and drift of the copper-

copper sulfate electrodes were not monitored, so no corrections to the data were made for these effects.

Self-potential measurements in the same area were repeated in September 1975, using a base electrode located at 4.2 km north on line A-A' and a reel holding 5 km of wire, allowing the base electrode to remain at the same location throughout the entire survey (including all the other survey lines shown in Figure 7). Survey electrode polarization was determined by periodically measuring the potential between the survey electrode and a portable reference electrode carried in a bath of copper sulfate solution. The readings were corrected by subtracting the polarization values from the observed measurements, with correction values linearly interpolated between polarization measurements.

The results of the 1975 survey along line A-A' are shown in Figure 6. Station locations were within a few meters of the 1974 ones, and readings generally were made every 100 m instead of the 50 m interval used for most of the 1974 survey. A change in the nature of the data between the two surveys is apparent, with the potentials for the 1975 data returning to a constant level on either side of a negative anomaly surrounding the hot springs area. Although many of the shorter-wavelength variations (up to 1 or 2 km) are similar for the two surveys, cumulative error in the earlier survey, caused by repeated movement of the base electrode and lack of correction for electrode polarization, resulted in a spurious offset of about 30 mV between the north and south ends of the line, and obscured the true nature of the negative anomaly surrounding the hot springs area.

Self-potential contours for the Leach Hot Springs area, based on



the smoothed 1975 data, are shown in Figure 7A. A negative anomaly of about 50 mV amplitude encloses the hot spring area and shows maximum activity close to the surface expression of a fault which is thought to act as a conduit for the thermal water (Olmsted et al., 1975). The boundary of the self-potential anomaly roughly coincides with the 2 HFU contour given by Olmsted et al. (1975), shown in Figure 7B, and with the boundary of a positive P-wave velocity anomaly and an electrically resistive silica zone surrounding the hot spring area (Beyer et al., 1976). Total hot spring flow at Leach Hot Springs is about 12 liters/sec at an average temperature of about 78°C (Olmsted et al., 1975). To date, no deep drilling has been done in the area, so the extent of any additional geothermal activity is not known.

The negative self-potential anomaly just to the north of the hot springs coincides with an area where the heat flow is high and the near-surface groundwater level drops sharply (Fig. 7B). Although not enough information is available to allow the contribution to the self-potential anomaly from these two effects to be separated, the similarity of the water table and self-potential contours in this area suggests an electrokinetic mechanism. The water table drops about 50 m, equivalent to a pressure difference of about 5 atm, in the vicinity of the springs. The resistivity of the spring water is about 12 ohm-m (Olmsted et al., 1975) and the rocks in the hot springs area are highly silicified, so an electrokinetic coupling coefficient of 10 mV/atm might not be unreasonable. Thus a 50 mV potential difference could be generated by the 5 atm pressure drop along the flow path, accounting for the similarity between the self-potential and water table contours in the vicinity of the fault.

2. Cerro Prieto geothermal field, Baja California, Mexico

Cerro Prieto, located in northern Baja California, Mexico, is a major geothermal field, presently producing 75 megawatts of electrical energy. Total fluid flow is about 750 metric tons/hr of steam and 2000 metric tons/hr of separated water (Noble et al., 1977). Well-head temperatures range from about 250°C to over 300°C and total dissolved solids (primarily NaCl) of the well water vary from about 9000 to 37,000 ppm (Mañon et al., 1977).

A self-potential profile, line B-B', run across the producing area of the field is shown in Figure 8. The location of the survey line, and the straight line onto which the data were projected to reduce geometric distortion, are shown in Figure 9. A striking dipolar anomaly with a peak-to-peak amplitude of about 150 mV is centered over the Cerro Prieto fault which is thought to act as a major conduit for the geothermal fluids (Noble et al., 1977).

A geologic profile along line B-B' is shown in the center of Figure 8, and an electrical model made in an attempt to define the source geometry of the self-potential anomaly is shown at the bottom of the figure. The model consists of a vertical sequence of ten horizontal current dipoles, separated by 500 m, in a half-space of 3 ohm-m resistivity. The dipole currents, which were chosen by trial and error to produce a potential field which roughly matches the measured data, increase linearly with depth. The dipoles extend from a depth of 1 km to 3.25 km; the zone of the fault along which thermal fluids are thought to flow into the shale and sandstone formation which comprises the geothermal reservoir. The dipoles are only in the plane of the section, and do not extend along the strike of the fault.

The potential field generated by the model corresponds reasonably well with the actual profile in the vicinity of the fault and near the ends of the line. The positive deviation of the actual profile from the theoretical curve beginning at about 1 km W probably is caused by higher resistivity material to the west of this point (well M-6 is not a producer, and the western boundary of the production zone lies between wells M-9 and M-6). The cause of the deviation centered at about 5 km E is not known, as little geologic information is available in this area.

Obviously, this model does not define the mechanism of generation of the anomaly. However, it does demonstrate that anomalies of very long wavelength may be produced by potentials generated in a relatively narrow fault zone, and that the existence of an extensive volume of elevated temperature or fluid circulation is not required for the generation of long-wavelength self-potential anomalies (although such a volume does exist in this case).

Considerable temperature and flow data, along with a number of reservoir core samples, are available for this field. We intend in the near future to measure the thermoelectric and electrokinetic coupling coefficients of the cores, and then to attempt to quantitatively model the potential generating mechanism using a technique presently being developed by D.V. Fitterman of the U.S. Geological Survey (personal communication, 1978). This technique, based on the approach of Nourbehecht (1963), allows the calculation of surface potential fields developed by temperature or pressure gradients in the vicinity of a vertical contact.

### 3. Paoha Island, Mono Lake, California

In 1976, an offshore self-potential survey was conducted in Mono

Lake, California, near a hot spring area on Paoha Island (Waring, 1965). The measurements were made between silver-silver chloride electrodes separated by 35 m, towed along the water surface behind a small boat (the equipment and procedures used are described by Corwin, 1976b). The survey line, shown in Figure 10, was about 15 m offshore, in water about 15 m deep.

A gradient anomaly with a maximum amplitude of 0.7 mV/35m and a length of 1200 m was measured directly offshore of the hot springs area (Fig. 10). Integration of this gradient anomaly gave a total field anomaly of about 2 mV maximum amplitude peak-to-peak. While the anomaly amplitude is small, it is well above the background noise level of about 0.05 mV/35m. The small amplitude of the anomaly is not surprising in view of the 0.1 ohm-m resistivity of the highly saline lake water.

Thermal gradient measurements made on the lake bottom indicate that the thermal activity continues offshore of the hot spring area on Paoha Island (Welday, 1977). A significant feature of this survey is that the anomaly was measured in homogeneous lake water, precluding possible electrode effects caused by varying soil chemistry, temperature, and moisture content (discussed previously) often encountered in an onshore survey;

#### 4. Roosevelt Hot Springs KGRA, Utah

The Roosevelt Hot Springs KGRA, located near Milford, Utah, is a water dominated geothermal system with maximum temperatures in excess of 265°C (Lenzer et al., 1977). Several production wells have been drilled in the area, and two of these wells are reported to be capable of producing a total mass flow of at least 450 metric tons/hr. The reservoir

consists of fractures within crystalline rock, and the depth to the top of the reservoir ranges from about 100 m to more than 1 km. The water contains about 6000 to 8000 ppm of dissolved solids, mainly NaCl. The Dome Fault, which strikes NNE through the area, appears to significantly influence the hydrology, and coincides with the axis of a thermal gradient anomaly (Lenzer et al., 1977; Sill and Bodell, 1977).

A self-potential profile run in early 1977 across the Dome Fault zone is shown in Figure 11. Also shown in the figure are thermal gradient data obtained by Sill and Bodell (1977) along a line roughly coincident with the self-potential line. A broad dipolar self-potential anomaly, extending from about 2.5 km west to about 1 km east, is roughly centered over the Dome fault. The broad anomaly is interrupted by a steep potential gradient centered directly over the surface trace of the Dome Fault. Some smaller self-potential variations correlate with faults or fault zones (indicated by arrows in Fig. 11) described by Ward and Sill (1976). The large-amplitude, short-wavelength self-potential activity to the east of 1 km east coincides with an area of steep topography and numerous outcrops of granitic rock. As discussed previously, high noise levels might be expected in such areas.

The correspondence between the broad self-potential and thermal gradient profiles suggests a geothermal origin for the self-potential. However, alunite (Ward and Sill, 1976) and pyrite (Parry et al., 1976) are known to be present in the Dome Fault zone. As discussed previously, self-potential activity may be associated with these minerals. The dipolar nature of this anomaly, however, is not typical of self-potential activity related to pyrite or alunite mineralization, which usually is of

negative polarity (Sato and Mooney, 1960; Gay, 1967). The shape of the dipolar anomaly is similar to that seen at Cerro Prieto (discussed earlier), and its coincidence with a major fault suggests a similar source geometry; electrical activity with a finite vertical extent concentrated in the fault zone. The short-wavelength dipolar anomaly superimposed on the longer wavelength variation and located directly over the surface trace of the fault could be caused by a separate, shallower zone of geothermally generated electrical activity along the fault.

#### 5. Steamboat Springs, Nevada

Reconnaissance electrical surveys, including self-potential measurements, were made by the U.S. Geological Survey in the Steamboat Springs area of Nevada in 1975 (Fig. 12). The surveys covered the Steamboat Hills, an area of about 21 km<sup>2</sup> west of Highway 395. Detailed self-potential studies were previously made in the eastern part of this area by White et al. (1964). The earlier survey reported considerable difficulty with "fluctuating conditions", which were attributed to "differences in chemical activity, weather, and soil moisture interacting with the porous pot (copper-copper sulfate) electrodes that were used." Station spacing was 50 ft (15.2 m) and positive and negative anomalies of several hundred mV amplitude and as much as 200 ft (61 m) in width were observed, "with no recognized geologic differences to distinguish positive from negative."

Examination of this earlier data shows that areas of opaline and chalcedonic sinter outcrop coincide with large-amplitude (about 100 mV) short-wavelength potential variations, in contrast to other areas where short-wavelength variations were of much smaller amplitude. It appears

that extreme electrode polarization effects were responsible for the noise, which tended to obscure other anomalies. White et al. (1964) state that no broad scale trends were found; however, one of their traverses (no. 8) crossed the north end of the principal anomaly found in the 1975 survey. Smoothing of their data shows a dipolar anomaly of 100 mV amplitude and 1200 m width, bounded by negative skirts, which corresponds well with the 1975 data.

In the 1975 reconnaissance survey, a station spacing of 300 m and a leapfrog method of traversing were used in order to cover the large area. As this technique is subject to cumulative errors, three sets of electrodes (one of copper-copper sulfate and two of silver-silver chloride) were used to check electrode polarization. Almost all of the lines were closed, and closure error did not exceed 13 mV with the silver-silver chloride electrodes. The copper-copper sulfate electrodes proved unsatisfactory for this survey because of large drifts, probably caused by polarization effects.

The self-potential contour map (Fig. 12) shows a north-trending positive zone flanked by negative skirts, suggesting a dipolar source, situated between the mud volcano basin and the high terrace. This area is about 1 km west of and 30 m higher in elevation than the Steamboat Springs fault zone, along which the present hot spring activity is concentrated. It is interesting to note that no major long-wavelength anomalies are associated with the Steamboat Springs fault zone although the northern part along the main hot spring terrace is positive with respect to the background. Fault patterns in the Steamboat Hills are rather complex. The faults trend predominantly northeast, northwest, and north, with north

trending faults being the most numerous and youngest (White et al., 1964). The negative skirts of the self-potential anomaly are associated with westerly dipping, north trending faults on the northern edge only.

Audio-magnetotelluric surveys and two telluric traverses (Fig. 12) were made in conjunction with the self-potential survey. These data sets all show a low-resistivity trough running north-south along the western edge of the self-potential anomaly and decreasing to the south, about where the self-potential anomaly ends.

### Conclusions

Both thermoelectric and electrokinetic coupling mechanisms may generate self-potential anomalies comparable to those observed in geothermal areas. If the local resistivity distribution is known, source geometry may be estimated using standard potential field techniques. Estimates of additional parameters such as the pressure and temperature distribution of the source may be made using an approach described by Nourbehecht (1963). When this approach is applied to a simple spherical source, electrokinetic coupling is seen to generate larger anomalies than thermoelectric coupling for reasonable values of the temperature, pressure, and coupling coefficients. Potentials generated by this model for both thermoelectric and electrokinetic coupling are smaller in amplitude than many observed self-potential anomalies in geothermal areas, implying that the model geometry or the laboratory-measured coupling coefficients are not realistic for geothermal sources. An important point of this analysis is that the size and polarity of self-potential anomalies generated by geothermal activity depend not only on source parameters such as temperature, pressure,



and geometry, but also on the magnitude and differences of the coupling coefficients.

Most self-potential measurements are reproducible within about  $\pm 5$  mV if proper field procedure and data reduction techniques are used. A better understanding of sources of geologic noise and electrode effects could lead to techniques for their removal from field data, allowing more reliable detection of anomalies of amplitude less than a few tens of millivolts. The possibility that observed anomalies may be related to non-geothermal sources, both geologic and cultural, must be considered. As with any other geophysical technique, all other available geological and geophysical information must be used when considering the significance of self-potential data.

Self-potential anomalies ranging in amplitude from about 50 mV to over 2V have been recorded in at least thirteen different geothermal areas around the world. Anomaly shapes show no consistent pattern, although the steepest gradients often are associated with faults thought to be conduits for thermal water, and broad-scale anomalies sometimes roughly coincide with areas of elevated heat flow. The short-wavelength, large amplitude anomalies that often appear to be related to faults in geothermal areas may be produced by relatively shallow thermal fluids in the fault zones, acting through an electrokinetic or thermoelectric coupling mechanism. Also, long-wavelength fields generated by deeper sources may exhibit locally steep gradients over near-surface lateral resistivity boundaries such as faults or contacts.

At this time the most promising uses of the self-potential method in geothermal exploration appear to be for the detection and tracing of

faults which control the flow of thermal fluids (often characterized by a dipolar anomaly centered over the fault or by a steep self-potential gradient), and as a reconnaissance technique in searching for areas of elevated heat flow, which may be roughly outlined by broad, relatively smooth self-potential anomalies interrupted by the steep gradients characteristic of fault zones or contacts.

Acknowledgments

This work was supported in part by the U.S. Department of Energy under Contract no. W-7405-ENG-48 to the Lawrence Berkeley Laboratory, University of California, Berkeley, and in part by the U.S. Geological Survey. We thank D.V. Fitterman, C.J. Zablocki, D.R. Mabey, H.F. Morrison, and M.H. Dorfman for their help and criticism. A.L. Lange of AMAX Exploration, Inc. kindly allowed us to use the Roosevelt Hot Springs data, and P. Wilde provided helpful support for the Mono Lake survey.

REFERENCES

- Ahmad, M.U., 1964, A laboratory study of streaming potentials: Geophys. Prosp., v. 12, no. 1, p. 49-64.
- Anderson, L.A., and Johnson, G.R., 1976, Application of the self-potential method to geothermal exploration in Long Valley, California, Jour. Geophys. Res., v. 81, no. 8, p. 1527-1532.
- Beyer, H., Dey, A., Liaw, A., Majer, E., McEvelly, T.V., Morrison, H.F., and Wollenberg, H., 1976, Preliminary open file report, geological studies in Grass Valley, Nevada: Lawrence Berkeley Laboratory report LBL-5262, Berkeley, California.
- Bogoslovsky, V.V., and Ogilvy, A.A., 1973, Deformations of natural electric fields near drainage structures: Geophys. Prosp., v. 21, no. 4, p. 716-723.
- Broughton Edge, A.B., and Laby, T.H., 1931, The principles and practice of geophysical prospecting: Cambridge Univ. Press, London.
- Combs, J., and Wilt, M., 1976, Telluric mapping, telluric profiling, and self-potential surveys of the Dunes geothermal anomaly, Imperial Valley, California: Proceedings, Second United Nations Symposium on the Development and Use of Geothermal Resources, San Francisco, Calif., U.S. Government Printing Office, Washington, D.C., v. 2, p. 917-928.
- Corwin, R.F., and Conti, U., 1973, A rugged silver-silver chloride electrode for field use: Rev. Sci. Instrum., v. 44, no. 6, p. 708-711.

- Corwin, R.F., 1976a, Self-potential exploration for geothermal reservoirs: Proceedings, Second United Nations Symposium on the Development and Use of Geothermal Resources, San Francisco, Calif., U.S. Government Printing Office, Washington, D.C., v. 2, p. 937-945.
- Corwin, R.F., 1976b, Offshore use of the self-potential method: Geophys. Prosp., v. 24, no. 1, p. 79-90.
- Dakhnov, V.N., 1962, Geophysical well logging: Colorado School of Mines Quarterly, v. 57, no. 2.
- Dorfman, M.H., Oskay, M.M., and Gaddis, M.P., 1977, Self-potential profiling-- a new technique for determination of heat movement in a thermal oil recovery flood: Preprint, paper presented at 52nd annual meeting, Society of Petroleum Engineers of AIME, Denver.
- Ewing, S., 1939, The copper-copper sulfate half-cell for measuring potentials in the earth: American Gas Association Proc. 624.
- Gay, S.P., Jr., 1967, A 1800 millivolt self-potential anomaly near Hualgayoc, Peru: Geophys. Prosp., v. 15, no. 2, p. 236-245.
- Goldstein, N.E., Beyer, H., Corwin, R., diSomma, D.E., Majer E., McEvelly, T.V., Morrison, H.F., Wollenberg, H.A., and Grannell, R., 1976, Open file report geoscience studies in Buena Vista Valley, Nevada: Lawrence Berkeley Laboratory report LBL-5913, Berkeley, Calif.
- Grant, F.S., and West, G.F., 1965, Interpretation theory in applied geophysics: McGraw-Hill, New York.
- Heikes, R.R., and Ure, R.W., 1961, Thermoelectricity: Science and Engineering: Interscience, New York.
- Hoogervorst, G.H.T.C., 1975, Fundamental noise affecting signal-to-noise ratio of resistivity surveys: Geophys. Prosp., v. 23, no. 2, p. 380-390.

- Jangi, B.L., Prakash, G., Dua, K.J.S., Thussu, J.L., Dimri, D.B., and Pathak, C.S., 1976, Geothermal exploration of the Parbati Valley geothermal field Kulu District, Himachal Pradesh, India: Proceedings, Second United Nations Symposium on the Development and Use of Geothermal Resources, San Francisco, Calif., U.S. Government Printing Office, Washington, D.C., v. 2, p. 1085-1094.
- Keller, G.V., and Frischknecht, F.C., 1966, Electrical methods in geophysical prospecting: Pergamon, New York.
- Klinkenberg, A., and van der Minne, J.L., 1958, Electrostatics in the petroleum industry: Elsevier, New York.
- Kruger, F.C., and Lacy, W.C., 1949, Geological explanation of geophysical anomalies near Cerro de Pasco, Peru: Econ. Geol., v. 44, no. 6, p. 485-491.
- Kruyt, H.R., 1952, Colloid science: Elsevier, New York.
- Lenzer, R.C., Crosby, G.W., and Berge, C.W., 1977, Recent developments at the Roosevelt Hot Springs KGRA: Proceedings, Amer. Nuclear Soc. topical meeting on energy and mineral resource recovery, April 1977, Colo. School of Mines, Golden, Colorado, p. 60-67.
- Mabey, D.R., Hoover, D.B., O'Donnell, J.E., and Wilson, C.W., ( ), Reconnaissance geophysical studies of the geothermal system in the southern Raft River Valley, Idaho (this volume).
- MacInnes, D.A., 1961, The principles of electrochemistry: Dover, New York.
- Mañon, A., Mazon, E., Jiménez, M., Sanchez, A., Fausto, J., and Zenizo, C., 1977, Extensive geochemical studies in the geothermal field of Cerro Prieto, Mexico: Lawrence Berkeley Laboratory Report LBL-7019.
- Noble, J.E., Mañon, A., Lippmann, M.J., and Witherspoon, P.A., 1977, A study of the structural control of fluid flow within the Cerro

- Prieto geothermal field, Baja California, Mexico: Preprint, 52nd Annual Meeting of the Society of Petroleum Engineers, AIME.
- Nourbehecht, B., 1963, Irreversible thermodynamic effects in inhomogeneous media and their application in certain geoelectric problems: Ph.D. thesis, Mass. Inst. of Tech., Cambridge.
- Ogilvy, A.A., Ayed, M.A., and Bogoslovsky, V.A., 1969, Geophysical studies of water leakages from reservoirs: Geophys. Prosp., v. 22, no.1, p. 36-62.
- Olmsted, F.H., Glancy, P.A., Harrill, J.R., Rush, F.E., and Van Denburgh, A.S., 1975, Preliminary hydrogeological appraisal of selected hydrothermal systems in northern and central Nevada: U.S. Geol. Survey Open File Report 75-76.
- Onodera, S., 1974, Geo-electric indications at the Otake geothermal field in the western part of the Kujyu Volcano Group, Kyushu, Japan: in Colp, J.L., and Furumoto, A.S., eds., Proceedings of a Conference, The Utilization of Volcano Energy: Sandia Laboratories, Albuquerque, N.M., p. 80-106.
- Parasnis, D.S., 1966, Mining geophysics: Elsevier, New York.
- Parasnis, D.S., 1970, Some recent geoelectric measurements in the Swedish sulfide ore fields illustrating scope and limitations of the methods concerned: Mining and Groundwater Geophysics, 1967, Geological Survey of Canada, Ottawa, Econ. Geol. Report No. 26, p. 290-301.
- Parry, W.T., Benson, N.L., and Miller, C.D., 1976, Geochemistry and hydrothermal alteration at selected Utah hot springs: Nat'l. Science Foundation Final Report, Contract G143741, Univ. of Utah, Salt Lake City.

- Poldini, E., 1939, Geophysical exploration by spontaneous polarization methods: *The Mining Magazine*, v. 60, p. 22-27.
- Rapolla, A., 1974, Natural electric field survey in three southern Italy geothermal areas: *Geothermics*, v. 3, no. 3, p. 118-121.
- Sato, M., and Mooney, H.M., 1960, The electrochemical mechanism of sulfide self-potentials: *Geophysics*, v. 25, no. 1, p. 226-249.
- Semenov, A.S., 1974, Electrical prospecting with the method of the natural electric field: *Nedra*, Leningrad.
- Sill, W.R. and Bodell, J., 1977, Thermal gradients and heat flow at Roosevelt Hot Springs: ERDA Technical Report, Vo. 77-3, Contract EY-76-S-07-1601, Univ. of Utah, Salt Lake City.
- Tuman, V.S., 1963, Thermo-telluric currents generated by an underground explosion and other geological phenomena: *Geophysics*, v. 28, no. 1, p. 91-98.
- Ward, S.H., and Sill, W.R., 1976, Dipole-dipole resistivity surveys, Roosevelt Hot Springs KGRA; Final Report, v. 2, to Nat'l Science Foundation, Contract G1-43741, Univ. of Utah, Salt Lake City.
- Waring, G.A., 1965, Thermal springs of the United States and other countries of the world: A summary. Revised by R.R. Blankenship and R. Bentall: U.S. Geological Survey Prof. Paper 492, U.S. Gov't. Printing Office, Washington, D.C.
- Welday, E.E., 1977, Thermal probe study of Mono Lake, California: in Geothermal investigations of California submerged lands and spherical flow in naturally fractured reservoirs: State Lands Commission, State of California, part D.



- White, D.E., Thompson, G.A., and Sandberg, C.H., 1964, Rocks, structure and geologic history of Steamboat Springs thermal area, Washoe County, Nevada: U.S. Geological Survey Prof. paper 458-B, U.S. Gov't. Printing Office, Washington, D.C.
- Williams, P.L., Mabey, D.R., Zohdy, A.A.R., Ackerman, H., Hoover, D.B., Pierce, K.L., and Oriel, S.S., 1976, Geology and geophysics of the southern Raft River Valley geothermal areas, Idaho, U.S.A.: Proceedings, Second United Nations Symposium on the Development and Use of Geothermal Resources, San Francisco, Calif., U.S. Government Printing Office, Washington, D.C., v. 2, p. 1273-1282.
- Yamashita, S., 1961, The electromotive force generated within the ore body by the temperature difference: J. Min. Coll; Akita Univ. (Japan), Ser. A., vol. 1, no. 1, p. 69-78.
- Zablocki, C.J., 1976, Mapping thermal anomalies on an active volcano by the self-potential method, Kilauea, Hawaii: Proceedings, Second United Nations Symposium on the Development and Use of Geothermal Resources, San Francisco, Calif., U.S. Government Printing Office, Washington, D.C., v. 2, p. 1299-1309.
- Zohdy, A.A.R., Anderson, L.A., and Muffler, L.J.P., 1973, Resistivity, self-potential and induced polarization surveys of a vapor-dominated geothermal system: Geophysics, v. 38, no. 6, p. 1130-1144.

FIGURES

- Figure 1  
(XBL 787-9595) Spherical model for thermoelectric or electrokinetic potential generation (after Nourbehecht, 1963). The boundary at depth  $d$  separates layers of different resistivity  $\sigma$  and coupling coefficient  $C$ . The sphere is at a temperature  $100^\circ\text{C}$  above the ambient temperature  $T_0$ , or at a pressure 5 atm above the ambient pressure  $P_0$ . The polarity of the self-potential anomaly depends on the sign of the coupling coefficient difference  $(C_1 - C_2)$ .
- Figure 2  
(XBL 787-9597) Self-potential distribution over a coal-mine fire, Marshall, Colorado. Contour interval is 20 mV. Open circles are survey stations.
- Figure 3  
(XBL 787-9594) Self-potential vs. ground elevation, Adagdak Volcano, Adak Island, Alaska.
- Figure 4  
(XBL 787-9592) Self-potential profile, line B-B', Kyle Hot Springs area, Buena Vista Valley, Nevada. KY-1 and KY-3 are drill-hole locations.
- Figure 5  
(XBL 787-9598) Variations in electrode potential caused by watering of copper-copper sulfate electrodes, Raft River, Idaho. Electrode separation was 200 m.
- Figure 6  
(XBL 787-9596) Self-potential profiles, line A-A', Leach Hot Springs area, Grass Valley, Nevada. Location of line A-A' is shown in Figure 7A. Upper profile was run in August 1974 and lower profile in September 1975, using improved field techniques described in text. Note typical desert soil background noise level of  $\pm 5$  to  $\pm 10$  mV toward north and south ends of 1975 profile.
- Figure 7  
(XBL 787-9599A) A. Self-potential distribution in Leach Hot Springs area, Grass Valley, Nevada, based on smoothed data taken in September 1975. SP-A through SP-E, A-A', and E-E' are traverse lines along which measurements were made. Electrode spacing usually was 100 m; contour interval is 10 mV. Faults dashed where inferred.
- B. Heat flow contours (dashed) and altitude of water table above sea level (solid lines) in the Leach Hot Springs area. (After Olmsted et al., 1975).

Figure 8  
(XBL 787-9600A)

Self-potential profile (December 1977 and March 1978), geologic cross-section (from Mañon et al., 1977), and electrical model for line B-B', Cerro Prieto geothermal field, Baja California, Mexico. The dashed line on the self-potential profile was generated by the model shown at the bottom of the figure. The location of line B-B' and the straight line onto which the data were projected are shown in Figure 9.

Figure 9  
(XBL 787-9593)

Line B-B', Cerro Prieto geothermal field, Baja California, Mexico. That data shown in Figure 8 were projected onto the straight dashed line connecting points B and B' to reduce geometric distortion. The indicated geothermal wells roughly outline the present production zone (the western boundary of the zone is between wells M-6 and M-9). The exact location and strike of the fault which passes between wells M-10 and M-53 are not yet established.

Figure 10  
(XBL 787-9601)

Gradient and total field self-potential anomaly in Mono Lake, California, near hot springs area on Paoha Island. Electrodes were towed along the water surface, and water depth was about 15 m.

Figure 11  
(XBL 787-9602)

Thermal gradient and self-potential profiles across the Dome Fault, Roosevelt Hot Springs KGRA, Utah. The 0-km point is at the intersection of sections 9, 10, 16, and 15, and the line runs due east-west. Thermal gradient data are from Sill and Bodell (1977). Arrows denote points at which faults mapped by Ward and Sill (1976) cross the self-potential survey line.

Figure 12  
(XBL 787-9603)

Self-potential distribution and relative telluric-voltage profiles in the Steamboat Hills area, Nevada. Open circles denote self-potential survey points; closed circles are stations on telluric traverses. Contour interval is 20 mV.

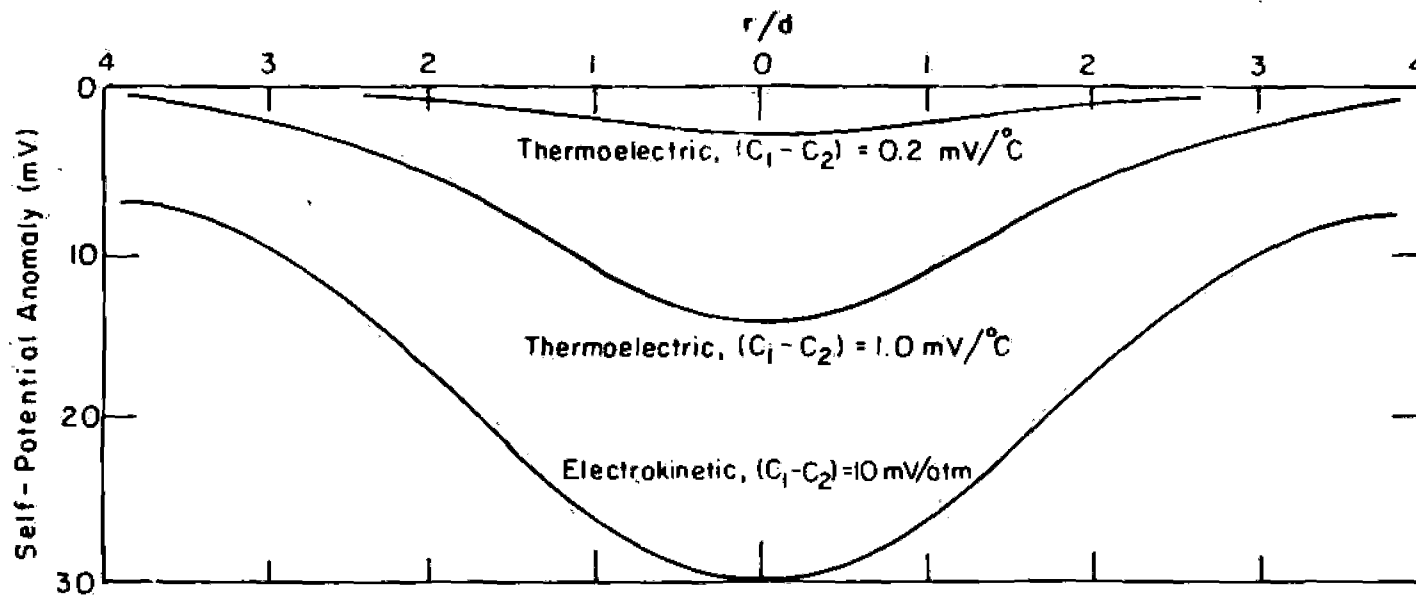
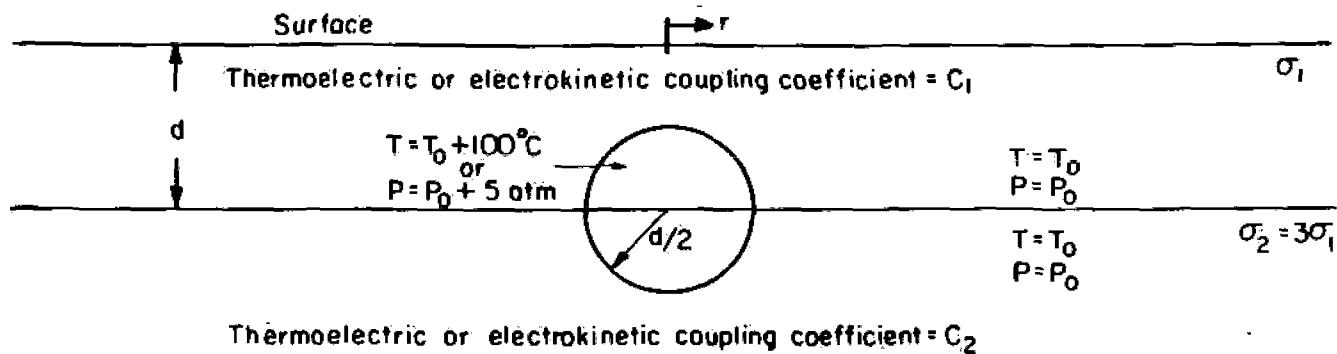


Figure 1

XBL 787-9595

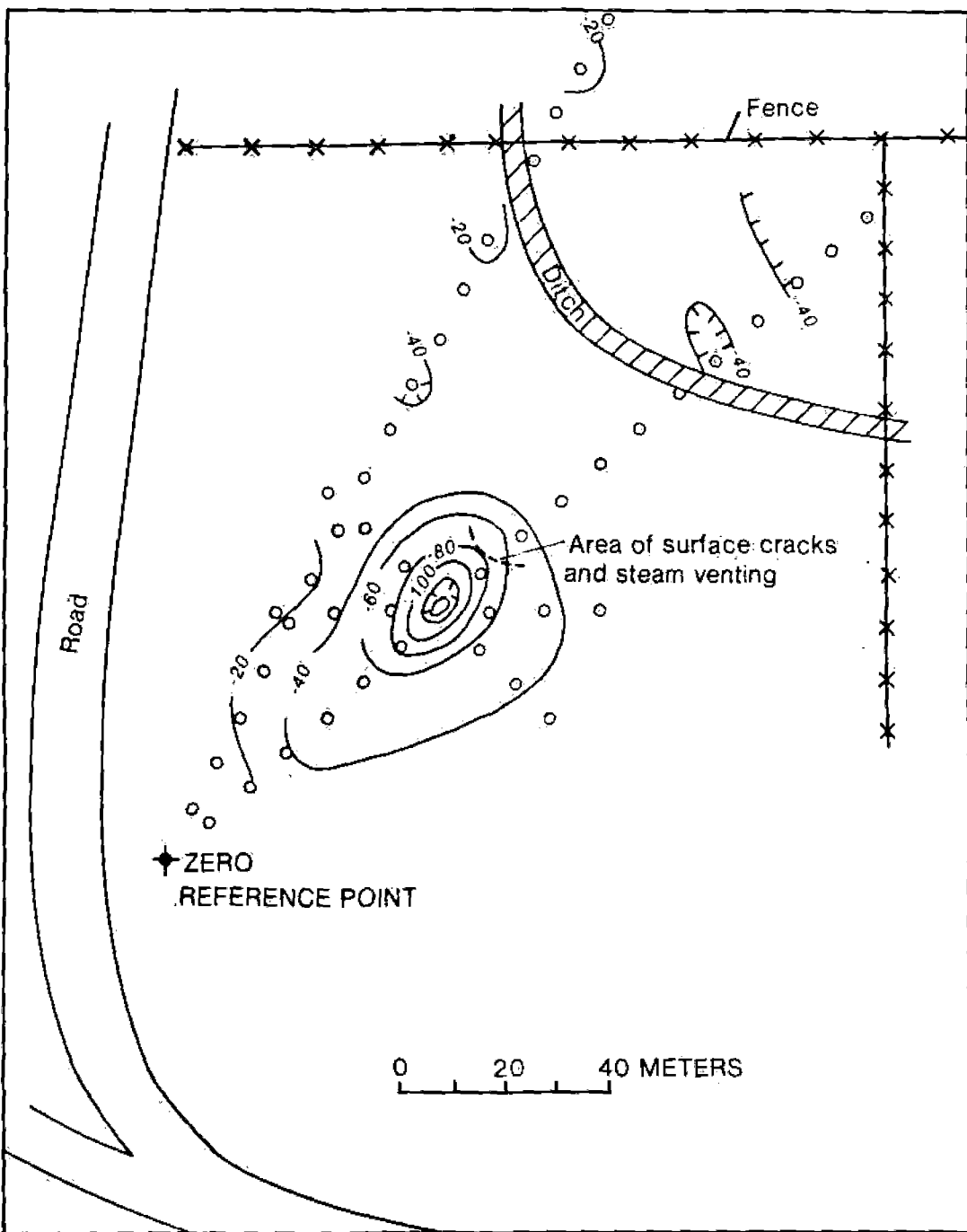


Figure 2

XBL 787-9597

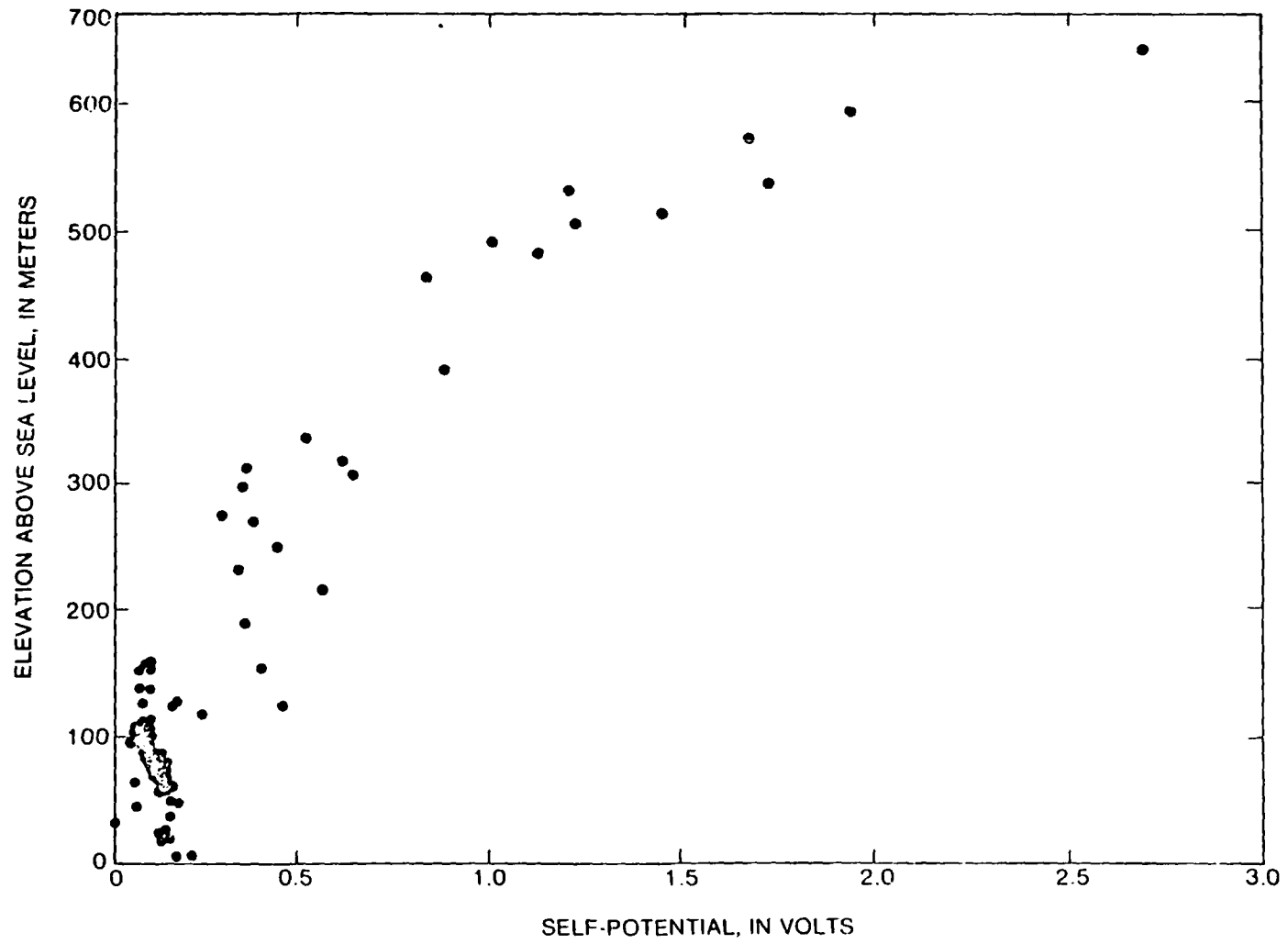


Figure 3

XBL 787-9594

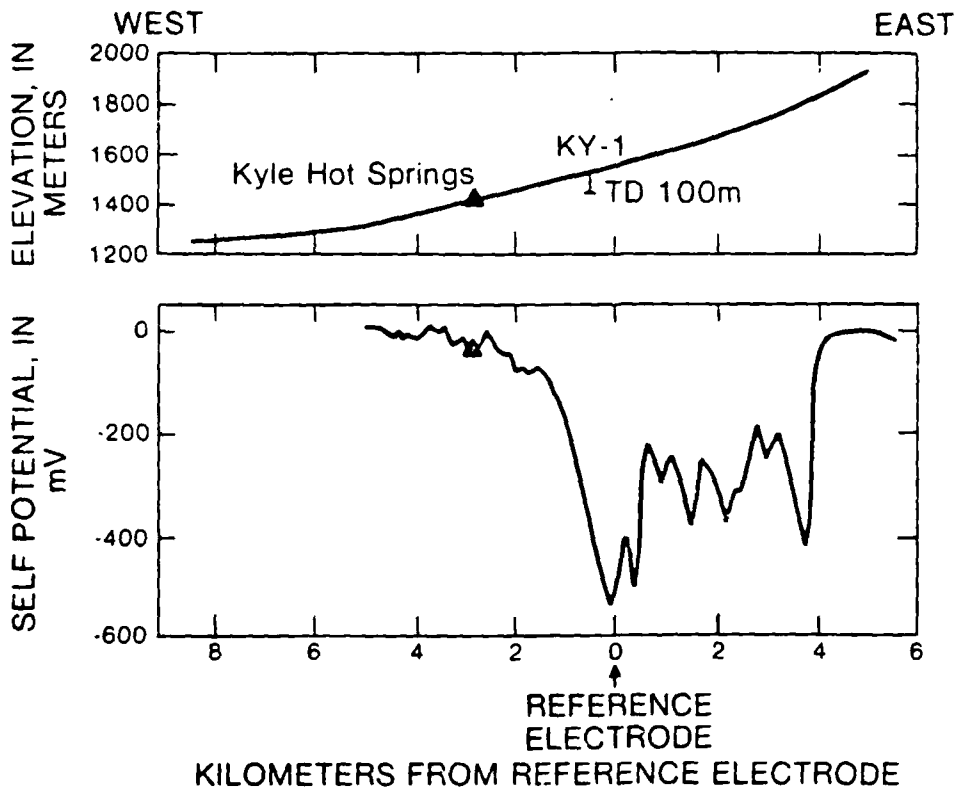
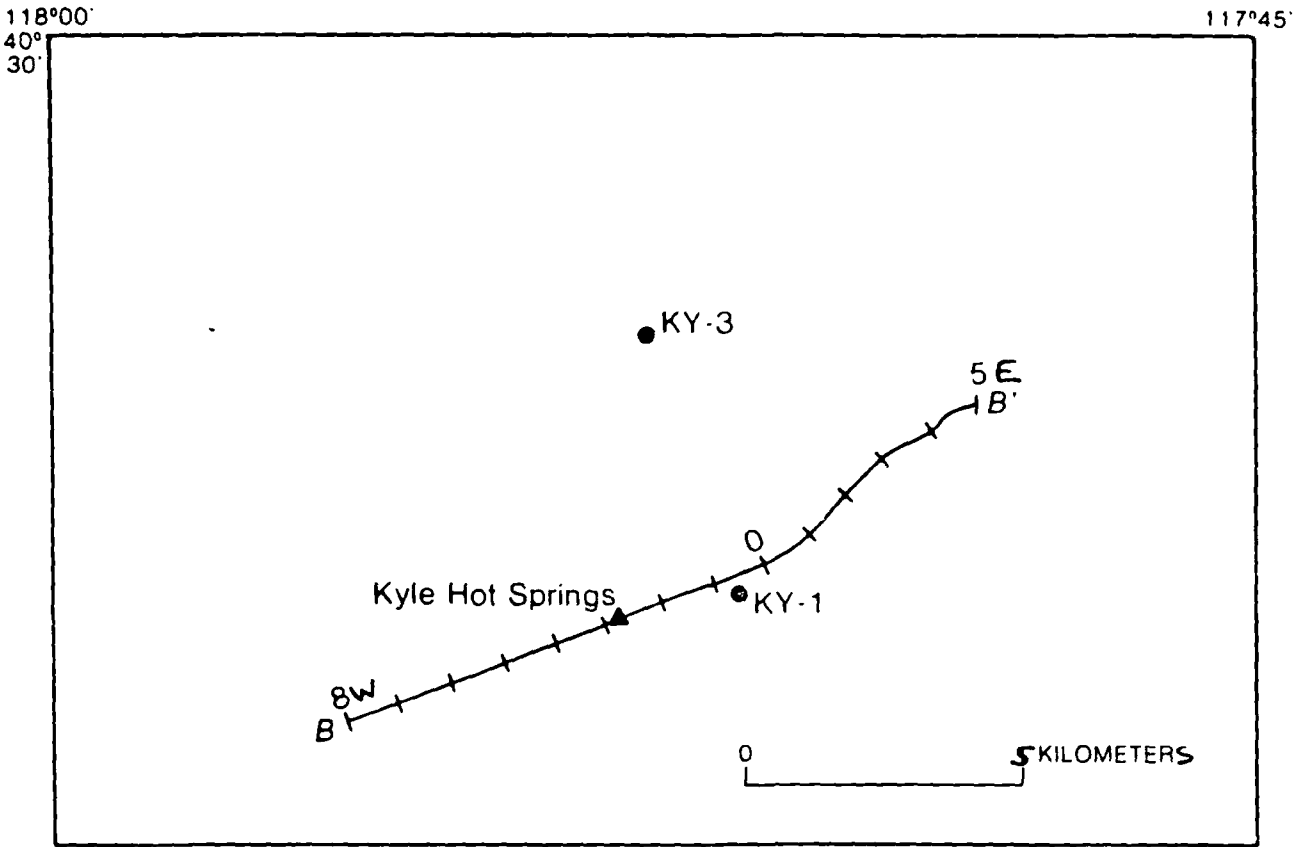
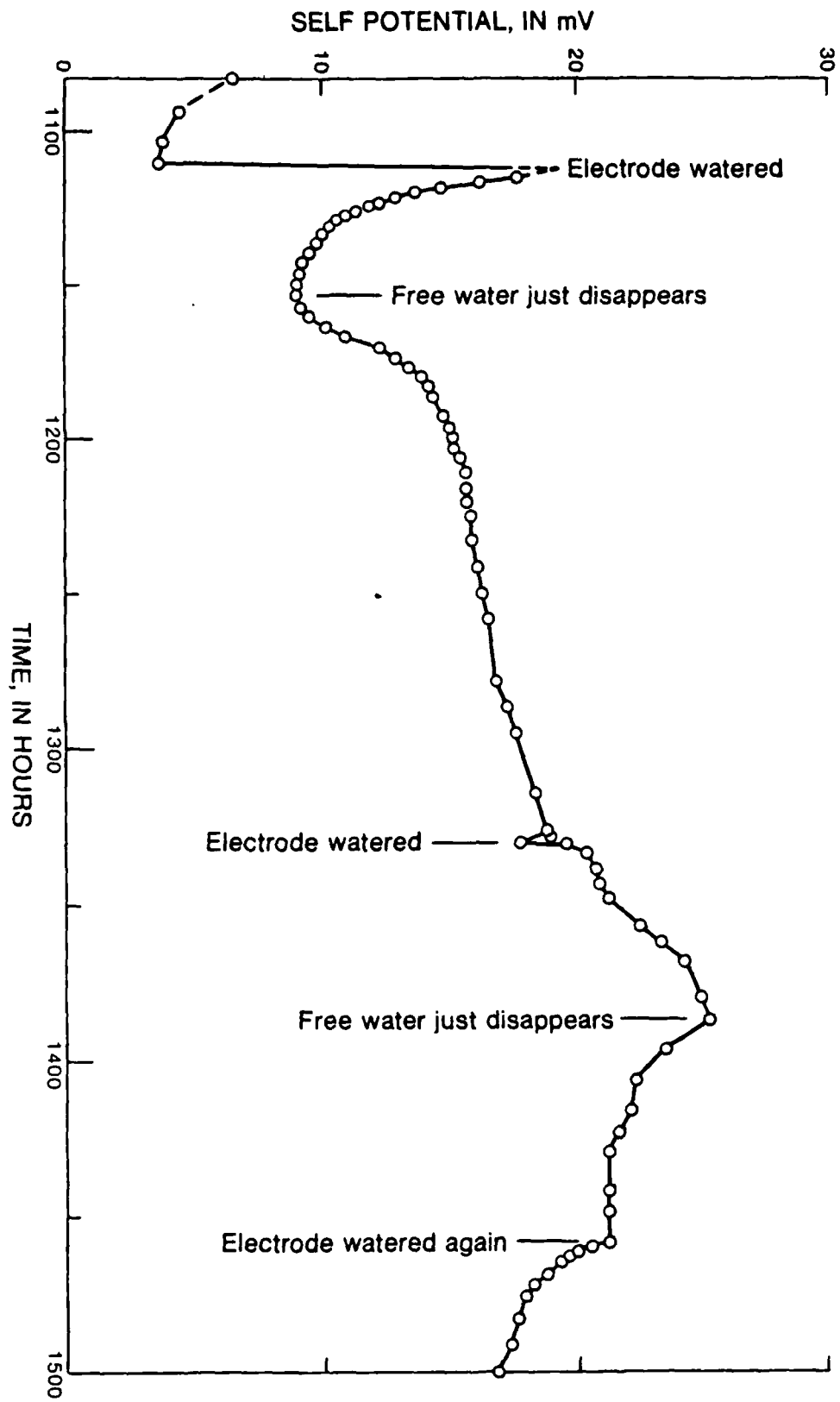


Figure 4

Figure 5



XBL 787-9598



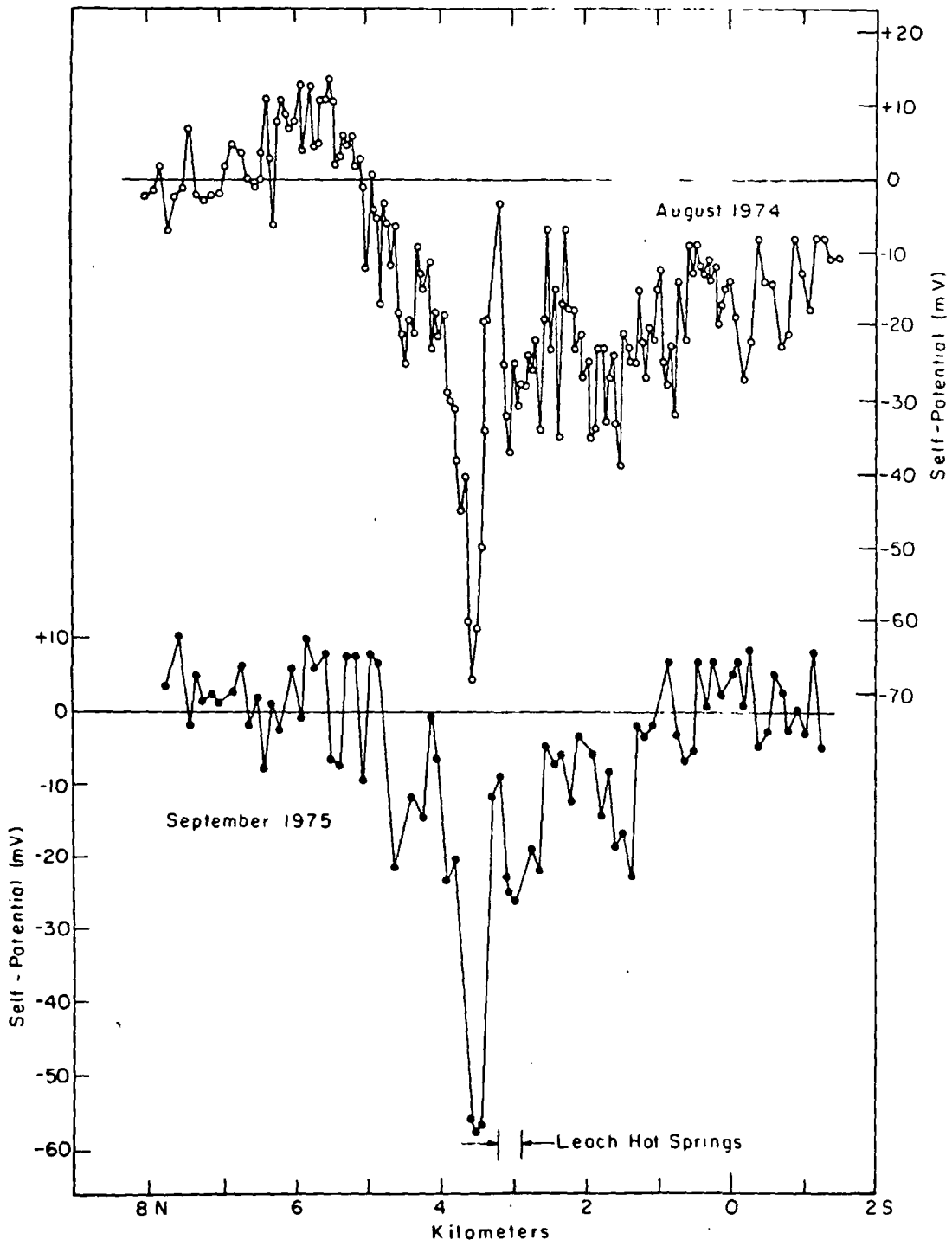


Figure 6

XBL 787-9596

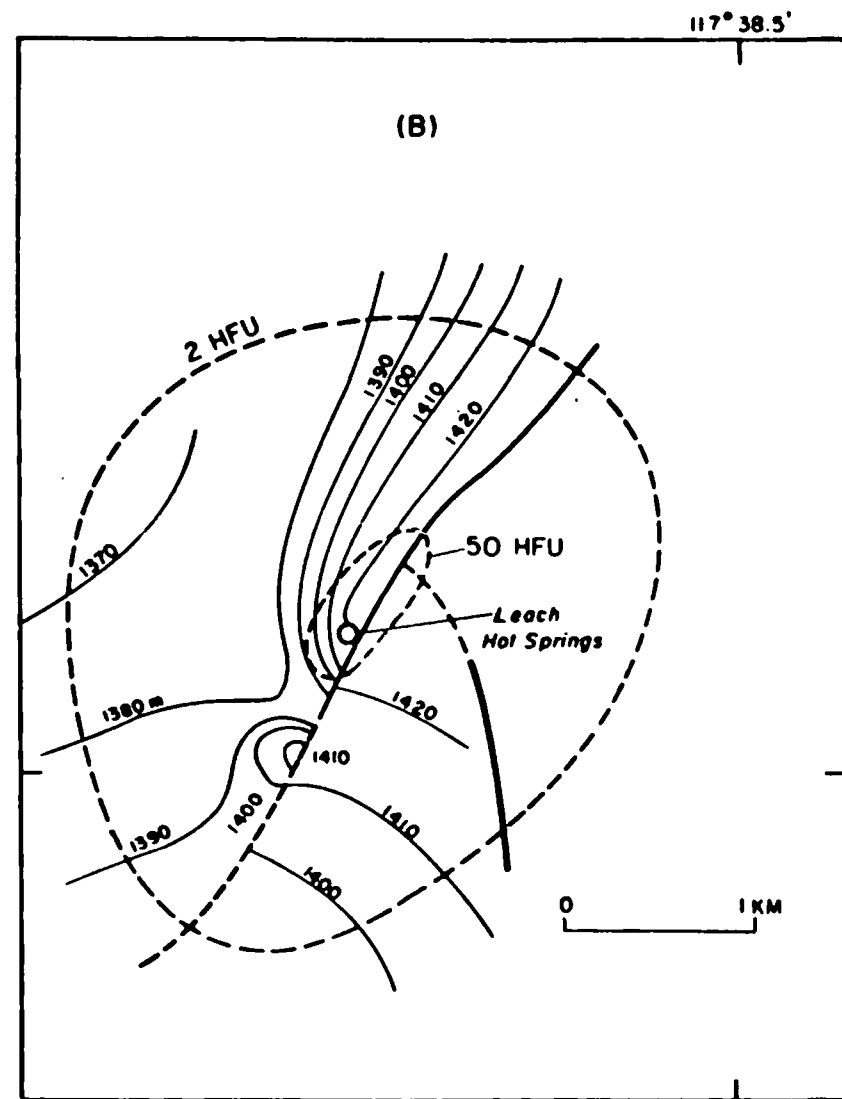
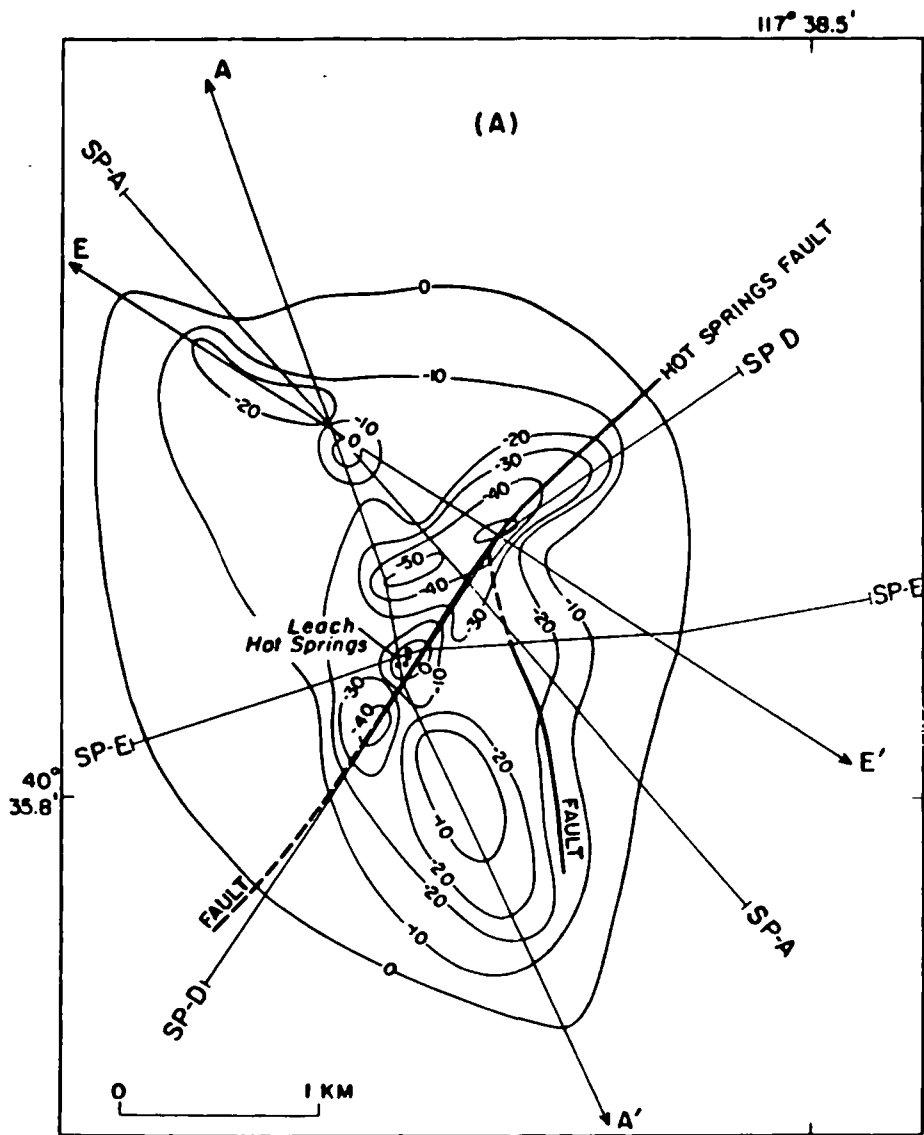


Figure 7

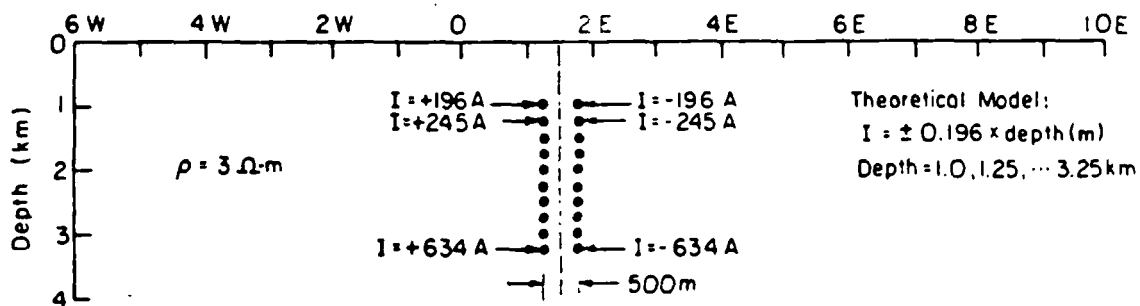
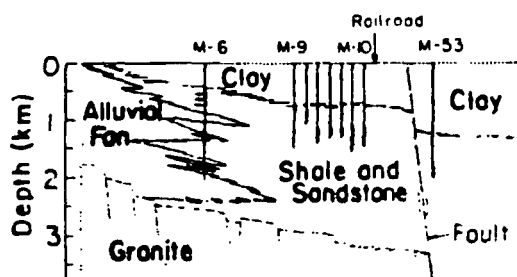
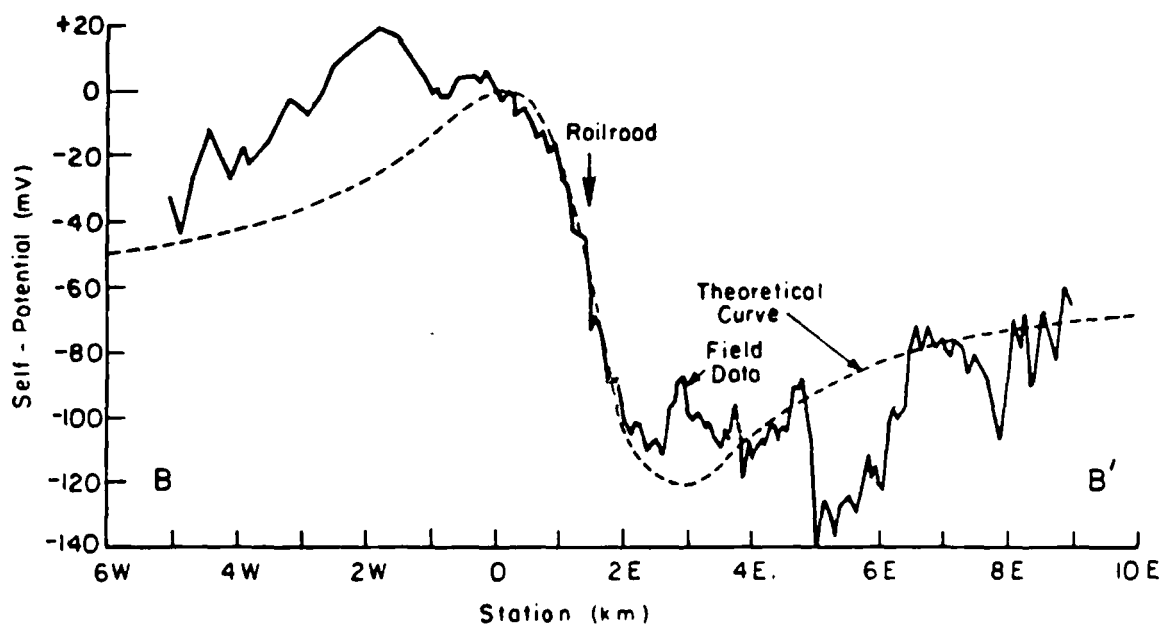


Figure 8

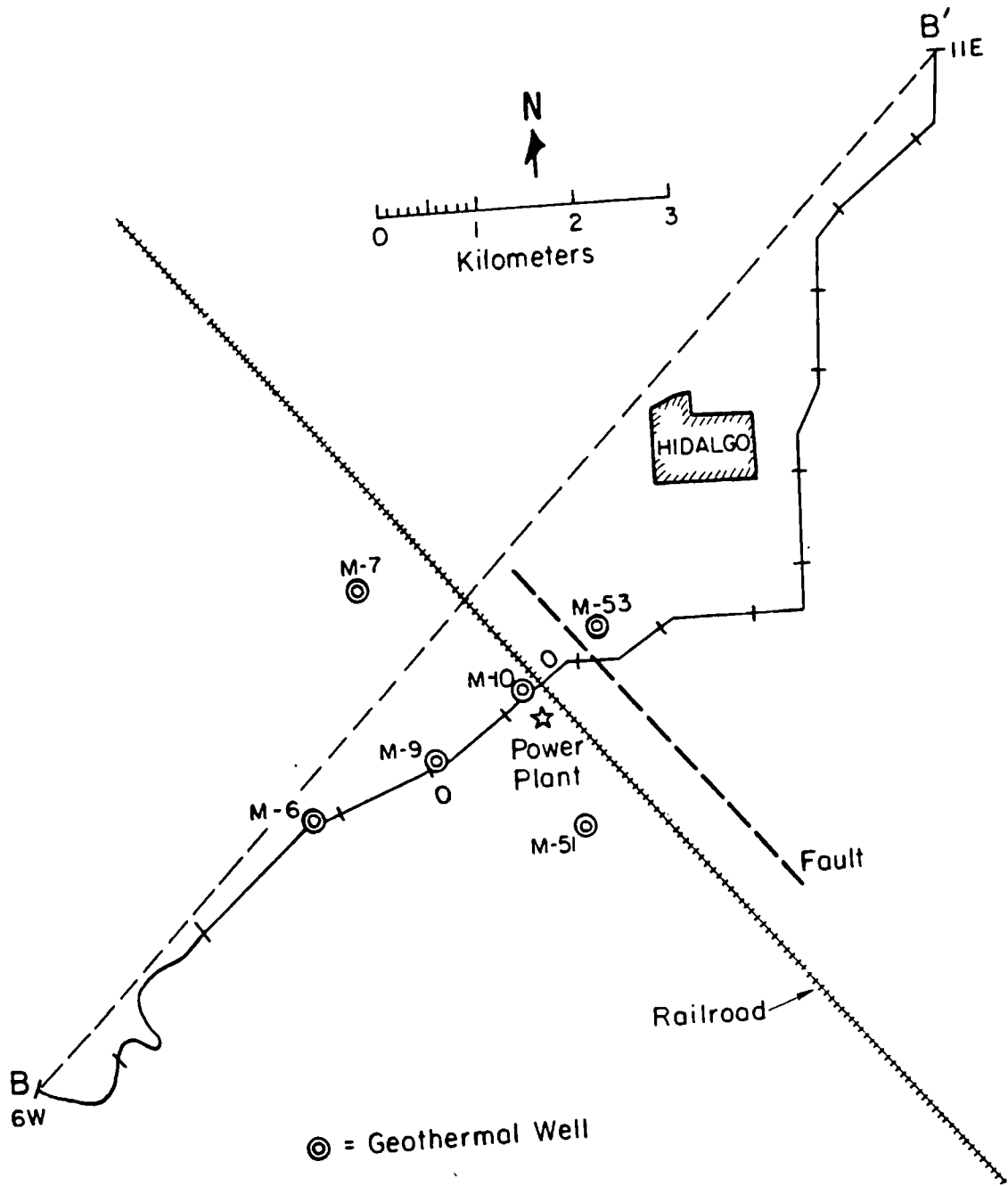


Figure 9

XBL 787-9593

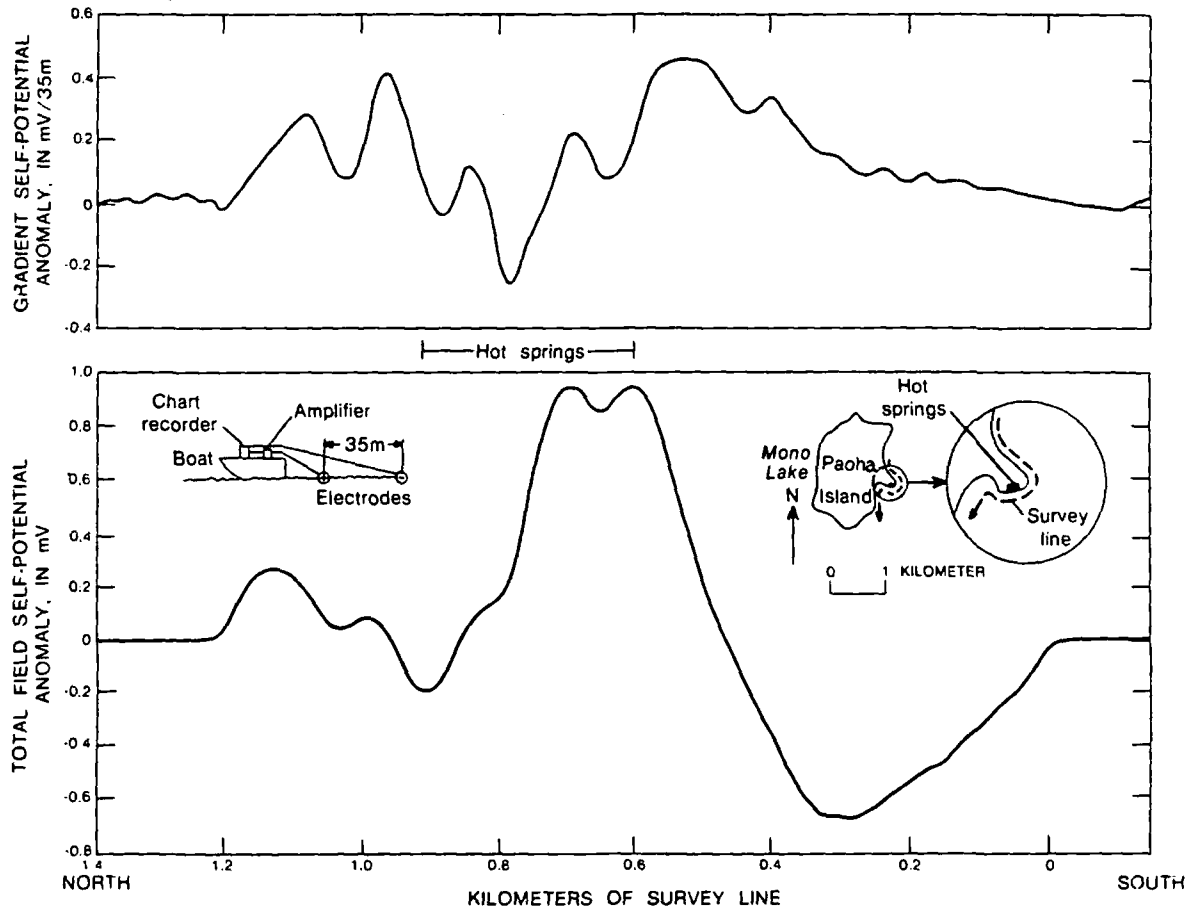


Figure 10

XBL 787-9601

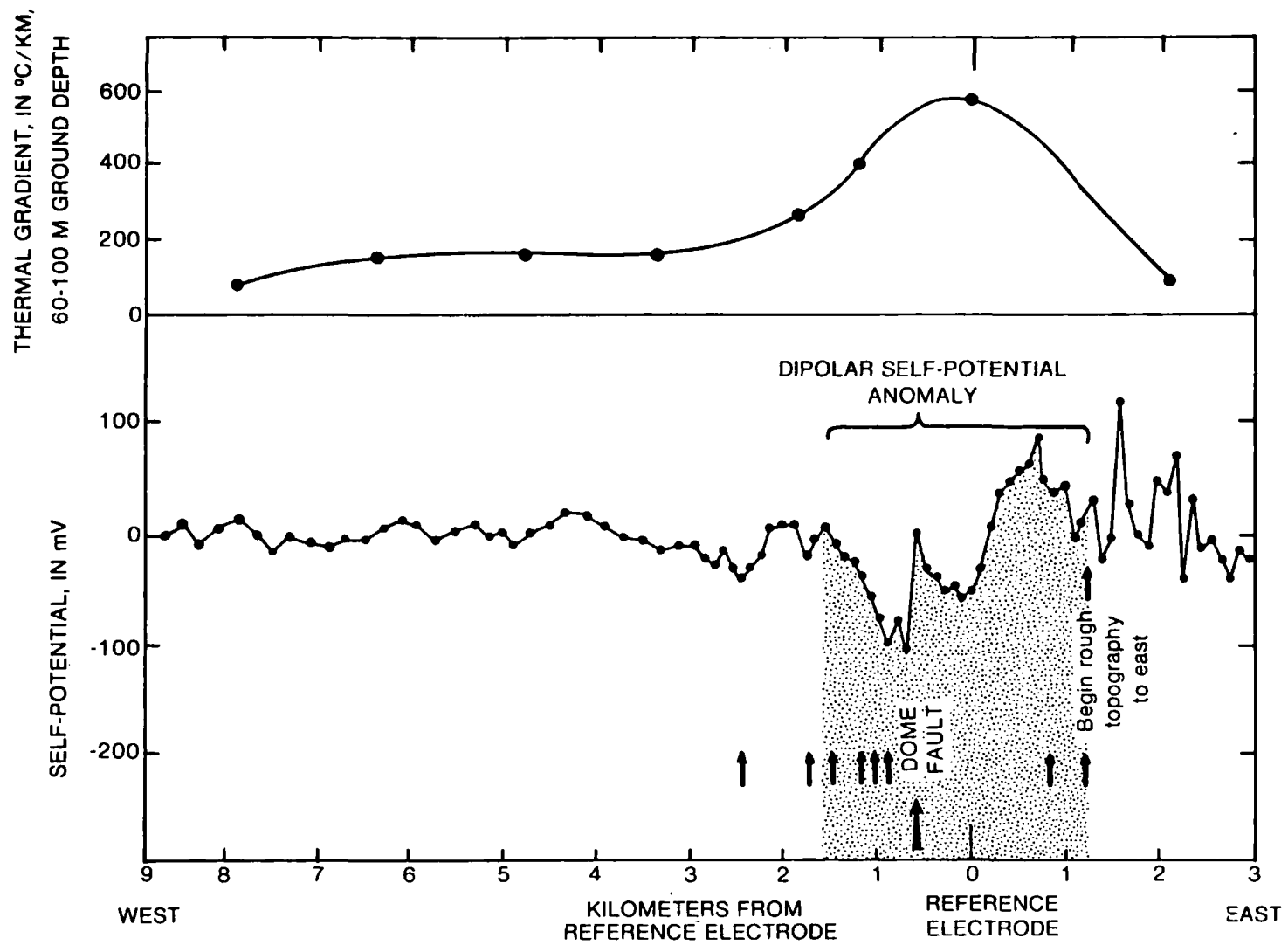


Figure 11

XBL 787-9602

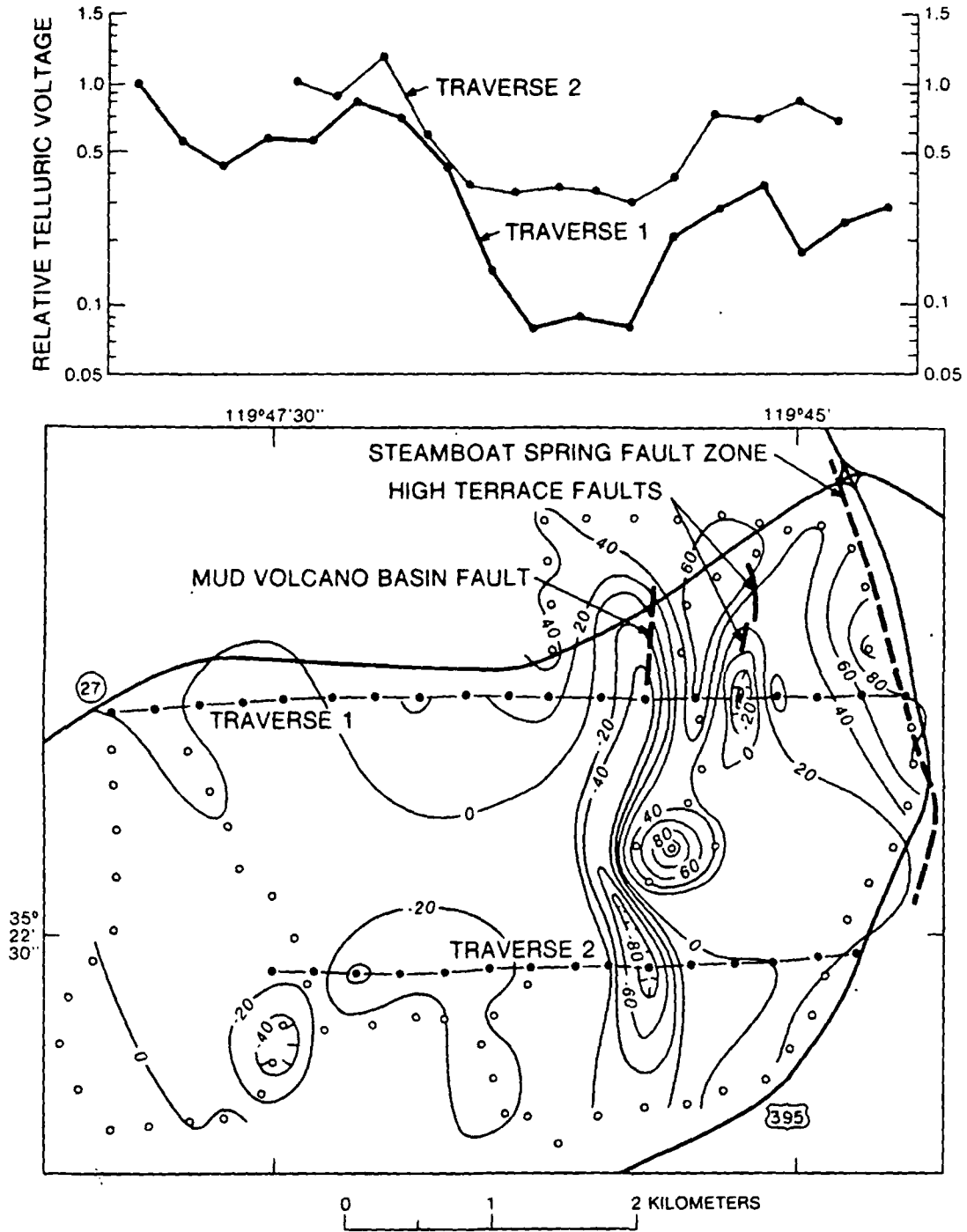


Figure 12

XBL 787-9603

SUBJ  
GTHM  
SQI

*in Bulletin Volcanologique*  
*Vol XXVII, 1964*  
*Napoli, Italy*

## Some quantitative indications of a recent hydrothermal process in volcanic areas.\*

V. V. AVERIEV

Institute of Volcanology of the Academy of Sciences of USSR

UNIVERSITY OF UTAH  
RESEARCH INSTITUTE  
EARTH SCIENCE LAB.

In the present meaning of the word postvolcanic activity embraces quite a vast number of processes. It is also generally assumed that it finds a most vivid expression in the hydrothermal process, which proceeds at an extremely wide range of temperatures. The existence of a general connection between hydrothermal activity and volcanism in volcanic areas does not exoke any doubts, however, their actual relations are not yet established with sufficient detail. On the other hand, our ideas on the formation of hydrothermae depend upon the completeness of our knowledge of geothermal and hydrogeological conditions. In respect to hydrothermae formed in volcanic areas, our data about these conditions are mostly of a most general character. This does not permit to formulate any exact concept regarding actual hydrothermal systems. This report deals with a justification and interpretation of some quantitative data on the recent hydrothermal process, which, in the author's opinion, should help the solution of the abovementioned problems.

Researches during recent years have shown that extensive hydrothermal systems of Kamchatka (Geyser Valley, Pauzhetka) are associated with intense heat anomalies with a specific heat evacuation up to 2-2.4 th.kcal/sec from 1 km<sup>2</sup>. These figures have been obtained by establishing the amount of heat evacuated by thermal springs and steam jets per the area on which they are formed (table 1). The territory of such anomalies comes to tens and, maybe, hundreds of square kilometers. They embrace an area with varying geological and structural conditions. They affect masses of old volcanoes with a low-temperature fumarolic activity, young extrusions and areas with ordinary non-volcanic structures. It is significant that heat evacuation on old

\* Paper read by B. I. PIIP at the IAV scientific session of Aug. 28, 1963 (XIII General Assembly, I.U.G.G.). Symposium on Post-Eruptive Processes in Regions of Active Volcanism.



TABLE 1 - Quantitative data on hydrothermae formation in the Geyser Valley area of Kamchatka.

Hydrothermal systems	Area in sq. km.	Character of hydrothermae	Evacuation of water mass in kg/sec	Average enthalpy in kcal/kg	Heat evacuation in kcal/sec	Specific heat evacuation in kcal/km <sup>2</sup> per sec	Assumed share of endogenous steam in kg/sec	Evacuation during 10000 years for entire area	
								of heat in kcal	of endogenous water in kg
Uzon caldera volcano	6	Boiling springs and steam jets	70	210	14700	2400	18		
Upper reaches of Geysernaia river: Lower complex	3.7	Boiling springs	7.5	200	1500	2000	2	2.8 × 10 <sup>10</sup>	35 × 10 <sup>11</sup>
Upper complex		Warm springs	100	55	5500		7		
Geyser Valley	35	Boiling springs, geysers, steam jets	275	250	68750	2000	86		

volcanic masses virtually does not differ from the average figures for the entire anomaly. Consequently, steam jets and fumaroles associated with such volcanoes can be regarded as phenomena not necessarily evoked by the volcanic structures themselves.

The given values of heat evacuation, 200 times exceeding the average figures for the Earth, can be provided only through a transport of the bulk of heat by steam. From this point of view heat anomalies can be regarded as gigantic drains, along which a concentrated rise of endogenetic steam is taking place in the top horizons of the crust, below the circulation base level of underground waters. (Under « endogenous steam » the author means water of any origin converted into steam in the interior of the Earth below the circulation base level of underground waters). Averaged values of such steaming are very high. For instance, for the Geyser Valley area it approaches the figure of 3 kg/sec for 1 km<sup>2</sup>.

Owing to the of infiltration su intensity. This is thermal manifest: ally — from low-t tion of high-temp sers and steam je filtration propert: ground waters a: strong infiltration can be reservoir c effectively sealed c

In the heat ar ifestations are as surface waters in these amounts of steam hydrotherm Springs with an a ter-bearing comple to 30 l/sec for 1 s

In areas with ferent types of hy relation between t

These data pe tionally powerful tively small and li drothermae of Ge 270 l/sec and evact on an area of 30-4

Inasmuch as endogenous steam, share of this stea enthalpy of steam kcal/kg, and, as sh means that in sprin enous water does maee feeding boiling deposits of hydrot to 60 % and more.

According to g

mal systems on Kamchatka in a whole number of cases coincides by time with the end of the last phase of Upper Quaternary glaciation. The duration of the postglacial period and, consequently, also of the « recent » hydrothermal activity comes to 10-13 th.years. It is characteristic that this figure agrees with the age of thermal springs in Iceland and in Yellowstone Park. The evacuation of heat and endogenous water masses during this period for separate hydrothermal systems is characterized by enormous figures. Thus, hydrothermae of the Geyser Valley area must have evacuated about  $3 \cdot 10^{16}$  kcal of heat, if we accept the time as 10,000 years and the intensity to be permanent (table 1). Such figures are fully comparable with the amount of heat that has been delivered to the surface during this period in the same area as result of volcanic eruptions. As to the evacuation of endogenous water masses it is estimated to be  $40 \cdot 10^{12}$  kg. If one assumes that all this water has been exsolved from the magma, this magmatic body, judging by the 5 weight percentage of volatile content, must have a volume of about 300 km<sup>3</sup>.

The figures quoted make one treat very critically the traditional concepts, which associate the evacuation of endogenous emanations with intrusive bodies disregarding both their sizes and their spatial position. Tentative computations indicate that steam exsolved from a magma at a temperature of 1200° and which reaches the circulation base level of underground waters with a temperature of 300-400°, must have an initial pressure of several thousands atmospheres, which corresponds a depth over 10 km. Small intrusions formed at small depths can, consequently, be at best in a paragenetic connection with a powerful hydrothermal activity and can not be regarded as an original source of the main mass of emanations.

Actually, purely volcanic events (if they are understood as eruptions of igneous material) and post-volcanic activity are two approximately equal branches from the point of view of energy. They might, possibly, be due to the same cause, the eruption of melted material (i.e. volcanicity) being a relatively rapid and short-lived reaction to this cause, whereas the post-volcanic process is characterized by a greater length and its manifestations in the upper horizons of the crust take place somewhat belatedly. The very term « post-volcanic process » in respect to hydrothermal activity is legitimate only in the sense of reflecting the time. However, at least at this stage of our knowledge of the problem, this term should not include any genetic meaning.

J. HEALY: A similar discharge from hot springs in the Tertiary. A magmatic magma can heat water if this is possible.  
K. J. MURATA: In the hydrothermal systems, can seawater be heated?  
B. L. PIIP: Yes, ma

### Discussion

J. HEALY: A similar relationship has been found between present day heat discharge from hot springs and that discharged by volcanism during the Pleistocene. A magmatic mass in cooling can lose only less than one sixth of its heat in water if this is 5% by weight.

K. J. MURATA: In the deep circulation of meteoric water in the hydrothermal systems, can seawater be involved in Kamchatka?

B. L. PIIP: Yes, may be. It is possible.

of cases coincides by  
aternary glaciation.  
requently, also of the  
h. years. It is charac-  
ermal springs in Ice  
heat and endogenous  
drothermal systems  
thermae of the Gey-  
kcal of heat, if we  
ty to be permanent  
the amount of heat  
period in the same  
acuation of endoge-  
kg. If one assumes  
gma, this magmatic  
latile content, must

cally the traditional  
ogenous emanations  
es and their spatial  
eam exsolved from  
ches the circulation  
ire of 300-400°, must  
spheres, which cor-  
ned at small depths  
ection with a pow-  
ded as an original

nderstood as erup-  
y are two approxi-  
nergy. They might,  
of melted material  
t-lived reaction to  
characterized by a  
orizons of the crust  
t-volcanic process »  
ly in the sense of  
of our knowledge  
enetic meaning.

## The Self-sealing Geothermal Field \*

Bulletin Volcanologique

V 30

1967

G. FACCA

Worldwide Geothermal Exploration Co., 10889 Wilshire Blvd. S 1460,  
Los Angeles, California; and 11, Vicolo Clementi (Portuense), Rome 8, Italy.

F. TONANI

Istituto di Mineralogia, University of Florence, Italy.

**Abstract**

A geothermal field producing dry steam or high temperature water is a trap for convection currents generated in an aquifer of high permeability and of sufficient thickness by a deep heat source. A basic implication of this concept is, that a geothermal field requires a cap-rock of more or less impermeable rocks above the producing aquifer.

In Larderello, Monte Amiata, and Salton Sea geothermal fields, a clearly reconnaissable tight formation overlies the producing zone and limits the upward movements of the convection currents.

In other fields, *i.e.* The Geysers (California), Wairakei and Waiotapu (New Zealand) we do not know a geologically well defined cap-rock formation, presenting a large difference in permeability in comparison with the reservoir formation.

The hot water circulating in a hydrothermal system without a cap-rock can produce deposits and rock alteration in proper places along the flow paths. The fracture and pore filling and any other permeability reducing factors increase resistance to the water circulation; those processes can originate an effective cap-rock. By such processes a hydrothermal system can become a self-sealed geothermal field.

The silica deposition is probably the main self-sealing process. In fact, 1) silica is very common, 2) it is available with almost no limitation, 3) its deposition is strictly related to temperature changes, and 4) it is likely to produce very effective patterns of deposition.

Where an unlimited CO<sub>2</sub> supply is available at depth, the calcium carbonate deposition appears to be a noticeable sealing process, which is controlled by

\* Paper presented at the IAV International Symposium on Volcanology (New Zealand) Nov. 1965.

pressure, at relatively shallow depth. In other cases  $\text{CaCO}_3$  precipitation should not be an important factor in the self-sealing of geothermal fields.

Argillization appears to be an important shallow process. It is especially effective in the acid environment of many thermal shows, thus determining their migration and/or extinction.

According to our analysis and to present evidence those three self-sealing processes are the most important ones.

In The Geysers Field, the wells penetrated the same formation, the Franciscan graywackes, from top to bottom. The Franciscan Formation has a very low primary permeability; secondary or fissure permeability is at the contrary very high. It is evident that there is no recognizable cap-rock in the accepted sense of petroleum geology.

The wells produce superheated steam; the producing zone begins at 300 m depth or so; the quantity of steam increases with the thickness of the producing zone penetrated by the holes.

Beginning in 1964, the wells have been drilled with air as circulating medium. No steam or water has been observed in the top few hundreds meters drilled: we can safely conclude that the graywackes are impervious in the upper section of the holes.

Cores and cuttings show frequent fissures filled with silica in different mineral forms and hydrothermally altered rocks are common.

In the Geysers area, hot springs, steam vents, carbon dioxide and hydrogen sulphide fumaroles are numerous, and wide zones of rocks, altered by past hydrothermal activity, are prominent features. As usual in many hyperthermal areas, also in The Geysers the manifestations of surface heat change frequently in place, in size, and in fluids discharge. The filling of rock fissures by mineral deposition seems the simplest and most natural explanation of the place changes of the individual springs.

The active faults continually generate new fissures, limit the sealing action, and account for the persistent surface thermal activity of the area.

The composition of the waters from the hot springs at The Geysers has been re-considered, in comparison with both surface waters and natural steam. The hot springs mainly originate by natural steam condensation, as Allen and Day stated in 1927. This conclusion is now strengthened and extended: the perched water table producing hot springs at The Geysers is purely condensed steam. Practically all its characteristics can be explained by this condition alone. Separation from other shallow water bodies is extremely sharp.

Let us summarize: the impermeability of the upper section of the holes is demonstrated by the lack of fluids in the Sulphur Bank area, whereas the geochemistry of the hot springs compared with shallow waters indicates that similar conditions occur in the Geysers and Little Geysers areas. Furthermore, silica and other fissure-filling processes occur all over the region, as well as argillization of graywackes.

We conclude that:

a) a cap-rock exists in The Geysers Field; this fact readily explains the production of dry steam;

b) the relative impermeability of the cap-rock is due to the hydrothermal

activity, which fills by i  
in places argillifies the c

c) the active fault  
ascending fluids; this pr

The numerous excell  
a similar explanation for

variations on the rocks pen  
details of the self-sealing

seems to anticipate som  
differences in general pri

Furthermore, in some  
active and we suggest th

outlook in geothermal exj

A self-sealing geother  
hydrothermal activity has

meable rocks into low p  
geometry, to constitute a

Field is a typical example

Thermal manifestatic  
through channels in an

manifestations». Their in  
ed, all the more that they

The sealing process  
ess of steam wells are

frequent and important s

Calcite deposition is l  
wells, where steam-water

duced also by soluble sal  
sulfate and other compos

acid carbonate with some

According to our think  
for the reservoir engineeri

The new concept bro  
areas with recent thermal

consideration as possible  
retical tool can be also us

tion and evaluation.

ases CaCO<sub>3</sub> precipitation should  
geothermal fields.

allow process. It is especially  
al shows, thus determining their

vidence those three self-sealing

he same formation, the Francis-  
iscan Formation has a very low  
neability is at the contrary very  
cap-rock in the accepted sense

producing zone begins at 300 m  
h the thickness of the producing

l with air as circulating medium.  
p few hundreds meters drilled:  
impervious in the upper section

filled with silica in different  
s are common.

ts, carbon dioxide and hydrogen  
ones of rocks, altered by past  
As usual in many hyperthermal  
surface heat change frequently  
ling of rock fissures by mineral  
explanation of the place changes

fissures, limit the sealing action.  
activity of the area.

ot springs at The Geysers has  
rface waters and natural steam.  
eam condensation, as Allen and  
trengthened and extended: the  
he Geysers is purely condensed  
be explained by this condition  
lies is extremely sharp.

e upper section of the holes is  
ur Bank area, whereas the geo-  
allow waters indicates that sim-  
eyers areas. Furthermore, silica  
r the region, as well as argilli-

; this fact readily explains the

rock is due to the hydrotherma-

activity, which fills by mineral deposition the fissures of the graywackes and  
in places argillifies the original sandstone;

c) the active fault movements provide temporary openings for the hot  
ascending fluids; this process explains the surface thermal activity.

The numerous excellent papers on the Wairakei and Waiotapu fields suggest  
a similar explanation for some New Zealand geothermal fields. Steiner's obser-  
vations on the rocks penetrated by drillholes in Waiotapu reveal many pertinent  
details of the self-sealing process. Grindley's paper on the structure of Waiotapu  
seems to anticipate some of our conclusions, notwithstanding the noticeable  
differences in general principles.

Furthermore, in some Iceland thermal areas the self-sealing process seems  
active and we suggest that further studies on this subject may provide a new  
outlook in geothermal exploration in that country.

A self-sealing geothermal field is defined as a geothermal field, in which  
hydrothermal activity has generated a cap-rock, by transforming originally per-  
meable rocks into low permeability rocks in such a manner and with such a  
geometry, to constitute an efficient trap for convection currents. The Geysers  
Field is a typical example of a self-sealing geothermal field.

Thermal manifestations related to vaporization-condensation processes  
through channels in an impervious capping formation can be named « leak  
manifestations ». Their interest for geothermal exploration cannot be overlook-  
ed, all the more that they are recognizable by geochemical investigations.

The sealing process of « leak manifestations » and the incrustation proc-  
ess of steam wells are expected to be similar. However, argillization is a  
frequent and important sealing process of natural channels.

Calcite deposition is likely to be important both in natural shows and in  
wells, where steam-water separation goes on poorly. Plugs in wells can be pro-  
duced also by soluble salts. Alkali and ammonium borates, boric acid, sodium  
sulfate and other compounds have been observed at Larderello; ammonium  
acid carbonate with some boron has been observed at the Geysers.

According to our thinking the study of the incrustation process is important  
for the reservoir engineering.

The new concept broadens the geothermal exploration possibilities: many  
areas with recent thermal rock alterations and mineral deposition deserve proper  
consideration as possible areas for self-sealed geothermal fields. The new theo-  
retical tool can be also usefully applied in rationalizing the geothermal exploi-  
tation and evaluation.

SUBJ  
GTHM  
SSGR

SITE SPECIFIC GEOTHERMAL RESERVOIR ENGINEERING ACTIVITIES (1978)

C.B. Goranson and R.C. Schroeder

*Lawrence Berkeley Laboratory*

UNIVERSITY OF UTAH  
RESEARCH INSTITUTE  
EARTH SCIENCE LAB.

Introduction

LBL personnel have been engaged in geothermal reservoir engineering since 1975, when T.N. Narasimhan and P.A. Witherspoon tested and analyzed RRGE-1 at Raft River (Narasimhan, et al., 1977). Since 1975 the LBL field capabilities have been expanded and improved. Our studies have included cooperative projects with several private companies, city governments, and federal agencies. Our purpose has been to develop new and improved techniques, tools, and analysis methods for use in assessing and modeling hydrothermal systems. The important tasks in carrying out these activities can be summarized as follows:

- Collect site specific data
- Develop field techniques
- Develop measurement tools
- Develop analysis methods
- Model site specific aquifers

Only the first of these activities will be covered in this report, and only work performed in FY 1978. A review of our analysis and data processing activities is given in a separate report (Benson, et al., 1978). A summary of equipment development and applications is also presented elsewhere (Goranson, et al., 1978).

The site specific studies include data from many sources, in addition to LBL field measurements. This data includes geological, geophysical, hydrological, and geochemical information about each site. The well testing requires well completion data, well logs, and wellbore geophysical

interpretations in order to carry out detailed analyses of the well test data. In general, the purpose for the well testing is:

- Determine hydrological parameters
- Identify aquifer limits (barriers)
- Identify aquifer recharge (if it exists)
- Determine well damage (if it exists)
- Determine thermal characteristics
- Obtain representative reservoir fluid sample

All of this information is used when a resource assessment is initiated and subsequent modeling is carried out. Clearly, the amount of information available for site specific resource evaluation determines the degree of confidence in estimating reserves and resource lifetime for proposed exploitation strategies.

The table below and Figure (1) show the specific geothermal sites at which (or for which) LBL personnel have played a role in the reservoir engineering measurements, evaluation, or planning during FY 1978.

Table 1

Locations of Site-Specific Reservoir Engineering Activities During FY 1978\*

Desert Hot Springs	-	well test analysis
Casa Diablo	-	well test planning
Coso Hot Springs	-	measurements, workover, and resource evaluation
Susánville	-	measurements, well siting, and resource evaluation
Klamath Falls	-	measurements, planning, and resource evaluation
Cerro Prieto	-	measurements and resource evaluation
East Mesa	-	measurements, workover, and resource evaluation

\* Minor activities included Valles Caldera, Salton Sea Geothermal Field, Raft River, and Heber.



Review of Specific Site Activities

I) Desert Hot Springs KGRA (Coranson and Schroeder, 1978)

LBL reviewed data from a well test carried out in June, 1977 by B.F. Russell, California State University at Fullerton. The test incorporated 3 wells in the Desert Hot Springs KGRA near Palm Springs, California. One well was produced at 110 gpm for 4.5 hours. Water level changes were measured in the production well and in two observation wells at distances of 102 and 212 feet from the flowing well. Maximum produced wellhead fluid temperature was 148°F.

The data was analyzed assuming that there is a partial penetration effect which yields a total reservoir height of 1,000 feet. Transmissivity values between  $1.7$  and  $3.7 \times 10^6$  md-ft/cp were calculated from the production and observation well data.

However, our confidence in the calculated transmissivity values is small. Analysis of data from well tests is directly dependent on geological and lithological information available for the reservoir. In this case little is known about the aquifer that was tested.

Lithologic and geophysical well logs were not available. Furthermore, the areal geology was not well defined. Our main conclusions were that the test was not of sufficient duration to estimate the total amount of heat available, maximum producible temperature, geologic extent of the resource, or maximum production capabilities. This anomaly appears to offer promise as a candidate for direct utilization applications. However, a modest

investment in well testing, geological studies, and their evaluation is necessary to provide estimates for the resource extent and its hydrothermal characteristics:

II) Mono-Long Valley KGRA - Casa Diablo Site (Long Valley Symposium, 1976)

LBL reservoir engineering personnel visited the Diablo Hot Springs geothermal area in June, 1977. We reviewed the site for possible well test activities that LBL could perform to delineate reservoir boundaries and maximum long term production rates for possible use in a Direct Heat Utilization program for the city of Mammoth Lakes. This reservoir has a maximum temperature of approximately 360°F at about 400 feet. The first well was drilled by Magma in 1957. Preliminary short term flow tests were reported to have flows between 300,000 to 500,000 lbs/hr. These rates and temperatures should be more than sufficient to supply space heating demands for the city of Mammoth Lakes. However, these short term tests do not indicate reservoir extent or total capacity of the reservoir.

LBL has no plans in the immediate future for extensive well testing. However, the heat load demands for the city of Mammoth Lakes have been illustrated (Sims and Racine, 1977), and relatively high temperature water is available from this relatively shallow aquifer. Therefore, drilling costs would be minimal and pipelines would be of reasonable length. These considerations make Diablo Hot Springs an interesting site for geothermal production. However, chemical precipitation during production or injection may be a problem (based on samples taken by Magma Power Co.).

The reservoir boundaries and reservoir capacity for long term production have not been determined, but the area shows promise. Additional testing and fluid sampling is required for initial resource evaluation.

III) Coso Hot Springs KGRA, China Lake, California (Goranson, et al., 1978)

An exploratory well - Coso Geothermal Exploratory Hole Number 1 (CGEH#1) was completed at the China Lake Naval Weapons Center on December 2, 1977 to a total depth of 4845 from ground level (CER completion report). The subsurface geology consists of a fractured granitic complex overlain with rhyolitic debris and intruded by rhyolitic dikes (Galbraith, 1977). LBL personnel monitored the downhole thermal equilibrium of the well. The first LBL temperature survey was performed on December 8, 1977. In all, eight temperature surveys were performed. Three downhole fluid samples were taken and one downhole pressure survey was made.

During drilling numerous fractures were encountered. These fractures are observable in Figure 2 as large mud losses along the length of the wellbore. Moreover, as seen in the temperature surveys, these fractures are also evident in the abnormally cooled portions along the well where mud entered the formation, thereby cooling it down (2,100, 2,700 and 3,500 feet). The well essentially had come to thermal equilibrium by June of 1978 as seen in Figure 3. The maximum temperature measured was 385°F at 2,000 feet, bottom hole temperature was 350°F.

On September 6, 1978 the well was stimulated with nitrogen using a one-inch diameter tubing placed downhole. After twelve-hours of nitrogen flow the well was dry with approximately 200 feet of fill. At this time the well stimulation operation was ended.

On November 2-6, 1978 well start-up and workover procedures commenced. The cleanout procedure consisted of pumping a nitrogen-foam - water mixture into the wellbore. The foam has the ability to entrain particles and float

them to the surface. The foam cleanout operation was successful and a large amount of material was brought to the surface. However, a blockage was encountered which prevented touching TD. The well again was dry after nitrogen stimulation. The water level buildup in the well was measured and indicated an inflow rate of approximately 4 gals/min.

Our conclusion is that there is not an appreciable amount of fluid in the formation from 3,500-4,845 feet. The small amount of fluid inflow seems to be originating outside the casing about 3,500 feet (CGEH#1 is cased to 3,500 feet). The zones of large mud losses in the cased portion mentioned above are the probable origin of the geothermal fluid in the well. The zone at 1900 feet had an influx of about 60 gpm while drilling with air and hydrothermally altered rock was encountered. This zone also has the highest recorded temperature of 385°F.

The well has proven to be useful in preliminary resource evaluation. To verify preliminary resource models there is a need for further drilling of wells in nearby areas to determine fracture orientations and resource characteristics in the Coso Hot Springs KGRA.

#### IV) Susanville Geothermal Anomaly, Susanville, California (BuRec, 1976)

The Bureau of Reclamation personnel are performing an extensive resource identification program in the Susanville - Honey Lake KGRA in Northern California (the location is shown in Figure 1). During the last three months the Bureau of Reclamation drilling crews have concentrated on the City of Susanville area, since the geothermal resource there is expected to be capable of meeting heat load demands within the City limits. Thermal waters are being used at this time to heat the city swimming pool. Other private

users include a greenhouse, a lumber company and a church. The maximum downhole temperature measured to date is 150°F at a depth of 350 feet, Figure 4.

There are 10 wells in the west side of the town of Susanville that were incorporated in a well test beginning November 27, 1978. Numerous drillers logs and geophysical well logs have been obtained from the Bureau of Reclamation. The approximate depth of the maximum temperature is known from well logs. However, the hydrothermal mechanism which maintains this resource is not known at this time. The interference test in early FY 1979 should outline the resource boundaries and yield information relative to the long-term production characteristics of the resource. The test will also yield information related to further well drilling activities in the area. After analysis of the well test data we will collaborate with the BuRec personnel to choose an optimum site for the first production well to supply fluid for the city of Susanville buildings. A productivity test is scheduled after the production well has been completed and developed. Injection and future production strategies will be studied using reservoir simulation computer programs.

V) Klamath Falls Geothermal Anomaly, Klamath Falls, Oregon (USGS, 1976)

Klamath Falls, Oregon has been designated as a known Geothermal Resource Area (KGRA). The city is one of the earliest large scale users of geothermal energy in the continental United States. There are approximately 350 hot water wells in the area used for space heating in about 450 structures. Downhole water well temperatures range from 30°C - 105°C (see Figure 5). Large quantities of data have been published by the Oregon

Institute of Technology Geo-Heat Utilization Center on the properties and characteristics of the Klamath Falls resource.

LBL has analyzed data from two well tests in the area performed by Oregon Institute of Technology. One test was performed in July, 1976, another test was carried out in July, 1978 with LBL participation. In the first test the museum well, located near the downtown area, was flowed and 12 nearby wells ranging from 129 to 1,425 feet from the pumped well and were monitored for water level changes. The museum well has been considered as a candidate for supplying makeup water during large heat load demands. No drawdowns were measured in the museum well and the maximum produced temperature was 84°C. Subsurface geology in the area is rather complex with alternating lacustrine and volcanic materials as the main geologic structures. This geologic complexity hampers data analysis in that tests were not of sufficient duration in time to uniquely define reservoir characteristics in terms of partial penetration, confined or unconfined aquifer behavior, leaky aquifer behavior, etc. Calculated values of effective transmissivity range from  $6 \times 10^6$  md-ft/cp at the observation well 130 feet from the production well to  $35 \times 10^6$  md-ft/cp at a distance of 1,000 feet. The differences in the values of transmissivity seem to indicate a partial penetration effect, however, there was not enough data available to obtain unique interpretations. Flow rate changes were made at the production well occurred before semi-steady state behavior had been reached, and hampered analytical analysis techniques.

The second well testing activity incorporated a well located on Old Fort Road about one mile from the center of town. This well is in an area where maximum downhole temperatures of 105°C exist, and may be penetrating a fault zone. The well was produced for two days at 250 gpm, shut in for

two days, then flowed for two days of production, with injection in a well 600 feet from the production well. The production well is 900 feet deep, the injection well was 200 feet in depth. Due to flow measurement problems and production well collapse, the flow time was limited to 24 hours (during the injection portion) of the test. 17 wells in the area were observed. However, all the observation wells had shallow completions (200-350 feet) while the production well was completed to 900 feet. The geology in the area of Old Fort Road is somewhat similar to that mentioned above. Draw-downs in the observation wells were quite small (15 cm) and the formation parameters have not been uniquely defined. However, a preliminary analysis indicates transmissivity values of the same order of magnitude as in the Museum Well test. Although production well data was obtained, the data shows complications which have not yet been identified (i.e. - partial penetration, leaky aquifer, fracture, etc.). The test again was not long enough in time to classify the reservoir from a hydrological standpoint. However, communication between producing and observation wells has been proven. Additional testing to determine the characteristics of the aquifer system is needed to confirm preliminary resource models of the area.

LBL reservoir engineering personnel plan to carry out production tests, and possibly a long term interference test in the area of Old Fort Road in FY 1979. These tests should hydrologically identify this resource. OIT personnel working with the Geo-Heat Utilization Center plan to drill two wells in the area of Old Fort Road in FY 1979. LBL plans to assist them in drilling and geophysical well logging to identify the lithology of the area. Continuous water-level monitoring in a few chosen wells will be important in the long-term resource evaluation at Klamath Falls.

VI) Cerro Prieto Geothermal Field, Baja California, Mexico (Proceedings of the 1st Annual Symposium on the Cerro Prieto Geothermal Field, 1978)

The Cerro Prieto Geothermal Field is located in the Mexicali Valley in the southern extension of the Salton Trough as shown in Figure 6. The field at this point in time has 18 wells supplying steam to generate 75 MWe. Well depths in the field vary between 1200-2200 m. Numerous hot water springs and fumaroles have existed in the area in the past, and some still exist today.

For testing purposes we have divided the field into four areas; west, south, east, north as shown in Figure 7. The western area encompasses the main producing field and well M-6. Data was available from a float type water level meter installed by the Mexican Department of Water Resources headquartered in Mexicali. The analysis of this data is difficult due to differences in the geologic regimes between M-6 and the main producing field (fanglomerates versus marine deltaic environment). This is indicated in lithologic and geophysical well logs. M-6 geological differences are also indicated in the low downhole temperatures relative to the main field ( $\approx 150^{\circ}\text{C}$ ). Another difficulty in the analysis arises from the elevation differences of the open intervals in M-6 and in wells in the field. The open interval in M-6 is between 500-700 m. Open intervals in the producing field in most cases are between 1100-1500 m. Since the temperature in M-6 is  $150^{\circ}\text{C}$  and the temperature in the main field is over  $300^{\circ}\text{C}$ , the viscosity of the fluids is vastly different. Due to these difficulties calculated transmissivity values using M-6 data indicates higher than actual permeability. Calculated transmissivity values are on the order of  $4.7 \times 10^6$  md-ft/cp ( $1.4 \times 10^{-6}$  m<sup>3</sup>/Pa·s).



From January 25 to March 15 LBL carried out an interference test in the southern portion of the field. Four wells were developed by CFE with maximum flow rates of 600,000 lbs/hr. Production temperatures varied from 290°C-300°C. Development intervals were staggered with flow periods ranging from four to ten days (see Figure 8). Well M-101 was chosen as the observation well while wells M-90, 91, 50, 51 were produced. Again the analysis is made difficult due to subsurface geological characteristics. The reservoir has recently been modeled (on the basis of well log interpretations) into three units - unconsolidated sediments, consolidated sediment, and basement rock. The consolidated unit has been divided essentially into four layers, layer 1, layer 2, reservoir A, and reservoir B. Reservoirs A and B are separated by a shale layer varying in thickness between 30 and 100 meters. The observation well penetrates partially into reservoir A. Production wells partially penetrate reservoirs A and B.

Downhole temperatures are approximately the same through this portion of the field. The data was analyzed using an isothermal, line source, isotropic, homogeneous, infinite aquifer, non-linear least squares fitting routine to match the observation well data. Figure 8 illustrates measured pressure response with flows superimposed. Figure 9 shows calculated pressures versus observed pressures. The calculated transmissivity is  $1.5 \times 10^6$  md-ft/cp ( $4.36 \times 10^{-7}$  m<sup>3</sup>/Pa·s). A storativity value of  $2.3 \times 10^{-2}$  ft/psi ( $1.017 \times 10^{-6}$  m/Pa) was also calculated. The calculated and observed pressure response fits rather well. However, due to the aforementioned subsurface geological characteristics, we feel our estimates are higher than they should be.

Another interference test was carried out in the eastern portion of the field. Well M-53 was developed during May. The well was then put on line to supply steam to the power plant. M-104 was chosen as an observation well near M-53. Well M-10 was also observed during this time. Observation in these wells began about the first of May and was concluded on July 27, 1978. Figures 10 and 11 show measured pressures in these wells. The initial pressure drop at M-10 was due to faulty equipment. This problem was fixed within a few days after the instrument was installed downhole. However, as noted in the figures, pressures began to increase immediately. Well M-10 is near the main producing field, and the measured pressure response should have been one of slow decline due to the nearby long-term production. M-104 was in an area of the field where no production had taken place within a few months prior to setting the instrument in the well. On May 5, 1978 an earthquake occurred with an epicenter approximately 20 km south of Cerro Prieto, magnitude 5.1 (Richter).

Pressures continued to rise after the earthquake, then began falling. On May 16, 1978 well M-53 began production. Note in Figure 11 that a change in the slope of the pressure buildup occurred about 2 days later. (Equipment was checked during these periods and found to be functioning correctly). The data obtained is not readily analyzable due to the unknown pressure buildup associated with the earthquake before flowing well M-53. However, using the transmissivity and storativity values obtained in the M-101 interference test, the pressure drop at the end of the observation period in M-104 should have been about 4 or 5 psi. The order of magnitude of the permeability, therefore is similar to that in the southern portion of the field. The subsurface geologic conditions are relatively the same in the eastern and southern portions of the field. However, another interference test

should be carried out to determine if this indeed is the case. In addition to the interference tests described above, there have been several productivity tests and two-rate flow tests performed during the development of the wells. Data has been examined for three two-rate tests. The wells M-51, M-90 and M-91 were varied in rate during their development. This was the period when M-101 was also monitored. The wells are all penetrating different aquifers, or combinations of aquifers. The presence of multiple aquifers, shale layers, or a combination of these is evident in the data, and makes unambiguous determination of the reservoir characteristics difficult. The use of reservoir simulation might allow a more acceptable model for the system to be developed.

The subsurface geological characteristics of the Cerro Prieto field are being clarified as new data becomes available from their extensive drilling program. We have introduced to CFE personnel our instrumentation for interference and production well testing and some of our computer programs for data analysis. CFE has begun an interference and production test in the southern and eastern portions of the field. Recent flowing pressure and temperature profiles in some of the wellbores may indicate two-phase flow in the well and possibly in the reservoir near the wellbore. One new well drilled in the eastern portion of the field exhibits bottomhole temperatures approaching 360°C. These are interesting aspects in terms of geothermal reservoir engineering problems.

Our plans in FY 1979 include the following:

- 1) Downhole reservoir fluid sampling.
- 2) Two-phase wellbore numerical modeling.

- 3) Numerical reservoir modeling to match subsurface geological and fluid characteristics.
- 4) Analysis of new interference and production well data.

All the information obtained to date, and new information becoming available will allow an understanding of the Cerro Prieto geothermal field and will help to define similar geothermal fields in the United States.

VII) East Mesa KGRA, Imperial Valley, California (Narasimhan, et al., 1977, Earth Science Division, LBL, 1979)

East Mesa is at the eastern edge of the Salton Trough in Southern California. In FY 1978 an Agreement was negotiated for well testing at the East Mesa site shown in Figure 1. The agreement included a review of all past well testing and analysis. In addition, productivity tests for wells 6-1, 6-2, 8-1 and 31-1 were agreed upon. The well 31-1 has no surface piping from the wellhead, and environmental restrictions prevented surface disposal. Hence, 31-1 was not subsequently tested, but the remaining tests were completed. A long term interference test was also completed using 8-1 as the flowing well while monitoring nearby wells.

The review of previous well testing at East Mesa provided estimates for the well productivity also. In tables 1, 2, 3 and 4 in the reference (Benson, et al., 1978), all of the data is summarized for the BuRec, Magma, and Republic wells from which the test data is available.

Summary

During FY 1979 the principle reservoir engineering activities will be at the geothermal sites indicated below in Table 2.

Table 2

Locations of Site-Specific Reservoir  
Engineering Activities During FY 1979\*

Susanville	-	measurements, well siting, and resource evaluation.
Klamath Falls	-	measurements, resource evaluation
Cerro Prieto	-	measurements, resource evaluation
Valles Caldera	-	resource evaluation
Others	-	measurements, resource evaluation

\* Minor activities are expected to continue at Niland, Raft River, East Mesa, and Heber.

The category in the table marked others is still vague, since final commitments at several geothermal sites has not been finalized at this time.

The first field test of FY 1979 is underway at Susanville where two flowing wells and 8 observation wells are being used to delineate aquifer continuity and material parameters. Computer modeling is underway to evaluate the resource. At Cerro Prieto the measurement program for FY 1979 is being negotiated to determine whether one long-term production test can be used to identify the non-homogeneities that have been identified from well logs and cores. Computer modeling using SHAFT78 (Pruess, et al., 1978) have been started to evaluate previous measurements and to estimate the future

two-phase behavior of the aquifers. All other activities are in the preparatory phase at this time.

References

- Benson, S., C. Goranson and R. Schroeder, 1979. Well Test Data Analysis Methods at LBL: Earth Sciences Division Annual Report, FY 1978, LBL-8648.
- Benson, S., C. Goranson, J. Haney, D. McEdwards, T.N. Narasimhan and R. Schroeder, 1979. A Summary of Well Tests and Analyses for the East Mesa Geothermal Site: LBL-8648.
- CER Corporation, 1978. Well Completion Report - COSO Geothermal Exploratory Hole No. 1 (CGEH#1).
- Earth Sciences Division, Lawrence Berkeley Laboratory, 1978. Resource and Reservoir Studies at the East Mesa KGRA: LBL-7094.
- Earth Sciences Division, Lawrence Berkeley Laboratory, 1976. Results of Reservoir Evaluation Tests, 1976, East Mesa Geothermal Field, California, LBL-5973.
- Galbraith, R., 1978. Geological and Geophysical Analysis of COSO Geothermal Exploratory Hole No. 1 (CGEH#1), COSO Hot Springs KGRA, California, University of Utah Research Institute, IDO/78-1701.b.4.2.
- Goranson, C. and R. Schroeder, 1978. Static Downhole Characteristics of Well CGEH-1 at COSO Hot Springs, California, Lawrence Berkeley Laboratory Report, LBL-7059.
- Goranson, C., R. Schroeder and J. Haney, 1978. Evaluation of COSO Geothermal Exploratory Hole No. 1 (CGEH-1), COSO Hot Springs KGRA, China Lake, California: Summaries, Fourth Workshop Geothermal Reservoir Engineering, Stanford University, Stanford, California.
- Goranson, C. and R. Schroeder, 1978. Recent Activities at the Cerro Prieto Field: Talk presented at the Fourth Annual Geothermal Workshop, in Proceedings of the First Annual Symposium on the Cerro Prieto Geothermal Field, September, 1978, San Diego, California.
- Goranson, C., J. Haney and R. Schroeder, 1978. A Review of Equipment for Use in Geothermal Field Measurements: Earth Sciences Division Annual Report FY 1978, LBL-8648.
- Goranson, C., D. McEdwards and R. Schroeder, 1976. Review of Desert Hot Springs Well Test: LBL-UCID-4028.
- Lund, J., P. Lienau, G. Culver and L. Svanevik, 1974. Klamath Falls Hot Water Well Study: Oregon Institute of Technology.
- Narasimhan, T.N., R. Schroeder, C. Goranson, D. Campbell and J. Barkman, 1977. Recent Results from Tests on the Republic Geothermal Field, East Mesa, California, LBL-7017.
- Narasimhan, T.N. and P.A. Witherspoon, 1977. Reservoir Evaluation Tests on RRGE-1 and RRGE-2, Raft River Geothermal Project, Idaho, LBL-5958.

- Narasimhan, T., R. Schroeder, C. Goranson and Sally Benson, 1977. Results of Reservoir Engineering Tests, 1977, East Mesa, California, SPE-7482.
- Pruess, K., R. Schroeder, P. Witherspoon and J. Zerzan, 1978. SHAFT78, A Two-Phase Multi-dimensional Computer Program for Geothermal Reservoir Simulation, LBL-8264.
- Sims, A. and W. Racine, 1977. Geothermal Space/Water Heating for City of Mammoth Lakes.
- U.S. Bureau of Reclamation - Mid Pacific Region, 1976. Water Quality Analysis, Inferred Geothermal Temperatures and Reservoir Evaluation Test.
- U.S. Bureau of Reclamation - Mid Pacific Region, 1976. Susanville Geothermal Investigations.
- U.S. Geological Survey, 1976. Hydrologic Reconnaissance of the Geothermal Area Near Klamath Falls, Oregon, with a section on "Preliminary Interpretation of Geophysical Data," Open File Report WRL-76-127.



Figure Captions

- Figure 1. Map showing locations of LBL reservoir engineering related activities for FY 1978.
- Figure 2. Summary of drillers log for CGEH-1, COSO Hot Springs, California. XBL 7812-13390
- Figure 3. Temperature versus depth for CGEH-1 at selected time intervals, COSO Hot Springs, California. XBL 784-7951
- Figure 4. Susanville geothermal well temperatures, Susanville, California.
- Figure 5. Well water temperatures at the 4000 foot elevation, Klamath Falls, Oregon.
- Figure 6. Salton Trough showing Imperial and Mexicali Valley (from Palmer, et al., 1975). XBL 764-1182
- Figure 7. Cerro Prieto Geothermal Field showing LBL reservoir engineering subdivisions. XBL 7811-12804
- Figure 8. Measured pressures in well M-101 with flow rates of four nearby wells superimposed.
- Figure 9. Calculated and observed pressure response of well M-101. XBL 786-1097
- Figure 10. Well M-104 pressure versus time with M-53 flow rates superimposed.
- Figure 11. Well M-10 pressure versus time with M-53 rates superimposed.

18

KLAMATH FALLS, ORE.

x

Sustitville, CA

Mono-Long Valley, CA

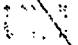

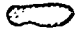
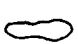
Coso Hot Springs CA

DESERT  
HOT  
SPRINGS  
CA

EAST  
MESA,  
CA

x  
L. CARRO PAIETO,  
MEXICO

**LEGEND**

-  CENOZOIC NONMARINE AND MARINE SEDIMENTARY ROCKS
-  OIL AND GAS FIELDS
-  GEOTHERMAL FIELDS
-  GEOTHERMAL AREAS UNDERGOING COMMERCIAL PRODUCTION TESTING AS OF (1-1-77)

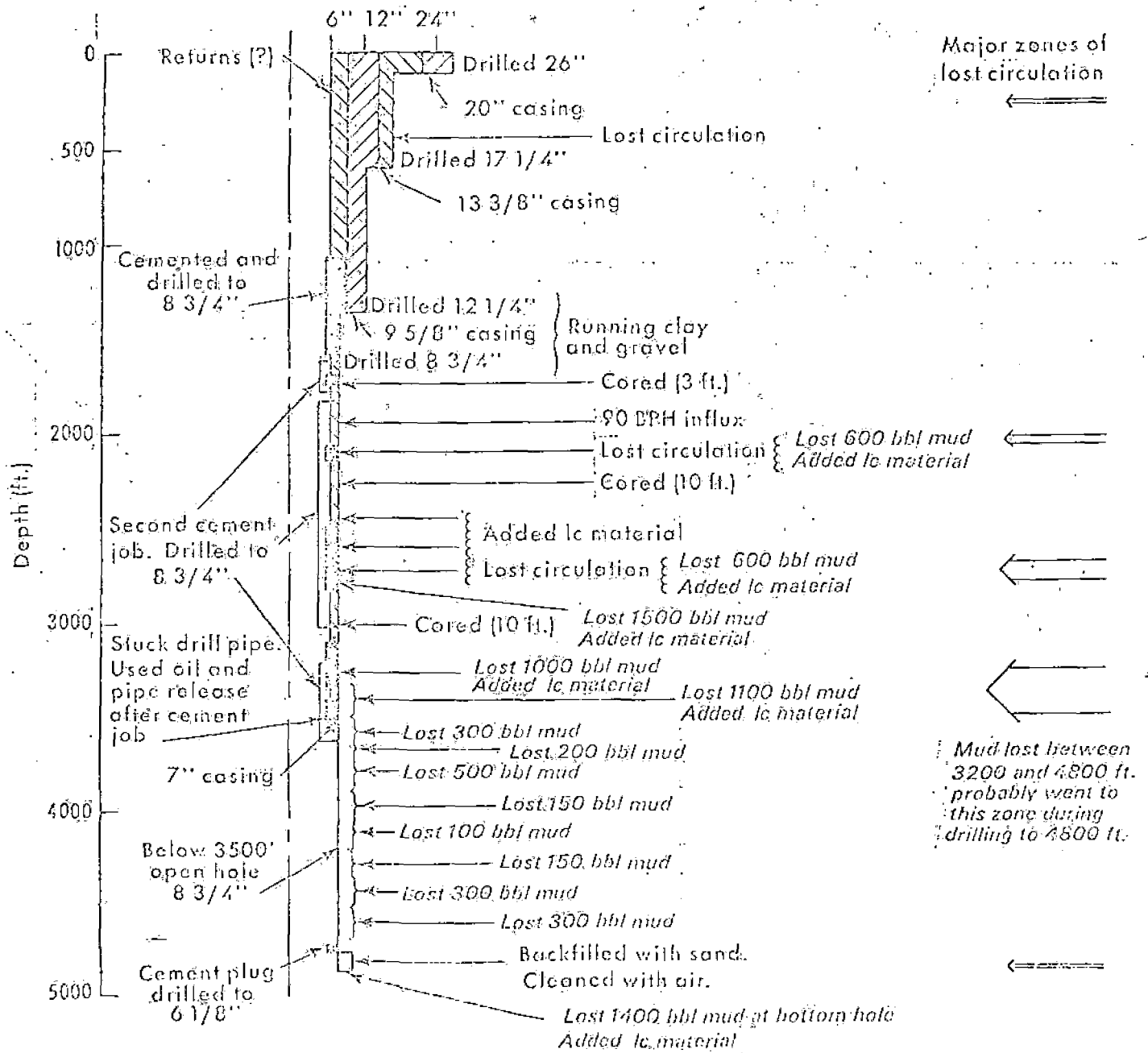
**COUNTIES WITH PRODUCTION**

<b>OIL &amp; GAS</b>	<b>GAS NOT ASSOCIATED WITH OIL PRODUCTION</b>
Alameda	Butte
Contra Costa	Colusa
Fresno	Glenn
Kern	Humboldt
Kings	Mariposa
Los Angeles	Merced
Monterey	Sacramento
Orange	San Joaquin
Riverside	Solano
San Benito	Sutter
San Bernardino	Tehama
San Luis Obispo	Yuba
San Mateo	
Santa Barbara	<b>GEOTHERMAL</b>
Ventura	Lake
	Sonoma

FIGURE I-5

OIL, GAS AND GEOTHERMAL FIELDS IN CALIFORNIA

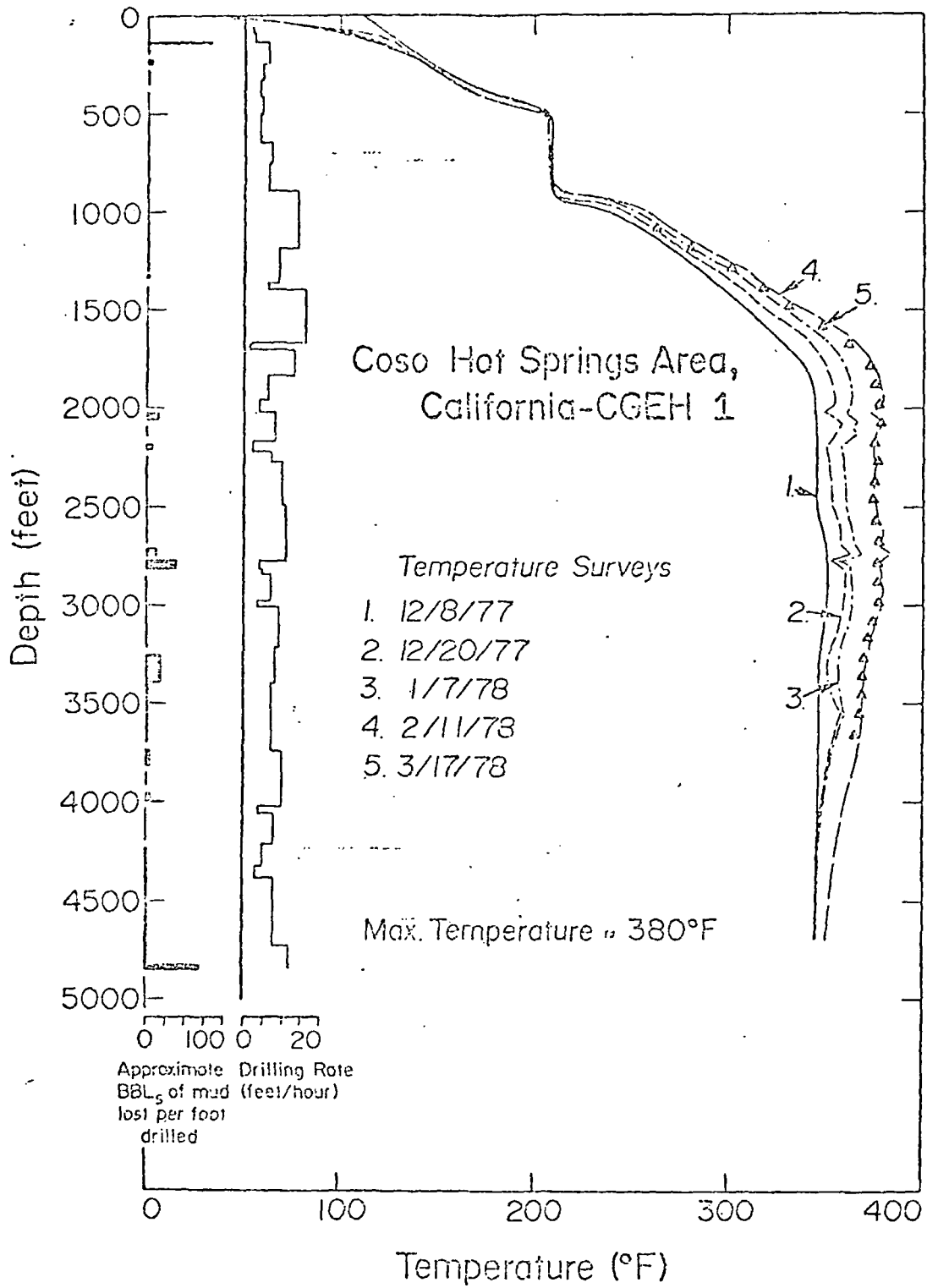
SOURCE: CALIFORNIA DIVISION OF OIL AND GAS, MAP OF OIL, GAS AND GEOTHERMAL FIELDS IN CALIFORNIA, 1977



Removed about 500 ft. of fill after cementing the final 7" casing. (Cement falling out?)

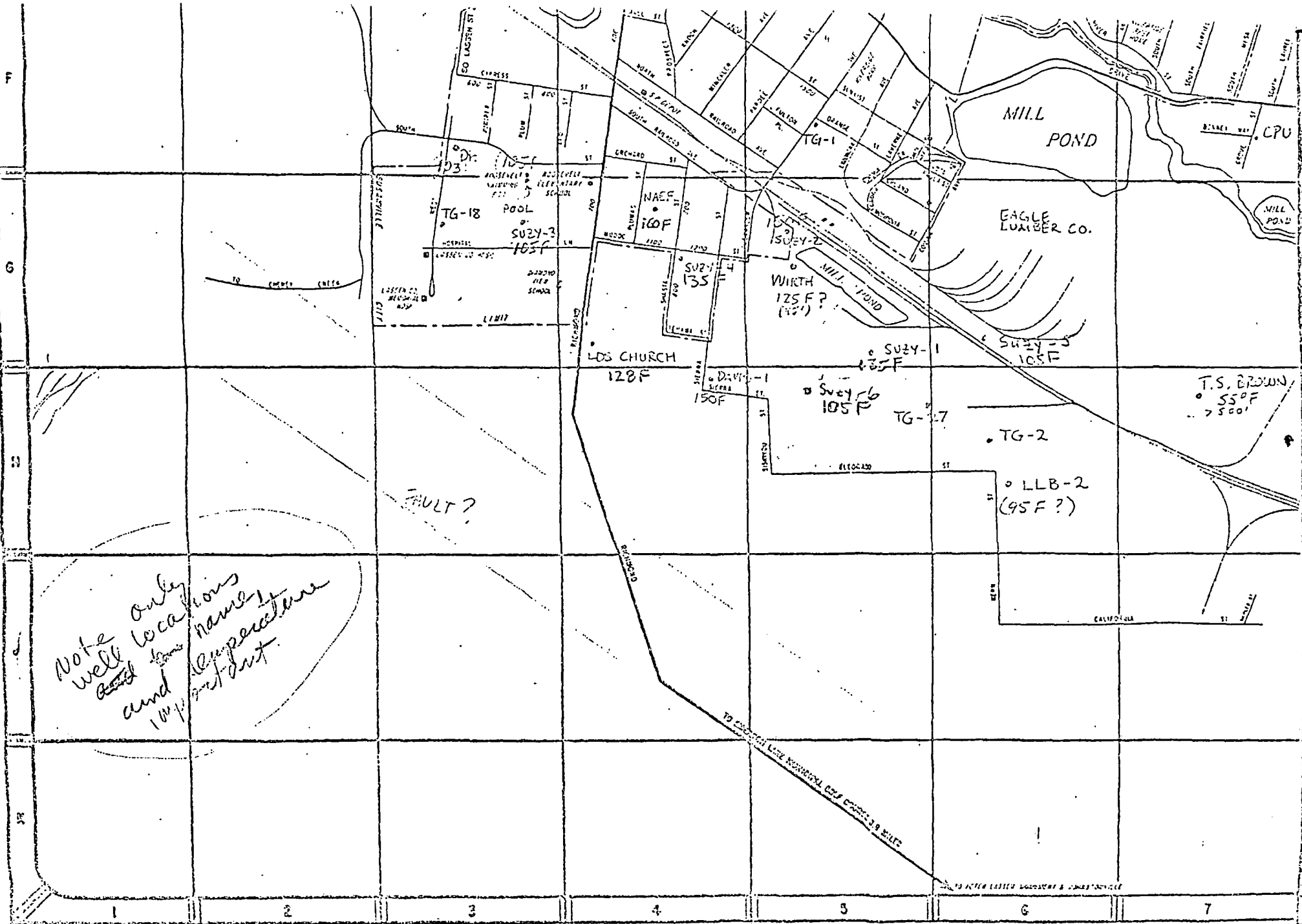
XBL 7812-13390

FIGURE 5



XBL 784-7951

~~Figure 6. Temperature Surveys in the Static Steam and Water Column at Coso Hot Springs.~~



Susanville Geothermal Well Temperatures - Susanville, CA Fig 4

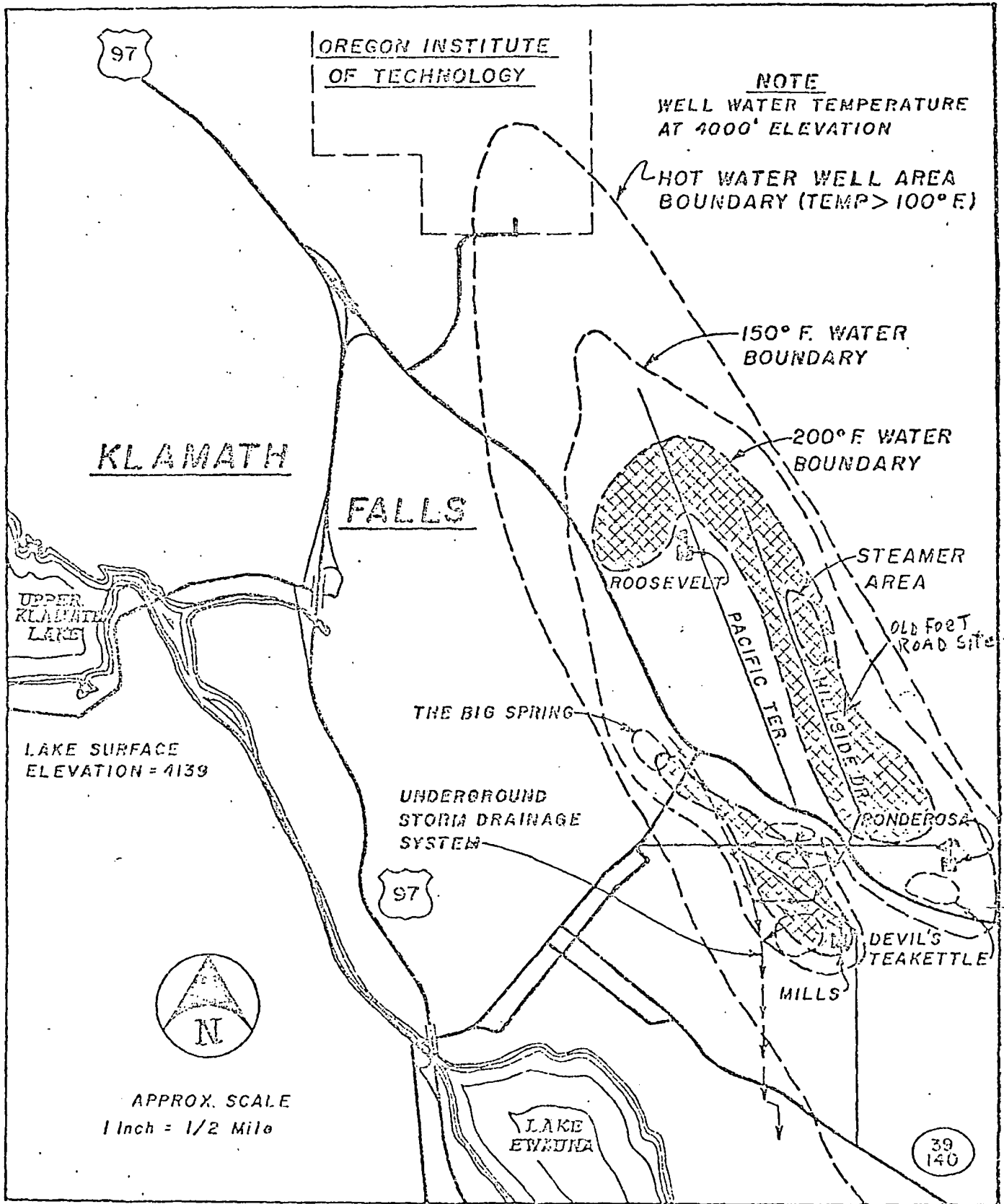
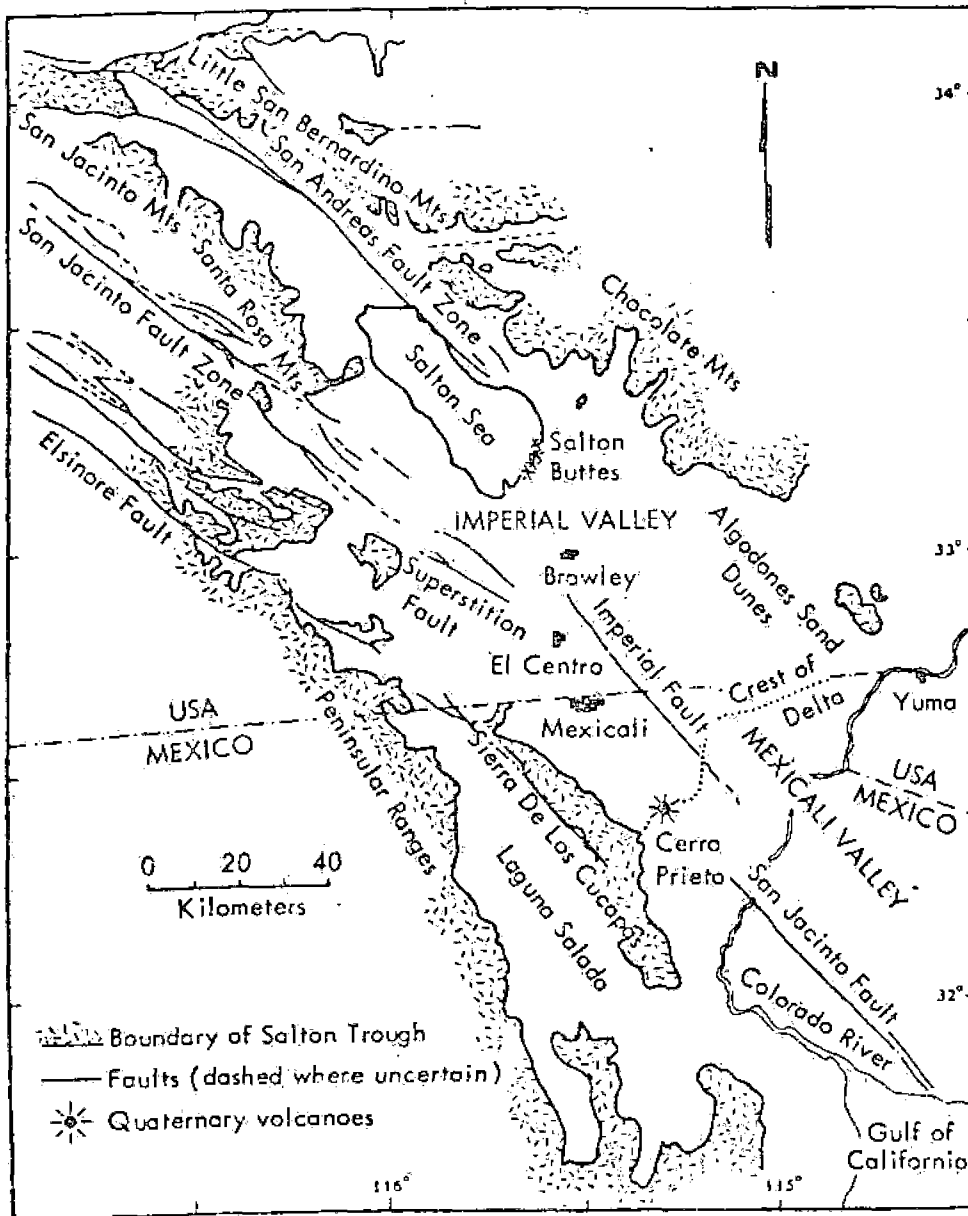


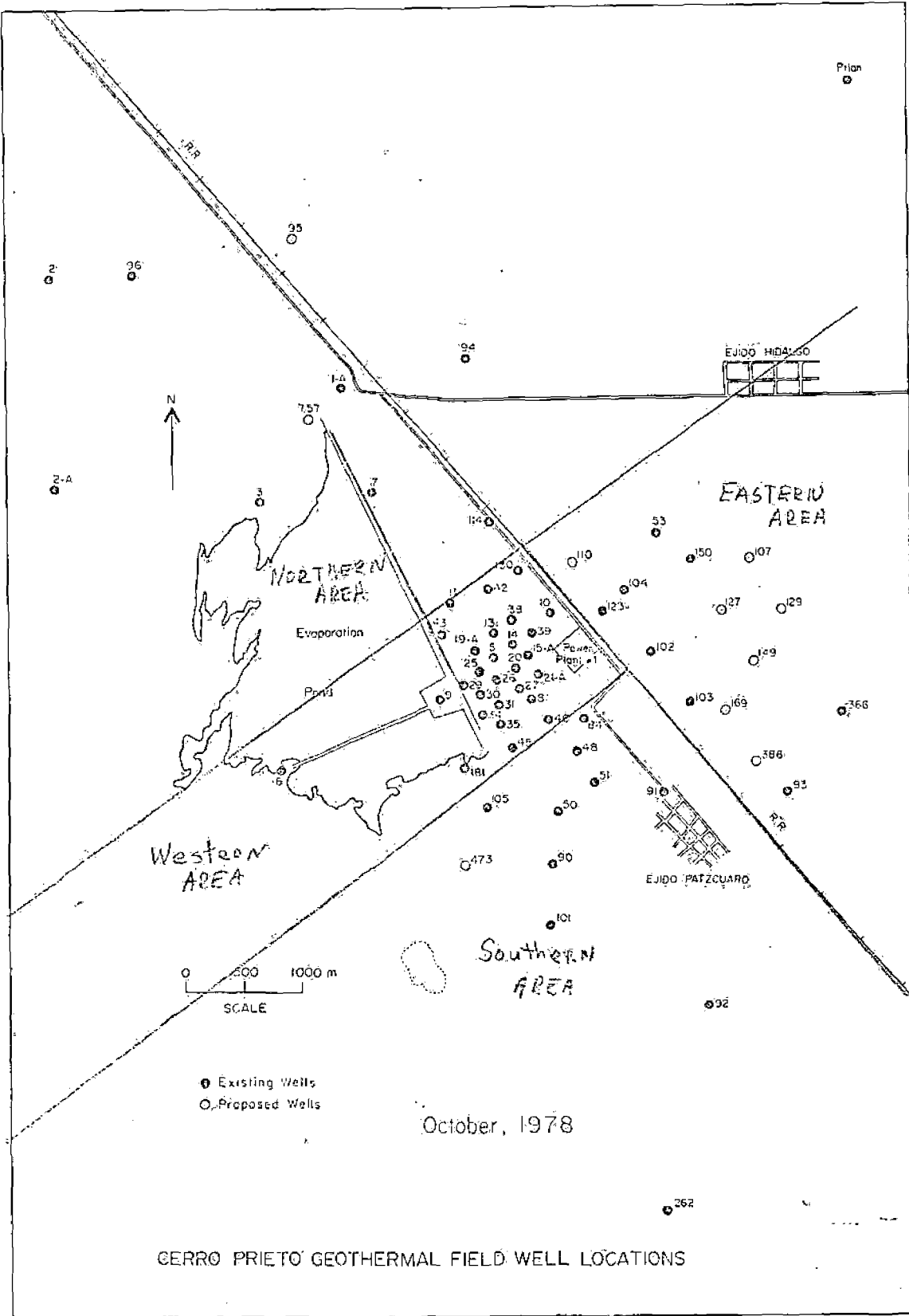
FIGURE 1. Well water temperature at 4000' elevation. - KLAMATH FALLS

Fig 5



XBL 764-1182

Fig. 2 Salton Trough (or Salton-Sea-Sea of Cortez Trough) showing Imperial and Mexicali Valleys (from Palmer et al., 1975).



CERRO PRIETO GEOTHERMAL FIELD WELL LOCATIONS

MSL 7811-12824

Fig. 2



AP vol. 4

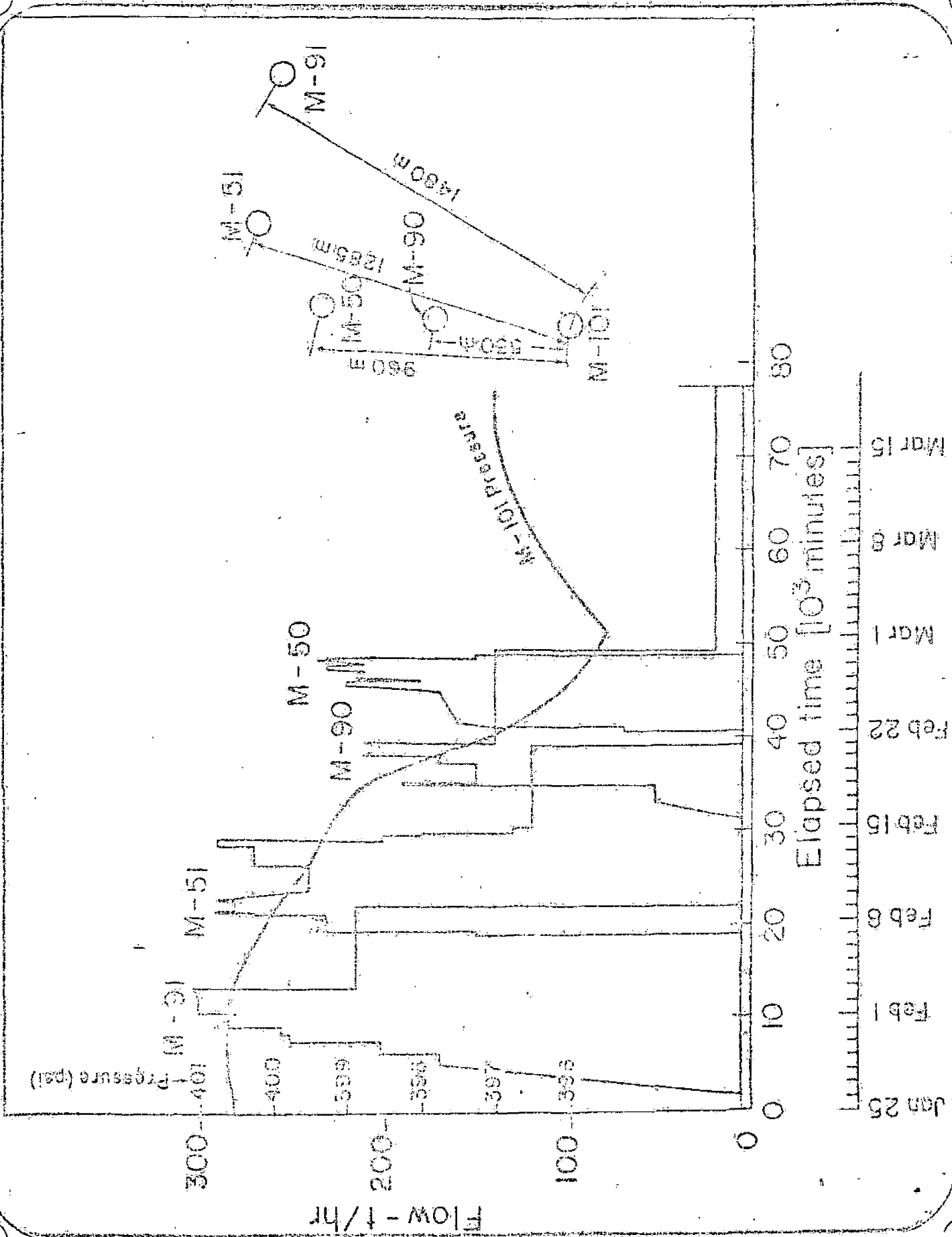
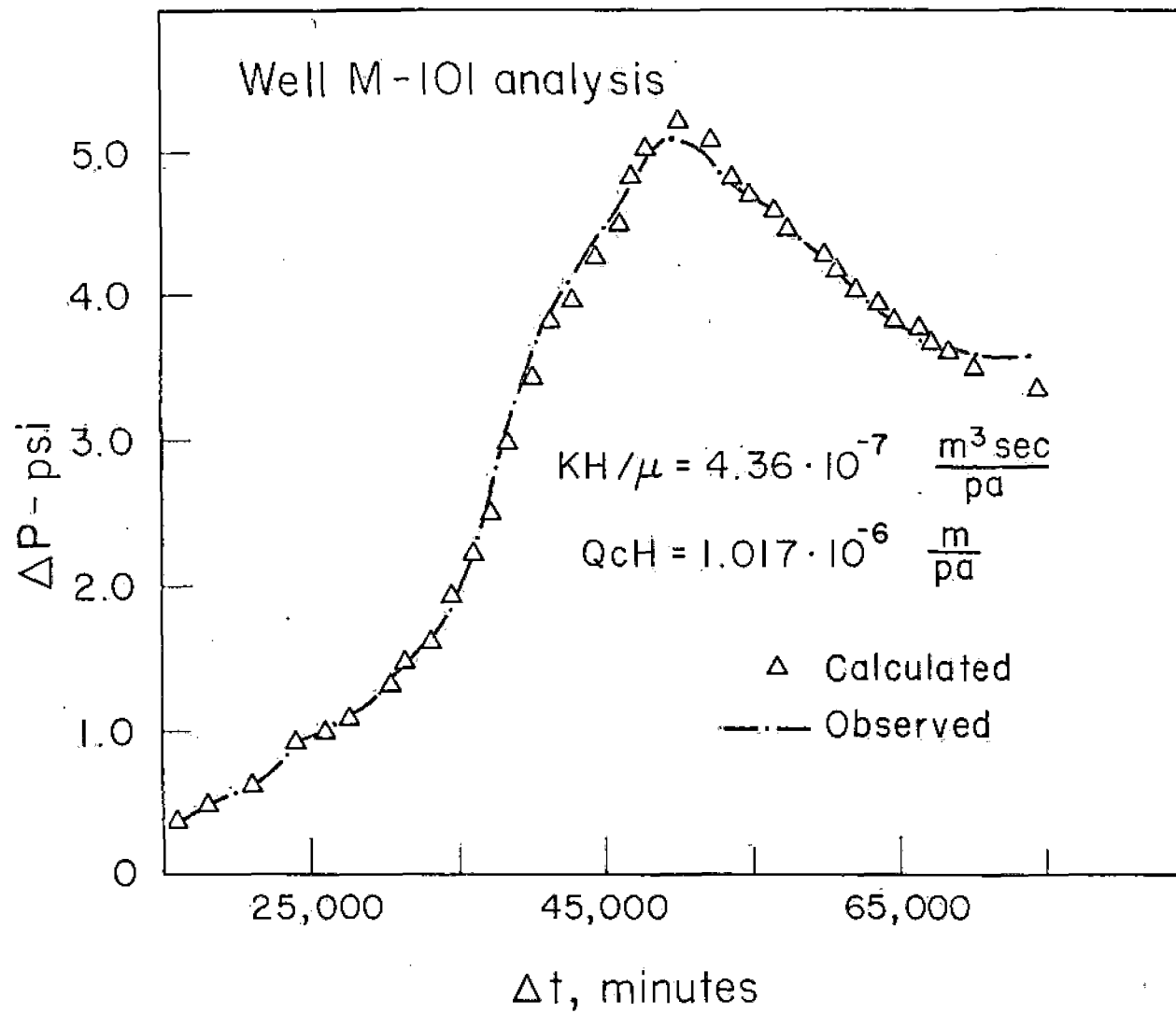
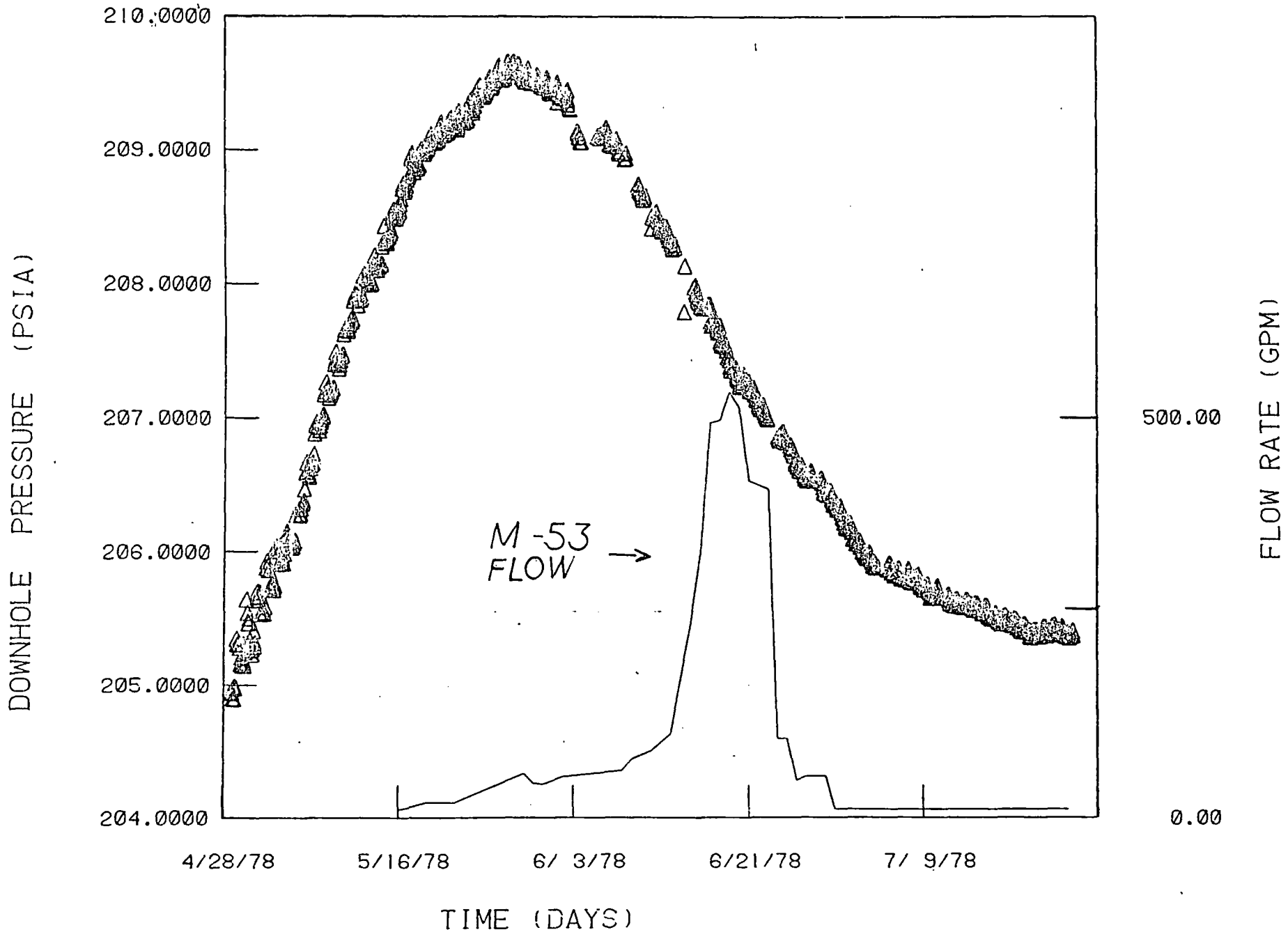


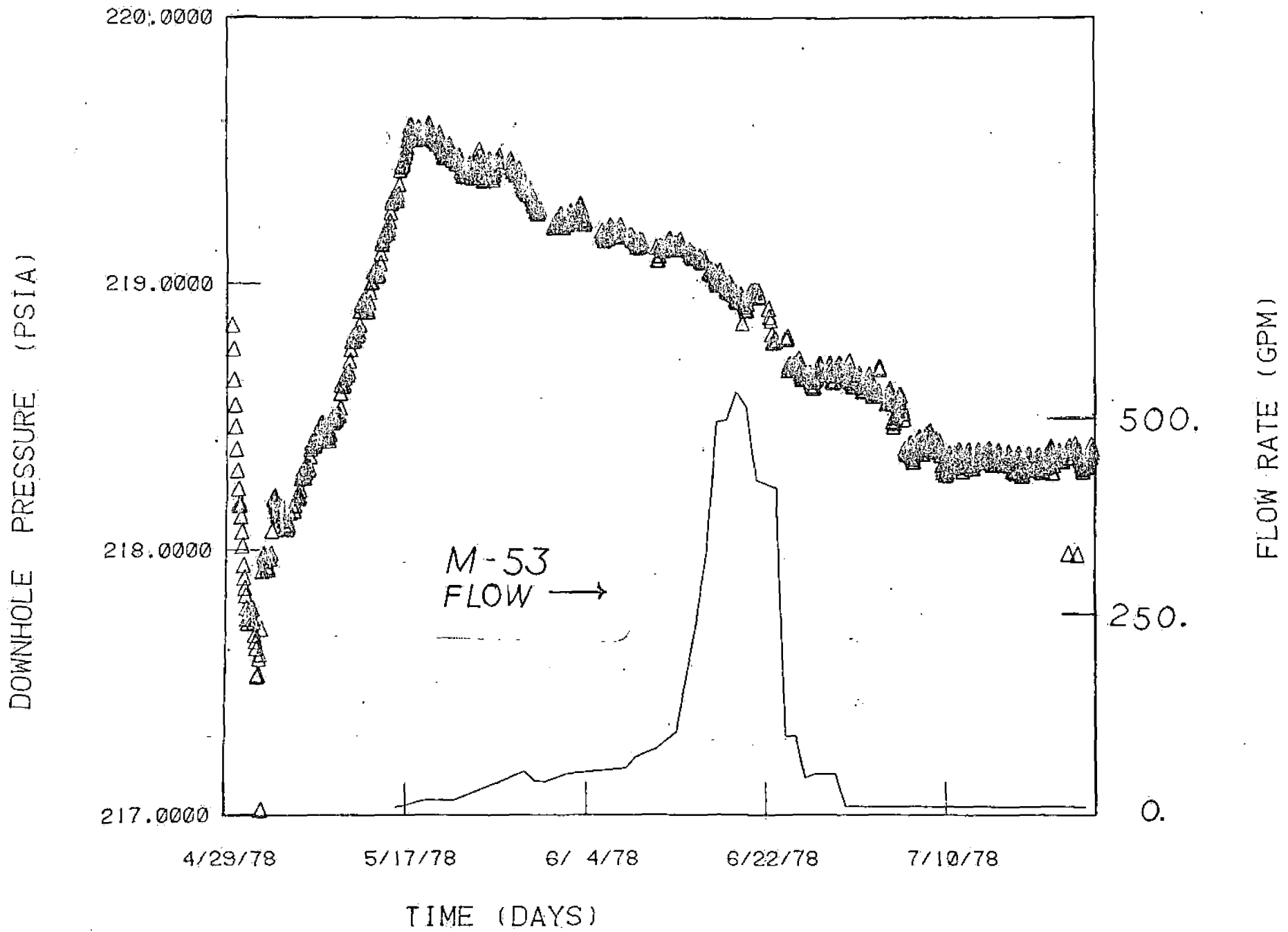
Fig. 8



XBL 786-1097



CERRO PRIETO WELL M-104



CERRO PRIETO WELL M-10

OREGON

KIND OF TAX	STATUTORY REFERENCE	MEASURE AND RATE OF TAX
Corporate Excise Tax	ORE. REV. STAT.  § 317.005 <u>et seq.</u>	Corporations (including utilities) doing or authorized to do business pay 6½% (Financial institutions 8%) of net income attributable to Oregon; minimum is \$10. Rate for year 1977: 7%; Rate for year 1978 and after: 7½%.  Offset allowed corporation primarily engaged in manufacturing, processing or assembling.
Corporate Income Tax	ORE. REV. STAT.  § 318.010 <u>et seq.</u>	Corporations not taxed under the excise tax deriving income from Oregon activities carried on in state pay tax of 6½% on net income allocated to state.
Business Corpora- tion License Fee	ORE. REV. STAT.  § 57.761 <u>et seq.</u>	Domestic corporation fee (§ 57.767): based on authorized capital stock at a graduated rate; maximum is \$200  Foreign corporation fee (§ 57.769): flat fee of \$200.
Property Tax	ORE. REV. STAT.  § 307.010 to  § 311.	Realty and tangible personalty taxed at 100% of true cash value as of January 1.  When mineral, coal, oil, and gas interests have been severed, they shall be taxed separately. (§ 308.115)  Unpatented mining claims exempt from taxation. (§ 307.080)

NEVADA

KIND OF TAX	STATUTORY REFERENCE	MEASURE AND RATE OF TAX
Domestic Corporation Organization Fee	NEV. REV. STAT. § 78.760	Based on authorized Capital Stock.
Foreign Corporation Organization Fee	NEV. REV. STAT. § 80.050	Rate is same as for domestic corporations but fees may not exceed \$25,000 for filing initial qualification documents; or \$25,000 for each subsequent filing of an amendment certificate increasing authorized capital stock.
Property Tax	NEV. REV. STAT. § 361.010 <u>et seq.</u>	<p>§ 361.225: All property is assessed at 35% of the full cash value.</p> <p><u>Mining property</u>: Computed on a net proceeds basis. Once the net proceeds for a mine are determined, the mine is then taxed at the same ad valorem rate as other property is taxed (§ 362.140).</p> <p>Unpatented mines and mining claims are exempt from taxation. (§ 361.075)</p> <p>Although the property tax for mines is computed on the value of the severed product, it is considered to be a lien on the mine or mining claims, from which ores or minerals are extracted for sale or reduction.</p>
Oil and Gas Conservation Tax	NEV. REV. STAT. § 522.150	5 mills per barrel of oil or 50,000 cubic feet of natural gas produced and sold, or bought.

IDAHO

KIND OF TAX	STATUTORY REFERENCE	MEASURE AND RATE OF TAX
Corporate Income Tax	IDAHO CODE § 63-3025, § 63-3025A	6.5% taxable income from instate sources
Corporate License Fee	IDAHO CODE § 30-601 to § 30-604	Based on authorized capital stock value Minimum is \$20; maximum is \$300 Exemption: all mining companies who do not own productive mines
Property Tax	IDAHO CODE § 63-2801 <u>et seq.</u>	<u>Productive mines:</u> Net annual profits, plus (1) price paid to U.S. for mines and claims or (2) separate value of surface ground used for other purposes plus value of machinery, property and surface improvements All other lands, realty, and personalty, assessed at 20% of the full market value.
Mining License Tax	IDAHO CODE § 47-1201 <u>et seq.</u>	2% of net proceeds of mine
Oil and Gas Production Tax	IDAHO CODE § 47-330	Rate is 5 mills per barrel of oil or per 50,000 cubic feet of gas produced. Levied for purposes of administering regulation of oil and gas industry.

UTAH

KIND OF TAX	STATUTORY REFERENCE	MEASURES AND RATE OF TAX
<p>Mining Occupation Tax</p>	<p>UTAH CODE § 59-5-66 <u>et seq.</u></p>	<p>1% of gross amount received for or gross value of ore or metal sold, or fissionable materials delivered. 2% of value at well or oil, gas, etc., sold or carried from production area.</p>
<p>Oil and Gas Production Tax</p>	<p>UTAH CODE § 40-6-14</p>	<p>Oil and gas produced, saved, sold or transported from production area, at rate fixed by Division of Oil and Gas Conservation, not over 2 mills per \$1 value at the well.</p>



UTAH

KIND OF TAX	STATUTORY REFERENCE	MEASURES AND RATE OF TAX
Corporate Income Tax	UTAH CODE § 59-13-65	6% of net income attributable to Utah, except income for a period requiring inclusion under the Corporate Franchise Tax, below.
Corporate Franchise Tax	UTAH CODE § 59-13-1 <u>et seq.</u>	6% of net income attributable to Utah. Minimum \$25. Income taxed under Franchise Tax offset against corporate income tax. (§ 59-13-70)
Property Tax	UTAH CODE § 59-5-57 <u>et seq.</u>	<p>§ 59-5-3 provides that mining property taxes (with some exceptions) are to be assessed by the State Tax Commission rather than by county assessors.</p> <p>§ 59-5-57 ("Severed Mineral Assessment"): if the surface lands and the mineral lands underlying such lands are owned by different individuals, such property rights shall be separately assessed to the respective owners.</p> <p><u>Metalliferous mines</u>: \$5 per acre, plus 2 times average net annual proceeds for past 3 years, plus 30% of value of machinery used in mining and other property not used for mining purposes.</p> <p><u>Non-metalliferous mines</u>: 30% of reasonable fair cash value and other realty and tangible personalty.</p> <p>§ 59-5-58: "net annual proceeds": the amount annually realized from the product of the mine over and above all costs and expenses of obtaining such proceeds and converting them into money.</p> <p>§ 59-5-58: Allowable deductions            § 59-5-59: Nonallowable deductions</p> <p><u>Coal and hydrocarbon lands</u>: 30% of their reasonable fair cash value</p>

NEW MEXICO

KIND OF TAX	STATUTORY REFERENCE	MEASURES AND RATE OF TAX
Oil and Gas Conservation Tax	N.M. STAT. ANN.  § 72-20-1 <u>et seq.</u>	Imposes a tax at the rate of 0.18% of taxable value on the following products: oil, natural gas or liquid hydrocarbon, individually or any combination thereof, uranium, coal and GEOTHERMAL ENERGY.  The purpose of this tax is to appropriate funds to the energy resources board of the state to be expended in the performance of its duties, the duties of the state geologist and the duties of the oil conservation commission.
Resources Excise Tax	N.M. STAT. ANN.  § 72-16A-20 to  § 72-16A- 29	For the privilege of severing natural resources: the rate is 3/4% of the market value except for potash; potash: 1/2 of 1%.  For the privilege of processing natural resources; the rate is 3/4% of the market value except for timber and potash. Timber: 3/8%. Potash: 1/8%.  Oil and gas are excluded from this tax and those subject to this tax are exempt from the Gross Receipts Tax.  No resources tax is due on the taxable value of any natural resource that is processed in New Mexico and on which the processors' tax has been paid.
Natural Gas Processors Tax	N.M. STAT. ANN.  § 72-23-1 <u>et seq.</u>	Imposes a tax at the rate of 45/100 of 1% of the value of manufactured products of natural gas or liquid hydrocarbon or in combination.  Those subject to this tax are exempt from the Gross Receipts Tax, the Oil and Gas Emergency School Act, and the Resources Excise Tax.

NEW MEXICO

KIND OF TAX	STATUTORY REFERENCE	MEASURES AND RATE OF TAX
Severance Tax	<p>N.M. STAT. ANN.</p> <p>§ 72-18-1 <u>et seq.</u></p>	<p>This tax has the effect of a license or occupation tax. It imposes a tax on the gross value of natural resources immediately after severance from the soil (but oil, gas, liquid hydrocarbon individually or any combination thereof or carbon dioxide are not included).</p> <p>Rates are as follows: for those products having a posted field or market price at the point of production, the value to be reported shall be its posted field or market price (for potash the value to be reported shall be 40% of such price) without any deductions except those expenses of hoisting, crushing and loading necessary to place the severed product in marketable form and at a marketable place; no deductions for hoisting, loading and crushing in excess of 50% of reported value shall be allowed. Rental or royalty payments belonging to the United States or the state of New Mexico shall be deducted from the gross value of the severed products.</p> <p>Class 1. Potash ----- 2 1/2%</p> <p>Class 2. Copper ----- 1/2%</p> <p>Class 3. Uranium and other material used primarily for its fissionable value ----- 1%</p> <p>Class 4. Timber ----- 1/8%</p> <p>Class 5. Coal ----- 1/2%</p> <p>Class 6. Pumice, gypsum, sand, gravel, clay, fluorspar and other nonmetallic minerals ----- 1/8%</p> <p>Class 7. Gold, silver, lead, zinc, thorium, molybdenum, manganese, rare earths and other metals ----- 1/8%</p>
Oil and Gas Severance Tax	<p>N.M. STAT. ANN.</p> <p>§ 72-19-1 <u>et seq.</u></p>	<p>Imposes a tax at the rate of 3 3/4% of taxable value on oil, natural gas, liquid hydrocarbon, individually or any combination thereof. Transportation expenses and any royalties paid to the government or Indian tribes may be deducted. Revenue collected under this tax is directed to the state's General Fund and is not subject to local control.</p>
Oil and Gas Emergency School (Privilege) Tax	<p>N.M. STAT. ANN.</p> <p>§ 72-21-1 <u>et seq.</u></p>	<p>Imposes an additional severance tax on the privilege of engaging in the business of severing oil, natural gas or liquid hydrocarbons from the soil of New Mexico. (This tax does not pertain to the production of minerals.)</p> <p>Rate is 2.55% of the taxable value of the product severed: oil, natural gas, or liquid hydrocarbon. Those subject to this tax are exempt from the Gross Receipts Tax and the Resources Excise Tax.</p>

NEW MEXICO

KIND OF TAX	STATUTORY REFERENCE	MEASURES AND RATE OF TAX
<p>Oil and Gas Production Equipment Ad Valorem Tax</p>	<p>N.M. STAT. ANN.  § 72-24-1 <u>et seq.</u></p>	<p>The tax is administered by the Oil and Gas Accounting Commission. The tax is on equipment used in oil, natural gas or liquid hydrocarbon production. The value of equipment of each production unit is set at an amount equal to 27% of the market value of the products of each production unit.</p> <p>The assessed value is determined by applying the uniform assessment rate of 33 1/3%.</p> <p>The Oil and Gas Production Equipment Tax and the Oil and Gas Ad Valorem Production Tax are the full and exclusive measure of <u>ad valorem</u> tax liability on the interest of all persons in the production of oil and gas.</p>
<p>Corporation Income Tax</p>	<p>N.M. STAT. ANN.  § 72-15A-1 <u>et seq.</u></p>	<p>Based on federal taxable income with adjustments.</p> <p>Tax rate is 5% of net income. Taxpayer may elect to allocate net income by Uniform Division of Income for Tax Purposes Act or Income Tax Act.</p>
<p>Corporate Franchise Tax</p>	<p>N.M. STAT. ANN.  § 51-13-1 <u>et seq.</u></p>	<p>Domestic corporations and foreign corporations for profit engaged in any business in New Mexico are taxed.</p> <p>Tax rate is \$.55 per \$1000, or fraction thereof, of the book value of that proportion of authorized and issued capital stock represented by property and business in the state. Minimum is \$10.</p>
<p>Gross Receipts (Sales) Tax</p>	<p>N.M. STAT. ANN.  § 72-16A-1 to § 72-16A-19</p>	<p>Rate is 4% of gross receipts for privilege of engaging in business. Oil, natural gas and liquid hydrocarbons covered by OIL AND GAS EMERGENCY SCHOOL TAX ACT and are specifically exempted from this tax by § 72-16A-12.20. Mineral interests are also exempt. Whenever the Oil and Gas Emergency School Tax, the Natural Gas Processors Tax or the Resources Excise Tax apply, then the Gross Receipts Tax does not apply.</p>
		<p>-49-</p>

NEW MEXICO

KIND OF TAX	STATUTORY REFERENCE	MEASURES AND RATE OF TAX
<p>Property Tax</p>	<p>N.M. STAT. ANN.            § 72-28-1 to            § 72-31-93             Mineral land valuation:            § 72-29-11 to            § 72-29-14</p>	<p>Valuation of mineral property is determined by the state Property Tax Department, not county assessors (§ 72-29-2-C(2)). Oil and gas property is not subject to valuation for property tax purposes under the Property Tax Code. Instead it is valued and taxed under the Oil and Gas Ad Valorem Production Tax (§ 72-22-1 <u>et seq.</u>) and the Oil and Gas Production Equipment Ad Valorem Tax (§ 72-24-1 <u>et seq.</u>).</p> <p>Property is assessed in proportion to its value. The current statewide uniform rate is 33 1/3% (§ 72-30-3).</p> <p>Mineral properties are classified as producing or nonproducing. Productive mineral property is taxed on the basis of net proceeds of production (the value for such mineral properties is an amount equal to 300% of the annual net production value). The value of class one nonproductive mineral property (nonoperated, privately owned mineral lands, reserves, interests and severed mineral products where the property is known to contain commercially workable quantities of minerals) is determined by applying a per acre value to the surface acres of the property being valued. The per acre value of such property is determined under regulations adopted by the Property Tax Department.</p> <p>"Annual net production value" for productive mineral property may be determined on an output basis, using either an average annual output for each of the previous five years, or, by election, only the prior year. Valuation is determined by the market value of the annual output, less the actual costs of producing and bringing the product to the surface, as well as the costs of milling, treating, transporting and selling the products. Alternatively, the Property Tax Department may value the property at 300% of the average annual output as determined under either the five year or one year method. If the productive property fails to produce a market value of average annual output above actual cost, then the Department may determine the taxable value of such property on the same basis as unproductive property.</p> <p>In addition to an ad valorem taxation on the value of mineral, the Property Tax Department assesses the value of all improvements, equipment, materials, supplies and personal property held or used in connection with the development of the mineral property. Also taxed is the value of any surface interests.</p>
<p>Oil and Gas Ad Valorem Production Tax</p>	<p>N.M. STAT. ANN.            § 72-22-1 <u>et seq.</u></p>	<p>Imposes an ad valorem tax on the assessed value of oil, natural gas and liquid hydrocarbon production severed and sold at certified local rates. The tax is initially administered by the Oil and Gas Accounting Commission which assesses the value of production units and collects the tax thereon.</p> <p>The taxable value of products is an amount equal to one hundred fifty per cent (150%) of the value of the products after deducting: (1) royalties paid or due the United States or the state of New Mexico; (2) royalties paid or due any Indian tribe, Indian pueblo, or Indian that is a ward of the United States; and (3) the reasonable expense of trucking any product from the production unit to the first place of market. The assessed value of the product is determined by applying the uniform assessment rate (33 1/3%) to the taxable value (150% of the market value) yielding an assessed valuation of 50% of the market value.</p>

CALIFORNIA

KIND OF TAX	STATUTORY REFERENCE	MEASURES AND RATE OF TAX
<p>Franchise (income) tax - business corporations, public utility companies and banks</p>	<p>CAL. REV. &amp; TAX CODE            § 23151            § 23503</p>	<p>Tax for the privilege of exercising a corporate franchise within the state. Insofar as the franchise tax overlaps the corporate income tax (below), the amount due under the franchise tax is offset against the amount due under the income tax.</p> <p>Tax rate is 9% of net income attributable to California. Minimum is \$200. Net income for California corporations is computed on an apportionment basis: the world wide income of a parent company and its subsidiaries is aggregated from which California net income is then determined.</p>
<p>Corporation Income Tax - All corporations except banking corporations</p>	<p>CAL. REV. &amp; TAX CODE            § 23501</p>	<p>Tax rate is 9% of net income attributable to California exclusive of income included in measure of franchise tax.</p> <p>Net income for California corporations computed on an apportionment basis: world wide income of parent company and its subsidiaries aggregated from which California net income then determined.</p>
<p>Oil &amp; Gas Production Charge</p>	<p>CAL. PUBLIC RESOURCES CODE            §§ 3402, 3403, 3423</p>	<p>Essentially a severance tax on the operation of oil and gas wells for the purpose of supervising and protecting deposits of oil and gas in California. The tax is levied per barrel of oil produced or per thousand cubic feet of gas produced. The Department of Conservation administers the tax and determines the annual rate on the basis of the annual amount required to support the Division of Oil and Gas. The assessments are a lien against the property of the person assessed and are made against the person operating the property. They are in addition to all other taxes and are payable on the first day in July of each year. Current rates as of July 1, 1976 are:</p>

CALIFORNIA

KIND OF TAX	STATUTORY REFERENCE	MEASURES AND RATE OF TAX
Property Tax	<p>CAL. CONST. Art. XIII, § 1; Art. XI, § 12</p> <p>CAL. REV. &amp; TAX CODE § 104-110, 201, 202, 401</p> <p>18 CAL. ADMIN. CODE §§ 27, 28</p>	<p>All property not exempt from taxation is taxable in proportion to its value. (CAL. CONST. Art. XIII, § 1)</p> <p>Although the Calif. Const. specifies that all property is to be assessed for taxation at its full cash value (Art. XI, § 12), § 401 of the Calif. Revenue and Tax Code provides that all property is to be assessed at 25% of the full cash value. Courts have upheld this assessment of property.</p> <p>Each county assessor, not a state agency, assess the value of oil, gas, mineral, and geothermal property and leaseholds. In practice assessment of oil and gas and geothermal leaseholds on private lands has differed from that on federal and state lands:</p> <ol style="list-style-type: none"> <li>1. Geothermal leaseholds on federal or state lands, when sold on a bonus bid basis, have been taxed as possessory interests, whether or not there is any production of power. (Note: where there have been title disputes over geothermal rights on state lands, the leaseholds on such lands have not been taxed as possessory interests, pending settlement of such disputes.)</li> <li>2. Geothermal leaseholds on private lands have not been taxed as possessory interests until there has been actual electrical production.</li> <li>3. Oil and gas leaseholds on state lands have been taxed as possessory interests, whether or not there is production.</li> <li>4. Oil and gas leaseholds on private lands have not been taxed as possessory interests until there has been production. (Often such leaseholds have not been recorded nor has there been a bonus bid price paid for the leasehold.)</li> </ol> <p>Once production has begun either for geothermal, oil and gas or mines, the property is then assessed on the basis of the present worth of future net income.</p> <p>Assessment problems are occurring on federal geothermal leaseholds where some development has taken place but there is no actual electrical generation or even a contract to sell power to a utility. The disputes center on what figure should be used for valuation purposes: total capital expended by the company to develop the leasehold up to the present time or some figure less than total capital expenditure.</p> <p>Unpatented mining claims are possessory interests and are, therefore, taxable.</p>

CHARTS OF STATE TAXES ARRANGED BY STATE



OIL AND GAS PRODUCTION OR CONSERVATION TAX

STATE	STATUTORY REFERENCE	MEASURES AND RATE OF TAX
CALIFORNIA	<p>CAL. PUBLIC RESOURCES CODE</p> <p>§§ 3402, 3403, 3423</p> <p>Oil &amp; Gas Production Charge</p>	<p>Essentially a severance tax on the operation of oil and gas wells for the purpose of supervising and protecting deposits of oil and gas in California. The tax is levied per barrel of oil produced or per thousand cubic feet of gas produced. The Department of Conservation administers the tax and determines the annual rate on the basis of the annual amount required to support the Division of Oil and Gas. The assessments are a lien against the property of the person assessed and are made against the person operating the property. They are in addition to all other taxes and are payable on the first day in July of each year. Current rates as of July 1, 1976 are:</p>
NEW MEXICO	<p>N.M. STAT. ANN.</p> <p>§ 72-20-1 et seq.</p> <p>Oil and Gas Conservation Tax</p>	<p>Imposes a tax at the rate of 0.18% of taxable value on the following products: oil, natural gas or liquid hydrocarbon, individually or any combination thereof, uranium, coal and GEOTHERMAL ENERGY.</p> <p>The purpose of this tax is to appropriate funds to the energy resources board of the state to be expended in the performance of its duties, the duties of the state geologist and the duties of the oil conservation commission.</p>
UTAH	<p>UTAH CODE</p> <p>§ 40-6-14</p> <p>Oil and Gas Production Tax</p>	<p>Oil and gas produced, saved, sold or transported from production area, at rate fixed by Division of Oil and Gas Conservation, not over 2 mills per \$1 value at the well.</p>
IDAHO	<p>IDAHO CODE</p> <p>§ 47-330</p> <p>Oil and Gas Production Tax</p>	<p>Rate is 5 mills per barrel of oil or per 50,000 cubic feet of gas produced.</p> <p>Levied for purposes of administering regulation of oil and gas industry.</p>
NEVADA	<p>NEV. REV. STAT.</p> <p>§ 522.150</p> <p>Oil and Gas Conservation Tax</p>	<p>5 mills per barrel of oil or 50,000 cubic feet of natural gas produced and sold, or bought.</p>

CORPORATE FRANCHISE, INCOME AND EXCISE TAXES

STATE	STATUTORY REFERENCE	MEASURES AND RATE OF TAX
UTAH	UTAH CODE § 59-13-65  Corporate Income Tax	6% of net income attributable to Utah, except income for a period requiring inclusion under the Corporate Franchise Tax, below.
	UTAH CODE § 59-13-1 <u>et seq.</u> Corporate Franchise Tax	6% of net income attributable to Utah. Minimum \$25. Income taxed under Franchise Tax offset against corporate income tax. (§ 59-13-70)
IDAHO	IDAHO CODE § 63-3025, § 63-3025A  Corporate Income Tax	6.5% taxable income from instate sources
OREGON	ORE. REV. STAT. § 317.005 <u>et seq.</u> Corporate Excise Tax	Corporations (including utilities) doing or authorized to do business pay 6½% (Financial institutions 8%) of net income attributable to Oregon; minimum is \$10. Rate for year 1977: 7%; Rate for year 1978 and after 7½%. Offset allowed corporation primarily engaged in manufacturing, processing or assembling.
	ORE. REV. STAT. § 318.010 <u>et seq.</u>  Corporate Income Tax	Corporations not taxed under the excise tax deriving income from Oregon from activities carried on instate pay a tax of 6½% on net income allocated to the state.

CORPORATE FRANCHISE, INCOME AND EXCISE TAXES

STATE	STATUTORY REFERENCE	MEASURES AND RATE OF TAX
CALIFORNIA	<p>CAL. REV. &amp; TAX CODE § 23151</p> <p>Franchise (income) tax - business corporations, public utility companies and banks</p>	<p>Tax for the privilege of exercising a corporate franchise within the state. Insofar as the franchise tax overlaps the corporate income tax (below), the amount due under the franchise tax is offset against the amount due under the income tax.</p> <p>Tax rate is 9% of net income attributable to California. Minimum is \$200. Net income for California corporations computed on an apportionment basis: world wide income of parent company and its subsidiaries aggregated from which California net income then determined.</p>
	<p>CAL. REV. &amp; TAX CODE § 23501</p> <p>Corporation Income Tax - All corporations except banking corporations</p>	<p>Tax rate is 9% of net income attributable to California exclusive of income included in measure of franchise tax.</p> <p>Net income for California corporations computed on an apportionment basis: world wide income of parent company and its subsidiaries aggregated from which California net income then determined.</p>
NEW MEXICO	<p>N.M. STAT. ANN. § 72-15A-1 et seq.</p> <p>Corporation Income Tax</p>	<p>Based on federal taxable income with adjustments.</p> <p>Tax rate is 5% of net income. Taxpayer may elect to allocate net income by Uniform Division of Income for Tax Purposes Act or Income Tax Act.</p>
	<p>N.M. STAT. ANN. § 51-13-1 et seq.</p> <p>Corporate Franchise Tax</p>	<p>Domestic corporations and foreign corporations for profit engaged in any business in New Mexico are taxed.</p> <p>Tax rate is \$.55 per \$1000, or fraction thereof, of the book value of that proportion of authorized and issued capital stock represented by property and business in the state. Minimum is \$10.</p>

SEVERENCE TAXES, LICENSE AND OCCUPATION TAXES

STATE	STATUTORY REFERENCE	MEASURES AND RATE OF TAX
IDAHO	<p>IDAHO CODE  § 47-1201 <u>et seq.</u>  Mining License  Tax</p>	<p>2% of net proceeds of mine</p>
	<p>IDAHO CODE  § 30-601 to  § 30-604    Corporate License  Fee</p>	<p>Based on authorized capital stock value  Minimum is \$20; maximum is \$300    Exemption: all mining companies who do not own productive mines</p>

SEVERENCE TAXES, LICENSE AND OCCUPATION TAXES

STATE	STATUTORY REFERENCE	MEASURES AND RATE OF TAX
<p>NEW MEXICO (continued)</p>	<p>N.M. STAT. ANN. § 72-16A-1 to § 72-16A-19  Gross Receipts (Sales) Tax</p>	<p>Rate is 4% of gross receipts for privilege of engaging in business. Oil, natural gas and liquid hydrocarbons covered by OIL AND GAS EMERGENCY SCHOOL TAX ACT and are specifically exempted from this tax by § 72-16A-12.20. Mineral interests are also exempt. Whenever the Oil and Gas Emergency School Tax, the Natural Gas Processors Tax or the Resources Excise Tax apply, then the Gross Receipts Tax does not apply.</p>
	<p>N.M. STAT. ANN. § 72-16A-20 to § 72-16A- 29  Resources Excise Tax</p>	<p>For the privilege of severing natural resources; the rate is 3/4% of the market value except for potash; potash: 4% .  For the privilege of processing natural resources; the rate is 3/4% of the market value except for timber and potash. Timber: 3/8%. Potash: 1/8%.  Oil and gas are excluded from this tax and those subject to this tax are exempt from the Gross Receipts Tax.  No resources tax is due on the taxable value of any natural resource that is processed in New Mexico and on which the processors' tax has been paid.</p>
	<p>N.M. STAT. ANN. § 72-23-1 <u>et seq.</u>  Natural Gas Processors Tax</p>	<p>Imposes a tax at the rate of 45/100 of 1% of the value of manufactured products of natural gas or liquid hydrocarbon or in combination.  Those subject to this tax are exempt from the Gross Receipts Tax, the Oil and Gas Emergency School Tax and the Resources Excise Tax.</p>
<p>UTAH</p>	<p>UTAH CODE § 59-5-66 <u>et seq.</u>  Mining Occupation  Tax</p>	<p>1% of gross amount received for or gross value of ore or metal sold, or fissionable materials delivered.  2% of value at well or oil, gas, etc., sold or carried from production area.</p>

SEVERANCE TAXES, LICENSE AND OCCUPATION TAXES

STATE	STATUTORY REFERENCE	MEASURES AND RATE OF TAX
<p>NEW MEXICO</p>	<p>N.M. STAT. ANN.</p> <p>§ 72-18-1 et seq.</p> <p>Severance Tax</p>	<p>This tax has the effect of a license or occupation tax. It imposes a tax on the gross value of natural resources immediately after severance from the soil (but oil, gas, liquid hydrocarbon individually or any combination thereof or carbon dioxide are not included).</p> <p>Rates are as follows: for those products having a posted field or market price at the point of production, the value to be reported shall be its posted field or market price (for potash the value to be reported shall be 40% of such price) without any deductions except those expenses of hoisting, crushing and loading necessary to place the severed product in marketable form and at a marketable place; no deductions for hoisting, loading and crushing in excess of 50% of reported value shall be allowed. Rental or royalty payments belonging to the United States or the state of New Mexico shall be deducted from the gross value of the severed products.</p> <p>Class 3. Uranium and other material used primarily for its fissionable value -----1%            Class 5. Coal-----1/2%            Class 6. Pumic, gypsum, sand, gravel, clay, flourspar and other nonmetallic minerals -----1/8%</p>
	<p>N.M. STAT. ANN.</p> <p>§ 72-19-1 et seq.</p> <p>Oil and Gas Severance Tax</p>	<p>Imposes a tax at the rate of 3 3/4% of taxable value on oil, natural gas, liquid hydrocarbon, individually or any combination thereof. Transportation expenses and any royalties paid to the government or Indian tribes may be deducted. Revenue collected under this tax is directed to the state's General Fund and is not subject to local control.</p>
	<p>N.M. STAT. ANN.</p> <p>§ 72-21-1 et seq.</p> <p>Oil and Gas Emergency School (Privilege) Tax</p>	<p>Imposes an additional severance tax on the privilege of engaging in the business of severing oil, natural gas or liquid hydrocarbons from the soil of New Mexico. (This tax does not pertain to the production of minerals.)</p> <p>Rate is 2.55% of the taxable value of the product severed: oil, natural gas, or liquid hydrocarbon. Those subject to this tax are exempt from the Gross Receipts Tax and the Resources Excise Tax.</p>

PROPERTY TAX

STATE	STATUTORY REFERENCE	MEASURES AND RATE OF TAX
IDAHO	<p>IDAHO CODE § 63-2801 <u>et seq.</u></p>	<p><u>Productive mines:</u> Net annual profits, plus (1) price paid to U.S. for mines and claims or (2) separate value of surface ground used for other purposes plus value of machinery, property and surface improvements</p> <p>All other lands , realty and personalty, assessed at 20% of full market value.</p>
NEVADA	<p>NEV. REV. STAT. § 361.010 <u>et seq.</u></p>	<p>§ 361.225: All property is assessed at 35% of the full cash value.</p> <p><u>Mining property:</u> Computed on a net proceeds basis. Once the net proceeds for a mine are determined, the mine is then taxed at the same ad valorem rate as other property is taxed (§ 362.140).</p> <p>Unpatented mines and mining claims are exempt from taxation. (§ 361.075)</p> <p>Although the property tax for mines is computed on the value of the severed product, it is considered to be a lien on the mine or mining claims, from which ores or minerals are extracted for sale or reduction.</p>
OREGON	<p>ORE. REV. STAT. § 307.010 to § 311.</p>	<p>Realty and tangible personalty taxed at 100% of true cash value as of January 1.</p> <p>When mineral, coal, oil, and gas interests have been severed, they shall be taxed separately. (§ 308.115)</p> <p>Unpatented mining claims exempt from taxation. (§ 307.080)</p>

PROPERTY TAX

STATE	STATUTORY REFERENCE	MEASURES AND RATE OF TAX
NEW MEXICO	<p>N.M. STAT. ANN.</p> <p>§ 72-24-1 <u>et seq.</u></p> <p>Oil and Gas Production Equipment Ad Valorem Tax</p>	<p>The tax is administered by the Oil and Gas Accounting Commission. The tax is on equipment used in oil, natural gas or liquid hydrocarbon production. The value of equipment of each production unit is set at an amount equal to 27% of the market value of the products of each production unit.</p> <p>The assessed value is determined by applying the uniform assessment rate of 33 1/3%.</p> <p>The Oil and Gas Production Equipment Tax and the Oil and Gas Ad Valorem Production Tax are the full and exclusive measure of <u>ad valorem</u> tax liability on the interest of all persons in the production of oil and gas.</p>
UTAH	<p>UTAH CODE</p> <p>§ 59-5-57 <u>et seq.</u></p>	<p>§ 59-5-3 provides that mining property taxes (with some exceptions) are to be assessed by the State Tax Commission rather than by county assessors.</p> <p>§ 59-5-57 ("Severed Mineral Assessment"): if the surface lands and the mineral lands underlying such lands are owned by different individuals, such property rights shall be separately assessed to the respective owners.</p> <p><u>Metalliferous mines</u>: \$5 per acre, plus 2 times average net annual proceeds for past 3 years, plus 30% of value of machinery used in mining and other property not used for mining purposes.</p> <p><u>Non-metalliferous mines</u>: 30% of reasonable fair cash value and other realty and tangible personalty.</p> <p>§ 59-5-58: Allowable deductions ; definition of "net annual proceeds"          § 59-5-59: Nonallowable deductions</p> <p><u>Coal and hydrocarbon lands</u>: 30% of their reasonable fair cash value</p>



PROPERTY TAX

STATE	STATUTORY REFERENCE	MEASURES AND RATE OF TAX
<p>NEW MEXICO</p>	<p>N.M. STAT. ANN.  § 72-28-1 to § 72-31-93  Mineral land valuation: § 72-29-11 to § 72-29-14</p>	<p>Valuation of mineral property is determined by the state Property Tax Department, not county assessors (§ 72-29-2-C(2)). Oil and gas property is not subject to valuation for property tax purposes under the Property Tax Code. Instead it is valued and taxed under the Oil and Gas Ad Valorem Production Tax (§ 72-22-1 <u>et seq.</u>) and the Oil and Gas Production Equipment Ad Valorem Tax (§ 72-24-1 <u>et seq.</u>).</p> <p>Property is assessed in proportion to its value. The current statewide uniform rate is 33 1/3% (§ 72-30-3).</p> <p>Mineral properties are classified as producing or nonproducing. Productive mineral property is taxed on the basis of net proceeds of production (the value for such mineral properties is an amount equal to 300% of the annual net production value). The value of class one nonproductive mineral property (nonoperated, privately owned mineral lands, reserves, interests and severed mineral products where the property is known to contain commercially workable quantities of minerals) is determined by applying a per acre value to the surface acres of the property being valued. The per acre value of such property is determined under regulations adopted by the Property Tax Department.</p> <p>"Annual net production value" for productive mineral property may be determined on an output basis, using either an average annual output for each of the previous five years, or, by election, only the prior year. Valuation is determined by the market value of the annual output, less the actual costs of producing and bringing the product to the surface, as well as the costs of milling, treating, transporting and selling the products. Alternatively, the Property Tax Department may value the property at 300% of the average annual output as determined under either the five year or one year method. If the productive property fails to produce a market value of average annual output above actual cost, then the Department may determine the taxable value of such property on the same basis as unproductive property.</p> <p>In addition to an ad valorem taxation on the value of mineral, the Property Tax Department assesses the value of all improvements, equipment, materials, supplies and personal property held or used in connection with the development of the mineral property. Also taxed is the value of any surface interests.</p>
	<p>N.M. STAT. ANN.  § 72-22-1 <u>et seq.</u>  Oil and Gas Ad Valorem Production Tax</p>	<p>Imposes an ad valorem tax on the assessed value of oil, natural gas and liquid hydrocarbon production severed and sold at certified local rates. The tax is initially administered by the Oil and Gas Accounting Commission which assesses the value of production units and collects the tax thereon.</p> <p>The taxable value of products is an amount equal to one hundred fifty per cent (150%) of the value of the products after deducting: (1) royalties paid or due the United States or the state of New Mexico; (2) royalties paid or due any Indian tribe, Indian pueblo, or Indian that is a ward of the United States; and (3) the reasonable expense of trucking any product from the production unit to the first place of market. The assessed value of the product is determined by applying the uniform assessment rate (33 1/3%) to the taxable value (150% of the market value) yielding an assessed valuation of 50% of the market value.</p>

PROPERTY TAX

STATE	STATUTORY REFERENCE	MEASURES AND RATE OF TAX
CALIFORNIA	<p>CAL. CONST. Art. XIII, § 1; Art. XI, § 12</p> <p>CAL. REV. &amp; TAX CODE § 104-110, 201, 202, 401</p> <p>18 CAL. ADMIN. CODE §§ 27, 28</p>	<p>All property not exempt from taxation is taxable in proportion to its value. (CAL. CONST. Art. XIII, § 1)</p> <p>Although the Calif. Const. specifies that all property is to be assessed for taxation at its full cash value (Art. XI, § 12), § 401 of the Calif. Revenue and Tax Code provides that all property is to be assessed at 25% of the full cash value. Courts have upheld this assessment of property.</p> <p>Each county assessor, not a state agency, assesses the value of oil, gas, mineral, and geothermal property and leaseholds. In practice assessment of oil and gas and geothermal leaseholds on private lands has differed from that on federal and state lands:</p> <ol style="list-style-type: none"> <li>1. Geothermal leaseholds on federal or state lands, when sold on a bonus bid basis, have been taxed as possessory interests, whether or not there is any production of power. (Note: where there have been title disputes over geothermal rights on state lands, the leaseholds on such lands have not been taxed as possessory interests, pending settlement of such disputes.)</li> <li>2. Geothermal leaseholds on private lands have not been taxed as possessory interests until there has been actual electrical production.</li> <li>3. Oil and gas leaseholds on state lands have been taxed as possessory interests, whether or not there is production.</li> <li>4. Oil and gas leaseholds on private lands have not been taxed as possessory interests until there has been production. (Often such leaseholds have not been recorded nor has there been a bonus bid price paid for the leasehold.)</li> </ol> <p>Once production has begun either for geothermal, oil and gas or mines, the property is then assessed on the basis of the present worth of future net income.</p> <p>Assessment problems are occurring on federal geothermal leaseholds where some development has taken place but there is no actual electrical generation or even a contract to sell power to a utility. The disputes center on what figure should be used for valuation purposes: total capital expended by the company to develop the leasehold up to the present time or some figure less than total capital expenditure.</p> <p>Unpatented mining claims are possessory interests and are, therefore, taxable.</p>

CHARTS OF STATE TAXES ARRANGED ACCORDING TO TYPE OF TAX

Washington (WASH. REV. CODE ANN. § 79.76.030, 79.76.040 (1974))

Geothermal resources means only that natural heat energy of the earth from which it is technologically practical to produce electricity commercially and the medium by which such heat energy is extracted from the earth, including liquids or gases, as well as any minerals contained in any natural or injected fluids, brines and associated gas, but excluding oil, hydrocarbon gas and other hydrocarbon substances.

Notwithstanding any other provision of law, geothermal resources are found and hereby determined to be sui generis, being neither a mineral resource nor a water resource.

Nevada (NEV. REV. STAT. § 361.027 (1975))

"Geothermal resource" means:

1. All products of geothermal processes, embracing indigenous steam, hot water and hot brines;
2. Steam and other gases, hot water and hot brines resulting from water, gas or other fluids artificially introduced into sub-surface formations;
3. Heat or other associated energy found beneath the surface of the earth; and
4. Byproducts of any of the items enumerated in subsections 1 to 3, inclusive, such as minerals (exclusive of oil, hydrocarbon gas that can be separately produced) which are found in solution or association with or derived from any of such items.

New Mexico (N.M. STAT. ANN. § 65-11-3(A) (Interim Supp. 1975))

"Geothermal resources" means the natural heat of the earth, or the energy, in whatever form, below the surface of the earth present in, resulting from, created by, or which may be extracted from, this natural heat, and all minerals in solution or other products obtained from naturally heated fluids, brines, associated gases, and steam, in whatever form, found below the surface of the earth, but excluding oil, hydrocarbon gas and other hydrocarbon substances.

Oregon (ORE. REV. STAT. § 522.050(7) (1975))

"Geothermal resources" means the natural heat of the earth, the energy, in whatever form, below the surface of the earth present in, resulting from, or created by, or which may be extracted from, the natural heat, and all minerals in solution or other products obtained from naturally heated fluids, brines, associated gases, and steam, in whatever form, found below the surface of the earth, exclusive of helium or of oil, hydrocarbon gas or other hydrocarbon substances, but including, specifically:

- (a) All products of geothermal processes, embracing indigenous steam, hot water and hot brines;
- (b) Steam and other gases, hot water and hot brines resulting from water, gas, or other fluids artificially introduced into geothermal formations;
- (c) Heat or other associated energy found in geothermal formations; and
- (d) Any byproduct derived from them.

Hawaii (HAWAII REV. STAT. § 182-1 et seq. (1968, Supp. 1975))

(1) "Minerals" means any or all of the oil, gas, coal, phosphate, sodium, sulphur, iron, titanium, gold, silver, bauxite, bauxitic clay, diaspore, boehmite, laterite, gibbsite, alumina, all ores of aluminum and, without limitation thereon, all other mineral substances and ore deposits whether solid, gaseous, or liquid, including all geothermal resources, in, on, or under any land, fast or submerged; but does not include sand, rock, gravel, and other materials suitable for use and used in general construction.

(9) "Geothermal resources" means the natural heat of the earth, the energy, in whatever form, below the surface of the earth present in, resulting from, or created by, or which may be extracted from, such natural heat, and all minerals in solution or other products obtained from naturally heated fluids, brines, associated gases and steam, in whatever form, found below the surface of the earth, but excluding oil, hydrocarbon gas or other hydrocarbon substances.

Idaho (IDAHO CODE § 42-4002(c) (Supp. 1975))

"Geothermal resource" means the natural heat energy of the earth, the energy, in whatever form, which may be found in any position and at any depth below the surface of the earth present in, resulting from, or created by, or which may be extracted from such natural heat, and all minerals in solution or other products obtained from the material medium of any geothermal resource. Geothermal resources are found and hereby declared to be sui generis, being neither a mineral resource nor a water resource, but they are also found and hereby declared to be closely related to and possibly affecting and affected by water and mineral resources in many instances.

Montana (MONT. REV. CODE § 81-2602(1) (Supp. 1975)).

"Geothermal resources" means the natural heat energy of the earth, including the energy, in whatever form, which may be found in any position and at any depth below the surface of the earth, either present in, resulting from, created by, or which may be extracted from, such natural heat, and all minerals in solution or other products obtained from the material medium of any geothermal resource. Geothermal resources are sui generis, being neither a mineral resource nor a water resource, but they are closely related to and possibly affecting and affected by water resources in many instances. No right to seek, obtain, or use geothermal resources has passed or shall pass with any existing or future lease of state or school lands.

Arizona (ARIZ. REV. STAT. ANN. § 27-651(5) (1973))

Geothermal resources means:

- (a) All products of geothermal processes embracing indigenous steam, hot water and hot brines.
- (b) Steam and other gases, hot water and hot brines resulting from water, other fluids or gas artificially introduced into geothermal formations.
- (c) Heat or other associated energy found in geothermal formations, including any artificial stimulation or induction thereof.
- (d) Any mineral or minerals, exclusive of fossil fuels and helium gas, which may be present in solution or in association with geothermal steam, water or brines.

California (CAL. PUB. RES. CODE § 6903 (1974))

For the purposes of this chapter, "geothermal resources" shall mean the natural heat of the earth, the energy in whatever form, below the surface of the earth, present in, resulting from, or created by, or which may be extracted from, such natural heat, and all minerals in solution or other products obtained from naturally heated fluids, brines, associated gases, and steam, in whatever form, found below the surface of the earth, but excluding oil, hydrocarbon gas or other hydrocarbon substances.

Colorado (COLO. REV. STAT. § 34-70-103 (4) & (6) (Supp. 1975)).

(6) (a) "Geothermal resources" means geothermal heat and associated geothermal resources, including but not limited to:

- (I) Indigenous steam, other gases, hot water, hot brine, and all other products of geothermal processes;
- (II) Steam, other gases, hot water, hot brine and all other products of geothermal processes resulting from water, brine, steam, air, gas, or other substances artificially introduced into subsurface formations; and
- (III) Natural heat, steam energy, and other similar thermal energy in whatever form found in subsurface formations.

(6) (b) For purposes of this article, such term shall not include thermal energy contained in mineral deposits (including deposits of coal, oil shale, crude oil, natural gas, and other hydrocarbon substances, and including other substances and materials associated and produced in connection with such minerals) which are explored for, developed, and produced primarily for the mineral value thereof and not primarily for the thermal energy contained therein.

(4) Geothermal by-product means any substances which remain after thermal energy has been removed from geothermal resources, including but not limited to cooled waters, solution minerals, chemical compounds, extractable salts, rare earths, and other mineral substances.

United States (30 U.S.C. § 1001(c) (1970))

Geothermal steam and associated geothermal resources means (i) all products of geothermal processes, embracing indigenous steam, hot water and hot brines; (ii) steam and other gases, hot water and hot brines resulting from water, gas or other fluids artificially introduced into geothermal formations; (iii) heat or other associated energy found in geothermal formations; and (iv) any byproduct derived from them;

(d) byproduct means any mineral or minerals (exclusive of oil, hydrocarbon gas, and helium) which are found in solution or in association with geothermal steam and which have a value of less than 75 per centum of the value of the geothermal steam or are not, because of quantity, quality or technical difficulties in extraction and production, of sufficient value to warrant extraction and production by themselves.

Alaska (ALASKA STAT. § 38.05.181(q) (1974))

(6) Geothermal resources means the natural heat of the earth, the energy, in whatever form, below the surface of the earth present in, resulting from, or created by, or which may be extracted from, the natural heat, and all minerals in solution or other products obtained from naturally heated fluids, brines, associated gases, and steam, in whatever form, found below the surface of the earth, exclusive of oil, hydrocarbon gas, helium or other hydrocarbon substances, but including, specifically:

- (a) all products of geothermal processes, embracing indigenous steam, hot water and hot brine;
- (b) steam and other gases, hot water and hot brines resulting from water, gas, or other fluids artificially introduced into geothermal formations;
- (c) heat or other associated energy found in geothermal formations; and
- (d) any byproducts derived from them.

(1) Byproduct means any mineral or minerals (exclusive of oil, hydrocarbon gas, helium or other hydrocarbon substances) which are found in solution or in association with geothermal resources and which have a value of less than 75 percent of the value of the geothermal resource or are not, because of quantity, quality or technical difficulties in extraction and production, of sufficient value to warrant extraction and production by themselves.



APPENDIX A

DEFINITIONS OF GEOTHERMAL RESOURCES AND BYPRODUCTS

Olpin, Owen, "The Law of Geothermal Resources," 14th Annual Rocky Mt. Mineral Law Institute, p. 123 (1968).

Public Land Law Review Commission, Energy, Fuel, Mineral Resources of the Public Lands (1970).

Root, T. E., "Contents of a Geothermal Lease: Some Suggestions," Natural Resources Lawyer, Vol. 8, p. 659 (1976)..

Schlauch and Worcester, "Geothermal Resources: A Primer for the Practitioner," Land and Water Law Review, Vol. 9, p. 327 (1974).

SELECTED BIBLIOGRAPHY

- Aidlin, Joseph, "Representing The Geothermal Resources Client," 19th Annual Rocky Mt. Mineral Law Institute, p. 27 (1973).
- Allen, Donald R., "Legal and Policy Aspects of Geothermal Resource Development," Water Resources Bulletin, Vol. 8, No. 2, p. 250 (April 1972).
- American Law of Mining, Vol. 4, esp. Title XXVI: "Valuation of Mining Properties," Title XXVII: "Ad Valorem and Production Taxation of Mining Properties," Title XXVIII: "The Income Taxation of Mining Operations," (1976).
- Arizona, University of, Symposium of Mine Taxation (1969).
- Bjorge, Kenneth R., "The Development of Geothermal Resources and the 1970 Geothermal Steam Act - Law in Search of Definition," University of Colorado Law Review, Vol. 46, p. 1, (1974).
- Brightwell, Thomas P., "State Property Taxation of Mineral Deposits," 15th Annual Rocky Mt. Mineral Law Institute, p.281 (1969).
- Brooks, Jr., John W., "Legal Problems of the Geothermal Industry," Natural Resources Journal, Vol. 6, p. 511 (1966).
- Eisenstat, Samuel M., "Tax Treatment of Exploring and Developing Geothermal Resources," Oil and Gas Tax Quarterly (1973).
- \_\_\_\_\_, "Geothermal Tax Considerations and Shelters," Financial Aspects of Geothermal Resources Development (Davis: Geothermal Resources Council, 1975) p. 49.
- \_\_\_\_\_, "Geothermal Exploration and Development in the United States: A Tax Analysis Under the Internal Revenue Code," Financial Aspects of Geothermal Resources Development, p. 59.
- Kirkham, W. G., and Brown, Susan J., State and Local Permit Study - An Analysis of Administrative Factors Affecting Geothermal Development at The Geysers, (Sacramento, Calif. Office of Planning & Research in the Governor's Office) 1976.
- Kruger and Otte, Geothermal Energy (1973).
- Lindsey, Michael, and Supton, Paul, Geothermal Energy: Legal Problems of Resource Development, (Stanford Environmental Law Society, 1975).
- Million, Stephen A., "The Application of Depletion to Geothermal Resources," University of Michigan Journal of Law Reform, Vol. 8, p. 233, (1976).

Two traditional tax incentives: percentage depletion allowances and immediate deduction of intangible drilling costs. - could be adopted by state legislatures for geothermal operations.<sup>69</sup> Percentage depletion allowances tend to encourage capital investment in exploration for and development of natural resources because such allowances are deductible from production income, up to a maximum of 50% of net income from such producing property. Immediate deduction of intangible drilling costs has attracted private investors to participate in joint venture exploratory drilling for oil and gas with the benefits of offsetting present income from other sources. However, both percentage depletion allowances and immediate deduction of intangible drilling expenses have come under increasing attack at both the federal and state levels.<sup>70</sup> It is likely that continued increases in the cost of other forms of energy minerals will reach the point where geothermal development is economically competitive without any tax incentives. Geothermal energy must, nonetheless, be competitive at the present time with other forms of energy that do have tax benefits. Society would be better served by encouraging the immediate development of alternative energy resources. For this to occur, other impediments besides tax problems would have to be removed for geothermal to develop rapidly.

Individual state taxes such as the ad valorem tax in California can be onerous but it is the combined tax burden of state taxes, coupled with federal taxes and a lack of a percentage depletion allowance and an "IDC" deduction, that must be considered in assessing the economic viability of an energy industry. Lack of tax incentives at the state level, combined with heavy taxes during these beginning years of geothermal development, suggests that geothermal development will continue at a slow pace.

---

<sup>69</sup>See discussion, supra footnote 61.

<sup>70</sup>Id.

lengthy wait before he will receive any income to offset this tax burden, private landowners have been deterred from developing the geothermal resources on their land and from leasing their land to others for development. Furthermore, the geothermal industry contends that this system of taxation has discouraged the entry of risk capital into geothermal ventures. . . ."<sup>65</sup>

Under the current statutory and constitutional requirements in California, there seems to be no way to postpone the ad valorem tax until production begins.<sup>66</sup> Several proposed constitutional amendments would allow deferral of ad valorem tax payments by producers of geothermal energy.<sup>67</sup> The California Legislature still has not passed any of these proposed amendments for submission to the electorate. However, the assessor's office in Imperial County "has classified geothermal operations as research and development operations because of the state of the art with liquid dominated resources, and has exempted the added value of any proven resources until there is commercial production."<sup>68</sup> Nonetheless, taxation of known or proven reserves before any steam can be sold has been and continues to be a particularly troublesome problem for geothermal developers.

A severance, occupation, license or excise tax would be one more tax for the geothermal producer to pay should such a tax be levied by a state on geothermal resources. Taxes are additional costs, and to the extent that they reduce profits, the profit to risk ratio and the return on investment are reduced, resulting in slower or less development of geothermal resources. None of the six states has a specific severance tax on geothermal resources although geothermal might come under Class 6 in New Mexico's Severance Tax as a "nonmetallic mineral."

---

<sup>65</sup>Lindsey and Supton, Geothermal Energy: Legal Problems of Resource Development, p. 97 (May, 1975),

<sup>66</sup>In fact, a California State Assemblyperson has proposed a bill that would penalize lessees of state leaseholds for not doing exploratory drilling on their leases within the five year lease period.

<sup>67</sup>At the present time under the California Constitution (Art. 13, Sec. 3) owners of timber and agricultural crops are allowed to defer property tax payments.

<sup>68</sup>Subcommittee on Geothermal Resources of the Joint Legislative Committee on Public Domain, Geothermal Resources in California: Much Heat and Some Light, p. 23 (1974), quoted in Lindsey and Supton, supra footnote 65, at p. 99.

## CONCLUSION

The timing of application of the state corporate income tax makes it generally the most equitable tax to the energy producer because there is no tax until there is a profit. Since most states with a corporate income tax pattern their systems after the federal tax system, depletion and intangible drilling deduction problems parallel those under the federal Internal Revenue Code.<sup>61</sup> California law allows a cost depletion for many natural resources,<sup>62</sup> a deduction of expenses for exploration for many natural resources,<sup>63</sup> and a percentage depletion of 22 percent on the gross income of oil and gas wells.<sup>64</sup> However, none of the six states studied have a specific depletion allowance and/or "IDC" deduction for geothermal.

The state property tax/ad valorem tax as applied in California seems to be the most restrictive tax to the geothermal producer because the tax is increased at every aspect of development to reflect the incremental value provided by the proven underlying reservoir. The tax is applied long before production begins and revenues are generated. "Since the owner can expect a

---

<sup>61</sup>There is no percentage depletion allowance and/or "IDC" deduction for geothermal resources under federal law. However, the following energy minerals have a percentage depletion allowance: uranium: 22%, oil shale: 15%, coal: 10%, oil and natural gas: 22% under certain restricted conditions. (26 U.S.C. § 613, 613A (1970).) See discussion *supra*, footnote 14. The 1976 Federal Tax Reform Act before the Senate/House Conference Committee has a provision that would allow a 22% percentage depletion allowance and an intangible drilling cost deduction for geothermal resources. Should this provision become federal law, many states probably will follow the federal law and will also grant a percentage depletion allowance and an "IDC" deduction for geothermal resources.

<sup>62</sup>CAL. REV. & TAX CODE §§ 24833, 24835 (West 1972, Supp. 1975).

<sup>63</sup>*Id.*, § 24837.5, but excluding, for the most part, oil and gas.

<sup>64</sup>*Id.*, § 24832. But where the total depletion taken by an oil and gas company exceeds the cost of the property and the 22 percent depletion computation produces a figure over \$1.5 million, the depletion allowance is reduced or eliminated. In effect, percentage depletion for oil and gas has been eliminated for the major producers.

NEVADA

Oil and Gas Conservation Tax.<sup>60</sup> The tax rate is 5 mills per barrel of oil or 50,000 cubic feet of natural gas produced and sold, or bought.

---

<sup>60</sup>NEV. REV. STAT. § 522.150 (1975).

CALIFORNIA

Oil and Gas Production Charge.<sup>56</sup> The tax is levied per barrel of oil produced or per thousand cubic feet of gas produced. The Department of Conservation administers the tax and determines the annual rate on the basis of the amount required to support the Division of Oil and Gas on an annual basis. The assessments are a lien against the property of the person assessed and are made against the person operating the property.

NEW MEXICO

Oil and Gas Conservation Tax.<sup>57</sup> The tax rate is 0.18% of the taxable value of the following products: oil, natural gas or liquid hydrocarbon, individually or any combination thereof, uranium, coal and geothermal energy.

UTAH

Oil and Gas Production Tax.<sup>58</sup> The tax is on oil and gas produced, saved, sold or transported from the production area at a rate fixed by the Division of Oil and Gas Conservation.

IDAHO

Oil and Gas Production Tax.<sup>59</sup> The tax rate is 5 mills per barrel of oil or per 50,000 cubic feet of gas produced.

---

<sup>56</sup>CAL. PUBLIC RES. CODE § 3402, 3403, 3423 (West 1972).

<sup>57</sup>N.M. STAT. ANN. § 72-20-1 et seq. (Interim Supp. 1975).

<sup>58</sup>UTAH CODE § 40-6-14 (1974).

<sup>59</sup>IDAHO CODE § 47-330 (1967).



## OREGON

Oregon has a Corporate Income Tax<sup>53</sup> and a Corporate Excise Tax.<sup>54</sup> Under the corporate excise tax corporations (including utilities) doing or authorized to do business in Oregon pay 6 1/2% of net income attributable to Oregon. Rate for year 1977: 7%, for year 1978 and after: 7 1/2%. Corporations not taxed under the excise tax must pay the corporate income tax on income from activities carried on in state at a rate of 6 1/2%. Rate for year 1977: 7%, for year 1978 and after: 7 1/2%.

## NEVADA

Nevada does not have a corporate income tax, a corporate franchise tax or a corporate excise tax.

## IV. OIL AND GAS PRODUCTION OR CONSERVATION TAXES<sup>55</sup>

Five of the Western states under study have an oil and gas production or conservation tax. The purpose of each of these taxes is to raise revenue to support the regulation of the industry itself. Its impact on the industries taxed is minimal. New Mexico's Oil and Gas Conservation Tax is the broadest: it taxes uranium, coal and geothermal energy as well as oil and natural gas. It is the only tax in any of the 6 states under study that specifically taxes geothermal energy. In California the oil and gas production charge tax pays for the supervision of geothermal drilling activities but the geothermal producers are not taxed.

---

<sup>53</sup>ORE. REV. STAT. § 318.010 et seq. (1975).

<sup>54</sup>ORE. REV. STAT. § 317.005 et seq. (1975).

<sup>55</sup>See Charts.

total business income to determine income subject to California tax.

#### NEW MEXICO

New Mexico has a Corporate Income Tax<sup>46</sup> and a Corporate Franchise Tax.<sup>47</sup> The franchise tax rate is \$.55 per \$1000, or fraction thereof, of the book value of that proportion of authorized and issued capital stock represented by property and business in the state. The corporate income tax rate is 5% of net income. The taxpayer may elect to allocate net income under the Uniform Division of Income for Tax Purposes Act<sup>48</sup> or the Income Tax Act.<sup>49</sup>

#### UTAH

Utah has a Corporate Income Tax<sup>50</sup> and a Corporate Franchise Tax.<sup>51</sup> The franchise tax rate is 6% of net income attributable to Utah. The corporate income tax applies only to interstate business and the rate is 6% of net income attributable to Utah, except for income requiring inclusion under the franchise tax.

#### IDAHO

Idaho's Corporate Income Tax<sup>52</sup> rate is 6.5% of taxable income from instate sources.

---

<sup>46</sup>N.M. STAT. ANN. § 72-15A-1 et seq. (Interim Supp. 1975).

<sup>47</sup>N.M. STAT. ANN. § 51-13-1 to 51-13-12 (Supp. 1975).

<sup>48</sup>N.M. STAT. ANN. § 72-15A-16 to 72-15A-36 (Supp. 1975).

<sup>49</sup>N.M. STAT. ANN. § 72-15A-1 to 72-15A-15 (Supp. 1975).

<sup>50</sup>UTAH CODE § 59-13-65 (1974).

<sup>51</sup>UTAH CODE § 59-13-1 et seq. (1974).

<sup>52</sup>IDAHO CODE § 63-3025 (1976).

### III. CORPORATE FRANCHISE, INCOME AND EXCISE TAXES<sup>43</sup>

Corporate income taxes are assessed only if the mine or oil and gas operation makes a profit. From industry's viewpoint this is perhaps the fairest of all taxing structures.

#### CALIFORNIA

California has a Franchise Tax<sup>44</sup> and a Corporate Income Tax.<sup>45</sup> The franchise tax is for the privilege of exercising a corporate franchise within the state. The tax rate is 9% of net income attributable to California. Minimum is \$200. Insofar as the franchise tax overlaps the corporate income tax, the amount due under the franchise tax is offset against the amount due under the income tax. The computation of income for both the franchise tax and the income tax follows generally the pattern of the federal income tax and interpretations of the federal law by the Treasury Department. The tax rate for the income tax is also 9%.

California taxes on corporate income are measured by income derived from or attributable to sources within California only. The law provides that allocation and apportionment of income is required where business activities are taxable within and without California. Detailed rules for apportionment of business income by formula are also provided by law. A three-factor formula is used. It consists of 1.) the average value of real and tangible personal property, 2.) gross sales, less returns allowances, and 3.) wages, salaries, commissions and other compensation of employees. For each factor, the total within and without the state is computed. From these figures, the percentage of each factor within the state is determined. The three percentages are totaled, and the average of the three computed. This average percentage is then applied to the

---

<sup>43</sup>See Charts.

<sup>44</sup>CAL. REV. & TAX CODE § 23151 (West 1970).

<sup>45</sup>CAL. REV. & TAX CODE § 23501 (West 1970).

### UTAH

Utah has no severance taxes on mines or on oil and gas production. It does have a Mining Occupation Tax<sup>40</sup> that covers both mine products and oil and gas. The tax rates are: 1% of the gross amount received for or the gross value of the ore or metal sold, or fissionable materials delivered; 2% of the value at the well of oil, gas, etc., sold or carried from the production area.

### IDAHO

Idaho has no severance taxes on mines or on oil and gas production. It does have a Mining License Tax.<sup>41</sup> The rate is 2% of the net proceeds of the mine. It also has a Corporate License Fee<sup>42</sup> that is based on the authorized capital stock value. The minimum fee is \$20; the maximum is \$300. All mining companies who do not own productive mines are exempt.

### OREGON

Oregon has no severance taxes.

### NEVADA

Nevada has no severance taxes.

---

<sup>40</sup>UTAH CODE § 59-5-66 et seq. (1974).

<sup>41</sup>IDAHO CODE § 47-1201 et seq. (Supp. 1975).

<sup>42</sup>IDAHO CODE § 30-601 et seq. (1967).

carbons from the soil of New Mexico. The rate is 2.55% of the taxable value of the product severed. Those subject to this tax are exempt from the Gross Receipts Tax and the Resources Excise Tax.

4. Resources Excise Tax (N.M. STAT. ANN. § 72-16A-20 et seq. (Interim Supp. 1975))

This tax is for the privilege of severing natural resources. The tax rate is 3/4% of the market value. For the privilege of processing natural resources, the tax rate is 3/4% of the market value. Oil and gas are excluded from this tax and those subject to it are exempt from the Gross Receipts Tax. No resources tax is due on the taxable value of any natural resource that is processed in New Mexico and on which the processors' tax has been paid.

5. Natural Gas Processors Tax (N.M. STAT. ANN. § 72-23-1 et seq. (Interim Supp. 1975))

This tax is on the value of manufactured products of natural gas or liquid hydrocarbon or in combination. The rate is 45/100 of 1%. Those processors subject to this tax are exempt from the Gross Receipts Tax, the Oil and Gas Emergency School (Privilege) Tax and the Resources Excise Tax.

In addition to these severance taxes New Mexico has a Gross Receipts (Sales) Tax.<sup>39</sup> This tax is for the privilege of engaging in business. The rate is 4% of gross receipts. Oil, natural gas and liquid hydrocarbons are covered by the Oil and Gas Emergency School (Privilege) Tax (above) and are specifically exempted from this tax by § 72-16A-12.20. When either the Oil and Gas Emergency School (Privilege) Tax, the Natural Gas Processors Tax or the Resources Excise Tax applies, then the Gross Receipts Tax does not apply.

---

<sup>39</sup> N.M. STAT. ANN. § 72-16A-1 et seq. (Interim Supp. 1975).

1. Severance Tax (N.M. STAT. ANN. § 72-18-1 et seq. (Interim Supp. 1975))

This tax has the effect of a license or occupation tax. It imposes a tax on the gross value of natural resources immediately after severance from the soil (but oil, gas, liquid hydrocarbon individually or any combination thereof or carbon dioxide are not included in this particular severance tax; they are taxed under the Oil and Gas Severance Tax and the Oil and Gas Emergency School (Privilege) Tax, discussed below).

Values are as follows: for those products having a posted field or market price at the point of production, the value to be reported shall be its posted field or market price without any deductions except those expenses of hoisting, crushing and loading necessary to place the severed product in marketable form and at a marketable place; no deductions are allowed for hoisting, loading and crushing in excess of 50% of the reported value.

Tax rates are as follows:

Class 3. Uranium and other material used primarily for its fissionable value-----	1%
Class 5. Coal-----	1/2%
Class 6. Pumice, gypsum, sand, gravel, clay, fluorspar and other nonmetallic minerals-----	1/8%

2. Oil and Gas Severance Tax (N.M. STAT. ANN. § 72-19-1 et seq. (Interim Supp. 1975))

Oil, natural gas, liquid hydrocarbon, individually or any combination thereof, are taxed at the rate of 3 3/4%. Transportation expenses and any royalties paid to the government or Indian tribes may be deducted from the tax base.

3. Oil and Gas Emergency School (Privilege) Tax (N.M. STAT. ANN. § 72-21-1 et seq. (Interim Supp. 1975))

This tax imposes an additional severance tax on the privilege of engaging in the business of severing oil, natural gas or liquid hydro-

## II. SEVERANCE TAXES<sup>38</sup>

A severance tax is a percentage tax on the gross value of what is produced. The amount of the tax depends upon the quantity of production (ore, coal, oil, gas) as well as the quality of the product. The tax generally is payable whether or not the mine or oil and gas field is operated at a profit. The severance tax may be levied in addition to the property (ad valorem) tax; generally state legislatures have found the severance tax to be easily raised without changing the state's overall taxing structure and without a great public outcry. Its main disadvantage is that it may not provide a steady flow of tax revenue to the taxing body.

### CALIFORNIA

California has no severance taxes on mines or on oil and gas production.

### NEW MEXICO

New Mexico has five (5) kinds of severance taxes:

1. Severance Tax
2. Oil and Gas Severance Tax
3. Oil and Gas Emergency School (Privilege) Tax
4. Resources Excise Tax
5. Natural Gas Processors Tax

---

<sup>38</sup> See Charts.

NEVADA

Mining property is taxed on a net proceeds basis (Net Proceeds Tax on Mine Operators and Royalty Recipients<sup>33</sup>). Once the net proceeds of a mine are determined, the mine is then assessed at the same ad valorem rate as other property is assessed (35%).<sup>34</sup> All other property is assessed at 35% of the full cash value.<sup>35</sup> Unpatented mines and mining claims are exempt from taxation. Geothermal properties are not assessed on a net proceeds basis.

OREGON

Realty and tangible personalty are assessed at 100% of the true cash value as of January 1st each year. When mineral, coal, oil and gas interests have been severed, they are taxed separately.<sup>36</sup> Unpatented mining claims are exempt from taxation.<sup>37</sup>

---

<sup>33</sup>NEV. REV. STAT. § 362.010 et seq. (1975).

<sup>34</sup>NEV. REV. STAT. §§ 361.225, 362.140 (1975).

<sup>35</sup>NEV. REV. STAT. § 361.225 (1975).

<sup>36</sup>ORE. REV. STAT. § 308.115 (1975).

<sup>37</sup>ORE. REV. STAT. § 307.080 (1975).



exclusive measure of ad valorem tax liability on the interests of all persons in the production of oil and gas.

The one geothermal area in northwestern New Mexico under active exploration by Union Oil Company is taxed as follows: the land itself is taxed as grazing land and the local county tax assessor assesses the value of all improvements, equipment, materials, supplies and personal property held or used by Union Oil in connection with the development of the geothermal resources. Note that there is no attempt to assess the present worth of the future net income from the property. Only with production would the land be taxed under New Mexico's net proceeds formula.

#### UTAH

Valuation of mineral property is determined by the State Tax Commission rather than by county assessors.<sup>30</sup> Non-metalliferous mines are assessed at 30% of the reasonable fair cash value along with other realty and tangible personalty. Coal and hydrocarbon lands are assessed at 30% of their reasonable fair cash value. Metalliferous mines including uranium are assessed at \$5 per acre, plus 2 times the average net annual proceeds for the past 3 years, plus 30% of the value of the machinery used in the mining operations and other property not used for mining purposes.<sup>31</sup>

#### IDAHO

Productive mines are taxed on the basis of annual net profits, plus (1) the price paid to the United States for mines and/or claims or (2) the separate value of the surface ground used for other purposes plus the value of machinery, property and surface improvements. All other lands, realty and personalty, are assessed at 20% of the full market value.<sup>32</sup>

---

<sup>30</sup>UTAH CODE § 59-5-3 (1974).

<sup>31</sup>UTAH CODE § 59-5-57 et seq. (1974).

<sup>32</sup>IDAHO CODE § 63-2801 et seq. (1976).

acres of the property being valued. The per acre value of such property is determined under regulations adopted by the Property Tax Department.

"Annual net production value" for productive mineral property may be determined on an output basis, using either an average annual output for each of the previous five years, or, by election, only for the prior year. Valuation is determined by the market value of the annual output, less the actual costs of producing and bringing the product to the surface, and less the costs of milling, treating, transporting and selling the products. Alternatively, the Property Tax Department may value the property at 300% of the average annual output as determined under either the five year or one year method. If the productive property fails to produce a market value of average annual output above actual cost, then the Department may determine the taxable value of such property on the same basis as nonproductive property. In addition to an ad valorem taxation of the value of the mineral, the Property Tax Department assesses the value of all improvements, equipment, materials, supplies and personal property held or used in connection with the development of the mineral property.

Under the Oil and Gas Ad Valorem Production Tax oil, natural gas and liquid hydrocarbon properties are taxed according to the value of the products severed and sold. The taxable value of such products is an amount equal to 150 percent of the value of the products after certain deductions (see Charts). The assessed value of the products is determined by applying the uniform assessment rate (33 1/3%) to the taxable value (150% of market value), yielding an assessed valuation of 50% of the market value.

The Oil and Gas Production Equipment Ad Valorem Tax is the second ad valorem tax on oil and natural gas properties and production. The tax is on equipment used in oil, natural gas or liquid hydrocarbon production. The value of equipment for each production unit is set at an amount equal to 27% of the market value of the products of each production unit. Then the assessed value is determined by applying the uniform assessment rate of 33 1/3%. The Oil and Gas Production Equipment Tax and the Oil and Gas Ad Valorem Production Tax are the full and

arrive at a fair market value for a geothermal property that has potential but no actual steam production or electrical generation?

In 1974 the Union Oil Company unit operation in Sonoma County had a market value of \$40,288,000 and paid \$805,000 that year in property taxes. Pacific Gas and Electric Company generating facilities had an investment of \$43,750,000 with an assessed value of \$8,200,000 and were taxed at a rate of \$7.66 per \$100, approximately \$628,000. Other geothermal operations in The Geysers and the landowners contributed about \$67,000 in taxes that year. Thus the total for 1974 in property taxes to Sonoma County was nearly \$1,500,000.

#### NEW MEXICO

Valuation of mineral property is determined by the state Property Tax Department, not by county assessors.<sup>25</sup> Oil and gas property is not subject to valuation for property tax purposes under the Property Tax Code,<sup>26</sup> but is valued and taxed under the Oil and Gas Ad Valorem Production Tax<sup>27</sup> and the Oil and Gas Production Equipment Ad Valorem Tax.<sup>28</sup> Property is assessed in proportion to its value. The current statewide uniform assessment rate is 33 1/3%.<sup>29</sup>

Mineral properties are classified as productive or nonproductive. Productive mineral property is taxed on the basis of net proceeds of production (the value for such mineral properties is an amount equal to 300% (3 times) of the annual net production value.) The value of class one nonproductive mineral property (nonoperated, privately owned mineral lands, reserves, interests and severed mineral products where the property is known to contain commercially workable quantities of minerals) is determined by applying a per acre value to the surface

---

<sup>25</sup>N.M. STAT. ANN. § 72-29-2-C(2) (Interim Supp. 1975).

<sup>26</sup>N.M. STAT. ANN. § 72-28-1 to § 72-31-93 (Interim Supp. 1975).

<sup>27</sup>N.M. STAT. ANN. § 72-22-1 et seq. (Interim Supp. 1975).

<sup>28</sup>N.M. STAT. ANN. § 72-24-1 et seq. (Interim Supp. 1975).

<sup>29</sup>N.M. STAT. ANN. § 72-30-3 (Interim Supp. 1975).

2. Geothermal leaseholds on private lands have not been taxed as possessory interests until there has been actual production of the resource. Often these leases have not been recorded nor has there been a bonus bid price paid for the leases.
3. Oil and gas leaseholds on state lands, when sold on a bonus bid basis, have been taxed as possessory interests, whether or not there is production.
4. Oil and gas leaseholds on private lands generally have not been taxed as possessory interests until there has been production. As with geothermal leaseholds on private lands, these leases often have not been recorded nor has there been a bonus bid price paid for the leases.

Once production has begun, either for geothermal, oil, gas, or mines, the property is then assessed on the basis of the present worth of future net income.

Assessment problems are occurring on federal geothermal leaseholds where some development has taken place but where there is no actual generation of power or even a contract to sell steam to a utility. In Lake and Sonoma counties the assessors are valuing such properties by projecting a future capitalized value of the income stream for the developments (usually wells) and then discounting it for the number of years estimated to put the wells into production. Another suggested method of valuation is to use the amount of total capital expended for the development as the assessment figure. Both of these methods of valuation are criticized because as the essential preproduction capital investment in development occurs, the taxes increase proportionately before such properties are in production and generating any revenues. Small and medium sized geothermal development companies are most affected by the increased taxes; the large capital investment they have tied up in development wells prior to income from the sale of production coupled with the increased taxes have forced some of them to sell their properties or take in large companies as partners.

Disputes over any method of valuation will continue and they demonstrate the problems of property tax valuation: how does one

specifies that all property is to be assessed for taxation purposes at its full cash value,<sup>22</sup> § 401 of the California Revenue and Tax Code provides that all property is to be assessed at 25% of the full cash value. Courts have upheld this assessment method of property.<sup>23</sup>

For mineral energy lands, each county assessor, not a state agency, determines the value of the property by computing the lifetime net proceeds from the property discounted to their present value. Assessment of geothermal properties has been evolving in the past several years. The California State Board of Equalization is charged with equalizing property assessments among the counties for all types of property. There is not yet in the Board of Equalization a written policy detailing how assessments among the counties on geothermal properties shall be equalized/reconciled. The Board thus far has dealt with varying county assessment techniques on a case by case basis.

Under the California Constitution, leaseholds are taxed as possessory interests.<sup>24</sup> In practice, assessment of oil, gas, and geothermal leaseholds on private lands has differed from that on federal and state lands:

1. Geothermal leaseholds on federal lands, when sold on a bonus bid basis, have been taxed as possessory interests, whether or not there is any production of power. (Where there have been title disputes over geothermal rights on federal or state lands, the leaseholds on such lands have not been taxed as possessory interests, pending settlement of such disputes.) Depending on the circumstances under which the winning bid was awarded, county assessors have used the bonus bid price or a portion thereof as the value of the leasehold for taxation purposes. The use of the full bid price is criticized on the grounds that some bonus bid prices are inflated, i.e., a company, in order to obtain a lease on what it considers to be a particularly desirable tract of land in a certain area, may bid up to the maximum amount that the economic evaluation indicates will yield the minimum acceptable return on its investment.

---

<sup>22</sup>CAL. CONST. Art. 11, Sec. 12.

<sup>23</sup>Sacramento County v. Hickman, 59 Cal.Rptr. 609, 66 Cal.2d 841, 428 P.2d 593 (1967).

<sup>24</sup>CAL. REV. & TAX CODE § 104(2) (West 1970).

the theory that the taxable value of the property can be ascertained solely with reference to the net proceeds from the property. Such "net proceeds" taxation for ad valorem tax purposes must be distinguished from severance taxes which are levied on a set amount per unit of production or on gross proceeds.

2. Gross Proceeds Method of Valuation (used by Colorado)

In Colorado mines are valued at one-fourth of the amount of the gross proceeds for the previous year. Alternatively, if net proceeds exceed one-fourth of the gross proceeds, then the mine is valued on the basis of net proceeds.<sup>17</sup> For Colorado purposes, gross value is defined as the value of the ore mined, not the value of the concentrates shipped.<sup>18</sup> Gross proceeds are computed by taking the gross value and deducting the costs of reduction, sale and transportation, but not the costs of extraction.<sup>19</sup>

3. Actual Cash Value/Fair Market Method of Valuation (used by California and Oregon)

Most often fair market value or full cash value of the property means the amount of money which can be realized by a sale of the property between a willing buyer and a seller both well informed and under no compulsion either to sell or buy. Since most energy mineral properties are not often sold, such properties are usually valued by computing the lifetime net proceeds from the property discounted to their present value. Some states have rather ad hoc formulations for computation of net proceeds; still others have statutorily defined methods of computation.<sup>20</sup>

CALIFORNIA

For mineral energy property, California uses the "actual cash value/fair market" method of valuation. All property not exempt from taxation is taxable in proportion to its value.<sup>21</sup> Although the California Constitution

---

<sup>17</sup>COLO. REV. STAT. ANN. § 137-6-5(2) (1973).

<sup>18</sup>Standard Chemical Co. v. Curtis, 77 Colo. 10, 233 P. 1112 (1925).

<sup>19</sup>Paxson v. Cresson Consol. Gold Mining and Mill Co., 56 Colo 206, 139 P. 531 (1914).

<sup>20</sup>See Brightwell, "Ad Valorem Taxation of Mining Properties," 15th Annual Rocky Mt. Mineral Law Institute, p. 281 (1969); American Law of Mining, Vol. 4, (1976), especially Title XXVI: "Valuation of Mining Properties," Title XXVII: "Ad Valorem and Production Taxation of Mining Properties."

<sup>21</sup>CAL. CONST. Art. 13, Sec. 1.

## STATE TAXATION

Taxation of energy minerals at the state level generally falls into one of five types: 1.) property or ad valorem taxes, 2.) severance taxes, 3.) occupation/license taxes, 4.) corporate income taxes, and 5.) oil and gas production or conservation taxes.

### I. PROPERTY TAX/AD VALOREM TAXES<sup>16</sup>

Property taxes on energy minerals are usually computed in one of three ways: 1.) on a net proceeds basis of the year's production, 2.) on a gross proceeds basis of the year's production, or 3.) on the basis of the actual cash or fair market value of the property, often computed from the present worth of future net income. Ad valorem taxes provide a steady source of tax revenues to the taxing body.

#### 1. Net Proceeds Method of Valuation (used by New Mexico, Utah, Idaho, and Nevada)

Net proceeds valuation of mineral energy resources is based on

---

for the production at The Geysers and the companies and the IRS are involved in a continuing controversy over this issue. An excellent discussion of geothermal deposits, their differing forms and the application of percentage and cost depletion can be found in Million, "The Application of Depletion to Geothermal Resources," University of Michigan Journal of Law Reform, Vol. 9, No. 2 (Winter), p. 233 (1976).

<sup>15</sup>At issue in a deduction for intangible drilling costs is the point at which such costs (those with no salvage value) can be taken. With a traditional "IDC" deduction the total costs may be deducted in the year in which they were incurred. Otherwise, such costs have to be capitalized and deducted over the life of the operation.

<sup>16</sup>See Charts.

The delays in meeting environmental impact report requirements and in obtaining the necessary drilling, land use, and construction permits significantly affect the property taxes of the developers in The Geysers area in California. Under the California Constitution and California statutes property taxes are increased at every aspect of development to reflect the incremental value provided by the proven underlying reservoir. The property tax is assessed before production begins. Thus, for example, if wells are drilled and shut-in until a power plant is built and then there are long delays in meeting EIR requirements and in obtaining the necessary permits, a company would have to pay property taxes on the increased value of the property for a number of years (due to the wells and/or any other developments) without any revenues being generated from the wells themselves.

In addition to the above constraints, attracting risk capital for geothermal exploration and development is a major problem, especially in view of the long delays from exploration to generation of electricity. Tax incentives have always been a significant means of attracting risk capital to infant industries. The lack of tax incentives for geothermal resources, such as a percentage depletion allowance<sup>14</sup> and a deduction for intangible drilling expenses,<sup>15</sup> can only adversely affect geothermal exploration and development. To the extent that state tax laws provide tax incentives, the geothermal industry may be able to attract more risk capital and to do more exploration and development.

---

<sup>14</sup>The Tax Court and the Ninth Circuit Court of Appeals held that the natural resource at The Geysers involved steam, which in turn was a "gas" within the meaning of § 263(c) and § 613(b) of the Internal Revenue Code. The courts also held that the geothermal resource was exhaustible. (Arthur E. Reich, 52 T.C. 700 (1969), aff'd, 454 F.2d 1157 (9th Cir. 1972). In a companion case, George D. Rowan, 28 T.C.M. 797 (1969), the Tax Court allowed immediate deduction of intangible drilling costs. The Ninth Circuit also affirmed this decision. In the Tax Reduction Act of 1975 Congress amended § 613 to read as follows: "any geothermal deposit in the United States or in a possession of the United States which is determined to be a gas within the meaning of 613 A(b) (1) (A)" qualifies for a 22 percent depletion allowance. (Int. Rev. Code of 1954, § 613 A(b) (1) (c).) However, the IRS continues to disallow a depletion allowance and a deduction for intangible drilling costs



3. Meeting environmental impact report or statement requirements (EIR or EIS) has taken longer periods of time and has become more expensive as more county, state and federal agencies impose requirements and as those requirements change and become more exacting. The lack of cooperation and coordination among the various county, state, and federal agencies requires the developer to make many duplicate EIR's for each agency involved. Furthermore, a developer must write an EIR on each well to be drilled; the developer may not file one EIR to cover all the wells to be drilled in a given area.
4. Many permits may be required from county and state agencies for geothermal exploration and drilling (for example, in California in The Geysers Field: county land use permit, county air quality permit, state Division of Oil and Gas drilling permit, Regional Water Quality Control Board waste discharge permit).<sup>11</sup> Obtaining permits has also taken longer periods of time and has become more expensive. In addition, the California Public Utilities Commission (CPUC)<sup>12</sup> must approve the environmental impact reports and construction plans of all proposed electrical power plants. Three years is an average time for obtaining this permit. For Unit 12 at The Geysers a permit was requested on July 19, 1972, and was approved on December 30, 1975. Construction on this power plant has still not begun because of delays in obtaining county permits. The permit for Unit 13, requested in March, 1974, has still not been approved. Unit 14 was approved after almost a 3 year delay: July, 1973, to April, 1976; Unit 15 was approved after more than a 2 year delay: March, 1974, to April, 1976. The federal government has not yet established procedures for geothermal power plant permitting on federal lands.

Since construction of a power plant requires at least two years, the total time for permitting and construction is at least five years, at The Geysers. Thus, the total time from initial geothermal exploration, to the drilling of wells, to EIR requirements, to CPUC approval and finally to plant operation is presently 7-10 years.

5. Technology for geothermal production from geopressured water and hot rock is still being evolved. In the United States only dry steam has evolved an economically feasible technology for extraction of the energy for electrical generation.<sup>13</sup> Hot water technology exists and the economic feasibility of development depends on several factors: temperature of the water, productivity of the individual wells, and depth of drilling to the reservoir.

---

<sup>11</sup>For a complete discussion of the permit problems see W. G. Kirkham and Susan J. Brown, State and Local Permit Study - An Analysis of Administrative Factors Affecting Geothermal Development at The Geysers, (Sacramento, Calif., Office of Planning and Research in the Governor's Office) 1976.

<sup>12</sup>The California Energy Resources Conservation and Development Commission will soon be the state agency processing power plant permit requests.

<sup>13</sup>Several other countries are producing electricity from either dry-steam or hot-water geothermal fields.

In dry steam geothermal systems steam and other gases (primarily CO<sub>2</sub> and H<sub>2</sub>S) are produced from the wells. The steam requires only minor cleaning before it is used directly in turbo-generators. Depending upon the chemical composition, which varies in different areas, noncondensable gases associated with the steam may need to be treated for removal of certain elements in order to meet environmental regulations. The chemical composition of the waters of hot water systems varies considerably from area to area. The concentration of solids in geothermal waters may create scaling conditions as well as corrosive conditions. Disposal of waste fluid can be accomplished by injecting the water back into the subsurface reservoir. Geopressured systems contain methane (natural gas) dissolved in hot water at abnormally high pressures. Considerable research needs to be done to evaluate the technology and economics of production from such systems. Disposal of spent water may be a problem. Hot, dry rock systems are largely unknown and technical development is still purely experimental.

As an infant energy industry geothermal faces many constraints, some of which may affect state tax treatment. Such constraints include:

1. The unclear tax treatment granted geothermal exploration expenditures by the Internal Revenue Service. See discussion infra in footnote 14.<sup>10</sup>
2. The slowness in processing federal competitive and noncompetitive lease applications. From January, 1974 to July 23, 1976, there have been 4,861 applications for noncompetitive leases for 10 million acres of federal lands across the country. 674 leases have been issued for 1,111,018.78 acres; 1027 applications were rejected; 1293 applications have been withdrawn by applicants; 1867 applications are awaiting action. During the same time period in the state of California there have been 925 applications for noncompetitive leases on federal lands within the state. 5 leases have been issued on 6,294 acres; 203 were rejected; 343 have been withdrawn; 374 applications are awaiting action. Delays are largely due to the environmental analysis of each area; each analysis requires a preparation period, review and comment period, and a Bureau of Land Management (BLM) decision period. The BLM decides whether or not to lease the area and whether or not certain stipulations will apply to the area. The Forest Service at the present time lacks the priorities in money and manpower to process the applications on National Forest lands.

---

<sup>10</sup> Jack McNamara, University of Southern California Law Center, is developing a computer model that analyzes the various federal taxes in combination and determines the impact of each on the economics of geothermal development.

legal problems. The following definitions used in statutes, case law and legal literature reflect the debate over the legal definition of geothermal resources.<sup>4</sup> Most significantly, the tax status of the resource may depend on its legal definition as well as its physical nature.

1. "Energy."<sup>5</sup>
2. "Gas" for the steam deposit at The Geysers.<sup>6</sup>
3. "Geothermal resources" means the natural heat of the earth, the energy, in whatever form, below the surface of the earth present in, resulting from, or created by, or which may be extracted from, the natural heat, and all minerals in solution or other products obtained from naturally heated fluids, brines, associated gases, and steam, in whatever form, found below the surface of the earth, exclusive of helium or of oil, hydrocarbon gas or other hydrocarbon substances, but including, specifically:
  - (a) All products of geothermal processes, embracing indigenous steam, hot water and hot brines;
  - (b) Steam and other gases, hot water and hot brines resulting from water, gas, or other fluids artificially introduced into geothermal formations;
  - (c) Heat or other associated energy found in geothermal formations; and
  - (d) Any byproduct derived from them.<sup>7</sup>
4. "For purposes of the Stockraising Homestead Act, geothermal rights are not mineral rights but are included with water rights."<sup>8</sup>
5. "Geothermal rights are retained with mineral (lease) rights, not with water rights."<sup>9</sup>

---

<sup>4</sup>Geothermal energy as a resource is not a familiar commodity which readily fits existing resource categories. It has been described at various times as water, gas, and a hard mineral. See Appendix A for a federal definition and for other state definitions of geothermal resources. Note that Hawaii defines geothermal as a mineral but that Washington, Idaho, and Montana declare that geothermal resources are sui generis, being neither a mineral or a water resource.

<sup>5</sup>Schlauch and Worcester in Land and Water Law Review, Vol. 9, No. 2, 1974.

<sup>6</sup>Reich v. Commissioner, 454 F.2d 1157 (9th Cir. 1972).

<sup>7</sup>ORE. REV. STAT. § 522.050(7) (1975).

<sup>8</sup>U.S. v. Union Oil Company of California, 369 F.Supp. 1289 (N.D. Cal. 1973), appeal docketed, No. 74-1574, 9th Cir., Jan. 11, 1974.

<sup>9</sup>Geothermal Kinetics, Inc. v. Union Oil Company of California, Intended Decision, No. 75314, Super. Ct. for County of Sonoma, California (1976).

## INTRODUCTION

This report compares state taxation of the energy minerals - coal, oil shale, uranium, oil and natural gas - to that of geothermal energy in six Western states: California, New Mexico, Utah, Idaho, Nevada, and Oregon. In the United States the only producing geothermal field for generation of electricity is The Geysers Field in northern California.<sup>1</sup> However, a discussion of state taxation of geothermal resources is appropriate since several areas in the states considered here may begin electrical generation in the next few years. The economics of development require a consideration of state taxes.

Increasing costs of conventional sources of energy and the dependence on foreign oil supplies have generated increased interest in geothermal resources as an alternative energy source. Up to 5 percent<sup>2</sup> of the nation's electrical generating capacity may be derived from geothermal resources.

Geothermal energy means heat from within the earth. While geothermal energy is present throughout the earth's crust, in most places this heat is too diffuse to be economically important. Wherever localized concentrations occur (that is, where the combination of high temperatures near the surface and porous rock that contains water produce extractable heat) a geothermal reservoir is created. Geothermal resources occur in four distinct types: dry steam systems, hot water systems, geopressured reservoir systems, and hot dry rock systems.<sup>3</sup> Each system presents unique technical, economic and

---

<sup>1</sup>There are approximately 400 geothermal wells and springs outside The Geysers that are used primarily for space heating and recreational purposes. One third of the homes in Klamath Falls, Oregon, are heated by geothermal energy.

<sup>2</sup>John E. Kilkenny, president of the American Association of Petroleum Geologists, in a speech before the annual meeting of the International Oil Scouts Association, July, 1976, reported in The Oil and Gas Journal, Vol. 74, No. 28, July 12, 1976, p. 26.

<sup>3</sup>Other potential systems include magma, normal gradient and salt dome.

## TABLE OF CONTENTS

Introduction -----	1
State Taxation-----	6
Property Taxes-----	6
Severance Taxes-----	14
Corporate Franchise, Income and Excise Taxes-----	18
Oil and Gas Production or Conservation Taxes-----	20
Conclusion-----	23
Selected References-----	26
Appendix A: Definitions of Geothermal Resources & Byproducts-----	28
Charts: State Taxes arranged according to type of tax-----	34
Charts: State Taxes arranged by state-----	45

#### ACKNOWLEDGMENTS

I would like to thank the following persons for their advice and assistance in preparing this study: Marshall J. Reed, U.S. Geological Survey, Conservation Division; Ed Coony, Dick Linwall and Tom Edwards, Union Oil Company of California, Los Angeles; Charles R. Garber, E. G. Dobrick, and Bob Greider, Chevron Oil Company, San Francisco; Samuel M. Eisenstat, Eisenstat & Gottesman, P.C.; New York; Robert D. Conover, Field Solicitor, United States Department of the Interior, Riverside; Robert H. Paschall and William Beacroft, California State Board of Equalization, Sacramento; Gary Vice, Sonoma County Assessor's Office, Santa Rosa; Michael Heays and Joseph Hyde, Coopers & Lybrand, San Francisco; Jep Hill, Research and Planning Consultants, Austin, Texas; Mel Schrecongost, California Division of Oil and Gas, Sacramento; Bev Hall and Dave Anderson, Geothermal Resources Council, Davis; Donald F. X. Finn, San Francisco.

Sharon C. Wagner  
August, 1976  
Palo Alto, California

SUBJ  
GTHM  
STGR

UNIVERSITY OF UTAH  
RESEARCH INSTITUTE  
EARTH SCIENCE LAB.

STATE TAXATION OF GEOTHERMAL RESOURCES  
COMPARED WITH  
STATE TAXATION OF OTHER ENERGY MINERALS

by  
SHARON C. WAGNER

A GEOTHERMAL RESOURCES COUNCIL PROJECT  
FOR THE  
U.S. GEOLOGICAL SURVEY, CONSERVATION DIVISION

AUGUST 1976

# Summary of United Nations Geothermal Exploration Experience, 1965 to 1975

JAMES R. McNITT

*United Nations, New York, N. Y. 10017, USA*

## ABSTRACT

In the period 1965 through 1975, the United Nations will have completed four geothermal exploration projects at an average cost of US\$3 000 000 each. The duration of a project is from four to seven years. Project work progresses through five phases.

Phase I is a reconnaissance survey designed to identify specific prospect areas and to determine priorities for detailed investigation. Hydrogeochemistry, interpreted within the framework of regional geology and hydrogeology, is the principle technique used. Aerial infrared imagery surveys have also been found useful.

Phase II consists of resistivity, microearthquake, and in some cases temperature-gradient surveys, whose objective is to locate sites for exploration drilling. The most effective technique has been found to be dc resistivity, using an in-line dipole-dipole configuration.

Phase III is exploration drilling. Holes are drilled to an average depth of 1500 m with an 8.5-inch bottom-hole opening. Water assisted with air has been found to be an effective circulating system.

Phase IV is reservoir evaluation and consists of drilling offset wells located about 200 m from the discovery well. They are drilled with the objective of proving sufficient production for the initial generating plant, and providing data for assessing the long-term production capacity of the reservoir.

Phase V is a feasibility study to determine the capital and operating cost of a power plant.

This work has resulted in one successful project, one failure, and two possibly successful projects, depending on the outcome of additional investigations. Finding high temperature has not been a problem. Siting productive wells in reservoirs having an erratic distribution of permeability has been the major problem.

did not result in the construction of a power plant because although a high temperature and high permeability reservoir was discovered, rapid deposition of carbonate in the wells prohibits development, at least within the restraints of present technology. Discoveries of high-temperature fluids have been made in Chile and Kenya, but permeability is irregularly distributed in both reservoirs and it is not yet known if development will be feasible. The Nicaraguan project is still in the exploration drilling stage, and drilling is not expected to begin in Ethiopia until 1976. The average cost of the projects is about US\$3 000 000 each.

This paper will describe in a general way how the work undertaken in these projects was organized and implemented, and will include an evaluation of those exploration techniques which were found to be particularly helpful as well as those which gave less conclusive results. The exploration philosophy presented here has not been applied in each of the UN-executed projects but has evolved over the years and is still evolving. Nor is it meant to be an inflexible approach. Each project has had its own specific difficulties, and the exploration programs have been modified to meet these problems as required.

The economic viability of a geothermal field depends on the following reservoir parameters: depth; temperature; pressure; permeability; porosity; thickness; areal extent; chemistry of the reservoir fluid; and, if not a volumetric reservoir, rate of recharge and ability to heat a recharging fluid. The objectives of an exploration project are to locate a geothermal reservoir, demonstrate that economically productive wells can be drilled, and to evaluate as many of the reservoir parameters as possible. The planning of an exploration program which will accomplish this task is hindered by the fact that standard exploration techniques, comparable to those used in the petroleum and mineral industries, have not yet been developed. Although techniques are not standardized, UN projects now tend to proceed through five consecutive phases, each with its specific objective:

## INTRODUCTION

During the decade 1965 to 1975, the United Nations (UN) executed geothermal exploration projects in cooperation with the governments of El Salvador, Chile, Turkey, Ethiopia, Kenya, and Nicaragua. In El Salvador, work has progressed to the stage where a 30-MW plant is scheduled to go on stream in the second quarter of 1975, which will be ten years after the commencement of exploration. The Turkish project, which began in 1967 and ended in 1973,

Phase I: Reconnaissance survey to identify specific prospect areas and to assign them priorities for more detailed investigation.

Phase II: Prospect investigations to locate drilling sites within a prospect area.

Phase III: Drilling to discover a geothermal reservoir.

Phase IV: Reservoir evaluation to prove sufficient production for the initial generating plant and provide data



for assessing the long-term production capacity of the reservoir.

Phase V: Economic feasibility study to determine capital and operating costs for a generating plant and to compare this cost with the cost of generating power from other available sources.

### PHASE I: RECONNAISSANCE

The objective of the reconnaissance phase is to select specific prospect areas for more detailed investigation, and the first step toward this goal is to establish selection criteria. Certainly, the one most common feature which makes a region attractive for geothermal prospecting is the presence of above-ambient temperatures in the ground-water regime. Intuition tells us that the more numerous these features and the higher their temperature, then the better are the prospects of finding even higher temperatures at depth. Even more convincing is the mutual association of hot springs and recent volcanism. This simple intuitive argument has been the basis for the selection of geothermal prospect areas throughout the world, including those areas explored by the UN.

Boiling springs, or fumaroles at or above boiling point, are present in all the prospect areas drilled by the UN; and with the exception of the Kizildere prospect in Turkey, all these are closely associated with volcanism of Pleistocene or younger age (no volcanic rocks occur within 50 km of the Kizildere prospect). Drilling results in these areas, at least in terms of finding high temperature, have been excellent: Ahuachapán, El Salvador, 237°C; El Tatio, Chile, 263°C; Kizildere, Turkey, 205°C; and Olkaria, Kenya, 286°C. Although the results of the drilling program in Nicaragua are not yet available, a temperature of 209°C has been reported from an earlier drilling program (Thigpen, 1971).

The practice of drilling geothermal exploration holes in the vicinity of boiling springs of high temperature fumaroles is so common that there is very little experience from which to assess the risk of drilling in areas without these high surface temperatures. Of the approximately 35 thermal areas for which both surface spring temperatures and subsurface temperature data are available (see particularly the compilation of White, 1970), it appears that only about four or five have been drilled where boiling temperatures were not present at the surface. However, the fact that the major geothermal reservoirs of Monte Amiata in Italy and the Imperial Valley in the United States fall into this group is compelling evidence that surface temperatures cannot be used as the sole selection criterion.

In the past few years a great deal of work has been done on the development of the silica and Na/K geothermometers for use as a reconnaissance tool. Although I am not aware of prospects which have been selected and drilled solely on the basis of this criterion, it is instructive to examine the data from drilled areas to see how successful the method would have been if used for that purpose.

The following general statements can be made concerning 30 areas for which both surface chemistry and subsurface temperatures are known (26 areas from White's 1970 compilation):

1. For the six reservoirs having temperatures ranging from 106 to 160°C, the silica temperatures are too high by an average of 18°C, the temperature difference ranging from +5 to +36°C.

2. Of the 22 reservoirs ranging from 160 to 300°C, 19 of the silica temperatures are too low by an average of 60°C, the difference ranging from -8 to -122°C.

3. Of the 28 reservoirs ranging from 106 to 300°C, 25 Na/K temperatures are too low by an average of 44°C, the difference ranging from -4°C to -128°C.

4. The two reservoirs over 300°C are the Salton Sea and the Cerro Prieto fields. The surface spring silica and Na/K temperatures of the Salton Sea area are too low by 252°C and 206°C respectively, and for the Cerro Prieto fields they are too low by 273°C and 170°C respectively.

In view of the marked tendency of the chemical method to underestimate reservoir temperatures, caution is required, particularly when chemical thermometers are used as a basis for rejecting prospect areas. For example, if chemically indicated temperatures were used as the sole criterion in assessing the 30 prospect areas discussed above, 5 of the 22 reservoirs above 180°C would not have been drilled, or 8 of the 20 reservoirs (40%) above 200°C would not have been drilled, including Wairakei, Olkaria, and the Salton Sea fields.

The difficulties encountered in applying temperature and chemical criteria arise from the fact that in very few cases do reservoir waters reach the surface undiluted with more shallow ground water or in the same state of chemical equilibrium that existed prior to their leaving the temperature environment of the reservoir. In order to assess the changes which take place during this journey from the reservoir to the surface, something must be known about the flow pattern and chemistry of the regional ground-water regime of which the thermal system is only a part. For example, if thermal springs occur in an area of ground-water recharge, one should suspect more contamination with near-surface ground-water than if the springs occurred in an area of regional ground-water discharge. In the latter case, modification of the chemistry due to long residence times should be considered more likely than the possibility of contamination with shallow ground-water. Furthermore, the chances are better that the subsurface location of a high temperature reservoir will be closer to the surface location of thermal springs, rising in an area of ground-water recharge, than to springs rising in an area of discharge.

In order to use hydrogeological arguments such as these in the preliminary evaluation of prospect areas, the UN now undertakes regional hydrogeological surveys in conjunction with the more standard temperature and geochemical surveys.

The minimum hydrogeologic data required before attempting a geochemical interpretation is 'a map of the catchment showing the ground-water flow net, as well as areas of recharge and discharge. Such maps are the product of standard hydrogeologic surveys, and their accuracy depends on the quality and quantity of both hydrologic and hydrogeologic data available for the area.

The hydrogeologic and geochemical data are collected and reduced simultaneously. The geochemical survey should be concerned not only with the collection and analysis of samples, but also with the reduction of the analytical results into concise graphical presentations which are designed to emphasize statistically significant regional trends as well as anomalies to these trends. Plots of the concentration variation of chemical constituents with respect to chloride have been found to be helpful in distinguishing normal chemical trends related to residence times from anomalous

trends related to abnormal processes such as heating. This trend analysis approach, based on a statistically significant number of samples and interpreted against a background knowledge of the hydrogeology of the area, can be an effective tool for selecting prospects for more detailed investigation. In addition, this approach can improve interpretations based mainly on chemical geothermometers.

## PHASE II: PROSPECT INVESTIGATIONS

The purpose of this phase is to provide information within specific prospect areas on which to base the selection of drilling sites. Depending on the individual prospect, both geochemical and geophysical surveys can be used. The geochemical techniques are the same as those used in the reconnaissance phase, and will not be discussed further. Although geophysical techniques are used principally for prospect evaluation rather than reconnaissance because of their high cost per unit of area surveyed relative to geochemical techniques, they can also be used as a reconnaissance tool where conditions are appropriate.

The geophysical methods which have been employed in the UN projects are infrared imagery, one-meter temperature probe, temperature gradient, resistivity, microearthquake, gravity, and magnetics. The following is a summary of UN experience with these methods and an evaluation of their ability to provide useful information for geothermal exploration.

### Aerial Infrared Surveys

This survey technique was employed in Ethiopia and Kenya.

In Ethiopia, approximately 30 000 km<sup>2</sup> were surveyed in the Awash Valley and the Dallol depression at a cost of US\$60 000. The purpose of the survey was to locate and map the large number of thermal areas which were known to exist in a sparsely populated and poorly accessible region. Two Bendix scanners were used, one equipped with a 3.0 to 5.5- $\mu$  detector and the other with an 8 to 14- $\mu$  detector. The output from both scanners was recorded on 70-mm film and on tape; and in addition, the signals were monitored on an oscilloscope. The 8 to 14- $\mu$  imagery was attenuated to show terrain detail as well as thermal anomalies, while the 3.0 to 5.5- $\mu$  scanner controls were set to show only those areas above ambient temperature. The equipment was flown in a DC-3 aircraft and data were collected between midnight and one hour before dawn.

The background imagery provided by the 8 to 14- $\mu$  scanner was used to locate and plot the above-ambient thermal imagery recorded by the 3.0 to 5.5- $\mu$  scanner. With this method, only the film output was needed to compile the results of the survey, and locations could be plotted as soon as the film was processed.

A contract was recently negotiated to process the taped data into isothermal maps to assist further evaluation of the geothermal potential of the region and also to provide a comparison of the two kinds of data reduction techniques.

In Kenya, 2200 km<sup>2</sup> were surveyed in the Lake Hannington and Lake Naivasha areas at a cost of US\$30 000. Unlike the Ethiopian survey, which was reconnaissance in nature, the objective of the Kenya survey was to obtain a detailed pattern of thermal activity within prospect areas where the major centers of activity were already known. The same equipment and data reduction techniques were used in Kenya as were used in Ethiopia.

Technically, the results of these surveys were excellent. Thermal manifestations of only a few meters in diameter were easily resolved and could be accurately plotted on aerial photographs in the case of Ethiopia, and on 1:25 000 topographic maps in the case of Kenya.

Obtaining this imagery data was of unquestioned value in the case of Ethiopia, as obtaining the same information by ground methods would have required several years and the results would not have been as comprehensive.

The results of the survey at Lake Naivasha were quite useful, although not as valuable as the Ethiopian data. Thermal activity at Naivasha is almost entirely in the form of low-pressure fumaroles and steaming ground rather than hot-water springs, and the location of these steam escapes is controlled by geologic structure rather than by surface drainage. Therefore, the thermal imagery obtained at Naivasha provided an accurate representation of the faults and volcanic vents controlling steam escape.

The imagery obtained from the Lake Hannington area only confirmed that there were no thermal manifestations in the prospect area that had not been previously known. Thermal activity at this location is in the form of hot-water springs rather than steam vents, and the drainage pattern is as dominant an element as geologic structure in controlling spring locations. The results of this survey, therefore, were of considerably less value than those obtained in the Ethiopian Rift and at Lake Naivasha.

### One-Meter Temperature Probe Surveys

This technique has been employed in almost all UN projects for the purpose of providing a quantitative map of surface activity.

If thermal activity is controlled by geologic structure, as in the steaming ground areas of Lake Naivasha, then the one-meter probe survey has much the same value as an infrared imagery survey; that is, it provides structural information for use in selecting drilling sites. If, on the other hand, the location of thermal activity is controlled by surface drainage patterns, the value of one-meter probe survey as an exploration tool is minimal. In either case, the results can be used for making semiquantitative estimates of heat flow from an area, and this in turn can be used as a criterion for prospect selection. In my opinion, however, this application is of more scientific than practical value.

Probably the most compelling reason for undertaking a one-meter probe survey is that in most cases it is an inexpensive and simple technique which may discover something that was not previously known. In UN experience, however, these surveys have discovered very little that was not already known, with the exception of those surveys carried out in areas of steaming ground.

In Chile, the pattern of the anomaly mapped by the one-meter probe method was duplicated by an "EM-GUN" survey (Macdonald, 1974). Therefore, if this type of shallow information is required in areas having a high water table, if time is not available for a one-meter probe survey, and if money is not available for an infrared imagery survey, then an "EM-GUN" survey could be used to obtain similar information.

### Temperature Gradient Surveys

Surveys of this type were carried out in three of the UN project areas: Kizildere, Ahuachapán, and El Tatio.

At Kızılder, 60 gradient holes were drilled to 100-m depth at a spacing density of 2 to 3 holes per kilometer (Duprat, 1970). The survey resulted in defining a west-trending anomaly 4 km long by 1 km wide having a maximum gradient of  $0.5^{\circ}\text{C}/\text{m}$  compared to a background gradient of  $0.2^{\circ}\text{C}/\text{m}$ . Although the survey was of value to the extent that it gave a fairly accurate indication of the size of the field that was eventually outlined by drilling, knowledge of the anomaly contributed little to the problem of selecting deep exploration well sites. Due to a structural complication, the center of the field was found to be 1 km south of the axis of the gradient anomaly, with the north boundary of the field corresponding with this axis. Knowledge of the anomaly, therefore, tended to mislead rather than to assist in the selection of deep drilling sites.

At Ahuachapán, approximately 24 gradient holes were drilled to a depth of 100 m over an area of 7 by 7 km. Two anomalies having values greater than  $0.4^{\circ}\text{C}/\text{m}$  were defined compared to a background value of  $0.1^{\circ}\text{C}/\text{m}$  (Gonzalez-Garcia, 1968). The southern anomaly, which was not closed to the south, measures 3.5 by 2.5 km; and the northern anomaly, which was not closed to the north, measures 1 by 3 km. The southern anomaly is on high ground, near the base of a volcanic range, and is associated with fumarolic activity, while the northern anomaly is on lower ground and is associated with a large hot spring. As drilling found subsurface temperatures up to  $237^{\circ}\text{C}$  in the southern anomaly and only  $100^{\circ}\text{C}$  in the northern anomaly, it was concluded that the northern anomaly was due to the northward flow of warm ground water originating from relatively shallow depths above the high-temperature reservoir to the south.

The main value of this survey was to delineate the sharp western boundary of the field, the presence of which was later confirmed by drilling. This boundary, however, was even more clearly indicated by a resistivity survey and its presence was also suggested by the surface distribution pattern of hydrothermally altered ground. A northern boundary to the field has now been determined by drilling (Cúellar, personal commun., 1975). This boundary is south of the northern boundary of the southern anomaly as defined by the gradient survey, and was not detected by the gradient survey because of the northward flow of warm ground water.

At El Tatio, 11 gradient holes were drilled, but at shallow depths ranging from only 11 to 33 m. The holes were located around the periphery of the thermal area, and gradients ranged from  $0.05^{\circ}\text{C}/\text{m}$  to  $1.9^{\circ}\text{C}/\text{m}$ . Generally, the larger gradients were found in the eastern and southeastern part of the field (Hochstein, 1968), which, on drilling, also proved to be the area having the higher subsurface temperature. Because of the limited number of holes, a gradient anomaly was not well defined, and consequently the survey did not contribute significantly to drill site selection.

As can be appreciated from the above examples, temperature gradient surveys must be interpreted with care. The method is most applicable to those prospect areas which are underlain by impermeable rock to at least the depth of the gradient holes, as at Monte Amiata in Italy and at Kızılder. This condition minimizes distortion of the gradient due to ground-water flow. Even under this favorable condition, however, no conclusion should be made from extrapolation of the measured gradient beyond the depth of the hole because, as can readily be appreciated, the same gradient could be caused by either a shallow, moderate-

temperature source, or a deep, high-temperature source. This fact is well-demonstrated by the two anomalies found at Ahuachapán.

The main cost of a temperature gradient survey is the cost of drilling which could be expected to average \$3000 per 100-meter hole.

### Resistivity Surveys

The major advantage of the infrared imagery, one-meter probe, and temperature gradient surveys is that they are all related directly to the main quantity being sought, that is, heat. The major disadvantage of these methods is that they give only superficial or shallow information when what is required is knowledge of conditions at a depth of about 1 km. Although under favorable conditions a resistivity survey can provide penetration to this depth, the parameter it measures is related not only to heat but also to porosity and formation fluid chemistry. Therefore, making geological interpretations of resistivity data can be just as difficult as interpreting thermal gradient data. Nevertheless, resistivity surveys have been by far the most effective of all the geophysical surveys used in the UN exploration program. Four types of direct current resistivity surveys have been used: (1) constant-spread Schlumberger; (2) Schlumberger soundings; (3) continuous, in-line dipole-dipole profiling; and (4) roving-dipole.

**Constant spread Schlumberger configuration.** Surveys with this configuration were undertaken at Ahuachapán, Momotombo, and El Tatio.

At Ahuachapán, the  $AB/2$  spacing was 1000 m and the distance between stations averaged about 1 km. Two anomalies of less than  $10\text{ ohm}\cdot\text{m}$ , compared to background values of greater than  $20\text{ ohm}\cdot\text{m}$ , were found to correspond, in general, to the two anomalies found by thermal gradient mapping (Gonzales-Garcia, 1968). On drilling, as mentioned above, the northern of the two anomalies was found to have a subsurface temperature of only  $100^{\circ}\text{C}$  as compared to  $237^{\circ}\text{C}$  in the southern anomaly. Neither the resistivity nor the temperature gradient survey could detect this difference.

Although a constant-spread Schlumberger survey was attempted at Momotombo, high contact resistances prevented the obtaining of sufficient data to determine if the thermal area is associated with a resistivity anomaly.

At El Tatio,  $AB/2$  spacings of 250 m, 500 m, and 1000 m were used at a station density of 250 and 500 m. The array with  $AB/2 = 250\text{ m}$  disclosed a  $5\text{-ohm}\cdot\text{m}$  anomaly, compared to a background value of over  $500\text{ ohm}\cdot\text{m}$ , covering an area of  $8\text{ km}^2$ . The anomaly coincides with the area of surface thermal activity. On increasing the  $AB/2$  spacing to 1000 m, the area enclosed within the  $5\text{-ohm}\cdot\text{m}$  contour increases to about  $16\text{ km}^2$  (Macdonald, 1974). Twelve of the 13 exploration holes drilled at El Tatio were located within the  $5\text{-ohm}\cdot\text{m}$  contour as defined by the survey with  $AB/2 = 1000\text{ m}$ , and all found temperatures in excess of  $210^{\circ}\text{C}$ . The one hole drilled outside the  $5\text{-ohm}\cdot\text{m}$  gradient contour found only  $176^{\circ}\text{C}$ ; but because it was sited on high ground and did not reach the elevation of the high-temperature zones found in the other wells, no significant conclusion can be drawn from this one low-temperature well.

**Schlumberger soundings.** Schlumberger soundings were done in all the project areas in order to study the

variation of resistivity with depth, and as a means of providing data for calculating true resistivity values. Only in Kızıldere and Olkaria, however, were attempts made to correlate the soundings and make a three-dimensional analysis of the data.

The results of the survey at Kızıldere are notable because the reservoir has been correlated with a resistivity high, rather than a resistivity low. This is because the reservoir is fractural metamorphic rock having a high resistance in comparison to the overlying unit of impermeable shale. Depth to the top of the reservoir is easy to interpret from Schlumberger soundings, and therefore the method was used to produce a structural contour map of that horizon (Duprat, 1970). Evidently, horizontal variation of resistivity within the reservoir due to variations in fluid temperature and salinity were not detectable.

The Schlumberger soundings made within the Olkaria thermal area gave very erratic results; and although attempts were made to correlate the soundings on profiles and maps, a convincing geologic interpretation could not be made from the data. In contrast to the complex sounding curves found within the Olkaria prospect, quite simple two- and three-layer curves were found outside the boundaries of the area. The reason for the complexity found within the thermal area became clear after obtaining data from continuous dipole-dipole profiles, the results of which are discussed below.

**Dipole-dipole configuration.** A few kilometers of dipole-dipole profiling were done in both the Ahuachapán and El Tatio areas in order to confirm the location of field boundaries, and to investigate specific problems, but the method was used extensively only at Olkaria because of the failure of other resistivity methods to give sufficiently consistent data on which a geologic interpretation could be based.

At Olkaria, 130 km of continuous, in-line (polar) dipole-dipole data were collected. Electrode separations for each dipole were kept constant at 250 m; and potentials from each current station were obtained for electrode separations ranging from  $n = 2$  to  $n = 8$ , giving a theoretical penetration of about 1 km. Centers for current electrode stations were spaced at 250-m intervals. With this method, a well-defined resistivity low was found closely associated with a northwest-trending volcanic zone. The boundaries of the anomaly are quite sharp, separating background values of apparent resistivity greater than 50 ohm·m from an average apparent resistivity of 20 to 30 ohm·m within the anomaly. At 18-km length of the anomaly was mapped, leaving the northwest and northeast ends open. The anomaly ranges in width from 4 to 10 km. Four low (<20 ohm·m) and two high (>30 ohm·m) anomalies occur within the major anomaly. These smaller anomalies range from about 3 to 10 km<sup>2</sup> in area. Drilling near one of these highs found subsurface temperatures of only 126°C, while temperatures of 240°C and 286°C were found by drilling near or within two of the low anomalies. No holes have been drilled outside of the large anomaly in ground having an apparent resistivity greater than 50 ohm·m.

It is the presence of these relatively small anomalies that makes interpretation of the Schlumberger soundings at Olkaria so difficult. Due to the distribution and size of these anomalies, all the expansions crossed one or more of their steeply dipping boundaries, mixing the effect of both vertical and horizontal resistivity changes. The great

advantage of the dipole-dipole profiling method is that it can discriminate between these two types of boundaries.

**Roving dipole configuration.** The roving dipole configuration was used at El Tatio, Momotombo, and Olkaria. This is basically a reconnaissance method in which the current dipole separation is on the order of several kilometers and sufficient current is used so that potentials can be read out to a distance of about 12 km from the center of the current dipole. Potential stations are located anywhere within a 24-km-diameter circle centered on the current electrodes, hence the name "roving dipole."

At El Tatio, the method was not used for reconnaissance but only for examining field boundaries, and no potential readings were obtained beyond about 4 km from the dipole.

As in the case of the constant-spread survey, the roving-dipole survey at Momotombo was hampered by high contact resistance, and no conclusion can be drawn because of insufficient data.

At Olkaria, approximately 300 km<sup>2</sup> were surveyed with the roving-dipole method, using three separate current electrode locations. There is practically no correlation of the results of the roving-dipole survey with those of the dipole-dipole survey. In place of the sharp boundary found by the dipole-dipole survey on the southwest side of the large, northwest-trending low, the roving dipole found a wide and diffuse gradient striking in the same direction as the boundary detected by the dipole-dipole survey, but with the position of the high and low sides reversed. Drilling has confirmed that there is a geothermal field on the northeast side of the boundary, and that the geothermal fluid contains 2000 ppm dissolved solids which are principally sodium chloride. The roving-dipole survey detected the small resistivity highs found within the dipole-dipole low, but not the small lows which drilling has shown to be high-temperature areas. The results of the roving-dipole survey at Olkaria cannot be considered very satisfactory.

In summary, UN project experience indicates that the most suitable resistivity technique for geothermal exploration is dipole-dipole profiling. Its principal advantage is that it produces better geologically interpretable results than the other three methods. In addition, the dipole-dipole array is easier to maneuver in rugged country than either the constant spread or expanding Schlumberger arrays. Its main disadvantage, compared to the Schlumberger array, is that it usually requires more current, and therefore a heavier generator, for the same penetration depth. Although the roving dipole is the most maneuverable of all the arrays (hence its growing popularity), this advantage, in my opinion, is not sufficient compensation for the difficulties encountered in making geologic interpretations from the resulting data.

### Microearthquake Surveys

The Ahuachapán and Olkaria projects have been surveyed by this method.

At Ahuachapán, a three-seismometer array was used (Ward and Jacob, 1971). The seismometers were positioned on the circumference of a circle 3 km in diameter and centered on a group of productive wells which had already been drilled. Although 150 events were recorded at a frequency of about one event per day, only 17 of these events could be located due to the problem of maintaining

the continuity of the cable which interconnected the stations. Epicenters of 14 of the 17 events plotted in a tight rectangular cluster measuring 1 km long by 0.5 km wide. Depths to the events ranged from 0 to 6 km. Ward and Jacob (1971) believe that all the events are located on a steeply-dipping fault plane which acts as a channel for the movement of geothermal fluid.

An array of eight seismometers was used at Olkaria, distributed first around the circumference of a circle 20 km in diameter, and then, due to a high signal attenuation, redistributed in an elliptical array 8 km long by 5 km wide. Radiotelemetry, rather than cables, was used for interconnection of the array; and although maintenance of the system required the daily attention of an electronics technician, signals were recorded from all the stations during almost 100% of the survey time. Twenty-three events were located during a monitoring period of 52 days on the first array and 20 events were located in 27 days by the second, smaller array (Hamilton, Smith, and Knapp, 1973). Of the 43 events, the epicenters of 29 define a north-trending zone 9 km long and ranging from 1 to 3 km in width. This zone corresponds to a linear trend of young lava domes and steaming vents. The depth to hypocenters along the trend ranges from 1 to 6 km.

The first deep test drilled at Olkaria was located on this trend of microearthquake events with negative results; that is, a temperature of only 126°C was found at a total drilled depth of 1000 m, and pumping tests indicated low permeability. The second hole drilled at Olkaria, located 2 km east of the microearthquake trend, found a temperature of 286°C but only moderate permeability.

In view of the mixed results obtained from these two surveys, we feel that the value of the technique still remains to be proven.

### Gravity and Magnetic Surveys

These surveys were carried out in several of the project areas at various station densities, the most extensive work having been done at Ahuachapán (gravity and magnetic) and Kızıdere (gravity only). As could be anticipated, the results of these surveys were useful for making regional structural interpretations, but no anomalies were found that could be directly related to geothermal fields.

### PHASE III: DRILLING

As drilling costs account for about three-quarters of the total exploration budget, this phase requires particularly careful planning in order to obtain the maximum footage for expenditure.

In order to plan a rational drilling program, first it is necessary to decide if information or production is the initial objective. There are compelling arguments that slim holes to 600 or 700 m should be drilled in order to verify temperature and permeability prior to committing funds for the heavier equipment capable of drilling production holes. However, studies have indicated that under the conditions of most UN projects, drilling slim holes offers very little savings, if any, over drilling larger-size production holes.

The Chilean project was an exception to this general rule due to the very high cost of preparing access roads to the El Tatio site, and therefore the drilling program was initiated with six slim holes drilled to 600 m. The information obtained

from these holes was quite valuable as it showed that temperature reversals occurred in the western part of the area, but not in the east; and consequently, deep test drilling was concentrated in the eastern part of the area. Unfortunately, the slim holes were not drilled deep enough to satisfactorily assess another problem, that is, permeability; and therefore, they gave little or no forewarning of the fact that only two of the seven deep tests would have sufficient permeability for economic production.

Prior to drilling full-size holes, it is necessary to decide on the size and depth of the holes and the casing program. Geologic and geophysical information is seldom sufficiently unambiguous to provide a reliable estimate of the depth to the potential reservoir. Therefore, hole and casing specifications often are based on experience rather than specific information concerning the area to be drilled. Knowing that the average depth of geothermal wells is on the order of 700 m, but also knowing that some wells are drilled to 2500 m before finding commercial production, UN projects tend to compromise with a depth objective of about 1500 m. If the well proves to be too shallow for production, it will hopefully still be deep enough to provide sufficient information for deciding either to abandon the prospect or to obtain heavier drilling equipment. A typical drilling and casing program for an initial exploration hole is shown in Table 1.

Whether or not wells can be completed without slotted liners cannot be known until after a well has been in production for several months. Liners are provided on the first few wells, however, to ensure that they will remain open for evaluation testing.

Next, it is necessary to decide on the circulation system to be used. In order to avoid the possibility of damaging reservoir permeability, water rather than mud is used to drill below the production string. As long as a pumping rate of approximately 400 gal/min is maintained, drilling with water as a circulating fluid has offered no particular problem when drilling in areas where formation fluid pressure approximates the pressure distribution in a hydrostatic column with its head located near the ground surface. On the other hand, major problems occur when drilling with water in areas where reservoir pressure is low compared to the hydrostatic column in the well. Ahuachapán and Olkaria, with static water rest levels at 150 m and 300 to 400 m respectively below the wellhead, are examples of such areas. Even rather limited formation permeability can cause a loss of circulation while drilling such low-pressure reservoirs, and in order to continue drilling under this condition one of the following alternative actions must be taken: (1) seal the loss with the risk of losing future production from the zone; (2) drill blind with the risk of sticking the drill string and also with the probable inconve-

Table 1. Typical UN drilling and casing program.

Depth (m)	Bit (inches)	Casing (inches)
10	26	20
200	17½	13⅜
600	12¼	9⅝
1500	8½	7*

\*slotted liner

nience of having to wait a long time for temperature recovery before evaluating the well; or (3) decrease the density of the fluid column with foam or air in order to regain circulation. Having experienced this problem at Ahuachapán and having anticipated it prior to drilling at Olkaria, capacity for foam drilling was included in the Olkaria drilling specifications. The equipment included a compressor with a capacity of 20 m<sup>3</sup>/min at a 17-bar delivery pressure and a booster with a delivery pressure of 100 bar. A locally available commercial detergent was used as the foaming agent. The system performed well until bottom-hole temperature reached about 120°C. Above this temperature, a stable foam could not be maintained due to steam flashing into the hole and the system had to be abandoned. However, a solution to the problem was found: after setting the production string, the 8.5-inch hole was drilled with water, at a pumping rate of 400 gal/min, plus air injected at a rate to maintain full water return. The air produces a pumping action in the annulus which is sufficient to lift the water and entrained cuttings to the surface. Although this method was successful in drilling to 1350 m, with static heads 300 m to 400 m below surface, higher compressor capacities would have been desirable when drilling below about 1200 m. In addition to the obvious advantages of this drilling method over either sealing, loss circulation zones or drilling blind, it also has several advantages over straight air drilling: (1) required air capacity is much less; (2) fluid velocities are much less, thereby greatly reducing the problem of equipment failure due to erosion; (3) the hole is kept cool, thereby reducing the hazard of uncontrolled blowouts; and (4) hole and formation pressures can be kept in balance.

As can be appreciated from the above discussion, the main source of drilling problems in UN projects has not been temperature, but loss of circulation due to low-pressure reservoirs. The temperature problem has been minimized by high fluid circulation rates, and with the introduction of a cooling tower into the circuit. The solution to the loss of circulation problem appears to be circulation assisted by air-lift.

Completed well costs for UN projects, where the drilling was contracted, have ranged from about US\$80 000 to US\$450 000. About half of this range, that is, from US\$80 000 to US\$250 000 is due to inflation in the drilling industry from 1968 to 1974. The other half of this range reflects varying drilling conditions and the varying degrees of efficiency with which operations were planned and executed.

#### PHASE IV: RESERVOIR EVALUATION

The basic measurements which must be made on a completed well are the variation of steam output with wellhead pressures and with time. To minimize standby charges on drilling equipment, it is desirable to have the well-testing equipment fabricated and in place by the time the well is completed. Even more time can be saved if a flow line for testing is connected to the wellhead below the blowout preventer stack so that tests can be made any time during drilling, and drawdown tests can be started even before the rig is moved off-site. This arrangement has the added advantage that in the event the well has to be stimulated, the rig is available for running tubing which can be used to air-lift the well into production. This system allows at least a quantitative assessment to be made within a day or two of completing the well.

This early assessment can only be quantitative because several weeks may be required before flow is reasonably stabilized. The time required for reaching stabilized conditions will depend on reservoir permeability and whether or not the reservoir fluid is depositing carbonate. If the reservoir is permeable and no carbonate is deposited, as at Ahuachapán, negligible decrease of flow will be noticed over the first few weeks. If permeability is moderate, flow rates will decrease but should become relatively stable after several weeks. For example, Olkaria No.2 had an initial steam production of about 60 ton/hr, but after about 3 weeks of decreasing production, the flow rate stabilized at 34 ton/hr. If permeability is low, the well will either not sustain flow, or flow will be cyclic. If carbonate deposition occurs, semistable conditions are never reached, and flow will continue to diminish indefinitely. The effect of carbonate deposition can be distinguished from the effect of poor permeability early in the testing period by looking for deposits in the casing.

Obtaining stabilized flow data as quickly as possible is essential for efficient project implementation because test results for a well just completed should be used to determine the location of the next well to be drilled in the series. In UN projects alternative well sites are prepared in advance of drilling. Prior to a discovery, holes are drilled at intervals of several kilometers in order to obtain a good distribution of test sites over the target area. On completing the first economically viable well, the remaining drilling budget is used to drill offsets from the discovery with the objective of proving as much steam as possible for use at the first plant site. Offset wells are spaced 100 to 300 m from the discovery well. Although this plan appears reasonable in theory, it often fails in practice because accurate well data are difficult to obtain before the drilling rig has to be moved to the next site.

At Ahuachapán, the second exploration hole was successful, having a capacity of 6.5 MW. Five offsets were then drilled under the next program. The first three wells were located 200 to 500 m from the discovery, and produced at capacities of 3.4, 6.4, and 3.0 MW. The other two wells were drilled about 1500 m from the discovery site and were nonproductive. Drilling which has been undertaken since termination of the UN program has established the northern and western boundaries of the field, but the eastern and northeastern boundaries are still unknown (Cuéllar, personal commun., 1975).

At El Tatio, the six slim holes were sited only for information purposes and were located along two sides of a rectangle measuring 2.5 by 4.5 km on a side, with the wells spaced at intervals of 1 to 2 km. Seven deep tests were then sited at distances ranging from 100 to 900 m from the best slim hole. Although all seven deep tests found adequate temperatures (220 to 262°C), only two, located 300 m apart, found adequate permeability for commercial production. A well located between these two wells has insufficient permeability for production.

At Olkaria, the second exploration well was successful. Two offset wells were drilled at a distance of 200 m from the discovery well, which has a stabilized output of 34 tons of steam and 8 tons of water per hour (Jonsson, personal commun., 1975). As yet, stabilized flows have not been measured in the offset wells, but it is believed that permeability is too low for commercial production.

At Kizildere, rather than drilling offsets from the discovery



well which was the first well drilled, an attempt was made to define the field boundaries by long step-outs. Eleven wells were drilled, five of which were found to be beyond the field boundary as defined by a minimum temperature of 190°C. The field, as outlined by this drilling program, is elliptical in shape, 4.5 km long by about 1.3 km wide. As mentioned earlier, although the Kızıldere reservoir has good permeability and acceptable temperature, deposition of carbonate in the wells has prevented development.

#### PHASE V: ECONOMIC FEASIBILITY STUDY

This phase of the project is relatively straightforward, and compared to the first four phases, requires little explanation.

In general, the feasibility study is designed to cover the following topics:

- Review of the well test data to verify production capacity and evaluate evidence for drawdown.
- Determination of capital cost and running charges of the optimum-size plant which could be operated from proven well capacities on the basis of a preliminary plant design.
- Comparison of these costs with the cost of alternative sources of power.
- Determination of possible economic uses of the resource for purposes other than power generation.
- Assessment of the environmental impact of development.

These are primarily desk studies which are contracted to consulting engineering firms and require about six months to complete. The principal purpose of the study is to provide an unbiased, "third-party" project evaluation which can be used by the governments concerned in soliciting investment for construction of a power plant.

#### CONCLUSION

After a decade of work during which two projects have been completed and two more nearly completed, the results are not all that the UN had hoped they would be: one successful project, one failure, and two possibly successful projects, but results are not yet certain.

Finding high temperature has not been a problem. This is partly due to using geochemical and geophysical exploration techniques, but also it is due to the fact that prospects have been chosen in the most obviously low-risk areas of the world. The UN has found that the problems are finding adequate permeability and avoiding carbonate deposition.

The failure at Kızıldere may yet be turned into a success if only one of the several suggested solutions to the problem of carbonate deposition is shown to be technically and economically viable. Until that time, it may be possible to avoid fruitless expenditures in such areas by careful examination of thermal water chemistry prior to drilling.

Inadequate permeability is a problem for which we see no easy solution. The magnitude of the problem can be better visualized by expressing the flow rates of a typical 5-MW geothermal well in the units used for petroleum wells: water must be produced at a rate of 34 000 barrels per day, or 1000 gal/min, from a wet field, and steam (reduced

to one atm at 100°C) at a rate of 64 million cu ft/day from a dry field. As petroleum prospectors know, these are very large flow rates and are not often achieved from semiconsolidated rock at depths of 1 km. As with the problem of carbonate deposition, many schemes for stimulating geothermal well production have been suggested (see particularly Kruger and Otte, 1973) but none of them, to our knowledge, have been tried in geothermal reservoirs.

If, because of the erratic distribution of permeability, the success ratio of development wells is going to be only one in four as suggested by the El Tatio and Olkaria results, then with the rising cost of drilling, the capital cost of providing steam for geothermal plants could rise to US\$400/KW. Either the cost of drilling must be reduced, the success ratio increased, or a viable stimulation technique found.

As rising drilling costs are related to the much larger problem of world-wide inflation, there is little that technicians can do to counteract this factor other than to develop more efficient drilling techniques and programs. Increasing success ratios should be possible, but in order to do so we must learn a great deal more than we know now about the nature and cause of permeability in geothermal reservoirs. With this knowledge, perhaps better exploration techniques can be found. In my opinion, the transfer of proven well stimulation technology from the petroleum industry to the geothermal industry, if it can be done successfully, would offer the most rational solution.

*The views and opinions expressed herein are those of the author and do not necessarily reflect those of the United Nations.*

#### REFERENCES CITED

- Duprat, A., 1970, Contribution de la géophysique a l'étude de la région géothermique de Denizli-Saraköy, Turquie: UN Symposium on the Development and Utilization of Geothermal Resources, Pisa, Proceedings (Geothermics, Spec. Iss. 2), v. 2, pt. 1, p. 275.
- Gonzalez-Garcia, J., 1968, Levantamientos geofísicos en el área geothermal de Ahuachapán: Unpub. UN project report.
- Hamilton, R. M., Smith, B. E., and Knapp, F., 1973, Earthquakes in geothermal areas near Lakes Naivasha and Hannington, Kenya: Unpub. UN project report.
- Hochstein, M. P., 1968, Geophysical studies for the geothermal development project in northern Chile during the period 24 February-18 June 1968, and 25 October-16 December 1968: Unpub. UN project report.
- Kruger, P., and Otte, C., eds., 1973, Geothermal energy, resources, production, and stimulation: Stanford, California, Stanford Univ. Press.
- Macdonald, W. J. P., 1974, Geophysical surveys of El Tatio geothermal field, 1968-1974: Unpub. UN project report.
- Thigpen, J. B., 1971, Deep borehole test south Volcan Momotombo fumarole area: Unpub. UN project report.
- Ward, P. L., and Jacob, K. H., 1971, Microearthquakes in the Ahuachapan geothermal field, El Salvador, Central America: Science, v. 173, p. 328.
- White, D. E., 1970, Geochemistry applied to the discovery, evaluation, and exploitation of geothermal energy resources: UN symposium on the Development and Utilization of Geothermal Resources, Pisa, Proceedings (Geothermics, Spec. Iss. 2), v. 1, p. 58.

THERMAL EXPANSION BEHAVIOR OF CERRO PRIETO SANDSTONES AND  
OTHER SEDIMENTARY ROCKS UNDER STRESS.

E. CONTRERAS

INSTITUTO DE INVESTIGACIONES  
ELECTRICAS. CUERNAVACA, MOR.,  
MEXICO.

F. BERMEJO

COMISION FEDERAL DE ELECTRICIDAD.  
CERRO PRIETO, B.C., MEXICO.

ABSTRACT

This paper describes the experimental work and presents the results of a research program - carried out to investigate the thermal expansion behavior of sedimentary rocks under high stress conditions. The aspects that were investigated include the effects of temperature, temperature cycling, and confining pressure. Furthermore, the validity of the usual assumption on thermal expansion isotropy was investigated. On the other hand, the matrix thermal expansion concept is analyzed and its physical meaning and applications are discussed. The effect of temperature on porosity is also a subject investigated regarding experimental methods for its estimation and comparison of earlier results.

The experiments carried out consisted basically of thermal stress versus temperature measurements on jacketed and unjacketed samples subjected to different confining pressures and covering the temperature range from 25°C to 280°C and the pressure range from 3.0 MPa to 34.4 MPa. A review of earlier work is included as a reference frame to discuss and compare the results of this work, as well as to emphasize the limited extent of the research on thermal expansion behavior of sedimentary rocks that had been accomplished.

Results are presented by means of thermal strain versus temperature curves and tabular data of thermal expansion coefficients. Several important conclusions for laboratory and field applications are reached from each of the aspects investigated.

The wide research scope of this work and the considerable amount of data reported may represent an important contribution to the knowledge of thermal expansion behavior of sedimentary rocks.

INTRODUCTION

The thermal expansion behavior of rocks is a subject of great interest in many reservoir engineering, geophysical, mining and similar underground applications where rocks are heated. The limited data available on thermal expansion of rocks are mostly bulk expansion data

for low porosity rocks, the majority of which are igneous, generally corresponding to either atmospheric pressure and wide temperature ranges, or high pressure and narrow temperature range conditions. That is, very few results have been reported in which samples were subjected simultaneously to high stress and a wide range of temperature variations

It is well known that sandstones constitute the main producing-horizons in various geothermal fields; therefore, the importance of the thermal expansion behavior of sedimentary rocks in geothermal applications is self-evident. However, this subject has not yet been covered extensively.

In order to obtain a good knowledge about the thermal expansion behavior of rocks, it is mandatory to understand the effects of parameters such as temperature, temperature cycling, heating rate, stress, saturation, expansion anisotropy, and effect of temperature on porosity. Such an understanding is also necessary to plan the experimental measurements more adequately, thus reducing considerably the amount of experimental work required. Concerning sedimentary rocks, the effects of only some of the above mentioned parameters have so far been partially investigated. A brief review of the existing studies on this subject is included in the following.

Ashqar (1979), Somerton (1980) and Somerton et al. (1981) reported the results of bulk thermal expansion of liquid-saturated specimens of Boise, Berea and Bandera sandstones that were subjected to 20.7 MPa confining pressure and 6.9 MPa pore pressure, while increasing the temperature from 30°C to 175°C at a rate of about 1°C/min. The samples were not subjected to temperature cycling, hence only heating strain-temperature curves were reported. These curves were compared with the strain-temperature curves for the same outcrop sandstones reported by Somerton and Selim (1961) run under dry and no confining or pore pressure conditions, and a fair agreement was found, indicating that thermal expansivities of Boise, Berea and Bandera sandstones were not strongly dependent of stress and fluid saturation.



Janah (1980), Somerton (1980) and Somerton et. al. (1981) reported results of a series of tests focused to investigate the influence of temperature on pore volume contraction for the same outcrop sandstones under stress. The specimens studied were subjected to 20.7 MPa confining pressure and 6.9 MPa pore pressure. Changes in pore volume were measured as temperature was increased from 30°C to 170°C. From their results, the authors concluded that the pore volume of liquid saturated sandstones under stress decreases with increasing temperature, and that the pore volume thermal contraction is a function of porosity, values decreasing with increased porosities. The fractional pore volume contractions reported by the authors for the Boise, Berea and Bandera sandstones for the 30°C to 170°C temperature range are 0.55%, 1.04% and 1.53%, respectively.

Janah (1980) also studied the effects of stress level on pore volume thermal contraction and noted that differences in confining stress level had little effect on it; on the other hand, increase in pore fluid pressure level had a marked effect, the pore volume contraction decreasing substantially with increased pore fluid pressure.

Greenwald et. al. (1982) presented a new set of results for exactly the same kind of experiments as carried out by Ashqar (1979) and Janah (1980) on bulk thermal expansion and thermal pore volume contraction of Boise, Berea and Bandera sandstones.

The strain-temperature curves reported by Greenwald et. al. (1982) differ to some extent from the ones obtained by Ashqar (1979), especially regarding Berea sandstone strain curves; the agreement for Boise and Bandera is fairly good. On the other hand, the fractional pore volume contractions reported by Greenwald et. al. for the Boise, Berea and Bandera sandstones for the 30°C to 170°C temperature increment are 3.0%, 3.7% and 4%, respectively, which compare badly to the 0.55%, 1.04% and 1.53% values reported by Janah (1980) and Somerton (1981). However no comments or explanations of these big dissimilarities were provided by the authors.

Assuming that all three sandstones are isotropic and thus, that the bulk volumetric strain is three times the axial strain, Greenwald et. al. (1982) combined their results of both pore volume contraction and axial thermal expansion measurements to calculate decrease in the original porosity. The results they reported are 3.0%, 3.8% and 4.4% porosity reduction for the 30°C - 170°C temperature range for the Boise, Berea and Bandera sandstones, respectively. Greenwald et. al. (1982) concluded that the inclusion of bulk volume thermal expansion values in porosity determinations is a second-order correction, which led to the observation that the calculated fractional changes in porosity resulted very similar to their results for fractional pore volume changes. The authors of the present work would like to point out that such

a conclusion is not always correct and would lead to significant errors in the cases where the fractional pore volume changes are of the same order of magnitude as the bulk volume thermal strain; such is the case if the pore volume contractions after Janah are considered instead of Greenwald's results.

Contreras et. al. (1982) measured the thermal strain of Berea sandstone and of a sandstone from Cerro Prieto Well M-94. The samples were tested at two different constant confining pressures of 3 MPa and 20.7 MPa, with the temperature being increased at a uniform rate of about 1.5°C/min. in the range from 20°C to 280°C. Thermal expansion measurements were made both on jacketed samples with no pore pressure, hence obtaining information about the usual bulk thermal strain, and on unjacketed samples with the confining fluid filling the rock pore volume, thus obtaining data about the so called "matrix thermal strain", a new concept that had not been introduced before in the scientific investigation on behavior of rocks. The results by Contreras et. al. (1982) showed that both, bulk and matrix thermal expansivities are dependent on the confining pressure applied to the rock. Further evidence was found that the bulk and the matrix thermal expansion coefficients depend of the temperature range itself. Furthermore, combining bulk and matrix thermal strain data and using a novel approach, Contreras et. al. (1982) presented estimates of the effect of temperature on porosity.

This short review of the existing literature clearly shows that there are several parameters whose influence on thermal expansion behavior of sedimentary rocks has not been investigated at all and that the effect of others has been investigated only in a very limited extension and mostly on outcrop sandstones.

The objectives of the present study were established to contribute to fill the main gaps of knowledge described above; consequently, in this work the following aspects are investigated in relation with thermal expansion behavior of sedimentary rocks: (1) effect of temperature cycling, (2) effect of heating rate, (3) effect of confining pressure, (4) effect of orientation with respect to the bedding plane, (5) comparison between bulk and matrix thermal strain and analysis of its significance, (6) effect of temperature on porosity. Furthermore, a big deal of data about thermal expansion coefficients of several sedimentary rocks is provided as another main result of the investigations accomplished. Unlike previous studies involving outcrop sandstones, the results presented in this paper correspond mostly to rocks from wells drilled in a very important geothermal region (the Cerro Prieto Geothermal Field area), thus increasing their importance for practical applications.

## EXPERIMENTAL ASPECTS

The identification, origin and porosity at room conditions of the samples used in this work are given in Table 1. The porosities reported were measured using the liquid saturation under vacuum method. The three kinds of outcrop sandstones were chosen so as to cover a wide range of porosities. The geothermal samples were obtained from wells M-94, M-127 and M-149 drilled in the Cerro Prieto Geothermal Field, located in Baja California, México. These geothermal samples were cut perpendicular to their bedding planes from field cores using a 2.5 cm. diameter diamond drill bit, except the sample M-127-HA that was drilled out parallel to its bedding plane. After cutting the samples to a length of approximately 5 cm., their ends were ground flat and parallel to within  $2.5 \times 10^{-3}$  cm.

TABLE 1. Origin and Porosity of the Sandstones Studied.

SAMPLE IDENTIFICATION	WELL	DEPTH (METERS)	POROSITY (%)
M94-A	M94	2417	15.8
M94-B	M94	2417	15.8
M127-A	M127	2195	20.2
M127-HA	M127	2195	20.2
M149-A	M149	2160	15
KAYENTA K1	OUTCROP	----	18.6
KAYENTA K2	OUTCROP	----	18.6
KAYENTA K3	OUTCROP	----	18.6
BEREA 1	OUTCROP	----	18.8
BEREA 2	OUTCROP	----	18.8
COLTON 1	OUTCROP	----	10.9
COLTON 2	OUTCROP	----	10.9

In order to fulfill the objectives established for this work, four basic types of tests were planned and run. Their description is presented below.

**Type A Tests.** Intended to investigate the effect of temperature cycling on the bulk thermal strain. For these tests, a constant confining pressure of 8 MPa was applied on dry jacketed samples that were then subjected to two heating-cooling cycles in the range from 25°C to 280°C, with the temperature being changed both for the heating and cooling parts at a uniform rate of about 2°C/min. Strain and temperature were recorded during the temperature cycles once every minute. Type A tests were run on samples M127-A and M127-HA.

**Type B Tests.** Intended to investigate the combined effect of heating rate and temperature cycling on the bulk thermal strain. These tests were run on dry jacketed samples subjected to a constant confining pressure of 8 MPa. Each sample tested was subjected to three consecutive temperature cycles at 1, 2 and 3°C/min in the range from 25°C to 280°C. Strain and temperature were recorded during the three cycles once every minute. Type B tests were run on samples M149-A and KAYENTA K1.

**Type C Tests.** Intended to investigate the effect of confining pressure and temperature cycling on the bulk thermal strain. These tests were run on dry jacketed samples subjected at two or three temperature cycles in the range 25°C to 280°C; for each consecutive cycle a different confining pressure was applied to the rock, keeping the heating and cooling rates constant at 2°C/min. The values of confined pressure chosen for these tests were 3, 17.2, 20.7 and 34.4 MPa. Samples M94-A and KAYENTA K2 were subjected to temperature cycles at 3, 17.2 and 34.4 MPa. Samples BEREA 1 and COLTON 1 were subjected only to heating from 25°C to 280°C at 3 and 20.7 MPa. Strain and temperature were recorded during the tests once a minute.

**Type D Test.** Intended to investigate the concept of matrix thermal expansion and determine the influence of confining pressure and temperature cycling on it. These tests were run on unjacketed samples, thus enabling the confining fluid to fill the rock pore volume. The samples tested were subjected to temperature variation in the range from 25°C to 280°C at two different confining pressures. Samples M94-B and KAYENTA K3 were subjected to temperature cycles at 3 and 34.4 MPa. Samples BEREA 2 and COLTON 2 were subjected only to heating from 25°C to 280°C at 3 and 20.7 MPa. Strain and temperature were recorded during the tests once a minute.

A summary of the tests description and the experimental work accomplished is shown in Table 2.

The experimental equipment used is shown schematically in Fig. 1. It consists primarily of the pressure vessel, a servocontrolled pressurizing system, an automatized heating system, strain and temperature sensors and transducers and a computer based data acquisition system.

Linear thermal expansion for both jacketed and unjacketed samples was measured along their axis by means of high resolution LVDT's (linearly variable differential transducers) attached to the top of the test specimen by quartz rods. Deformation of up to  $2.5 \times 10^{-2}$  cm. can be measured with an accuracy of  $\pm 6.2 \times 10^{-3}$  cm. Averaging the outputs of the two LVDT's removes any false strain due to tilting. More details

TABLE 2. Summary of Testing Conditions and Experimental Work Carried Out.

TEST TYPE (SAMPLES TESTED)	SAMPLE CONDITION	CONFINING PRESS MPa	TEMPERATURE VARIATION (°C)	HEATING RATE °C/MIN.
A (M127-A, M127-HA)	JACKETED	8	25-280-25	2
			25-280-25	2
B (M149-A, KAYENTA K1)	JACKETED	8	25-280-25	1
		8	25-280-25	2
		8	25-280-25	3
C (M94-A, KAYENTA K2)	JACKETED	3	25-280-25	2
		17.2	25-280-25	2
		34.4	25-280-25	2
C (BEREA 1, COLTON 1)	JACKETED	3	25-280	2
		20.7	25-280	2
D (M94-B, KAYENTA K3)	UNJACKETED	3	25-280-25	2
		34.4	25-280-25	2
D (BEREA 2, COLTON 2)	UNJACKETED	3	25-280	2
		20.7	25-280	2

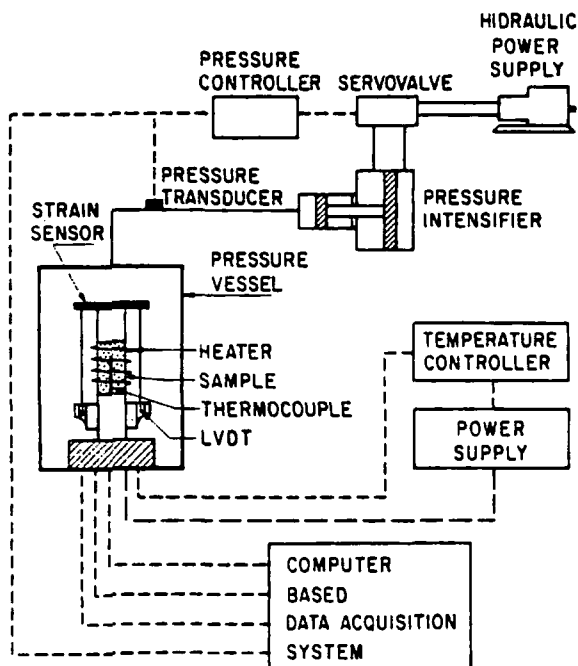


Figure 1. Schematic of experimental equipment.

on the experimental configuration used are given by Ennis et. al. (1979).

The temperature cycles and heating rates were tailored by means of a Honeywell programmable controller that regulated the power to an electric heater located inside the pressure vessel around the sample. By using the servocontrolled pressurizing system, confining pressure was kept constant at the chosen values within  $\pm .01$  MPa.

Data collected during the tests consisted of deformation output from the two LVDT's, sample temperature and confining pressure. Data was collected once every minute and stored by means of a computer based acquisition system.

In order to take into account the thermal expansion of the measuring system, calibration tests were run using fused quartz as the standard.

## RESULTS AND DISCUSSION

### Effect of Repeated Temperature Cycles on Bulk Thermal Expansion:

The results of type A tests carried out to investigate the effect of two consecutive temperature cycles on the bulk thermal expansion of sandstones are shown graphically in figures 2 and 3 by means of strain versus temperature curves. Description of the test conditions were given before and are also included as inset in the figures. The general strain-temperature behavior exhibited by the samples M127-A and M127-HA is very similar, as it can be inferred from figures 2 and 3. Several interesting features of the strain-temperature curves can be appreciated and will be analyzed and discussed in the following.

For both samples, the heating and cooling strain-temperature curves of the first cycle show significant differences, with the cooling curve lying below the heating curve almost for the whole temperature range, resulting in a negative strain or compaction at the end of the first cycle. On the other hand, the strain-temperature behavior for the second cycle is highly reversible, since the discrepancies between its heating and cooling curves are almost inexistente; further, the compactions observed after completion of the second cycle are smaller than the ones for the first cycle. Using the strain marks drawn on figures 2 and 3, it is also noted that for both temperature cycles, the sum of the heating thermal strain,  $\epsilon_T$ , and the corresponding compaction,  $\epsilon_C$ , is almost a constant value,  $\epsilon$ , for each sample. The parameter  $\epsilon$  physically represents the cooling thermal strain experimented by the rock.

From these observations, we can draw an important conclusion, although still somewhat preliminary, concerning the strain-temperature behavior of sandstones. It appears that after a few temperature cycles, the rock will become thermomechanically stabilized, and that further recycling will not cause additional compaction in it. Under these circumstances, bulk thermal strain of sedimentary rocks would be reversible provided the rock has been previously subjected to a few temperature cycles. More experimental evidence supporting the conclusion of reversibility will be presented in the forthcoming subsection.

Further, since the parameter  $\epsilon$  is the cooling thermal strain experimented by the rock, and such a parameter has the same value for both cycles as was noted before, it would be reasonable to propose that the thermal strain versus temperature curve of the cooling part of the temperature cycle does not depend on the thermal history of the rock, (as opposed to the heating strain-temperature curve that does depend on the thermal history). The validity of the above proposed concept is strong-

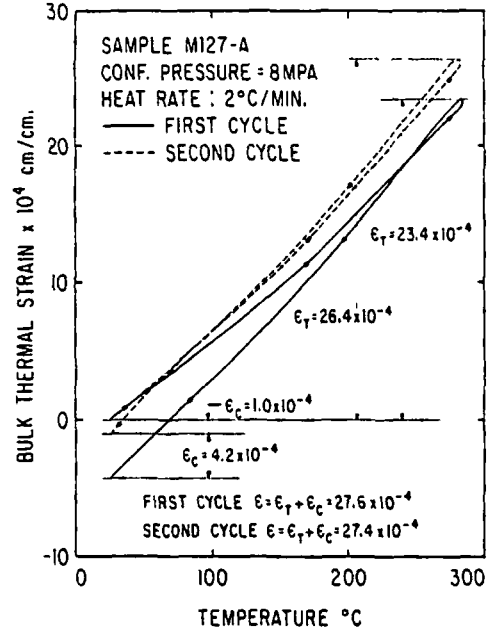


Figure 2. Effect of repeated temperature cycles on bulk thermal expansion of sample M127-A.

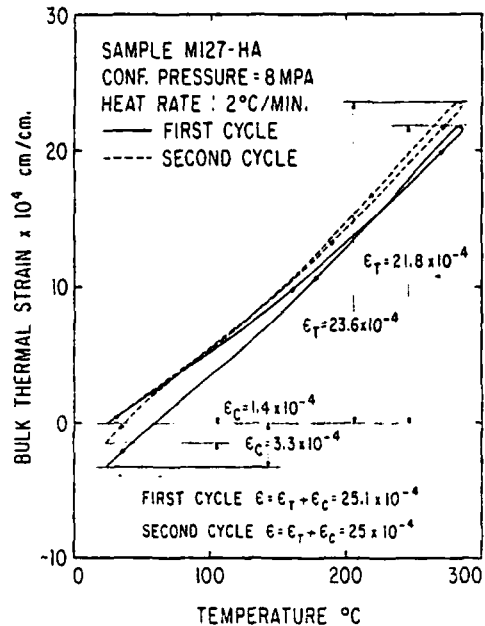


Figure 3. Effect of repeated temperature cycles on bulk thermal expansion of sample M127-HA.

ly supported by the experimental evidence that will be presented later in this work.

Combining the concept about the invariability of the cooling strain-temperature curve with the conclusion on the reversibility of the bulk thermal strain after a few temperature cycles, it is possible to determine the bulk thermal strain versus temperature behavior of a thermomechanically stabilized rock from the knowledge of any cooling strain curve, even the one corresponding to the first cycle. The importance of this conclusion is evident for the planning of experimental measurements as well as for analysis and application of results.

**Effect of Heating Rate and Temperature Cycling on Bulk Thermal Expansion.**

The results of type B tests carried out to investigate the effect of different heating rate values are shown in figures 4 and 5 for the samples M149-A and KAYENTA K1, respectively. Again, it is observed that for both samples the heating strain and the cooling strain versus temperature curves of the first cycle differ to a large extent, and a considerable compaction results at the end of this cycle. However, this compaction is more noticeable for sample KAYENTA K1 than for sample M149-A.

Both the latter strain-temperature cycles (two and three) differ markedly from cycle one. However, discrepancies between the cycles two and three are nearly indistinguishable from each other, thus providing evidence that the change in heating rate from 2°C/min to 3°C/min does not affect the strain-temperature pattern.

Furthermore, thermal expansion for cycles two and three is highly reversible upon cooling; the heating and cooling curves show only a small hysteresis loop, which can be related to the existence during the heating period of a lag of the inside-the-sample temperature with respect to the temperature sensed by the thermocouple attached to the external surface of the sample. The opposite phenomenon occurs during the cooling period. This observation is supported by the fact that the hysteresis loop is wider for the 3°C/min heating rate than for the 2°C/min heating rate.

The notorious similarity between cycles two and three provides enough evidence so as to reasonably conclude that their discrepancy from cycle one is not due to the different heating rates, but to the compaction mechanism, which was discussed before. Therefore, it can be concluded that differences in heating rates in the range from 1°C/min to 3°C/min do not affect the thermal strain-temperature behavior of sedimentary rocks nor do they produce irreversible structural damage. As it is noted, the actual value of the heating rate influences only the extension of the hysteresis loop. A 2°C/min heating rate is recom-

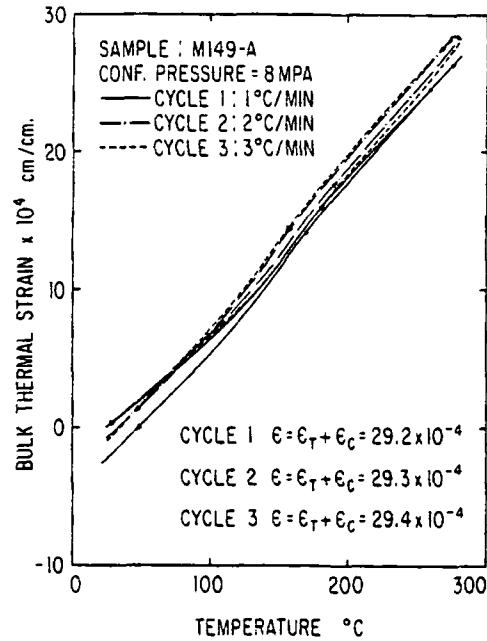


Figure 4. Effect of heating rate and temperature cycling on bulk thermal expansion of sample M149-A.

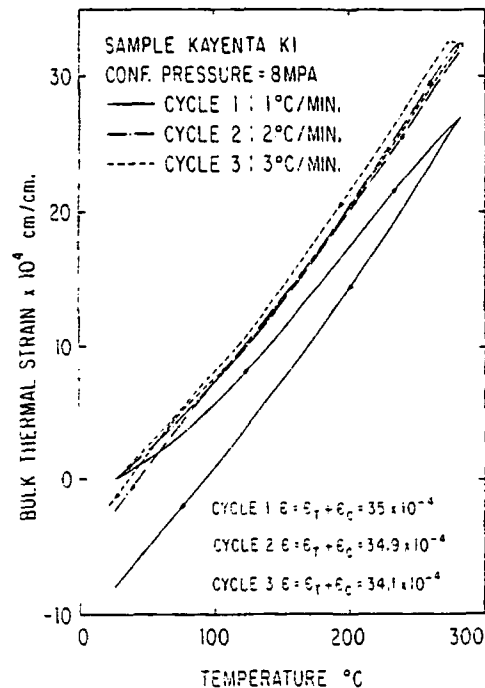


Figure 5. Effect of heating rate and temperature cycling on bulk thermal expansion of sample KAYENTA K1.

mended by the authors of this work, since the hysteresis loop associated to it is small enough so as to avoid significant experimental errors.

Concerning the heating and cooling thermal strains for the three cycles, it is interesting to note that for each sample the cooling thermal strain associated to the total temperature range covered is practically constant, regardless of the cycle considered. The same conclusion was drawn in the earlier subsection as well. The numerical values of the cooling thermal strain for the three cycles of both samples studied, M149-A and KAYENTA K1, are shown on figures 4 and 5, respectively.

#### Invariability of the Cooling Thermal Strain-Temperature Curve.

The observations that have been made regarding the constant value exhibited by the cooling thermal strain in the total temperature range for a given sample, regardless of its thermal history, strongly suggest the possibility that, provided the stress conditions on the rock are kept constant, the cooling thermal strain versus temperature curves exhibit the same pattern independently of the thermal history of the rock. In order to confirm such an assumption, the cooling strain-temperature curves of the cycles shown in figures 2 - 5 were redrawn using a common origin at 280°C, and the results are shown in figures 6 - 9, which provide enough experimental evidence in favor of the proposed concept about the invariability of the cooling thermal strain.

A practical application of this concept, as it was mentioned before, is the inference of the thermal expansion behavior corresponding to a stabilized rock from the cooling thermal strain-temperature curve of any cycle. This means that all the information regarding the thermal expansion behavior of a rock subjected to a given confining pressure, can be obtained from a single first cycle, but not from the heating thermal strain versus temperature curve only, since this curve is dependent on the thermal history of the rock. Another application of the invariability of the cooling thermal strain-temperature curve will be shown in the next subsection.

#### Effect of Confining Pressure on Bulk Thermal Expansion.

Type C tests were carried out to investigate the effect of confining pressure on bulk thermal expansion behavior. Information on the experimental conditions and the samples tested was given before and is summarized in table 2. The results for samples M94-A and KAYENTA K2 are shown in figures 10 and 11, respectively. The bulk thermal strain versus temperature cycles for the confining pressures of 3 MPa, 17.2 MPa and 34.4 MPa are plotted using a common origin at 25°C.

The problem involved in analyzing the effect of confining pressure on bulk thermal expansion from figures 10 and 11, is that the heating strain-temperature curves are influenced by the previous thermal treatment underwent by the rock sample. Thus, the differences that may exist between any two heating curves are the sum of the influence of confining pressure itself plus the effect associated to the thermal history of the rock. Therefore, an analysis of the effect of confining pressure from heating strain-temperature curves requires that these effects be separated. On the other hand, the invariability of the cooling strain-temperature curves with respect to the thermal history was demonstrated before; thus, any observable discrepancies between cooling strain curves can be attributed to the effect of the confining pressure only. Using this approach and taking into account that for a thermomechanically stabilized rock at a given pressure, the heating strain curve is very similar to its corresponding cooling strain curve (see figures 2 - 5), the isolated effect of confining pressure on bulk thermal expansion can be estimated by plotting the cooling strain-temperature curves from a common origin at 25°C. Applying this method to the cases under study, samples M94-A and KAYENTA K2, the results shown in figures 12 and 13 were obtained. For sample M94-A, the effect of confining pressure on bulk thermal expansion in the range from 3 MPa to 34.4 MPa is rather small and erratic. On the other hand, for sample KAYENTA K2 the effect of increasing confining pressure is to reduce the thermal strain at a given temperature. At high temperatures (> 150°C), this effect is more significant for the 3 MPa to 17.2 MPa interval than for the 17.2 MPa to 34.4 MPa interval.

Bulk thermal expansion measurements at 3 MPa and 20.7 MPa were also carried out on samples BERE A 1 and COLTON 1 in the range from 25°C to 280°C with no temperature cycling. The results of these measurements are presented in table 3 by means of average thermal expansion coefficients for the 25°C to 280°C range, from which the effect of confining pressure on bulk thermal expansion can be inferred.

#### The Matrix Thermal Expansion Concept:

In the following, the concept of matrix thermal expansion introduced by Contreras et. al. (1982) is analyzed with relation to its physical significance and applications. It has been pointed out by some authors, Somerton et. al. (1981) among others, that it is the expansion of mineral grains into the pore space that causes the decrease in pore volume with increased temperature, since there is less resistance to grain expansion into the pore space than to displacing adjacent grains. From this observation it can be inferred that for a confined sample, that is a jacketed sample subjected to a confining pressure higher than a pore pressure, the observable bulk thermal expansion should be

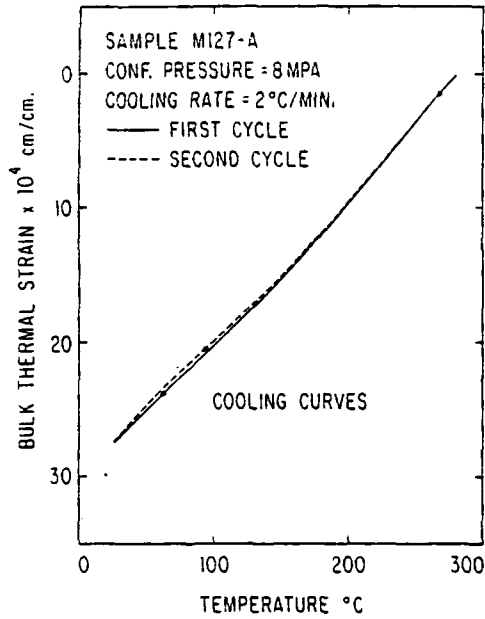


Figure 6. Strain-temperature cooling curves of sample M127-A. (Redrawn from Fig.2 using a common origin at 280°C).

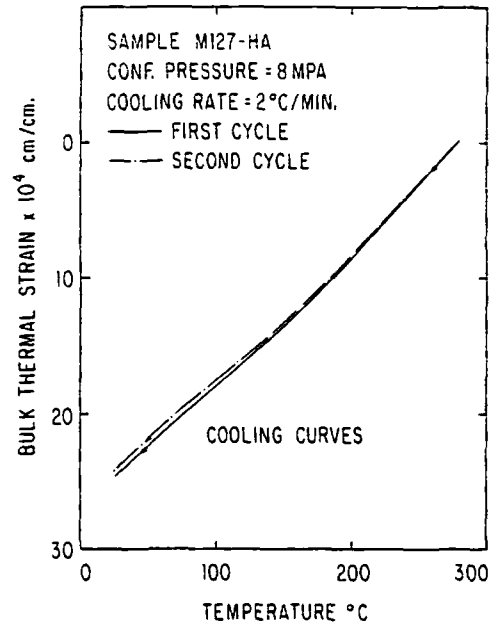


Figure 7. Strain-temperature cooling curves of sample M127-HA. (Redrawn -- from Fig.3 using a common origin at 280°C).

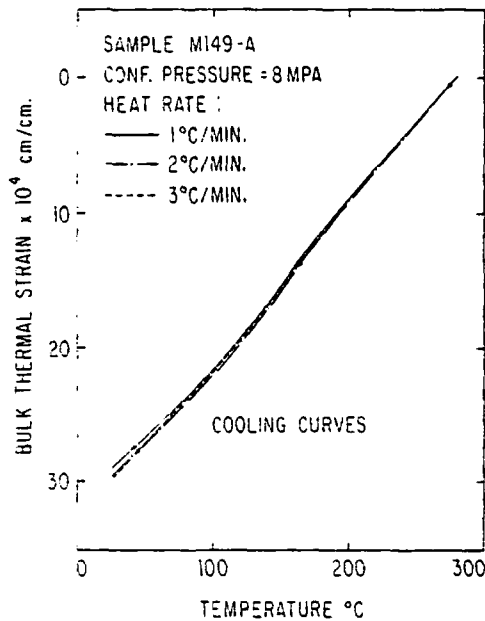


Figure 8. Strain-temperature cooling curves of sample M149-A. (Redrawn from Fig.4 using a common origin at 280°C).

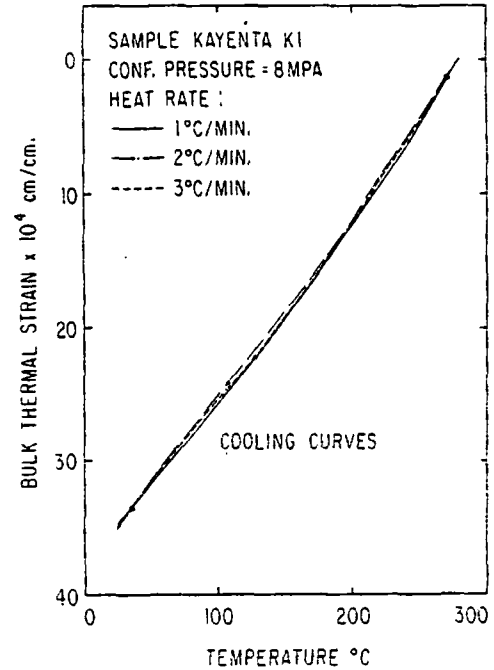


Figure 9. Strain-temperature cooling curves of sample KAYENTA K1. (Redrawn from Fig.5 using a common origin at 280°C).

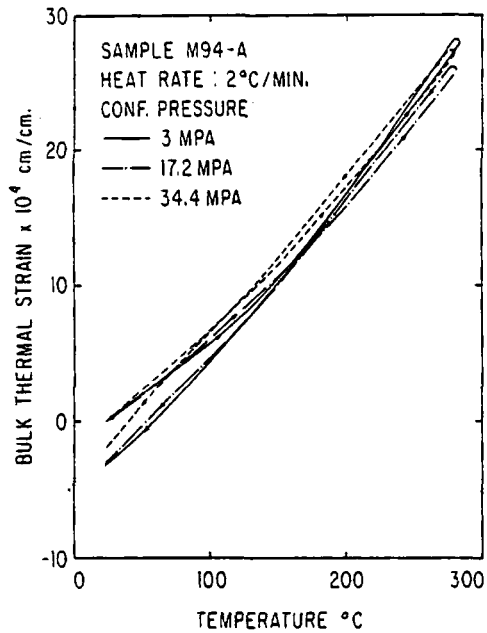


Figure 10. Combined effect of confining pressure and temperature cycling on bulk thermal expansion of sample M94-A.

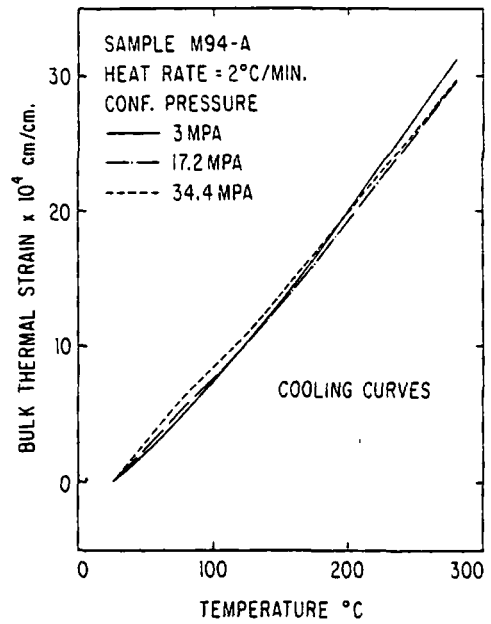


Figure 12. Isolated effect of confining pressure on bulk thermal expansion of sample M94-A. (As inferred from strain-temperature cooling curves).

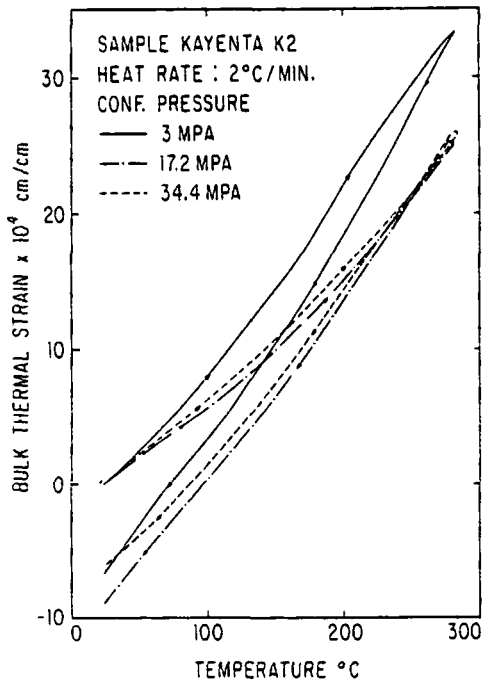


Figure 11. Combined effect of confining pressure and temperature cycling on bulk thermal expansion of sample KAYENTA K2.

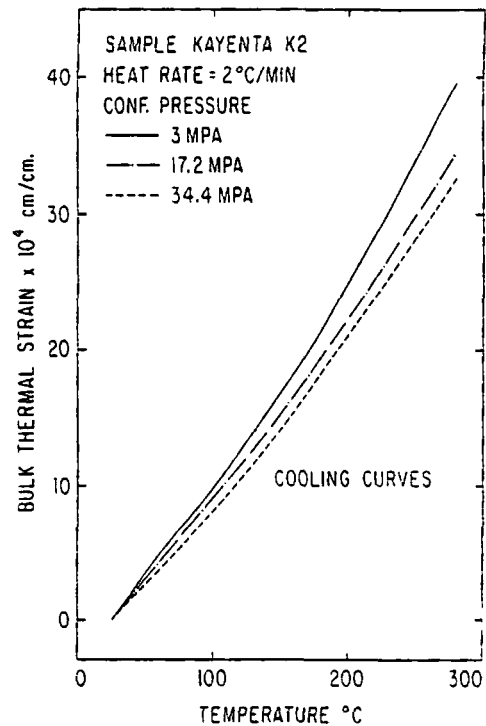


Figure 13. Isolated effect of confining pressure on bulk thermal expansion of sample KAYENTA K2. (As inferred from strain-temperature cooling curves).



smaller than the thermal expansion experimented by the solid material or rock matrix.

In order to evaluate the matrix thermal expansion of a confined rock subjected to given confining pressure  $P_c$  and pore pressure  $P_p$ , it is required to suppress the preferential expansion of the mineral grains into the pore space by making the resistance opposed to the expansion of grains equal towards any direction. This can be accomplished if a pressure equal to the mean isotropic stress in the rock is applied in the pore space in such a way that the isotropic stress is kept constant to avoid any stress difference which could affect the matrix thermal expansion to be determined. It can be shown that these conditions are achieved by increasing both the confining pressure and the pore pressure up to a common value  $P_o$  given by

$$(1) P_o = \frac{P_c - \phi P_p}{1 - \phi}$$

where  $\phi$  is the porosity of the rock. Therefore the matrix thermal expansion behavior of a rock subjected to  $P_c$  and  $P_p$  can be inferred from thermal expansion measurements carried out either on the jacketed rock subjected to  $P' = P_c = P_p$  or on theunjacketed rock subjected to a hydrostatic pressure equal to  $P_o$ .

The matrix thermal expansion behavior of some sandstones was determined by running tests type D. In order to provide a comparison frame to analyze differences between matrix and bulk thermal expansions, matrix tests were run on samples obtained from the same piece of rock as the samples used for type C bulk tests. The effect of temperature cycling and confining pressure on matrix thermal expansion behavior of samples M94-B and KAYENTA K2 is shown in figures 14 and 15 respectively. It is interesting to note that at the end of the first temperature cycle (confining pressure = 3 MPa) a permanent positive strain results, which is probably indicative that some kind of irreversible microstructural alteration occurs in the rock. On the other hand, the thermal strain versus temperature behavior for the second cycle (confining pressure = 34.4 MPa) is highly reversible. This suggests that the assumed microstructural damage is temperature-dependent only.

Matrix and bulk thermal strain-temperature curves for the heating part of temperature cycles are shown in Fig. 16 for samples M94-A (matrix data) and M94-B (bulk data). The differences that exist between matrix strain and bulk strain for the same confining pressure at given temperature, provide evidence in favor of the concept that preferential expansion of the mineral grains occurs towards the pore space. To this point, it has to be pointed out in accordance with the discussion of the latter subsection, that to accomplish a better comparison with bulk thermal expansion data for 3MPa and 34.4 confining pressure matrix thermal expansion measurements should have been carried out at 3.6 MPa and 40.9 MPa respectively.

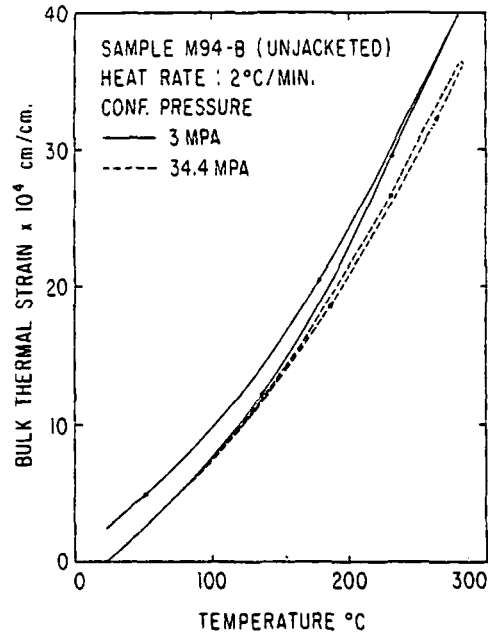


Figure 14. Effect of confining pressure and temperature cycling on matrix thermal expansion of sample -- M94-B.

#### Estimation of the Effect of Temperature on Porosity from Bulk and Matrix Thermal Expansion Measurements.

Determination of the effect of temperature on porosity is a subject of interest because of its practical implications in reservoir engineering. The traditional approach proposed to investigate this effect consists of calculating the fractional change in porosity  $\Delta\phi/\phi_o$  from experimental data on fractional change in bulk volume  $\Delta V_B/V_B$  (normally considered to be three times the linear bulk strain) and fractional change in pore volume  $\Delta V_P/V_P$ . The basic equation used is

$$(2) \frac{\Delta\phi}{\phi_o} = 1 - \frac{1 - \frac{\Delta V_P}{V_P}}{\frac{\Delta V_B}{V_B}}$$

Greenwald et. al. (1982) used this method to calculate the effect of temperature in the range from 40° to 170°C on fractional porosity change for Boise, Berea and Bandera sandstones under 20.7 MPa confining pressure and 6.9 MPa pore pressure. The result reported by Greenwald for the Berea sandstone is shown in Fig. 17. Further, from data on linear thermal expansion and pore volume contraction for the same outcrop rock by Somerton (1980) and Somerton et. al.

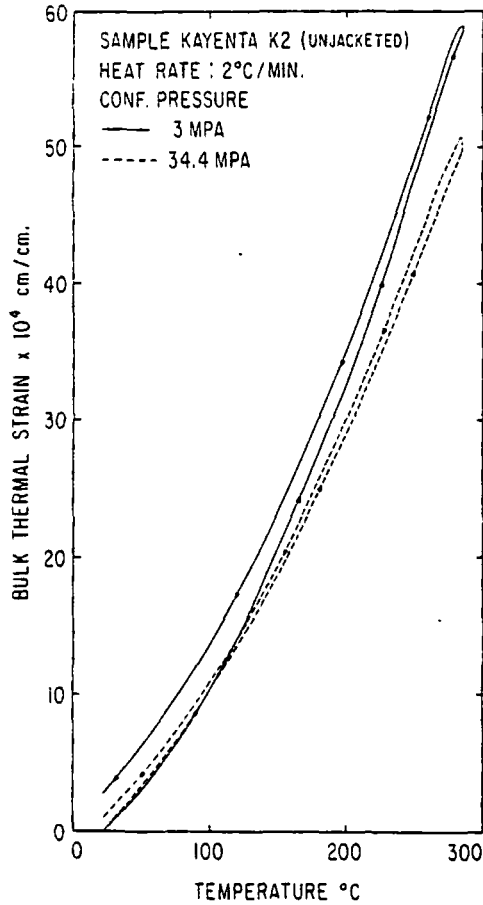


Figure 15. Effect of confining pressure and temperature cycling on matrix thermal expansion of sample KAYENTA K2.

(1981), we calculate the effect of temperature on porosity and the result is also shown in Fig. 17. The discrepancy exhibited by the results shown arises from the differences between the pore volume contraction data used by Greenwald and the data presented by Somerton. This matter was referred to in the literature review of the present work.

On the other hand, provided the rock is isotropic, the effect of temperature on porosity may also be expressed mathematically as

$$(3) \frac{\phi_T}{\phi_{T_0}} = \frac{1}{\phi_0} \{1 + (\phi_0 - 1) e^{3(E_s - E_B)}\}$$

where:

$\phi_T$  = Porosity at temperature T

$\phi_{T_0}$  = Porosity at temperature  $T_0$

$E_s$  = Linear matrix thermal strain at temperature T

$E_B$  = Linear bulk thermal strain at temperature T.

Using matrix and bulk linear thermal expansion data obtained from type C and D tests, we calculated through equation (3) the effect of temperature on porosities for sandstones BEREA and KAYENTA and the results are presented in Figs. 17 and 18 respectively. Our results for BEREA sandstone show a fair agreement with the values we calculated from Somerton's data, but they differ considerably from the results reported by Greenwald.

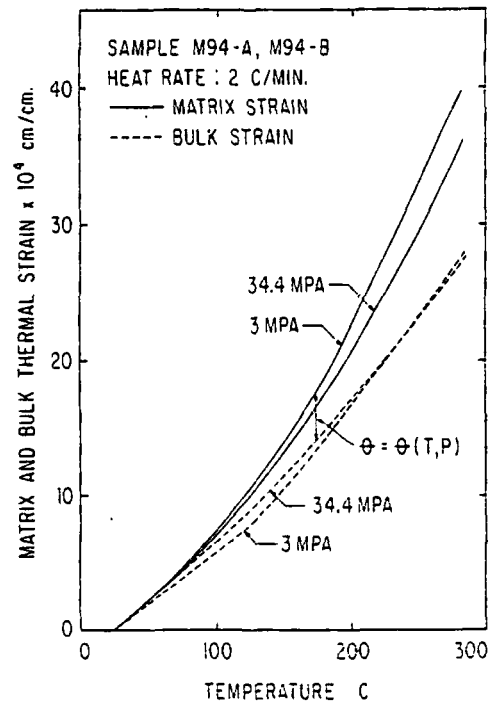


Figure 16. Comparison between matrix and Bulk thermal strain of samples M94-A and M94-B.

Results of Research on Thermal Expansion Isotropy:

The assumption that sedimentary rocks are isotropic concerning thermal expansion behavior is very frequently adopted; for example when it is considered that the volumetric strain equals three times the linear strain. The validity of

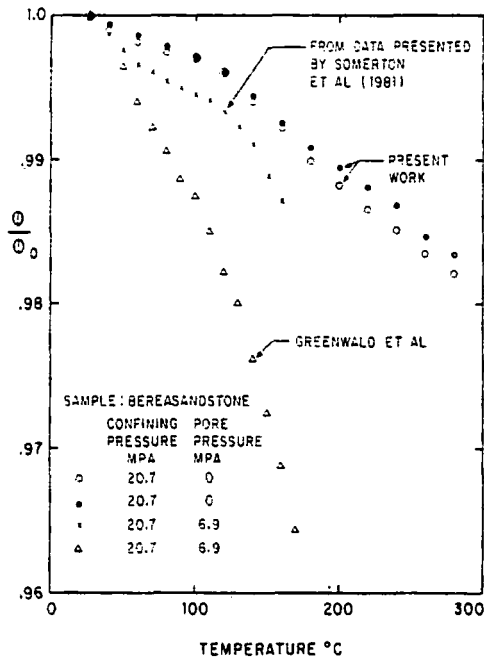


Figure 17. Effect of temperature on porosity of Berea sandstone as reported by different authors.

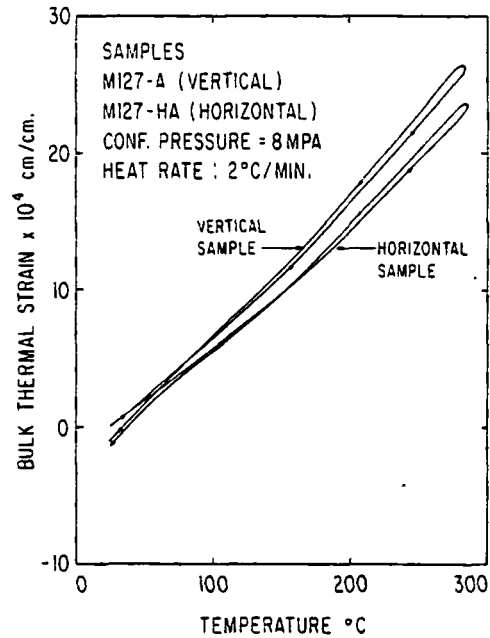


Figure 19. Effect of orientation with respect to the bedding plane on bulk thermal expansion. (From data presented in Figs. 2 and 3).

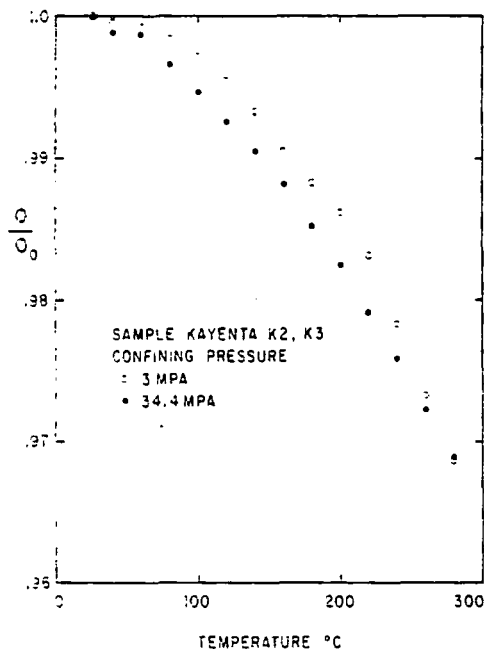


Figure 18. Effect of temperature on porosity of sample KAYENTA K2, K3.

this assumption was investigated in the present work by measuring the bulk thermal expansion of two twin samples obtained from the same piece of rock; one of them was cut parallel to the bedding plane (sample M127-HA) and the other one was cut perpendicular to the bedding plane (sample M127-A). These samples were also used to investigate temperature cycling effects and the results obtained were presented before (see Figs. 2 and 3). Overlapping the thermal strain versus temperature curves for the second cycles of samples M127-A and M127-HA, as taken from Figs. 2 and 3, the result shown in Fig. 19 is obtained. The thermal strain exhibited by the vertical sample is higher than the thermal strain exhibited by the horizontal sample at a given temperature, thus suggesting that the thermal expansion isotropy assumption for sedimentary rocks may not be a good approach to simplify analysis. Of course, more investigation has to be conducted to determine the extent of thermal expansion anisotropy in sedimentary rocks.

#### Thermal Expansion Coefficients:

The results of some of the tests carried out are not presented explicitly by means of thermal strain-temperature curves. However, thermal expansion coefficients were calculated from thermal strain versus temperature data for all of the tests carried out. The results are presented in Table 3.

TABLE 3. Thermal Expansion Coefficients of the Samples Tested.

SAMPLE	CONFINING PRESSURE MPa		LINEAR THERMAL EXPANSION COEFFICIENTS °C <sup>-1</sup> X 10 <sup>6</sup>							
			BULK				MATRIX			
			TEMPERATURE INTERVAL °C				TEMPERATURE INTERVAL °C			
			40-70	140-170	240-270	AVG(25-280)	40-70	140-170	240-270	AVG(25-280)
M94-A (1)	3	H-2	7.2	12.3	13.5	10.8				
		C-2	9.9	12.8	14.3	12.3				
	17.2	H-2	8.2	10.5	12.7	10.0				
		C-2	10.7	11.7	13.0	11.5				
	34.4	H-2	9.0	10.7	12.7	10.7				
		C-2	11.9	11.7	12.2	11.7				
M94-B (2)	3	H-2					10.1	15.9	20.6	
	34.4	H-2					9.4	13.6	19.7	
M127-A (3)	8	H-2	7.8	9.4	10.3	10.0				
		C-2	9.7	10.9	12.9	10.7				
		H-2	8.9	10.2	11.3	8.1				
		C-2	10.7	10.6	12.3	9.7				
M127-HA (4)	8	H-2	7.5	8.2	9.4	8.1				
		C-2	9.5	9.7	11.3	9.7				
		H-2	7.9	8.3	9.8	8.9				
		C-2	9.4	9.4	11.1	9.7				
M149-A (5)	8	H-2	8.3	13.5	10.9	10.5				
		C-2	9.9	13.8	10.9	11.5				
		H-2	8.7	14.0	12.0	11.0				
		C-2	11.3	13.8	11.9	11.6				
		H-3	8.7	13.3	12.6	11.0				
		C-3	11.6	14.7	11.0	11.7				
KAYENTA K1 (6)	8	H-1	7.7	12.1	11.3	10.6				
		C-1	12.0	14.3	16.1	13.8				
		H-2	9.0	14.3	12.1	12.4				
		C-2	13.1	14.0	15.9	13.7				
		H-3	9.9	14.2	15.3	12.6				
		C-3	13.0	14.1	16.1	13.8				
KAYENTA K2 (7)	3	H-2	10.9	14.6	11.7	12.9				
		C-2	14.2	15.1	20.1	15.5				
	17.2	H-2	7.9	10.3	13.0	9.9				
		C-2	12.8	13.8	15.2	13.5				
	34.4	H-2	8.8	10.4	12.2	10.1				
		C-2	10.7	13.5	14.9	13.0				
KAYENTA K3 (8)	3	H-2					13.5	24.3	33.4	22.1
	34.4	H-2					12.6	20.2	25.1	18.9
BEREA 1 (9)	3	H-2	10.2	14.5	15.4	12.8				
	20.7	H-2	10.6	13.0	15.8	12.5				
BEREA 2 (10)	3	H-2					12.1	21.9	20.5	18.0
	20.7	H-2					13.1	19.6	18.4	17.3
COLTON 1 (11)	3	H-2	10.9	17.1	16.3	14.8				
	20.7	H-2	9.8	12.5	13.6	11.7				
COLTON 2 (12)	3	H-2					12.7	18.5	14.8	15.9
	20.7	H-2					12.7	14.8	17.2	14.3

Note: H and C in the confining pressure column indicate whether the reported data in the row correspond to the heating or to the cooling part of the temperature cycling respectively.

Thermal expansion coefficients were calculated both for heating and cooling curves in the intervals of 40°C to 70°C, 140°C to 170°C and 240°C to 270°C, using a linear regression scheme with at least ten experimental data points for each interval. The correlation coefficient was higher than 0.99 in all the cases. Furthermore, average thermal expansion coefficients for the total temperature range covered (25°C to 280°C) were also calculated and the results are also reported in Table 3.

#### SUMMARY AND CONCLUSIONS

An extensive experimental program focused to investigate the thermal expansion behavior of sedimentary rocks has been carried out. The significant findings and conclusions from this work can be summarized as follows:

1. At a given confining pressure, after a first irreversible thermal strain-temperature cycle samples become thermomechanically stabilized and further cycles are almost reversible, repeatable and with no considerable hysteresis. However, a rock sample stabilized at a given pressure will again exhibit an irreversible thermal strain-temperature behavior if the confining pressure is increased up to a new value. This suggests that the compaction experimented by the rock arises from a combined effect of temperature and pressure.
2. Differences in heating rates in the range from 1°C/min to 3°C/min do not affect the thermal expansion behavior of the sedimentary rocks studied.
3. At a given confining pressure, the cooling thermal strain versus temperature curves show the same pattern independently of the thermal history of the rock (as opposed to the heating curves that exhibit thermal history dependence).
4. The bulk thermal expansion behavior that a stabilized rock at a given pressure would exhibit, can be inferred from the cooling thermal strain-temperature curve of any cycle, even the first one, but not from the first heating strain temperature curve.
5. The effect of confining pressure on bulk thermal expansion is significant and well behaved for one of the two samples studied, but is rather small and erratic for the other sample. More investigation on this aspect has to be carried out to obtain further evidence to support some sort of conclusion.
6. The matrix thermal expansion behavior corresponding to a rock subjected to given confining pressure  $P_c$  and pore pressure  $P_p$ , can be inferred by measuring the thermal expansion of the rock subjected to confining pres-

sure  $P_c^*$  and to a pore pressure  $P_p^*$  given by

$$P_p^* = P_c^* = \frac{P_c - \phi P_p}{1 - \phi}$$

where  $\phi$  is the porosity of the rock.

7. For a rock subjected to given pressure conditions, the matrix thermal strain is higher than the bulk thermal strain at a given temperature; this is in agreement with the concept of preferential thermal expansion of mineral grains into the pore space.
8. The matrix thermal expansion behavior exhibited by the samples studied shows that strain remains in the rock after completion of the first temperature cycle. On the other hand, for the second cycle the thermal strain versus temperature behavior is highly reversible and with no hysteresis, even though a different confining pressure was applied on the samples during the second cycle. This suggests that the remaining strain of the first cycle arises because of structural damage caused by differential thermal expansion of the mineral grains when are heated during the first cycle. This structural damage is temperature dependent and occurs during the first temperature cycle only. Furthermore, it can be noted that the effect of increased confining pressure is to reduce the matrix thermal expansion at a given temperature.
9. The effect of temperature on porosity was estimated from matrix and bulk thermal expansion data for two sandstones and results were compared with earlier available data calculated from pore volume contraction and bulk thermal expansion data. Although the observed effect is rather small, more investigation on this particular subject should be conducted to establish ranges of porosity change as well as to determine a pattern of influence upon variable confining pressure.
10. Thermal expansion isotropy for sedimentary rocks is an assumption that should be adopted cautiously.
11. A big deal of data about thermal expansion coefficients of the samples tested is reported. Information concerning magnitudes and variation ranges of this parameter may be useful for reservoir engineering calculations that involve the thermal expansion behavior of sedimentary rocks.

#### ACKNOWLEDGEMENTS

We wish to thank Ing. Alfredo Mañón M. at Comisión Federal de Electricidad, Coordinadora Ejecutiva de Cerro Prieto, for his interest in this work. We also thank Ing. Sergio Mercado G., at Instituto de Investigaciones Eléctricas,

for his permission to accomplish the experimental program leading to this paper as part of project IIE-1663. Martín Uribe collaborated in the experimental work, Adrián Patiño drafted the figures and Mrs. María Eugenia Calderón and Mrs. Ma. de Lourdes Calderón made the typing; their participation is duly acknowledged.

#### REFERENCES

- Ashqar, P. I., (1979), "Thermal Expansion of Porous Rocks Under Stress". Master of Science Project Report, University of California, Berkeley, December 1979.
- Contreras, E., Iglesias, E., Bermejo, F. (1982), "Effects of Temperature and Stress on the Compressibilities, Thermal Expansivities, and Porosities of Cerro Prieto and Berea Sandstones to 9000 psi and 280°C". Proceedings 8th Workshop on Geothermal Reservoir Engineering. Stanford, California, December 14-16, 1982.
- Ennis, D. O., Butters, S. W., Lingle, R., Van Buskirk, R. G., Prater, F. R. (1979). "Capabilities to Measure Geothermal Material Properties at Simulated In-Situ Conditions". Terratek Report TR79-49.
- Greenwald, R. F., Ashqar, P. I., Somerton, W.H., (1982). "Thermal Expansion Behavior of Porous Rocks Under Stress". Proceedings of the Thermal Expansion Conference N° 7. Plenum Press, 1982. David C. Larsen, Editor.
- Janah, A., (1980). "Pore Volume Variation with Temperature for Porous Rocks Under Stress". M. S. Report, University of California, Berkeley. Department of Mechanical Engineering.
- Somerton, W. H., Selim, M. A., (1961). "Additional Thermal Data for Porous Rocks-Thermal Expansion and Heat of Reaction". 31st Annual California Regional Meeting of SPE, October 21-22, 1961.
- Somerton, W. H., (1980). "The Behavior of Rock-Fluid Systems at Elevated Temperatures and Pressures". Annual Report 1981, Earth Sciences Division. Lawrence Berkeley Laboratory. University of California.
- Somerton, W. H., Janah, A. H., Ashqar, P. I., (1981). "Thermal Expansion of Fluid Saturated Rocks Under Stress". SPWLA Twenty-Second Annual Logging Symposium. June 23-26, 1981.

SUBJ  
GTHM  
TGE

I

UNIVERSITY OF UTAH  
RESEARCH INSTITUTE  
EARTH SCIENCE LAB.

## TAXATION OF GEOTHERMAL ENERGY

Sharon Wagner

### INTRODUCTION

Whenever the issues of taxes, tax credits, tax incentives, depletion allowances, and/or intangible deductions are raised, it must be remembered that there are 51 tax systems in this country: one federal and 50 state. State corporate and personal income tax structures may or may not parallel the federal corporate and personal income tax structure. Generally the states have followed the federal government's lead in constructing their own tax systems. However, in the post-Proposition 13 mood of the electorate, it is not clear that states will adopt tax incentives for geothermal resources. Moreover, since the geothermal tax incentives adopted as part of the 1978 Energy Tax Act are so new, there will be some uncertainty as to their application until the IRS promulgates its Treasury Regulations for these new internal Revenue Code (IRC) sections. Until that time, it is safe to assume that the IRS will follow (with certain exceptions) the Treasury Regulations and court cases that are applied to the oil and gas industry. Most of the Treasury Regulations cited in the footnotes in the text below were written for the oil and gas industry but they are generally applicable to geothermal.

### THE FEDERAL TAX SYSTEM

Prior to the passage of the Energy Tax Act of 1978,<sup>1</sup> the federal tax treatment of geothermal resources was based mainly on judicial decisions; not statutory authority. In 1969 the 9th Circuit Court of Appeals<sup>2</sup> held that the federal intangible drilling deduction<sup>3</sup> and the percentage depletion allowance<sup>4</sup> applied to the geothermal drilling at The Geysers. To reach this result the Court held that geothermal steam was "gas" within the meaning of §263(c) and §613(b) (1) of the IRC.

In 1975 the Code was revised to provide a 22% percentage depletion allowance for any geothermal deposit in the U.S., or a U.S. possession that was determined to be gas.<sup>5</sup> But the IRS refused to follow either the Court decisions or the new Code provision and contested both the intangible drilling deduction and depletion allowance on activities and income from The Geysers. Furthermore, because of the IRS intransigence the tax treatment of drilling a geothermal deposit that was hot water instead of the steam was even less clear.<sup>6</sup>

---

<sup>1</sup>P.L. 95-618, §403(b), amending IRC, §613A(b).

<sup>2</sup>Arthur E. Reich, 52 T.C. 700 (1969), aff'd, 454 F. 2d 1157 (9th Cir. 1972) and George D. Rowan, 28 T.C.M. 797 (1969).

<sup>3</sup>IRC §263(c).

<sup>4</sup>IRC §613.

<sup>5</sup>P.L. 94-455.

<sup>6</sup>In Miller v. United States, 78-1 U.S.T.C. P9127 (D.C.C.D. Cal. 1977) the federal district court denied the intangible drilling deduction to investors who drilled geothermal wells in Nevada in an area of hot water, not steam, reservoirs.

The Energy Tax Act of 1978 has eliminated most of the uncertainties of tax treatment of geothermal exploration and development. The new tax provisions can be used to promote capital investment and to generate for the investor certain tax savings which reduce the risk of investment. Furthermore, the definition of geothermal deposits<sup>7</sup> is broad enough to include all the various forms of geothermal energy including dry steam, hot water or dry hot rocks. The act covers three basic subjects: intangible drilling costs, depletion allowance, and tax credits.

## I. INTANGIBLE DRILLING COSTS

### A. Option to Deduct Intangible Drilling Costs

§402 of the Energy Tax Act amends §263(c) of the IRC to allow a taxpayer the option to deduct as expenses intangible drilling costs (called "intangibles" or IDCs)<sup>8</sup> The costs of drilling and completing a geothermal well are divided for tax purposes into two classes: intangible drilling costs and equipment costs. The equipment costs must be capitalized and "recovered" through depreciation or depletion. Intangible drilling costs may be treated in two ways.<sup>9</sup>

<sup>7</sup>"A geothermal reservoir consisting of natural heat which is stored in rocks or in an aqueous liquid or vapor (whether or not under pressure)."

<sup>8</sup> Intangible drilling costs are defined by Part 5A, Temporary Income Tax Regulations for the Energy Tax Act, 45 Fed. Reg. 6779 (1980) (to be codified in 26 CFR Part 1) as any cost incurred which in itself has no salvage value and which is "incident to and necessary for the drilling of wells and the preparation of wells for the production of geothermal steam or hot water." Such expenditures expressly include "labor, fuel, repairs, hauling, supplies etc." that are used (1) in the drilling, shooting and cleaning of wells; (2) in such clearing of ground, road making, surveying, and geological works as are necessary in preparation for the drilling of wells; and (3) in the construction of such derricks, tanks, pipelines, and other physical structures as are necessary for the drilling of wells and the preparation of wells for the production of geothermal steam or hot water.

<sup>9</sup> Since the geothermal provision for the option to expense intangibles is separate from oil and gas activities, a taxpayer may make one kind of election for his geothermal deposits and a different one for his oil and gas wells. For example, he could decide to expense intangibles for both geothermal and oil and gas properties or he could capitalize oil and gas and expense geothermal intangibles.



They may be deducted as expenses (in tax terminology they may be expensed) in the year in which they are incurred or they may be capitalized and deducted over a certain period of time as depreciation or depletion.<sup>10</sup> Allowing a taxpayer to expense (deduct) all the intangibles in the year in which they were incurred gives the taxpayer a kind of "accelerated depreciation."

The taxpayer must make his election to expense or to capitalize intangibles in his first taxable year in which he incurs such costs.<sup>11</sup> Once the election is made, the taxpayer must treat such expenditures on all geothermal properties in the same manner for all future years.<sup>12</sup> For example, if Taxpayer (T)<sup>13</sup> has spent \$50,000 of intangible costs, T may claim as a deduction on his income tax return the \$50,000 of intangible costs. But if T decides to capitalize intangible drilling costs T will not take \$50,000 for 1978, but instead will deduct this amount over a given period of time as depreciation or depletion. However, if the taxpayer elects to capitalize his intangibles, he is granted a second election for dry or productive wells.<sup>14</sup>

<sup>10</sup>Part 5A, Temp. Reg. supra note 8, states that intangibles, if capitalized, are to be separated and recovered as depreciation or depletion. Intangibles not represented by physical property (clearing ground, draining, road making, surveying geological work, excavating, grading, and the drilling, shooting, and cleaning of wells) are to be recovered through depletion. But intangible expenditures represented by physical properties (wages, fuel, repairs, hauling, supplies, etc.) are to be recovered through depreciation.

<sup>11</sup>A taxpayer must make a clear election either to expense or to capitalize. If he does not, the IRS will hold that he elected to capitalize intangibles. It is best that if a taxpayer desires to expense intangibles, he include with his income tax return an express statement of election to expense in accordance with the option.

<sup>12</sup>U.S. Treasury Regulation §1.611-4(e)

<sup>14</sup>But this second election need not have to be exercised until the first year in which a dry hole is drilled.

<sup>13</sup>The owner of the operating rights in a property who has the responsibility to develop the property is granted the option of expensing intangibles. But each taxpayer, regardless of his relationship to another taxpayer, is entitled to a separate election. Thus each partner in a partnership is entitled to a separate election. Trusts as separate taxpayers are entitled to an election regardless of the kind of election made by the beneficiaries.

The costs incurred in drilling a nonproductive well may be deducted by the taxpayer as an ordinary loss provided a proper election is made. But the taxpayer must make a clear statement of election to deduct as ordinary losses intangible drilling and development costs of nonproductive wells. If a clear statement is not made, such costs can be recovered only through depreciation and depletion.

But a noncorporate taxpayer, a Subchapter S corporation or a personal holding company that decides to expense intangibles instead of capitalizing them, may be subject to one of the following: the minimum tax (see "B"); a limitation on deductions to the amount "at risk" (see "C"); recapture of intangible deductions if the property is sold at a profit (see "D").

#### B. Preference Income-Minimum Tax

Some types of income are given preferential treatment by special provisions of the tax law. A minimum tax applies to a number of items that are considered to be of a tax preference nature. These types of income include capital gains, stock options, and income offset by depletion, amortization, and intangible drilling costs. The tax is computed by totaling all the items of tax preference, then reducing this amount by the greater of \$10,000 or one-half a taxpayer's regular income tax after reduction by credits. A flat 15% rate is then applied against the balance.<sup>15</sup>

---

<sup>15</sup>A taxpayer may be able to claim the unused part of certain credits against his minimum tax. Also if a taxpayer has a net operating loss that remains to be carried forward to a succeeding tax year, the minimum tax otherwise due may be deferred in an amount of up to 15% of the net operating loss to be carried forward to subsequent tax years when the loss is absorbed. In the years when the loss is absorbed, the taxpayer will be liable for the minimum tax deferred in an amount equal to 15% of the net operating loss absorbed in each year. See IRC §57(a)(11).

If taxpayer has "excess intangible drilling costs" that exceed net geothermal income, he will have preference income subject to the minimum tax. Intangible drilling costs are considered to be excessive when the intangible drilling and development costs of a geothermal well allowable for the tax year are greater than the sum of (1) the amount allowable if the costs had been capitalized and straight-line recovery of the intangibles had been used and (2) the net income for the tax year from the geothermal property.

Straight-line recovery means the rateable amortization of such intangibles over the 120 month period beginning with the month in which production from the well begins (or, if elected, any method which would be permitted for purposes of determining cost depletion). Net income from all such property reduced by any deductions allocable to the properties, except intangible drilling and development costs in excess of straight recovery.

This preference does not apply to taxpayers who elect to capitalize by straight-line recovery their intangibles. Nor does it apply to nonproductive wells.<sup>16</sup>

Special rules apply to corporations in computing their minimum tax<sup>17</sup>. And the IRS will publish rules under which items of tax preference of both individuals and corporations are to be properly adjusted where the tax treatment that gave rise to the preference does not result in a reduction of the taxpayer's income tax for any tax year.

In effect what this provision does is to lessen the benefit of the option to expense intangible drilling costs. Few taxpayers now have geothermal income and if they chose to expense intangibles, they will have preference income (that is, the amount they deduct by expensing intangibles will definitely be greater than the sum of intangibles capitalized and net geothermal income).

#### C. Losses Limited to Amount at Risk. <sup>18</sup>

---

<sup>16</sup>Nonproductive wells are those which are plugged and abandoned without having produced steam or hot water in commercial quantities for any substantial period of time.

<sup>17</sup>See IRS Publication 542, Corporations and the Federal Income Tax.

<sup>18</sup>See IRC §465(c).

The 1976 Tax Reform Act limited the tax benefits available to persons engaging in oil and gas operations. These same limitations with some changes were extended to geothermal operations by the 1978 Energy Tax Act.

Before passage of the 1976 Act a taxpayer could take deductions up to the amount of this cost (or "basis") in a business or investment venture. But the basis of a taxpayer often included expenditures financed by nonrecourse loans for which the taxpayer had no personal liability (i.e., he had nothing "at risk" because of the way the loan was made to him or to an investment group). Such leveraged nonrecourse loans were often employed by investors to finance drilling and development costs of oil and gas activities. Since a taxpayer could elect to expense intangible drilling costs, he could take deductions far in excess of his own actual investment. This kind of investment was desirable for a high bracket taxpayer because the large deductions for intangibles could be used to offset income earned from other sources.

The 1976 law added §465 to the IRC and limited the amount of losses<sup>19</sup> deductible by a taxpayer engaged in exploring for and exploiting oil and gas. The taxpayer's deduction cannot exceed the total amount the taxpayer has at risk in the venture. Deductions taken for intangibles are considered losses for purposes of this section.

The Revenue Act of 1978 changed the "at risk" rules for years beginning after December 31, 1978. The most significant change is that previously allowed losses must be recaptured when the taxpayer's "at risk" amount is reduced below zero. But only the excess of the losses previously allowed in a particular "at risk" activity over any amounts previously recaptured will be recaptured under this provision. However, such recaptured losses may be deductible in a later year if at the "at risk" is later increased.

The practical effect of these "at risk" provisions is to eliminate the use of nonrecourse financing to increase available deductions.

#### D. Recapture of Intangible Costs Expenses As Ordinary Income on Disposition of Geothermal Property.

Probably the most far-reaching change of the 1976 Tax Reform Act affecting corporate and noncorporate taxpayers is the requirement that upon the disposition of oil and gas property taxpayers are required to recapture all or some part of the intangible costs incurred as ordinary income if the property is disposed of at a gain (a profit). These recapture provisions were extended by the Energy Tax Act of 1978 to intangible drilling costs incurred in connection with geothermal deposits.<sup>20</sup>

---

<sup>19</sup>A loss is the excess of allowable deductions allocable to a particular activity over the income derived from the activity during the taxable year.

<sup>20</sup>P.L. 95-618, §402(c), amending IRC §1254(a).

This recapture provision applies only to intangibles which the taxpayer elects to expense in the year in which they were incurred and does not apply to intangibles which were capitalized. The amount of intangibles recaptured as ordinary income (instead of as capital gains) is the lesser of (1) the intangible costs incurred (reduced by an amount which would have been allowed as cost depletion had such intangibles been capitalized) or (2) the gain realized on the disposition. Or, in other words, the amount recaptured and taxed as ordinary income is the amount that the intangibles deducted exceed that which would have been allowed had the intangibles been capitalized and amortized on a straight-line basis (120 months) from the time the property went into production.<sup>21</sup>

## II. PERCENTAGE DEPLETION

The IRC provides two methods of computing a depletion allowance: cost depletion and percentage depletion. Cost depletion provides for a deduction for the taxpayer's basis (cost) in the property in relation to the production and sale of minerals from the property. On the other hand, percentage depletion is a statutory concept that provides for a deduction of specified percentages of the gross income from the property. The deduction, however, cannot exceed 50% of the net income from the property. A taxpayer is required to compute depletion both ways and to claim the larger of the two amounts.

A depletion allowance reduces the taxpayer's basis in a property but the total amount taken as a depletion allowance is not restricted to the taxpayer's basis. Even though cost depletion will be zero after the taxpayer's initial basis has been recovered (for example, T deducts \$5,000 per year for five years for a total of \$25,000 - the amount of his original investment), the taxpayer may continue to claim a percentage depletion based on income from the property.<sup>22</sup>

§403 of the 1978 Energy Tax Act grants percentage depletion on income from geothermal deposits. The rate through 1980 is 22%. It decreases by 2% yearly until 1983 and thereafter the rate is 15%.

---

<sup>21</sup>It should be noted that there are questions as to the proper method of calculating the reduction of recapturable intangibles under this section.

<sup>22</sup>A depletion allowance on the income derived from production and sale of the minerals from a property is available only to the owner of an economic interest in that property. An owner of an economic interest can be an owner of mineral interests, royalties, working interests, overriding royalties, net profits interests or certain kinds of production payments.

This percentage depletion allowance is much more favorable than the one allowed oil and gas. It is not limited in any way to a specified amount of production. It has no 65% of taxable income limitation nor is it restricted to independent producers. However, the percentage depletion cannot exceed 50% of the taxable income from the property and is subject to the minimum tax-preference income rules.<sup>23</sup>

There is some question about the availability of depletion on minerals which are consumed by the producer of such minerals. Many manufacturers are now exploring and developing their own sources of energy supplies, particularly natural gas reserves and in some areas geothermal. But the depletion allowance is dependent upon the sale of a mineral. Some courts have held that no depletion is allowable for minerals consumed in the operation of the producing energy property. It is not clear, however, if a depletion allowance is precluded with respect to gas used in manufacturing operations. For example, the IRS ruled in 1968 that the value of dry gas manufactured from wet, gas and used as fuel for gasoline absorption plant is includible in determining "gross income from the property" for percentage depletion purposes, but the value of dry gas reinjected into the geological formation is not includible. One way for the corporate taxpayer to avoid the problem is to conduct its exploration and development activities through a wholly-owned subsidiary. The subsidiary could sell the gas to the parent at an arm's length price and create depletable gross income.

### III. TAX CREDITS

#### A. Residential Energy Credit

§101 of the 1978 Energy Tax Act provides for a nonrefundable tax credit for certain expenditures incurred for equipment which uses geothermal energy in a taxpayer's principal residence in the United States. The equipment must be new and must meet certain performance and quality standards; it must reasonably be expected to remain in production for five years. The credit is as follows: (a) 30% of the expenditure up to \$2000, (b) 20% of the expenditure from \$2000 to \$10,000. The maximum credit is \$2200. The credit may be carried over to future years for equipment purchased after April 20, 1977 and before January 1, 1986.

#### B. Additional Investment Tax Credit for Alternative Energy Property

A 10% investment tax credit in addition to the existing investment tax credit is available for geothermal equipment which qualifies as either "alternative energy property" or "specially defined energy property." Public utilities cannot benefit to the extent of "alternative energy property" but can use the credit for "specially defined energy property."

The business energy credit is limited to 100% of tax liability, except for solar or wind energy property on which the credit is refundable. Until the IRS issues its regulations on this new section it will not be completely clear what kind of equipment qualifies.

<sup>23</sup>The excess of the depletion deduction over the adjusted basis of the property at the end of the year (determined without regard to the depletion deduction for the year) is what would be preference income.

STATE TAX SYSTEMS<sup>24</sup>

Of the fifteen states with known geothermal resources Nevada, Texas, Washington and Wyoming have no state personal or corporate income tax. Alaska, Colorado, Hawaii, Idaho, Montana, and New Mexico apply their income tax levies to adjusted gross income as calculated for federal income tax. But five states have an independently determined income tax: Arizona, California, Louisiana, Oregon and Utah. Their differences from the federal law are largely due to the state provisions concerning percentage depletion for resources extraction industries.

Two states, California and Arizona, provide two examples of how complex the state tax picture can be. California has a franchise tax and a corporate income tax. The franchise is for the privilege of exercising a corporate franchise within the state. The tax rate is 9.6% for calendar or fiscal years ending in 1980. For subsequent years the rate is dependent on bank and corporation tax revenues. The following chart gives these rates.

1981	
Revenues Collected in 1979-80	Corporation Tax Rate for 1981
Less than \$2,950,000,000	9.6%
\$2,950,000,000--\$3,025,000,000	9.5%
\$3,025,000,000--\$3,100,000,000	9.45%
Greater than \$3,100,000,000	9.40%
1982	
Sum of Revenues Collected in 1979-80 and 1980-81	Corporation Tax Rate for 1982
Less than \$6,000,000,000	9.6%
\$6,000,000,000--\$6,075,000,000	9.50%
\$6,075,000,000--\$6,150,000,000	9.45%
\$6,150,000,000--\$6,225,000,000	9.40%
Greater than \$6,225,000,000	9.35%
1983	
Sum of Revenues Collected in 1979-81, 1980-81 and 1981-82	Corporation Tax Rate for 1983
Less than \$9,450,000,000	9.6%
\$9,450,000,000--\$9,525,000,000	9.50%
\$9,525,000,000--\$9,600,000,000	9.45%
\$9,600,000,000--\$9,675,000,000	9.40%
\$9,675,000,000--\$9,750,000,000	9.35%
Greater than \$9,750,000,000	9.30%

<sup>24</sup> For an extensive analysis of state tax systems see State Taxation of Geothermal Resources Compared with State Taxation of Other Energy Minerals, Sharon C. Wagner, published by the Geothermal Resources Council, Davis, CA.

Established in 1818 by Benjamin Silliman

THE FIRST SCIENTIFIC JOURNAL IN THE  
UNITED STATES

DEVOTED TO THE GEOLOGICAL SCIENCES  
AND TO RELATED FIELDS

Editors: JOHN ROGERS — JOHN H. OSTROM

Managing Editor: MARIE C. CASEY

Second-class postage PAID at New Haven, Conn. Published monthly, except July and September, at Kline Geology Laboratory, Yale University, New Haven, Conn. 06520.

Subscription rate \$15 per year (\$2.00 a number). Student rate \$10 per year (application blanks available on request). Postage prepaid to the Americas; 60 cents per year outside the Americas.

The JOURNAL completed its first series of 50 volumes in 1845, its second series of 50 volumes in 1870, its third series of 50 volumes in 1905, its fourth series of 50 volumes in 1920, its fifth series of 36 volumes in 1938. Since 1938 the numbering by series has been discontinued, and volumes are annual and bear the whole numbers as of 1818, that for 1950 being volume 237.

Available back numbers and volumes to 1955, also cumulative indices, may be obtained from *Walter J. Johnson, Inc.*, 141 Fifth Avenue, New York, N.Y. 10003; more recent numbers and volumes from the office of the AMERICAN JOURNAL OF SCIENCE, Kline Geology Laboratory, Box 2161, Yale Station, New Haven, Conn. 06520.

#### INSTRUCTIONS TO CONTRIBUTORS

Typescripts of articles submitted should be double-spaced (three copies), should follow the recommendations in the pamphlet *Suggestions to Authors*, 5th ed. (see below), and should be preceded by brief abstracts. They should be checked with special care before being submitted, to avoid changes in proof other than printer's errors. All measurements should be given in SI (metric) units.

References to literature should be listed alphabetically by authors at the end of the article; all references should be complete. For articles in journals or other serial publications, the reference should give in order: Author's name, year of publication, full title: name of periodical or series, volume number, inclusive pages. For books or other unnumbered publications, it should give: Author's name, year of publication, full title: place of publication, publisher, total number of pages. This form follows the recommendations in "Suggestions to Authors of the Reports of the United States Geological Survey," 5th ed. Washington, D. C., 1958 (Government Printing Office, \$1.75), which is also the standard used for abbreviating names of periodicals, etc. Citations within an article should be to author and year, with specific pages wherever appropriate.

Illustrations should be neat and legible and should include explanation of symbols used. Copy that cannot be reproduced cannot be accepted; it should be capable of reduction to not more than 4 by 7 inches, all lettering being at least 1/16 inch high after reduction. When necessary, one large map or table can be accepted, if it will not exceed 7 inches in width after reduction. Line drawings should be in black India ink on white drawing board, tracing cloth, or coordinate paper printed in blue and should be accompanied by clear originals or reduced photographs for use by the reviewers. Photographs should be positive prints. Photostatic and typewritten material cannot be accepted as copy for illustrations. Plates (photographs) and figures (line drawings) should each be numbered consecutively through each article, using arabic numerals. If two photographs form one plate, they are figures A and B of that plate.

Reprints. Thirty separate copies of each article will be furnished to the author free of cost and without previous notice from him; these will be without a cover. The cost of additional copies will, of course, be greater if the article is accompanied by plates involving unusual expense. Copies will be furnished with a printed cover giving the title, author, volume, page, and year, when specially ordered.

Page charges. Each institution sponsoring research reported in an article accepted for the JOURNAL will be asked to pay a charge of \$30.00 per printed page, due when galley proof is returned. Institutions or authors paying such charges will be entitled to 100 free reprints without covers (over and above the 30 free reprints furnished the author). No charge will be made if the author indicates that his institution is unable to pay them, and payment of page charges on an article will not in any case be a condition for its acceptance.

SUBJ  
GTHM  
THS

# American Journal of Science

SUMMER 1969

## THERMODYNAMICS OF HYDROTHERMAL SYSTEMS AT ELEVATED TEMPERATURES AND PRESSURES

HAROLD C. HELGESON

Department of Geology,

Northwestern University, Evanston, Illinois 60201

**ABSTRACT.** Chemical relations in hydrothermal systems can be described in terms of the thermodynamic properties of minerals, aqueous species, gases, and concentrated sodium chloride solutions. Sufficient thermodynamic data are available to permit calculation of equilibrium constants for a large number of hydrothermal reactions at high temperatures and pressures. Where these data are incomplete, the calculations involve entropy estimates, application of average heat capacities, and/or assumptions concerning the temperature dependence of thermodynamic variables and the relative importance of electrostatic and non-electrostatic interaction among the aqueous species in hydrothermal solutions. High temperature stoichiometric activity coefficients for individual ions can be calculated using deviation functions computed from osmotic coefficients for concentrated sodium chloride solutions. The results of such calculations, together with computed heat capacities, enthalpies, entropies, and equilibrium constants for many hydrothermal species and reactions at high temperatures are presented in tables and diagrams. The methods, assumptions, and equations employed in the calculations are summarized in general notation. The numerical information contained in the tables permits calculation of the solubilities of silicates, sulfides, carbonates, sulfates, and oxides in multicomponent hydrothermal solutions containing high concentrations of sodium chloride at elevated temperatures, and evaluation of the mass transfer accompanying irreversible reactions responsible for metasomatism and ore deposition in hydrothermal systems.

#### INTRODUCTION

The chemistry of electrolyte solutions at high temperatures has received considerable attention in recent years, and it is now possible to predict with confidence the thermodynamic characteristics of hydrothermal solutions to  $> 300^{\circ}\text{C}$  (Criss and Cobble, 1964a and b; Cobble, 1964, 1966a and b; Helgeson, 1967a). It is the purpose of this paper to summarize the equations and methods involved in applying such predictions to hydrothermal equilibria and to compute an internally consistent set of values for the thermodynamic properties of hydrothermal systems at high temperatures. The results of the calculations are presented in tables as well as diagrams to facilitate extrapolation to the supercritical region and to enable the reader to use the numerical values in his own investigations.

Most of the species and reactions considered below are important in hydrothermal processes involving "acid" aqueous solutions containing high sodium chloride concentrations. Electrolyte solutions of this kind occur in the Salton Sea geothermal system (White, Anderson, and Grubbs, 1963; Helgeson, 1968a), and they are commonly found in fluid inclusions in vein minerals (Roedder, 1963, 1965, 1967). Chloride-rich acid solutions are responsible for high temperature metasomatism (Orville, 1963; Helgeson, 1967b) and hydrothermal-rock alteration (Hemley, 1959; Hem-

UNIVERSITY OF UTAH  
RESEARCH INSTITUTE  
EARTH SCIENCE LAB.

729

UNIVERSITY OF UTAH  
RESEARCH INSTITUTE  
EARTH SCIENCE LAB.



ley, Meyer, and Richter, 1961; Hemley and Jones, 1964; Meyer and Hemley, 1967). In addition, both experimental (Barnard and Christopher, 1966; Hemley and others, 1967; Cloke, 1969) and theoretical (Helgeson, 1964, 1967c; Helgeson and Garrels, 1968; Helgeson, Garrels, and MacKenzie, 1969) evidence indicates that these solutions are capable of transporting and precipitating metals and sulfides in ore-forming concentrations at elevated temperatures.

Aqueous species contributing to hydrothermal processes involving acid chloride-rich solutions include  $\text{HCO}_3^-$ ,  $\text{HSO}_4^-$ ,  $\text{HS}^-$ ,  $\text{H}_2\text{CO}_3$  and  $\text{CO}_2(\text{aq})$ ,  $\text{H}_2\text{S}(\text{aq})$ ,  $\text{KCl}$ ,  $\text{NaCl}$ ,  $\text{HCl}$ ,  $\text{CaSO}_4$ ,  $\text{MgSO}_4$ ,  $\text{H}_2\text{SiO}_4$ , and chloride and sulfate complexes of the ore forming metals. There is little evidence that polynuclear metal ion complexes are important, or that chloride complexes of ferrous iron, calcium, magnesium, or aluminum form to significant degrees below  $\sim 300^\circ\text{C}$  (Sillén and Martell, 1964; Helgeson, 1964). Bicarbonate and bisulfate metal ion complexes and carbonate, bicarbonate, sulfate, and bisulfate complexes of sodium and potassium exhibit minor association below this temperature (Quist and others, 1963; Quist and Marshall, 1966; Helgeson, 1967a; Lafon, ms). Aluminum ion forms stable complexes with fluoride and (to a much lesser extent) sulfate ions in aqueous solutions. However, thermodynamic calculations indicate that fluoride and sulfate complexes probably contribute only slightly to the transport of aluminum in hydrothermal solutions at high temperatures, even where the pH of the solution is low. At low temperatures, aluminum fluoride complexes may be important in acid solutions (Hem, 1968). Aluminum hydroxide complexes appear to be the primary agents of aluminum transport in "acid" as well as "alkaline" hydrothermal solutions at high temperatures. Hydroxide complexes of calcium, sodium, potassium, magnesium, and most other metal ions are important only in alkaline solutions below  $300^\circ\text{C}$ , but ferrous hydroxide may associate to a significant extent in acid solutions above  $200^\circ\text{C}$ . Of the several oxidation states of gold, iron, and copper that form, aurous, ferrous, and cuprous ions and complexes predominate in hydrothermal solutions.  $\text{Zn}^{++}$ ,  $\text{Pb}^{++}$ ,  $\text{Cu}^+$ ,  $\text{Cu}^{++}$ ,  $\text{Fe}^{+++}$ ,  $\text{Ag}^+$ ,  $\text{Au}^+$ , and  $\text{Au}^{+++}$  ions associate primarily with  $\text{Cl}^-$  in chloride-rich solutions. Although concentrations of metal-carbonate, sulfide, bisulfide, and polysulfide complexes are negligible in acid low-sulfide solutions, metal-sulfate complexes may be important contributors to mineral solubilities in such solutions at temperatures below  $\sim 200^\circ\text{C}$ .

For temperatures below  $300^\circ\text{C}$ , the standard state adopted for the aqueous phase is an hypothetical 1 molal solution at 1 atm and any specified temperature. For gases and solids the standard state is unit activity for the ideal gas and the pure solid, respectively, at 1 atm and any specified temperature. The pressure dependence of hydrothermal equilibria are slight (considered negligible in this contribution) below  $300^\circ\text{C}$ . For this reason, pressure is regarded as a variable only where higher temperatures are considered. In these instances, the standard states apply to any specified temperature and pressure.

LIST OF SYMBOLS

- A — molal Debye-Hückel parameter defined by equation (39).
- $a$  — coefficient in equations (16) and (17), equal to 0.01875.
- $\hat{a}$  — coefficient (in the Debye-Hückel equation) assumed to represent the distance of closest approach of ions in an electrolyte solution.
- $d_1, d_2$  — coefficients in equation (26).
- $a'$  — coefficient in equations (28) and (31).
- $a''$  — coefficient in equations (10), (11), and (12).
- $a_i$  — activity of the  $i$ th species.
- $a_{\text{H}_2\text{O}}$  — activity of  $\text{H}_2\text{O}$ .
- $\alpha$  — degree of association defined by equations (33), (34), and (54).
- $\alpha'$  — coefficient in equation (17).
- $\alpha''$  — coefficient in equation (5).
- B — molal Debye-Hückel parameter defined by equation (10).
- $B'$  — deviation function describing the departure of the mean ionic activity coefficient of an electrolyte from that predicted by the Debye-Hückel expression.
- $b$  — coefficient in equations (16) and (17), equal to  $-12.741$ .
- $b_1, b_2$  — coefficients in equation (4).
- $b'$  — coefficient in equations (28) and (31).
- $b''$  — coefficient in equations (10), (11), and (12).
- $\beta$  — overall dissociation constant for complexes, or equilibrium constant for gas-aqueous reactions.
- $\beta'$  — coefficient in equation (17).
- $\beta''$  — coefficient in equation (5).
- $\epsilon$  — representation of cations.
- $\epsilon L_{\gamma}$  — representation of a mononuclear complex involving cation  $\epsilon$  and  $\gamma$  moles of anion L.
- $c$  — coefficient in equations (16) and (17), equal to  $7.84 \times 10^{-4}$ .
- $\check{c}$  — integer index for complexes in equations (18), (20), (21), (24), (36), and (54).
- $c'$  — coefficient in equations (28) and (31).
- $c''$  — coefficient in equations (10), (11), and (12).
- $C_{P,i}^\circ$  — standard heat capacity of the  $i$ th species.
- $\left. \begin{matrix} T \\ C_{P,i}^\circ \end{matrix} \right\}$  — average standard heat capacity of the  $i$ th species from temperature  $T_r$  to temperature  $T$ .
- $\Delta C_{P,r}^\circ$  — standard heat capacity of reaction.
- $\left. \begin{matrix} T \\ \Delta C_{P,r}^\circ \end{matrix} \right\}$  — average standard heat capacity of reaction from temperature  $T_r$  to temperature  $T$ .
- $\gamma_{\check{c}}$  — activity coefficient in the  $\check{c}$ th complex.

- $\gamma_i$  — stoichiometric individual ion activity coefficient of the  $i$ th ion in a multicomponent electrolyte solution containing a predominant concentration of a given salt (defined by eq 45).
- $\gamma_i^*$  — individual ion activity coefficient of the  $i$ th ion.
- $\gamma_{\pm}$  — stoichiometric mean activity coefficient.
- $\gamma_{\pm}^*$  — mean ionic activity coefficient.
- $\gamma_{+}^*$  — individual ion activity coefficient of a cation.
- $\gamma_{-}^*$  — individual ion activity coefficient of an anion.
- $d$  — integer index for the difference expressed by equation (20).
- $d'$  — coefficient in equations (28) and (31).
- $\hat{e}$  — integer index for anions in equations (21), (22), (25), (26), (50), (51), and (52).
- $\epsilon$  — dielectric constant.
- $f_i$  — fugacity of the  $i$ th species.
- $\Delta G_{f,i}^{\circ}$  — standard Gibbs free energy of formation from the elements of the  $i$ th species.
- $\Delta G_r^{\circ}$  — standard Gibbs free energy of reaction.
- $h$  — average number of water molecules associated with  $\nu$  ions.
- $H_i^{\circ}$  — standard enthalpy of the  $i$ th species.
- $\Delta H_i^{\circ}$  — standard enthalpy of formation from the elements of the  $i$ th species at the reference temperature plus the enthalpy change for the  $i$ th species associated with an increase in temperature from  $T_r$  to  $T$ .
- $\Delta H_{f,i}^{\circ}$  — standard enthalpy of formation from the elements of the  $i$ th species.
- $\Delta H_r^{\circ}$  — standard enthalpy of reaction.
- $\theta$  — coefficient in equations (16) and (17), equal to 219.0.
- $I$  — stoichiometric ionic strength.
- $\bar{I}$  — true ionic strength.
- $i$  — integer index for chemical species.
- $i$  — integer index for cations in equations (19), (20), (21), (24), (26), and (27).
- $j$  — integer index for reaction products.
- $K$  — equilibrium constant.
- $k$  — Henry's law coefficient.
- $K_{sp}$  — activity product constant.
- $L$  — representation of anions.
- $l$  — integer index for reactants.
- $\lambda'$  — coefficient in equation (17).
- $M_i$  — molarity of the  $i$ th species.
- $m_i$  — molality of the  $i$ th species.
- $m_{t,i}$  — total molality of the  $i$ th ion or salt.
- $n$  — number of moles of a given cation in a mineral.
- $\hat{n}$  — sum of the exponents in the Law of Mass Action equation.
- $\nu$  — number of moles of ions in 1 mole of a given salt.
- $\nu_+$  — number of moles of the cation in 1 mole of a given salt.
- $\nu_-$  — number of moles of the anion in 1 mole of a given salt.

- $P$  — pressure in atmospheres.
- $P_r$  — reference pressure in atmospheres (1 atm).
- $q$  — integer index for mononuclear complexes involving a common ligand in equations (26) and (27).
- $R$  — gas constant, equal to 1.9872 cal mole<sup>-1</sup> deg<sup>-1</sup> or 82.0575 cm<sup>3</sup> atm mole<sup>-1</sup> deg<sup>-1</sup>.
- $r_{\hat{e}}$  — ion radius of the  $\hat{e}$ th anion.
- $r_i$  — ion radius of the  $i$ th cation.
- $\rho$  — density.
- $S^*$  — sum of the entropies of 1 mole of an aqueous species and its coordinated water molecules.
- $S_i^{\circ}$  — standard conventional third law entropy of the  $i$ th species.
- $S_i^{\circ(\text{abs})}$  — standard absolute third law entropy of the  $i$ th species.
- $S^{\circ d}$  — difference in the sum of the entropies of 1 mole of an aqueous complex and its coordinated water molecules and the sum of the entropies of the free cation and its coordinated water molecules.
- $\Delta S_e^{\circ}$  — standard electrostatic entropy of dissociation.
- $\Delta S_r^{\circ}$  — standard entropy of reaction.
- $S\psi$  — solubility of the  $\psi$ th mineral (in molality units) defined by equation (51).
- $\sigma$  — exponential coefficient in equation (36).
- $T$  — temperature in degrees Kelvin.
- $T_r$  — reference temperature in degrees Kelvin (298.15°K).
- $u$  — integer index in equation (48).
- $\hat{u}$  — number of water molecules coordinated to a cation.
- $\Delta V_r^{\circ}$  — standard volume of reaction.
- $\phi$  — stoichiometric osmotic coefficient.
- $x$  — number of water molecules coordinated to a complex.
- $y$  — number of moles of ligand L coordinated in a mononuclear complex of the form  $CL_y$ .
- $\nu$  — number of moles of a given anion in a mineral.
- $\psi$  — integer index for minerals.
- $z$  — limit of the range of integer index  $y$  in equations (46), (47), and (49).
- $Z_i$  — charge on the  $i$ th species.
- $\omega$  — coefficient in equations (16) and (17), equal to 1.00322.

## PREDICTIVE METHODS

In the present state of knowledge, limitations imposed by the amounts and kinds of data available for hydrothermal reactions dictate the "best" methods for predicting thermodynamic properties of hydrothermal systems at elevated temperatures. A variety of approximations, each with its own uncertainties, can be used for this purpose. Because the reliability of numerical values obtained from such approximations reflects the method as well as the data used in the calculations, the computational methods applicable under various circumstances are summarized below.

## Equilibrium Constants

The basic thermodynamic equation describing the temperature dependence of the equilibrium constant is

$$\log K(T) = \log K(T_r) - \frac{\Delta H^\circ_r(T_r)}{2.303R} \left( \frac{1}{T} - \frac{1}{T_r} \right) - \frac{1}{2.303RT} \int_{T_r}^T \Delta C^\circ_{p,r}(T) dT + \frac{1}{2.303R} \int_{T_r}^T \Delta C^\circ_{p,r}(T) d \ln T \quad (1)$$

in which  $\Delta H^\circ_r$  and  $\Delta C^\circ_{p,r}$  are, respectively, the standard enthalpy and heat capacity of reaction,  $R$  is the gas constant,  $K$  the equilibrium constant,  $T$  the temperature of interest (in  $^\circ\text{K}$ ), and  $T_r$  the reference temperature (298.15 $^\circ\text{K}$  in this commun.). For most reactions involving aqueous solutions, the integrals in equation (1) cannot be evaluated rigorously because the required heat capacity functions are not available. To integrate the last two terms in equation (1), the assumption is frequently made that  $\Delta C^\circ_{p,r}(T)$  is zero or constant, but this practice often leads to serious errors in computed  $\log K(T)$  values at elevated temperatures (Cobble, 1964; Helgeson, 1964, 1967a). In many cases, ambiguities and uncertainties resulting from these assumptions can be avoided by adopting one or another of the alternate approaches summarized below.

*Calculation from average heat capacities.*—Average heat capacities

$\left( \frac{C^\circ_p}{T_r} \right)_T$  for ions can be computed from absolute entropies by evaluating

$$\left( \frac{C^\circ_p}{T_r} \right)_T = \frac{S^\circ_i(\text{abs})(T) - S^\circ_i(\text{abs})(T_r)}{\ln T/T_r} \quad (2)$$

where  $S^\circ_i(\text{abs})$  is the absolute entropy of the  $i$ th species. The absolute entropy is related to the conventional entropy ( $S^\circ$ ) by

$$S^\circ_i(\text{abs})(T) = S^\circ_i(T) + Z_i S^\circ_{\text{H}^+}(\text{abs})(T) \quad (3)$$

where  $Z_i$  represents the charge on the  $i$ th species and  $S^\circ_{\text{H}^+}(\text{abs})(T)$  is the absolute entropy of the hydrogen ion at temperature  $T$ . Criss and Cobble (1964a) have shown that the absolute entropies of ions at high temperatures can be calculated from

$$S^\circ_i(\text{abs})(T) = b_1(T) + b_2(T) S^\circ_i(\text{abs})(T_r) \quad (4)$$

where  $b_1$  and  $b_2$  are temperature dependent coefficients characteristic of simple cations, simple anions, oxy-anions, or acid oxy-anions. The relation expressed in equation (4) was obtained by assigning absolute entropies to the hydrogen ion at various specified temperatures. Equation

(1) can be combined with equation (2) to define a similar relation for average heat capacities. This expression appears as

$$\left( \frac{C^\circ_{p,i}}{T_r} \right)_T = \alpha''(T) + \beta''(T) S^\circ_i(\text{abs})(T_r) \quad (5)$$

where  $\alpha''(T) = b_1(T)/\ln(T/T_r)$  and  $\beta''(T) = (b_2(T)-1)/\ln(T/T_r)$ . Values of  $b_1$ ,  $b_2$ ,  $\alpha''$ , and  $\beta''$  have been computed by Criss and Cobble (1964a and b) for 60 $^\circ$ , 100 $^\circ$ , 150 $^\circ$ , 200 $^\circ$ , 250 $^\circ$ , and 300 $^\circ\text{C}$ . These coefficients allow absolute entropies and average heat capacities to be calculated for a large number of aqueous species at elevated temperatures.

When average heat capacities can be computed for all reactants and products in a given reaction, the equilibrium constant at temperature  $T$  can be predicted directly from

$$\log K(T) = \log K(T_r) - \frac{\Delta H^\circ_r(T_r)}{2.303R} \left( \frac{1}{T} - \frac{1}{T_r} \right) - \frac{\Delta C^\circ_{p,r} \left( \frac{T-T_r}{T_r} \right)}{2.303RT} + \frac{\left( \frac{C^\circ_{p,r}}{T_r} \right)_T \ln T/T_r}{2.303R} \quad (6)$$

in which

$$\Delta C^\circ_{p,r} \left( \frac{T-T_r}{T_r} \right) = \sum_j \left( \frac{C^\circ_{p,j}}{T_r} \right)_T - \sum_l \left( \frac{C^\circ_{p,l}}{T_r} \right)_T \quad (7)$$

where  $j$  and  $l$  represent the products and reactants, respectively.

*Calculation from a combination of average and actual heat capacities.*—In cases where the actual heat capacities for some (but not all) of the reactants or products in a given reaction are defined by empirical power functions of temperature, equilibrium constants can be computed by first evaluating (for those species)

$$\Delta H^\circ_i(T) = \Delta H^\circ_{f,i}(T_r) + \int_{T_r}^T C^\circ_{p,i}(T) dT \quad (8)$$

and

$$S^\circ_i(T) = S^\circ_i(T_r) + \int_{T_r}^T C^\circ_{p,i}(T) d \ln T \quad (9)$$

in which  $\Delta H^\circ_{f,i}(T_r)$  is the standard enthalpy of formation from the elements of the  $i$ th species at the reference temperature [ $\Delta H^\circ_{f,i}(T_r)$ ] plus the enthalpy change for the  $i$ th species associated with an increase in

temperature from  $T_r$  to temperature  $T$ . Heat capacities of solids and gases are usually described by power functions of the form

$$C_{p,i}^{\circ}(T) = a'' + b''T + c''/T^2 \quad (10)$$

so that equations (8) and (9) will normally appear as

$$\Delta H^{\circ}_i(T) = \Delta H^{\circ}_{f,i}(T_r) + a''(T-T_r) + \frac{b''}{2}(T^2-T_r^2) - c''\left(\frac{1}{T} - \frac{1}{T_r}\right) \quad (11)$$

and

$$S^{\circ}_i(T) = S^{\circ}_i(T_r) + a'' \ln T/T_r + b''(T-T_r) - \frac{c''}{2}\left(\frac{1}{T^2} - \frac{1}{T_r^2}\right) \quad (12)$$

Where average heat capacities are known for the remaining reactants and products, standard enthalpies and entropies at a given temperature can be calculated by evaluating

$$\Delta H^{\circ}_i(T) = \Delta H^{\circ}_{f,i}(T_r) + C_{p,i}^{\circ} \left[ \frac{T}{T_r} \right] (T-T_r) \quad (13)$$

and

$$S^{\circ}_i(T) = S^{\circ}_i(T_r) + C_{p,i}^{\circ} \left[ \frac{T}{T_r} \right] \ln T/T_r \quad (14)$$

High temperature equilibrium constants for the reaction can then be computed from

$$\log K(T) = \frac{T \left( \sum_j S^{\circ}_j(T) - \sum_l S^{\circ}_l(T) \right) - \sum_j \Delta H^{\circ}_j(T) + \sum_l \Delta H^{\circ}_l(T)}{2.303RT} \quad (15)$$

where  $j$  and  $l$  again refer to the products and reactants, respectively. When equation (15) is employed, care must be exercised to avoid confusion between relative and absolute entropies in the summation terms of the equation. If heat capacity power functions are known for all reactants and products, high temperature equilibrium constants can be computed simply by combining equations (11), (12), and (15).

*Prediction of dissociation constants.*—In geochemical problems it is quite common to find that no heat capacity data of any kind are available for one or more of the reactants or products in a given reaction. This is particularly true for complexes in aqueous solution. Despite this handicap, dissociation constants often can be closely approximated to  $\sim 200^{\circ}\text{C}$  by evaluating (Helgeson, 1967a)

$$\log K(T) = \frac{\Delta S^{\circ}_e(T_r)}{2.303RT} \left[ T_r - \frac{\theta}{\omega} \left( 1 - \exp[\exp(b+aT) - c + (T-T_r)/\theta] \right) \right] - \frac{\Delta H^{\circ}_e(T_r)}{2.303RT} \quad (16)$$

where  $\theta$ ,  $\omega$ ,  $a$ ,  $b$ , and  $c$  are temperature independent constants characteristic of the solvent. For aqueous solutions these coefficients have the values 219.0, 1.00322, 0.01875,  $-12.741$ , and  $7.84 \times 10^{-3}$ , respectively (Helgeson, 1967a). The method of approximation afforded by equation (16) involves the assumption that  $\Delta C_{p,r}^{\circ}(T)$  changes monotonically but nonlinearly with temperature;  $\Delta C_{p,r}^{\circ}(T)$  is implicitly defined in terms of  $\Delta S^{\circ}_e(T_r)$  in the equation. Dissociation constants computed from equation (16) are often much closer approximations of actual dissociation constants at high temperatures than those computed by assuming  $\Delta C_{p,r}^{\circ}(T) = 0$  or  $\Delta C_{p,r}^{\circ}(T) = \text{a constant}$ . Equation (16) is an approximation modified from equation (17) below.

Where dissociation constants are known over a restricted temperature range, experimental  $\log K(T)$  values can be fit by the method of least squares to

$$\begin{aligned} \log K(T) = & \frac{\Delta S^{\circ}_e(T_r)}{2.303RT} \left[ T_r - T - \frac{\theta}{\omega} \left( 1 - \exp[\exp(b+aT) - c + (T-T_r)/\theta] \right) \right] \\ & - \frac{\Delta H^{\circ}_e(T_r)}{2.303RT} + \frac{\Delta S^{\circ}_e(T_r)}{2.303R} + \frac{\alpha'}{2.303R} (\ln T/T_r - 1 + T_r/T) \\ & + \frac{\beta'(T-T_r)^2}{4.606RT} + \frac{\lambda'}{4.606RT} (T^3/3 - T_r^3/3 - T_r^2T + T_r^3) \quad (17) \end{aligned}$$

where  $\theta$ ,  $\omega$ ,  $a$ ,  $b$ , and  $c$  are constants with the values given above,  $\Delta S^{\circ}_e(T_r)$  is the electrostatic entropy of dissociation at the reference temperature ( $T_r$ ), and  $\alpha'$ ,  $\beta'$ , and  $\lambda'$  are temperature independent coefficients characteristic of the reaction (Helgeson, 1967a). Values of the reaction-dependent parameters defined by the low temperature fits can then be used to predict  $\log K$  values at higher temperatures. However, care must be exercised to avoid overfitting. Where only a few experimental values are available, or the data are highly uncertain, all of the reaction-dependent coefficients should not be included in the least squares fit routine; that is,  $\lambda'$ , or  $\lambda'$  and  $\beta'$  should be set to zero.

#### Entropy and Heat Capacity Estimates

For many reactions in aqueous solution, equilibrium constants are known only at  $25^{\circ}\text{C}$ . In such cases it is common to find that insufficient entropy or enthalpy data are available for the species involved in the reaction to permit calculation of high temperature equilibrium constants using the approaches described above. This problem often can be overcome in a first approximation by estimating entropies of dissociation or the entropies and heat capacities of reactant or product species.

*Dissociational reactions in aqueous solution.*—Entropies of dissociation for complexes in aqueous solution at  $25^{\circ}\text{C}$  can be estimated from entropy correlation plots. These entropies can then be used in conjunction with equation (16) to approximate dissociation constants at higher temperatures. The approach summarized below for making such esti-

mates is a modification of that employed by Cobble (1953b) for estimating the entropies of complex ions.

For convenience, let us define the sum of the entropies of 1 mole of an aqueous species and its coordinated water molecules as  $S^*$ ; that is, for a given temperature,

$$S^* [\text{EL}_y(\text{H}_2\text{O})_x \text{Z}_c] \equiv S^\circ [\text{EL}_y \text{Z}_c] + x S^\circ [\text{H}_2\text{O}] \quad (18)$$

and

$$S^* [\text{E}(\text{H}_2\text{O})_u \text{Z}_i] \equiv S^\circ [\text{E} \text{Z}_i] + u S^\circ [\text{H}_2\text{O}] \quad (19)$$

in which  $S^\circ$  is the conventional third law entropy,  $\text{EL}_y$  is a mono-nuclear complex involving cation  $\text{E}$  and  $y$  moles of anion  $\text{L}$ ,  $x$  and  $u$  represent the number of water molecules coordinated to the complex and cation, respectively, and  $\text{Z}_c$  and  $\text{Z}_i$  are the respective charges on the complex and the cation. Subtracting equation (19) from equation (18) gives

$$S^* [\text{EL}_y(\text{H}_2\text{O})_x \text{Z}_c] - S^* [\text{E}(\text{H}_2\text{O})_u \text{Z}_i] = \Delta S^*_d = S^\circ [\text{EL}_y \text{Z}_c] - S^\circ [\text{E} \text{Z}_i] + (x - u) S^\circ [\text{H}_2\text{O}] \quad (20)$$

where  $\Delta S^*_d$  is the difference in the sums of the entropies expressed in equations (18) and (19). Equation (20) can now be combined with the expression for the entropy of dissociation of the complex written as

$$\Delta S^\circ_r = S^\circ [\text{E} \text{Z}_i] + y S^\circ [\text{L} \text{Z}_c] - S^\circ [\text{EL}_y \text{Z}_c] \quad (21)$$

to give

$$\Delta S^\circ_r = y S^\circ [\text{L} \text{Z}_c] + (x - u) S^\circ [\text{H}_2\text{O}] - \Delta S^*_d \quad (22)$$

where  $\text{Z}_c$  is the charge on the anion. If as a first approximation we assume,

$$x = u - y \quad (23)$$

then equations (20) and (22) reduce, respectively, to

$$\Delta S^*_d = S^\circ [\text{EL}_y \text{Z}_c] - S^\circ [\text{E} \text{Z}_i] - y S^\circ [\text{H}_2\text{O}] \quad (24)$$

and

$$\Delta S^\circ_r = y \left( S^\circ [\text{L} \text{Z}_c] - S^\circ [\text{H}_2\text{O}] \right) - \Delta S^*_d \quad (25)$$

For complexes involving a common ligand at 25°C, empirical considerations indicate that  $\Delta S^*_d$  can be described by

$$\Delta S^*_d(q) = a_1 + a_2 / (r_{i(q)} + r_{c(q)}) \quad (26)$$

in which  $a_1$  and  $a_2$  are coefficients characteristic of the group of complexes, and  $r_{i(q)}$  and  $r_{c(q)}$  are the radii of the cation and ligand, respectively, in the  $q$ th complex. The validity of equation (26) can be

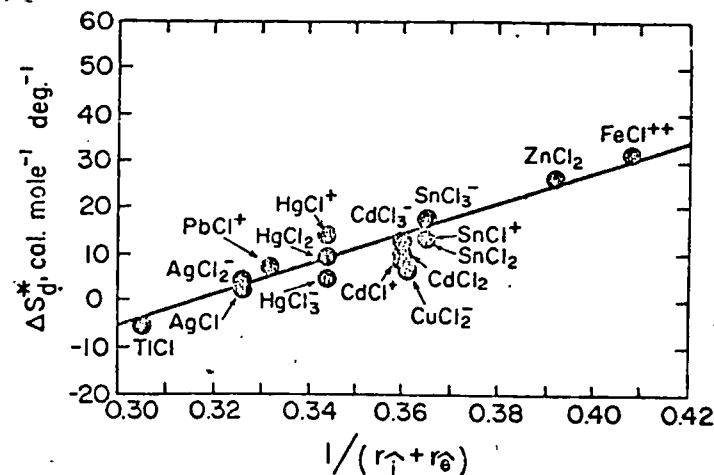


Fig. 1. Correlation plot of  $\Delta S^*_d$  (see text—eqs 20 and 24) for metal chloride complexes at 25°C and 1 atm against the reciprocal of the sum of the radii of the ions in the complex. The plotted values of  $\Delta S^*_d$  and the sources of data from which they were calculated (see text) are given in table 1. The curve shown above is consistent with equation (27).

assessed for chloride complexes in figure 1. The data used in computing the  $\Delta S^*_d$  values plotted in figure 1 are given in table 1 along with the sources from which they were obtained. The maximum deviation from the linear curve of the points in figure 1 is 8 cal mole<sup>-1</sup> deg<sup>-1</sup> (for  $\text{CuCl}_2^-$ ), but the average deviation is only 3 cal mole<sup>-1</sup> deg<sup>-1</sup>, which is well within the experimental uncertainty of the data. The specific statement of equation (26) for the curve in figure 1 is

$$\Delta S^*_d(q) = -102.5 + 325 / (r_{i(q)} + 1.81) \quad (27)$$

where 1.81 is the radius of the chloride ion (Sienko and Plane, 1963). Values of  $\Delta S^\circ_r$  computed from equations (25) and (27) for the species shown in figure 1 are given in table 1 to afford a numerical comparison with those based on experimental data.

The procedure summarized above for estimating dissociational entropies is of general applicability; that is, expressions similar to equations (26) and (27) can be developed for various groups of dissociational reactions for which data are incomplete. Entropy estimates obtained in this manner permit approximations of high temperature dissociation constants for a large number of complexes of interest in geochemistry. For many of these, only experimental dissociation constants at 25°C are available, but estimates of  $\Delta S^\circ_r(T_r)$  allow approximations of  $\Delta H^\circ_r(T_r)$  [from  $\Delta H^\circ_r(T_r) = T_r \Delta S^\circ_r(T_r) - 2.303RT_r \log K(T_r)$ ] and thus estimation of high temperature dissociation constants from equation (16). In cases where sufficient data are not available to estimate dissociational

entropies from correlation plots, it may be possible to estimate directly the entropy of a particular complex, neutral species, or ion, which will then permit calculation of dissociational entropies at 25°C. A number of techniques for making such estimates have been summarized by Latimer (1952), Cobble (1953a and b), and others.

TABLE I  
Entropies of dissociation for chloride complexes  
in aqueous solution at 25°C and 1 atm

Reaction.	Cation radius <sup>a</sup> , (Å)	Experimental $\Delta S^\circ_f$ (cal mole <sup>-1</sup> deg <sup>-1</sup> )	Calculated <sup>b</sup> $\Delta S^\circ_f$ (cal mole <sup>-1</sup> deg <sup>-1</sup> )	Calculated <sup>c</sup> $\Delta S^\circ_f$ (cal mole <sup>-1</sup> deg <sup>-1</sup> )
$\text{AgCl} \rightleftharpoons \text{Ag}^+ + \text{Cl}^-$	1.26	-6 <sup>d</sup>	2.6	-6.6
$\text{AgCl}_2^- \rightleftharpoons \text{Ag}^+ + 2\text{Cl}^-$	1.26	-11 <sup>d</sup>	4.4	-9.8
$\text{CuCl}_2^- \rightleftharpoons \text{Cu}^+ + 2\text{Cl}^-$	0.96	-13.0 <sup>e</sup>	6.6	-21.2
$\text{PbCl}^+ \rightleftharpoons \text{Pb}^{2+} + \text{Cl}^-$	1.20	-11.6 <sup>f</sup>	7.4	-8.6
$\text{ZnCl}_2 \rightleftharpoons \text{Zn}^{2+} + 2\text{Cl}^-$	0.74	-32.7 <sup>g</sup>	26.3	-31.3
$\text{HgCl}^+ \rightleftharpoons \text{Hg}^{2+} + \text{Cl}^-$	1.10	-17 <sup>h</sup>	13.8	-12.5
$\text{HgCl}_2 \rightleftharpoons \text{Hg}^{2+} + 2\text{Cl}^-$	1.10	-16 <sup>i</sup>	9.6	-15.7
$\text{HgCl}_3^- \rightleftharpoons \text{Hg}^{2+} + 3\text{Cl}^-$	1.10	-13.7 <sup>j</sup>	4.1	-18.9
$\text{CdCl}^+ \rightleftharpoons \text{Cd}^{2+} + \text{Cl}^-$	0.97	-11.4 <sup>k</sup>	8.2	-17.6
$\text{CdCl}_2 \rightleftharpoons \text{Cd}^{2+} + 2\text{Cl}^-$	0.97	-16.4 <sup>l</sup>	10.0	-20.8
$\text{CdCl}_3^- \rightleftharpoons \text{Cd}^{2+} + 3\text{Cl}^-$	0.97	-22.3 <sup>m</sup>	12.7	-24.0
$\text{SnCl}^+ \rightleftharpoons \text{Sn}^{2+} + \text{Cl}^-$	0.93	-15.4 <sup>n</sup>	12.2	-19.3
$\text{SnCl}_2 \rightleftharpoons \text{Sn}^{2+} + 2\text{Cl}^-$	0.93	-18.9 <sup>n</sup>	12.5	-22.5
$\text{SnCl}_3^- \rightleftharpoons \text{Sn}^{2+} + 3\text{Cl}^-$	0.93	-27.4 <sup>n</sup>	17.8	-25.7
$\text{FeCl}^+ \rightleftharpoons \text{Fe}^{2+} + \text{Cl}^-$	0.64	-35 <sup>m</sup>	31.8	-33.3
$\text{TlCl} \rightleftharpoons \text{Tl}^+ + \text{Cl}^-$	1.74	2.2 <sup>i</sup>	5.4	0.2
$\text{AuCl}_2^- \rightleftharpoons \text{Au}^+ + 2\text{Cl}^-$	1.37			-6.0
$\text{AuCl}_3^- \rightleftharpoons \text{Au}^{3+} + 4\text{Cl}^-$	0.9			-30.2
$\text{SnCl}_4^- \rightleftharpoons \text{Sn}^{4+} + 4\text{Cl}^-$	0.71			-39.2

<sup>a</sup> Sienko and Plane (1963). <sup>b</sup> Computed from equation (25) using the experimental entropies shown above together with 16.7 cal mole<sup>-1</sup> deg<sup>-1</sup> for  $S^\circ_{\text{H}_2\text{O}}$  (Wagman and others, 1968) and 13.51 for  $S^\circ_{\text{Cl}^-}$  (Ahlqvist and Cobble, 1964). <sup>c</sup> Calculated from equations (25) and (27). <sup>d</sup> Jonte and Martin (1952). <sup>e</sup> Calculated from  $S^\circ_{\text{CuCl}_2^-}$  (Latimer 1952) and the ionic entropies in table 3. <sup>f</sup> Austin, Matheson, and Parton (1959). <sup>g</sup> Based on least squares fits of log  $K(T)$  values at 150° and 115°C (Kraus and Raridon, 1966) and 25°C (Marcus and Mayden, 1963) using equation (16). <sup>h</sup> Malcolm, Parton, and Watson (1961). <sup>i</sup> Williams (1954). <sup>j</sup> Helgeson (1967a). <sup>k</sup> Vanderzee and Dawson (1953). <sup>l</sup> Wagman and others (1966). <sup>m</sup> Rabinowitch and Stockmayer (1942). <sup>n</sup> Latimer (1952).

**Minerals.**—Although thermodynamic data are now available for a large number of minerals (Robie, 1966; Robie and Waldbaum, 1968), only free energy data (derived from solubility studies) at 25°C exist for many minerals of interest in hydrothermal and metamorphic studies. Approximation of the standard enthalpies of formation of these minerals at 25°C permits calculation of provisional equilibrium constants for high temperature hydrothermal reactions that could not otherwise be evaluated in the present state of knowledge. As a rule, direct estimation of the standard enthalpies of formation of minerals involves prohibitive uncertainties owing to the lack of adequate general models for calculating bond energies in minerals. In contrast, third law entropies of minerals can be approximated closely by direct estimation, which permits calculation of  $\Delta H^\circ_f(T_r)$  from  $\Delta H^\circ_f(T_r) = \Delta G^\circ_f(T_r) + T_r \Delta S^\circ_f(T_r)$ , where  $\Delta S^\circ_f(T_r)$  is the standard entropy of formation of the mineral from its elements.

Entropies of silicates, sulfates, and carbonates can be approximated by summing the entropies of the oxide components of the minerals (Latimer, 1952; Fyfe and others, 1958). Although such a summation does not provide for all of the configurational entropy contribution, the uncertainty attending this procedure rarely exceeds 10 percent and more often than not is less than a few cal mole<sup>-1</sup> deg<sup>-1</sup>. Close estimates can be made for clay minerals if the entropy of  $\text{H}_2\text{O}$  is taken to be that of ice at 25°C (10.68 cal mole<sup>-1</sup> deg<sup>-1</sup>, Robie and Waldbaum, 1968) or assigned a value of 9.4 cal mole<sup>-1</sup> deg<sup>-1</sup> (Latimer, 1952). For example, the entropy of muscovite obtained from the sum of the entropies of its oxide components at 25°C is 69.8 cal mole<sup>-1</sup> deg<sup>-1</sup> if  $\text{H}_2\text{O}$  is represented by ice, and 68.5 cal mole<sup>-1</sup> deg<sup>-1</sup> if Latimer's value for the entropy of hydrate water is used; the experimental entropy of muscovite is 69.0 cal mole<sup>-1</sup> deg<sup>-1</sup> (Robie and Waldbaum, 1968). An error of a few cal mole<sup>-1</sup> deg<sup>-1</sup> in the entropy of a mineral rarely introduces significant error in high temperature calculations of mineral equilibria. In contrast to summing the entropies of oxide components, entropies of minerals can also be estimated with confidence by summing the values tabulated by Latimer (1952) for the entropy contributions of elements and ions in solid compounds. This procedure is particularly useful for estimating the entropies of multicomponent sulfides.

As in the case of entropy, heat capacities of minerals can be approximated closely by summing the heat capacities of the components of the minerals. This is true also for heat capacities of minerals expressed by power functions of temperature (eq 10). For example, the heat capacity power function for muscovite obtained by summing the power functions for its oxide components is  $89.95 + 33.23 \times 10^{-3}T - 20.67 \times 10^{-5}T^{-2}$  when ice (9.0 cal mole<sup>-1</sup> deg<sup>-1</sup>) is used to represent  $\text{H}_2\text{O}$  (see footnote n, table 8). The experimentally derived function is  $97.56 + 26.38 \times 10^{-3}T - 25.44 \times 10^{-5}T^{-2}$  (Kelley, 1960). At 25°C, the estimated heat capacity defined by the first of these power functions is 77 cal mole<sup>-1</sup> deg<sup>-1</sup> compared to the experimental value of 77 cal mole<sup>-1</sup> deg<sup>-1</sup>. At

300°C the corresponding values are 103 cal mole<sup>-1</sup> deg<sup>-1</sup> compared to 105 cal mole<sup>-1</sup> deg<sup>-1</sup>. Discrepancies of this order of magnitude are insignificant with respect to calculated equilibrium constants at high temperature.

Estimates of entropies and heat capacity power functions of temperature make it possible to compute standard enthalpies of formation for minerals at 25°C from high temperature phase equilibrium data. For example, the  $\Delta H^\circ_f(T_r)$  value for annite used to compute the high temperature hydrolytic equilibrium constants for this mineral in table 12 were calculated from the high temperature equilibrium  $P_{H_2O}$  and  $f_{O_2}$  for sanidine + magnetite +  $H_2O_{(l)} \rightleftharpoons$  annite +  $\frac{1}{2}O_{2(g)}$  (Eugster and Wones, 1962) at 500°C and 2070 atm. An estimated entropy (table 12) and heat capacity power function (table 8) for annite permitted calculation of the high temperature values for the entropy of annite (eq 9). The same calculations for the other species in the assemblage (for which thermodynamic data are known) permitted calculation of  $\Delta S^\circ_r(T)$  for the equilibrium assemblage at 500°C. From the values of  $f_{O_2}$  and  $P_{H_2O}$  given by Eugster and Wones, and fugacity coefficients for  $H_2O^1$  (Anderson, 1967),  $\Delta G^\circ_r(T)$  could also be computed, which made it possible to calculate  $\Delta H^\circ_r(T)$ , and hence,  $\Delta H^\circ_{annite}(T)$ . Application of the estimated heat capacity power function resulted in the value of  $\Delta H^\circ_f(T_r)$  for annite given in table 12.<sup>2</sup>

#### Activity Coefficients in Sodium Chloride Solutions

Because the solute in many hydrothermal solutions is composed largely of sodium chloride, the thermodynamic properties of aqueous solutions of this salt can be used to compute activity coefficients in concentrated hydrothermal solutions at elevated temperatures. Thermodynamic properties of concentrated sodium chloride solutions are summarized in table 2. The methods used in computing the values shown in the table are outlined briefly below.

<sup>1</sup> Fugacity coefficients for other gases involved in similar calculations can be computed from data given by Garrels and Christ (1965).

<sup>2</sup> The effects of pressure were disregarded in the calculation of the enthalpy of formation of annite described above. The volume changes for reactions used in such calculations are commonly small, and the pressure corrections are thus often smaller than the uncertainty in the experimental data. Where this is not true the experimental equilibrium constants should first be corrected for pressure by evaluating

$$\log K(T, P_r) = \log K(T, P) - \frac{1}{2.303RT} \int_{P_r}^P \Delta V^\circ_r(T, P) dP$$

where  $P_r$  refers to the reference pressure (1 atm in this context),  $\Delta V^\circ_r$  is the standard change in volume for the reaction in  $cm^3$  mole<sup>-1</sup>, and  $R$  is the gas constant expressed as 82.0575  $cm^3$  atm mole<sup>-1</sup> deg<sup>-1</sup>. In many instances this equation can be approximated closely by

$$\log K(T, P_r) = \log K(T, P) - \frac{\Delta V^\circ_r(T, P_r)(P - P_r)}{2.303RT}$$

*Analysis of vapor pressure data.*—Stoichiometric osmotic coefficients for sodium chloride solutions from 25° to 270°C have been fit (Helgeson, 1967b; Helgeson and James, 1968) with a least squares computer routine employing a Debye-Hückel power function for activity coefficients suggested by Lietzke and Stoughton (1961). The activity coefficient power function is

$$\ln \gamma_{\pm}(T, I) = \frac{-2.303 A(T) |Z_1 Z_2| I^{1/2}}{1 + a'(T) I^{1/2}} + b'(T) I + c'(T) I^2 + d'(T) I^3 \quad (28)$$

where  $\gamma_{\pm}(T, I)$  represents the stoichiometric mean activity coefficient at temperature  $T$  and stoichiometric ionic strength  $I$ ,  $a'(T)$ ,  $b'(T)$ ,  $c'(T)$ , and  $d'(T)$  are temperature-dependent coefficients,  $Z$  is the charge on the subscripted cation (1) and anion (2), and  $A(T)$  is the Debye-Hückel parameter defined below by equation (39).

The stoichiometric mean activity coefficient of NaCl is related to the stoichiometric osmotic coefficient ( $\phi$ ) by

$$\phi(T, I) = 1 + \frac{1}{I} \int_0^I I d \ln \gamma_{\pm}(T, I) \quad (29)$$

Equation (29) can also be written as

$$\phi(T, I) = 1 + \ln \gamma_{\pm}(T, I) - \frac{1}{I} \int_0^I \ln \gamma_{\pm}(T, I) dI \quad (30)$$

and integrated with the aid of equation (28) to give the following power function for the stoichiometric osmotic coefficient:

$$\phi(T, I) = 1 - \frac{2.303 A(T) |Z_1 Z_2|}{a'^3(T) I} \left[ (1 + a'(T) I^{1/2}) - 2 \ln(1 + a'(T) I^{1/2}) - \frac{1}{1 + a'(T) I^{1/2}} \right] + \frac{b'(T) I}{2} + \frac{2c'(T) I^2}{3} + \frac{3d'(T) I^3}{4} \quad (31)$$

The values of the power series coefficients defined by the fits of the osmotic coefficients of NaCl with equation (31) were used in equation (28) to calculate the stoichiometric mean activity coefficients shown in table 2. Because experimental osmotic coefficients are available for NaCl at only three concentrations above 100°C (table 2), the  $d'$  coefficient was set to zero in the least squares fits.<sup>3</sup>

*Calculations providing for complexing.*—The stoichiometric mean activity coefficient of sodium chloride at a given temperature is related to the mean ionic activity coefficient ( $\gamma^*_{\pm}$ ) by

$$\gamma_{\pm NaCl} = (1 - \alpha_{NaCl}) \gamma^*_{\pm NaCl} \quad (32)$$

<sup>3</sup> Since these calculations were carried out, Lindsay and Liu (1968) have presented osmotic coefficient data for NaCl at concentration intervals of 0.1  $m$  from 0.05 to 3.50  $m$  and temperatures from 125° to 300°C. Least squares fits of their data yield activity coefficients in close agreement with those computed above.

in which  $\alpha_{\text{NaCl}}$  is the degree of association of the solute, defined by

$$\alpha_{\text{NaCl}} = \frac{m_{\text{NaCl}}}{m_{t,\text{NaCl}}} \quad (33)$$

where  $m_{\text{NaCl}}$  is the molality of the complex and  $m_{t,\text{NaCl}}$  is the stoichiometric (total) molality of the salt. Combining equation (33) with the Law of Mass Action for the dissociation of NaCl leads to

$$\alpha_{\text{NaCl}} = \frac{\gamma_{\pm}^2 m_{t,\text{NaCl}}}{K_{\text{NaCl}} \gamma_{\text{NaCl}}} \quad (34)$$

where  $K_{\text{NaCl}}$  and  $\gamma_{\text{NaCl}}$  are, respectively, the dissociation constant and activity coefficient of the complex. Equation (34) can be used to compute values of  $\alpha_{\text{NaCl}}$  (and consequently values of  $\gamma_{\pm}^*$ —eq 32) from stoichiometric mean activity coefficients if dissociation constants and activity coefficients for the complex are known.

Although sodium chloride solutions are essentially completely dissociated at low temperatures, above  $\sim 200^\circ\text{C}$  this is no longer true. Experi-

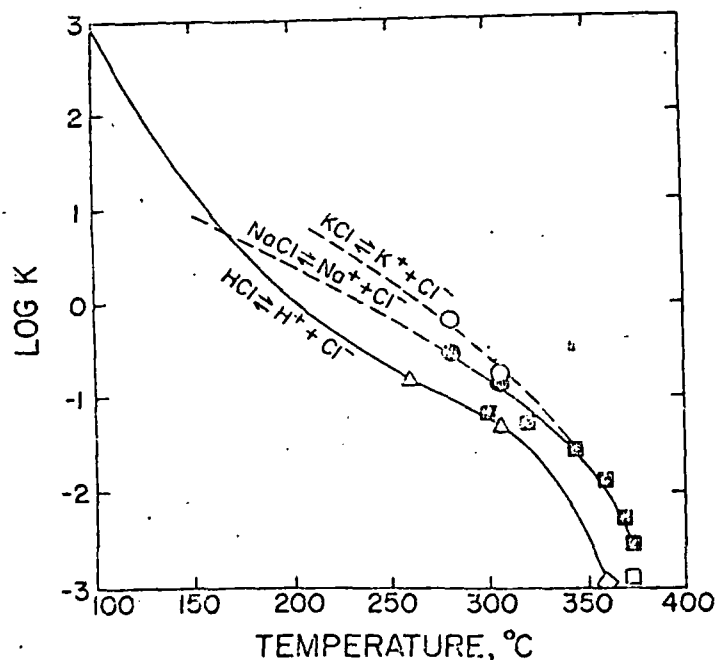


Fig. 2. Dissociation constants for NaCl, KCl, and HCl at high temperatures (see table 4). Open circle = KCl—Wright, Lindsay, and Druga (1961) after Noyes (1907); filled circle = NaCl—Wright, Lindsay, and Druga (1961) after Noyes (1907); triangle = HCl—Wright, Lindsay, and Druga (1961) after Noyes (1907); open square = KCl—extrapolated from supercritical data (Franck, 1951); filled square = NaCl—Pearson, Copeland, and Benson (1962a); diamond = HCl—Pearson, Copeland, and Benson (1962b). The smooth curve for HCl is based on a least squares fit of low and high temperature  $\log K(T)$  values (Helgeson, 1967a) using equation (17), but those for KCl and NaCl are based on simple interpolation. The dissociation constants plotted above are consistent with molal units of concentration.

mental dissociation constants for aqueous NaCl below  $281^\circ\text{C}$  are not available; those reported in the literature for higher (but subcritical)<sup>4</sup> temperatures are plotted together with comparative values of  $\log K(T)$  for KCl and HCl in figure 2. Calculated degrees of association and mean ionic activity coefficients for sodium chloride at elevated temperatures are given in table 2. The values shown in table 2 for these parameters were computed from equations (32) and (34) using extrapolated values of  $K_{\text{NaCl}}$  (table 2)<sup>5</sup>. The extrapolated dissociation constants are those corresponding to the dashed curve for NaCl in figure 2. The activity coefficient of the complex was represented in the calculations by  $\gamma_{\text{CO}_2}$  in NaCl solutions (table 2). Values of  $\gamma_{\text{CO}_2}$  were computed from Henry's law coefficients (Ellis and Golding, 1963) by evaluating (for each temperature and molality of sodium chloride)

$$\gamma_{\text{CO}_2} = k_{m_i}/k \quad (35)$$

where  $k$  and  $k_{m_i}$  are the Henry's law coefficients in pure water and in a sodium chloride solution of total molality,  $m_t$ . Because Henry's law coefficients are not available for concentrations of NaCl over 2 molal at high temperatures, extrapolations of  $\gamma_{\text{CO}_2}$  were also necessary. These extrapolations were accomplished for each temperature with the aid of an empirical equation, which can be written in general notation as

$$\gamma_{\chi} = 10^{\sigma \bar{I}} \quad (36)$$

where  $\gamma_{\chi}$  is the activity coefficient of a neutral complex,  $\sigma$  is the slope constant on semi-logarithmic coordinates, and  $\bar{I}$  is the true ionic strength of the solution. The true ionic strength of a sodium chloride solution is given by

$$\bar{I} = \frac{1}{2} \sum_i Z_i^2 m_i = (1 - \alpha_{\text{NaCl}}) I \quad (37)$$

where  $i$  designates the charged species in solution and  $I$  is the stoichiometric ionic strength (equiv. to  $m_{t,\text{NaCl}}$ ).

Equation (36) closely approximates the activity coefficients of a large number of molecular species in aqueous electrolyte solutions at  $25^\circ\text{C}$  (Randall and Failey, 1927a-c), and it also describes  $\gamma_{\text{CO}_2}$  in NaCl solutions up to 2  $m$  at high temperatures (Helgeson, 1967b; Helgeson and James, 1968). Because the activity coefficients of different molecular species in a given salt solution are similar (Randall and Failey, 1927a-c),

<sup>4</sup> Supercritical dissociation constants for NaCl over a wide range of temperature and pressure are also now available (Quist and Marshall, 1968a).

<sup>5</sup> At present, there is little alternative to graphic extrapolation of high temperature  $\log K(T)$  data to obtain estimates below  $281^\circ\text{C}$ . The uncertainties in the high temperature data are sufficiently large to preclude definitive least squares fits using theoretical  $\log K(T)$  expressions (Helgeson, 1967a). Attempts to obtain values of  $\log K_{\text{NaCl}}$  and  $\gamma_{\text{NaCl}}$  from least squares fits of the stoichiometric activity coefficients using equations providing for complexing have been only partly successful owing to the limited data available for the temperature range where NaCl associates to a significant degree (Helgeson and James, 1968).



TABLE 2  
Thermodynamic properties of concentrated sodium chloride solutions at elevated temperatures<sup>1</sup>

	$m, \text{NaCl}$	Temperature, °C							
		25°	50°	100°	150°	200°	250°	270°	300°
Osmotic coefficient ( $\beta_{\text{NaCl}}$ ) <sup>a</sup>	1.0	0.935	0.940	0.935	0.900	0.855	0.797	0.769 <sup>a</sup>	
	2.0	0.983	0.996	0.986	0.953	0.900	0.824	0.786	
	3.0	1.045	1.059	1.042	0.991	0.920	0.852	0.784 <sup>a</sup>	
Stoichiometric mean activity coefficient ( $\gamma_{\pm\text{NaCl}}$ ) <sup>b</sup>	1.0	0.656	0.656	0.622	0.532	0.443	0.356	0.318	0.25 <sup>p</sup>
	2.0	0.670	0.678	0.641	0.532	0.425	0.320	0.277	0.22 <sup>p</sup>
	3.0	0.719	0.728	0.687	0.546	0.419	0.301	0.254	0.20 <sup>p</sup>
Standard state dissociation constant ( $K_{\text{NaCl}}$ )					9.4°	2.63°	0.71°	0.40°	0.15 <sup>m</sup>
Degree of association ( $\alpha_{\text{NaCl}}$ ) <sup>d</sup>	1.0	0.00	0.00	0.00	0.025	0.061	0.133	0.178	0.29 <sup>p</sup>
	2.0	0.00	0.00	0.00	0.043	0.093	0.173	0.209	0.32 <sup>p</sup>
	3.0	0.00	0.00	0.00	0.056	0.115	0.206	0.238	0.34 <sup>p</sup>
True ionic strength ( $\bar{I}_{\text{NaCl}}$ ) <sup>e</sup>	1.0	1.0	1.0	1.0	0.975	0.939	0.867	0.822	0.71
	2.0	2.0	2.0	2.0	1.914	1.814	1.654	1.582	1.36
	3.0	3.0	3.0	3.0	2.832	2.655	2.382	2.285	1.98
Mean ionic activity coefficient ( $\gamma_{\pm\text{NaCl}}$ ) <sup>f</sup>	1.0	0.656	0.656	0.622	0.546	0.472	0.410	0.387	0.36 <sup>a</sup>
	2.0	0.670	0.678	0.641	0.556	0.468	0.387	0.349	0.32 <sup>a</sup>
	3.0	0.719	0.728	0.687	0.578	0.473	0.379	0.333	0.30 <sup>a</sup>
Debye-Hückel activity coefficient ( $\gamma_{\pm\text{NaCl,D-H}}$ ) <sup>g</sup>	1.0	0.599	0.598	0.566	0.497	0.429	0.384	0.388	0.36
	2.0	0.556	0.556	0.524	0.449	0.378	0.335	0.339	0.32
	3.0	0.534	0.535	0.503	0.425	0.352	0.311	0.308	0.30
Deviation function (B) <sup>h</sup>		0.041	0.043 <sub>s</sub>	0.046	0.047 <sub>s</sub>	0.047	0.034	0.015	0.0 <sup>a</sup>
Activity coefficient of carbon dioxide in NaCl solutions ( $\gamma_{\text{CO}_2}$ ) <sup>i</sup>	1.0	1.27	1.24	1.20	1.19	1.23	1.34	1.42 <sup>m</sup>	1.50
	2.0	1.57	1.50	1.44	1.40	1.47	1.67	1.83 <sup>m</sup>	2.00
	3.0	1.93	1.80	1.74 <sup>a</sup>	1.70 <sup>a</sup>	1.74 <sup>a</sup>	1.86 <sup>a</sup>	2.03 <sup>a</sup>	2.29 <sup>a</sup>

Activity of water ( $a_w$ ) <sup>j</sup>	1.0	0.9669 <sup>l</sup>	0.9667	0.9669	0.968	0.970	0.972	0.973	
	2.0	0.9316 <sup>l</sup>	0.9308	0.9315	0.934	0.937	0.942	0.945	
	3.0	0.8932 <sup>l</sup>	0.8919	0.8930	0.898	0.905	0.914	0.919	
A (Debye-Hückel) <sup>k</sup>		0.5095	0.5354	0.6019	0.6915	0.8127	0.9907	1.0905	1.2979
B (Debye-Hückel) $\times 10^{-8k}$		0.3284	0.3329	0.3425	0.3536	0.3659	0.3807	0.3879	0.4010
$\bar{a}$ (Debye-Hückel term in the Stokes-Robinson expression—eq 41)		3.94 <sup>r</sup>	4.19 <sup>r</sup>						
		3.89 <sup>q</sup>	4.20 <sup>q</sup>	4.19 <sup>q</sup>	3.58 <sup>q</sup>	3.22 <sup>q</sup>	3.43 <sup>q</sup>	3.79 <sup>q</sup>	4.4 <sup>q</sup>
h (hydration parameter—eq 41)		3.61 <sup>r</sup>	3.70 <sup>r</sup>						
		3.67 <sup>q</sup>	3.69 <sup>q</sup>	3.90 <sup>m</sup>	4.01 <sup>q</sup>	4.22 <sup>q</sup>	3.61 <sup>q</sup>	2.22 <sup>q</sup>	1.2 <sup>q</sup>

<sup>a</sup> Values at 25° and 100° are from Robinson and Stokes (1959), at 50° from Harned (1961), and at 150° and above from Gardner, Jones, and de Nordwall (1963). <sup>b</sup> The values at 25°, 50°, and 100° were taken from Harned and Owen (1958); for 150° to 270°, the values were computed from equation (28) after performing least squares fits of the osmotic coefficients using equation (31). <sup>c</sup> Extrapolated from higher temperature data (fig. 2). The values of K are consistent with molal units of concentration. <sup>d</sup> Computed from the stoichiometric activity coefficients, dissociation constants, and values of  $\gamma_{\text{CO}_2}$  in NaCl solutions (to represent  $\gamma_{\text{NaCl}}$ ) using equation (34). <sup>e</sup> Computed from the degrees of association using equation (37). <sup>f</sup> Computed from the degrees of association and the stoichiometric activity coefficients using equation (32). <sup>g</sup> Computed from  $\log \gamma_{\pm, \text{D-H}} = -A(T) |Z_+ Z_-| \bar{I}^{1/2} / (1 + \bar{a}(T)B(T)\bar{I}^{1/2})$  using the values of  $\bar{a}(T)$ ,  $A(T)$ ,  $B(T)$ , and  $\bar{I}$  given above. <sup>h</sup> Smoothed (fig. 3) values computed (using eq 38) from the mean ionic activity coefficients and those calculated from the Debye-Hückel equation. <sup>i</sup> Computed (using eq 35) from Henry's Law coefficients for CO<sub>2</sub> in water and NaCl solutions at elevated temperatures (Ellis and Golding, 1963). <sup>j</sup> Computed from the osmotic coefficients using equation (42). <sup>k</sup> Computed (Helgeson, 1967b) from equations (39) and (40) using density and dielectric constant data for water taken, respectively, from Keenan and Keyes (1936) and Akerlof and Oshry (1950). <sup>l</sup> Robinson and Stokes (1959). <sup>m</sup> Interpolated. <sup>n</sup> Extrapolated. <sup>o</sup> Computed from the values of  $K_{\text{NaCl}}$ ,  $\gamma_{\text{CO}_2}$  in NaCl solutions (to represent  $\gamma_{\text{NaCl}}$ ), and extrapolated values of the mean ionic activity coefficient (eqs 32 and 34). <sup>p</sup> Calculated from least squares fits of the mean ionic activity coefficients in the concentration range 1.0 to 3.0 m using the Stokes-Robinson equation (eq 41). <sup>q</sup> Obtained from least squares fits (eq 41) in the concentration range 0.1 to 3.0 m. <sup>r</sup> Computed from the Stokes-Robinson equation (eq 41) using the values of  $A(T)$ ,  $B(T)$ ,  $\bar{I}$ ,  $B(T)$ , and the extrapolated mean ionic activity coefficients shown above. <sup>s</sup> All values given in this table are consistent with molal units of concentration.

the assumption that  $\gamma_{\text{NaCl}} \approx \gamma_{\text{CO}_2}$  in NaCl solutions probably introduces negligible error into mean ionic activity coefficient calculations.

*Deviation function.*—The departure of the log of the mean ionic activity coefficient from that predicted by the Debye-Hückel expression at 25°C has been described by Scatchard (1936) and others with a deviation function. Pitzer and Brewer (1961) designate this function with the symbol  $B'$  to distinguish it from the limiting function at zero concentration. The deviation function at a given temperature can be defined by writing

$$B'(\bar{I}) = \frac{\log \gamma_{\pm}^* + A|Z_1 Z_2| \bar{I}^{1/2} / (1 + \bar{a} B \bar{I}^{1/2})}{\bar{I}} \quad (38)$$

in which  $\bar{a}$  is the "distance of closest approach" of the ions in solution, and  $A$  and  $B$  are the molal Debye-Hückel coefficients given by

$$A(T) = \frac{1.8246 \times 10^6 (\rho_{\text{H}_2\text{O}}(T))^{1/2}}{(\epsilon_{\text{H}_2\text{O}}(T)T)^{3/2}} \quad (39)$$

and

$$B(T) = \frac{50.29 \times 10^8 (\rho_{\text{H}_2\text{O}}(T))^{1/2}}{(\epsilon_{\text{H}_2\text{O}}(T)T)^{1/2}} \quad (40)$$

where  $\rho_{\text{H}_2\text{O}}$  is the density, and  $\epsilon_{\text{H}_2\text{O}}$  the dielectric constant of water at temperature  $T$ . Values of the  $A$  and  $B$  coefficients in equation (38) at 10 degree intervals from 25° to 350°C have been presented elsewhere (Helgeson, 1967b).

The definition of the deviation function expressed by equation (38) differs somewhat from that used previously by Scatchard (1936), Pitzer and Brewer (1961), and others to analyze the behavior of electrolyte solutions at low temperatures. The function employed by these investigators is defined by an expression of equation (38) in which stoichiometric ionic strength is used, and the product  $\bar{a}B$  is set to unity. Although this simplification is useful for considering the behavior of electrolyte solutions at low temperatures, it is desirable to include explicit provision for  $\bar{a}$  and true ionic strength in calculations of  $B'$  at high temperatures.

The deviation function,  $B'$ , is essentially independent of concentration at ionic strengths of  $\sim 0.5$  or more in most electrolyte solutions at 25°C. Cobble (1964) assumed this function to be temperature independent as well, and he employed 25°C values of  $B'$  to calculate high temperature activity coefficients. It is shown below that Cobble's assumption is invalid for concentrated sodium chloride solutions at elevated temperatures.

Prediction of the deviation function for high temperature sodium chloride solutions requires values of the Debye-Hückel  $\bar{a}$  parameter at each temperature. Because of the high sensitivity of the deviation function to small errors in the  $\bar{a}$  values used in the equation, this parameter

must be known accurately in order to define adequately the temperature dependence of the deviation function. The required values of  $\bar{a}$  were obtained by fitting the mean ionic activity coefficients in table 2 with a least squares computer routine involving the Stokes-Robinson equation (Stokes and Robinson, 1948; Robinson and Stokes, 1959).

The Stokes-Robinson equation closely describes the concentration dependence of the mean ionic activity coefficients of a large number of strong electrolytes to high concentrations at 25°C. For a given electrolyte at temperature  $T$  and true ionic strength  $\bar{I}$ , this expression appears as

$$\log \gamma_{\pm}^*(T, \bar{I}) = - \frac{A(T) |Z_1 Z_2| \bar{I}^{1/2}}{1 + \bar{a}(T) B(T) \bar{I}^{1/2}} - \frac{h(T)}{\nu} \log a_w(T, \bar{I}) - \log [1 - 0.018m(\nu - h(T))] \quad (41)$$

in which  $a_w$  is the activity of  $\text{H}_2\text{O}$ ,  $m$  is the molality of the completely dissociated solute (equivalent to  $\bar{I}$  in the case of NaCl),  $\bar{a}$  is the "distance of closest approach" of the ions in solution,  $\nu$  is the number of ions per mole of solute, and  $h$  is the average number of water molecules coordinated to  $\nu$  ions in solution. The Stokes-Robinson equation provides for the effects of ion hydration on the activity coefficient of the solute. It can be derived rigorously from equations describing the Gibbs free energy of the solution in terms of the chemical potentials of  $\text{H}_2\text{O}$  and the hydrated and unhydrated solute. Two assumptions are involved in the derivation: (1) that the coefficient  $h$  is independent of concentration, and (2) that the Debye-Hückel term in the equation accurately describes the part of the departure of activity from molality due to electrostatic interaction of the solvated ions. The excellent fits obtained by Stokes and Robinson (1948) of observed activity coefficients in a large number of concentrated electrolytes at 25°C suggest that these assumptions are valid.

Equation (41) was used to compute least squares fits of the mean ionic activity coefficients for sodium chloride solutions shown in table 2 (Helgeson and James, 1968). The values of  $\bar{I}$  in equation (41) were computed from equation (37) using the degrees of association ( $\alpha_{\text{NaCl}}$ ) given in table 2. The activities of water employed in the calculation were computed from the stoichiometric osmotic coefficient ( $\phi$ ) for each temperature and total concentration of NaCl ( $m_t$ ) by evaluating

$$\ln a_w = - \frac{\nu m_t \phi}{55.55} \quad (42)$$

The osmotic coefficients and computed activities of water are given in table 2 along with the values of  $\bar{a}(T)$  and  $h(T)$  for NaCl obtained from the least squares fits. The deviation functions calculated (eq 38) from the  $\bar{a}$  and  $\gamma_{\pm}^*$  values are also shown in table 2.

It can be seen in figure 3 that  $B'_{\text{NaCl}}$  passes through a maximum with increasing temperature, but that at each temperature  $B'_{\text{NaCl}}$  is only slightly dependent on concentration at molalities of NaCl between one and three. The maximum variation in  $B'_{\text{NaCl}}$  with concentration in the

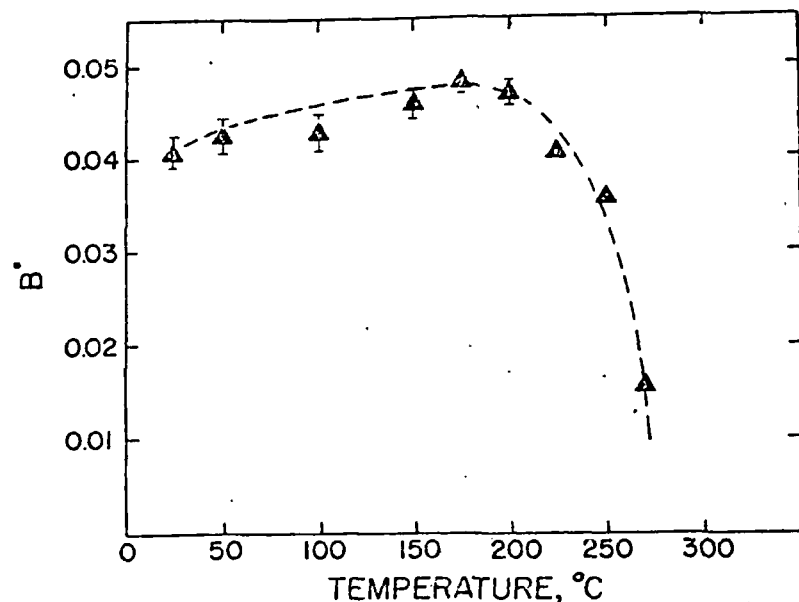


Fig. 3. Plot of the deviation function,  $B$ , against temperature for 1, 2, and 3 molal NaCl solutions. The symbols represent the mean values of  $B$  at each temperature computed from equation (38); the vertical bars on the symbols depict the maximum variation in  $B$  in 1 to 3 molal solutions. Where no vertical bar is shown, the maximum variation is within the limits of the symbol.

range 1.0 to 3.0  $m_{\text{NaCl}}$  from 25° to 270°C is  $\pm 0.002$  from the values represented by the symbols in figure 3; this variation represents a slight increase in  $B$  with increasing concentration. However, it can be seen in figure 3 that the uncertainty in the data from which the  $B$  values were calculated exceeds the extent of this variation. Although mean ionic activity coefficients for NaCl are not available above 270°C (see footnote 3, p. 743), it appears likely that  $B$  approaches zero in the region of 300°C.  $B$  also becomes small in HCl solutions at high temperatures (Helgeson and James, 1968). The behavior of  $B$  in figure 3 suggests that the simple Debye-Hückel expression in the Stokes-Robinson equation for  $\gamma_{\pm}^*$  (eq 41) is sufficient to describe the mean ionic activity coefficient of NaCl in 1 to 3 molal solutions in the region of 300°C. This is not surprising because the hydration entropies of ions at 25°C are relatively large negative numbers that would be expected to become substantially less negative with increasing temperature, and the bulk of the solute in sodium chloride solutions is associated above 300°C.

From a practical standpoint, the fact that the Debye-Hückel expression can be used to predict accurately mean ionic activity coefficients in concentrated electrolytes at high temperatures is extremely useful. Note, however, that such calculations are valid only when true (and not stoichiometric) ionic strength is used in the equation. It can be demonstrated that the product  $\bar{a}B$  (where  $B$  is the Debye-Hückel co-

efficient) for NaCl solutions is essentially independent of temperature from 25° to 270°C. Also,  $B$  is closely related to  $\gamma_{\text{CO}_2}$  in NaCl solutions, which is reflected by the relative success of the Delta approximation (Helgeson, 1964) in predicting activity coefficients at elevated temperatures. Various theoretical implications of the behavior of  $\gamma_{\text{CO}_2}$ ,  $\gamma_{\pm}^*$ ,  $\gamma_{\pm}^*$ ,  $\bar{a}$ ,  $h$ , and  $B$  for NaCl solutions and other electrolytes at elevated temperatures together with empirical correlations of these parameters with thermodynamic variables have been considered in detail elsewhere (Helgeson and James, 1968).

*True individual ion activity coefficients.*—In the derivation of the Stokes-Robinson equation (eq 41), the departure of activity from molality for the completely dissociated solute over and above that described by the Debye-Hückel term for the solvated ions is attributed to ion hydration; that is, as the concentration of the solute increases at a given temperature, the product  $B\bar{I}$ , which is numerically equivalent to the sum of the second and third terms on the right side of the Stokes-Robinson equation, is a function only of the decrease in the number of uncoordinated solvent molecules per 1000 g of water. At constant concentration in sodium chloride solutions of 1 to 3 molal, the number of uncoordinated water molecules apparently first decreases and then increases with increasing temperature above 25°C.

In a concentrated multicomponent electrolyte solution consisting predominantly of sodium chloride, ions present in small concentrations (compared to that of the sodium-chloride) should contribute negligibly to the ionic strength and total coordination of water molecules in the solution. In such an electrolyte, close approximations of individual ion activity coefficients for the species present in small concentrations can be calculated from

$$\log \gamma_{\pm}^*(T, \bar{I}) = \frac{-A(T)Z_i^2\bar{I}^{1/2}}{1 + \bar{a}_i(T)B(T)\bar{I}^{1/2}} + B(T)\bar{I} \quad (43)$$

where  $\gamma_{\pm}^*$  is the activity coefficient of the  $i$ th ion present in small concentrations in the solution,  $\bar{I}$  and  $B$  are the true ionic strength and deviation functions, respectively, for pure solutions of the supporting electrolyte, and  $\bar{a}_i$  refers to the "distance of closest approach" of the  $i$ th ion. Equation (43) can also be written for mean ionic activity coefficients of salts present in small concentrations in a sodium chloride solution. This requires only that the relation

$$\gamma_{\pm}^* = \left( \gamma_{+}^{*v_{+}} \gamma_{-}^{*v_{-}} \right)^{1/v} \quad (44)$$

be satisfied for the dissociated part of the salt in question.

Provided appropriate  $\bar{a}$  values are known for each temperature, equation (43) and the data in table 2 permit calculation of activity coefficients of ions present in small concentrations in sodium chloride solutions at high temperatures and concentrations of NaCl. Unfortunately, values of  $\bar{a}$  for most ions at high temperatures are not available, nor

can they be calculated with confidence. It appears that the best approximation that can be made in the present state of knowledge is to assume that  $\bar{a}$  coefficients for ions are independent of temperature and employ the values at 25°C in calculations of high temperature activity coefficients from equation (43). It can be seen in table 2 that  $\bar{a}$  for NaCl solutions from 25° to 300°C varies between -0.7 and 0.5 angstroms from its value at 25°C. If the  $\bar{a}$  values for other salts behave in a similar fashion, the error involved in calculating high temperature activity coefficients by assuming  $\bar{a}$  values at 25°C to be constant should be negligible compared to other uncertainties attending geochemical calculations. On the other hand, if the temperature variation of  $\bar{a}$  coefficients for other salts is similar to that exhibited by the  $\bar{a}$  for HCl, the error may be substantial at high temperatures. The  $\bar{a}$  coefficient for HCl is essentially constant from 25° to 150°C, but it increases rapidly with increasing temperature between 150° and 275°C (Helgeson and James, 1968). Nevertheless, it appears likely that the temperature dependence of  $\bar{a}$  coefficients for metal ions and metal ion complexes will prove to be more like NaCl than HCl.

Because  $\bar{a}$  coefficients tend to increase at high temperatures, high temperature activity coefficients computed from equation (43) assuming constant  $\bar{a}$  values equal to their values at 25°C should be minimal approximations. Where such approximations render individual ion activity coefficients less than  $\sim 0.1$ , the effect of small errors in the activity coefficients on calculations of solution equilibria may be large. For this reason, approximations of individual ion activity coefficients at high temperatures and concentrations of sodium chloride should be confined to monovalent and possibly divalent species. Predictions of high temperature activity coefficients in concentrated solutions of mixed electrolytes in which more than  $\sim 20$  percent of the solute is not sodium chloride requires use of Harned's rule coefficients or coefficients for a similar but higher order power function (Lietzke, Hupf, and Stoughton, 1965; Helgeson, 1967b).

*Stoichiometric individual ion activity coefficients.*—Calculations of high temperature mineral solubilities in concentrated hydrothermal solutions in which the solute is predominately sodium chloride can be simplified considerably by first computing stoichiometric individual ion activity coefficients for the solution. The stoichiometric individual ion activity coefficient,  $\gamma_i$ , is defined as

$$\gamma_i = \frac{a_i}{m_{i,i}} \quad (45)$$

where  $a_i$  and  $m_{i,i}$  designate the activity and total molality of the  $i$ th ion present in small concentrations in the sodium chloride solution. Garrels and Thompson (1962) used the symbol  $\gamma_T$  for stoichiometric individual ion activity coefficients. The  $\gamma_T$  used by Garrels and Thompson differs from the  $\gamma_i$  in equation (45) only to the extent that the latter specifically refers to the presence of the  $i$ th ion in an electrolyte solution containing a predominant concentration of some other salt.

Values of  $\gamma_i$  can be calculated for a given temperature and concentration of sodium chloride (or some other supporting electrolyte) by evaluating one of several possible mass balance relations that can be written for the  $i$ th ion, depending on its identity. For example, if  $\mathbf{C}$  represents a cation associated in a series of  $z$  mononuclear complexes involving  $y$  moles of anion L ( $y = 1, 2, 3, \dots, z$ ), we can write

$$m_{i,\mathbf{C}} = m_{\mathbf{C}} + \sum_y^z m_y \quad (46)$$

where  $m_{\mathbf{C}}$  and  $m_y$  are the molalities, respectively, of cation  $\mathbf{C}$  and the  $y$ th complex, which has the form  $\mathbf{C}L_y$ . Expressing equation (46) in terms of activities leads to

$$m_{i,\mathbf{C}} = \frac{a_{\mathbf{C}}}{\gamma_{\mathbf{C}}^*} + \sum_y^z \frac{a_{\mathbf{C}} a_{L^y}}{\beta_y \gamma_y} = a_{\mathbf{C}} \left( \frac{1}{\gamma_{\mathbf{C}}^*} + \sum_y^z \frac{a_{L^y}}{\beta_y \gamma_y} \right) \quad (47)$$

where  $\gamma_y$  is the activity coefficient of the  $y$ th complex,  $a_{\mathbf{C}}$  and  $a_L$  are the activities of the cation and anion, respectively,  $\gamma^*$  represents the true individual ion activity coefficient of the subscripted species, and  $\beta_y$  is the overall dissociation constant for the  $y$ th complex defined as

$$\beta_y = \prod_u^y K_u \quad (48)$$

where  $u$  is an integer index ( $u = 1, 2, 3, \dots, y$ ) and  $K_u$  represents the stepwise dissociation constant for the  $u$ th complex. Combining equations (45) and (47) leads to

$$\gamma_{\mathbf{C}} = \frac{1}{\frac{1}{\gamma_{\mathbf{C}}^*} + \sum_y^z \frac{a_{L^y}}{\beta_y \gamma_y}} = \frac{1}{\frac{1}{\gamma_{\mathbf{C}}^*} + \sum_y^z \frac{m_{L^y} \gamma_{L^y}^*}{\beta_y \gamma_y}} \quad (49)$$

If the total molality ( $m_i$ ) of cation  $\mathbf{C}$  is small compared to that of sodium chloride, the values of  $\gamma_{\mathbf{C}}^*$  and  $\gamma_{L^y}^*$  (and  $\gamma_y$  when the  $y$ th complex is a charged species) in equation (49) can be calculated from equation (43). The values of  $\bar{I}$  and  $B'$  used in the calculations are those obtained from equations (37) and (38) for the supporting electrolyte; the  $\beta$  values in equation (49) can be predicted from the thermodynamic relations discussed above. If the  $y$ th complex is a nonpolar neutral species,  $\gamma_y$  can be approximated as  $\gamma_{\text{CO}_2}$ ; if it is more like  $\text{H}_2\text{SiO}_4$ ,  $\gamma_y$  can be regarded as unity (Helgeson, 1964; 1967b). Where the ligand involved is chloride in a concentrated sodium chloride solution containing small concentrations of other species, the mean ionic activity of sodium chloride in a pure sodium chloride solution can be used as a close approximation of  $a_L$ . In such cases,  $m_{L^y} \gamma_{L^y}^*$  in equation (49) can be replaced by  $m_{i,\text{NaCl}}$   $\gamma_{\pm \text{NaCl}}$  and (because  $\gamma_{\pm \text{NaCl}}$  is known—table 2)  $\gamma_{\mathbf{C}}$  can then be computed as

a function of  $m_{L,NaCl}$ . Where L does not correspond to  $Cl^-$ ,  $\gamma_{\epsilon}$  can be calculated as a function of  $m_L$ . In many cases  $m_L$  in hydrothermal solutions can be approximated as  $m_{L,L}$ .

Expressions analogous to equations (46) to (49) can be derived to calculate values of  $\gamma_L$ . Such expressions are particularly useful where the anion L is associated predominantly with the hydrogen ion. Under these conditions,  $\gamma_L$  can be computed as a function of pH. By rearranging equation (45), precomputed values of  $\gamma_{\epsilon}$  and  $\gamma_L$  permit calculation of the activities of the free  $\epsilon$  and L ions in concentrated hydrothermal solutions directly from analytical data. Consequently, hydrothermal mineral solubilities can be predicted without further consideration of complexes in solution; that is, provided all important complexes are included in the calculations of the  $\gamma_{\epsilon}$  and  $\gamma_L$  values.

#### Solubility Calculations

By specifying values for such variables as pH and the total molality of NaCl in concentrated sodium chloride solutions at a particular temperature, values of  $\gamma$  for  $S^{--}$ ,  $SO_4^{--}$ ,  $CO_3^{--}$ ,  $Ag^+$ ,  $Fe^{+++}$ ,  $Cu^{++}$ , and other ions that may be present in small concentrations in hydrothermal solutions can be calculated from expressions of equation (49) or the corresponding equation for anions. Provided these calculations include provision for a realistic distribution of aqueous species, the solubility of a given mineral in the solution can then be computed from the activity product relation,

$$m_{L,i}^n m_{L,\epsilon}^v \gamma_i^n \gamma_{\epsilon}^v = K_{sp,\psi} \quad (50)$$

where  $K_{sp,\psi}$  is the activity product constant of the  $\psi$ th mineral, which consists of  $n$  moles of the  $i$ th cation and  $v$  moles of the  $\epsilon$ th anion in the system. The stoichiometric solubility (where  $\nu m_{L,i} = n m_{L,\epsilon}$ ) is then given by

$$S_{\psi} = \frac{m_{L,i}}{n} = \frac{1}{n} \left( \frac{n^v K_{sp,\psi}}{v^v \gamma_i^n \gamma_{\epsilon}^v} \right)^{1/(n+v)} \quad (51)$$

in which  $S_{\psi}$  is the solubility (in molality units) of the  $\psi$ th phase. If  $m_{L,\epsilon}$  (the total molality of the  $\epsilon$ th anion) is specified, non stoichiometric solubilities can be computed from

$$S_{\psi} = \frac{m_{L,i}}{n} = \frac{1}{n} \left( \frac{K_{sp,\psi}}{m_{L,\epsilon}^v \gamma_i^n \gamma_{\epsilon}^v} \right)^{1/n} \quad (52)$$

If more than one solid phase is in equilibrium with the solution, expressions analogous to equations (51) and (52) can be derived by combining statements of equation (50) for each solid and writing a mass balance expression relating the total molalities of each cation in solution. The mutual solubilities of the minerals in the solution can then be computed from these equations.

#### Pressure as a Variable

As indicated earlier, the pressure dependence of equilibrium constants for most hydrothermal reactions is slight (considered negligible in this discussion) at temperatures below  $\sim 300^{\circ}C$ . This is true for solid phase equilibria even at much higher temperatures, but for dissociational reactions in aqueous solution, pressure effects become significant as temperature increases above  $\sim 300^{\circ}C$ .

The need for a general method of computing equilibrium constants at high pressures and temperatures has become more acute in recent years. Experimental data for hydrothermal systems are frequently obtained at temperatures and pressures greater than  $300^{\circ}C$  and 1000 atm. The dependence of equilibrium constants on pressure is a volume function, but few ionic volumes are known for aqueous electrolytes at high temperatures and pressures, and those data that exist (Owen and Brinkley, 1941; Couture and Laidler, 1956; Zen, 1957; Hepler, 1965; Ellis, 1966, 1967, 1968) are rarely definitive with respect to the volumes of individual ions and complexes. Despite this handicap, the effect of pressure on dissociation constants in aqueous solutions of electrolytes can be closely approximated from the temperature and pressure dependence of the dielectric constant of water.

Consideration of the thermodynamic characteristics of dissociational reactions as a function of temperature suggests that the dielectric constant of water essentially controls the stabilities of complexes in aqueous solutions of electrolytes at high temperatures (Helgeson, 1967a). It can be shown that the conventional molal dissociation constant for a neutral complex in the supercritical pressure-temperature region for water can be described within the uncertainty of the experimental data by a monotonic function of the dielectric constant of the solvent; that is, the molal  $\log K(T,P)$  for a given neutral complex is essentially a constant for all pressure-temperature combinations that result in the same value of the dielectric constant of water in the supercritical region. Data are not available to determine whether the same relation exists for charged complexes in the supercritical region, but theoretical considerations suggest that the stabilities of these species should also vary monotonically with the dielectric constant of the solvent.

\*The conventional dissociation constant does not provide explicitly for the participation of the solvent in the dissociational reaction. If the reaction is written to include the correct degree of participation by the solvent, then the *isothermal* dissociation constant becomes independent of the dielectric constant of the medium (Quist and Marshall, 1968b). Most supercritical dissociation constants reported in the literature are consistent with molar units of concentration (for example, Franck, 1961; Quist and Marshall, 1966, 1968a and c). These data can be converted to be consistent with molal units of concentration by solving  $\log K_m = \log K_M - (\bar{n} - 1) \log \rho_{w,20}$  where  $K_m$  and  $K_M$  are the molal and molar dissociation constants, respectively,  $\rho_{w,20}$  represents the density of water, and  $\bar{n}$  is equal to the sum of the exponents in the Law of Mass Action equation for the dissociational reaction. Despite recent arguments to the contrary (Quist and Marshall, 1968a) dissociation constants consistent with molal units of concentration and the molal scale of concentration itself are perfectly appropriate for calculations pertaining to the supercritical region. Molal units of concentration are commonly more useful than molar units in geochemical calculations.

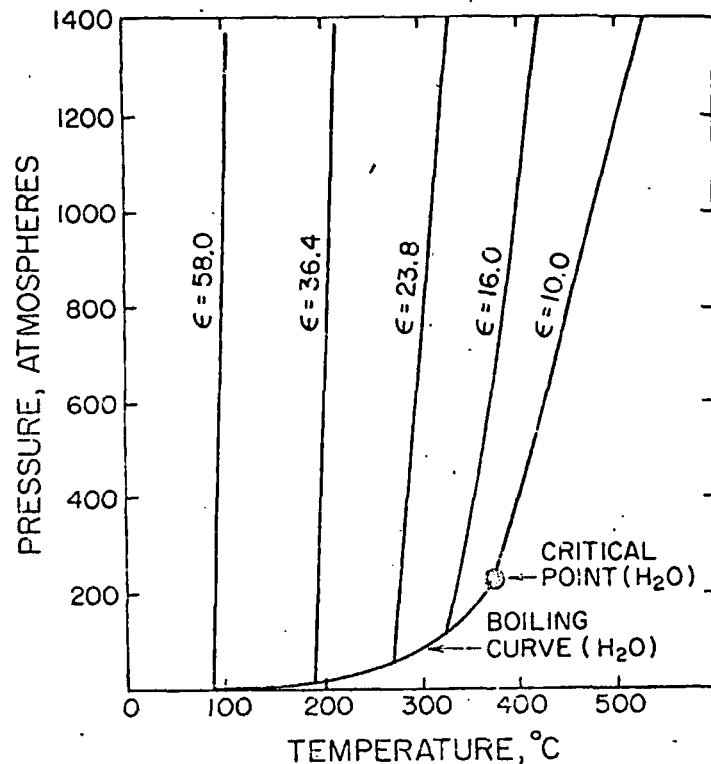
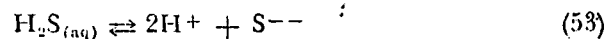


Fig. 4. Isodielectric curves for water in the liquid and supercritical phase regions. The curves were drawn from dielectric constant values taken from Quist and Marshall (1965) and density data for water obtained from Holser and Kennedy (1958).

Isodielectric curves for water are plotted in figure 4 to illustrate the order of magnitude of pressure effects on dissociation constants. For example, suppose that the molal dissociation constant for



at 1000 atm and 400°C is required for a given geochemical calculation. In figure 4 it can be seen that the dielectric constant of water under these conditions is the same as it is at 120 atm and 325°C on the boiling curve. Pressure effects contribute only slightly to dissociation constants calculated for a 1 atm standard state from high temperature experimental data obtained along the vapor + liquid pressure-temperature curve for water to ~325°C. For this reason, and also because appropriate ionic volumes are rarely available, the pressure correction (119 atm in this case) is commonly neglected, and the experimental  $\log K(T)$  values obtained from such experiments are assigned to the 1 atm standard state. Because the molal value of  $\log K(T)$  for the dissociation of a neutral complex in water at high temperatures is essentially constant along an isodielectric curve, the molal dissociation constant computed for 325°C

and 1 atm (or more accurately, 120 atm) is approximately equivalent to that at 400°C and 1000 atms.

The relation described above between  $\log K(T,P)$  and the dielectric constant of the solvent is more useful for the purpose of estimating molal  $\log K(T,P)$  values at high temperatures and pressures than density relations. This is true because  $\log K(T,P)$  for a given reaction cannot be characterized as a single monotonic function of density at all pressure and temperature combinations contributing to constant density. On the other hand, isentropes for water are essentially coincident with the isodielectric curves shown in figure 4, which means that  $\log K(T,P)$  can also be approximated as a monotonic function of the entropy of the solvent (Helgeson, 1964).

If a molar scale of concentration is used and the dissociational reaction is written to include the correct degree of solvation of the participating species in solution, the corresponding supercritical dissociation constant is independent of pressure (Quist and Marshall, 1968a). Consequently, these dissociation constants can be computed for any pressure-temperature condition solely from predictive equations involving temperature, such as those presented in the preceding pages. However, in practice this approach is usually precluded by the dearth of information concerning the actual extent of solvation (hydration numbers) of the various species in hydrothermal solutions at high temperatures.

#### COMPUTER CALCULATIONS AND RESULTS

The equations and methods of calculation summarized in the preceding pages have been programmed for machine computation. The results of calculations carried out with the aid of these computer programs are discussed below and presented in tables 1 to 14 and figures 5 to 21. The data employed in the calculations are also presented in the tables, along with references to the sources from which they were taken. In certain cases (noted in the footnotes in the tables) thermodynamic values reported in the literature have been changed (within the margins of uncertainty reported in the source references) to agree with other experimental and geologic observations, and estimates of thermodynamic properties are given for a number of species for which data are incomplete. The values listed in the tables are the result of a critical compilation, and they are intended to constitute an internally consistent array of thermodynamic data.

#### Dissociation Constants

Thermodynamic data at 25°C and 1 atm for various species and dissociational reactions of interest in hydrothermal studies are summarized in tables 3 and 4 along with calculated average heat capacities and  $\log K(T)$  values for higher temperatures. The dissociation constants, which were computed from equations (11) to (17) using thermodynamic data given in tables 3 and 4, are also plotted in figure 5 to illustrate the changes in the stabilities of hydrothermal species with increasing temperature.

TABLE 3  
Thermodynamic data for species in aqueous solution at 25°C and 1 atm

Species	$\Delta H_f^\circ$ <sup>a</sup> (cal mole <sup>-1</sup> )	$S^\circ$ (cal mole <sup>-1</sup> deg <sup>-1</sup> )	Average heat capacity <sup>a</sup> (cal mole <sup>-1</sup> deg <sup>-1</sup> )					
			60°C	100°C	150°C	200°C	250°C	300°C
H <sub>4</sub> SiO <sub>4</sub>	-348,060 <sup>b</sup>	45.84 <sup>b</sup>	49 <sup>p</sup>	49 <sup>p</sup>	46 <sup>p</sup>	46 <sup>p</sup>	46 <sup>p</sup>	45 <sup>p</sup>
H <sub>2</sub> S	-9,030 <sup>c</sup>	30.9 <sup>d</sup>	46 <sup>m</sup>	39 <sup>m</sup>	35 <sup>m</sup>	32 <sup>m</sup>	33 <sup>n</sup>	35.5 <sup>n</sup>
HS <sup>-</sup>	-4,230 <sup>c</sup>	15.0 <sup>e</sup>	-52	-58	-62	-66	-70	-76
S <sup>2-</sup>	9,070 <sup>f</sup>	-4.0 <sup>e</sup>	-48	-58	-61	-65	-69	-75
SO <sub>4</sub> <sup>2-</sup>	-217,320 <sup>c</sup>	4.8 <sup>g</sup>	-99	-108	-105	-114	-120	-126
CO <sub>3</sub> <sup>2-</sup>	-161,840 <sup>c</sup>	-13.6 <sup>g</sup>	-132	-146	-138	-151	-162	-171
OH <sup>-</sup>	-54,970 <sup>c</sup>	-2.57 <sup>g</sup>	-47	-58	-61	-65	-69	-76
Cl <sup>-</sup>	-39,950 <sup>c</sup>	13.51 <sup>g</sup>	-51	-58	-62	-66	-70	-76
F <sup>-</sup>	-79,500 <sup>c</sup>	-3.3 <sup>g</sup>	-47	-58	-61	-65	-69	-75
H <sub>2</sub> O <sub>(l)</sub>	-68,315 <sup>c</sup>	16.71 <sup>g</sup>	18	18	18	18	18	18
H <sup>+</sup>	0.0	0.0	23	31	33	35	37	39
Ag <sup>+</sup>	25,310 <sup>c</sup>	17.69 <sup>g</sup>	30	39	39	43	45	47
Cu <sup>+</sup>	16,930 <sup>b</sup>	9.4 <sup>g</sup>	33	44	43	47	50	53
Cu <sup>2+</sup>	15,390 <sup>c</sup>	-23.6 <sup>g</sup>	49	65	66	71	75	79
Pb <sup>2+</sup>	-400 <sup>c</sup>	2.5 <sup>g</sup>	37	49	49	54	58	61
Zn <sup>2+</sup>	-36,780 <sup>c</sup>	-26.0 <sup>g</sup>	50	66	67	73	77	81
Hg <sup>2+</sup>	41,590 <sup>c</sup>	-5.4 <sup>g</sup>	41	54	55	60	63	67
Fe <sup>2+</sup>	-21,000 <sup>c</sup>	-27.1 <sup>g</sup>	50	66	68	73	78	82

Species	$\Delta H_f^\circ$ <sup>a</sup> (cal mole <sup>-1</sup> )	$S^\circ$ (cal mole <sup>-1</sup> deg <sup>-1</sup> )	Average heat capacity <sup>a</sup> (cal mole <sup>-1</sup> deg <sup>-1</sup> )					
			60°C	100°C	150°C	200°C	250°C	300°C
Fe <sup>3+</sup>	-11,400 <sup>c</sup>	-70.1 <sup>c</sup>	70	93	96	105	109	115
Ca <sup>2+</sup>	-129,770 <sup>c</sup>	-13.2 <sup>c</sup>	45	59	60	66	68	72
Mg <sup>2+</sup>	-110,410 <sup>c</sup>	-28.2 <sup>c</sup>	51	67	69	75	79	83
Ba <sup>2+</sup>	-128,670 <sup>c</sup>	3.0 <sup>c</sup>	38	50	50	55	58	61
K <sup>+</sup>	-60,040 <sup>c</sup>	24.5 <sup>c</sup>	27	35	35	39	41	43
Na <sup>+</sup>	-57,279 <sup>c</sup>	14.4 <sup>c</sup>	35	41	41	45	47	49
Al <sup>3+</sup>	-127,000 <sup>c</sup>	-76.9 <sup>c</sup>	72	95	99	108	114	120
Au <sup>+</sup>		22.0 <sup>k</sup>	29	37	37	41	45	45
Au <sup>3+</sup>		-23.0 <sup>l</sup>	50	67	69	74	78	82

<sup>a</sup> Computed from equations (2) to (5) and the entropies shown above (Criss and Cobble, 1964a and b). <sup>b</sup> Computed from a constant  $\Delta C_p$  least squares fit of quartz solubilities measured by Morey, Fournier, and Rowe (1962) and Kennedy (1950) using the thermodynamic data for quartz given in table 7. <sup>c</sup> Computed from  $\Delta H_f^\circ$  for  $\text{H}_2\text{S}_{(g)} = -4930$  cal mole<sup>-1</sup> (Wagman and others, 1968) and a value of  $\Delta H_f^\circ$  for  $\text{H}_2\text{S}_{(aq)} \rightleftharpoons \text{H}_2\text{S}_{(g)}$  of  $-4100$  cal mole<sup>-1</sup> (Pohl, 1961; table 10). <sup>d</sup> Computed from  $S^\circ$  for  $\text{H}_2\text{S}_{(g)} = 49.16$  cal mole<sup>-1</sup> deg<sup>-1</sup> (Wagman and others, 1968) and a value of  $\Delta S^\circ$  for  $\text{H}_2\text{S}_{(g)} \rightleftharpoons \text{H}_2\text{S}_{(aq)}$  of  $-18.3$  cal mole<sup>-1</sup> deg<sup>-1</sup> (Pohl, 1961; Wright and Maass, 1932; table 10). <sup>e</sup> Wagman and others (1965, 1966, 1968). <sup>f</sup> Calculated from  $\log K_{HS^-} = -13.9$  (Maronny, 1959; Muhammed and Sundaram, 1961) and the entropy values shown above for HS<sup>-</sup> and S<sup>2-</sup>. This value of  $\Delta H_f^\circ$  for S<sup>2-</sup>, which is consistent with the other data given above for species involving S<sup>2-</sup>, differs from that (7900 cal mole<sup>-1</sup>) reported by Wagman and others (1968). <sup>g</sup> Latimer (1952). <sup>h</sup> Calculated from  $\log K(T)$  for the disproportionation of the cuprous ion (Fenwick, 1926; table 10) using the values of  $S^\circ_{\text{Cu}^+}$ ,  $S^\circ_{\text{Cu}^{2+}}$ , and  $\Delta H_f^\circ$  for Cu<sup>2+</sup> shown above together with the data for Cu<sup>+</sup> given in table 6. <sup>i</sup> Wagman (1951). <sup>j</sup> Wulff (1957). <sup>k</sup> Computed from a prediction of the dissociational entropy for AuCl from equations (25) and (27).  $S^\circ_{\text{AuCl}} = 13.51$  (Ahluwalia and Cobble, 1964), and a value of  $S^\circ_{\text{AuCl}}$  computed from Cobble's (1953) equation for neutral species. <sup>l</sup> Calculated from the predicted dissociational entropy for AuCl<sup>-</sup> in table 1 using  $S^\circ_{\text{AuCl}_2^-} = 61$  cal mole<sup>-1</sup> deg<sup>-1</sup> (Latimer, 1952). <sup>m</sup> Helgeson (1967a). <sup>n</sup> Computed (Helgeson, 1967a) from least squares fits of equation (17) to equilibrium constants for  $\text{H}_2\text{S}_{(g)} \rightleftharpoons \text{H}_2\text{S}_{(aq)}$  at elevated temperatures (Kozinsteva, 1964). The high temperature values of  $\Delta H_f^\circ$  for  $\text{H}_2\text{S}_{(g)}$  used in the calculations were computed from a heat capacity power function (eq 10, table 8) and the value of  $\Delta H_f^\circ$  for  $\text{H}_2\text{S}_{(g)}$  at 25°C given in footnote c above. <sup>o</sup> Calculated from quartz solubilities (Morey, Fournier, and Rowe, 1962; Kennedy, 1950) and the thermodynamic data given in table 7 for quartz. <sup>p</sup> Enthalpy of formation from the elements. <sup>q</sup> Compared to  $-3.5$  cal mole<sup>-1</sup> deg<sup>-1</sup> (Wagman and others, 1968). <sup>r</sup> Ahluwalia and Cobble (1964). <sup>s</sup> Compared to  $-26.8$  cal mole<sup>-1</sup> deg<sup>-1</sup> (Wagman and others, 1968).

TABLE 4  
Thermodynamic data for dissociational equilibria in aqueous solution<sup>bbb</sup>

Reaction <sup>a</sup>	$\Delta H^\circ$ , (T <sub>r</sub> ) (cal mole <sup>-1</sup> )	$\Delta S^\circ$ , (T <sub>r</sub> ) (cal mole <sup>-1</sup> deg <sup>-1</sup> )	log K(T) <sup>11</sup>							
			25°C	50°C	60°C	100°C	150°C	200°C	250°C	300°C
H <sub>2</sub> O <sub>(liq)</sub> ⇌ H <sup>+</sup> + OH <sup>-</sup>	13,335 <sup>b</sup>	-19.31 <sup>c</sup>	-14.00 <sup>d,ff</sup>	-13.27 <sup>d,ff</sup>	-13.03 <sup>d,ff</sup>	-12.26 <sup>d,ff</sup>	-11.64 <sup>d,ff</sup>	-11.27 <sup>d,ff</sup>	-11.13 <sup>d,ff</sup>	-11.50 <sup>d</sup>
H <sub>2</sub> S ⇌ H <sup>+</sup> + HS <sup>-</sup>	4,800 <sup>a</sup>	-15.9 <sup>f</sup>	-6.92 <sup>g</sup>	-6.77 <sup>h,gg</sup>	-6.72 <sup>h,gg</sup>	-6.63 <sup>h,gg</sup>	-6.72 <sup>h</sup>	-6.96 <sup>h</sup>	-7.35 <sup>h</sup>	-8.66 <sup>h</sup>
HS <sup>-</sup> ⇌ H <sup>+</sup> + S <sup>2-</sup>	13,300 <sup>a</sup>	-19.0 <sup>f</sup>	-13.90 <sup>i</sup>	-13.13 <sup>h,gg</sup>	-12.84 <sup>h,gg</sup>	-11.78 <sup>h,gg</sup>	-10.62 <sup>h</sup>	-9.57 <sup>h</sup>	-8.61 <sup>h</sup>	-7.72 <sup>h</sup>
HSO <sub>3</sub> <sup>-</sup> ⇌ H <sup>+</sup> + SO <sub>3</sub> <sup>2-</sup>	-3,850 <sup>l</sup>	-22.0 <sup>j</sup>	-1.99 <sup>k,l</sup>	-2.27 <sup>l</sup>	-2.40 <sup>d,ff</sup>	-2.99 <sup>l</sup>	-3.74 <sup>l</sup>	-4.49 <sup>l</sup>	-5.41 <sup>d,ff</sup>	-7.06 <sup>d</sup>
H <sub>2</sub> SO <sub>4</sub> <sup>-</sup> ⇌ H <sup>+</sup> + HSO <sub>4</sub> <sup>-</sup>									0.6 <sup>m</sup>	0.5 <sup>m</sup>
H <sub>2</sub> CO <sub>(app)</sub> <sup>na</sup> ⇌ H <sup>+</sup> + HCO <sub>3</sub> <sup>-</sup>	1,840 <sup>n</sup>	-22.9 <sup>o</sup>	-6.35 <sup>p</sup>	-6.31 <sup>d,ff</sup>	-6.52 <sup>d,ff</sup>	-6.45 <sup>d,ff</sup>	-6.73 <sup>d,ff</sup>	-7.05 <sup>d,ff</sup>	-7.63 <sup>d,ff</sup>	-8.36 <sup>d</sup>
HCO <sub>3</sub> <sup>-</sup> ⇌ H <sup>+</sup> + CO <sub>3</sub> <sup>2-</sup>	3,600 <sup>n</sup>	-35.16 <sup>c</sup>	-19.52 <sup>q</sup>	-10.17 <sup>d,ff</sup>	-10.15 <sup>d,ff</sup>	-10.16 <sup>d,ff</sup>	-10.29 <sup>d,ff</sup>	-10.68 <sup>d,ff</sup>	-11.43 <sup>d,ff</sup>	-13.38 <sup>d</sup>
HAs(OH) <sub>3</sub> ⇌ H <sup>+</sup> + H <sub>2</sub> As(OH) <sub>2</sub> <sup>-</sup>	3,430 <sup>rr</sup>	-82.9 <sup>rr</sup>	-20.6 <sup>ww</sup>	-20.5 <sup>t</sup>	-20.5 <sup>t</sup>	-20.8 <sup>t</sup>	-21.8 <sup>t</sup>	-23.6 <sup>t</sup>		
HAs(OH) <sub>2</sub> <sup>-</sup> ⇌ H <sup>+</sup> + HAS(OH) <sub>2</sub> <sup>-</sup>	5,120 <sup>rr</sup>	-66.9 <sup>rr</sup>	-18.4 <sup>ww</sup>	-18.2 <sup>t</sup>	-18.1 <sup>t</sup>	-18.2 <sup>t</sup>	-18.8 <sup>t</sup>	-20.1 <sup>t</sup>		
HAs(OH) <sub>2</sub> <sup>-</sup> ⇌ H <sup>+</sup> + As(OH) <sub>4</sub> <sup>-</sup>	4,350 <sup>rr</sup>	-98.9 <sup>rr</sup>	-11.7 <sup>ww</sup>	-11.5 <sup>t</sup>	-11.4 <sup>t</sup>	-11.4 <sup>t</sup>	-11.7 <sup>t</sup>	-12.3 <sup>t</sup>		
HAs(OH) <sub>3</sub> ⇌ H <sup>+</sup> + As(OH) <sub>4</sub> <sup>-</sup>	6,560 <sup>rr</sup>	-20.2 <sup>rr</sup>	-9.2 <sup>ww</sup>	-8.9 <sup>t</sup>	-8.8 <sup>t</sup>	-8.4 <sup>t</sup>	-8.3 <sup>t</sup>	-8.4 <sup>t</sup>		
As(OH) <sub>3</sub> ⇌ As(OH) <sub>2</sub> + OH <sup>-</sup>	6,800 <sup>rr</sup>	0.7 <sup>rr</sup>	-4.8 <sup>ww</sup>	-4.4 <sup>t</sup>	-4.3 <sup>t</sup>	-3.8 <sup>t</sup>	-3.3 <sup>t</sup>	-2.9 <sup>t</sup>		
Al(OH) <sub>3</sub> ⇌ Al <sup>3+</sup> + 4OH <sup>-</sup>	10,300 <sup>x</sup>	-115.2 <sup>yy</sup>	-32.73 <sup>zz</sup>	-32.3 <sup>t</sup>	-32.2 <sup>t</sup>	-32.2 <sup>t</sup>	-33.0 <sup>tt,xx</sup>	-34.6 <sup>tt,xx</sup>	-36.7 <sup>tt,xx</sup>	-39.5 <sup>tt</sup>
Al(OH) <sub>3</sub> ⇌ Al <sup>3+</sup> + OH <sup>-</sup>	-1,990 <sup>x</sup>	-49.0 <sup>yy</sup>	-9.25 <sup>zz</sup>	-9.4 <sup>t</sup>	-9.5 <sup>t</sup>	-10.0 <sup>t</sup>	-10.8 <sup>tt,xx</sup>	-11.9 <sup>tt,xx</sup>	-13.1 <sup>tt,xx</sup>	-14.7 <sup>tt</sup>
KSO <sub>4</sub> <sup>-</sup> ⇌ K <sup>+</sup> + SO <sub>4</sub> <sup>2-</sup>	-2,655 <sup>tt,xx</sup>	12.7 <sup>tt,xx</sup>	0.84 <sup>tt,xx</sup>	-1.06 <sup>tt,xx</sup>	-1.06 <sup>tt,xx</sup>	-1.30 <sup>tt,xx</sup>	-1.60 <sup>tt,xx</sup>	-1.94 <sup>tt,xx</sup>		
KH <sub>2</sub> O ⇌ K <sup>+</sup> + HSO <sub>4</sub> <sup>-</sup>									0.8 <sup>r</sup>	-0.3 <sup>r</sup>
CaSO <sub>4</sub> ⇌ Ca <sup>2+</sup> + SO <sub>4</sub> <sup>2-</sup>	-1,760 <sup>d,pp</sup>	16.5 <sup>d,pp</sup>	2.31 <sup>d,pp</sup>	2.4 <sup>d,t,pp</sup>	2.5 <sup>d,t,pp</sup>	2.7 <sup>d,t,pp</sup>	3.1 <sup>d,t,pp</sup>	3.6 <sup>d,t,pp</sup>		
MgSO <sub>4</sub> ⇌ Mg <sup>2+</sup> + SO <sub>4</sub> <sup>2-</sup>	-4,920 <sup>d,pp</sup>	26.8 <sup>d,pp</sup>	2.25 <sup>d,pp</sup>	2.6 <sup>d,t,pp</sup>	2.7 <sup>d,t,pp</sup>	3.2 <sup>d,t,pp</sup>	3.9 <sup>d,t,pp</sup>	4.8 <sup>d,t,pp</sup>		
MnSO <sub>4</sub> ⇌ Mn <sup>2+</sup> + SO <sub>4</sub> <sup>2-</sup>	-3,700 <sup>d</sup>	22.7 <sup>d</sup>	2.25 <sup>t</sup>	2.5 <sup>d,t</sup>	2.6 <sup>d,t</sup>	3.0 <sup>d,t</sup>	3.6 <sup>d,t</sup>	4.3 <sup>d,t</sup>		

ZnSO <sub>4</sub> ⇌ Zn <sup>2+</sup> + SO <sub>4</sub> <sup>2-</sup>	-4,090 <sup>d</sup>	24.5 <sup>d</sup>	2.38 <sup>n</sup>	2.6 <sup>d,t</sup>	2.7 <sup>d,t</sup>	3.2 <sup>d,t</sup>	3.8 <sup>d,t</sup>	4.6 <sup>d,t</sup>		
Ag <sub>2</sub> SO <sub>4</sub> ⇌ 2Ag <sup>+</sup> + SO <sub>4</sub> <sup>2-</sup>	-1,500 <sup>w</sup>	11.0 <sup>w</sup>	1.30 <sup>w</sup>	1.4 <sup>t</sup>	1.4 <sup>t</sup>	1.6 <sup>t</sup>	1.9 <sup>t</sup>	2.2 <sup>t</sup>		
CaCO <sub>3</sub> ⇌ Ca <sup>2+</sup> + CO <sub>3</sub> <sup>2-</sup>	-3,130 <sup>n</sup>	25.1 <sup>s</sup>	3.20 <sup>t</sup>	3.4 <sup>t,xx</sup>	3.5 <sup>t,xx</sup>	3.9 <sup>t,xx</sup>	4.5 <sup>t,xx</sup>	5.2 <sup>t,xx</sup>		
NaCl ⇌ Na <sup>+</sup> + Cl <sup>-</sup>							0.97 <sup>aa,bb</sup>	0.42 <sup>aa,bb</sup>	-0.15 <sup>aa,bb</sup>	-0.82 <sup>tt</sup>
KCl ⇌ K <sup>+</sup> + Cl <sup>-</sup>								0.9 <sup>aa,cc</sup>	0.3 <sup>aa,cc</sup>	-0.6 <sup>tt</sup>
HCl ⇌ H <sup>+</sup> + Cl <sup>-</sup>	-18,630 <sup>d</sup>	34.4 <sup>d</sup>	6.1 <sup>dd</sup>	5.0 <sup>dd</sup>	4.56 <sup>d,ff</sup>	2.90 <sup>d,ff</sup>	1.23 <sup>d,ff</sup>	0.06 <sup>ff</sup>	-0.67 <sup>d,ff</sup>	-1.24 <sup>d,ff</sup>
Mg(OH) <sub>2</sub> ⇌ Mg <sup>2+</sup> + OH <sup>-</sup>	-2,140 <sup>x</sup>	19.0 <sup>uu</sup>	2.60 <sup>vv</sup>	2.7 <sup>t</sup>	2.8 <sup>t</sup>	3.1 <sup>t</sup>	3.6 <sup>t</sup>	4.1 <sup>t,yy</sup>		
Fe(OH) <sub>3</sub> ⇌ Fe <sup>3+</sup> + OH <sup>-</sup>	2,700 <sup>x</sup>	17.0 <sup>uu</sup>	5.7 <sup>aa</sup>	5.6 <sup>t</sup>	5.5 <sup>t</sup>	5.4 <sup>t</sup>	5.5 <sup>t</sup>	5.7 <sup>t,yy</sup>		

<sup>a</sup> All species shown in this column are aqueous, and H<sub>2</sub>O refers to liquid water. <sup>b</sup> Hale, Izat, and Christensen (1963) and Vanderzee and Swanson (1963). <sup>c</sup> Calculated from log K(T<sub>r</sub>) and ΔH<sup>o</sup>(T<sub>r</sub>). <sup>d</sup> Helgeson (1967a). <sup>e</sup> Computed from data given in table 3. <sup>f</sup> Cobble (1964). <sup>g</sup> Ellis and Goldin (1959) and Muhammad and Sundaram (1961). <sup>h</sup> Computed from data given in table 3 using equation (6). <sup>i</sup> Marony (1959) and Muhammad and Sundaram (1961). <sup>j</sup> Criss and Cobble (1951b). <sup>k</sup> Young and Irish (1962). <sup>l</sup> Lietzke and Stoughton (1961). <sup>m</sup> Extrapolated as a dielectric constant function from supercritical log K(T,P) values published by Quist and Marshall (1965). <sup>n</sup> Pitzer (1937). <sup>o</sup> Harned and Davis (1943). <sup>p</sup> Harned and Scholes (1944). <sup>q</sup> Extrapolated as a dielectric constant function from supercritical log K(T,P) values published by Quist and Marshall (1966). <sup>r</sup> Bell and George (1953). <sup>s</sup> Estimates calculated from equation (16). <sup>t</sup> Nair and Nancollas (1958). <sup>u</sup> Nair and Nancollas (1959). <sup>v</sup> Hopkins and Wulff (1965). <sup>w</sup> Calculated from log K(T<sub>r</sub>) and ΔS<sup>o</sup>(T<sub>r</sub>). <sup>x</sup> Estimated from an entropy correlation plot by Lafon (ms). <sup>y</sup> Garrels and Thompson (1962). <sup>z</sup> Extrapolated. <sup>aa</sup> Figure 2 in table 2. <sup>ab</sup> Figure 2. <sup>ac</sup> Robinson (1936). <sup>ad</sup> Pearson, Copeland, and Benson (1963b) and a value of 28.0 cal mole<sup>-1</sup> deg<sup>-1</sup> for S<sup>o</sup><sub>Al(OH)<sub>3</sub></sub> (Wagman and others, 1968). <sup>ae</sup> Computed from the free energy of formation of crystalline gibbsite (table 12), the hydrolysis equilibrium constant for crystalline gibbsite (Al(OH)<sub>3</sub>(cr) + H<sub>2</sub>O<sub>(liq)</sub> ⇌ Al(OH)<sub>4</sub><sup>-</sup> + H<sup>+</sup>; log K(T<sub>r</sub>) = -15.3, Kittrick, 1966), and the ΔG<sup>o</sup>(T<sub>r</sub>) values for Al<sup>3+</sup> and OH<sup>-</sup> given by Wagman and others (1968). <sup>af</sup> Estimated entropy of dissociation calculated from an expression analogous to equation (25) and an entropy correlation plot for hydroxyl complexes similar to that shown in figure 1 for chloride species but including provision for charge. <sup>ag</sup> Calculated by applying correction factors to log values computed from equation (16). The correction factors were taken to be equivalent to those for ammonium hydroxide (0.86 at 300°C, Helgeson, 1967a). <sup>ah</sup> Computed from ΔH<sup>o</sup>(T<sub>r</sub>) and ΔS<sup>o</sup>(T<sub>r</sub>). <sup>ai</sup> Computed by the method of least squares from log K(T) values reported by Truesdell and Hettler (1968) and Quist and others (1963). <sup>aj</sup> Computed from the equilibrium constant for Al<sup>3+</sup> + H<sub>2</sub>O<sub>(liq)</sub> ⇌ Al(OH)<sub>3</sub> + H<sup>+</sup> (10<sup>-5.2</sup>; Hem and Hershon, 1967). <sup>ak</sup> Hostetler (1963). <sup>al</sup> Leussing and Kolthoff (1953). <sup>am</sup> Dissociation constants for NaCO<sub>3</sub>, MgCO<sub>3</sub>, MgHCO<sub>3</sub>, CaHCO<sub>3</sub>, and NaSO<sub>4</sub> which are not included in this table, have been computed recently by Lafon (ms) for temperatures from 0° to 100°C.



TABLE 5  
Predicted dissociation constants for metal chloride complexes in aqueous solution at elevated temperatures

Dissociational Reaction	$\Delta H^\circ_r(T_r)^a$ (cal mole <sup>-1</sup> )	$\Delta S^\circ_r(T_r)^b$ (cal mole <sup>-1</sup> deg <sup>-1</sup> )	log $\beta(T)^c$						
			25°C	50°C	100°C	150°C	200°C	250°C	300°C
$\text{AgCl} \rightleftharpoons \text{Ag}^+ + \text{Cl}^-$	2,540	-6.6	-3.31 <sup>d</sup>	-3.17	-2.99	-2.92	(-2.9)	(-3.0) <sup>e</sup>	(-3.4) <sup>f</sup>
$\text{AgCl}_2^- \rightleftharpoons \text{Ag}^+ + 2\text{Cl}^-$	4,230	-9.8	-5.25 <sup>d</sup>	-5.02	-4.71	-4.57	(-4.6)	(-4.7) <sup>e</sup>	(-5.2) <sup>f</sup>
$\text{AgCl}_3^{2-} \rightleftharpoons \text{Ag}^+ + 3\text{Cl}^-$	3,280	-13.2	-5.25 <sup>d</sup>	-5.08	-4.88	-4.85	(-5.0)	(-5.3) <sup>e</sup>	(-6.0) <sup>f</sup>
$\text{AgCl}_4^{3-} \rightleftharpoons \text{Ag}^+ + 4\text{Cl}^-$	2,680	-16.4	-5.51 <sup>d</sup>	-5.38	-5.26	-5.31	(-5.6)	(-6.0) <sup>e</sup>	(-6.9) <sup>f</sup>
$\text{CuCl}_2^- \rightleftharpoons \text{Cu}^+ + 2\text{Cl}^-$	420	-21.2	-4.94 <sup>d</sup>	-4.94	-5.06	-5.35	(-5.8)	(-6.5) <sup>e</sup>	(-7.4) <sup>f</sup>
$\text{CuCl}_3^{2-} \rightleftharpoons \text{Cu}^+ + 3\text{Cl}^-$	-260	-24.4	-5.14 <sup>d</sup>	-5.18	-5.39	-5.77	(-6.4)	(-7.2) <sup>e</sup>	(-8.3) <sup>f</sup>
$\text{CuCl}_4^{3-} \rightleftharpoons \text{Cu}^+ + 4\text{Cl}^-$	-8,650	-29.1	-0.01 <sup>h</sup>	-0.53	-1.54	-2.57	(-3.7)	(-4.8) <sup>e</sup>	(-6.0) <sup>f</sup>
$\text{CuCl}_2 \rightleftharpoons \text{Cu}^{2+} + 2\text{Cl}^-$	-10,560	-32.2	0.69 <sup>i</sup>	0.06	-1.15	-2.36	(-3.7)	(-4.9) <sup>e</sup>	(-6.5) <sup>f</sup>
$\text{CuCl}_3^- \rightleftharpoons \text{Cu}^{2+} + 3\text{Cl}^-$	-13,690	-35.4	2.29 <sup>i</sup>	1.48	-0.04	-1.52	(-3.1)	(-4.6) <sup>e</sup>	(-6.5) <sup>f</sup>
$\text{CuCl}_4^{2-} \rightleftharpoons \text{Cu}^{2+} + 4\text{Cl}^-$	-17,780	-38.6	4.59 <sup>i</sup>	3.54	1.63	-0.16	(-2.0)	(-3.9) <sup>e</sup>	(-6.1) <sup>f</sup>
$\text{PbCl} \rightleftharpoons \text{Pb}^{2+} + \text{Cl}^-$	-380	-8.6	-1.60 <sup>j</sup>	-1.63	-1.73	-1.88	(-2.1)	(-2.4) <sup>e</sup>	(-3.0) <sup>f</sup>
$\text{PbCl}_2 \rightleftharpoons \text{Pb}^{2+} + 2\text{Cl}^-$	-1,080	-11.8	-1.78 <sup>j</sup>	-1.85	-2.04	-2.29	(-2.6)	(-3.1) <sup>e</sup>	(-3.9) <sup>f</sup>
$\text{PbCl}_3^- \rightleftharpoons \text{Pb}^{2+} + 3\text{Cl}^-$	-2,170	-15.0	-1.62 <sup>j</sup>	-1.81	-2.13	-2.50	(-3.0)	(-3.6) <sup>e</sup>	(-4.6) <sup>f</sup>
$\text{PbCl}_4^{2-} \rightleftharpoons \text{Pb}^{2+} + 4\text{Cl}^-$	-3,530	-18.2	-1.33 <sup>j</sup>	-1.59	-2.05	-2.57	(-3.2)	(-4.0) <sup>e</sup>	(-5.3) <sup>f</sup>
$\text{ZnCl} \rightleftharpoons \text{Zn}^{2+} + \text{Cl}^-$	-7,790	-28.1	-0.43 <sup>k</sup>	-0.90	-1.82	-2.78	(-3.9)	(-4.8) <sup>e</sup>	(-6.0) <sup>f</sup>
$\text{ZnCl}_2 \rightleftharpoons \text{Zn}^{2+} + 2\text{Cl}^-$	-8,500 <sup>l</sup>	-31.3	-0.61 <sup>k</sup>	-1.12	-2.13	-3.19	(-4.4)	(-5.5) <sup>e</sup>	(-6.9) <sup>f</sup>
$\text{ZnCl}_3^- \rightleftharpoons \text{Zn}^{2+} + 3\text{Cl}^-$	-9,560	-34.5	-0.53 <sup>k</sup>	-1.14	-2.25	-3.34	(-4.8)	(-6.0) <sup>e</sup>	(-7.7) <sup>f</sup>

$\text{ZnCl}_4^{2-} \rightleftharpoons \text{Zn}^{2+} + 4\text{Cl}^-$	-10,960	-37.7	-0.20 <sup>k</sup>	-0.89	-2.14	-3.35	(-5.0)	(-6.4) <sup>e</sup>	(-8.3) <sup>f</sup>
$\text{HgCl} \rightleftharpoons \text{Hg}^{2+} + \text{Cl}^-$	4,800 <sup>m</sup>	-12.5	-6.25 <sup>n</sup>	-5.99	-5.65	-5.50	(-5.5)	(-5.8) <sup>e</sup>	(-6.4) <sup>f</sup>
$\text{HgCl}_2 \rightleftharpoons \text{Hg}^{2+} + 2\text{Cl}^-$	13,400 <sup>n</sup>	-15.7	-13.25 <sup>n</sup>	-12.51	-11.41	-10.71	(-10.4)	(-10.3) <sup>e</sup>	(-10.8) <sup>f</sup>
$\text{HgCl}_3^- \rightleftharpoons \text{Hg}^{2+} + 3\text{Cl}^-$	15,300 <sup>n</sup>	-18.9	-15.35 <sup>n</sup>	-14.50	-13.25	-12.46	(-12.1)	(-12.1) <sup>e</sup>	(-12.7) <sup>f</sup>
$\text{FeCl} \rightleftharpoons \text{Fe}^{3+} + \text{Cl}^-$	-7,910	-33.3	-1.48 <sup>n</sup>	-1.96	-2.94	-3.98	(-5.1) <sup>e</sup>	(-6.2) <sup>e</sup>	(-7.5) <sup>f</sup>
$\text{FeCl}_2 \rightleftharpoons \text{Fe}^{3+} + 2\text{Cl}^-$	-7,970	-36.5	-2.13 <sup>n</sup>	-2.62	-3.63	-4.72	(-5.9)	(-7.1) <sup>e</sup>	(-7.7) <sup>f</sup>
$\text{FeCl}_3 \rightleftharpoons \text{Fe}^{3+} + 3\text{Cl}^-$	-10,290	-39.7	-1.13 <sup>n</sup>	-1.76	-3.00	-4.30	(-5.7)	(-7.1) <sup>e</sup>	(-8.0) <sup>f</sup>
$\text{FeCl}_4^- \rightleftharpoons \text{Fe}^{3+} + 4\text{Cl}^-$	-13,860	-42.9	0.79 <sup>r</sup>	-0.05	-1.63	-3.23	(-4.9)	(-6.6) <sup>e</sup>	(-7.8) <sup>f</sup>
$\text{AuCl}_2^- \rightleftharpoons \text{Au}^+ + 2\text{Cl}^-$	10,490	-6.0	-9 <sup>s</sup>	-8.4	-7.5	-6.9	(-6.4)	(-6.2) <sup>e</sup>	(-6.2) <sup>f</sup>
$\text{AuCl}_4^- \rightleftharpoons \text{Au}^{3+} + 4\text{Cl}^-$	26,460	-30.2	-26 <sup>s</sup>	-24.5	-22.4	-21.0	(-20.2)	(-20.2) <sup>e</sup>	(-21.1) <sup>f</sup>

<sup>a</sup> Except where otherwise indicated, values in this column were computed from log  $K(T_r)$  and  $\Delta S^\circ_r(T_r)$ . <sup>b</sup> All  $\Delta S^\circ_r(T_r)$  values were calculated from equations (25) and (27) using ionic radii (table 1) and the values of  $S^\circ_{\text{Cl}^-}$  and  $S^\circ_{\text{H}_2\text{O}}$  at 25°C given in footnote b, table 1. <sup>c</sup> The values of the overall dissociation constants were computed from log  $K(T)$  values (eq. 48) predicted from equation (16) using the  $\Delta S^\circ_r(T_r)$  and  $\Delta H^\circ_r(T_r)$  values shown above. The dissociation constants are consistent with molal units of concentration—those that are more uncertain are given in parentheses. <sup>d</sup> Jonte and Martin (1952). <sup>e</sup> Leden (1952); Berne and Leden (1953). <sup>f</sup> Chalytkian (1948). <sup>g</sup> Hurlen (1961). <sup>h</sup> Näsänen (1953). <sup>i</sup> Bjerrum (1946). <sup>j</sup> Nelson and Kraus (1954); Marcus (1956). <sup>k</sup> Marcus and Mayden (1963). <sup>l</sup> This value is consistent with high temperature log  $K(T)$  values (Kraus and Raridon, 1960)—see footnote g, table 1. <sup>m</sup> Malcolm, Parton, and Watson (1961). <sup>n</sup> Calculated from  $\Delta H^\circ_r(T_r)$  and  $\Delta S^\circ_r(T_r)$ . <sup>o</sup> Williams (1954). <sup>p</sup> Rabinowitch and Stockmayer (1942). <sup>q</sup> Marcus (1960). <sup>r</sup> Computed from the free energy of formation of  $\text{Au}^+$  (Latimer, 1952) and the oxidation potential for the reaction  $\text{AuCl}_2^- + e^- \rightleftharpoons \text{Au}_{(s)} + 2\text{Cl}^-$  (Bjerrum and Kirschner, 1948; Bjerrum, 1948). <sup>s</sup> Extrapolated. <sup>t</sup> Computed from the free energy of formation of  $\text{Au}^{3+}$  (Latimer, 1952) and the oxidation potential for  $\text{AuCl}_4^- + 3e^- \rightleftharpoons \text{Au}_{(s)} + 4\text{Cl}^-$  (Bjerrum and Kirschner, 1948; Bjerrum, 1948). <sup>u</sup> These values are actually for 18°C, but they are uncertain to the extent that a 7 degree correction to 25°C is unwarranted.

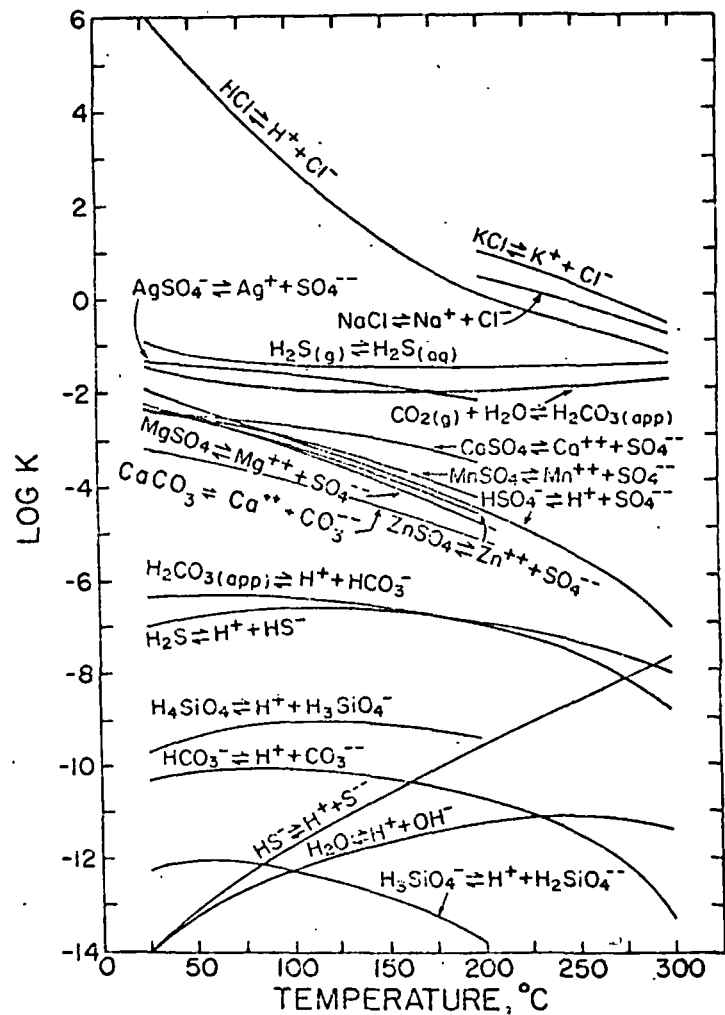


Fig. 5. Dissociation constants for complexes in hydrothermal solutions at elevated temperatures (table 4). The curves shown for the dissociation of  $\text{H}_2\text{SiO}_4$  and  $\text{H}_3\text{SiO}_4^-$  are those computed by Cobble (1964); the log K values defined by these curves are more consistent with low temperature thermodynamic data than those obtained at high temperatures by Ryzhenko (1967).

Predicted high temperature dissociation constants for chloride complexes of the ore-forming metals are shown in table 5. Log  $K(T)$  curves for these reactions are plotted in figures 6 and 7. Because the uncertainty resulting from calculation of log  $K(T)$  values with equation (16) increases substantially above 200°C (Helgeson, 1967a), and because entropy estimates (eqs 25 and 27) were used in the calculations, the numerical values for log  $\beta(T)$  given in table 5 as well as the log  $K(T)$  curves in figures 6 and 7 should be regarded as approximations.

It can be deduced from figures 5 to 7 that high temperature electrolyte solutions are highly associated. The high degree of formation attained by metal-ion chloride complexes is particularly significant with respect to the transport and deposition of the ore-forming metals in hydrothermal systems. As indicated above, calculations of sulfide solubilities in sodium chloride solutions at elevated temperatures suggest that more than adequate quantities of these metals can be carried in hydrothermal solutions to account for major ore deposits (Helgeson, 1964, 1967c; Helgeson, Garrels, and MacKenzie, 1969; Helgeson and Garrels, 1968). The results of a few such calculations involving thermodynamic values given in the tables are presented in later pages of this communication.

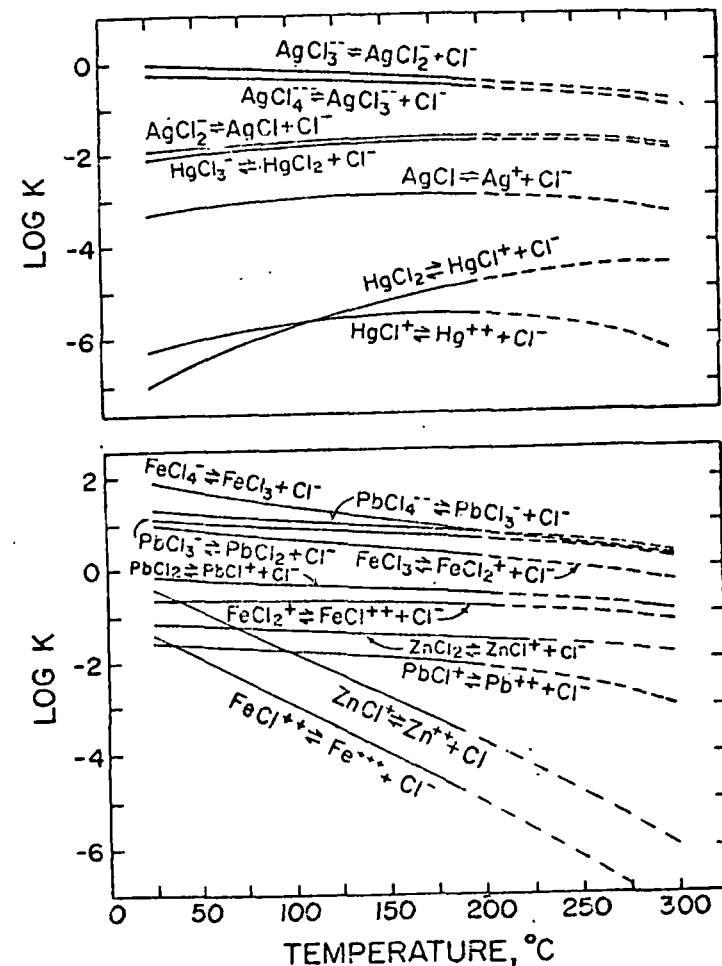


Fig. 6. Predicted dissociation constants for metal chloride complexes at elevated temperatures (table 5). The curves below 200°C were computed from equation (16) using entropy estimates from equations (25) and (27)—see text. The dashed extensions of the curves are extrapolations.

TABLE 6

Enthalpies<sup>a</sup> and entropies<sup>b</sup> of elements of interest in hydrothermal studies<sup>c</sup>

Element	Temperature, °C												
	25	50	60	100	150	200	250	300	350	400	450	500	
Au <sub>(c)</sub>	H°(T)–H°(T <sub>0</sub> )	0.0	151	212	456	763	1074	1388	1705	2025	2348	2675	3004
	S°	11.31 <sup>d</sup>	11.80	11.98	12.67	13.45	14.14	14.77	15.35	15.88	16.38	16.85	17.29
Ag <sub>(c)</sub>	H°(T)–H°(T <sub>0</sub> )	0.0	152	213	457	764	1075	1386	1702	2033	2347	2677	3011
	S°	10.20 <sup>d</sup>	10.69	10.88	11.57	12.34	13.03	13.66	14.23	14.77	15.27	15.74	16.19
Hg <sub>(l,g)</sub>	H°(T)–H°(T <sub>0</sub> )	0.0	166	232	496	824	1151	1476	1802	2126	2450	2774	3094
	S°	18.2 <sup>d</sup>	18.7	18.9	19.7	20.5	21.2	21.9	22.5	23.0	23.5	24.0	24.4
Cu <sub>(c)</sub>	H°(T)–H°(T <sub>0</sub> )	0.0	147	206	443	744	1048	1356	1667	1983	2302	2625	2951
	S°	7.97 <sup>d</sup>	8.44	8.62	9.30	10.05	10.73	11.35	11.92	12.45	12.94	13.40	13.84
O <sub>2(c)</sub>	H°(T)–H°(T <sub>0</sub> )	0.0	176	247	535	900	1271	1645	2024	2407	2792	3181	3572
	S°	48.996 <sup>d,e</sup>	49.56	49.78	50.60	51.51	52.34	53.09	53.79	54.43	55.02	55.58	56.16
H <sub>2(c)</sub>	H°(T)–H°(T <sub>0</sub> )	0.0	172	241	517	862	1208	1556	1906	2257	2609	2964	3320
	S°	31.21 <sup>d,e</sup>	31.76	31.97	32.76	33.62	34.40	35.10	35.73	36.32	36.87	37.37	37.85

<sup>a</sup> In cal mole<sup>-1</sup> where T<sub>0</sub> refers to 298.15°K. <sup>b</sup> In cal mole<sup>-1</sup> deg<sup>-1</sup>. <sup>c</sup> The values shown in this table are for a standard state of 1 atm and the indicated temperature. The subscripts (c), (liq), and (g) refer to crystalline, liquid, and gas respectively. All the enthalpies and entropies for temperatures of 50°C and above were computed from a statement of equation (11) written in terms of H°, and equation (12), respectively, using the coefficients shown in table 8. <sup>d</sup> Robie (1966); Robie and Waldbaum (1968). <sup>e</sup> Wagman and others (1965, 1968).

#### Standard Enthalpies, Entropies, and Heat Capacities

High temperature thermodynamic data for a variety of solids and gases of interest in hydrothermal studies are summarized in tables 6 and 7. The values shown in the tables were computed from equations (11) and (12) using the heat capacity power function coefficients for equation (10) shown in table 8. Average heat capacities of ions and several neutral species in aqueous solution are given in table 3 for temperatures from 25° to 300°C.

#### Equilibrium Constants for Oxidation-Reduction and Dissolution Reactions

Thermodynamic data for a variety of hydrothermal oxidation-reduction and solubility reactions are presented in tables 9 to 12. The log K(T) values shown in these tables were computed from equations (11) to (17) and data presented in tables 3, 6, 8, and 9 to 12. A number of the activity product constants are plotted against temperature in figure 8. Although reactions involving a large number of minerals are presented in table 12, the fact that a reaction is included in the table is not meant to imply that the mineral involved is necessarily stable in the presence of H<sub>2</sub>O at the temperatures indicated. The log K values given in table 12 are "idealized"; they can be used to describe stable or metastable

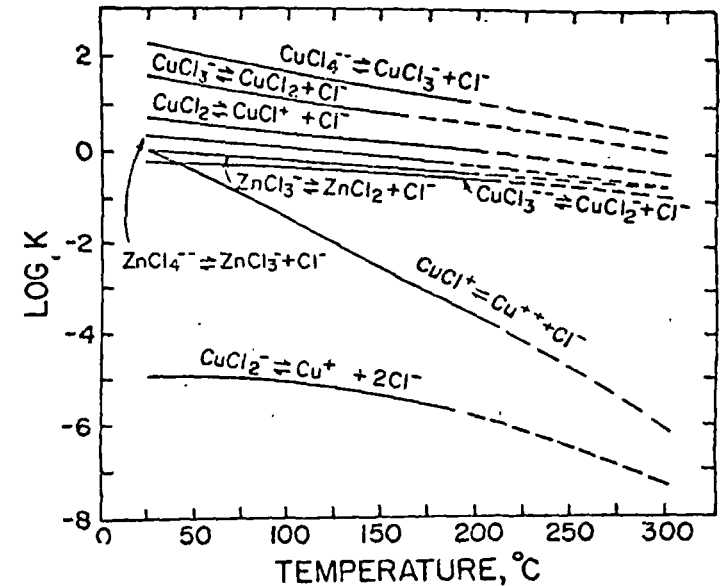


Fig. 7. Predicted dissociation constants for metal chloride complexes at elevated temperatures (table 5). The curves below 200°C were computed from equation (16) using entropy estimates from equations (25) and (27)—see text. The dashed extensions of the curves are extrapolations.

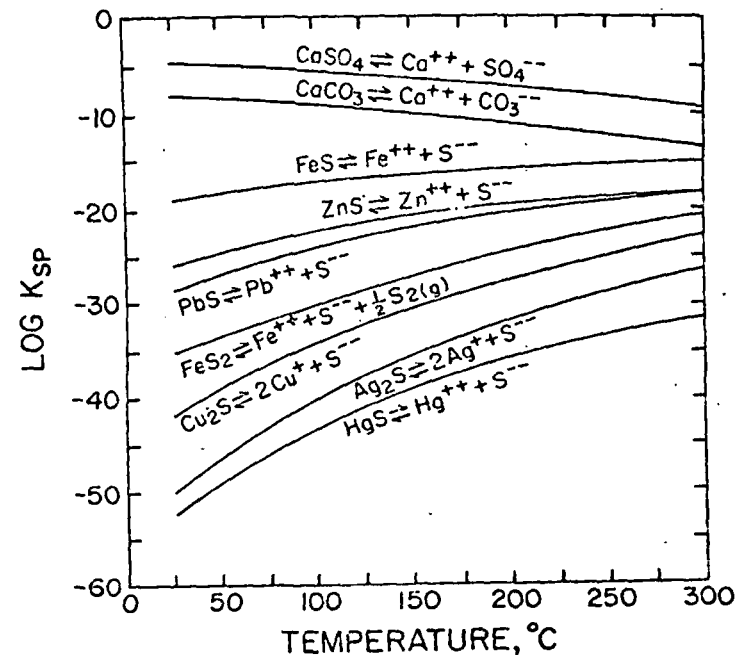


Fig. 8. Activity product constants for anhydrite, calcite, and various sulfides at elevated temperatures (table 11). HgS refers to metacinnabar.

TABLE 7

Standard entropies<sup>a</sup> and enthalpies<sup>b</sup> for various minerals and gases of interest in hydrothermal studies<sup>c</sup>

Species		Temperature, °C				
		25°	50°	60°	100°	150°
$\alpha$ Ag <sub>2</sub> S (acanthite)	$\Delta H^\circ$	-7,731 <sup>d</sup>	-7,273	-7,085	-6,307	-5,275
	S°	34.14 <sup>d</sup>	35.62	36.19	38.39	40.97
$\alpha$ Cu <sub>2</sub> S (chalcocite)	$\Delta H^\circ$	-19,148 <sup>d</sup>	-18,660	-18,465	-17,635	-16,710
	S°	28.86 <sup>d</sup>	30.43	31.02	33.23	35.69
CuS (covellite)	$\Delta H^\circ$	-11,610 <sup>d</sup>	-11,324	-11,210	-10,748	-10,166
	S°	15.93 <sup>d</sup>	16.85	17.20	18.51	19.97
PbS (galena)	$\Delta H^\circ$	-23,350 <sup>d</sup>	-23,053	-22,934	-22,452	-21,841
	S°	21.84 <sup>d</sup>	22.80	23.16	24.55	26.05
ZnS (sphalerite)	$\Delta H^\circ$	-49,750 <sup>d</sup>	-49,475	-49,365	-48,914	-48,337
	S°	13.77 <sup>d</sup>	14.67	14.99	16.27	17.72
HgS (metacinnabar)	$\Delta H^\circ$	-11,058 <sup>d</sup>	-10,869	-10,743	-10,261	-9,643
	S°	23.00 <sup>d</sup>	23.97	24.34	25.72	27.27
FeS (pyrrhotite)	$\Delta H^\circ$	-24,130 <sup>d</sup>	-23,795	-23,657	-23,076	-22,291
	S°	14.42 <sup>d</sup>	15.50	15.92	17.56	19.54
FeS <sub>2</sub> (pyrite)	$\Delta H^\circ$	-41,000 <sup>d</sup>	-40,620	-40,470	-39,830	-39,010
	S°	12.65 <sup>d</sup>	13.87	14.34	16.14	18.21
$\alpha$ Fe <sub>2</sub> O <sub>3</sub> (hematite)	$\Delta H^\circ$	-197,360 <sup>d</sup>	-196,660	-196,397	-195,309	-194,877
	S°	30.39 <sup>d</sup>	22.95	23.75	26.83	30.43
$\alpha$ Fe <sub>3</sub> O <sub>4</sub> (magnetite)	$\Delta H^\circ$	-267,400 <sup>d</sup>	-266,480	-266,100	-264,550	-262,490
	S°	36.03 <sup>d</sup>	39.00	40.14	44.55	49.71
CaCO <sub>3</sub> (calcite)	$\Delta H^\circ$	-288,420 <sup>d</sup>	-287,916	-287,766	-286,832	-285,676
	S°	22.15 <sup>d</sup>	23.77	24.41	26.39	29.79
CaSO <sub>4</sub> (anhydrite)	$\Delta H^\circ$	-343,321 <sup>d</sup>	-342,718	-342,473	-341,468	-340,150
	S°	25.5 <sup>d</sup>	27.44	28.19	31.03	34.32
$\alpha$ SiO <sub>2</sub> (quartz)	$\Delta H^\circ$	-217,650 <sup>d</sup>	-217,380	-217,260	-216,780	-216,140
	S°	9.88 <sup>d</sup>	10.76	11.11	12.46	14.07
KAlSi <sub>3</sub> O <sub>8</sub> (microcline)	$\Delta H^\circ$	-945,600 <sup>d, e, f, g</sup>	-944,720	-944,224	-942,037	-939,129
	S°	52.47 <sup>d</sup>	56.50	58.10	64.29	71.60
NaAlSi <sub>3</sub> O <sub>8</sub> (low albite)	$\Delta H^\circ$	-937,300 <sup>d, e, f, g</sup>	-936,040	-935,510	-933,330	-930,450
	S°	50.2 <sup>d</sup>	54.26	55.85	62.03	69.29
CaAl <sub>2</sub> Si <sub>2</sub> O <sub>8</sub> (anorthite)	$\Delta H^\circ$	-1,009,300 <sup>d</sup>	-1,008,020	-1,007,490	-1,005,260	-1,002,300
	S°	43.45 <sup>d</sup>	52.57	54.20	60.50	67.93

	Temperature, °C						
	200°	250°	300°	350°	400°	450°	500°
	-4,176	-3,012	-1,782	-486	876	2,304	3,793
	43.44	45.76	48.02	50.19	52.29	54.35	56.33
	-15,735	-14,760	-13,785	-12,810	-11,835	-10,860	-9,885
	37.86	39.82	41.60	43.23	44.74	46.14	47.44
	-9,577	-8,981	-8,379	-7,770	-7,154	-6,532	-5,903
	21.29	22.48	23.58	24.60	25.55	26.44	27.28
	-21,220	-20,589	-19,949	-19,319	-18,639	-17,969	-17,289
	27.45	28.72	29.88	30.97	31.99	32.95	33.86
	-47,749	-47,153	-46,549	-45,939	-45,323	-44,703	-44,073
	19.03	20.23	21.33	22.35	23.30	24.19	25.03
	-9,016	-8,380	-7,735	-7,081	-6,418	-5,745	-5,064
	28.67	29.95	31.13	32.22	33.24	34.21	35.12
	-21,440	-20,523	-19,540	-18,491	-17,376	-16,195	-14,943
	21.44	23.28	25.07	26.83	28.55	30.24	31.90
	-38,160	-37,295	-36,420	-35,525	-34,620	-33,720	-32,800
	20.10	21.84	23.45	24.94	26.33	27.63	28.85
	-192,374	-190,808	-189,183	-187,002	-185,767	-183,980	-182,141
	33.79	36.93	39.90	42.71	45.39	47.95	50.41
	-260,320	-258,020	-255,610	-253,070	-250,420	-247,610	-244,740
	54.57	59.18	63.58	67.82	71.92	75.90	79.77
	-284,464	-283,210	-281,920	-280,602	-279,267	-277,830	-276,499
	32.50	35.02	37.37	39.58	41.65	43.61	45.47
	-338,792	-337,365	-335,878	-334,334	-332,260	-331,058	-329,346
	37.38	40.24	42.96	45.54	48.01	50.40	52.70
	-215,470	-214,760	-214,020	-213,250	-212,450	-211,630	-210,790
	15.58	17.01	18.36	19.64	20.87	22.05	23.17
	-936,074	-932,966	-929,645	-926,306	-922,900	-919,433	-915,912
	78.42	84.79	90.74	96.82	101.58	106.55	111.25
	-927,430	-924,300	-921,080	-917,790	-914,435	-911,020	-907,550
	76.04	82.32	88.19	93.69	98.87	103.77	108.41
	-999,200	-995,930	-992,660	-989,270	-985,800	-982,230	-978,760
	74.87	81.34	87.39	93.07	98.41	103.46	108.25

TABLE 7 (continued)

Species		Temperature, °C				
		25°	50°	60°	100°	150°
Al <sub>2</sub> Si <sub>2</sub> O <sub>7</sub> (OH) <sub>2</sub> (kaolinite)	ΔH°	-980,020 <sup>a,b,c</sup>	-978,530	-977,920	-975,370	-972,030
	S°	48.53 <sup>d</sup>	53.33	55.20	62.41	70.81
KAl <sub>3</sub> Si <sub>3</sub> O <sub>10</sub> (OH) <sub>2</sub> (muscovite)	ΔH°	-1,420,900 <sup>a,c</sup>	-1,418,920	-1,418,090	-1,414,630	-1,410,040
	S°	69.0 <sup>d</sup>	75.39	77.90	87.70	99.25
NaAlSi <sub>3</sub> O <sub>8</sub> · H <sub>2</sub> O (analcime)	ΔH°	-786,300 <sup>a,c</sup>	-785,050	-784,540	-782,540	-780,030
	S°	56.03 <sup>d</sup>	60.07	61.60	67.29	73.69
CaMg(SiO <sub>3</sub> ) <sub>2</sub> (diopside)	ΔH°	-767,400 <sup>a,c</sup>	-766,430	-766,020	-761,300	-762,000
	S°	34.20 <sup>d</sup>	37.34	38.58	43.45	49.23
MgSiO <sub>3</sub> (clinocstatite)	ΔH°	-370,100 <sup>a,c</sup>	-369,610	-369,410	-368,560	-367,440
	S°	16.22 <sup>d</sup>	17.79	18.41	20.81	23.63
Ca <sub>2</sub> Mg <sub>3</sub> Si <sub>5</sub> O <sub>22</sub> (OH) <sub>2</sub> (tremolite)	ΔH°	-2,952,900 <sup>a,c</sup>	-2,948,980	-2,947,410	-2,941,150	-2,933,310
	S°	131.19 <sup>d</sup>	143.81	148.53	166.35	186.03
KAlSi <sub>3</sub> O <sub>8</sub> (leucite)	ΔH°	-721,700 <sup>a,c</sup>	-720,720	-720,230	-718,760	-716,800
	S°	44.95 <sup>d</sup>	47.21	48.40	52.85	57.80
NaAlSi <sub>3</sub> O <sub>8</sub> (α nepheline)	ΔH°	-498,500 <sup>a,c</sup>	-497,790	-497,490	-496,230	-494,490
	S°	29.72 <sup>d</sup>	32.02	32.93	36.50	40.87
Mg <sub>3</sub> Si <sub>2</sub> O <sub>10</sub> (OH) <sub>2</sub> (talc)	ΔH°	-1,415,200 <sup>a,c</sup>	-1,413,280	-1,412,510	-1,409,430	-1,405,590
	S°	62.34 <sup>d</sup>	68.53	70.87	79.59	89.26
KMg <sub>3</sub> AlSi <sub>3</sub> O <sub>10</sub> F <sub>2</sub> (fluorophlogopite)	ΔH°	-1,498,100 <sup>a</sup>	-1,496,000	-1,495,140	-1,491,550	-1,486,850
	S°	75.90 <sup>d</sup>	82.65	85.30	95.45	107.28
Mg <sub>2</sub> SiO <sub>4</sub> (forsterite)	ΔH°	-519,000 <sup>a</sup>	-518,270	-517,970	-516,720	-515,070
	S°	22.75 <sup>d</sup>	25.08	26.00	29.54	33.09
Fe <sub>2</sub> SiO <sub>4</sub> (fayalite)	ΔH°	-353,500 <sup>a,c</sup>	-352,690	-352,350	-350,930	-349,180
	S°	35.45 <sup>d</sup>	38.06	39.08	42.98	47.51
Mg(OH) <sub>2</sub> (brucite)	ΔH°	-221,200 <sup>d</sup>	-220,750	-220,570	-219,820	-218,860
	S°	15.09 <sup>d</sup>	16.52	17.09	19.20	21.63
Mg <sub>5</sub> Si <sub>8</sub> O <sub>22</sub> (OH) <sub>2</sub> (chrysotile)	ΔH°	-1,043,950 <sup>a</sup>	-1,041,360 <sup>a</sup>	-1,040,070 <sup>a</sup>	-1,037,750 <sup>a</sup>	-1,033,890 <sup>a</sup>
	S°	52.9 <sup>a</sup>	58.32 <sup>a</sup>	60.45 <sup>a</sup>	68.71 <sup>a</sup>	78.42 <sup>a</sup>
S <sub>2(g)</sub>	ΔH°	30,680 <sup>a</sup>	30,876	30,955	31,277	31,688
	S°	54.51 <sup>a</sup>	55.14	55.38	56.29	57.33
H <sub>2</sub> S <sub>(g)</sub>	ΔH°	-4,930 <sup>a</sup>	-4,724	-4,640	-4,301	-3,866
	S°	49.16 <sup>a</sup>	49.82	50.03	51.04	52.13
H <sub>2</sub> O <sub>(g)</sub>	ΔH°	-57,796 <sup>a</sup>	-57,954	-57,513	-57,186	-56,773
	S°	45.10 <sup>a</sup>	45.75	46.00	46.93	47.97

	Temperature, °C						
	200°	250°	300°	350°	400°	450°	500°
	-968,540	-964,950	-961,250	-957,480	-953,620	-949,690	-945,700
	78.59	85.82	92.56	98.88	104.83	110.45	115.79
	-1,405,200	-1,400,180	-1,395,000	-1,389,700	-1,384,260	-1,378,730	-1,373,090
	110.04	120.13	129.58	138.46	146.84	154.79	162.31
	-775,520	-773,010	-772,500	-769,990	-767,490	-764,980	-762,470
	79.20	84.24	88.82	93.01	96.88	100.48	103.84
	-759,570	-757,050	-754,450	-751,800	-749,090	-746,330	-743,540
	54.65	59.71	64.45	68.90	73.08	77.03	80.77
	-366,260	-365,040	-363,790	-362,510	-361,200	-359,880	-358,530
	26.26	28.70	30.99	33.13	35.15	37.05	38.86
	-2,925,480	-2,917,640	-2,909,810	-2,901,970	-2,894,140	-2,886,300	-2,878,470
	203.56	219.30	233.60	246.71	258.80	270.03	280.50
	-714,830	-712,870	-710,910	-708,950	-706,990	-705,030	-703,070
	62.17	66.11	69.69	72.97	76.00	78.81	81.43
	-492,580	-490,490	-488,220	-485,780	-483,160	-480,360	-477,390
	45.14	49.33	53.47	57.55	61.59	65.60	69.57
	-1,401,740	-1,397,900	-1,394,050	-1,390,210	-1,386,370	-1,382,520	-1,378,630
	97.85	105.57	112.59	119.02	124.96	130.47	135.61
	-1,481,950	-1,476,920	-1,471,760	-1,466,500	-1,461,160	-1,455,740	-1,450,250
	113.20	123.30	137.70	146.50	154.80	162.50	169.90
	-512,350	-511,570	-509,740	-507,870	-505,970	-504,040	-502,050
	57.54	41.12	44.46	47.58	50.51	53.23	55.90
	-347,310	-345,390	-343,420	-341,400	-339,360	-337,270	-335,160
	51.68	55.54	59.14	62.50	65.66	68.65	71.48
	-217,850	-216,810	-215,720	-214,600	-213,430	-212,230	-210,990
	23.88	25.98	27.46	29.84	31.63	33.56	35.02
	-1,020,830 <sup>a</sup>	-1,025,610 <sup>a</sup>	-1,021,240 <sup>a</sup>	-1,016,750 <sup>a</sup>	-1,012,150 <sup>a</sup>	-1,007,430 <sup>a</sup>	-1,002,620 <sup>a</sup>
	87.50 <sup>a</sup>	95.96 <sup>a</sup>	103.93 <sup>a</sup>	111.44 <sup>a</sup>	118.55 <sup>a</sup>	125.30 <sup>a</sup>	131.74 <sup>a</sup>
	32,105	32,527	32,932	33,380	33,811	34,243	34,677
	58.26	59.11	59.88	60.60	61.26	61.88	62.46
	-3,420	-2,966	-2,562	-2,029	-1,548	-1,059	-5,619
	53.13	54.04	54.89	55.63	56.42	57.12	57.79
	-56,352	-55,926	-55,494	-55,055	-54,610	-54,160	-53,702
	48.91	49.76	50.55	51.28	51.97	52.62	53.23

TABLE 7 (continued)

Species	Temperature, °C				
	25 <sup>a</sup>	50 <sup>a</sup>	60 <sup>a</sup>	100 <sup>a</sup>	150 <sup>a</sup>
$\Delta H^\circ$	-94,050 <sup>a</sup>	-92,457	-93,235	-92,392	-91,440
$S^\circ$	51.05 <sup>a</sup>	52.97	53.65	56.04	58.44

<sup>a</sup> In cal mole<sup>-1</sup> deg<sup>-1</sup>. <sup>b</sup> The enthalpies given in the table ( $\Delta H^\circ$ ) are equal to the sum of the standard enthalpy of formation from the elements of the respective compounds and gases at the reference temperature ( $T_r$ ) plus the enthalpy change for the compound or gas resulting from a temperature increase from  $T_r$  to temperature  $T$ ; the units are cal mole<sup>-1</sup>. The values shown for the silicates (and brucite) above 25°C have been rounded to the nearest 10 cal mole<sup>-1</sup>. <sup>c</sup> The values shown in this table are for a standard state of 1 atm at the indicated temperature. All the enthalpies and entropies for temperatures of 50° and above were computed from equations (11) and (12), respectively, using the heat capacity power function coefficients shown in table 8.

TABLE 8

Heat capacity power function coefficients (eq 10) for solids and gases<sup>a</sup>

Species <sup>c</sup>	$a''$	$b'' \times 10^3$	$c'' \times 10^{-4}$
$\alpha$ Ag <sub>2</sub> S (acanthite)	10.13	26.4	0.0
$\alpha$ Cu <sub>2</sub> S (chalcocite)	19.50	0.0	0.0
CuS (covellite)	10.60	2.5 <sup>d</sup>	0.0
PbS (galena)	10.65	3.92	0.0
ZnS (sphalerite)	11.77 <sup>d</sup>	1.26 <sup>d</sup>	-1.16 <sup>d</sup>
ZnS (wurtzite)	11.82 <sup>d</sup>	1.16 <sup>d</sup>	-1.04 <sup>d</sup>
HgS (metacinnabar)	10.30	3.65	0.0
HgS (cinnibar)	11.57 <sup>e,m</sup>		
FeS (pyrrhotite)	5.19	26.4	0.0
CuFeS <sub>2</sub> (chalcopyrite)	15.6 <sup>d</sup>	21.6 <sup>d</sup>	0.6 <sup>d</sup>
FeS <sub>2</sub> (pyrite)	17.38	1.32	-3.05
Cu <sub>2</sub> FeS <sub>3</sub> (bornite)	44.4 <sup>d</sup>	40.0 <sup>d</sup>	0.6 <sup>d</sup>
Ag <sub>(s)</sub> (native silver)	5.09	2.04	0.36
Au <sub>(s)</sub> (native gold)	5.66	1.24	0.0
Cu <sub>(s)</sub> (native copper)	5.41	1.50	0.0
Hg <sub>(l)</sub> (native mercury)	6.44	0.6	0.19
$\alpha$ Fe <sub>2</sub> O <sub>3</sub> (hematite)	23.49	18.6	-3.55
$\alpha$ Fe <sub>3</sub> O <sub>4</sub> (magnetite)	21.88	48.2	0.0
$\alpha$ SiO <sub>2</sub> (quartz)	11.22	8.20	-2.70
CuO (tenorite)	9.27	4.80	0.0
Cu <sub>2</sub> O (cuprite)	14.90	5.70	0.0
CaCO <sub>3</sub> (calcite)	24.98	5.24	-6.20
CaMg(CO <sub>3</sub> ) <sub>2</sub> (dolomite)	37.65 <sup>e,n</sup>		
ZnCO <sub>3</sub> (smithsonite)	9.36	33.0	0.0
PbCO <sub>3</sub> (cerussite)	12.39	28.66	0.0
FeCO <sub>3</sub> (siderite)	11.63	26.80	0.0
$\alpha$ CaF <sub>2</sub> (fluorite)	14.35	7.28	0.47
CaSO <sub>4</sub> (anhydrite)	16.78	23.60	0.0
BaSO <sub>4</sub> (barite)	33.80	0.0	-8.43
PbSO <sub>4</sub> (anglesite)	10.96	31.0	4.29
KAlSi <sub>3</sub> O <sub>8</sub> (microcline, orthoclase, adularia, and sanidine)	63.83	12.90	-17.65
NaAlSi <sub>3</sub> O <sub>8</sub> (low albite)	61.70	13.99	-15.01
CaAl <sub>2</sub> Si <sub>2</sub> O <sub>8</sub> (anorthite)	64.42	13.70	-16.89
Al <sub>2</sub> Si <sub>2</sub> (OH) <sub>2</sub> (kaolinite)	67.93 <sup>d,b</sup>	19.22 <sup>d,b</sup>	-13.78 <sup>d,b</sup>
KAl <sub>2</sub> Si <sub>2</sub> O <sub>7</sub> (OH) <sub>2</sub> (muscovite)	87.56 <sup>d</sup>	26.38 <sup>d</sup>	-25.42 <sup>d</sup>
KFe <sub>3</sub> AlSi <sub>3</sub> O <sub>10</sub> (OH) <sub>2</sub> (illite)	87.91 <sup>d</sup>	35.01 <sup>d</sup>	-19.51 <sup>d</sup>
KFe <sub>3</sub> AlSi <sub>3</sub> O <sub>10</sub> (OH) <sub>2</sub> (annite)	100.41 <sup>d</sup>	36.41 <sup>d</sup>	-14.31 <sup>d</sup>
Mg <sub>2</sub> Al <sub>2</sub> Si <sub>2</sub> O <sub>10</sub> (OH) <sub>2</sub> (chlorite)	96.31 <sup>d</sup>	36.11 <sup>d</sup>	-23.91 <sup>d</sup>

1485

Species	Temperature, °C						
	200 <sup>a</sup>	250 <sup>a</sup>	300 <sup>a</sup>	350 <sup>a</sup>	400 <sup>a</sup>	450 <sup>a</sup>	500 <sup>a</sup>
$\Delta H^\circ$	-90,563	-89,739	-88,952	-88,192	-87,451	-86,726	-86,011
$S^\circ$	60.40	62.05	63.40	64.76	65.91	66.94	67.90

<sup>a</sup> Robie and Waldbaum (1968). <sup>b</sup> Computed from the enthalpy of formation from the oxides (Robie, 1966) using enthalpies of formation of the oxides from the elements reported by Robie and Waldbaum (1968). <sup>c</sup> Waldbaum (1966). <sup>d</sup> Rounded to the nearest even 50 cal mole<sup>-1</sup>. <sup>e</sup> Barany and Kelley (1961). <sup>f</sup> Barany (1964). <sup>g</sup> Weller and King (1963). <sup>h</sup> Wagman and others (1965, 1968). <sup>i</sup> Kelley and others (1959). <sup>j</sup> King and others (1967). <sup>k</sup> Computed using the heat capacity power function for antigorite (table 8). <sup>l</sup> Computed from the entropy given above for calcite and an activity product constant of 10<sup>-30</sup> (Berner, 1967) at 25°C and 1 atm. <sup>m</sup> Adjusted (within the uncertainty range reported in the source reference) to achieve internal consistency among equilibrium constants describing mineral assemblages at 25°C.

TABLE 8 (continued)

Heat capacity power function coefficients (eq 10) for solids and gases<sup>a</sup>

Species <sup>c</sup>	$a''$	$b'' \times 10^3$	$c'' \times 10^{-4}$
Na <sub>0.33</sub> Al <sub>2.33</sub> Si <sub>2.67</sub> O <sub>10</sub> (OH) <sub>2</sub> (montmorillonite)	84.9 <sup>d</sup>	24.3 <sup>d</sup>	-19.7 <sup>d</sup>
K <sub>0.33</sub> Al <sub>2.33</sub> Si <sub>2.67</sub> O <sub>10</sub> (OH) <sub>2</sub> (montmorillonite)	85.31 <sup>d</sup>	24.91 <sup>d</sup>	-19.71 <sup>d</sup>
Ca <sub>0.167</sub> Al <sub>2.33</sub> Si <sub>2.67</sub> O <sub>10</sub> (OH) <sub>2</sub> (montmorillonite)	84.2 <sup>d</sup>	33.6 <sup>d</sup>	-20.0 <sup>d</sup>
Mg <sub>0.333</sub> Al <sub>2.33</sub> Si <sub>2.67</sub> O <sub>10</sub> (OH) <sub>2</sub> (montmorillonite)	84.0 <sup>d</sup>	33.7 <sup>d</sup>	-19.9 <sup>d</sup>
NaAlSi <sub>3</sub> O <sub>8</sub> ·H <sub>2</sub> O (amalcime)	50.17 <sup>e</sup>		
CaMg(SiO <sub>3</sub> ) <sub>2</sub> (diopside)	52.87	7.54	-15.74
MgSiO <sub>3</sub> (clinopyroxene)	24.55	4.74	-6.23
Ca <sub>2</sub> Mg <sub>3</sub> Si <sub>8</sub> O <sub>22</sub> (OH) <sub>2</sub> (tremolite)	156.7 <sup>e</sup>		
KAlSi <sub>3</sub> O <sub>8</sub> (leucite)	39.23 <sup>e</sup>		
NaAlSi <sub>3</sub> O <sub>8</sub> (α nepheline)	6.63	70.60	0.0
Mg <sub>2</sub> Si <sub>4</sub> O <sub>11</sub> (OH) <sub>2</sub> (talc)	76.89 <sup>e</sup>		
KMg <sub>2</sub> Al <sub>2</sub> Si <sub>2</sub> O <sub>10</sub> F <sub>2</sub> (fluorophlogopite)	100.86	17.16	-21.46
Mg <sub>2</sub> SiO <sub>4</sub> (forsterite)	35.81	6.54	-8.52
Fe <sub>2</sub> SiO <sub>4</sub> (fayalite)	36.51	9.36	-6.70
Mg(OH) <sub>2</sub> (brucite)	13.04	15.30	0.0
Al(OH) <sub>3</sub> (gibbsite)	8.65	45.6	0.0
Mg <sub>3</sub> Si <sub>2</sub> O <sub>7</sub> (OH) <sub>2</sub> (antigorite)	75.82 <sup>a</sup>	31.6 <sup>b</sup>	-17.58 <sup>b</sup>
S <sub>2(g)</sub>	8.72	0.16	-0.90
H <sub>2</sub> S <sub>2(g)</sub>	7.81	2.96	-0.46
Fe <sub>2</sub> O <sub>4(g)</sub>	7.30	2.46	0.0
O <sub>2(g)</sub>	7.16	1.0	-0.40
H <sub>2</sub> O <sub>2(g)</sub>	6.52	0.78	0.12
CO <sub>2(g)</sub>	10.57	2.10	-2.06

<sup>a</sup> Kelley (1960). <sup>b</sup> The estimated power-function coefficients for kaolinite give 58.16 cal mole<sup>-1</sup> deg<sup>-1</sup> for the heat capacity of kaolinite at 25°C, compared to 58.62 cal mole<sup>-1</sup> deg<sup>-1</sup> reported by King and Weller (1961). <sup>c</sup> Heat capacity at 25°C (cal mole<sup>-1</sup> deg<sup>-1</sup>). When this quantity is used as the  $a''$  coefficient in equations (11) and (12) with  $b''$  and  $c''$  set to zero, the heat capacity is treated as a constant. <sup>d</sup> Pankratz (1964). <sup>e</sup> Robie and Stout (1963). <sup>f</sup> The subscripts (c), (liq), and (g) refer to crystalline, liquid, and gas, respectively. <sup>g</sup> King and others, 1967. <sup>h</sup> Estimated by summing (in appropriate proportions) the coefficients in the heat capacity power functions for the elements (Kelley, 1966) in the mineral (see text). <sup>i</sup> Estimated by summing (in mole proportions) the coefficients in the heat capacity power functions of the oxide components (Kelley, 1960) in the mineral using ice ( $C_p = a'' = 9.0$  cal mole<sup>-1</sup> deg<sup>-1</sup>) to represent H<sub>2</sub>O (see text). <sup>j</sup> Stout and Robie (1965). <sup>k</sup> Pankratz and King (1965). <sup>l</sup> King and Weller (1962). Computed using  $C_p = 18.1 + 8.8 \times 10^{-5} T$  obtained by fitting the enthalpies for K<sub>2</sub>O between 400° and 1000°K reported by Robie and Waldbaum (1968).

mineral assemblages, define mineral stabilities, and predict (by controlled extrapolation) higher temperature stability regions.

### Activity Coefficients and Degrees of Formation of Complexes

Stoichiometric individual ion activity coefficients for  $Al^{+++}$ ,  $S^{--}$ ,  $SO_4^{--}$ ,  $CO_3^{--}$ , and various ore-forming metals in concentrated NaCl solutions to 300°C are shown in tables 13 and 14 and plotted in figures 9 to 14. These values, together with the activity coefficients for  $Na^+$ ,  $K^+$ , and  $Ca^{++}$  in tables 13 and 14, were computed from equilibrium constants given in tables 4 and 5, mass balance expressions of the kind shown in equation (49), true individual ion activity coefficients computed from equation (43) using 25°C  $\bar{a}$  values<sup>7</sup>, and the data in table 2. Values of  $\gamma_{CO_2}$  in NaCl solutions (table 2) were used in the calculations to represent the activity coefficients of the neutral species. Also,  $a_{Cl-}$ ,  $\bar{Y}$ , and  $B^*$  in the calculations were taken to be those in pure NaCl solutions (table 2) because other constituents in hydrothermal solutions are commonly present in small concentrations compared to NaCl. The stoichiometric individual ion activity coefficients shown in table 14 are conservative values; that is, they do not include provision for divalent and trivalent complexes of the metal ions (see discussion above and footnote a, table 14). The complexes with the higher charges were omitted to preclude any substantial errors that might be introduced by the assumption of constant  $\bar{a}$  values.

The degrees of formation achieved by metal chloride complexes in concentrated sodium chloride solutions at high temperatures are depicted in figure 15. The distribution of species shown in figure 15 is based on evaluation of

$$\alpha_{\check{c}} = \frac{a_{Cl-}^y \gamma_i}{\beta_{\check{c}} \gamma_{\check{c}}} \quad (54)$$

where  $\alpha_{\check{c}}$  is the degree of formation of the  $\check{c}$ th mononuclear complex containing  $y$  moles of chloride and 1 mole of the  $i$ th cation. The curves for the respective metal ions in figure 15 include provision for all of the reactions and species involving those ions shown in table 5; the  $\beta_{\check{c}}$ ,  $\gamma_{\check{c}}$ , and  $\gamma_i$  values used in the calculations were computed in the manner described above. Because 25°C  $\bar{a}$  values were used to compute the activity coefficients required to evaluate equation (54), appreciable error may have been incorporated into the calculations of  $\alpha_{\check{c}}$  for the divalent complexes at the higher temperatures. Figure 15 thus illustrates only the distribution of species in solution that occurs if the  $\bar{a}$  values for the ions remain essentially constant from 25°C to 300°C. If they in fact increase significantly, the diagrams in figure 15 will change substantially, but the  $\gamma_i$  values presented in tables 13 and 14 and figures 9 to 14 will be affected only slightly owing to the fact that the divalent (and higher

<sup>7</sup> The values of  $\bar{a}$  were assigned on the basis of Kielland's (1937)  $\bar{a}$  values assuming equalities for similar complexes.

TABLE 9  
Equilibrium constants for hydrothermal oxidation-reduction reactions involving aqueous species at high temperatures

Reaction <sup>a</sup>	$\Delta H^\circ(T)^\circ$ (cal mole <sup>-1</sup> )	$\Delta S^\circ(T)^\circ$ (cal/mole- deg <sup>-1</sup> )	$\log K(T)^\circ$									
			25°C	50°C	60°C	100°C	150°C	200°C	250°C	300°C		
$2H_2S + O_{2(aq)} \rightleftharpoons S_{2(aq)} + 2H_2O^d$	-87,890	-22.9	59.44	54.4*	52.57	46.27	39.99	35.05	30.6*	27.21		
$H_2S + 2O_{2(aq)} \rightleftharpoons H^* + HSO_3^-$	-204,440	-102.2	127.54	115.5*	111.71	97.30	83.05	71.62	62.5*	55.61		
$H_2S + 2O_{2(aq)} \rightleftharpoons 2H^* + SO_3^{--}$	-208,290	-124.2	125.55	113.2*	109.31	94.31	79.31	67.13	57.1*	48.35		
$HS^- + 2O_{2(aq)} \rightleftharpoons H^* + SO_3^{--}$	-213,090	-108.4	132.33	120.0*	116.02	100.93	86.03	74.09	64.4*	56.61		
$2H^* + S^{--} + \frac{1}{2}O_{2(aq)} \rightleftharpoons \frac{1}{2}S_{2(aq)} + H_2O^d$	-62,040	23.5	50.62	47.1*	45.85	41.54	37.33	34.05	31.3*	29.39		
$2HS^- + O_{2(aq)} + 2H^* \rightleftharpoons S_{2(aq)} + 2H_2O^d$	-97,490	8.9	73.42	68.0*	65.01	59.53	53.43	48.97	45.3*	43.33		
$S^{--} + 2O_{2(aq)} \rightleftharpoons SO_3^{--}$	-220,390	-89.4	146.43	133.9*	128.86	112.70	96.68	83.74	72.7*	64.26		
$Fe^{+++} + \frac{1}{2}H_2O \rightleftharpoons Fe^{++} + \frac{1}{4}O_{2(aq)} + H^*$	24,357	46.89	-7.75	-6.35*	-5.87	-4.16	-2.48	-1.15	-0.1*	0.84		
$Cu^{++} + \frac{1}{2}H_2O \rightleftharpoons Cu^+ + \frac{1}{4}O_{2(aq)} + H^*$	35,697	36.89	-18.10	-16.1*	-15.35	-12.83	-10.34	-8.35	-6.64*	-5.33		
$S^{--} + 4H_2O^d \rightleftharpoons SO_3^{--} + 4H_{2(aq)}$	46,870	68.80	-19.76	-17.15*	-16.26	-13.30	-10.69	-8.92	-7.6*	-6.87		
$8Fe^{+++} + 4H_2O^d + S^{--} \rightleftharpoons 8Fe^{++} + SO_3^{--} + 8H^*$	29,930	285.72	84.45	83.1*	81.90	79.42	76.84	74.62	71.9*	70.93		
$8Cu^{++} + 4H_2O^d + S^{--} \rightleftharpoons 8Cu^+ + SO_3^{--} + 8H^*$	59,190	203.72	1.63	5.1*	6.06	10.06	13.95	16.70	19.6*	21.62		
$Cu^+ + Fe^{+++} \rightleftharpoons Cu^{++} + Fe^{++}$	-11,140	10.00	10.35	9.7*	9.48	8.67	7.85	7.20	6.6*	6.17		

<sup>a</sup> All reactants and products are aqueous unless otherwise indicated by the subscript (aq) for gas. <sup>b</sup> Computed from thermodynamic data given in tables 3, 6, and 7. <sup>c</sup> The  $\log K(T)$  values shown for 25°C were computed from the  $\Delta H^\circ(T)^\circ$  and  $\Delta S^\circ(T)^\circ$  values shown in the table; those for 60°C and above were calculated using  $\Delta H^\circ_{25}(T)^\circ$ ,  $S^\circ_{25}(T)^\circ$  and average heat capacity values for the ions,  $H_2S_{(aq)}$ , and  $H_2O_{(liq)}$  (table 3) to first compute  $\Delta H^\circ(T)^\circ$  and  $S^\circ(T)^\circ$  for these species at elevated temperatures (eqs 13 and 14). These values were then used together with those for gases in tables 6 and 7 to evaluate equation (15). All the  $\log K(T)$  values are consistent with molal units of concentration. <sup>d</sup> Liquid water. <sup>e</sup> Interpolated.

TABLE 10

Equilibrium constants for the disproportionation of aqueous ions, oxidation-reduction of hydrothermal minerals, and dissolution of gases in aqueous solution at elevated temperatures

Reaction <sup>a</sup>	$\Delta H^\circ_f(T_r)^b$ (cal mole <sup>-1</sup> )	$\Delta S^\circ_f(T_r)^b$ (cal mole <sup>-1</sup> deg <sup>-1</sup> )	log K(T) <sup>c</sup>								
			25°C	50°C	60°C	100°C	150°C	200°C	250°C	300°C	
$2\text{Cu}^+ \rightleftharpoons \text{Cu}^{2+}_{(c)} + \text{Cu}^0$	-18,470	-34.45	6.01	4.92 <sup>d</sup>	4.57	3.20	1.84	0.66	0.37	1.27	
$3\text{Au}^+ \rightleftharpoons 2\text{Au}^{3+}_{(c)} + \text{Au}^0$	-53,260 <sup>e</sup>	-66.4	9.82 <sup>e</sup>	7.91 <sup>b</sup>	7.22 <sup>b</sup>	4.76 <sup>b</sup>	2.21 <sup>b</sup>	0.16 <sup>b</sup>	1.60 <sup>b</sup>	3.11 <sup>b</sup>	
$\text{Cu}_2\text{FeS}_4 + 4\text{FeS}_2 \rightleftharpoons 5\text{CuFeS}_2 + \text{S}_{2(g)}$	56,750 <sup>f</sup>	68.91 <sup>g</sup>	-26.5	-23.2 <sup>d</sup>	-22.2	-18.2	-14.2	-11.1	-8.5	-6.4 <sup>h</sup>	
$4\text{FeS}_2 + 4\text{H}_2\text{O} \rightleftharpoons 4\text{Fe}^{2+} + 7\text{S}^{2-} + \text{SO}_4^{2-} + 8\text{H}^+$	199,430	-249.04	-200.57	-189.7 <sup>d</sup>	-185.46	-171.89	-158.96	-149.17	-141.49	-135.04	
$3\text{Fe}_2\text{O}_3(c) \rightleftharpoons 2\text{Fe}_3\text{O}_4(c) + \frac{1}{2}\text{O}_2(g)$	57,100	33.89	-34.43	-31.13 <sup>d</sup>	-30.04	-26.02	-22.07	-18.95	-16.44	-14.35	
$\text{FeS}_{2(c)} \rightleftharpoons \text{FeS}_{(c)} + \frac{1}{2}\text{S}_{2(g)}$	32,210	29.02	-17.26	-15.42 <sup>d</sup>	-14.78	-12.50	-10.25	-8.48	-7.03	-5.81	
$\text{FeS}_{(c)} + \text{FeS}_{2(c)} + \frac{3}{2}\text{O}_2(g) \rightleftharpoons \text{Fe}_2\text{O}_3(c) + \frac{3}{2}\text{S}_{2(g)}$	307,350	7.49	63.69	58.67 <sup>d</sup>	56.96	50.89	44.92	40.20	36.38	33.22	
$\text{FeS}_{2(c)} + \frac{3}{2}\text{O}_2(g) \rightleftharpoons \text{Fe}_2\text{O}_3(c) + 2\text{S}_{2(g)}$	-53,940	31.12	46.33	43.18 <sup>d</sup>	42.18	38.39	34.66	31.72	29.35	28.19	
$3\text{FeS}_{2(c)} + 2\text{O}_2(g) \rightleftharpoons \text{Fe}_3\text{O}_4(c) + 3\text{S}_{2(g)}$	-52,360	63.98	52.27	49.13 <sup>d</sup>	48.24	44.57	40.95	38.11	35.81	33.93	
$\text{Cu}_2\text{S}_{(c)} + \frac{1}{2}\text{S}_{2(g)} \rightleftharpoons 2\text{CuS}_{(c)}$	-19,412	24.20	8.92	7.71 <sup>d</sup>	7.32	6.06	4.72	3.66	2.77	2.09	
$\text{Cu}^{2+}_{(c)} + 2\text{H}^+ + \frac{1}{2}\text{O}_2(g) \rightleftharpoons \text{Cu}^+ + \text{H}_2\text{O}_{(liq)}$	-52,925	-39.34	30.19	27.1 <sup>d</sup>	26.13	22.45	18.84	16.04	13.78	11.94	
$2\text{Cu}^{2+}_{(c)} + \frac{1}{2}\text{S}_{2(g)} \rightleftharpoons \text{Cu}_2\text{S}_{(c)}$	-34,488	-14.29	22.15	20.20 <sup>d</sup>	19.50	17.09	14.78	12.88	11.38	10.16	
$\text{Cu}^{2+}_{(c)} + \text{H}^+ + \frac{1}{4}\text{O}_2(g) \rightleftharpoons \text{Cu}^+ + \frac{1}{2}\text{H}_2\text{O}_{(liq)}$	-17,227	-2.44	12.09	11.1 <sup>d</sup>	10.78	9.63	8.50	7.69	7.07	6.61	
$\text{Cu}^{2+}_{(c)} + \frac{1}{2}\text{S}_{2(g)} \rightleftharpoons \text{CuS}_{(c)}$	-26,945	-19.27	15.54	14.01 <sup>d</sup>	13.46	11.58	11.35	9.94	7.09	6.13	
$\text{Ag}^{2+}_{(c)} + \text{H}^+ + \frac{1}{4}\text{O}_2(g) \rightleftharpoons \text{Ag}^+ + \frac{1}{2}\text{H}_2\text{O}_{(liq)}$	-8,847	3.60	7.27	6.74 <sup>d</sup>	6.60	6.01	5.44	5.06	4.74	4.50	
$2\text{Ag}^{2+}_{(c)} + \frac{1}{2}\text{S}_{2(g)} \rightleftharpoons 2\text{AgS}_{(c)}$	-23,077	-13.51	13.95	12.65 <sup>d</sup>	12.19	10.57	9.00	7.77	6.79	5.99	
$\text{Hg}^{2+}_{(liq)} + 2\text{H}^+ + \frac{1}{2}\text{O}_2(g) \rightleftharpoons \text{Hg}^+ + \text{H}_2\text{O}_{(liq)}$	-26,725	-31.69	12.66	11.13 <sup>d</sup>	10.61	8.72	6.84	5.37	4.15	3.14	

$\text{Hg}^{2+}_{(liq)} + \frac{1}{2}\text{S}_{2(g)} \rightleftharpoons \text{HgS}_{(c)}^1$	-26,500	-22.75	14.43	12.86 <sup>d</sup>	12.40	10.55	8.73	7.30	6.14	5.19
$\text{Au}^{3+}_{(c)} + \frac{3}{4}\text{O}_2(g) + 3\text{H}^+ \rightleftharpoons \text{Au}^+ + \frac{3}{2}\text{H}_2\text{O}_{(liq)}$	4,850 <sup>e</sup>	-46.0	-13.61 <sup>e</sup>	-13.34 <sup>b</sup>	-13.24 <sup>b</sup>	-12.91 <sup>b</sup>	-12.59 <sup>b</sup>	-12.35 <sup>b</sup>	-12.17 <sup>b</sup>	-12.02 <sup>b</sup>
$\text{Au}^{3+}_{(c)} + \frac{1}{2}\text{O}_2(g) + \text{H}^+ \rightleftharpoons \text{Au}^+ + \frac{1}{2}\text{H}_2\text{O}_{(liq)}$	12,680 <sup>e</sup>	6.8	-7.81 <sup>e</sup>	-7.08 <sup>b</sup>	-6.82 <sup>b</sup>	-5.89 <sup>b</sup>	-4.94 <sup>b</sup>	-4.17 <sup>b</sup>	-3.52 <sup>b</sup>	-2.97 <sup>b</sup>
$\text{CO}_2(g) + \text{H}_2\text{O}_{(liq)} \rightleftharpoons \text{H}_2\text{CO}_3(\text{app})^g$	4,650	-22.3	-1.46	-1.70 <sup>d</sup>	-1.78	-1.97	-2.07	-2.06	-1.98	-1.83
$\text{H}_2\text{S}_{(g)} \rightleftharpoons \text{H}_2\text{S}_{(aq)}$	-4,100	-18.3	-0.99	-1.20 <sup>d</sup>	-1.26	-1.43	-1.52	-1.54	-1.52	-1.46

<sup>a</sup> All reactants and products are aqueous unless otherwise indicated by the subscripts (c) for crystalline or (g) for gas; the subscript (liq) refers to liquid. The crystalline compounds correspond to the mineral designations given in tables 7 and 8. <sup>b</sup> Except where noted otherwise, these values were computed from thermodynamic data given in tables 3, 6, and 7. <sup>c</sup> Except where noted otherwise, the log K(T) values for 25°C were computed from the values of  $\Delta H^\circ_f(T_r)$  and  $\Delta S^\circ_f(T_r)$  shown in the table; those for 60°C and above were calculated using  $\Delta H^\circ_f(T_r)$ ,  $S^\circ_f(T_r)$ , and average heat capacities for the ions,  $\text{H}_2\text{O}_{(liq)}$ , and  $\text{H}_2\text{S}_{(aq)}$  (table 5) to first compute  $\Delta H^\circ_f(T)$  and  $S^\circ_f(T)$  for these species at elevated temperatures (eqs 13 and 14). These values were then used together with those computed from equations (11) and (12) using data given in tables 6, 7, and 8 for minerals and gases to evaluate equation (15). The enthalpies of formation and entropies of chalcopyrite used in the calculations are given in footnotes j and k below. All the log K(T) values are consistent with molal units of concentration. <sup>d</sup> Interpolated. <sup>e</sup> The subscript (app) indicates that the species referred to is the undifferentiated sum of  $\text{H}_2\text{CO}_3(\text{app})$  and  $\text{CO}_2(\text{app})$ . <sup>f</sup> Computed from  $\Delta S^\circ_f(T_r)$  and log K(T<sub>r</sub>). <sup>g</sup> Computed from free energies of formation from the elements (Latimer, 1952). <sup>h</sup> Predicted assuming a constant  $\Delta C^\circ_{p,r}(T)$  equal to a mean value computed from average heat capacities for the respective ions (table 5) and the true heat capacities of the other species calculated from equation (10) using the coefficients in table 8. <sup>i</sup> Metacinnibar. <sup>j</sup> Computed from entropies given in table 7 and estimates of the entropy of chalcopyrite (31.2 cal mole<sup>-1</sup> deg<sup>-1</sup>) and bornite (91 cal mole<sup>-1</sup> deg<sup>-1</sup>) at 25°C obtained by summing (in appropriate proportions) the values tabulated by Latimer (1952) for the entropies of formation of iron, copper, and sulfide in solids—see text. <sup>k</sup> Computed from enthalpies of formation given in table 7 and those for chalcopyrite (-44,550 cal mole<sup>-1</sup>) and bornite (-84,820 cal mole<sup>-1</sup>) calculated from estimated free energies of formation for these minerals (-45,000 cal mole<sup>-1</sup> and -89,000 cal mole<sup>-1</sup>, respectively) at 25°C (Bartholomé, 1958) together with corresponding entropies of formation of the minerals from the elements calculated from the entropy estimates given in footnote j above and data for the elements taken from Robie and Waldbaum (1968). Bartholomé's values for the free energies of chalcopyrite and bornite appear to be more consistent with high temperature equilibrium data for the sulfides (Barton and Skinner, 1967) than do Young's (1967). <sup>l</sup> This value compares favorably with that (-6.9) reported by Barton and Skinner (1967), but the slope of log K(T) is more positive. Barton and Skinner assumed the heat capacity of reaction to be zero; the present calculations indicate that the heat capacity is neither zero nor constant.



TABLE 11  
Activity products for hydrothermal minerals and equilibrium constants for various silicate reactions involving an aqueous phase at high temperatures

Reaction <sup>a</sup>	$\Delta H^{\circ}_f(T_r)^b$ (cal mole <sup>-1</sup> )	$\Delta S^{\circ}_f(T_r)^b$ (cal mole <sup>-1</sup> deg <sup>-1</sup> )	log K(T) <sup>c</sup>							
			25°C	50°C	60°C	100°C	150°C	200°C	250°C	300°C
$\text{Cu}_2\text{FeS}_4(\text{bornite}) \rightleftharpoons 4\text{Cu}^+ + \text{Cu}^{2+} + \text{Fe}^{2+} + 4\text{S}^{--}$	183,210 <sup>d</sup>	-120.10 <sup>d</sup>	-160.5	-150.0 <sup>e</sup>	-146.4	-133.4	-120.8	-110.6	-102.3	-95.6
$\text{CuFeS}_2(\text{chalcopyrite}) \rightleftharpoons \text{Cu}^{2+} + \text{Fe}^{2+} + 2\text{S}^{--}$	57,080 <sup>d</sup>	-89.90 <sup>d</sup>	-61.5	-58.4 <sup>e</sup>	-57.1	-53.1	-49.2	-46.2	-43.7	-41.9
$\text{PbS} \rightleftharpoons \text{Pb}^{2+} + \text{S}^{--}$	32,030	-23.34	-28.57	-26.67 <sup>e</sup>	-26.14	-23.96	-21.93	-20.36	-19.14	-18.31
$\text{ZnS}(\text{sphalerite}) \rightleftharpoons \text{Zn}^{2+} + \text{S}^{--}$	22,040	-43.77	-25.72	-24.44 <sup>e</sup>	-24.03	-22.48	-21.01	-19.81	-18.86	-18.17
$\text{ZnS}(\text{marcasite}) \rightleftharpoons \text{Zn}^{2+} + \text{S}^{--}$	18,385 <sup>d</sup>	-46.56 <sup>d</sup>	-23.65	-22.58 <sup>e</sup>	-22.24	-20.96	-19.73	-18.73	-17.95	-17.39
$\text{Ag}_2\text{S} \rightleftharpoons 2\text{Ag}^+ + \text{S}^{--}$	67,427	-2.76	-50.02	-46.17 <sup>e</sup>	-44.83	-40.08	-35.45	-31.71	-28.74	-26.36
$\text{Cu}_2\text{S} \rightleftharpoons 2\text{Cu}^+ + \text{S}^{--}$	62,080	-14.06	-48.57	-45.05 <sup>e</sup>	-43.79	-39.37	-35.05	-31.54	-28.65	-26.32
$\text{CuS} \rightleftharpoons \text{Cu}^{2+} + \text{S}^{--}$	36,070	-43.53	-35.96	-33.91 <sup>e</sup>	-33.18	-30.66	-28.21	-26.28	-24.73	-23.56
$\text{HgS}(\text{mercurianthracite}) \rightleftharpoons \text{Hg}^{2+} + \text{S}^{--}$	61,830	-32.40	-52.37	-48.84 <sup>e</sup>	-47.64	-43.36	-39.23	-35.98	-33.42	-31.45
$\text{HgS}(\text{cinnabar}) \rightleftharpoons \text{Hg}^{2+} + \text{S}^{--}$	64,560 <sup>d</sup>	-20.12 <sup>d</sup>	-53.68	-50.02 <sup>e</sup>	-48.73	-44.25	-39.91	-36.51	-33.65	-31.72
$\text{FeS} \rightleftharpoons \text{Fe}^{2+} + \text{S}^{--}$	12,200	-42.52	-18.39	-18.17 <sup>e</sup>	-17.96	-17.12	-16.33	-15.71	-15.22	-14.94
$\text{FeS}_2 \rightleftharpoons \text{Fe}^{2+} + \text{S}^{--} + \frac{1}{2}\text{S}_2(\text{g})$	29,070	-43.75	-36.15	-33.50 <sup>e</sup>	-32.74	-30.17	-26.60	-24.19	-22.25	-20.75
$\text{CaSO}_4 \rightleftharpoons \text{Ca}^{2+} + \text{SO}_4^{--}$	-3,755	-34.10	-4.70 <sup>n</sup>	-4.99 <sup>n</sup>	-5.09 <sup>n</sup>	-5.63 <sup>n</sup>	-6.35 <sup>n</sup>	-7.18 <sup>n</sup>	-8.12 <sup>n</sup>	-9.05 <sup>n</sup>
$\text{BaSO}_4(\text{barite}) \rightleftharpoons \text{Ba}^{2+} + \text{SO}_4^{--}$	6,140 <sup>d</sup>	-23.80 <sup>d</sup>	-5.70	-9.42 <sup>e</sup>	-9.34	-9.22	-9.34	-9.76	-10.34	-11.05
$\text{PbSO}_4(\text{anglesite}) \rightleftharpoons \text{Pb}^{2+} + \text{SO}_4^{--}$	220 <sup>d</sup>	-28.2 <sup>d</sup>	-7.75	-7.70 <sup>e</sup>	-7.70	-7.85	-8.26	-8.88	-9.60	-10.44
$\text{CaCO}_3 \rightleftharpoons \text{Ca}^{2+} + \text{CO}_3^{--}$	-3,190	-49.0	-8.37	-8.62 <sup>e</sup>	-8.74	-9.39	-10.25	-11.37	-12.72	-14.10

$\text{CaMg}(\text{CO}_3)_2(\text{dolomite}) \rightleftharpoons \text{Ca}^{2+} + \text{Mg}^{2+} + 2\text{CO}_3^{--}$	-8,290 <sup>d</sup>	-105.69 <sup>d</sup>	-17.02 <sup>e</sup>	-17.63 <sup>e</sup>	-17.92	-19.28	-21.02	-23.26	-25.83	-28.46
$\text{ZnCO}_3(\text{smithsonite}) \rightleftharpoons \text{Zn}^{2+} + \text{CO}_3^{--}$	4,420 <sup>d</sup>	-59.30 <sup>d</sup>	-9.72	-10.05 <sup>e</sup>	-10.19	-10.88	-11.77	-12.90	-14.18	-15.52
$\text{PbCO}_3(\text{cerussite}) \rightleftharpoons \text{Pb}^{2+} + \text{CO}_3^{--}$	5,710 <sup>d</sup>	-42.40 <sup>d</sup>	-13.45	-13.19 <sup>e</sup>	-13.16	-13.21	-13.54	-14.30	-15.31	-16.50
$\text{FeCO}_3(\text{siderite}) \rightleftharpoons \text{Fe}^{2+} + \text{CO}_3^{--}$	5,030 <sup>d</sup>	-65.8 <sup>d</sup>	-10.69	-11.04 <sup>e</sup>	-11.21	-11.95	-12.86	-14.05	-15.32	-16.67
$\text{CaF}_2(\text{fluorite}) \rightleftharpoons \text{Ca}^{2+} + 2\text{F}^-$	1,530 <sup>d</sup>	-36.26 <sup>d</sup>	-9.04	-9.01 <sup>e</sup>	-9.01	-9.20	-9.66	-10.26	-11.08	-12.13
$\text{KAlSi}_3\text{O}_8 + \text{Na}^+ \rightleftharpoons \text{NaAlSi}_3\text{O}_8 + \text{K}^+$	5,939	7.83	-2.64	-2.29 <sup>e</sup>	-2.19	-1.80	-1.43	-1.15	-0.95	-0.79
$3\text{KAlSi}_3\text{O}_8 + 2\text{H}^+ \rightleftharpoons \text{KAl}_2\text{Si}_2\text{O}_{10}(\text{OH})_2 + 2\text{K}^+ + 6\text{SiO}_2(\text{qtz})$	8,880	19.87	10.85	10.31 <sup>e</sup>	10.17	9.55	8.91	8.49	8.12	7.82
$2\text{KAl}_2\text{Si}_2\text{O}_{10}(\text{OH})_2 + 2\text{H}^+ + 3\text{H}_2\text{O}^* \rightleftharpoons 3\text{Al}_2\text{Si}_2\text{O}_7(\text{OH})_4 + 2\text{K}^+$	13,395	6.46	11.22	10.45 <sup>e</sup>	10.16	9.12	7.96	7.01	6.20	5.44
$4\text{CaMg}(\text{SiO}_3)_2 + \text{Mg}^{2+} + 2\text{H}^+ \rightleftharpoons \text{Ca}_2\text{Mg}_2\text{Si}_2\text{O}_{10}(\text{OH})_2 + 2\text{Ca}^{2+}$	32,430	3.81	22.93	21.03 <sup>e</sup>	20.42	18.08	15.62	13.63	11.76	10.13
$\text{NaAlSi}_3\text{O}_8 + \text{K}^+ + \text{H}_4\text{SiO}_4 \rightleftharpoons \text{KAlSi}_3\text{O}_8 + \text{Na}^+ + 2\text{H}_2\text{O}$	9,009	8.19	4.81	4.32 <sup>e</sup>	4.13	3.50	2.92	2.45	2.05	1.75
$2\text{Al}(\text{OH})_3^{\text{m}} + 2\text{H}_4\text{SiO}_4 \rightleftharpoons \text{Al}_2\text{Si}_2\text{O}_7(\text{OH})_4 + 5\text{H}_2\text{O}^*$	9,275	6.90	8.29	7.8 <sup>e</sup>	7.59	6.97	6.44	6.02	5.70	5.54
$\text{Mg}_3\text{Al}_2\text{Si}_2\text{O}_{10}(\text{OH})_2 + 10\text{H}^+ \rightleftharpoons \text{Al}_2\text{Si}_2\text{O}_7(\text{OH})_4 + 5\text{Mg}^{2+} + \text{H}_4\text{SiO}_4 + 5\text{H}_2\text{O}^*$	111,865	75.08	65.57	59.6 <sup>e</sup>	57.15	49.81	42.86	37.95	34.18	31.26

TABLE 11 (continued)

Reaction <sup>a</sup>	$\Delta H_f^\circ(T_r)^b$ (cal mole <sup>-1</sup> )	$\Delta S_f^\circ(T_r)^b$ (cal mole <sup>-1</sup> deg <sup>-1</sup> )	log K(T) <sup>c</sup>							
			25°C	50°C	60°C	100°C	150°C	200°C	250°C	300°C
4CaAl <sub>2</sub> Si <sub>2</sub> O <sub>8</sub> + 5Mg <sup>++</sup> + 18H <sup>+</sup> ⇌ Ca <sub>2</sub> Mg <sub>5</sub> Si <sub>2</sub> O <sub>22</sub> (OH) <sub>2</sub> + 2Ca <sup>++</sup> + 8Al <sup>+++</sup> + 8H <sub>2</sub> O <sup>o</sup>	-185,710	-429.53	42.25	39.1 <sup>f</sup>	28.06	15.28	2.74	6.65	14.48	20.79
Mg <sub>6</sub> Al <sub>2</sub> Si <sub>2</sub> O <sub>16</sub> (OH) <sub>8</sub> + 2Ca <sup>++</sup> + 5H <sub>2</sub> SiO <sub>4</sub> + 2H <sup>+</sup> ⇌ Ca <sub>2</sub> Mg <sub>6</sub> Si <sub>2</sub> O <sub>22</sub> (OH) <sub>2</sub> + 2Al <sup>+++</sup> + 14H <sub>2</sub> O <sup>o</sup>	-53,630	-103.47	16.69	13.6 <sup>f</sup>	12.68	9.96 <sup>g</sup>	6.32	4.22	2.84	1.97
Mg <sub>3</sub> Si <sub>2</sub> O <sub>10</sub> (OH) <sub>2</sub> + 5H <sub>2</sub> O <sup>o</sup> ⇌ Mg <sub>3</sub> Si <sub>2</sub> O <sub>7</sub> (OH) <sub>2</sub> <sup>h</sup> + 2H <sub>2</sub> SiO <sub>4</sub>	17,605	-1.31	-13.19	-12.20 <sup>f</sup>	-11.83 <sup>g</sup>	-10.60 <sup>g</sup>	-9.43 <sup>g</sup>	-8.47 <sup>g</sup>	-7.68 <sup>g</sup>	-7.03 <sup>g</sup>

<sup>a</sup> Where no indication is given, all reactants and products except liquid water, H<sub>2</sub>SiO<sub>4</sub>, and ionic species correspond to the mineral designations given in table 7. H<sub>2</sub>SiO<sub>4</sub> and all ionic species are in the aqueous standard state. <sup>b</sup> Except where noted otherwise, the values in these columns were computed from thermodynamic data given in tables 3, 7, and 10 (footnotes j and k). <sup>c</sup> Except where noted otherwise, the log K(T) values for 25°C were computed from the values of  $\Delta H_f^\circ(T_r)$  and  $\Delta S_f^\circ(T_r)$  shown in the table; those for 60°C and above were calculated using  $\Delta H_f^\circ(T_r)$ ,  $S_f^\circ(T_r)$ , and average heat capacity values for the ions, H<sub>2</sub>O<sub>(110)</sub>, and H<sub>2</sub>SiO<sub>4</sub> (table 3) to first compute  $\Delta H_f^\circ(T)$  and  $S_f^\circ(T)$  for these species at elevated temperatures (eqs 13 and 14). These values were then used together with those computed from eq (11) and (12) using data given in tables 7, 8, and 10 (footnotes j and k) for the solids and  $S_{298}$  to evaluate equation (15). With the exception of dolomite (see footnote l below), values of  $\Delta H_f^\circ(T_r)$  and  $S_f^\circ(T_r)$  for minerals not included in tables 7 and 10 were taken from Robie and Waldbaum (1968). All the log K(T) values are consistent with molal units of concentration. <sup>d</sup> See footnotes j and k, table 10. <sup>e</sup> Liquid water. <sup>f</sup> Interpolated. <sup>g</sup> Computed using the heat capacity power function for antigonite (table 8) to represent chrysotile. <sup>h</sup> Chrysotile. <sup>i</sup> Computed from data given in table 3 for the ionic species and, except where noted otherwise, the enthalpies of formation and entropies of the minerals at 25°C tabulated by Robie and Waldbaum (1968). <sup>j</sup> Computed using the entropy for dolomite reported by Stout and Robie (1963). <sup>k</sup> Langmuir (1954); Hsu (1967); Berner (1967). <sup>l</sup> The  $\Delta H_f^\circ(T_r)$  value for dolomite used in the calculations was computed from the activity product constant for dolomite and a calculated entropy of formation of dolomite from the elements at 25°C (see footnote j above). <sup>m</sup> See footnote p, table 7. <sup>n</sup> These values differ from those reported by Yeats and Marshall (1969), who did not take into account explicitly the effects of calcium sulfate complexing in their calculation of the activity product for anhydrite. <sup>o</sup> Crystalline gibbsite.

TABLE 12  
Equilibrium constants for the hydrolysis of silicates and  
various oxide, hydroxide, and carbonate minerals at elevated temperatures<sup>a</sup>

Reaction <sup>a</sup>	$\Delta H_f^\circ(T_r)^b$ (cal mole <sup>-1</sup> )	$\Delta S_f^\circ(T_r)^b$ (cal mole <sup>-1</sup> deg <sup>-1</sup> )	log K(T) <sup>c,d</sup>						
			25°C	60°C	100°C	150°C	200°C	250°C	300°C
SiO <sub>2</sub> + 2H <sub>2</sub> O ⇌ H <sub>2</sub> SiO <sub>4</sub>	6,220	2.54	-4.00	-3.52	-2.08	-2.67	-2.35	-2.11	-1.94
KAlSi <sub>3</sub> O <sub>8</sub> (intermediate) + 4H <sup>+</sup> + 4H <sub>2</sub> O ⇌ K <sup>+</sup> + Al <sup>+++</sup> + 3H <sub>2</sub> SiO <sub>4</sub>	-11,960	34.19	1.29	0.42	-0.32	-1.14	-1.57	-1.95	-2.38
KAlSi <sub>3</sub> O <sub>8</sub> (adularite) + 4H <sup>+</sup> + 4H <sub>2</sub> O ⇌ K <sup>+</sup> + Al <sup>+++</sup> + 3H <sub>2</sub> SiO <sub>4</sub>	-12,960 <sup>e</sup>	-37.71 <sup>e</sup>	1.26	0.30	-0.50	-1.37	-1.83	-2.31	-2.77
KAlSi <sub>3</sub> O <sub>8</sub> (high and low) + 4H <sup>+</sup> + 4H <sub>2</sub> O ⇌ K <sup>+</sup> + Al <sup>+++</sup> + 3H <sub>2</sub> SiO <sub>4</sub>	-13,580 <sup>e</sup>	-38.65 <sup>e</sup>	1.51	0.50	-0.34	-1.25	-1.80	-2.26	-2.74
NaAlSi <sub>3</sub> O <sub>8</sub> (low albite) + 4H <sup>+</sup> + 4H <sub>2</sub> O ⇌ Na <sup>+</sup> + Al <sup>+++</sup> + 3H <sub>2</sub> SiO <sub>4</sub>	-17,900	-42.02	3.94	2.61	1.48	0.31	-0.41	-1.01	-1.59
NaAlSi <sub>3</sub> O <sub>8</sub> (high albite) + 4H <sup>+</sup> + 4H <sub>2</sub> O ⇌ Na <sup>+</sup> + Al <sup>+++</sup> + 3H <sub>2</sub> SiO <sub>4</sub>	-20,690 <sup>e</sup>	-46.49 <sup>e</sup>	5.00	3.46 <sup>g</sup>	2.13 <sup>g</sup>	0.75 <sup>g</sup>	-0.17 <sup>g</sup>	-0.91 <sup>g</sup>	-1.65 <sup>g</sup>
NaAlSi <sub>3</sub> O <sub>8</sub> ·H <sub>2</sub> O + 4H <sup>+</sup> + H <sub>2</sub> O ⇌ Na <sup>+</sup> + Al <sup>+++</sup> + 2H <sub>2</sub> SiO <sub>4</sub>	-25,780	-43.56	9.37	7.45	5.79	4.18	3.13	2.31	1.63
CaAl <sub>2</sub> Si <sub>2</sub> O <sub>8</sub> + 8H <sup>+</sup> ⇌ Ca <sup>++</sup> + 2Al <sup>+++</sup> + 2H <sub>2</sub> SiO <sub>4</sub>	-70,590	-123.77	24.09	19.32	14.53	9.79	6.34	3.47	1.12
Al <sub>2</sub> Si <sub>2</sub> O <sub>7</sub> (OH) <sub>2</sub> (andinite) + 6H <sup>+</sup> ⇌ 2Al <sup>+++</sup> + H <sub>2</sub> O + 2H <sub>2</sub> SiO <sub>4</sub>	-38,415	-93.94	7.63	4.75	2.27	-0.12	-1.72	-2.98	-4.02
Al <sub>2</sub> Si <sub>2</sub> O <sub>7</sub> (OH) <sub>2</sub> (dialite) + 6H <sup>+</sup> ⇌ 2Al <sup>+++</sup> + H <sub>2</sub> O + 2H <sub>2</sub> SiO <sub>4</sub>	-39,270 <sup>e</sup>	-92.51 <sup>e</sup>	8.56	5.63 <sup>m</sup>	3.10 <sup>m</sup>	0.69 <sup>m</sup>	-0.90 <sup>m</sup>	-2.13 <sup>m</sup>	-3.09 <sup>m</sup>
Al <sub>2</sub> Si <sub>2</sub> O <sub>7</sub> (OH) <sub>2</sub> (hollandite) + 6H <sup>+</sup> ⇌ 2Al <sup>+++</sup> + H <sub>2</sub> O + 2H <sub>2</sub> SiO <sub>4</sub>	-43,440 <sup>e</sup>	-94.01 <sup>e</sup>	11.29	8.03 <sup>m</sup>	5.21 <sup>m</sup>	2.50 <sup>m</sup>	0.67 <sup>m</sup>	-0.75	-1.89 <sup>m</sup>
KAl <sub>2</sub> Si <sub>2</sub> O <sub>7</sub> (OH) <sub>2</sub> + 10H <sup>+</sup> ⇌ K <sup>+</sup> + 3Al <sup>+++</sup> + 3H <sub>2</sub> SiO <sub>4</sub>	-64,320	-137.68	17.05	12.21	7.97	3.80	0.93	-1.38	-3.31
K <sub>0.6</sub> Mg <sub>0.25</sub> Al <sub>2.35</sub> Si <sub>2.35</sub> O <sub>10</sub> (OH) <sub>2</sub> (111111) + 8H <sup>+</sup> + 2H <sub>2</sub> O ⇌ 0.6K <sup>+</sup> + 0.25Mg <sup>++</sup> + 2.35Al <sup>+++</sup> + 3.5H <sub>2</sub> SiO <sub>4</sub>	-46,486 <sup>f</sup>	-108.60 <sup>f</sup>	10.34	6.85	3.82	0.81	-1.23	-2.87	-4.29

TABLE 12 (continued)

Reaction <sup>a</sup>	$\Delta H_f^\circ(T_r)^b$ (cal mole <sup>-1</sup> )	$\Delta S_f^\circ(T_r)^b$ (cal mole <sup>-1</sup> deg <sup>-1</sup> )	log K(T) <sup>c,d</sup>						
			25°C	60°C	100°C	150°C	200°C	250°C	300°C
$KFe_3AlSi_3O_{10}(OH)_{2(\text{montmorillonite})} + 10H^+ \rightleftharpoons K^+ + 3Fe^{2+} + Al^{3+} + 3H_4SiO_4$	-60,470 <sup>e</sup>	-96.2 <sup>e,f</sup>	23.3	18.7	14.7	10.8	8.0	5.8	3.9
$NaAlSi_3O_8 + 4H^+ \rightleftharpoons Na^+ + Al^{3+} + H_4SiO_4$	-33,840	-46.33	14.66	12.11	9.84	7.62	6.05	4.76	3.70
$KAlSi_3O_8 + 4H^+ + 2H_2O \rightleftharpoons K^+ + Al^{3+} + 2H_4SiO_4$	-24,830	-32.19	9.85	7.98	6.34	4.70	3.60	2.71	1.95
$Mg_3Al_2Si_2O_{10}(OH)_2(\text{chlorite}) + 16H^+ \rightleftharpoons 5Mg^{2+} + 2Al^{3+} + 3H_4SiO_4 + 6H_2O$	-150,280 <sup>g</sup>	-169.02 <sup>g</sup>	73.20	61.90	52.08	42.74	36.23	31.20	27.24
$3Na_{0.33}Al_{2.33}Si_{3.67}O_{10}(OH)_2(\text{montmorillonite})^k + 22H^+ + 8H_2O \rightleftharpoons 3Na^+ + 7Al^{3+} + 11H_4SiO_4$	-127,900 <sup>g</sup>	-341.74 <sup>g</sup>	19.06	9.48	1.18	-7.03	-12.56	-17.00	-20.89
$3K_{0.33}Al_{2.33}Si_{3.67}O_{10}(OH)_2(\text{montmorillonite})^k + 22H^+ + 8H_2O \rightleftharpoons 3K^+ + 7Al^{3+} + 11H_4SiO_4$	-124,420 <sup>g</sup>	-335.44 <sup>g</sup>	18.32	9.00	0.92	-7.11	-12.51	-16.57	-20.70
$6Ca_{0.10}Al_{2.70}Si_{3.30}O_{10}(OH)_2(\text{montmorillonite})^k + 44H^+ + 16H_2O \rightleftharpoons 6Ca^{2+} + 14Al^{3+} + 22H_4SiO_4$	-264,170 <sup>g</sup>	-715.88 <sup>g</sup>	37.10	17.34	-0.11	-17.00	-28.68	-38.13	-46.89
$6Mg_{0.10}Al_{2.70}Si_{3.30}O_{10}(OH)_2(\text{montmorillonite})^k + 44H^+ + 16H_2O \rightleftharpoons 6Mg^{2+} + 14Al^{3+} + 22H_4SiO_4$	-267,850 <sup>g</sup>	-730.88 <sup>g</sup>	36.60	16.49	-0.96	-18.25	-30.09	-39.53	-47.81
$MgSiO_3 + 2H^+ + H_2O \rightleftharpoons Mg^{2+} + H_4SiO_4$	-20,055	-15.29	11.36	9.83	8.48	7.14	6.16	5.37	4.70
$CaMg(SiO_3)_2 + 4H^+ + 2H_2O \rightleftharpoons Ca^{2+} + Mg^{2+} + 2H_4SiO_4$	-32,270	-17.34	19.86	17.41	15.23	13.01	11.41	10.03	8.85
$Ca_2Mg_2Si_2O_{10}(OH)_2 + 14H^+ + 8H_2O \rightleftharpoons 2Ca^{2+} + 5Mg^{2+} + 8H_4SiO_4$	-96,650	-65.55	56.51	49.22	42.84	36.42	32.01	28.36	25.27
$Mg_3Si_2O_8(OH)_2 + 6H^+ + 4H_2O \rightleftharpoons 3Mg^{2+} + 4H_4SiO_4$	-35,010	-30.42	19.01	16.40	14.17	11.96	10.53	9.42	8.45
$Mg_2Si_2O_7(OH)_{2(\text{heyrlandite})} + 6H^+ \rightleftharpoons 3Mg^{2+} + 2H_4SiO_4 + H_2O$	-52,615	-29.11	32.20 <sup>p</sup>	28.23 <sup>n,p</sup>	24.77 <sup>n,p</sup>	21.39 <sup>n,p</sup>	19.00 <sup>n,p</sup>	17.10 <sup>n</sup>	15.58 <sup>n</sup>
$Fe_2SiO_4 + 4H^+ \rightleftharpoons 2Fe^{2+} + H_4SiO_4$	-36,560	-43.81	17.22	14.43	11.96	9.50	7.67	6.25	5.05

$Mg_2SiO_4 + 4H^+ \rightleftharpoons 2Mg^{2+} + H_4SiO_4$	-49,880	-33.31	29.28	25.47	22.08	18.74	16.26	14.26	12.61
$Fe_2O_3 + 6H^+ \rightleftharpoons 2Fe^{3+} + 3H_2O$	-30,445	-110.96	-1.93	-4.24	-6.28	-8.22	-9.69	-10.36	-11.81
$Fe_3O_4 + 8H^+ \rightleftharpoons Fe^{2+} + 2Fe^{3+} + 4H_2O$	-49,660	-136.49	6.57	2.79	-0.57	-3.77	-6.21	-8.13	-9.69
$CuO_{(\text{tenorite})} + 2H^+ \rightleftharpoons Cu^{2+} + H_2O$	-15,785 <sup>d</sup>	-17.08 <sup>d</sup>	7.84	6.63	5.56	4.50	3.72	3.09	2.59
$Cu_2O_{(\text{cuprite})} + 2H^+ \rightleftharpoons 2Cu^+ + H_2O$	5,945 <sup>d</sup>	13.11 <sup>d</sup>	-1.49	-1.01	-0.48	0.05	0.62	1.16	1.70
$Mg(OH)_2 + 2H^+ \rightleftharpoons Mg^{2+} + 2H_2O$	-25,820	-9.81	16.78	14.84	13.10	11.41	10.09	9.08	8.53
$Al(OH)_{3(\text{crystalline gibbsite})} + 3H^+ \rightleftharpoons Al^{3+} + 3H_2O^h$	-23,845 <sup>t</sup>	-43.52 <sup>d,1</sup>	7.96	6.17 <sup>1</sup>	4.62 <sup>1</sup>	3.16 <sup>1</sup>	2.15 <sup>1</sup>	1.36 <sup>1</sup>	0.76 <sup>1</sup>
$Al(OH)_{3(\text{microcrystalline gibbsite})} + 3H^+ \rightleftharpoons Al^{3+} + 3H_2O^h$	-25,560 <sup>d</sup>	-43.52 <sup>d</sup>	9.23	7.30	5.63	4.05	2.94	2.08	1.41
$CaCO_3 + 2H^+ \rightleftharpoons Ca^{2+} + H_2O + CO_{2(g)}$	-4,020	32.37	9.76	9.48	9.25	9.04	8.95	8.81	8.73

<sup>a</sup> Where no indication is given, all reactants other than H<sub>2</sub>O and H<sup>+</sup> correspond to the mineral designations given in table 7. H<sub>4</sub>SiO<sub>4</sub> and all ionic species are in the aqueous standard state, and H<sub>2</sub>O refers to liquid water. The subscript (g) refers to gas. <sup>b</sup> Except where noted otherwise, the values in these columns were computed from data given in tables 3 and 7. <sup>c</sup> The log K(T) values for 25°C were computed from the values of  $\Delta H_f^\circ(T_r)$  and  $\Delta S_f^\circ(T_r)$  shown in the table; those for 60°C and above were calculated using  $\Delta H_f^\circ(T_r)$ ,  $S_f^\circ(T_r)$ , and average heat capacities for the ions, H<sub>2</sub>O<sub>(l)</sub>, and H<sub>4</sub>SiO<sub>4</sub> (table 3) to first compute  $\Delta H_f^\circ(T)$  and  $S_f^\circ(T)$  for these species at elevated temperatures (eqs 13 and 14). These values were then used together with those computed from equations (11) and (12) using data given in tables 7 and 8 for the solids to evaluate equation (15). Values of  $\Delta H_f^\circ(T_r)$  and  $S_f^\circ(T_r)$  for minerals not included in table 7 were taken from Robie and Waldbaum (1968), as were data used to compute average heat capacities for high albite. All the log K(T) values are consistent with molal units of concentration. <sup>d</sup> Computed from data given in table 3 for ionic species, H<sub>2</sub>O, and H<sub>4</sub>SiO<sub>4</sub>, and the enthalpies of formation and entropies of the minerals at 25°C tabulated by Robie and Waldbaum (1968). <sup>e</sup> Computed from data given in table 3 and an estimated third law entropy for the mineral at 25°C obtained by summing (in appropriate proportions) the entropies of the oxide components of the minerals using 9.4 cal mole<sup>-1</sup> deg<sup>-1</sup> (Latimer, 1952) for H<sub>2</sub>O—see text and footnotes f and g below. <sup>f</sup> Computed from data given in table 3 together with the free energies of formation of the minerals obtained from solubility studies and entropies of formation

TABLE 12 (continued)

calculated from the third law entropy estimates for the minerals given below. The calculated free energies and enthalpies of formation and estimated entropies of the minerals at 25°C are (per mole of the mineral with the composition given above):

Mineral	$\Delta H_f^\circ(T_r)$ (cal mole <sup>-1</sup> )	$S^\circ(T_r)$ (cal mole <sup>-1</sup> deg <sup>-1</sup> )	$\Delta G_f^\circ(T_r)$ (cal mole <sup>-1</sup> )	Source of $\Delta G_f^\circ(T_r)$
Illite	-1,390,820	66.4	-1,300,980	Computed from the solubilities of illite and kaolinite in sea water reported by Mackenzie and Garrels (1965).
Mg-chlorite	-2,109,840	112	-1,954,800	Calculated from the solubilities of chlorite and kaolinite in sea water reported by Mackenzie and Garrels (1965).
Ca-montmorillonite	-1,367,980	61.2	-1,279,240	Computed from the composition of Sierra Nevada waters (Feth, Roberson, and Polzer, 1964) considered to be in equilibrium with calcium montmorillonite (Garrels and Mackenzie, 1967).
Na-montmorillonite	-1,366,840	62.8	-1,277,760	Calculated from the free energy of formation of calcium montmorillonite assuming $\log(a_{Na^+}^2/a_{Ca^{++}}) = 1.1$ for the exchange of calcium for sodium (computed by R. M. Garrels (personal commun.) from data reported by Schachtschabel, 1940).
K-montmorillonite	-1,368,920	63.4	-1,279,600	Calculated from the free energy of formation of sodium montmorillonite assuming $\log(a_{Na^+}/a_{K^+}) = 0.5$ for the exchange of sodium for potassium (computed by R. M. Garrels (personal commun.) from data reported by Schachtschabel, 1940).
Mg-montmorillonite	-1,364,140	61.2	-1,275,340	Calculated from the free energy of formation of calcium montmorillonite assuming $\log(a_{Mg^{++}}/a_{Ca^{++}}) = 0.4$ for the exchange of calcium for magnesium (computed by R. M. Garrels (personal commun.) for data reported by Schachtschabel, 1940).
Crystalline gibbsite	-308,100	16.75 <sup>1</sup>	-275,200	Computed from the solubility of crystalline gibbsite reported by Kittrick (1966) using data given by Wagman and others (1968)—see footnote tt, table 4.

\* Computed from the equilibrium constant obtained by Eugster and Wones (1962) for  $Fe_2O_3(\text{magnetite}) + KAlSi_3O_8(\text{kaolinite}) + H_2O(l) \rightleftharpoons KFe_2AlSi_2O_{10}(OH)_2(\text{annite}) + \frac{1}{2}O_2(g)$  at 500°C and 2070 bars using data taken from tables 6, 7, and 8, Anderson (1967), and Robie and Waldbaum (1968). The procedure used in the calculation is described in the text. The estimated third law entropy of annite at 25°C is

100 cal mole<sup>-1</sup> deg<sup>-1</sup> (see footnote c above), and the calculated values of  $\Delta G_f^\circ(T_r)$  and  $\Delta H_f^\circ(T_r)$  for annite are -1,150,100 and -1,233,750 cal mole<sup>-1</sup>, respectively. <sup>b</sup> It can be deduced from comparison of various equilibrium constants given above that the assemblage gibbsite + quartz is not stable with respect to kaolinite + H<sub>2</sub>O in the temperature range 25° to 300°C. However, calculations of high temperature equilibrium constants for the hydrolysis of corundum, boehmite, and diaspore using solubilities determined by Apps (ms) or thermodynamic data compiled by Robie and Waldbaum (1968) result in values that require kaolinite to be unstable with respect to each of these minerals + quartz + H<sub>2</sub>O at temperatures well below 500°C. In view of experimental evidence indicating that kaolinite is stable up to ~ 300°C (Hemley and Jones, 1964) it appears that the thermodynamic data for corundum, boehmite, and diaspore at 25°C are in error. On the other hand, the crystallinities of kaolinite, gibbsite, diaspore, and boehmite produced experimentally are quite variable, and thus (see footnote r below) the substantial agreement that exists between the results of solubility studies involving kaolinite and the thermodynamic data (table 7) used to compute the log K values for kaolinite given above is not necessarily a definitive criterion for resolving the conflict. <sup>1</sup> The illite in this reaction is close to an illitic end member composition in the montmorillonite-mixed layer illite solid solution series (Hower and Mowatt, 1966). <sup>2</sup> Computed using the heat capacity of cryptocrystalline gibbsite to represent that of crystalline gibbsite. <sup>3</sup> Idealized end members in the beidellite solid solution series. <sup>4</sup> The entropy of crystalline gibbsite at 25°C was assumed to be equivalent to that of cryptocrystalline gibbsite in the calculations. <sup>5</sup> Computed using  $C_p(T_r)$  for halloysite and dickite (58.86 and 57.24 cal mole<sup>-1</sup> deg<sup>-1</sup>, respectively, King and Weller, 1961) as constants. <sup>6</sup> Computed using the heat capacity of antigorite to represent that of chrysotile. <sup>7</sup> These values are consistent with those reported by Hostetler and Christ (1963). <sup>8</sup> Computed using average heat capacities for high albite—see footnote c above. <sup>9</sup> Owing to the significant effect of crystallinity on the thermodynamic behavior of the clay minerals, the actual hydrolysis of these minerals in geochemical processes cannot necessarily be described in terms of the log K values shown in this table: the hydrolysis constants given in the table are "idealized" values. <sup>10</sup> Hydrolysis constants are given in this table for a number of minerals that are not stable in the presence of H<sub>2</sub>O at the temperatures indicated, (for example, enstatite, forsterite, et cetera). These reactions were included to enable additive calculation of equilibrium constants for stable assemblages and to facilitate extrapolation to higher temperatures. <sup>11</sup> Constant heat capacity fits of the log K values given in the table results in the following estimates of equilibrium constants for the reactions (in the above order) at 0°C: -4.4, 2.1, 2.1, 2.4, 5.1, 6.3, 11.1, 29.4, 10.2, 11.2, 14.2, 21.4, 13.5, 26.4, 16.9, 11.5, 83.3, 27.4, 26.6, 54.5, 54.4, 12.7, 22.0, 62.8, 21.4, 35.7, 19.7, 32.6, 0.1, 9.9, 8.9, -1.9, 18.5, 9.6, 11.0, 10.0.

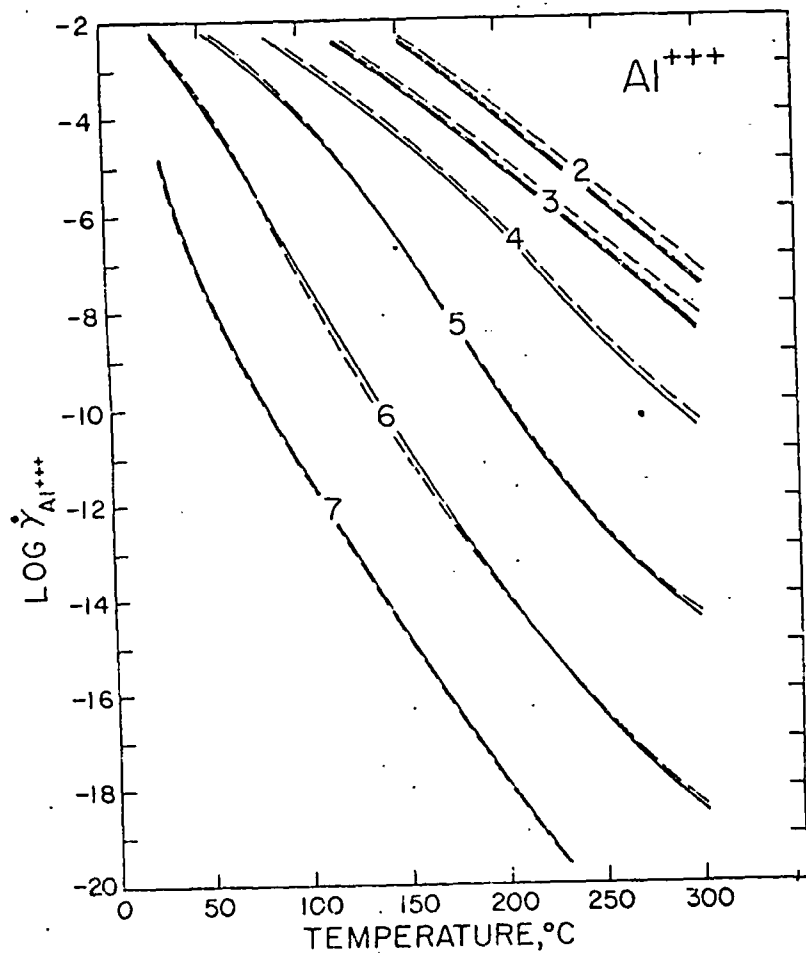


Fig. 9. Stoichiometric individual ion activity coefficients ( $\gamma_i$ ) for the aluminum ion as a function of temperature at constant pH (indicated by the numbers on the curves) in 1 (---), 2 (---), and 3 (—) molal NaCl solutions (see text and table 13).

charged) complexes were omitted from the calculations represented in the tables.

Distribution diagrams are presented in figures 16 and 17 for aluminum hydroxide species and complexes involving the hydrogen ion and carbonate, sulfide, and sulfate ligands, respectively. Unlike the curves in figure 15, those in figures 16 and 17 represent the equilibrium pH at a given temperature for equal activities of the species shown on either side of the curves. Similar distribution diagrams for sulfur, copper, and iron species in terms of fugacity of oxygen and pH at two temperatures are shown in figures 18 and 19. The relation between fugacity of oxygen and the ratio of the concentration of total sulfate to that of total sulfide

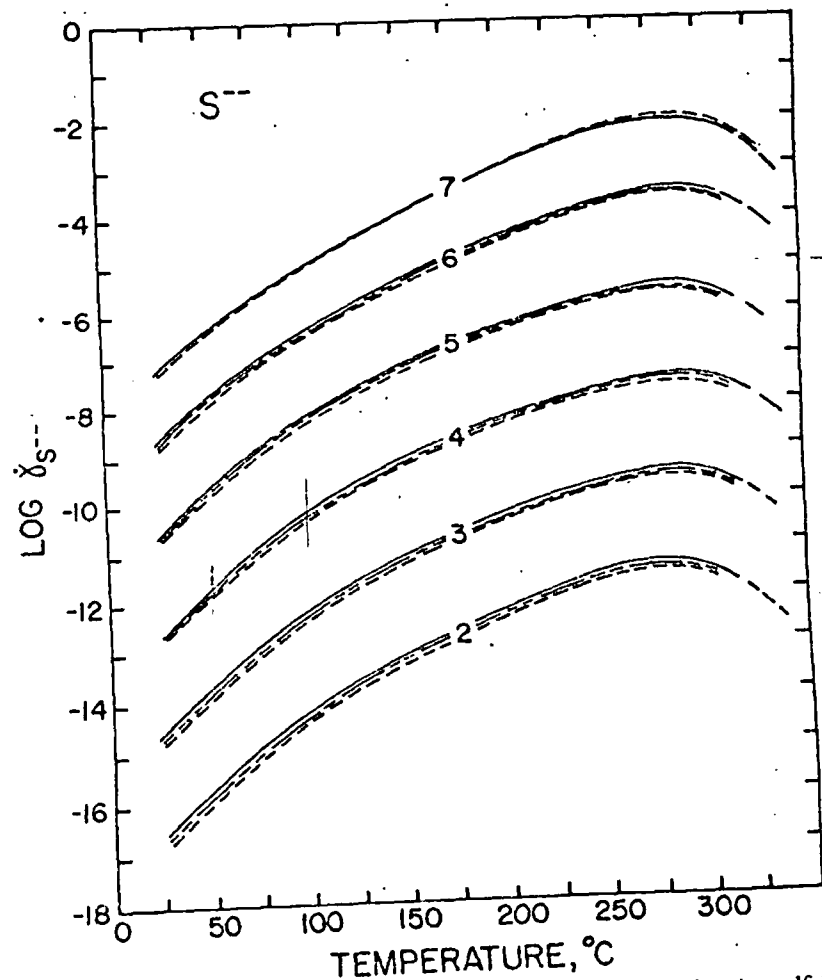


Figure 10. Stoichiometric individual ion activity coefficients ( $\gamma_i$ ) for the sulfide ion as a function of temperature at constant pH (indicated by the numbers of the curves) in 1 (---), 2 (---), and 3 (—) molal NaCl solutions (see text and table 13).

in a 3 molal NaCl solution with a pH of 5 at elevated temperatures is depicted in figure 20. The curves shown in figures 16 to 20 were computed from data given in tables 4, 6, and 9.

#### CONCLUDING REMARKS

Although many equilibria are considered in the preceding pages, all hydrothermal reactions of interest in hydrothermal geochemistry could not be included in this communication. On the other hand, the data and equations summarized above permit other high temperature equilibrium constants to be calculated to suit the requirements of one or another investigation. In many instances, a desired equilibrium constant can be

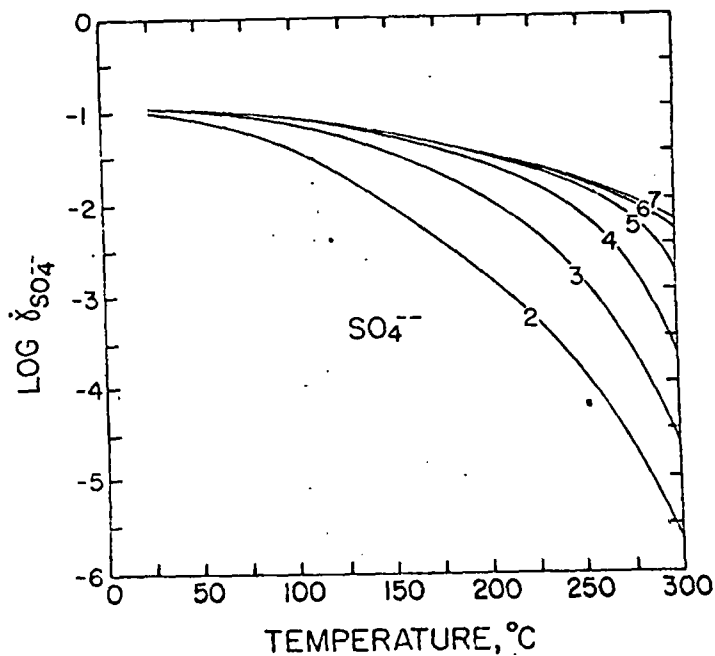


Fig. 11. Stoichiometric individual ion activity coefficients ( $\gamma_i$ ) for the sulfate ion as a function of temperature at constant pH (indicated by the numbers on the curves) in 3 molal NaCl solutions (see text and table 13).

obtained by combining various reactions for which  $\log K(T)$  values are given in the tables. Values of  $\gamma_i$  can be taken directly from the tables and graphs, and values of  $\gamma_i^*$  can be computed as needed from the data and equations given in the foregoing discussion.

The information contained in the tables permits quantitative calculations for hydrothermal systems and processes at high temperatures without the aid of a computer. As an example, calculated sulfide solubilities are plotted against temperature in figure 21. Note that with the exception of metacinnibar, the computed solubilities of the individual sulfides in a 3 molal NaCl solution with a pH of 5 are more than sufficient at high temperatures to account for hydrothermal ore deposits of the metals considered. It can also be seen in figure 21 that the solubilities of a number of the sulfides are similar at high temperatures, but change differentially with decreasing temperatures. Many other conclusions, observations, and implications of considerable geologic significance can be drawn from similar calculations involving the thermodynamics of hydrothermal reactions summarized above. Discussion of these is beyond the scope of the present paper, but in future communications the thermodynamic relations presented here will be used to define phase relations among silicates in hydrothermal systems and to evaluate polyphase equilibrium states and the mass transfer involved in hydrothermal vein for-

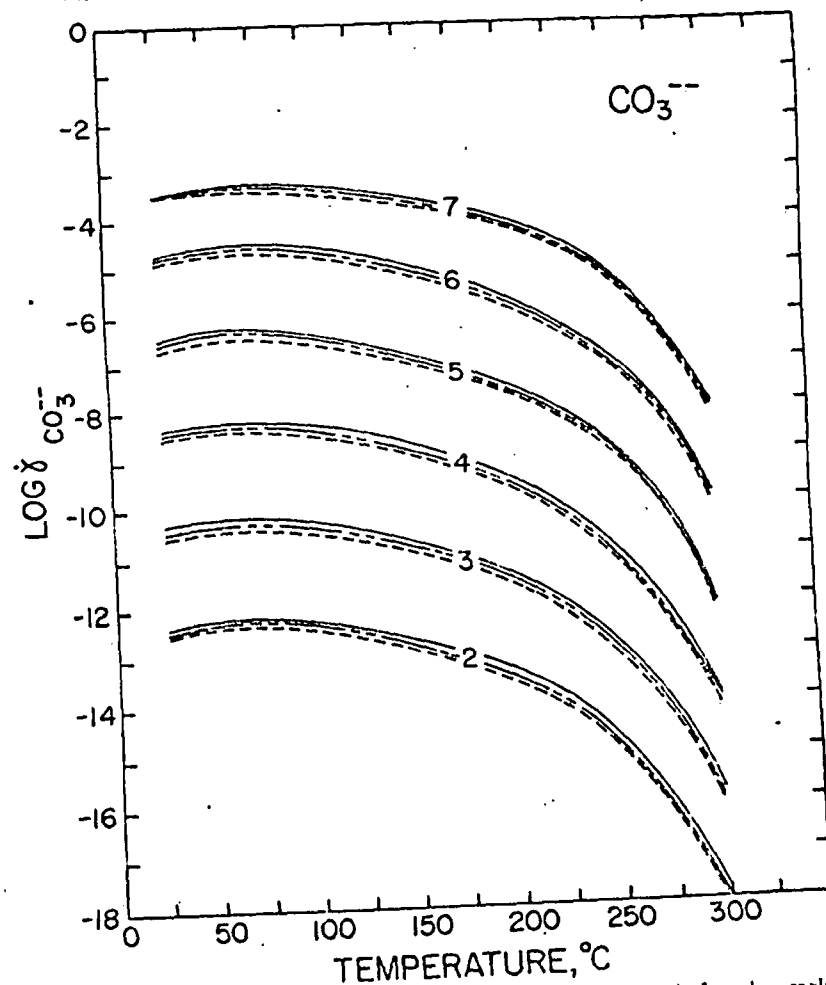


Fig. 12. Stoichiometric individual ion activity coefficients ( $\gamma_i$ ) for the carbonate ion as a function of temperature at constant pH (indicated by the numbers on the curves) in 1 (---), 2 (---), and 3 (—) molal NaCl solutions (see text and table 13).

Such calculations make it possible to characterize quantitatively the mutual solubilities of sulfides and silicates at high temperatures. Irreversible reactions responsible for metasomatism and the paragenesis, replacement, and zoning of hydrothermal minerals have been programmed for machine evaluation. The methods employed in the calculations and idealized models of the mass transfer involved in various geochemical processes have been presented elsewhere (Helgeson, 1968b; Helgeson, Garrels, and Mackenzie, 1969; Helgeson and Garrels, 1968).

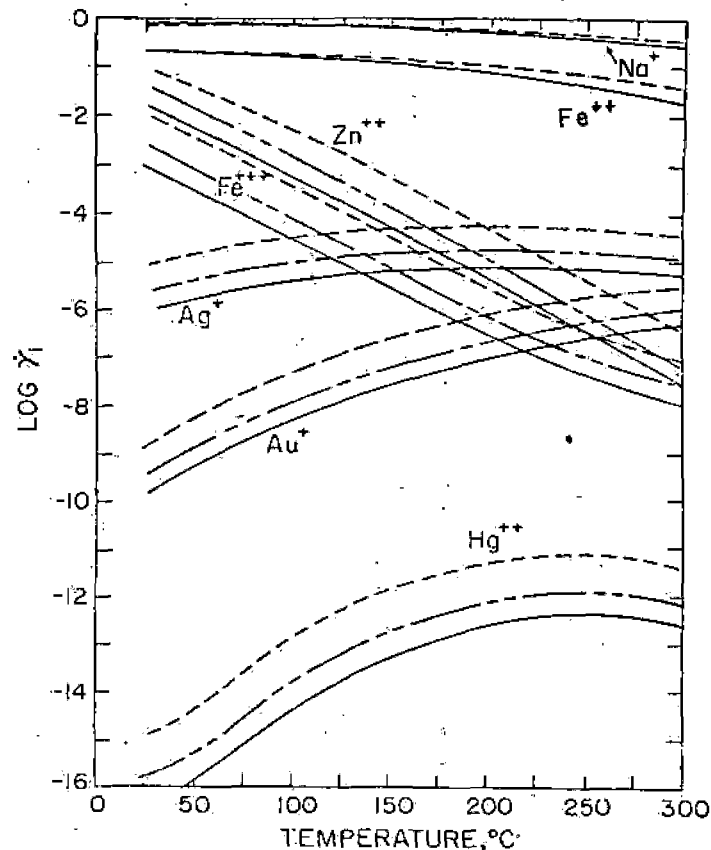


Fig. 13. Stoichiometric individual ion activity coefficients ( $\gamma_i$ ) for metal ions in 1 (---), 2 (— — —), and 3 (—) molal NaCl solutions at elevated temperatures (see text and table 14).

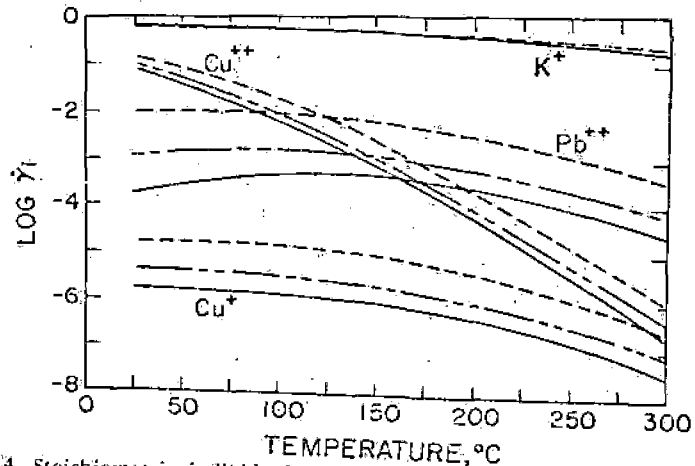


Fig. 14. Stoichiometric individual ion activity coefficients ( $\gamma_i$ ) for metal ions in 1 (---), 2 (— — —), and 3 (—) molal NaCl solutions at elevated temperatures (see text and table 14).

TABLE 13

Stoichiometric individual ion activity coefficients ( $\gamma_i$ ) for aluminum, sulfide, carbonate, sulfate, and calcium ions present in relatively small concentrations in 3.0 molal sodium chloride solutions

Ion	pH	$\log \gamma_i^a$						
		25°C	50°C	100°C	150°C	200°C	250°C	300°C
Al <sup>+++</sup> (assuming the presence of Al(OH) <sup>++</sup> and Al(OH) <sub>3</sub> <sup>-</sup> )	2	-1.17	-1.22	-1.46	-2.49	-4.07	-5.71	-7.55
	3	-1.17	-1.25	-1.94	-3.45	-5.04	-6.71	-8.56
	4	-1.21	-1.47	-2.83	-4.45	-6.27	-8.65	-10.50
	5	-1.49	-2.18	-3.94	-6.72	-9.83	-12.60	-14.45
	6	-2.26	-3.54	-7.34	-10.70	-13.83	-16.60	-18.45
	7	-4.87	-7.33	-11.34	-14.70	-17.83	-20.60	-22.45
	8	-8.86	-11.33	-15.34	-18.70	-21.83	-24.60	-26.45
	9	-12.86	-15.33	-19.34	-22.70	-25.83	-28.60	-30.45
	10	-16.86	-19.33	-23.34	-26.70	-29.83	-32.60	-34.45
	11	-20.86	-23.33	-27.34	-30.70	-33.83	-36.60	-38.45
	12	-24.86	-27.33	-31.34	-34.70	-37.83	-40.60	-42.45
	S <sup>---</sup> (assuming the presence of HS <sup>-</sup> and H <sub>2</sub> S <sub>(aq)</sub> )	2	-16.60	-15.64	-14.17	-13.11	-12.29	-11.69
3		-14.60	-13.64	-12.17	-11.11	-10.29	-9.69	-9.42
4		-12.61	-11.65	-10.17	-9.11	-8.29	-7.69	-7.42
5		-10.62	-9.66	-8.20	-7.13	-6.30	-5.70	-5.42
6		-8.71	-7.81	-6.39	-5.30	-4.43	-3.78	-3.47
7		-7.20	-6.30	-5.04	-3.93	-2.98	-2.27	-2.11
CO <sub>3</sub> <sup>---</sup> (assuming the presence of HCO <sub>3</sub> <sup>-</sup> , H <sub>2</sub> CO <sub>3(aq)</sub> , and CO <sub>2(aq)</sub> <sup>b</sup> )		2	-12.38	-12.22	-12.37	-12.79	-13.52	-14.79
	3	-10.38	-10.22	-10.37	-10.79	-11.52	-12.79	-15.88
	4	-8.39	-8.23	-8.37	-8.79	-9.52	-10.79	-13.88
	5	-6.43	-6.28	-6.41	-6.81	-7.53	-8.79	-11.88
	6	-4.73	-4.58	-4.65	-4.97	-5.62	-6.83	-9.83
	7	-3.50	-3.35	-3.38	-3.58	-4.03	-5.10	-7.93
	SO <sub>4</sub> <sup>---</sup> (assuming the presence of HSO <sub>4</sub> <sup>-</sup> in the absence of calcium)	2	-1.01	-1.09	-1.43	-2.03	-2.77	-3.79
3		-0.96	-1.00	-1.14	-1.42	-1.92	-2.82	-4.62
4		-0.95	-0.99	-1.10	-1.26	-1.51	-2.07	-3.64
5		-0.95	-0.99	-1.10	-1.25	-1.42	-1.79	-2.77
6		-0.95	-0.99	-1.10	-1.24	-1.43	-1.75	-2.33
7		-0.95	-0.99	-1.10	-1.24	-1.43	-1.75	-2.25
$a_{Ca^{++}}$		SO <sub>4</sub> <sup>---</sup> (assuming the presence of HSO <sub>4</sub> <sup>-</sup> and CaSO <sub>4(aq)</sub> at a pH of 5)	0.001	-0.95	-1.0	-1.1	-1.3	-1.5
	0.01	-1.04	-1.1	-1.2	-1.4	-1.7	*	
$a_{SO_4^{---}}$	Ca <sup>++</sup> (assuming the presence of CaSO <sub>4(aq)</sub> and CaCO <sub>3(aq)</sub> at a pH of 5) <sup>c</sup>	0.001	-0.67	-0.7	-0.8	-0.9	-1.2	
	0.01	-0.75	-0.8	-1.0	-1.2	-1.5		

<sup>a</sup> Computed from equation (49) or expressions for anions analogous to equation (49) using data given in tables 2 and 4 (see text). <sup>b</sup> If the total molality of calcium present in the solution is one or less, the computed values of  $\gamma_{CO_3^{---}}$  are not affected by the formation of CaCO<sub>3(aq)</sub>. <sup>c</sup> Where total CO<sub>2(aq)</sub> is less than 1 molal, the CaCO<sub>3(aq)</sub> species has a negligible effect on  $\gamma_{Ca^{++}}$  at pH 6 and below.

TABLE 14

Stoichiometric individual ion activity coefficients ( $\gamma_i$ ) for  $\text{Na}^+$  and cations present in relatively small concentrations in 1.0, 2.0, and 3.0 molal sodium chloride solutions

Ion	$m_{\pm, \text{NaCl}}$	$\log \gamma_i^a$						
		25°C	50°C	100°C	150°C	200°C	250°C	300°C
Ag <sup>+</sup>	1.0	-5.07	-4.8	-4.5	-4.3	-4.3	-4.2 <sup>b</sup>	-4.5 <sup>b</sup>
	2.0	-5.68	-5.5	-5.1	-4.8	-4.8	-4.7 <sup>b</sup>	-5.0 <sup>b</sup>
	3.0	-6.06	-5.8	-5.5	-5.2	-5.1	-5.0 <sup>b</sup>	-5.5 <sup>b</sup>
Cu <sup>+</sup>	1.0	-4.75	-4.8	-4.9	-5.0	-5.1	-6.0 <sup>b</sup>	-6.6 <sup>b</sup>
	2.0	-5.36	-5.4	-5.5	-5.6	-6.0	-6.5 <sup>b</sup>	-7.1 <sup>b</sup>
	3.0	-5.75	-5.8	-5.9	-6.0	-6.3	-6.8 <sup>b</sup>	-7.5 <sup>b</sup>
Cu <sup>2+</sup>	1.0	-0.91	-1.0	-1.7	-2.6	-3.7 <sup>b</sup>	-4.8 <sup>b</sup>	-6.0 <sup>b</sup>
	2.0	-1.03	-1.2	-2.0	-3.0	-4.1 <sup>b</sup>	-5.2 <sup>b</sup>	-6.4 <sup>b</sup>
	3.0	-1.10	-1.3	-2.2	-3.2	-4.3 <sup>b</sup>	-5.4 <sup>b</sup>	-6.7 <sup>b</sup>
Pb <sup>2+</sup>	1.0	-2.07	-2.0	-2.2	-2.3	-2.5	-2.9 <sup>b</sup>	-3.5 <sup>b</sup>
	2.0	-2.09	-2.6	-2.8	-3.0	-3.2	-3.5 <sup>b</sup>	-4.2 <sup>b</sup>
	3.0	-3.75	-3.1	-3.3	-3.4	-3.6	-3.9 <sup>b</sup>	-4.6 <sup>b</sup>
Zn <sup>2+</sup>	1.0	-1.00	-1.1	-2.3	-3.2	-4.3	-5.2 <sup>b</sup>	-6.5 <sup>b</sup>
	2.0	-1.43	-1.9	-2.9	-3.8	-5.0	-5.8 <sup>b</sup>	-7.2 <sup>b</sup>
	3.0	-1.84	-2.4	-3.4	-4.3	-5.4	-6.3 <sup>b</sup>	-7.6 <sup>b</sup>
Hg <sup>2+</sup>	1.0	-14.98	-14.4	-12.8	-11.8	-11.3	-11.1 <sup>b</sup>	-11.4 <sup>b</sup>
	2.0	-15.90	-15.3	-13.7	-12.7	-12.1	-11.9 <sup>b</sup>	-12.2 <sup>b</sup>
	3.0	-16.50	-15.9	-14.3	-13.3	-12.6	-12.3 <sup>b</sup>	-12.6 <sup>b</sup>
Fe <sup>3+</sup>	1.0	-2.62	-2.5	-3.4	-4.4	-5.5 <sup>b</sup>	-6.6 <sup>b</sup>	-7.1 <sup>b</sup>
	2.0	-2.60	-3.1	-4.1	-5.1	-6.1 <sup>b</sup>	-7.2 <sup>b</sup>	-7.6 <sup>b</sup>
	3.0	-2.98	-3.5	-4.5	-5.5	-6.5 <sup>b</sup>	-7.5 <sup>b</sup>	-8.0 <sup>b</sup>
Fe <sup>2+</sup>	1.0	-0.64	-0.67	-0.7	-0.8	-1.0	-1.2 <sup>b</sup>	-1.4 <sup>b</sup>
	2.0	-0.68	-0.71	-0.8	-0.9	-1.0	-1.2 <sup>b</sup>	-1.6 <sup>b</sup>
	3.0	-0.67	-0.70	-0.8	-0.9	-1.0	-1.3 <sup>b</sup>	-1.7 <sup>b</sup>
Au <sup>+</sup>	1.0	-8.8	-8.2	-7.3	-6.6	-6.0	-5.6 <sup>b</sup>	-5.5 <sup>b</sup>
	2.0	-9.4	-8.9	-7.9	-7.2	-6.6	-6.2 <sup>b</sup>	-6.0 <sup>b</sup>
	3.0	-9.8	-9.2	-8.3	-7.5	-6.9	-6.5 <sup>b</sup>	-6.3 <sup>b</sup>
Au <sup>3+</sup>	1.0	-25.4	-24.0	-21.7	-20.1	-19.1	-18.7 <sup>b</sup>	-19.2 <sup>b</sup>
	2.0	-26.7	-25.2	-23.0	-21.3	-20.2	-19.8 <sup>b</sup>	-20.2 <sup>b</sup>
	3.0	-27.5	-26.0	-23.8	-22.0	-20.9	-20.1 <sup>b</sup>	-20.8 <sup>b</sup>
Na <sup>+</sup>	1.0	-0.18	-0.19	-0.21	-0.25	-0.31	-0.41 <sup>b</sup>	-0.61 <sup>b</sup>
	2.0	-0.17	-0.18	-0.20	-0.25	-0.33	-0.46 <sup>b</sup>	-0.63 <sup>b</sup>
	3.0	-0.15	-0.15	-0.17	-0.24	-0.33	-0.49 <sup>b</sup>	-0.73 <sup>b</sup>
K <sup>+</sup>	1.0	-0.22	-0.22	-0.25	-0.29	-0.35	-0.44 <sup>b</sup>	-0.62 <sup>b</sup>
	2.0	-0.22	-0.23	-0.25	-0.30	-0.37	-0.49 <sup>b</sup>	-0.71 <sup>b</sup>
	3.0	-0.20	-0.21	-0.24	-0.28	-0.37	-0.51 <sup>b</sup>	-0.76 <sup>b</sup>

<sup>a</sup> The dissociation constants for the metal chloride complexes used in calculating the values of  $\gamma_i$  in this table from equation (49) are shown in table 5. To insure minimal uncertainty and conservative values (see text), divalent and trivalent metal chloride complexes were not considered in the calculations; that is,  $q$  in equation (49) was assigned a value of  $Z_i + 1$  for each metal ion. Because all the metal ions considered above, with the exception of  $\text{Fe}^{2+}$ , associate with the chloride ion to a significant degree, the individual ion activity coefficients for the ions themselves have no significant effect, except in the case of  $\text{Na}^+$ ,  $\text{K}^+$ , and  $\text{Fe}^{2+}$ , on the  $\gamma_i$  values shown above. <sup>b</sup> These values have a higher uncertainty than the others given in the table owing to extrapolation of equilibrium constants and activity coefficients used

in the calculations. <sup>c</sup> No  $\log K(T)$  data are available for  $\text{CuCl}_{(aq)}$ , so this species was not considered specifically in the calculations. <sup>d</sup> The term for  $\text{FeCl}_2^{2+}$  was omitted from equation (49) to eliminate the influence of the divalent charge on this species, which is the most stable of the ferric chloride complexes. The degree of formation achieved by this species is represented by the magnitude of the overall dissociation constants for the higher order ferric chloride complexes considered in the calculations. <sup>e</sup> There is little indication that chloride complexes of  $\text{Fe}^{2+}$  form to significant degrees, at least at low temperatures. The values shown for  $\text{Fe}^{2+}$  are thus equivalent to individual ion activity coefficients. Because the ion is divalent and a 25°C  $\lambda$  was used in the calculations, the activity coefficients shown for this species at high temperatures are probably too small. On the other hand, there are indirect indications from solubility data that  $\text{Fe}^{2+}$  may form stable complexes with chloride in the region of 300°, and that the overall stability constant is of the order of  $10^2$  or  $10^3$ . In view of these uncertainties, the activity coefficients shown above for  $\text{Fe}^{2+}$  should be considered provisional estimates. <sup>f</sup> The values shown for these ions are based on the dissociational reactions for the gold species shown in table 5.

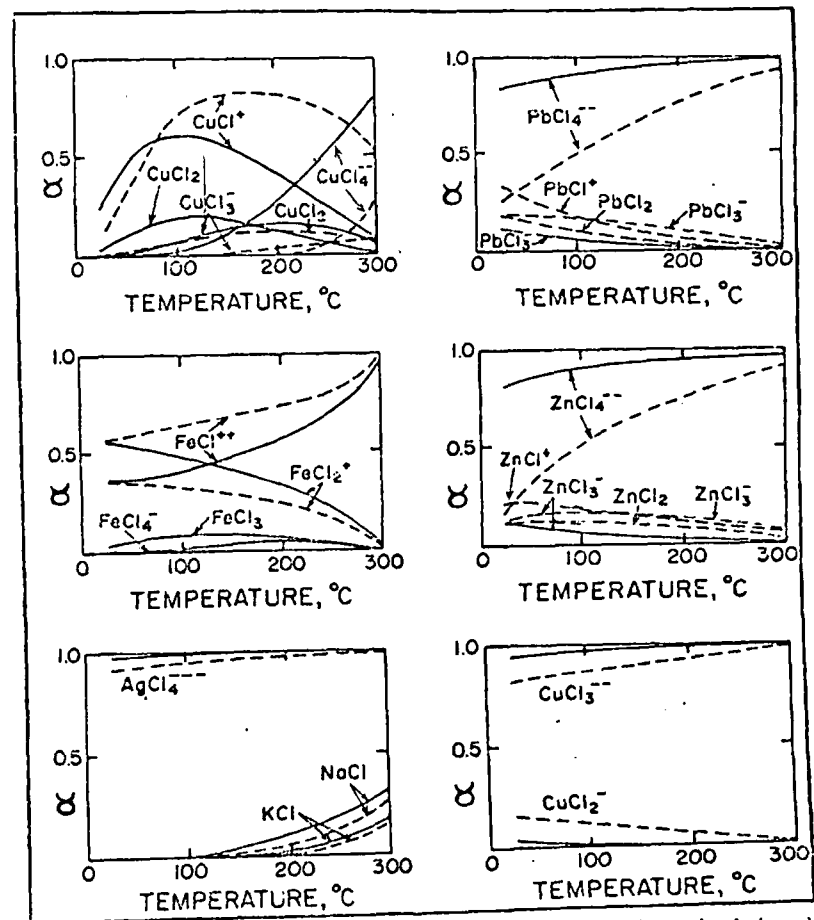


Fig. 15. Degrees of formation ( $\alpha$ ) for metal chloride complexes in 1 (---) and 3 (—) molal  $\text{NaCl}$  solutions at elevated temperatures (see text—eq 54). Mercury is not shown because the species  $\text{HgCl}_2^-$  accounts for >98 percent of the mercury in solution. Complexes that form to less than a few percent have been omitted from the diagrams. Unlike the  $\gamma_i$  values shown in table 14 and figures 13 and 14, the  $\alpha$  values shown above were calculated (eq 54) assuming the presence of all chloride complexes (of each cation) in table 5 (see text).



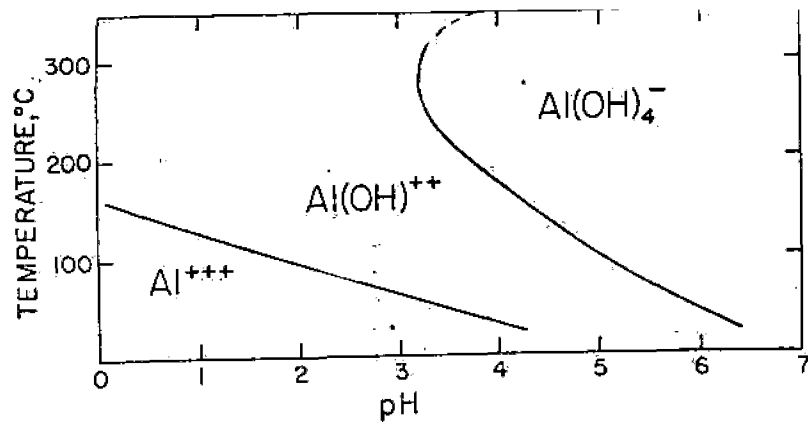


Fig. 16. Distribution of aluminum species in aqueous solution as a function of temperature and solution pH. The curves represent equal activities of the species shown in adjoining fields in the diagram. The positions of the curves are defined by dissociation constants in table 4.

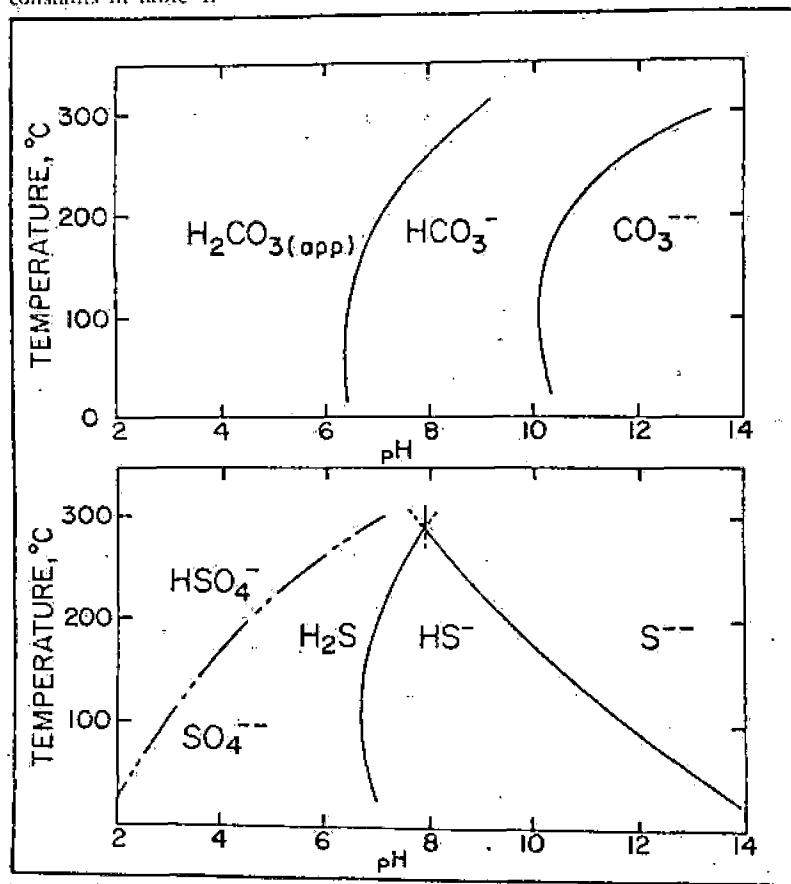


Fig. 17. Distribution of carbonate, sulfide, and sulfate species in aqueous solution as a function of temperature and solution pH. The curves represent equal activities of the species shown in adjoining fields in the diagrams. The positions of the curves are defined by dissociation constants in table 4. The subscript (app) indicates that the species referred to is the undifferentiated sum of  $H_2CO_3$  and  $CO_{2(aq)}$ .

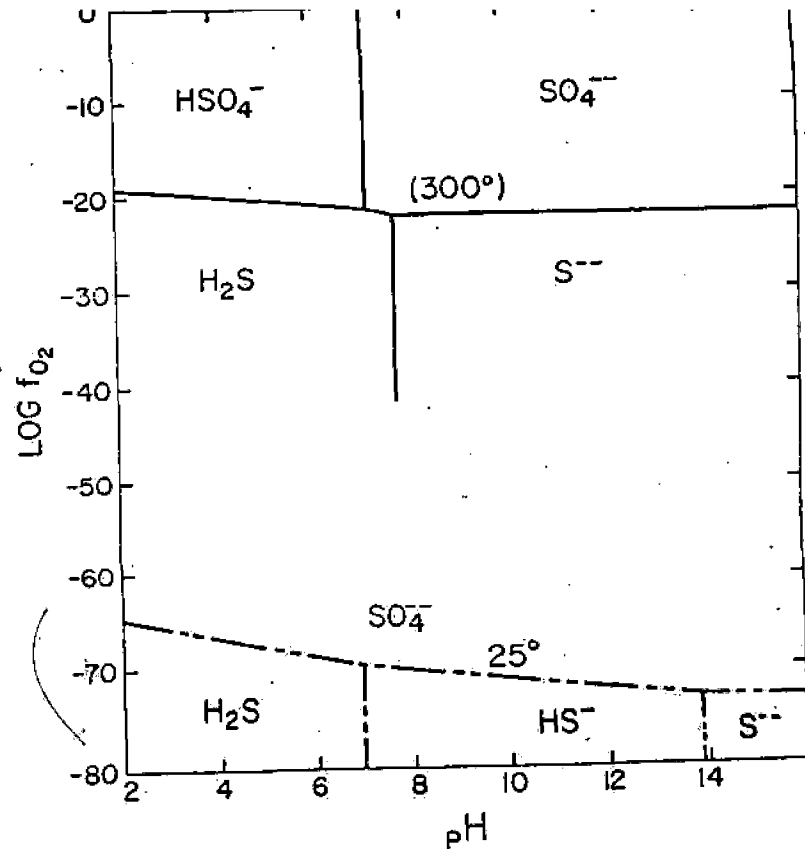


Fig. 18. Distribution of sulfur species at 25°C (---) and 300°C (—) as a function of  $f_{O_2}$  and solution pH. The curves, which define the positions of equal activities of the species in adjoining fields in the diagram, were computed from the equilibrium constants given in table 9. The field for  $HSO_4^-$  at 25°C lies to the left of the diagram.

#### ACKNOWLEDGMENTS

I am indebted to R. M. Garrels, F. T. Mackenzie, C. L. Christ, and J. J. Henley for their encouragement, helpful suggestions, and constructive criticism during the preparation of this paper, and to C. L. Christ and John Haas for reviewing the manuscript. The impetus to undertake this task came from stimulating discussions with J. J. Henley. Also I would like to acknowledge the invaluable assistance and suggestions I received from the following students: T. H. Brown, A. Nigrini, T. A. Jones, W. R. James, J. R. Riehle, and G. M. Lafon. The work reported here was supported in part by NSF Grants GU-1700, GA-828, GA-11285.

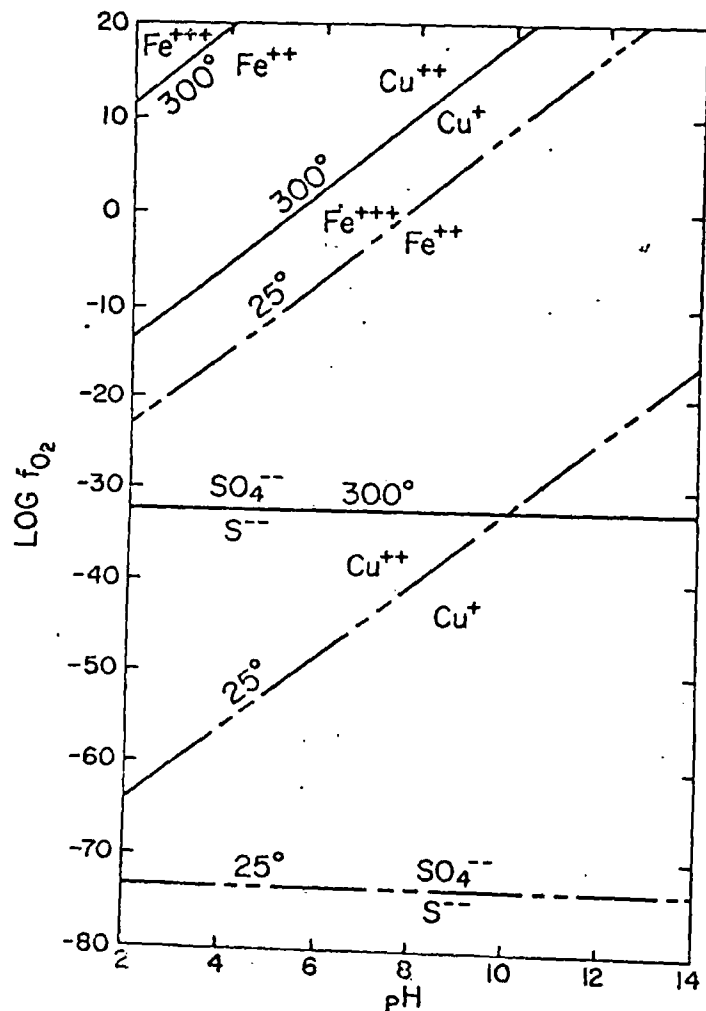


Fig. 19. Distribution of iron, copper, and sulfur species at 25°C (---) and 300°C (—) as a function of  $f_{O_2}$  and solution pH. The curves, which define the positions of equal activities of the species in adjoining fields in the diagram, were computed from the equilibrium constants given in table 9.

GA-9758, and GU-2190, together with funds made available by the office of Research Coordination at Northwestern University, and the Petroleum Research Fund of the American Chemical Society. The help of J. M. Klyce, W. R. James, P. Abrams, K. Vonesh, and especially R. H. Leeper in assisting with the computer calculations is also acknowledged with thanks. Finally, I would like to express my appreciation to Mrs. E. J. Faulkner for many hours spent in typing and retyping the manuscript.

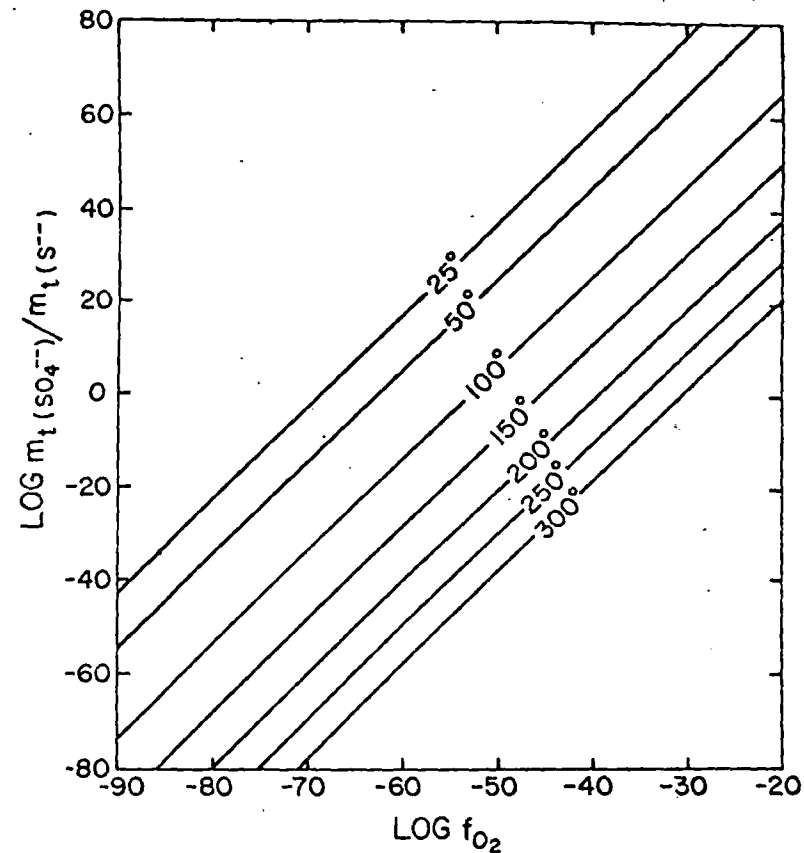


Fig. 20. Ratio of the total concentration of sulfate to sulfide in a 3.0 molal NaCl solution as a function of  $f_{O_2}$  from 25° to 300°C at a pH of 5. The positions of the isotherms were computed from the data given in tables 9 and 13.

#### REFERENCES

- Akerlof, G. C., and Oshry, H. I., 1950, The dielectric constant of water at high temperatures and in equilibrium with its vapor: *Am. Chem. Soc. Jour.*, v. 72, p. 2844-2847.
- Ahluwalia, J. C. and Cobble, J. W., 1964, The thermodynamic properties of high temperature aqueous solutions. III. The partial molal heat capacities of hydrochloric acid from 0°-100° and the Third-Law potentials of the silver chloride and calomel electrodes from 0°-100°: *Am. Chem. Soc. Jour.*, v. 86, p. 5381-5384.
- Anderson, G. M., 1967, Specific volumes and fugacities of water, in Barnes, H. L., ed., *Geochemistry of Hydrothermal Ore Deposits*: New York, Holt, Rinehart, and Winston, Inc., p. 632-635.
- Apps, J. A., ms, 1959, The system albite, analcime, and montmorillonite at 25°C and one atmosphere: Ph.D. thesis, Harvard Univ., Dept. of Geol. Sci., Cambridge, Mass.
- Austin, J. M., Matheson, R. A., and Parton, H. N., 1959, Some thermodynamic properties of solutions of salts of bivalent metals, in Hamer, W. J., ed., *Structure of electrolytic solutions*: New York, John Wiley & Sons, p. 365-379.
- Barany, R., 1964, Heat and free energy of formation of muscovite: *U.S. Bur. Mines Rept. Inv.* 6356, 6 p.
- Barany, R., and Kelley, K. K., 1961, Heats and free energies of formation of gibbsite, kaolinite, halloysite, and dickite: *U.S. Bur. Mines Rept. Inv.*, no. 5825, 13 p.
- Barnard, W. M., and Christopher, P. A., 1966, Hydrothermal synthesis of chalcopyrite: *Econ. Geology*, v. 61, p. 897-902.

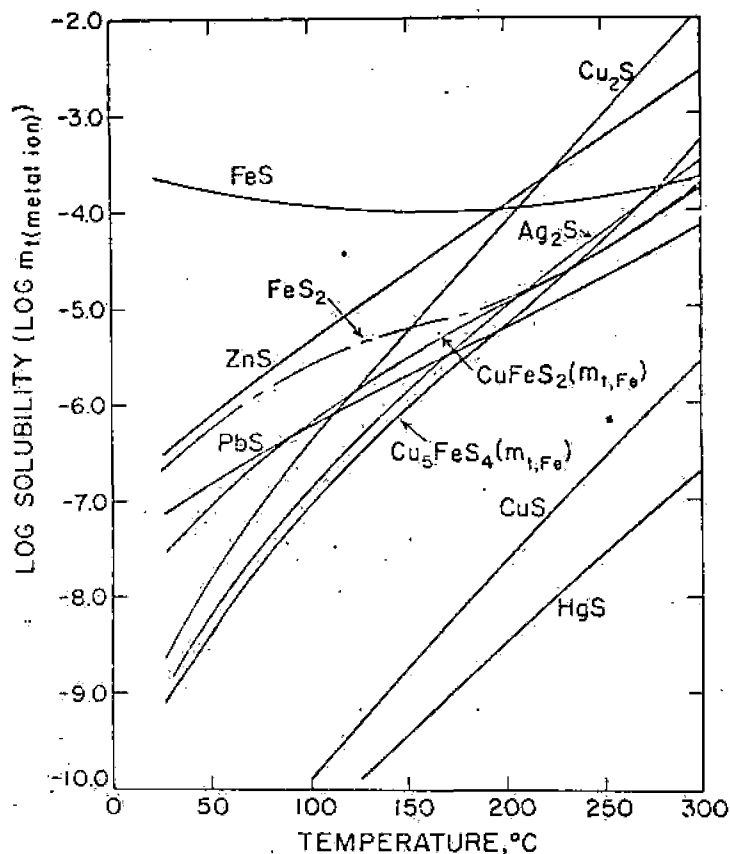


Fig. 21. Calculated stoichiometric solubilities (in terms of the total molality of the metal ion) of various individual sulfides in a 3 molal sodium chloride solution with a pH of 5, at elevated temperatures. HgS refers to metacinnabar. Except for pyrite, chalcopyrite, and bornite, the solubilities were computed from equation (51) and the data presented in tables 11, 13, and 14. Pyrite solubilities were calculated by evaluating  $4\text{FeS}_2 + 8\text{H}^+ + 4\text{H}_2\text{O} = 8\text{H}_2\text{S} + 4\text{Fe}^{2+} + 8\text{OH}^-$  and  $4\text{FeS}_2 + 7\text{H}^+ + 4\text{H}_2\text{O} = 7\text{HS} + 4\text{Fe}^{2+} + 4\text{SO}_4^{2-}$  with the aid of the data in tables 10, 13, and 14. The solubilities of chalcopyrite and bornite were computed from oxidation-reduction equations analogous to those given above for pyrite, which are written in terms of the predominant species in the aqueous phase. This procedure permits the molalities of all species in the reactions to be defined in terms of the molality of  $\text{Fe}^{2+}$ , and therefore the solubilities of the minerals can be computed directly from the Law of Mass Action equations for the reactions. Owing to the limitation imposed by the computed stoichiometric individual ion activity coefficients (see footnote a, table 13), all solubilities depicted above should be regarded as minimal approximations of the true mineral solubilities.

- Banholomé, P., 1958, On the paragenesis of copper ores: Léopoldville, Belgian Congo, *Studia Univ. Lovanium*.
- Barton, P. B., and Skinner, B. T., 1967, Sulfide mineral stabilities, in Barnes, H. L., ed., *Geochemistry of hydrothermal ore deposits*; New York, Holt, Rinehart, and Winston, Inc., p. 236-333.
- Bell, R. P., and George, J. H. B., 1953, Incomplete dissociation of some thallous and calcium salts at different temperatures: *Faraday Soc. Trans.*, v. 49, p. 619-627.
- Berne, E., and Leden, I., 1953, Solubility of silver chloride and the formation of complexes between silver and chloride ions; *Svensk. Kem. tidskr.*, v. 65, p. 88-97.

- Berner, R. A., 1967, Comparative dissolution characteristics of carbonate minerals in the presence and absence of aqueous magnesium ion: *Am. Jour. Sci.*, v. 265, p. 45-70.
- Bjerrum, J., 1946, Acidic complex formation I. Optical investigations on cupric chloride in mixtures with other chlorides: *Kgl. Danske Vidensk. Selsk. Mat-fys. Medd.*, v. 22, no. 18, 43 p.
- Bjerrum, N., 1948, La stabilité des chlorures d'or: *Soc. Chimie Belge Bull.*, v. 57, p. 432-445.
- Bjerrum, N., and Kirschlmer, A., 1918, Die Rhodanide des Goldes und das freie Rhodan mit einem Anhang über das Goldchlorid: *Kgl. Danske Vidensk. Selsk.-Skr., Naturvidensk. math. Afdel.*, v. 5, p. 1-77.
- Chaltykai, O., 1948, Properties of cuprous complexes: *Zhur. obshchei Khim.*, v. 18, p. 1625-1638.
- Clake, P. L., 1969, Solubility of ZnS, PbS, Cu<sub>2</sub>S, and MoS<sub>2</sub> in NaCl solutions: *Econ. Geology*, v. 64, in press.
- Cobbie, J. W., 1953a, Empirical considerations of entropy. I. The entropies of the oxy-anions and related species: *Jour. Chem. Physics*, v. 21, p. 1443-1446.
- , 1953b, Empirical considerations of entropy. II. The entropies of inorganic complex ions: *Jour. Chem. Physics*, v. 21, p. 1446-1450.
- , 1964, The thermodynamic properties of high temperature aqueous solutions. VI. Applications of entropy correspondence to thermodynamics and kinetics: *Am. Chem. Soc. Jour.*, v. 86, p. 5394-5401.
- , 1966a, High temperature aqueous solutions: *Science*, v. 152, p. 1479-1485.
- , 1966b, Thermodynamics, in Eyring, H., ed. *Annual Review of Physical Chemistry*; Palo Alto, California: Annual Review Inc., p. 15-36.
- Couture, A. M., and Laidler, K. J., 1956, The partial molal volumes of ions in aqueous solution. I. Dependence on charge and radius: *Canadian Jour. Chemistry*, v. 34, p. 1209-1216.
- Criss, C. M., and Cobble, J. W., 1964a, The thermodynamic properties of high temperature aqueous solutions. IV. Entropies of the ions up to 200° and the correspondence principle: *Am. Chem. Soc. Jour.*, v. 86, p. 5385-5390.
- , 1964b, The thermodynamic properties of high temperature aqueous solutions. V. The calculation of ionic heat capacities up to 200°: Entropies and heat capacities above 200°: *Am. Chem. Soc. Jour.*, v. 86, p. 5390-5393.
- Ellis, A. J., 1966, Partial molal volumes of alkali chlorides in aqueous solution to 200°: *Chem. Soc. [London] Jour.*, p. 1579-1584.
- , 1967, Partial molal volumes of MgCl<sub>2</sub>, CaCl<sub>2</sub>, SiCl<sub>2</sub>, and BaCl<sub>2</sub> in aqueous solution to 200°: *Chem. Soc. [London] Jour.*, p. 660-664.
- , 1968, Partial molal volumes in high-temperature water. Pt. 3. Halide and oxyanion salts: *Chem. Soc. London Jour. A*, p. 1138-1143.
- Ellis, A. J., and Golding, R. M., 1959, Spectrophotometric determination of the acid dissociation constants of hydrogen sulfide: *Chem. Soc. [London] Jour.*, p. 127-130.
- , 1963, The solubility of carbon dioxide above 100°C in water and in sodium chloride solutions: *Am. Jour. Sci.*, v. 261, p. 47-60.
- Ellis, A. J., and Milstone, N. B., 1967, The ionization constants of hydrogen sulfide from 20° to 90°C: *Geochim. et Cosmochim. Acta*, v. 31, p. 615-620.
- Eugster, H. P., and Wones, D. R., 1962, Stability of the ferruginous biotite, amite: *Jour. Petrology*, v. 3, p. 82-123.
- Fenwick, E., 1926, The equilibrium between cupric ion, cuprous ion, and metallic copper: *Am. Chem. Soc. Jour.*, v. 48, p. 860-870.
- Ferh, J. H., Roberson, C. E., and Polzer, W. L., 1964, Sources of mineral constituents in water from granitic rocks, Sierra Nevada, California and Nevada: *U. S. Geol. Survey Water-Supply Paper 1535-I*, 170 p.
- Franck, E. U., 1961, Überkritisches Wasser als elektrolytisches Lösungsmittel: *Angew. Chemie*, v. 73, p. 309-322.
- Fyfe, W. S., Turner, F. J., and Verhoogen, John, 1958, Metamorphic reactions and metamorphic facies: *Geol. Soc. America Mem.*, 73, 259 p.
- Gardner, E. R., Jones, B. J., and de Nordvall, H. J., 1963, Osmotic coefficients of some aqueous sodium chloride solutions at high temperatures: *Faraday Soc. Trans.*, v. 59, p. 1994-2000.
- Garrick, R. M., and Christ, C. L., 1965, *Solutions, minerals and equilibria*: New York, Harper and Row, 450 p.
- Garrels, R. M., and Mackenzie, F. T., 1967, Origin of the chemical composition of some springs and lakes, in Gould, R. F., ed., *Equilibrium concepts in natural water systems*: Washington, D. C., Am. Chem. Soc. Pubs., p. 222-242.

- Garrels, R. M., and Thompson, M. E., 1962, Chemical model for sea water at 25°C and 1 atmosphere total pressure: *Am. Jour. Sci.*, v. 260, p. 57-66.
- Gron, M., Marcus, Y., and Shiloh, M., 1963, A modified Debye theory of salting of non-electrolytes in electrolyte solutions: *Jour. Phys. Chemistry*, v. 67, p. 2495-2497.
- Halc, J. D., Izat, R. M., and Christensen, J. J., 1963, The calorimetric study of the heat of ionization of water at 25°: *Jour. Phys. Chemistry*, v. 67, p. 2605-2608.
- Harned, H. S., 1961, Osmotic coefficients of hydrochloric acid, potassium and sodium chloride from 0° to 40° or 50°: U.S. Atomic Energy Comm., Doc. TID-12096.
- Harned, H. S., and Davis, R., 1943, The ionization constant of  $H_2CO_3$  in water and the solubility of  $CO_2$  in water and aqueous solutions from 0 to 50°: *Am. Chem. Soc. Jour.*, v. 65, p. 2030-2037.
- Harned, H. S., and Owen, B. B., 1958, The physical chemistry of electrolyte solutions, 3d ed.: New York, Reinhold, 803 p.
- Harned, H. S., and Scholes, S. R., 1941, The ionization constant of  $HCO_3^-$  from 0 to 50°: *Am. Chem. Soc. Jour.*, v. 63, p. 1706-1709.
- Helgeson, H. C., 1964, Complexing and hydrothermal ore deposition: New York, Pergamon Press, 128 p.
- 1967a, Thermodynamics of complex dissociation in aqueous solution at elevated temperatures: *Jour. Phys. Chemistry*, v. 71, p. 3121-3136.
- 1967b, Solution chemistry and metamorphism, in Abelson, P. H., ed., *Researches in Geochemistry*, v. 2: New York, John Wiley & Sons, p. 362-404.
- 1967c, Silicate metamorphism in sediments and the genesis of hydrothermal ore solutions, in Brown, J. S., ed., *Genesis of stratiform lead-zinc-barite-fluorite deposits*: *Econ. Geology*, Mon. 3, p. 333-342.
- 1968a, Geologic and thermodynamic characteristics of the Salton Sea geothermal system: *Am. Jour. Sci.*, v. 266, p. 129-166.
- 1968b, Evaluation of irreversible reactions in geochemical processes involving minerals and aqueous solutions: I. Thermodynamic relations: *Geochim. et Cosmochim. Acta*, v. 32, p. 853-877.
- Helgeson, H. C., and Garrels, R. M., 1968, Hydrothermal transport and deposition of gold: *Econ. Geology*, v. 63, p. 622-635.
- Helgeson, H. C., Garrels, R. M., and Mackenzie, F. T., 1969, Evaluation of irreversible reactions in geochemical processes involving minerals and aqueous solutions. II. Applications: *Geochim. et Cosmochim. Acta*, v. 33, p. 455-481.
- Helgeson, H. C., and James, W. R., 1968, Activity coefficients in concentrated electrolyte solutions at high temperatures: *Am. Chem. Soc., 155th Natl. Mtg.*, San Francisco, California, April 1968, Abs., p. 5-130.
- Hem, J. D., 1968, Graphical methods for studies of aqueous aluminum hydroxide, fluoride, and sulfate complexes: U. S. Geol. Survey Water-Supply Paper 1827-B, 33 p.
- Hem, J. D., and Roberson, C. E., 1967, Form and stability of aluminum hydroxide complexes in illite solution: U. S. Geol. Survey Water-Supply Paper 1827-A, 35 p.
- Hemley, J. J., 1959, Some mineralogical equilibria in the system  $K_2O-Al_2O_3-SiO_2-H_2O$ : *Am. Jour. Sci.*, v. 257, p. 241-270.
- Hemley, J. J., and Jones, W. R., 1964, Chemical aspects of hydrothermal alteration with emphasis on hydrogen metasomatism: *Econ. Geology*, v. 59, p. 538-569.
- Hemley, J. J., Meyer, Charles, Hodgson, C. J., and Thatcher, A. B., 1967, Some sulfide solubilities in alteration-controlled systems: *Science*, v. 158, p. 1580-1582.
- Hemley, J. J., Meyer, Charles, and Richter, D. H., 1961, Some alteration reactions in the system  $Na_2O-Al_2O_3-SiO_2-H_2O$ : U.S. Geol. Survey Prof. Paper 424D, p. D338-D340.
- Hepler, L. C., 1965, Entropy and volume changes on ionization of aqueous acids: *Jour. Phys. Chemistry*, v. 69, p. 965-967.
- Holser, W. T., and Kennedy, G. C., 1958, Properties of water. IV: Pressure-volume-temperature relations of water in the range 100 to 400°C. and 100 to 1400 bars: *Am. Jour. Sci.*, v. 256, p. 744-753.
- Hopkins, H. P., and Wulff, C. A., 1965, The solution thermochemistry of polyvalent electrolytes. II. Silver sulfate: *Jour. Phys. Chemistry*, v. 69, p. 9-11.
- Hostetler, P. B., 1963, The stability and surface energy of brucite in water at 25°C: *Am. Jour. Sci.*, v. 261, p. 238-258.
- Hostetler, P. B., and Christ, C. L., 1968, Studies in the system  $MgO-SiO_2-CO_2-H_2O$  (I): The activity-product constant of chrysotile: *Geochim. et Cosmochim. Acta*, v. 32, p. 485-497.
- Hower, J., and Mowatt, T. G., 1966, The mineralogy of illite and mixed-layer illite/montmorillonites: *Am. Mineralogist*, v. 51, p. 825-834.
- Hsu, K. J., 1967, Chemistry of dolomite formation, in Chilingar, G. V., Bissell, H. J., and Fairbridge, R. W., eds., *Carbonate Rocks*: New York Elsevier, p. 170-191.
- Hugus, Z. Z., 1951, The partial molal entropy of the cuprous ion: *Am. Chem. Soc. Jour.*, v. 73, p. 5459-5460.
- Hurlen, T., 1961, Electrochemical behavior of copper in acid chloride solutions: *Acta Chem. Scandinavica*, v. 15, p. 1231-1238.
- Jönte, H. H., and Martin, D. S., 1952, Solubility of silver chloride and the formation of complexes in chloride solution: *Am. Chem. Soc. Jour.*, v. 74, p. 2052-2054.
- Keenan, J. H., and Keyes, F. G., 1936, Thermodynamic properties of steam: New York, John Wiley & Sons, 90 p.
- Kelley, K. K., 1960, Contributions to the data on theoretical metallurgy: XIII. High temperature heat content, heat capacity and entropy data for the elements and inorganic compounds: U.S. Bur. Mines Bull. 584, 232 p.
- Kelley, K. K., Barany, R., King, E. G., and Christensen, A. U., 1959, Some thermodynamic properties of fluorophlogopite mica: U.S. Bur. Mines Rept. Inv. 5436, 16 p.
- Kelley, K. K., and King, E. G., 1961, Contributions to the data on theoretical metallurgy: U.S. Bur. Mines Bull. 592, 149 p.
- Kennedy, G. C., 1950, A portion of the system silica-water: *Econ. Geology*, v. 45, p. 629-653.
- Kielland, J., 1937, Individual ion activity coefficients of ions in aqueous solutions: *Am. Chem. Soc. Jour.*, v. 59, p. 1675-1678.
- King, E. G., Barany, R., Weller, W. W., and Pankrauz, I. B., 1967, Thermodynamic properties of forsterite and serpentine: U.S. Bur. Mines Rept. Inv. 6962, 19 p.
- King, E. G., and Weller, W. W., 1961, Low temperature heat capacities and entropies at 298.15° K of diaspor, kaolinite, dickite, and halloysite: U.S. Bur. Mines Rept. Inv. 5810, 6 p.
- 1962, Low temperature heat capacity and entropy at 298.15° K of red mercuric sulfide: U.S. Bur. Mines Rept. Inv. 6001, 4 p.
- Kittrick, J. A., 1966, The free energy of formation of gibbsite and  $Al(OH)_3$  from solubility measurements: *Soil Sci. Soc. America Proc.*, v. 30, p. 595-598.
- Kozintseva, T. N., 1964, Solubility of hydrogen sulfide in water at elevated temperatures: *Geokhimiya*, v. 8, p. 758-765.
- Kraus, K. A., and Rardon, R. J., 1960, Anion exchange studies. XXXI. Adsorption of Zn (II) and Ga (III) from HCl solutions in the temperature range 25°-150°: *Am. Chem. Soc. Jour.*, v. 82, p. 3271-3276.
- Lafon, G. M., ms, 1969, Some quantitative aspects of the chemical evolution of the oceans: Ph.D. thesis, Northwestern Univ., Dept. Geol. Sci., Evanston, Ill.
- Langmuir, D., ms 1964, Stability of carbonates in the system  $CaO-MgO-CO_2-H_2O$ : Ph.D. thesis, Harvard Univ., Cambridge, Mass.
- Latimer, W. M., 1952, The oxidation states of the elements and their potentials in aqueous solutions: Englewood Cliffs, N.J., Prentice-Hall, Inc., 392 p.
- Leden, I., 1952, The use of anion-exchange resin to prove the presence of anionic complexes in some calcium and copper salts: *Svensk. kem. tidskr.*, v. 64, p. 145-149.
- Leussing, D. L., and Kolthoff, I. M., 1953, The solubility product of ferrous hydroxides and the ionization of the aquo-ferrous ion: *Am. Chem. Soc. Jour.*, v. 75, p. 2476-2479.
- Lietzke, M. H., Hupf, H. B., and Stoughton, R. W., 1965, Electromotive force studies in aqueous solution at elevated temperatures. VI. The thermodynamic properties of HCl-NaCl mixtures: *Jour. Phys. Chemistry*, v. 69, p. 2395-2399.
- Lietzke, M. H., and Stoughton, R. W., 1961, The calculation of activity coefficients from osmotic coefficient data: *Jour. Phys. Chemistry*, v. 65, p. 508-509.
- Lietzke, M. H., Stoughton, R. W., and Young, T. F., 1961, The bisulfate acid constant from 25 to 225° as computed from solubility data: *Jour. Phys. Chemistry*, v. 65, p. 2247-2249.
- Lindsay, W. T., Jr., and Liu, C. T., 1968, Vapor pressure lowering of aqueous solutions at elevated temperatures: Final report, Contract no. 14-01-0001-407, Division of Chemistry, Office of Saline Water, U. S. Dept. Interior, Washington, D.C., 235 p.
- Mackenzie, F. T., and Garrels, R. M., 1965, Silicates: reactivity with sea water: *Science*, v. 150, p. 57-58.
- Malcolm, G. N., Parton, H. N., and Watson, J. D., 1961, Enthalpies and entropies of formation of Hg (II) halide 1 : 1 complex ions: *Jour. Phys. Chemistry*, v. 65, p. 1900-1902.
- Marcus, Y.: 1955, "personal communication," cited in *Stability constants of metal-ion complexes* by Sillescu, L. G., and Martell, A. E., 1964: London, Chem. Soc., 308 p.
- 1960, The anion exchange of metal complexes. IV. Iron (III) chloride system: *Jour. Inorganic Nuclear Chemistry*, v. 12, p. 287-296.

- Marcus, Y., and Mayden, D., 1963, The anion exchange of metal complexes. VIII. The effect of the secondary cation. The zinc-chloride system: *Jour. Phys. Chemistry*, v. 67, p. 979-983.
- Marouney, G., 1959, Constantes de dissociation de l'hydrogene sulfure: *Electrochim. Acta*, v. 1, p. 58-59.
- Marshall, W. L., 1967, Aqueous systems at high temperature. XX. The dissociation constant and thermodynamic functions for magnesium sulfate to 200°: *Jour. Phys. Chemistry*, v. 71, p. 3584-3588.
- Meyer, Charles, and Henley, J. J., 1967, Wall rock alteration, in Barnes, H. L., ed., *Geochemistry of hydrothermal ore deposits*: New York, Holt, Rinehart, and Winston, Inc., p. 166-235.
- Morey, G. W., Fournier, R. O., and Rowe, J. J., 1962, The solubility of quartz in water in the temperature interval from 25° to 300°C: *Geochim. et Cosmochim. Acta*, v. 26, p. 1029-1043.
- Mulhamed, S. S., and Sundaram, E. V., 1961, The spectrophotometric determination of the dissociation constants of hydrogen sulfide: *Jour. Sci. Ind. Research*, v. 20B, p. 16-18.
- Nair, V. S. K., and Nancollas, G. H., 1958, Thermodynamics of ion association. VI. Magnesium and zinc sulfates: *Chem. Soc. [London] Jour.*, p. 3706-3710.
- , 1959, Thermodynamics of ion association. VII. Some transition metal sulfates: *Chem. Soc. [London] Jour.*, p. 1458-1462.
- Nasänen, R., 1953, cited in *Stability constants of metal-ion complexes* by L. G. Sillén, and A. E. Martell, 1954: London, Chem. Soc., 306 p.
- Nelson, F., and Kraus, K. A., 1954, Anion-exchange studies. XI. Lead (II) and bismuth (III) in chloride and nitrate solutions: *Am. Chem. Soc. Jour.*, v. 76, p. 5916-5920.
- Noyes, A. A., 1907, The electrical conductivity of aqueous solutions: Washington, D.C., Carnegie Inst. Washington Pub. 63, 352 p.
- Noyes, A. A., Kato, Y., and Sosman, R. B., 1910, The hydrolysis of ammonium acetate and the ionization of water at high temperatures: *Am. Chem. Soc. Jour.*, v. 32, p. 159-178.
- Orville, P. M., 1963, Alkali ion exchange between vapor and feldspar phases: *Am. Jour. Sci.*, v. 261, p. 201-237.
- Owen, B. B., and Brinkley, S. R., Jr., 1941, Calculation of the effect of pressure upon ionic equilibria in pure water and salt solutions: *Chem. Rev.*, v. 29, p. 461-474.
- Pärkkäiz, L. B., 1961, High-temperature heat contents and entropies of muscovite and dehydrated muscovite: *U.S. Bur. Mines Rept. Inv.* 6371, 6 p.
- Pärkkäiz, L. B., and King, E. G., 1965, High-temperature heat contents and entropies of two zinc sulfides and four solid solutions of zinc and iron sulfides: *U.S. Bur. Mines Rept. Inv.* 6708, 8 p.
- Pearson, D., Copeland, C. S., and Benson, S. W., 1963a, The electrical conductance of aqueous sodium chloride in the range 300 to 383°: *Am. Chem. Soc. Jour.*, v. 85, p. 1044-1047.
- , 1963b, The electrical conductance of aqueous hydrochloric acid in the range 300 to 383°: *Am. Chem. Soc. Jour.*, v. 85, p. 1044-1047.
- Pitzer, K. S., 1937, The heats of ionization of water, ammonium hydroxide, carbonic, phosphoric and sulfuric acids. The variations of ionization constants with temperature and the entropy change with ionization: *Am. Chem. Soc. Jour.*, v. 59, p. 2865-2871.
- Pitzer, K. S., and Brewer, L., 1961, *Thermodynamics*, 2nd ed. of *Revision of thermodynamics* by G. N. Lewis, and M. Randall: New York, McGraw-Hill, 723 p.
- Pohl, H. A., 1961, Thermodynamics of the hydrogen sulfide-water system relevant to the dual temperature process for production of heavy water: *Chem. Eng. Data Jour.*, v. 6, p. 515-518.
- Quist, A. S., Franck, E. G., Jolley, H. R., and Marshall, W. L., 1963, Electrical conductances of aqueous solutions at high temperature and pressure. I. The conductances of potassium sulfate-water solutions from 25 to 800° and at pressures up to 4000 bars: *Jour. Phys. Chemistry*, v. 67, p. 2453-2459.
- Quist, A. S., and Marshall, W. L., 1965, Estimation of the dielectric constant of water to 800°: *Jour. Phys. Chemistry*, v. 69, p. 3165-3167.
- , 1966, Electrical conductances of aqueous solutions at high temperatures and pressures. III. The conductances of potassium bisulfate solutions from 0° to 700° and at pressures to 4000 bars: *Jour. Phys. Chemistry*, v. 70, p. 3714-3725.
- , 1968a, Electrical conductances of aqueous sodium chloride solutions from 0° to 800° and at pressures to 4000 bars: *Jour. Phys. Chemistry*, v. 72, p. 684-703.
- , 1968b, The independence of isothermal equilibria in electrolyte solutions on changes in dielectric constant: *Jour. Phys. Chemistry*, v. 72, p. 1536-1544.
- , 1968c, Electrical conductances of aqueous hydrogen bromide solutions from 0° to 800° and at pressures to 4000 bars: *Jour. Phys. Chemistry*, v. 72, p. 1545-1552.
- Rabinowitch, E., and Stockmayer, W. H., 1942, Associations of ferric ions with chloride, bromide, and hydroxyl ions (a spectroscopic study): *Am. Chem. Soc. Jour.*, v. 64, p. 335-347.
- Randall, M., and Fittley, C. F., 1927a, The activity coefficient of gases in aqueous salt solutions: *Chem. Rev.*, v. 4, p. 271-284.
- , 1927b, The activity coefficient of non-electrolytes in aqueous salt solutions from solubility measurements. The salting-out order of the ions: *Chem. Rev.*, v. 4, p. 285-290.
- , 1927c, The activity coefficient of the undissociated part of weak electrolytes: *Chem. Rev.*, v. 4, p. 291-317.
- Robie, R. A., 1966, Thermodynamic properties of minerals, in Clark, S. P., ed., *Handbook of physical constants*: *Geol. Soc. America Mem.* 97, p. 437-458.
- Robie, R. A., and Stout, J. W., 1963, Heat capacity from 12° to 305°K and entropy of talc and tremolite: *Jour. Phys. Chemistry*, v. 67, p. 2252-2256.
- Robie, R. A., and Waldbaum, D. R., 1968, Thermodynamic properties of minerals and related substances at 298.15°K (25°C) and one atmosphere (1.013 bars) pressure and at higher temperatures: *U.S. Geol. Survey Bull.* 1259, 256 p.
- Robinson, R. A., 1936, The dissociation constant of hydrochloric acid: *Faraday Soc. Trans.*, v. 32, p. 743-744.
- Robinson, R. A., and Stokes, R. M., 1959, *Electrolyte solutions*, 2d ed.: London, Butterworths, 559 p.
- Röedder, E., 1962, Studies of fluid inclusions III. Extractions and quantitative analysis of inclusions in the milligram range: *Econ. Geology*, v. 58, p. 353-374.
- , 1965, Report on S. E. G. Symposium on the Chemistry of the Ore-Forming Fluids: *Econ. Geology*, v. 60, p. 1380-1403.
- , 1967, Fluid inclusions as samples of ore fluids, in Barnes, H. L., ed., *Geochemistry of hydrothermal ore deposits*: New York, Holt, Rinehart, and Winston, Inc., p. 515-574.
- Ryzhenko, B. N., 1967, Determination of hydrolysis of sodium silicate and calculation of dissociation constants of orthosilicic acid at elevated temperatures: *Geochim. Internat.*, v. 4, p. 99-107.
- Scatchard, G., 1936, Concentrated solutions of strong electrolytes: *Chem. Rev.*, v. 19, p. 309-327.
- Schäferschädel, P., 1940, Untersuchungen über die Sorption der Tonminerale und Bödenkolloide und die Bestimmung des Anteils dieser Kolloide und der Sorption im Boden: *Kolloid Beitr.*, v. 51, p. 199.
- Sienko, M. J., and Plane, R. A., 1963, *Physical-inorganic chemistry*: New York, W. A. Benjamin, Inc., 166 p.
- Sillén, L. G., and Martell, A. E., 1964, *Stability constants of metal-ion complexes*: London, Chem. Soc., 754 p.
- Stokes, R. H., and Robinson, R. A., 1948, Ionic hydration and activity in electrolyte solutions: *Am. Chem. Soc. Jour.*, v. 70, p. 1870-1878.
- Stout, J. W., and Robie, R. A., 1963, Heat capacity from 11° to 300°K entropy, and heat of formation of dolomite: *Jour. Phys. Chemistry*, v. 67, p. 2248-2252.
- Truesdell, A. H., and Höstetler, P. B., 1968, Dissociation constants of KSO<sub>3</sub>— from 10-50°C: *Geochim. et Cosmochim. Acta*, v. 32, p. 1019-1022.
- Vanderzee, C. E., and Dawson, H. J., 1953, The stability constants of cadmium chloride complexes; variation with temperature and ionic strength: *Am. Chem. Soc. Jour.*, v. 75, p. 5659-5663.
- Vanderzee, C. E., and Swanson, J. A., 1963, The heat of ionization of water: *Jour. Phys. Chemistry*, v. 67, p. 2608-2612.
- Wagman, D. D., 1931, The heat of formation and entropy of aqueous cuprous ion: *Am. Chem. Soc. Jour.*, v. 53, p. 5463.
- Wagman, D. D., Evans, W. H., Halow, I., Parker, V. B., Bailey, S. M., and Schumm, R. H., 1965, Selected values of chemical thermodynamic properties, Part 1: *Natl. Bur. Standards Tech. Note* 270-1, 124 p.
- , 1966, Selected values of chemical thermodynamic properties, Part 2: *Natl. Bur. Standards Tech. Note* 270-2, 62 p.
- , 1968, Selected values of chemical thermodynamic properties, Part 3: *Natl. Bur. Standards Tech. Note* 270-3, 264 p.

- University, Cambridge, Mass.
- White, D. E., and King, E. G., 1963, Low-temperature heat capacity and entropy at deep hole may tap ore-bearing magmatic water and rocks undergoing metamorphism: *Science*, v. 139, p. 919-922.
- Williams, R. J. P., 1954, The stability of complex ions with special reference to hydration: *Jour. Phys. Chemistry*, v. 58, p. 121-126.
- Wright, R. H., and Maass, O., 1932, Electrical conductivity of aqueous solutions of hydrogen sulfide: *Canadian Research Jour.*, v. 6, p. 588-595.
- Wright, J. M., Lindsay, W. T., and Brugá, T. R., 1961, The behavior of electrolytic solutions at elevated temperatures as derived from conductance measurements: Washington, D.C., U.S. Atomic Energy Comm., WAPP-TM-204.
- Wulff, G. A., 1967, Entropies of the aqueous  $Zn^{2+}$ ,  $Cd^{2+}$ ,  $Hg^{2+}$  ions: *Jour. Chem. Eng. Data*, v. 12, p. 82-85.
- Yeats, L. B., and Marshall, W. L., 1969, Apparent invariance of activity coefficients of calcium sulfate at constant ionic strength and temperature in the system  $CaSO_4-Na_2SO_4-NaNO_3-H_2O$  to the critical temperature of water: *Associated equilibria: Jour. Phys. Chemistry*, v. 73, p. 91-90.
- Young, P. A., 1967, The stability of the copper-iron sulfides: *Amdel Bull.*, no. 3, p. 1-13.
- Young, T. F., and Irish, D. E., 1962, Solutions of Electrolytes, in *Annual Review of Phys. Chemistry: Palo Alto, California*, Ann. Reviews Inc., v. 13, p. 435-458.
- Zen, E-an, 1957, Partial molar volumes of some salts in aqueous solutions: *Geochim. et Cosmochim. Acta*, v. 12, p. 103-122.

[AMERICAN JOURNAL OF SCIENCE, VOL. 267, SUMMER 1969, P. 807-824]

THE TETRAPOD-BEARING CONTINENTAL TRIASSIC SEDIMENTS OF SOUTH AMERICA

WILLIAM D. SILL

Peabody Museum of Natural History and Department of Geology and Geophysics, Yale University, New Haven, Conn. 06520

**ABSTRACT.** The Triassic period marked one of the most important transitions in the history of tetrapods: the change from a therapsid-dominated fauna to one dominated by archosaurs. Yet because of a general lack of sediments representing the transitional period, documentation of the change has been difficult and controversial. The recent discoveries of highly fossiliferous sequential continental strata in western Argentina together with the previously known sediments of Brazil and East Africa may hold the key for documenting this transition. Interpretation of the Middle and Upper Triassic is unsettled, but it is apparent that part and perhaps most of the Middle and Upper Triassic is represented. Differences of opinion about correlation exist between and among geologists and paleontologists, depending on the emphasis given to vertebrate remains, fossil plants, and regional stratigraphy. More field studies and fossil discoveries are needed to evaluate accurately the temporal position of the sediments.

INTRODUCTION

The Triassic constitutes one of the more enigmatic chapters in the history of tetrapod evolution. Early Triassic faunas were essentially continuations of Late Permian mammal-like reptile and amphibian faunas with the addition of a few primitive archosaurs. In contrast, the Late Triassic was marked by the first stage of the great archosaur radiation that was to dominate the remainder of the Mesozoic. Tetrapod-bearing sediments of definite Middle Triassic age are lacking in most parts of the world or are represented only by marine strata. As the early and late faunas are radically different from each other, this serious gap in our knowledge of terrestrial life has veiled one of the major events in tetrapod evolution.

Although continental deposits, bearing faunas in part intermediate between the Early and Late Triassic assemblages, have long been known—for example, Manda, Maleri, Elgin, and Santa Maria Formations—these are relatively isolated in terms of vertical and horizontal continuity, making correlation difficult and long a matter of dispute. The recent discoveries in Argentina of sequential tetrapod-bearing sediments representing at least part, and perhaps most, of the Middle Triassic promises to provide the key for documenting the faunal transition of the "Triassic interregnum". Unfortunately, translation of the biological information into a time sequence to match the European or Pethyan type areas is still a matter of disension. There is some disagreement between and among paleozoologists, paleobotanists, and geologists regarding the interpretation of the South American Triassic. But it is a dynamic disagreement, serving to stimulate further study and exploration. Because of the potential importance of the South American Triassic in resolving the long-standing problem of the therapsid-to-archosaur transition, and because of the divergent interpretations of the new discoveries, a review and synthesis of current work is desirable.



# American Journal of Science

SUMMER 1969

## THERMODYNAMICS OF HYDROTHERMAL SYSTEMS AT ELEVATED TEMPERATURES AND PRESSURES

HAROLD C. HELGESON

Department of Geology,  
Northwestern University, Evanston, Illinois 60201

**ABSTRACT.** Chemical relations in hydrothermal systems can be described in terms of the thermodynamic properties of minerals, aqueous species, gases, and concentrated sodium chloride solutions. Sufficient thermodynamic data are available to permit calculation of equilibrium constants for a large number of hydrothermal reactions at high temperatures and pressures. Where these data are incomplete, the calculations involve entropy estimates, application of average heat capacities, and/or assumptions concerning the temperature dependence of thermodynamic variables and the relative importance of electrostatic and non-electrostatic interaction among the aqueous species in hydrothermal solutions. High temperature stoichiometric activity coefficients for individual ions can be calculated using deviation functions computed from osmotic coefficients for concentrated sodium chloride solutions. The results of such calculations, together with computed heat capacities, enthalpies, entropies, and equilibrium constants for many hydrothermal species and reactions at high temperatures are presented in tables and diagrams. The methods, assumptions, and equations employed in the calculations are summarized in general notation. The numerical information contained in the tables permits calculation of the solubilities of silicates, sulfides, carbonates, sulfates, and oxides in multicomponent hydrothermal solutions containing high concentrations of sodium chloride at elevated temperatures, and evaluation of the mass transfer accompanying irreversible reactions responsible for metasomatism and ore deposition in hydrothermal systems.

### INTRODUCTION

The chemistry of electrolyte solutions at high temperatures has received considerable attention in recent years, and it is now possible to predict with confidence the thermodynamic characteristics of hydrothermal solutions to  $> 300^{\circ}\text{C}$  (Criss and Cobble, 1964a and b; Cobble, 1964, 1966a and b; Helgeson, 1967a). It is the purpose of this paper to summarize the equations and methods involved in applying such predictions to hydrothermal equilibria and to compute an internally consistent set of values for the thermodynamic properties of hydrothermal systems at high temperatures. The results of the calculations are presented in tables as well as diagrams to facilitate extrapolation to the supercritical region and to enable the reader to use the numerical values in his own investigations.

Most of the species and reactions considered below are important in hydrothermal processes involving "acid" aqueous solutions containing high sodium chloride concentrations. Electrolyte solutions of this kind occur in the Salton Sea geothermal system (White, Anderson, and Grubbs, 1963; Helgeson, 1968a), and they are commonly found in fluid inclusions in vein minerals (Roedder, 1963, 1965, 1967). Chloride-rich acid solutions are responsible for high temperature metasomatism (Orville, 1963; Helgeson, 1967b) and hydrothermal rock alteration (Hemley, 1959; Hem-

SUBJ  
GTHM  
THS

UNIVERSITY OF UTAH  
RESEARCH INSTITUTE  
EARTH SCIENCES

ley, Meyer, and Richter, 1961; Hemley and Jones, 1964; Meyer and Hemley, 1967). In addition, both experimental (Barnard and Christopher, 1966; Hemley and others, 1967; Cloke, 1969) and theoretical (Helgeson, 1964, 1967c; Helgeson and Garrels, 1968; Helgeson, Garrels, and MacKenzie, 1969) evidence indicates that these solutions are capable of transporting and precipitating metals and sulfides in ore-forming concentrations at elevated temperatures.

Aqueous species contributing to hydrothermal processes involving acid chloride-rich solutions include  $\text{HCO}_3^-$ ,  $\text{HSO}_4^-$ ,  $\text{HS}^-$ ,  $\text{H}_2\text{CO}_3$  and  $\text{CO}_2(\text{aq})$ ,  $\text{H}_2\text{S}(\text{aq})$ ,  $\text{KCl}$ ,  $\text{NaCl}$ ,  $\text{HCl}$ ,  $\text{CaSO}_4$ ,  $\text{MgSO}_4$ ,  $\text{H}_4\text{SiO}_4$ , and chloride and sulfate complexes of the ore forming metals. There is little evidence that polynuclear metal ion complexes are important, or that chloride complexes of ferrous iron, calcium, magnesium, or aluminum form to significant degrees below  $\sim 300^\circ\text{C}$  (Sillén and Martell, 1964; Helgeson, 1964). Bicarbonate and bisulfate metal ion complexes and carbonate, bicarbonate, sulfate, and bisulfate complexes of sodium and potassium exhibit minor association below this temperature (Quist and others, 1963; Quist and Marshall, 1966; Helgeson, 1967a; Lafon, ms). Aluminum ion forms stable complexes with fluoride and (to a much lesser extent) sulfate ions in aqueous solutions. However, thermodynamic calculations indicate that fluoride and sulfate complexes probably contribute only slightly to the transport of aluminum in hydrothermal solutions at high temperatures, even where the pH of the solution is low. At low temperatures, aluminum fluoride complexes may be important in acid solutions (Hem, 1968). Aluminum hydroxide complexes appear to be the primary agents of aluminum transport in "acid" as well as "alkaline" hydrothermal solutions at high temperatures. Hydroxide complexes of calcium, sodium, potassium, magnesium, and most other metal ions are important only in alkaline solutions below  $300^\circ\text{C}$ , but ferrous hydroxide may associate to a significant extent in acid solutions above  $200^\circ\text{C}$ . Of the several oxidation states of gold, iron, and copper that form, aurous, ferrous, and cuprous ions and complexes predominate in hydrothermal solutions.  $\text{Zn}^{++}$ ,  $\text{Pb}^{++}$ ,  $\text{Cu}^+$ ,  $\text{Cu}^{++}$ ,  $\text{Fe}^{+++}$ ,  $\text{Ag}^+$ ,  $\text{Au}^+$ , and  $\text{Au}^{+++}$  ions associate primarily with  $\text{Cl}^-$  in chloride-rich solutions. Although concentrations of metal-carbonate, sulfide, bisulfide, and polysulfide complexes are negligible in acid low-sulfide solutions, metal-sulfate complexes may be important contributors to mineral solubilities in such solutions at temperatures below  $\sim 200^\circ\text{C}$ .

For temperatures below  $300^\circ\text{C}$ , the standard state adopted for the aqueous phase is an hypothetical 1 molal solution at 1 atm and any specified temperature. For gases and solids the standard state is unit activity for the ideal gas and the pure solid, respectively, at 1 atm and any specified temperature. The pressure dependence of hydrothermal equilibria are slight (considered negligible in this contribution) below  $300^\circ\text{C}$ . For this reason, pressure is regarded as a variable only where higher temperatures are considered. In these instances, the standard states apply to any specified temperature and pressure.

## LIST OF SYMBOLS

A	— molal Debye-Hückel parameter defined by equation (39).
a	— coefficient in equations (16) and (17), equal to 0.01875.
$\bar{a}$	— coefficient (in the Debye-Hückel equation) assumed to represent the distance of closest approach of ions in an electrolyte solution.
$\bar{a}_1, \bar{a}_2$	— coefficients in equation (26).
$a'$	— coefficient in equations (28) and (31).
$a''$	— coefficient in equations (10), (11), and (12).
$a_i$	— activity of the <i>i</i> th species.
$a_{\text{H}_2\text{O}}$	— activity of $\text{H}_2\text{O}$ .
$\alpha$	— degree of association defined by equations (33), (34), and (54).
$\alpha'$	— coefficient in equation (17).
$\alpha''$	— coefficient in equation (5).
B	— molal Debye-Hückel parameter defined by equation (40).
B'	— deviation function describing the departure of the mean ionic activity coefficient of an electrolyte from that predicted by the Debye-Hückel expression.
b	— coefficient in equations (16) and (17), equal to $-12.741$ .
$b_1, b_2$	— coefficients in equation (4).
$b'$	— coefficient in equations (28) and (31).
$b''$	— coefficient in equations (10), (11), and (12).
$\beta$	— overall dissociation constant for complexes, or equilibrium constant for gas-aqueous reactions.
$\beta'$	— coefficient in equation (17).
$\beta''$	— coefficient in equation (5).
C	— representation of cations.
$\text{CL}_\nu$	— representation of a mononuclear complex involving cation C and $\nu$ moles of anion L.
c	— coefficient in equations (16) and (17), equal to $7.84 \times 10^{-4}$ .
$\check{c}$	— integer index for complexes in equations (18), (20), (21), (24), (36), and (54).
$c'$	— coefficient in equations (28) and (31).
$c''$	— coefficient in equations (10), (11), and (12).
$C^\circ_{P,i}$	— standard heat capacity of the <i>i</i> th species.
$\left. \begin{matrix} T \\ C^\circ_{P,i} \end{matrix} \right\}$	— average standard heat capacity of the <i>i</i> th species from temperature $T_r$ to temperature T.
$\Delta C^\circ_{P,r}$	— standard heat capacity of reaction.
$\left. \begin{matrix} T \\ \Delta C^\circ_{P,r} \end{matrix} \right\}$	— average standard heat capacity of reaction from temperature $T_r$ to temperature T.
$\gamma_{\check{c}}$	— activity coefficient in the $\check{c}$ th complex.



- $\gamma_i$  — stoichiometric individual ion activity coefficient of the  $i$ th ion in a multicomponent electrolyte solution containing a predominant concentration of a given salt (defined by eq 45).
- $\gamma_i^*$  — individual ion activity coefficient of the  $i$ th ion.
- $\gamma_{\pm}$  — stoichiometric mean activity coefficient.
- $\gamma_{\pm}^*$  — mean ionic activity coefficient.
- $\gamma_{+}^*$  — individual ion activity coefficient of a cation.
- $\gamma_{-}^*$  — individual ion activity coefficient of an anion.
- $d$  — integer index for the difference expressed by equation (20).
- $d'$  — coefficient in equations (28) and (31).
- $\hat{e}$  — integer index for anions in equations (21), (22), (25), (26), (50), (51), and (52).
- $\epsilon$  — dielectric constant.
- $f_i$  — fugacity of the  $i$ th species.
- $\Delta G_{f,i}^{\circ}$  — standard Gibbs free energy of formation from the elements of the  $i$ th species.
- $\Delta G_r^{\circ}$  — standard Gibbs free energy of reaction.
- $h$  — average number of water molecules associated with  $\nu$  ions.
- $H_i^{\circ}$  — standard enthalpy of the  $i$ th species.
- $\Delta H_i^{\circ}$  — standard enthalpy of formation from the elements of the  $i$ th species at the reference temperature plus the enthalpy change for the  $i$ th species associated with an increase in temperature from  $T_r$  to  $T$ .
- $\Delta H_{f,i}^{\circ}$  — standard enthalpy of formation from the elements of the  $i$ th species.
- $\Delta H_r^{\circ}$  — standard enthalpy of reaction.
- $\theta$  — coefficient in equations (16) and (17), equal to 219.0.
- $I$  — stoichiometric ionic strength.
- $\bar{I}$  — true ionic strength.
- $i$  — integer index for chemical species.
- $\hat{i}$  — integer index for cations in equations (19), (20), (21), (24), (26), and (27).
- $j$  — integer index for reaction products.
- $K$  — equilibrium constant.
- $k$  — Henry's law coefficient.
- $K_{sp}$  — activity product constant.
- $L$  — representation of anions.
- $l$  — integer index for reactants.
- $\lambda'$  — coefficient in equation (17).
- $M_i$  — molarity of the  $i$ th species.
- $m_i$  — molality of the  $i$ th species.
- $m_{t,i}$  — total molality of the  $i$ th ion or salt.
- $n$  — number of moles of a given cation in a mineral.
- $\bar{n}$  — sum of the exponents in the Law of Mass Action equation.
- $\nu$  — number of moles of ions in 1 mole of a given salt.
- $\nu_+$  — number of moles of the cation in 1 mole of a given salt.
- $\nu_-$  — number of moles of the anion in 1 mole of a given salt.

- $P$  — pressure in atmospheres.
- $P_r$  — reference pressure in atmospheres (1 atm).
- $q$  — integer index for mononuclear complexes involving a common ligand in equations (26) and (27).
- $R$  — gas constant, equal to 1.9872 cal mole<sup>-1</sup> deg<sup>-1</sup> or 82.0575 cm<sup>3</sup> atm mole<sup>-1</sup> deg<sup>-1</sup>.
- $r_{\hat{e}}$  — ion radius of the  $\hat{e}$ th anion.
- $r_i$  — ion radius of the  $i$ th cation.
- $\rho$  — density.
- $S^*$  — sum of the entropies of 1 mole of an aqueous species and its coordinated water molecules.
- $S_i^{\circ}$  — standard conventional third law entropy of the  $i$ th species.
- $S_i^{\circ(\text{abs})}$  — standard absolute third law entropy of the  $i$ th species.
- $S_d^*$  — difference in the sum of the entropies of 1 mole of an aqueous complex and its coordinated water molecules and the sum of the entropies of the free cation and its coordinated water molecules.
- $\Delta S_e^{\circ}$  — standard electrostatic entropy of dissociation.
- $\Delta S_r^{\circ}$  — standard entropy of reaction.
- $S_{\psi}$  — solubility of the  $\psi$ th mineral (in molality units) defined by equation (51).
- $\sigma$  — exponential coefficient in equation (36).
- $T$  — temperature in degrees Kelvin.
- $T_r$  — reference temperature in degrees Kelvin (298.15°K).
- $u$  — integer index in equation (48).
- $\bar{u}$  — number of water molecules coordinated to a cation.
- $\Delta V_r^{\circ}$  — standard volume of reaction.
- $\phi$  — stoichiometric osmotic coefficient.
- $x$  — number of water molecules coordinated to a complex.
- $y$  — number of moles of ligand  $L$  coordinated in a mononuclear complex of the form  $CL_y$ .
- $\nu$  — number of moles of a given anion in a mineral.
- $\psi$  — integer index for minerals.
- $z$  — limit of the range of integer index  $y$  in equations (46), (47), and (49).
- $Z_i$  — charge on the  $i$ th species.
- $\omega$  — coefficient in equations (16) and (17), equal to 1.00322.

## PREDICTIVE METHODS

In the present state of knowledge, limitations imposed by the amounts and kinds of data available for hydrothermal reactions dictate the "best" methods for predicting thermodynamic properties of hydrothermal systems at elevated temperatures. A variety of approximations, each with its own uncertainties, can be used for this purpose. Because the reliability of numerical values obtained from such approximations reflects the method as well as the data used in the calculations, the computational methods applicable under various circumstances are summarized below.

## Equilibrium Constants

The basic thermodynamic equation describing the temperature dependence of the equilibrium constant is

$$\log K(T) = \log K(T_r) - \frac{\Delta H^{\circ}_r(T_r)}{2.303R} \left( \frac{1}{T} - \frac{1}{T_r} \right) - \frac{1}{2.303RT} \int_{T_r}^T \Delta C^{\circ}_{P,r}(T) dT + \frac{1}{2.303R} \int_{T_r}^T \Delta C^{\circ}_{P,r}(T) d \ln T \quad (1)$$

in which  $\Delta H^{\circ}_r$  and  $\Delta C^{\circ}_{P,r}$  are, respectively, the standard enthalpy and heat capacity of reaction,  $R$  is the gas constant,  $K$  the equilibrium constant,  $T$  the temperature of interest (in  $^{\circ}K$ ), and  $T_r$  the reference temperature (298.15 $^{\circ}K$  in this commu.). For most reactions involving aqueous solutions, the integrals in equation (1) cannot be evaluated rigorously because the required heat capacity functions are not available. To integrate the last two terms in equation (1), the assumption is frequently made that  $\Delta C^{\circ}_{P,r}(T)$  is zero or constant, but this practice often leads to serious errors in computed  $\log K(T)$  values at elevated temperatures (Cobble, 1964; Helgeson, 1964, 1967a). In many cases, ambiguities and uncertainties resulting from these assumptions can be avoided by adopting one or another of the alternate approaches summarized below.

*Calculation from average heat capacities.*—Average heat capacities

$\left( \begin{matrix} T \\ C^{\circ}_P \\ T_r \end{matrix} \right)$  for ions can be computed from absolute entropies by evaluating

$$C^{\circ}_{P,i} \left( \begin{matrix} T \\ T_r \end{matrix} \right) = \frac{S^{\circ}_i(\text{abs})(T) - S^{\circ}_i(\text{abs})(T_r)}{\ln T/T_r} \quad (2)$$

where  $S^{\circ}_i(\text{abs})$  is the absolute entropy of the  $i$ th species. The absolute entropy is related to the conventional entropy ( $S^{\circ}$ ) by

$$S^{\circ}_i(\text{abs})(T) = S^{\circ}_i(T) + Z_i S^{\circ}_{H^+}(\text{abs})(T) \quad (3)$$

where  $Z_i$  represents the charge on the  $i$ th species and  $S^{\circ}_{H^+}(\text{abs})(T)$  is the absolute entropy of the hydrogen ion at temperature  $T$ . Criss and Cobble (1964a) have shown that the absolute entropies of ions at high temperatures can be calculated from

$$S^{\circ}_i(\text{abs})(T) = b_1(T) + b_2(T) S^{\circ}_i(\text{abs})(T_r) \quad (4)$$

where  $b_1$  and  $b_2$  are temperature dependent coefficients characteristic of simple cations, simple anions, oxy-anions, or acid oxy-anions. The relation expressed in equation (4) was obtained by assigning absolute entropies to the hydrogen ion at various specified temperatures, Equation

(4) can be combined with equation (2) to define a similar relation for average heat capacities. This expression appears as

$$C^{\circ}_{P,i} \left( \begin{matrix} T \\ T_r \end{matrix} \right) = \alpha''(T) + \beta''(T) S^{\circ}_i(\text{abs})(T_r) \quad (5)$$

where  $\alpha''(T) = b_1(T)/\ln(T/T_r)$  and  $\beta''(T) = (b_2(T)-1)/\ln(T/T_r)$ . Values of  $b_1$ ,  $b_2$ ,  $\alpha''$ , and  $\beta''$  have been computed by Criss and Cobble (1964a and b) for 60 $^{\circ}$ , 100 $^{\circ}$ , 150 $^{\circ}$ , 200 $^{\circ}$ , 250 $^{\circ}$ , and 300 $^{\circ}C$ . These coefficients allow absolute entropies and average heat capacities to be calculated for a large number of aqueous species at elevated temperatures.

When average heat capacities can be computed for all reactants and products in a given reaction, the equilibrium constant at temperature  $T$  can be predicted directly from

$$\log K(T) = \log K(T_r) - \frac{\Delta H^{\circ}_r(T_r)}{2.303R} \left( \frac{1}{T} - \frac{1}{T_r} \right) - \frac{\Delta C^{\circ}_{P,r} \left( \begin{matrix} T \\ T_r \end{matrix} \right) (T-T_r)}{2.303RT} + \frac{\Delta C^{\circ}_{P,r} \left( \begin{matrix} T \\ T_r \end{matrix} \right) \ln T/T_r}{2.303R} \quad (6)$$

in which

$$\Delta C^{\circ}_{P,r} \left( \begin{matrix} T \\ T_r \end{matrix} \right) = \sum_j C^{\circ}_{P,j} \left( \begin{matrix} T \\ T_r \end{matrix} \right) - \sum_l C^{\circ}_{P,l} \left( \begin{matrix} T \\ T_r \end{matrix} \right) \quad (7)$$

where  $j$  and  $l$  represent the products and reactants, respectively.

*Calculation from a combination of average and actual heat capacities.*—In cases where the actual heat capacities for some (but not all) of the reactants or products in a given reaction are defined by empirical power functions of temperature, equilibrium constants can be computed by first evaluating (for those species)

$$\Delta H^{\circ}_i(T) = \Delta H^{\circ}_{f,i}(T_r) + \int_{T_r}^T C^{\circ}_{P,i}(T) dT \quad (8)$$

and

$$S^{\circ}_i(T) = S^{\circ}_i(T_r) + \int_{T_r}^T C^{\circ}_{P,i}(T) d \ln T \quad (9)$$

in which  $\Delta H^{\circ}_i(T)$  is the standard enthalpy of formation from the elements of the  $i$ th species at the reference temperature [ $\Delta H^{\circ}_{f,i}(T_r)$ ] plus the enthalpy change for the  $i$ th species associated with an increase in

temperature from  $T_r$  to temperature  $T$ . Heat capacities of solids and gases are usually described by power functions of the form

$$C_{P,i}^{\circ}(T) = a'' + b''T + c''/T^2 \quad (10)$$

so that equations (8) and (9) will normally appear as

$$\Delta H_{i,i}^{\circ}(T) = \Delta H_{i,i}^{\circ}(T_r) + a''(T - T_r) + \frac{b''}{2}(T^2 - T_r^2) - c'' \left( \frac{1}{T} - \frac{1}{T_r} \right) \quad (11)$$

and

$$S_{i,i}^{\circ}(T) = S_{i,i}^{\circ}(T_r) + a'' \ln T/T_r + b''(T - T_r) - \frac{c''}{2} \left( \frac{1}{T^2} - \frac{1}{T_r^2} \right) \quad (12)$$

Where average heat capacities are known for the remaining reactants and products, standard enthalpies and entropies at a given temperature can be calculated by evaluating

$$\Delta H_{i,i}^{\circ}(T) = \Delta H_{i,i}^{\circ}(T_r) + C_{P,i}^{\circ} \left[ \frac{T}{T_r} \right] (T - T_r) \quad (13)$$

and

$$S_{i,i}^{\circ}(T) = S_{i,i}^{\circ}(T_r) + C_{P,i}^{\circ} \left[ \frac{T}{T_r} \right] \ln T/T_r \quad (14)$$

High temperature equilibrium constants for the reaction can then be computed from

$$\log K(T) = \frac{T \left( \sum_j S_{j,i}^{\circ}(T) - \sum_l S_{l,i}^{\circ}(T) \right) - \sum_j \Delta H_{j,i}^{\circ}(T) + \sum_l \Delta H_{l,i}^{\circ}(T)}{2.303RT} \quad (15)$$

where  $j$  and  $l$  again refer to the products and reactants, respectively. When equation (15) is employed, care must be exercised to avoid confusion between relative and absolute entropies in the summation terms of the equation. If heat capacity power functions are known for all reactants and products, high temperature equilibrium constants can be computed simply by combining equations (11), (12), and (15).

*Prediction of dissociation constants.*—In geochemical problems it is quite common to find that no heat capacity data of any kind are available for one or more of the reactants or products in a given reaction. This is particularly true for complexes in aqueous solution. Despite this handicap, dissociation constants often can be closely approximated to  $\sim 200^{\circ}\text{C}$  by evaluating (Helgeson, 1967a)

$$\log K(T) = \frac{\Delta S_{r,i}^{\circ}(T_r)}{2.303RT} \left[ T_r - \frac{\theta}{\omega} \left( 1 - \exp[\exp(b + aT) - c + (T - T_r)/\theta] \right) \right] - \frac{\Delta H_{r,i}^{\circ}(T_r)}{2.303RT} \quad (16)$$

where  $\theta$ ,  $\omega$ ,  $a$ ,  $b$ , and  $c$  are temperature independent constants characteristic of the solvent. For aqueous solutions these coefficients have the values 219.0, 1.00322, 0.01875,  $-12.741$ , and  $7.84 \times 10^{-4}$ , respectively (Helgeson, 1967a). The method of approximation afforded by equation (16) involves the assumption that  $\Delta C_{P,r}^{\circ}(T)$  changes monotonically but nonlinearly with temperature;  $\Delta C_{P,r}^{\circ}(T)$  is implicitly defined in terms of  $\Delta S_{r,i}^{\circ}(T_r)$  in the equation. Dissociation constants computed from equation (16) are often much closer approximations of actual dissociation constants at high temperatures than those computed by assuming  $\Delta C_{P,r}^{\circ}(T) = 0$  or  $\Delta C_{P,r}^{\circ}(T) = \text{a constant}$ . Equation (16) is an approximation modified from equation (17) below.

Where dissociation constants are known over a restricted temperature range, experimental  $\log K(T)$  values can be fit by the method of least squares to

$$\begin{aligned} \log K(T) = & \frac{\Delta S_{r,i}^{\circ}(T_r)}{2.303RT} \left[ T_r - T - \frac{\theta}{\omega} \left( 1 - \exp[\exp(b + aT) - c + (T - T_r)/\theta] \right) \right] \\ & - \frac{\Delta H_{r,i}^{\circ}(T_r)}{2.303RT} + \frac{\Delta S_{r,i}^{\circ}(T_r)}{2.303R} + \frac{\alpha'}{2.303R} (\ln T/T_r - 1 + T_r/T) \\ & + \frac{\beta'(T - T_r)^2}{4.606RT} + \frac{\lambda'}{4.606RT} (T^3/3 - T_r^3/3 - T_r^2T + T_r^3) \quad (17) \end{aligned}$$

where  $\theta$ ,  $\omega$ ,  $a$ ,  $b$ , and  $c$  are constants with the values given above,  $\Delta S_{r,i}^{\circ}(T_r)$  is the electrostatic entropy of dissociation at the reference temperature ( $T_r$ ), and  $\alpha'$ ,  $\beta'$ , and  $\lambda'$  are temperature independent coefficients characteristic of the reaction (Helgeson, 1967a). Values of the reaction-dependent parameters defined by the low temperature fits can then be used to predict  $\log K$  values at higher temperatures. However, care must be exercised to avoid overfitting. Where only a few experimental values are available, or the data are highly uncertain, all of the reaction-dependent coefficients should not be included in the least squares fit routine; that is,  $\lambda'$ , or  $\lambda'$  and  $\beta'$  should be set to zero.

#### Entropy and Heat Capacity Estimates

For many reactions in aqueous solution, equilibrium constants are known only at  $25^{\circ}\text{C}$ . In such cases it is common to find that insufficient entropy or enthalpy data are available for the species involved in the reaction to permit calculation of high temperature equilibrium constants using the approaches described above. This problem often can be overcome in a first approximation by estimating entropies of dissociation or the entropies and heat capacities of reactant or product species.

*Dissociational reactions in aqueous solution.*—Entropies of dissociation for complexes in aqueous solution at  $25^{\circ}\text{C}$  can be estimated from entropy correlation plots. These entropies can then be used in conjunction with equation (16) to approximate dissociation constants at higher temperatures. The approach summarized below for making such esti-

mates is a modification of that employed by Cobble (1953b) for estimating the entropies of complex ions.

For convenience, let us define the sum of the entropies of 1 mole of an aqueous species and its coordinated water molecules as  $S^*$ ; that is, for a given temperature,

$$S^* [\text{CL}_y(\text{H}_2\text{O})_x^z] \equiv S^\circ [\text{CL}_y^z] + xS^\circ [\text{H}_2\text{O}] \quad (18)$$

and

$$S^* [\text{C}(\text{H}_2\text{O})_u^z] \equiv S^\circ [\text{C}^z] + uS^\circ [\text{H}_2\text{O}] \quad (19)$$

in which  $S^\circ$  is the conventional third law entropy,  $\text{CL}_y$  is a mononuclear complex involving cation C and y moles of anion L, x and u represent the number of water molecules coordinated to the complex and cation, respectively, and  $Z_c$  and  $Z_l$  are the respective charges on the complex and the cation. Subtracting equation (19) from equation (18) gives

$$S^* [\text{CL}_y(\text{H}_2\text{O})_x^z] - S^* [\text{C}(\text{H}_2\text{O})_u^z] = \Delta S_d^* = S^\circ [\text{CL}_y^z] - S^\circ [\text{C}^z] + (x - u)S^\circ [\text{H}_2\text{O}] \quad (20)$$

where  $\Delta S_d^*$  is the difference in the sums of the entropies expressed in equations (18) and (19). Equation (20) can now be combined with the expression for the entropy of dissociation of the complex written as

$$\Delta S_r^\circ = S^\circ [\text{C}^z] + yS^\circ [\text{L}^z] - S^\circ [\text{CL}_y^z] \quad (21)$$

to give

$$\Delta S_r^\circ = yS^\circ [\text{L}^z] + (x - u)S^\circ [\text{H}_2\text{O}] - \Delta S_d^* \quad (22)$$

where  $Z_c$  is the charge on the anion. If as a first approximation we assume,

$$x = u - y \quad (23)$$

then equations (20) and (22) reduce, respectively, to

$$\Delta S_d^* = S^\circ [\text{CL}_y^z] - S^\circ [\text{C}^z] - yS^\circ [\text{H}_2\text{O}] \quad (24)$$

and

$$\Delta S_r^\circ = y \left( S^\circ [\text{L}^z] - S^\circ [\text{H}_2\text{O}] \right) - \Delta S_d^* \quad (25)$$

For complexes involving a common ligand at 25°C, empirical considerations indicate that  $\Delta S_d^*$  can be described by

$$\Delta S_d^*_{d(q)} = \hat{a}_1 + \hat{a}_2 / (r_{i(q)} + r_{\hat{e}(q)}) \quad (26)$$

in which  $\hat{a}_1$  and  $\hat{a}_2$  are coefficients characteristic of the group of complexes, and  $r_{i(q)}$  and  $r_{\hat{e}(q)}$  are the radii of the cation and ligand, respectively, in the qth complex. The validity of equation (26) can be

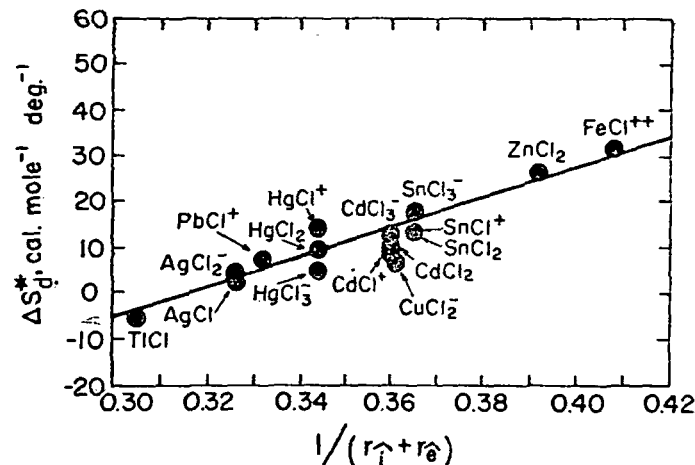


Fig. 1. Correlation plot of  $\Delta S_d^*$  (see text—eqs 20 and 24) for metal chloride complexes at 25°C and 1 atm against the reciprocal of the sum of the radii of the ions in the complex. The plotted values of  $\Delta S_d^*$  and the sources of data from which they were calculated (see text) are given in table 1. The curve shown above is consistent with equation (27).

assessed for chloride complexes in figure 1. The data used in computing the  $\Delta S_d^*$  values plotted in figure 1 are given in table 1 along with the sources from which they were obtained. The maximum deviation from the linear curve of the points in figure 1 is 8 cal mole<sup>-1</sup> deg<sup>-1</sup> (for  $\text{CuCl}_2^-$ ), but the average deviation is only 3 cal mole<sup>-1</sup> deg<sup>-1</sup>, which is well within the experimental uncertainty of the data. The specific statement of equation (26) for the curve in figure 1 is

$$\Delta S_d^*_{d(q)} = -102.5 + 325 / (r_{i(q)} + 1.81) \quad (27)$$

where 1.81 is the radius of the chloride ion (Sienko and Plane, 1963). Values of  $\Delta S_r^\circ$ , computed from equations (25) and (27) for the species shown in figure 1 are given in table 1 to afford a numerical comparison with those based on experimental data.

The procedure summarized above for estimating dissociational entropies is of general applicability; that is, expressions similar to equations (26) and (27) can be developed for various groups of dissociational reactions for which data are incomplete. Entropy estimates obtained in this manner permit approximations of high temperature dissociation constants for a large number of complexes of interest in geochemistry. For many of these, only experimental dissociation constants at 25°C are available, but estimates of  $\Delta S_r^\circ(T_r)$  allow approximations of  $\Delta H_r^\circ(T_r)$  [from  $\Delta H_r^\circ(T_r) = T_r \Delta S_r^\circ(T_r) - 2.303RT_r \log K(T_r)$ ] and thus estimation of high temperature dissociation constants from equation (16). In cases where sufficient data are not available to estimate dissociational

entropies from correlation plots, it may be possible to estimate directly the entropy of a particular complex, neutral species, or ion, which will then permit calculation of dissociational entropies at 25°C. A number of techniques for making such estimates have been summarized by Latimer (1952), Cobble (1953a and b), and others.

TABLE I  
Entropies of dissociation for chloride complexes  
in aqueous solution at 25°C and 1 atm.

Reaction	Cation radius <sup>a</sup> (Å)	Experimental $\Delta S^\circ_f$ (cal mole <sup>-1</sup> deg <sup>-1</sup> )	Calculated <sup>b</sup> $\Delta S^\circ_f$ (cal mole <sup>-1</sup> deg <sup>-1</sup> )	Calculated <sup>c</sup> $\Delta S^\circ_f$ (cal mole <sup>-1</sup> deg <sup>-1</sup> )
$\text{AgCl} \rightleftharpoons \text{Ag}^+ + \text{Cl}^-$	1.26	-6 <sup>d</sup>	2.6	-6.6
$\text{AgCl}_2^- \rightleftharpoons \text{Ag}^+ + 2\text{Cl}^-$	1.26	-11 <sup>d</sup>	4.4	-9.8
$\text{CuCl}_2^- \rightleftharpoons \text{Cu}^+ + 2\text{Cl}^-$	0.96	-13.0 <sup>e</sup>	6.6	-21.2
$\text{PbCl}^+ \rightleftharpoons \text{Pb}^{2+} + \text{Cl}^-$	1.20	-11.6 <sup>f</sup>	7.4	-8.6
$\text{ZnCl}_2 \rightleftharpoons \text{Zn}^{2+} + 2\text{Cl}^-$	0.74	-32.7 <sup>g</sup>	26.3	-31.3
$\text{HgCl}^+ \rightleftharpoons \text{Hg}^{2+} + \text{Cl}^-$	1.10	-17 <sup>h</sup>	13.8	-12.5
$\text{HgCl}_2 \rightleftharpoons \text{Hg}^{2+} + 2\text{Cl}^-$	1.10	-16 <sup>i</sup>	9.6	-15.7
$\text{HgCl}_3^- \rightleftharpoons \text{Hg}^{2+} + 3\text{Cl}^-$	1.10	-13.7 <sup>j</sup>	4.1	-13.9
$\text{CdCl}^+ \rightleftharpoons \text{Cd}^{2+} + \text{Cl}^-$	0.97	-11.4 <sup>k</sup>	8.2	-17.6
$\text{CdCl}_2 \rightleftharpoons \text{Cd}^{2+} + 2\text{Cl}^-$	0.97	-16.4 <sup>k</sup>	10.0	-20.8
$\text{CdCl}_3^- \rightleftharpoons \text{Cd}^{2+} + 3\text{Cl}^-$	0.97	-22.3 <sup>k</sup>	12.7	-24.0
$\text{SnCl}^+ \rightleftharpoons \text{Sn}^{2+} + \text{Cl}^-$	0.93	-15.4 <sup>l, n</sup>	12.2	-19.3
$\text{SnCl}_2 \rightleftharpoons \text{Sn}^{2+} + 2\text{Cl}^-$	0.93	-18.9 <sup>l, n</sup>	12.5	-22.5
$\text{SnCl}_3^- \rightleftharpoons \text{Sn}^{2+} + 3\text{Cl}^-$	0.93	-27.4 <sup>l, n</sup>	17.8	-25.7
$\text{FeCl}^{2+} \rightleftharpoons \text{Fe}^{3+} + \text{Cl}^-$	0.64	-35 <sup>m</sup>	31.8	-33.3
$\text{TlCl} \rightleftharpoons \text{Tl}^+ + \text{Cl}^-$	1.74	2.2 <sup>i</sup>	5.4	0.2
$\text{AuCl}_2^- \rightleftharpoons \text{Au}^+ + 2\text{Cl}^-$	1.37			-6.0
$\text{AuCl}_4^- \rightleftharpoons \text{Au}^{3+} + 4\text{Cl}^-$	0.9			-30.2
$\text{SnCl}_4^- \rightleftharpoons \text{Sn}^{4+} + 4\text{Cl}^-$	0.71			-39.2

<sup>a</sup> Sienko and Plane (1963). <sup>b</sup> Computed from equation (25) using the experimental entropies shown above together with 16.7 cal mole<sup>-1</sup> deg<sup>-1</sup> for  $S^\circ_{\text{H}_2\text{O}}$  (Wagman and others, 1968) and 13.51 for  $S^\circ_{\text{Cl}^-}$  (Ahluwalia and Cobble, 1964). <sup>c</sup> Calculated from equations (25) and (27). <sup>d</sup> Jonte and Martin (1952). <sup>e</sup> Calculated from  $S^\circ_{\text{CuCl}_2^-}$  (Latimer 1952) and the ionic entropies in table 3. <sup>f</sup> Austin, Matheson, and Parton (1959). <sup>g</sup> Based on least squares fits of  $\log K(T)$  values at 150° and 115°C (Kraus and Raridon, 1960) and 25°C (Marcus and Mayden, 1963) using equation (16). <sup>h</sup> Malcolm, Parton, and Watson (1961). <sup>i</sup> Williams (1954). <sup>j</sup> Helgeson (1967a). <sup>k</sup> Vanderzee and Dawson (1953). <sup>l</sup> Wagman and others (1966). <sup>m</sup> Rabinowitch and Stockmayer (1942). <sup>n</sup> Latimer (1952).

*Minerals.*—Although thermodynamic data are now available for a large number of minerals (Robie, 1966; Robie and Waldbaum, 1968), only free energy data (derived from solubility studies) at 25°C exist for many minerals of interest in hydrothermal and metamorphic studies. Approximation of the standard enthalpies of formation of these minerals at 25°C permits calculation of provisional equilibrium constants for high temperature hydrothermal reactions that could not otherwise be evaluated in the present state of knowledge. As a rule, direct estimation of the standard enthalpies of formation of minerals involves prohibitive uncertainties owing to the lack of adequate general models for calculating bond energies in minerals. In contrast, third law entropies of minerals can be approximated closely by direct estimation, which permits calculation of  $\Delta H^\circ_f(T_r)$  from  $\Delta H^\circ_f(T_r) = \Delta G^\circ_f(T_r) + T_r \Delta S^\circ_f(T_r)$ , where  $\Delta S^\circ_f(T_r)$  is the standard entropy of formation of the mineral from its elements.

Entropies of silicates, sulfates, and carbonates can be approximated by summing the entropies of the oxide components of the minerals (Latimer, 1952; Fyfe and others, 1958). Although such a summation does not provide for all of the configurational entropy contribution, the uncertainty attending this procedure rarely exceeds 10 percent and more often than not is less than a few cal/mole deg. Close estimates can be made for clay minerals if the entropy of H<sub>2</sub>O is taken to be that of ice at 25°C (10.68 cal mole<sup>-1</sup> deg<sup>-1</sup>, Robie and Waldbaum, 1968) or assigned a value of 9.4 cal/mole deg<sup>-1</sup> (Latimer, 1952). For example, the entropy of muscovite obtained from the sum of the entropies of its oxide components at 25°C is 69.8 cal mole<sup>-1</sup> deg<sup>-1</sup> if H<sub>2</sub>O is represented by ice, and 68.5 cal mole<sup>-1</sup> deg<sup>-1</sup> if Latimer's value for the entropy of hydrate water is used; the experimental entropy of muscovite is 69.0 cal mole<sup>-1</sup> deg<sup>-1</sup> (Robie and Waldbaum, 1968). An error of a few cal mole<sup>-1</sup> deg<sup>-1</sup> in the entropy of a mineral rarely introduces significant error in high temperature calculations of mineral equilibria. In contrast to summing the entropies of oxide components, entropies of minerals can also be estimated with confidence by summing the values tabulated by Latimer (1952) for the entropy contributions of elements and ions in solid compounds. This procedure is particularly useful for estimating the entropies of multicomponent sulfides.

As in the case of entropy, heat capacities of minerals can be approximated closely by summing the heat capacities of the components of the minerals. This is true also for heat capacities of minerals expressed by power functions of temperature (eq 10). For example, the heat capacity power function for muscovite obtained by summing the power functions for its oxide components is  $89.95 + 33.23 \times 10^{-3}T - 20.67 \times 10^5 T^{-2}$  when ice (9.0 cal mole<sup>-1</sup> deg<sup>-1</sup>) is used to represent H<sub>2</sub>O (see footnote n, table 8). The experimentally derived function is  $97.56 + 26.38 \times 10^{-3}T - 25.44 \times 10^5 T^{-2}$  (Kelley, 1960). At 25°C, the estimated heat capacity defined by the first of these power functions is 77 cal mole<sup>-1</sup> deg<sup>-1</sup> compared to the experimental value of 77 cal mole<sup>-1</sup> deg<sup>-1</sup>. At

300°C the corresponding values are 103 cal mole<sup>-1</sup> deg<sup>-1</sup> compared to 105 cal mole<sup>-1</sup> deg<sup>-1</sup>. Discrepancies of this order of magnitude are insignificant with respect to calculated equilibrium constants at high temperature.

Estimates of entropies and heat capacity power functions of temperature make it possible to compute standard enthalpies of formation for minerals at 25°C from high temperature phase equilibrium data. For example, the  $\Delta H^\circ_f(T_r)$  value for annite used to compute the high temperature hydrolytic equilibrium constants for this mineral in table 12 were calculated from the high temperature equilibrium  $P_{H_2O}$  and  $f_{O_2}$  for sanidine + magnetite +  $H_2O_{(aq)} \rightleftharpoons$  annite +  $\frac{1}{2}O_{2(g)}$  (Eugster and Wones, 1962) at 500°C and 2070 atm. An estimated entropy (table 12) and heat capacity power function (table 8) for annite permitted calculation of the high temperature values for the entropy of annite (eq 9). The same calculations for the other species in the assemblage (for which thermodynamic data are known) permitted calculation of  $\Delta S^\circ_f(T)$  for the equilibrium assemblage at 500°C. From the values of  $f_{O_2}$  and  $P_{H_2O}$  given by Eugster and Wones, and fugacity coefficients for  $H_2O^1$  (Anderson, 1967),  $\Delta G^\circ_f(T)$  could also be computed, which made it possible to calculate  $\Delta H^\circ_f(T)$ , and hence,  $\Delta H^\circ_{\text{annite}}(T)$ . Application of the estimated heat capacity power function resulted in the value of  $\Delta H^\circ_f(T_r)$  for annite given in table 12.<sup>2</sup>

#### Activity Coefficients in Sodium Chloride Solutions

Because the solute in many hydrothermal solutions is composed largely of sodium chloride, the thermodynamic properties of aqueous solutions of this salt can be used to compute activity coefficients in concentrated hydrothermal solutions at elevated temperatures. Thermodynamic properties of concentrated sodium chloride solutions are summarized in table 2. The methods used in computing the values shown in the table are outlined briefly below.

<sup>1</sup> Fugacity coefficients for other gases involved in similar calculations can be computed from data given by Garrels and Christ (1965).

<sup>2</sup> The effects of pressure were disregarded in the calculation of the enthalpy of formation of annite described above. The volume changes for reactions used in such calculations are commonly small, and the pressure corrections are thus often smaller than the uncertainty in the experimental data. Where this is not true the experimental equilibrium constants should first be corrected for pressure by evaluating

$$\log K(T, P_r) = \log K(T, P) - \frac{1}{2.303RT} \int_{P_r}^P \Delta V^\circ_r(T, P) dP$$

where  $P_r$  refers to the reference pressure (1 atm in this column),  $\Delta V^\circ_r$  is the standard change in volume for the reaction in cm<sup>3</sup> mole<sup>-1</sup>, and  $R$  is the gas constant expressed as 82.0575 cm<sup>3</sup> atm mole<sup>-1</sup> deg<sup>-1</sup>. In many instances this equation can be approximated closely by

$$\log K(T, P_r) = \log K(T, P) - \frac{\Delta V^\circ_r(T, P_r)(P - P_r)}{2.303RT}$$

*Analysis of vapor pressure data.*—Stoichiometric osmotic coefficients for sodium chloride solutions from 25°C to 270°C have been fit (Helgeson, 1967b; Helgeson and James, 1968) with a least squares computer routine employing a Debye-Hückel power function for activity coefficients suggested by Lietzke and Stoughton (1961). The activity coefficient power function is

$$\ln \gamma_{\pm}(T, I) = \frac{-2.303 A(T) |Z_1 Z_2| I^{1/2}}{1 + a'(T) I^{1/2}} + b'(T) I + c'(T) I^2 + d'(T) I^3 \quad (28)$$

where  $\gamma_{\pm}(T, I)$  represents the stoichiometric mean activity coefficient at temperature  $T$  and stoichiometric ionic strength  $I$ ,  $a'(T)$ ,  $b'(T)$ ,  $c'(T)$ , and  $d'(T)$  are temperature-dependent coefficients,  $Z$  is the charge on the subscripted cation (1) and anion (2), and  $A(T)$  is the Debye-Hückel parameter defined below by equation (39).

The stoichiometric mean activity coefficient of NaCl is related to the stoichiometric osmotic coefficient ( $\phi$ ) by

$$\phi(T, I) = 1 + \frac{1}{I} \int_0^I I d \ln \gamma_{\pm}(T, I) \quad (29)$$

Equation (29) can also be written as

$$\phi(T, I) = 1 + \ln \gamma_{\pm}(T, I) - \frac{1}{I} \int_0^I \ln \gamma_{\pm}(T, I) dI \quad (30)$$

and integrated with the aid of equation (28) to give the following power function for the stoichiometric osmotic coefficient:

$$\phi(T, I) = 1 - \frac{2.303 A(T) |Z_1 Z_2|}{a'^3(T) I} \left[ (1 + a'(T) I^{1/2}) - 2 \ln(1 + a'(T) I^{1/2}) - \frac{1}{1 + a'(T) I^{1/2}} \right] + \frac{b'(T) I}{2} + \frac{2c'(T) I^2}{3} + \frac{3d'(T) I^3}{4} \quad (31)$$

The values of the power series coefficients defined by the fits of the osmotic coefficients of NaCl with equation (31) were used in equation (28) to calculate the stoichiometric mean activity coefficients shown in table 2. Because experimental osmotic coefficients are available for NaCl at only three concentrations above 100°C (table 2), the  $d'$  coefficient was set to zero in the least squares fits.<sup>3</sup>

*Calculations providing for complexing.*—The stoichiometric mean activity coefficient of sodium chloride at a given temperature is related to the mean ionic activity coefficient ( $\gamma^*_{\pm}$ ) by

$$\gamma_{\pm \text{NaCl}} = (1 - \alpha_{\text{NaCl}}) \gamma^*_{\pm \text{NaCl}} \quad (32)$$

<sup>3</sup> Since these calculations were carried out, Lindsay and Liu (1968) have presented osmotic coefficient data for NaCl at concentration intervals of 0.1  $m$  from 0.05 to 3.50  $m$  and temperatures from 125°C to 300°C. Least squares fits of their data yield activity coefficients in close agreement with those computed above.

in which  $\alpha_{\text{NaCl}}$  is the degree of association of the solute, defined by

$$\alpha_{\text{NaCl}} = \frac{m_{\text{NaCl}}}{m_{t,\text{NaCl}}} \quad (33)$$

where  $m_{\text{NaCl}}$  is the molality of the complex and  $m_{t,\text{NaCl}}$  is the stoichiometric (total) molality of the salt. Combining equation (33) with the Law of Mass Action for the dissociation of NaCl leads to

$$\alpha_{\text{NaCl}} = \frac{\gamma_{\pm}^2 m_{t,\text{NaCl}}}{K_{\text{NaCl}} \gamma_{\text{NaCl}}} \quad (34)$$

where  $K_{\text{NaCl}}$  and  $\gamma_{\text{NaCl}}$  are, respectively, the dissociation constant and activity coefficient of the complex. Equation (34) can be used to compute values of  $\alpha_{\text{NaCl}}$  (and consequently values of  $\gamma_{\pm}^*$ —eq 32) from stoichiometric mean activity coefficients if dissociation constants and activity coefficients for the complex are known.

Although sodium chloride solutions are essentially completely dissociated at low temperatures, above  $\sim 200^\circ\text{C}$  this is no longer true. Experi-

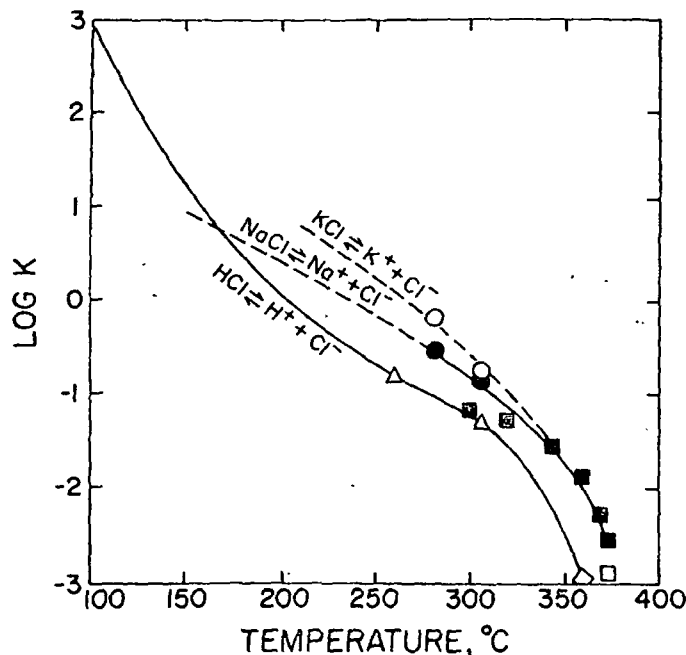


Fig. 2. Dissociation constants for NaCl, KCl, and HCl at high temperatures (see table 4). Open circle = KCl—Wright, Lindsay, and Druga (1961) after Noyes (1907); filled circle = NaCl—Wright, Lindsay, and Druga (1961) after Noyes (1907); triangle = HCl—Wright, Lindsay, and Druga (1961) after Noyes (1907); open square = KCl—extrapolated from supercritical data (Franck, 1961); filled square = NaCl—Pearson, Copeland, and Benson (1963a); diamond = HCl—Pearson, Copeland, and Benson (1963b). The smooth curve for HCl is based on a least squares fit of low and high temperature  $\log K(T)$  values (Helgeson, 1967a) using equation (17), but those for KCl and NaCl are based on simple interpolation. The dissociation constants plotted above are consistent with molal units of concentration.

mental dissociation constants for aqueous NaCl below  $281^\circ\text{C}$  are not available; those reported in the literature for higher (but subcritical)\* temperatures are plotted together with comparative values of  $\log K(T)$  for KCl and HCl in figure 2. Calculated degrees of association and mean ionic activity coefficients for sodium chloride at elevated temperatures are given in table 2. The values shown in table 2 for these parameters were computed from equations (32) and (34) using extrapolated values of  $K_{\text{NaCl}}$  (table 2)<sup>5</sup>. The extrapolated dissociation constants are those corresponding to the dashed curve for NaCl in figure 2. The activity coefficient of the complex was represented in the calculations by  $\gamma_{\text{CO}_2}$  in NaCl solutions (table 2). Values of  $\gamma_{\text{CO}_2}$  were computed from Henry's law coefficients (Ellis and Golding, 1963) by evaluating (for each temperature and molality of sodium chloride)

$$\gamma_{\text{CO}_2} = k_{m_i}/k \quad (35)$$

where  $k$  and  $k_{m_i}$  are the Henry's law coefficients in pure water and in a sodium chloride solution of total molality,  $m_t$ . Because Henry's law coefficients are not available for concentrations of NaCl over 2 molal at high temperatures, extrapolations of  $\gamma_{\text{CO}_2}$  were also necessary. These extrapolations were accomplished for each temperature with the aid of an empirical equation, which can be written in general notation as

$$\gamma_{\xi} = 10^{\sigma \bar{I}} \quad (36)$$

where  $\gamma_{\xi}$  is the activity coefficient of a neutral complex,  $\sigma$  is the slope constant on semi-logarithmic coordinates, and  $\bar{I}$  is the true ionic strength of the solution. The true ionic strength of a sodium chloride solution is given by

$$\bar{I} = \frac{1}{2} \sum_i Z_i^2 m_i = (1 - \alpha_{\text{NaCl}}) I \quad (37)$$

where  $i$  designates the charged species in solution and  $I$  is the stoichiometric ionic strength (equiv. to  $m_{t,\text{NaCl}}$ ).

Equation (36) closely approximates the activity coefficients of a large number of molecular species in aqueous electrolyte solutions at  $25^\circ\text{C}$  (Randall and Failey, 1927a-c), and it also describes  $\gamma_{\text{CO}_2}$  in NaCl solutions up to 2  $m$  at high temperatures (Helgeson, 1967b; Helgeson and James, 1968). Because the activity coefficients of different molecular species in a given salt solution are similar (Randall and Failey, 1927a-c),

\* Supercritical dissociation constants for NaCl over a wide range of temperature and pressure are also now available (Quist and Marshall, 1968a).

<sup>5</sup> At present, there is little alternative to graphic extrapolation of high temperature  $\log K(T)$  data to obtain estimates below  $281^\circ\text{C}$ . The uncertainties in the high temperature data are sufficiently large to preclude definitive least squares fits using theoretical  $\log K(T)$  expressions (Helgeson, 1967a). Attempts to obtain values of  $\log K_{\text{NaCl}}$  and  $\gamma_{\text{NaCl}}$  from least squares fits of the stoichiometric activity coefficients using equations providing for complexing have been only partly successful owing to the limited data available for the temperature range where NaCl associates to a significant degree (Helgeson and James, 1968).

TABLE 2  
Thermodynamic properties of concentrated sodium chloride solutions at elevated temperatures<sup>1</sup>

	$m_i, \text{NaCl}$	Temperature, °C							
		25°	50°	100°	150°	200°	250°	270°	300°
Osmotic coefficient ( $\phi_{\text{NaCl}}$ ) <sup>a</sup>	1.0	0.935	0.940	0.935	0.900	0.855	0.797	0.769 <sup>m</sup>	
	2.0	0.983	0.996	0.986	0.953	0.900	0.824	0.786	
	3.0	1.045	1.059	1.048	0.991	0.920	0.832	0.784 <sup>m</sup>	
Stoichiometric mean activity coefficient ( $\gamma_{\pm, \text{NaCl}}$ ) <sup>b</sup>	1.0	0.656	0.656	0.622	0.532	0.443	0.356	0.318	0.25 <sup>p</sup>
	2.0	0.670	0.678	0.641	0.532	0.425	0.320	0.277	0.22 <sup>p</sup>
	3.0	0.719	0.728	0.687	0.546	0.419	0.301	0.254	0.20 <sup>p</sup>
Standard state dissociation constant ( $K_{\text{NaCl}}$ )					9.4 <sup>c</sup>	2.63 <sup>c</sup>	0.71 <sup>c</sup>	0.40 <sup>c</sup>	0.15 <sup>m</sup>
Degree of association ( $\alpha_{\text{NaCl}}$ ) <sup>d</sup>	1.0	0.00	0.00	0.00	0.025	0.061	0.133	0.178	0.29 <sup>p</sup>
	2.0	0.00	0.00	0.00	0.043	0.093	0.173	0.209	0.32 <sup>p</sup>
	3.0	0.00	0.00	0.00	0.056	0.115	0.206	0.238	0.34 <sup>p</sup>
True ionic strength ( $\bar{I}_{\text{NaCl}}$ ) <sup>e</sup>	1.0	1.0	1.0	1.0	0.975	0.939	0.867	0.822	0.71
	2.0	2.0	2.0	2.0	1.914	1.814	1.654	1.582	1.36
	3.0	3.0	3.0	3.0	2.832	2.655	2.382	2.286	1.98
Mean ionic activity coefficient ( $\gamma_{\pm, \text{NaCl}}$ ) <sup>f</sup>	1.0	0.656	0.656	0.622	0.546	0.472	0.410	0.387	0.36 <sup>g</sup>
	2.0	0.670	0.678	0.641	0.556	0.468	0.387	0.349	0.32 <sup>g</sup>
	3.0	0.719	0.728	0.687	0.578	0.473	0.379	0.333	0.30 <sup>g</sup>
Debye-Hückel activity coefficient ( $\gamma_{\pm, \text{NaCl, D.-H.}}$ ) <sup>h</sup>	1.0	0.599	0.598	0.566	0.497	0.429	0.384	0.388	0.36
	2.0	0.556	0.556	0.524	0.449	0.378	0.335	0.330	0.32
	3.0	0.534	0.535	0.503	0.425	0.352	0.311	0.308	0.30
Deviation function (B) <sup>h</sup>		0.041	0.043 <sub>k</sub>	0.046	0.047 <sub>k</sub>	0.047 <sup>i</sup>	0.034	0.015	0.0 <sup>n</sup>
Activity coefficient of carbon dioxide in NaCl solutions ( $\gamma_{\text{CO}_2}$ ) <sup>j</sup>	1.0	1.27	1.24	1.20	1.19	1.23	1.34	1.42 <sup>m</sup>	1.50
	2.0	1.57	1.50	1.44	1.40	1.47	1.67	1.83 <sup>m</sup>	2.00
	3.0	1.93	1.80	1.74 <sup>n</sup>	1.70 <sup>n</sup>	1.74 <sup>n</sup>	1.86 <sup>n</sup>	2.03 <sup>n</sup>	2.29 <sup>n</sup>

Activity of water ( $a_w$ ) <sup>j</sup>	1.0	0.9669 <sup>l</sup>	0.9667	0.9669	0.968	0.970	0.972	0.973	
	2.0	0.9316 <sup>l</sup>	0.9308	0.9315	0.934	0.937	0.942	0.945	
	3.0	0.8932 <sup>l</sup>	0.8919	0.8930	0.898	0.905	0.914	0.919	
A (Debye-Hückel) <sup>k</sup>		0.5095	0.5354	0.6019	0.6915	0.8127	0.9907	1.0905	1.2979
B (Debye-Hückel) $\times 10^{-8k}$		0.3284	0.3329	0.3425	0.3536	0.3659	0.3807	0.3879	0.4010
$\beta$ (Debye-Hückel term in the Stokes-Robinson expression—eq 41)		3.94 <sup>r</sup>	4.19 <sup>r</sup>						
		3.89 <sup>n</sup>	4.20 <sup>n</sup>	4.19 <sup>n</sup>	3.58 <sup>n</sup>	3.22 <sup>n</sup>	3.43 <sup>n</sup>	3.79 <sup>n</sup>	4.4 <sup>n</sup>
$h$ (hydration parameter—eq 41)		3.61 <sup>r</sup>	3.70 <sup>r</sup>						
		3.67 <sup>n</sup>	3.69 <sup>n</sup>	3.90 <sup>m</sup>	4.01 <sup>n</sup>	4.22 <sup>n</sup>	3.61 <sup>n</sup>	2.22 <sup>n</sup>	1.2 <sup>n</sup>

<sup>a</sup> Values at 25° and 100° are from Robinson and Stokes (1959), at 50° from Harned (1961), and at 150° and above from Gardner, Jones, and de Nordwall (1963). <sup>b</sup> The values at 25°, 50°, and 100° were taken from Harned and Owen (1958); for 150° to 270°, the values were computed from equation (28) after performing least squares fits of the osmotic coefficients using equation (31). <sup>c</sup> Extrapolated from higher temperature data (fig. 2). The values of K are consistent with molal units of concentration. <sup>d</sup> Computed from the stoichiometric activity coefficients, dissociation constants, and values of  $\gamma_{\text{CO}_2}$  in NaCl solutions (to represent  $\gamma_{\text{NaCl}}$ ) using equation (34). <sup>e</sup> Computed from the degrees of association using equation (37). <sup>f</sup> Computed from the degrees of association and the stoichiometric activity coefficients using equation (32). <sup>g</sup> Computed from  $\log \gamma_{\pm, \text{D.-H.}}$  ( $T, \bar{I} = -A(T) | Z_+ Z_- | \bar{I}^{1/2} / (1 + \beta(T)B(T)\bar{I}^{1/2})$ ) using the values of  $\beta(T)$ ,  $A(T)$ ,  $B(T)$ , and  $\bar{I}$  given above. <sup>h</sup> Smoothed (fig. 3) values computed (using eq 38) from the mean ionic activity coefficients and those calculated from the Debye-Hückel equation<sup>h</sup>. <sup>i</sup> Computed (using eq 35) from Henry's Law coefficients for CO<sub>2</sub> in water and NaCl solutions at elevated temperatures (Ellis and Golding, 1963). <sup>j</sup> Computed from the osmotic coefficients using equation (42). <sup>k</sup> Computed (Helgeson, 1967b) from equations (39) and (40) using density and dielectric constant data for water taken, respectively, from Keenan and Keyes (1936) and Akerlof and Oshry (1950). <sup>l</sup> Robinson and Stokes (1959). <sup>m</sup> Interpolated. <sup>n</sup> Extrapolated. <sup>p</sup> Computed from the values of  $K_{\text{NaCl}}$ ,  $\gamma_{\text{CO}_2}$  in NaCl solutions (to represent  $\gamma_{\text{NaCl}}$ ), and extrapolated values of the mean ionic activity coefficient (eqs 32 and 34). <sup>q</sup> Calculated from least squares fits of the mean ionic activity coefficients in the concentration range 1.0 to 3.0 m using the Stokes-Robinson equation (eq 41). <sup>r</sup> Obtained from least squares fits (eq 41) in the concentration range 0.1 to 3.0 m. <sup>s</sup> Computed from the Stokes-Robinson equation (eq 41) using the values of  $A(T)$ ,  $B(T)$ ,  $\bar{I}$ ,  $B(T)$ , and the extrapolated mean ionic activity coefficients shown above. <sup>t</sup> All values given in this table are consistent with molal units of concentration.



the assumption that  $\gamma_{\text{NaCl}} \approx \gamma_{\text{CO}_2}$  in NaCl solutions probably introduces negligible error into mean ionic activity coefficient calculations.

*Deviation function.*—The departure of the log of the mean ionic activity coefficient from that predicted by the Debye-Hückel expression at 25°C has been described by Scatchard (1936) and others with a deviation function. Pitzer and Brewer (1961) designate this function with the symbol  $B'$  to distinguish it from the limiting function at zero concentration. The deviation function at a given temperature can be defined by writing

$$B'(\bar{I}) = \frac{\log \gamma_{\pm}^* + A|Z_1 Z_2| \bar{I}^{1/2} / (1 + \bar{a} B \bar{I}^{1/2})}{\bar{I}} \quad (38)$$

in which  $\bar{a}$  is the "distance of closest approach" of the ions in solution, and A and B are the molal Debye-Hückel coefficients given by

$$A(T) = \frac{1.8246 \times 10^6 (\rho_{\text{H}_2\text{O}}(T))^{1/2}}{(\epsilon_{\text{H}_2\text{O}}(T) T)^{3/2}} \quad (39)$$

and

$$B(T) = \frac{50.29 \times 10^3 (\rho_{\text{H}_2\text{O}}(T))^{1/2}}{(\epsilon_{\text{H}_2\text{O}}(T) T)^{1/2}} \quad (40)$$

where  $\rho_{\text{H}_2\text{O}}$  is the density, and  $\epsilon_{\text{H}_2\text{O}}$  the dielectric constant of water at temperature T. Values of the A and B coefficients in equation (38) at 10 degree intervals from 25° to 350°C have been presented elsewhere (Helgeson, 1967b).

The definition of the deviation function expressed by equation (38) differs somewhat from that used previously by Scatchard (1936), Pitzer and Brewer (1961), and others to analyze the behavior of electrolyte solutions at low temperatures. The function employed by these investigators is defined by an expression of equation (38) in which stoichiometric ionic strength is used, and the product  $\bar{a}B$  is set to unity. Although this simplification is useful for considering the behavior of electrolyte solutions at low temperatures, it is desirable to include explicit provision for  $\bar{a}$  and true ionic strength in calculations of  $B'$  at high temperatures.

The deviation function,  $B'$ , is essentially independent of concentration at ionic strengths of  $\sim 0.5$  or more in most electrolyte solutions at 25°C. Cobble (1964) assumed this function to be temperature independent as well, and he employed 25°C values of  $B'$  to calculate high temperature activity coefficients. It is shown below that Cobble's assumption is invalid for concentrated sodium chloride solutions at elevated temperatures.

Prediction of the deviation function for high temperature sodium chloride solutions requires values of the Debye-Hückel  $\bar{a}$  parameter at each temperature. Because of the high sensitivity of the deviation function to small errors in the  $\bar{a}$  values used in the equation, this parameter

must be known accurately in order to define adequately the temperature dependence of the deviation function. The required values of  $\bar{a}$  were obtained by fitting the mean ionic activity coefficients in table 2 with a least squares computer routine involving the Stokes-Robinson equation (Stokes and Robinson, 1948; Robinson and Stokes, 1959).

The Stokes-Robinson equation closely describes the concentration dependence of the mean ionic activity coefficients of a large number of strong electrolytes to high concentrations at 25°C. For a given electrolyte at temperature T and true ionic strength  $\bar{I}$ , this expression appears as

$$\log \gamma_{\pm}^*(T, \bar{I}) = - \frac{A(T) |Z_1 Z_2| \bar{I}^{1/2}}{1 + \bar{a}(T) B(T) \bar{I}^{1/2}} - \frac{h(T)}{\nu} \log a_w(T, \bar{I}) - \log [1 - 0.018m(\nu - h(T))] \quad (41)$$

in which  $a_w$  is the activity of  $\text{H}_2\text{O}$ ,  $m$  is the molality of the completely dissociated solute (equivalent to  $\bar{I}$  in the case of NaCl),  $\bar{a}$  is the "distance of closest approach" of the ions in solution,  $\nu$  is the number of ions per mole of solute, and  $h$  is the average number of water molecules coordinated to  $\nu$  ions in solution. The Stokes-Robinson equation provides for the effects of ion hydration on the activity coefficient of the solute. It can be derived rigorously from equations describing the Gibbs free energy of the solution in terms of the chemical potentials of  $\text{H}_2\text{O}$  and the hydrated and unhydrated solute. Two assumptions are involved in the derivation: (1) that the coefficient  $h$  is independent of concentration, and (2) that the Debye-Hückel term in the equation accurately describes the part of the departure of activity from molality due to electrostatic interaction of the solvated ions. The excellent fits obtained by Stokes and Robinson (1948) of observed activity coefficients in a large number of concentrated electrolytes at 25°C suggest that these assumptions are valid.

Equation (41) was used to compute least squares fits of the mean ionic activity coefficients for sodium chloride solutions shown in table 2 (Helgeson and James, 1968). The values of  $\bar{I}$  in equation (41) were computed from equation (37) using the degrees of association ( $\alpha_{\text{NaCl}}$ ) given in table 2. The activities of water employed in the calculation were computed from the stoichiometric osmotic coefficient ( $\phi$ ) for each temperature and total concentration of NaCl ( $m_t$ ) by evaluating

$$\ln a_w = - \frac{\nu m_t \phi}{55.55} \quad (42)$$

The osmotic coefficients and computed activities of water are given in table 2 along with the values of  $\bar{a}(T)$  and  $h(T)$  for NaCl obtained from the least squares fits. The deviation functions calculated (eq 38) from the  $\bar{a}$  and  $\gamma_{\pm}^*$  values are also shown in table 2.

It can be seen in figure 3 that  $B'_{\text{NaCl}}$  passes through a maximum with increasing temperature, but that at each temperature  $B'_{\text{NaCl}}$  is only slightly dependent on concentration at molalities of NaCl between one and three. The maximum variation in  $B'_{\text{NaCl}}$  with concentration in the

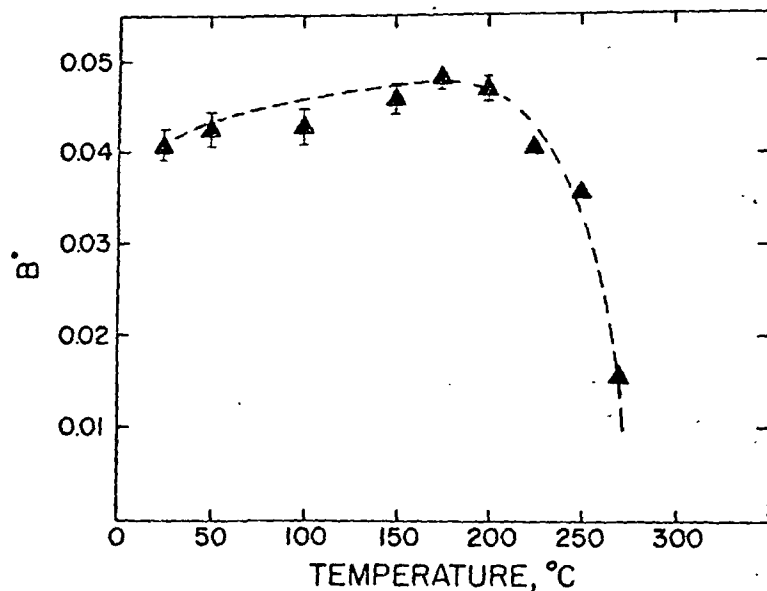


Fig. 3. Plot of the deviation function,  $B'$ , against temperature for 1, 2, and 3 molal NaCl solutions. The symbols represent the mean values of  $B'$  at each temperature computed from equation (38); the vertical bars on the symbols depict the maximum variation in  $B'$  in 1 to 3 molal solutions. Where no vertical bar is shown, the maximum variation is within the limits of the symbol.

range 1.0 to 3.0  $m_{\text{NaCl}}$  from 25° to 270°C is  $\pm 0.002$  from the values represented by the symbols in figure 3; this variation represents a slight increase in  $B'$  with increasing concentration. However, it can be seen in figure 3 that the uncertainty in the data from which the  $B'$  values were calculated exceeds the extent of this variation. Although mean ionic activity coefficients for NaCl are not available above 270°C (see footnote 3, p. 743), it appears likely that  $B'$  approaches zero in the region of 300°C.  $B'$  also becomes small in HCl solutions at high temperatures (Helgeson and James, 1968). The behavior of  $B'$  in figure 3 suggests that the simple Debye-Hückel expression in the Stokes-Robinson equation for  $\gamma_{\pm}^*$  (eq 41) is sufficient to describe the mean ionic activity coefficient of NaCl in 1 to 3 molal solutions in the region of 300°C. This is not surprising because the hydration entropies of ions at 25°C are relatively large negative numbers that would be expected to become substantially less negative with increasing temperature, and the bulk of the solute in sodium chloride solutions is associated above 300°C.

From a practical standpoint, the fact that the Debye-Hückel expression can be used to predict accurately mean ionic activity coefficients in concentrated electrolytes at high temperatures is extremely useful. Note, however, that such calculations are valid only when true (and not stoichiometric) ionic strength is used in the equation. It can be demonstrated that the product  $\bar{a}B$  (where  $B$  is the Debye-Hückel co-

efficient) for NaCl solutions is essentially independent of temperature from 25° to 270°C. Also,  $B'$  is closely related to  $\gamma_{\text{CO}_2}$  in NaCl solutions, which is reflected by the relative success of the Delta approximation (Helgeson, 1964) in predicting activity coefficients at elevated temperatures. Various theoretical implications of the behavior of  $\gamma_{\text{CO}_2}$ ,  $\gamma_{\pm}^*$ ,  $\bar{a}$ ,  $h$ , and  $B'$  for NaCl solutions and other electrolytes at elevated temperatures together with empirical correlations of these parameters with thermodynamic variables have been considered in detail elsewhere (Helgeson and James, 1968).

*True individual ion activity coefficients.*—In the derivation of the Stokes-Robinson equation (eq 41), the departure of activity from molality for the completely dissociated solute over and above that described by the Debye-Hückel term for the solvated ions is attributed to ion hydration; that is, as the concentration of the solute increases at a given temperature, the product  $B'\bar{I}$ , which is numerically equivalent to the sum of the second and third terms on the right side of the Stokes-Robinson equation, is a function only of the decrease in the number of uncoordinated solvent molecules per 1000 g. of water. At constant concentration in sodium chloride solutions of 1 to 3 molal, the number of uncoordinated water molecules apparently first decreases and then increases with increasing temperature above 25°C.

In a concentrated multicomponent electrolyte solution consisting predominantly of sodium chloride, ions present in small concentrations (compared to that of the sodium chloride) should contribute negligibly to the ionic strength and total coordination of water molecules in the solution. In such an electrolyte, close approximations of individual ion activity coefficients for the species present in small concentrations can be calculated from

$$\log \gamma_{i}^*(T, \bar{I}) = \frac{-A(T)Z_i^2 \bar{I}^{1/2}}{1 + \bar{a}_i(T)B(T)\bar{I}^{1/2}} + B'(T)\bar{I} \quad (43)$$

where  $\gamma_{i}^*$  is the activity coefficient of the  $i$ th ion present in small concentrations in the solution,  $\bar{I}$  and  $B'$  are the true ionic strength and deviation functions, respectively, for pure solutions of the supporting electrolyte, and  $\bar{a}_i$  refers to the "distance of closest approach" of the  $i$ th ion. Equation (43) can also be written for mean ionic activity coefficients of salts present in small concentrations in a sodium chloride solution. This requires only that the relation

$$\gamma_{\pm}^* = \left( \gamma_{+}^{*v_{+}} \gamma_{-}^{*v_{-}} \right)^{1/v} \quad (44)$$

be satisfied for the dissociated part of the salt in question.

Provided appropriate  $\bar{a}$  values are known for each temperature, equation (43) and the data in table 2 permit calculation of activity coefficients of ions present in small concentrations in sodium chloride solutions at high temperatures and concentrations of NaCl. Unfortunately, values of  $\bar{a}$  for most ions at high temperatures are not available, nor

can they be calculated with confidence. It appears that the best approximation that can be made in the present state of knowledge is to assume that  $\bar{a}$  coefficients for ions are independent of temperature and employ the values at 25°C in calculations of high temperature activity coefficients from equation (43). It can be seen in table 2 that  $\bar{a}$  for NaCl solutions from 25° to 300°C varies between -0.7 and 0.5 angstroms from its value at 25°C. If the  $\bar{a}$  values for other salts behave in a similar fashion, the error involved in calculating high temperature activity coefficients by assuming  $\bar{a}$  values at 25°C to be constant should be negligible compared to other uncertainties attending geochemical calculations. On the other hand, if the temperature variation of  $\bar{a}$  coefficients for other salts is similar to that exhibited by the  $\bar{a}$  for HCl, the error may be substantial at high temperatures. The  $\bar{a}$  coefficient for HCl is essentially constant from 25° to 150°C, but it increases rapidly with increasing temperature between 150° and 275°C (Helgeson and James, 1968). Nevertheless, it appears likely that the temperature dependence of  $\bar{a}$  coefficients for metal ions and metal ion complexes will prove to be more like NaCl than HCl.

Because  $\bar{a}$  coefficients tend to increase at high temperatures, high temperature activity coefficients computed from equation (43) assuming constant  $\bar{a}$  values equal to their values at 25°C should be minimal approximations. Where such approximations render individual ion activity coefficients less than  $\sim 0.1$ , the effect of small errors in the activity coefficients on calculations of solution equilibria may be large. For this reason, approximations of individual ion activity coefficients at high temperatures and concentrations of sodium chloride should be confined to monovalent and possibly divalent species. Predictions of high temperature activity coefficients in concentrated solutions of mixed electrolytes in which more than  $\sim 20$  percent of the solute is not sodium chloride requires use of Harned's rule coefficients or coefficients for a similar but higher order power function (Lietzke, Hupf, and Stoughton, 1965; Helgeson, 1967b).

*Stoichiometric individual ion activity coefficients.*—Calculations of high temperature mineral solubilities in concentrated hydrothermal solutions in which the solute is predominately sodium chloride can be simplified considerably by first computing stoichiometric individual ion activity coefficients for the solution. The stoichiometric individual ion activity coefficient,  $\dot{\gamma}_i$ , is defined as

$$\dot{\gamma}_i = \frac{a_i}{m_{i,i}} \quad (45)$$

where  $a_i$  and  $m_{i,i}$  designate the activity and total molality of the  $i$ th ion present in small concentrations in the sodium chloride solution. Garrels and Thompson (1962) used the symbol  $\gamma_T$  for stoichiometric individual ion activity coefficients. The  $\gamma_T$  used by Garrels and Thompson differs from the  $\dot{\gamma}_i$  in equation (45) only to the extent that the latter specifically refers to the presence of the  $i$ th ion in an electrolyte solution containing a predominant concentration of some other salt.

Values of  $\dot{\gamma}_i$  can be calculated for a given temperature and concentration of sodium chloride (or some other supporting electrolyte) by evaluating one of several possible mass balance relations that can be written for the  $i$ th ion, depending on its identity. For example, if  $\text{C}$  represents a cation associated in a series of  $z$  mononuclear complexes involving  $y$  moles of anion L ( $y = 1, 2, 3, \dots, z$ ), we can write

$$m_{i,\text{C}} = m_{\text{C}} + \sum_y^z m_y \quad (46)$$

where  $m_{\text{C}}$  and  $m_y$  are the molalities, respectively, of cation C and the  $y$ th complex, which has the form  $\text{CL}_y$ . Expressing equation (46) in terms of activities leads to

$$m_{i,\text{C}} = \frac{a_{\text{C}}}{\gamma_{\text{C}}^*} + \sum_y^z \frac{a_{\text{C}} a_{\text{L}}^y}{\beta_y \gamma_y} = a_{\text{C}} \left( \frac{1}{\gamma_{\text{C}}^*} + \sum_y^z \frac{a_{\text{L}}^y}{\beta_y \gamma_y} \right) \quad (47)$$

where  $\gamma_y$  is the activity coefficient of the  $y$ th complex,  $a_{\text{C}}$  and  $a_{\text{L}}$  are the activities of the cation and anion, respectively,  $\gamma^*$  represents the true individual ion activity coefficient of the subscripted species, and  $\beta_y$  is the overall dissociation constant for the  $y$ th complex defined as

$$\beta_y = \prod_u^y K_u \quad (48)$$

where  $u$  is an integer index ( $u = 1, 2, 3, \dots, y$ ) and  $K_u$  represents the stepwise dissociation constant for the  $u$ th complex. Combining equations (45) and (47) leads to

$$\dot{\gamma}_{\text{C}} = \frac{1}{\frac{1}{\gamma_{\text{C}}^*} + \sum_y^z \frac{a_{\text{L}}^y}{\beta_y \gamma_y}} = \frac{1}{\frac{1}{\gamma_{\text{C}}^*} + \sum_y^z \frac{m_{\text{L}}^y \gamma_{\text{L}}^*}{\beta_y \gamma_y}} \quad (49)$$

If the total molality ( $m_i$ ) of cation C is small compared to that of sodium chloride, the values of  $\gamma_{\text{C}}^*$  and  $\gamma_{\text{L}}^*$  (and  $\gamma_y$  when the  $y$ th complex is a charged species) in equation (49) can be calculated from equation (43). The values of  $\bar{I}$  and  $B'$  used in the calculations are those obtained from equations (37) and (38) for the supporting electrolyte; the  $\beta$  values in equation (49) can be predicted from the thermodynamic relations discussed above. If the  $y$ th complex is a nonpolar neutral species,  $\gamma_y$  can be approximated as  $\gamma_{\text{CO}_2}$ ; if it is more like  $\text{H}_4\text{SiO}_4$ ,  $\gamma_y$  can be regarded as unity (Helgeson, 1964; 1967b). Where the ligand involved is chloride in a concentrated sodium chloride solution containing small concentrations of other species, the mean ionic activity of sodium chloride in a pure sodium chloride solution can be used as a close approximation of  $a_{\text{L}}$ . In such cases,  $m_{\text{L}}^y \gamma_{\text{L}}^*$  in equation (49) can be replaced by  $m_{\text{L,NaCl}} \gamma_{\text{NaCl}}$  and (because  $\gamma_{\pm\text{NaCl}}$  is known—table 2)  $\dot{\gamma}_{\text{C}}$  can then be computed as

a function of  $m_{t,NaCl}$ . Where L does not correspond to  $Cl^-$ ,  $\gamma_C$  can be calculated as a function of  $m_L$ . In many cases  $m_L$  in hydrothermal solutions can be approximated as  $m_{t,L}$ .

Expressions analogous to equations (46) to (49) can be derived to calculate values of  $\gamma_L$ . Such expressions are particularly useful where the anion L is associated predominantly with the hydrogen ion. Under these conditions,  $\gamma_L$  can be computed as a function of pH. By rearranging equation (45), precomputed values of  $\gamma_C$  and  $\gamma_L$  permit calculation of the activities of the free C and L ions in concentrated hydrothermal solutions directly from analytical data. Consequently, hydrothermal mineral solubilities can be predicted without further consideration of complexes in solution; that is, provided all important complexes are included in the calculations of the  $\gamma_C$  and  $\gamma_L$  values.

#### Solubility Calculations

By specifying values for such variables as pH and the total molality of NaCl in concentrated sodium chloride solutions at a particular temperature, values of  $\gamma$  for  $S^{--}$ ,  $SO_4^{--}$ ,  $CO_3^{--}$ ,  $Ag^+$ ,  $Fe^{+++}$ ,  $Cu^{++}$ , and other ions that may be present in small concentrations in hydrothermal solutions can be calculated from expressions of equation (49) or the corresponding equation for anions. Provided these calculations include provision for a realistic distribution of aqueous species, the solubility of a given mineral in the solution can then be computed from the activity product relation,

$$m_{t,i}^n m_{t,\hat{e}}^v \gamma_i^n \gamma_{\hat{e}}^v = K_{sp,\psi} \quad (50)$$

where  $K_{sp,\psi}$  is the activity product constant of the  $\psi$ th mineral, which consists of  $n$  moles of the  $i$ th cation and  $v$  moles of the  $\hat{e}$ th anion in the system. The stoichiometric solubility (where  $vm_{t,i} = nm_{t,\hat{e}}$ ) is then given by

$$S_{\psi} = \frac{m_{t,i}}{n} = \frac{1}{n} \left( \frac{n^v K_{sp,\psi}}{v^v \gamma_i^n \gamma_{\hat{e}}^v} \right)^{1/(n+v)} \quad (51)$$

in which  $S_{\psi}$  is the solubility (in molality units) of the  $\psi$ th phase. If  $m_{t,\hat{e}}$  (the total molality of the  $\hat{e}$ th anion) is specified, non stoichiometric solubilities can be computed from

$$S_{\psi} = \frac{m_{t,i}}{n} = \frac{1}{n} \left( \frac{K_{sp,\psi}}{m_{t,\hat{e}}^v \gamma_i^n \gamma_{\hat{e}}^v} \right)^{1/n} \quad (52)$$

If more than one solid phase is in equilibrium with the solution, expressions analogous to equations (51) and (52) can be derived by combining statements of equation (50) for each solid and writing a mass balance expression relating the total molalities of each cation in solution. The mutual solubilities of the minerals in the solution can then be computed from these equations.

#### Pressure as a Variable

As indicated earlier, the pressure dependence of equilibrium constants for most hydrothermal reactions is slight (considered negligible in this discussion) at temperatures below  $\sim 300^\circ C$ . This is true for solid phase equilibria even at much higher temperatures, but for dissociational reactions in aqueous solution, pressure effects become significant as temperature increases above  $\sim 300^\circ C$ .

The need for a general method of computing equilibrium constants at high pressures and temperatures has become more acute in recent years. Experimental data for hydrothermal systems are frequently obtained at temperatures and pressures greater than  $300^\circ C$  and 1000 atm. The dependence of equilibrium constants on pressure is a volume function, but few ionic volumes are known for aqueous electrolytes at high temperatures and pressures, and those data that exist (Owen and Brinkley, 1941; Couture and Laidler, 1956; Zen, 1957; Hepler, 1965; Ellis, 1966, 1967, 1968) are rarely definitive with respect to the volumes of individual ions and complexes. Despite this handicap, the effect of pressure on dissociation constants in aqueous solutions of electrolytes can be closely approximated from the temperature and pressure dependence of the dielectric constant of water.

Consideration of the thermodynamic characteristics of dissociational reactions as a function of temperature suggests that the dielectric constant of water essentially controls the stabilities of complexes in aqueous solutions of electrolytes at high temperatures (Helgeson, 1967a). It can be shown that the conventional molal<sup>o</sup> dissociation constant for a neutral complex in the supercritical pressure-temperature region for water can be described within the uncertainty of the experimental data by a monotonic function of the dielectric constant of the solvent; that is, the molal  $\log K(T,P)$  for a given neutral complex is essentially a constant for all pressure-temperature combinations that result in the same value of the dielectric constant of water in the supercritical region. Data are not available to determine whether the same relation exists for charged complexes in the supercritical region, but theoretical considerations suggest that the stabilities of these species should also vary monotonically with the dielectric constant of the solvent.

\* The conventional dissociation constant does not provide explicitly for the participation of the solvent in the dissociational reaction. If the reaction is written to include the correct degree of participation by the solvent, then the *isothermal* dissociation constant becomes independent of the dielectric constant of the medium (Quist and Marshall, 1968b). Most supercritical dissociation constants reported in the literature are consistent with molar units of concentration (for example, Franck, 1961; Quist and Marshall, 1966, 1968a and c). These data can be converted to be consistent with molal units of concentration by solving  $\log K_m = \log K_M - (\bar{n} - 1) \log \rho_{H_2O}$ , where  $K_m$  and  $K_M$  are the molal and molar dissociation constants, respectively,  $\rho_{H_2O}$  represents the density of water, and  $\bar{n}$  is equal to the sum of the exponents in the Law of Mass Action equation for the dissociational reaction. Despite recent arguments to the contrary (Quist and Marshall, 1968a) dissociation constants consistent with molal units of concentration and the molal scale of concentration itself are perfectly appropriate for calculations pertaining to the supercritical region. Molal units of concentration are commonly more useful than molar units in geochemical calculations.

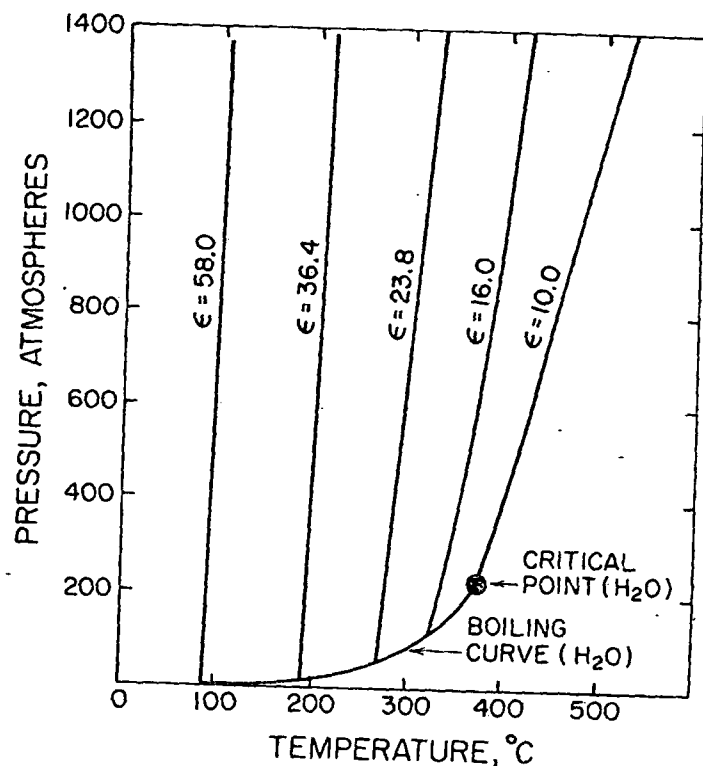
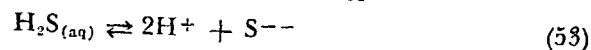


Fig. 4. Isodielectric curves for water in the liquid and supercritical phase regions. The curves were drawn from dielectric constant values taken from Quist and Marshall (1965) and density data for water obtained from Holser and Kennedy (1958).

Isodielectric curves for water are plotted in figure 4 to illustrate the order of magnitude of pressure effects on dissociation constants. For example, suppose that the molal dissociation constant for



at 1000 atm and 400°C is required for a given geochemical calculation. In figure 4 it can be seen that the dielectric constant of water under these conditions is the same as it is at 120 atm and 325°C on the boiling curve. Pressure effects contribute only slightly to dissociation constants calculated for a 1 atm standard state from high temperature experimental data obtained along the vapor + liquid pressure-temperature curve for water to ~325°C. For this reason, and also because appropriate ionic volumes are rarely available, the pressure correction (119 atm in this case) is commonly neglected, and the experimental log  $K(T)$  values obtained from such experiments are assigned to the 1 atm standard state. Because the molal value of log  $K(T)$  for the dissociation of a neutral complex in water at high temperatures is essentially constant along an isodielectric curve, the molal dissociation constant computed for 325°C

and 1 atm (or more accurately, 120 atm) is approximately equivalent to that at 400°C and 1000 atm.

The relation described above between log  $K(T,P)$  and the dielectric constant of the solvent is more useful for the purpose of estimating molal log  $K(T,P)$  values at high temperatures and pressures than density relations. This is true because log  $K(T,P)$  for a given reaction cannot be characterized as a single monotonic function of density at all pressure and temperature combinations contributing to constant density. On the other hand, isentropes for water are essentially coincident with the isodielectric curves shown in figure 4, which means that log  $K(T,P)$  can also be approximated as a monotonic function of the entropy of the solvent (Helgeson, 1964).

If a molar scale of concentration is used and the dissociational reaction is written to include the correct degree of solvation of the participating species in solution, the corresponding supercritical dissociation constant is independent of pressure (Quist and Marshall, 1968a). Consequently, these dissociation constants can be computed for any pressure-temperature condition solely from predictive equations involving temperature, such as those presented in the preceding pages. However, in practice this approach is usually precluded by the dearth of information concerning the actual extent of solvation (hydration numbers) of the various species in hydrothermal solutions at high temperatures.

#### COMPUTER CALCULATIONS AND RESULTS

The equations and methods of calculation summarized in the preceding pages have been programmed for machine computation. The results of calculations carried out with the aid of these computer programs are discussed below and presented in tables 1 to 14 and figures 5 to 21. The data employed in the calculations are also presented in the tables, along with references to the sources from which they were taken. In certain cases (noted in the footnotes in the tables) thermodynamic values reported in the literature have been changed (within the margins of uncertainty reported in the source references) to agree with other experimental and geologic observations, and estimates of thermodynamic properties are given for a number of species for which data are incomplete. The values listed in the tables are the result of a critical compilation, and they are intended to constitute an internally consistent array of thermodynamic data.

#### Dissociation Constants

Thermodynamic data at 25°C and 1 atm for various species and dissociational reactions of interest in hydrothermal studies are summarized in tables 3 and 4 along with calculated average heat capacities and log  $K(T)$  values for higher temperatures. The dissociation constants, which were computed from equations (11) to (17) using thermodynamic data given in tables 3 and 4, are also plotted in figure 5 to illustrate the changes in the stabilities of hydrothermal species with increasing temperature.

TABLE 3  
Thermodynamic data for species in aqueous solution at 25°C and 1 atm

Species	$\Delta H_f^\circ$ <sup>a</sup> (cal mole <sup>-1</sup> )	$S^\circ$ (cal mole <sup>-1</sup> deg <sup>-1</sup> )	Average heat capacity <sup>a</sup> (cal mole <sup>-1</sup> deg <sup>-1</sup> )					
			60°C	100°C	150°C	200°C	250°C	300°C
H <sub>2</sub> SiO <sub>4</sub>	-348,060 <sup>b</sup>	45.84 <sup>b</sup>	49 <sup>b</sup>	49 <sup>b</sup>	46 <sup>b</sup>	46 <sup>b</sup>	46 <sup>b</sup>	45 <sup>b</sup>
H <sub>2</sub> S	-9,030 <sup>c</sup>	30.9 <sup>d</sup>	46 <sup>m</sup>	39 <sup>m</sup>	35 <sup>m</sup>	32 <sup>m</sup>	33 <sup>n</sup>	35.5 <sup>n</sup>
HS <sup>-</sup>	-4,230 <sup>e</sup>	15.0 <sup>e</sup>	-52	-58	-62	-66	-70	-76
S <sup>2-</sup>	9,070 <sup>f</sup>	-4.0 <sup>e, f</sup>	-48	-58	-61	-65	-69	-75
SO <sub>4</sub> <sup>2-</sup>	-217,320 <sup>g</sup>	4.3 <sup>g</sup>	-99	-108	-105	-114	-120	-126
CO <sub>3</sub> <sup>2-</sup>	-161,840 <sup>g</sup>	-13.6 <sup>g</sup>	-132	-146	-138	-151	-162	-171
OH <sup>-</sup>	-54,970 <sup>g</sup>	-2.57 <sup>g</sup>	-47	-58	-61	-65	-69	-76
Cl <sup>-</sup>	-39,950 <sup>g</sup>	13.51 <sup>g</sup>	-51	-58	-62	-66	-70	-76
F <sup>-</sup>	-79,500 <sup>g</sup>	-3.3 <sup>g</sup>	-47	-58	-61	-65	-69	-75
H <sub>2</sub> O <sub>(l)</sub>	-68,315 <sup>g</sup>	16.71 <sup>g</sup>	18	18	18	18	18	18
H <sup>+</sup>	0.0	0.0	23	31	33	35	37	39
Ag <sup>+</sup>	25,310 <sup>h</sup>	17.69 <sup>h</sup>	30	39	39	43	45	47
Cu <sup>+</sup>	16,930 <sup>b</sup>	9.4 <sup>i</sup>	33	44	43	47	50	53
Cu <sup>2+</sup>	15,390 <sup>h</sup>	-23.6 <sup>h</sup>	49	65	66	71	75	79
Pb <sup>2+</sup>	-400 <sup>h</sup>	2.5 <sup>h</sup>	37	49	49	54	58	61
Zn <sup>2+</sup>	-36,780 <sup>h</sup>	-26.0 <sup>j, k</sup>	50	66	67	73	77	81
Hg <sup>2+</sup>	41,590 <sup>h</sup>	-5.4 <sup>j</sup>	41	54	55	60	63	67
Fe <sup>2+</sup>	-21,000 <sup>h</sup>	-27.1 <sup>h</sup>	50	66	68	73	78	82

Species	$\Delta H_f^\circ$ <sup>a</sup> (cal mole <sup>-1</sup> )	$S^\circ$ (cal mole <sup>-1</sup> deg <sup>-1</sup> )	Average heat capacity <sup>a</sup> (cal mole <sup>-1</sup> deg <sup>-1</sup> )					
			60°C	100°C	150°C	200°C	250°C	300°C
Fe <sup>3+</sup>	-11,400 <sup>h</sup>	-70.1 <sup>h</sup>	70	93	96	105	109	115
Ca <sup>2+</sup>	-129,770 <sup>h</sup>	-13.2 <sup>h</sup>	45	59	60	66	68	72
Mg <sup>2+</sup>	-110,410 <sup>h</sup>	-28.2 <sup>h</sup>	51	67	69	75	79	83
Ba <sup>2+</sup>	-128,670 <sup>h</sup>	3.0 <sup>h</sup>	38	50	50	55	58	61
K <sup>+</sup>	-60,040 <sup>h</sup>	24.5 <sup>h</sup>	27	35	35	39	41	43
Na <sup>+</sup>	-57,279 <sup>h</sup>	14.4 <sup>h</sup>	35	41	41	45	47	49
Al <sup>3+</sup>	-127,000 <sup>h</sup>	-76.9 <sup>h</sup>	72	95	99	108	114	120
Au <sup>+</sup>		22.0 <sup>h</sup>	29	37	37	41	43	45
Au <sup>3+</sup>		-23.0 <sup>l</sup>	50	67	69	74	78	82

<sup>a</sup> Computed from equations (2) to (5) and the entropies shown above (Criss and Cobble, 1964a and b). <sup>b</sup> Computed from a constant  $\Delta C_p$ , least squares fit of quartz solubilities measured by Morey, Fournier, and Rowe (1962) and Kennedy (1950) using the thermodynamic data for quartz given in table 7. <sup>c</sup> Computed from  $\Delta H_f^\circ$  for H<sub>2</sub>S(g) = -4930 cal mole<sup>-1</sup> (Wagman and others, 1968) and a value of  $\Delta H_f^\circ$  for H<sub>2</sub>S(aq) = H<sub>2</sub>S(l) of -4100 cal mole<sup>-1</sup> (Pohl, 1961; table 10). <sup>d</sup> Computed from  $S^\circ$  for H<sub>2</sub>S(g) = 49.16 cal mole<sup>-1</sup> deg<sup>-1</sup> (Wagman and others, 1968) and a value of  $\Delta S_f^\circ$  for H<sub>2</sub>S(g) = H<sub>2</sub>S(aq) of -18.3 cal mole<sup>-1</sup> deg<sup>-1</sup> (Pohl, 1961; Wright and Maass, 1932; table 10). <sup>e</sup> Wagman and others (1965, 1966, 1968). <sup>f</sup> Calculated from log K<sub>HS<sup>-</sup>} = -13.9 (Maronny, 1959; Muhammed and Sundaram, 1961) and the entropy values shown above for HS<sup>-</sup> and S<sup>2-</sup>. This value of  $\Delta H_f^\circ$  for S<sup>2-</sup>, which is consistent with the other data given above for species involving S<sup>2-</sup>, differs from that (7900 cal mole<sup>-1</sup>) reported by Wagman and others (1968). <sup>g</sup> Latimer (1952). <sup>h</sup> Calculated from log K(T<sub>r</sub>) for the disproportionation of the cuprous ion (Fenwick, 1926; table 10) using the values of  $S^\circ$  for Cu<sup>+</sup>, S<sup>0</sup>, and Cu<sup>2+</sup> shown above together with the data for Cu<sub>2</sub>O given in table 6. <sup>i</sup> Wagman (1951). <sup>j</sup> Wulff (1957). <sup>k</sup> Computed from a prediction of the dissociational entropy for AuCl from equations (25) and (27),  $S^\circ$  for AuCl<sup>-</sup> = 13.51 (Ahluwalia and Cobble, 1964), and a value of  $S^\circ$  for AuCl<sub>2</sub> computed from Cobble's (1953) equation for neutral species. <sup>l</sup> Calculated from the predicted dissociational entropy for AuCl<sub>2</sub> in table 1 using  $S^\circ$  for AuCl<sub>2</sub> = 61 cal mole<sup>-1</sup> deg<sup>-1</sup> (Latimer, 1952). <sup>m</sup> Computed (Helgeson, 1967a). <sup>n</sup> Computed (Helgeson, 1967a) from least squares fits of equation (17) to equilibrium constants for H<sub>2</sub>S(g) = H<sub>2</sub>S(aq) at elevated temperatures (Kozinsteva, 1964). The high temperature values of  $\Delta H_f^\circ$  for H<sub>2</sub>S(g) used in the calculations were computed from a heat capacity power function (eq 10, table 8) and the value of  $\Delta H_f^\circ$  for H<sub>2</sub>S(g) at 25°C given in footnote c above. <sup>o</sup> Calculated from quartz solubilities (Morey, Fournier, and Rowe, 1962; Kennedy, 1950) and the thermodynamic data given in table 7 for quartz. <sup>p</sup> Enthalpy of formation from the elements. <sup>q</sup> Compared to -3.5 cal mole<sup>-1</sup> deg<sup>-1</sup> (Wagman and others, 1968). <sup>r</sup> Ahluwalia and Cobble (1964). <sup>s</sup> Compared to -26.8 cal mole<sup>-1</sup> deg<sup>-1</sup> (Wagman and others, 1968).</sub>

TABLE 4  
Thermodynamic data for dissociational equilibria in aqueous solution<sup>bbb</sup>

Reaction <sup>a</sup>	$\Delta H^\circ_f(T_r)$ (cal mole <sup>-1</sup> )	$\Delta S^\circ_f(T_r)$ (cal mole <sup>-1</sup> deg <sup>-1</sup> )	$\log K(T)^{jj}$							
			25°C	50°C	60°C	100°C	150°C	200°C	250°C	300°C
$H_2O_{(l)} \rightleftharpoons H^+ + OH^-$	13,335 <sup>b</sup>	-19.31 <sup>c</sup>	-14.00 <sup>d,ee</sup>	-13.27 <sup>d,ee</sup>	-13.03 <sup>d,ee</sup>	-12.26 <sup>d,ee</sup>	-11.64 <sup>d,ee</sup>	-11.27 <sup>d,ee</sup>	-11.13 <sup>d,ee</sup>	-11.1
$H_2S \rightleftharpoons H^+ + HS^-$	4,800 <sup>e</sup>	-15.9 <sup>f</sup>	-6.99 <sup>g</sup>	-6.77 <sup>h,gg</sup>	-6.72 <sup>h,gg</sup>	-6.63 <sup>h,gg</sup>	-6.72 <sup>h</sup>	-6.96 <sup>h</sup>	-7.35 <sup>h</sup>	-8.1
$HS^- \rightleftharpoons H^+ + S^{2-}$	13,300 <sup>e</sup>	-19.0 <sup>f</sup>	-13.90 <sup>i</sup>	-13.13 <sup>h,gg</sup>	-12.84 <sup>h,gg</sup>	-11.78 <sup>h,gg</sup>	-10.62 <sup>h</sup>	-9.57 <sup>h</sup>	-8.61 <sup>h</sup>	-7.7
$HSO_4^- \rightleftharpoons H^+ + SO_4^{2-}$	-3,850 <sup>d</sup>	-22.0 <sup>i</sup>	-1.99 <sup>k,t</sup>	-2.27 <sup>t</sup>	-2.40 <sup>d,ee</sup>	-2.99 <sup>t</sup>	-3.74 <sup>t</sup>	-4.49 <sup>t</sup>	-5.41 <sup>d,ee</sup>	-7.0
$H_2SO_4 \rightleftharpoons H^+ + HSO_4^-$										0.6 <sup>m</sup> 0.5
$H_2CO_{3(aq)}^{bb} \rightleftharpoons H^+ + HCO_3^-$	1,840 <sup>n</sup>	-22.9 <sup>e</sup>	-6.35 <sup>p</sup>	-6.31 <sup>d,ee</sup>	-6.32 <sup>d,ee</sup>	-6.45 <sup>d,ee</sup>	-6.73 <sup>d,ee</sup>	-7.08 <sup>d,ee</sup>	-7.03 <sup>d,ee</sup>	-8.8
$HCO_3^- \rightleftharpoons H^+ + CO_3^{2-}$	3,600 <sup>n</sup>	-35.16 <sup>e</sup>	-10.32 <sup>u</sup>	-10.17 <sup>d,ee</sup>	-10.15 <sup>d,ee</sup>	-10.16 <sup>d,ee</sup>	-10.29 <sup>d,ee</sup>	-10.68 <sup>d,ee</sup>	-11.43 <sup>d,ee</sup>	-13.3
$HAs(OH)_3 \rightleftharpoons H^+ + H_2As(OH)_2^-$	3,430 <sup>rr</sup>	-82.9 <sup>rr</sup>	-20.6 <sup>ww</sup>	-20.5 <sup>t</sup>	-20.5 <sup>t</sup>	-20.8 <sup>t</sup>	-21.8 <sup>t</sup>	-23.6 <sup>t</sup>		
$H_2As(OH)_2^- \rightleftharpoons H^+ + HAs(OH)_2^-$	5,120 <sup>rr</sup>	-66.9 <sup>rr</sup>	-18.4 <sup>ww</sup>	-18.2 <sup>t</sup>	-18.1 <sup>t</sup>	-18.2 <sup>t</sup>	-18.8 <sup>t</sup>	-20.1 <sup>t</sup>		
$HAs(OH)_2^- \rightleftharpoons H^+ + As(OH)_2^-$	4,350 <sup>rr</sup>	-83.9 <sup>rr</sup>	-11.7 <sup>ww</sup>	-11.5 <sup>t</sup>	-11.4 <sup>t</sup>	-11.4 <sup>t</sup>	-11.7 <sup>t</sup>	-12.3 <sup>t</sup>		
$HAs(OH)_2 \rightleftharpoons H^+ + As(OH)_2^-$	6,560 <sup>rr</sup>	-20.2 <sup>rr</sup>	-9.2 <sup>ww</sup>	-8.9 <sup>t</sup>	-8.8 <sup>t</sup>	-8.4 <sup>t</sup>	-8.3 <sup>t</sup>	-8.4 <sup>t</sup>		
$As(OH)_2^- \rightleftharpoons As(OH)_2 + OH^-$	6,800 <sup>s,rr</sup>	0.7 <sup>rr</sup>	4.8 <sup>ww</sup>	4.4 <sup>t</sup>	4.3 <sup>t</sup>	3.8 <sup>t</sup>	3.3 <sup>t</sup>	2.9 <sup>t</sup>		
$Al(OH)_3 \rightleftharpoons Al^{3+} + 3OH^-$	10,300 <sup>x</sup>	-115.2 <sup>aa</sup>	-32.73 <sup>cc</sup>	-32.3 <sup>t</sup>	-32.2 <sup>t</sup>	-32.2 <sup>t</sup>	-33.0 <sup>t,yy</sup>	-34.6 <sup>t,yy</sup>	-36.7 <sup>t,yy</sup>	-39.5 <sup>t</sup>
$Al(OH)_3 \rightleftharpoons Al^{3+} + OH^-$	-1,990 <sup>x</sup>	-49.0 <sup>uu</sup>	9.25 <sup>rr</sup>	9.4 <sup>t</sup>	9.5 <sup>t</sup>	10.0 <sup>t</sup>	10.8 <sup>t,yy</sup>	11.9 <sup>t,yy</sup>	13.1 <sup>t,yy</sup>	14.7 <sup>t</sup>
$KSO_4 \rightleftharpoons K^+ + SO_4^{2-}$	-2,635 <sup>ff,xx</sup>	12.7 <sup>ff,xx</sup>	0.84 <sup>ff,xx</sup>	1.00 <sup>ff,xx</sup>	1.06 <sup>ff,xx</sup>	1.30 <sup>ff,xx</sup>	1.60 <sup>ff,xx</sup>	1.94 <sup>ff,xx</sup>		
$KHSO_4 \rightleftharpoons K^+ + HSO_4^-$									0.8 <sup>r</sup>	0.3 <sup>r</sup>
$CaSO_4 \rightleftharpoons Ca^{2+} + SO_4^{2-}$	-1,760 <sup>ii,pp</sup>	16.5 <sup>d,pp</sup>	2.31 <sup>o,pp</sup>	2.4 <sup>d,t,pp</sup>	2.5 <sup>d,t,pp</sup>	2.7 <sup>d,t,pp</sup>	3.1 <sup>d,t,pp</sup>	3.6 <sup>d,t,pp</sup>		
$MgSO_4 \rightleftharpoons Mg^{2+} + SO_4^{2-}$	-4,920 <sup>d,pp</sup>	26.8 <sup>d,pp</sup>	2.25 <sup>d,pp</sup>	2.6 <sup>d,t,pp</sup>	2.7 <sup>d,t,pp</sup>	3.2 <sup>d,t,pp</sup>	3.9 <sup>d,t,pp</sup>	4.8 <sup>d,t,pp</sup>		
$MnSO_4 \rightleftharpoons Mn^{2+} + SO_4^{2-}$	-3,700 <sup>d</sup>	22.7 <sup>d</sup>	2.25 <sup>v</sup>	2.5 <sup>d,t</sup>	2.6 <sup>d,t</sup>	3.0 <sup>d,t</sup>	3.6 <sup>d,t</sup>	4.3 <sup>d,t</sup>		

$ZnSO_4 \rightleftharpoons Zn^{2+} + SO_4^{2-}$	-4,090 <sup>d</sup>	24.5 <sup>d</sup>	2.38 <sup>u</sup>	2.6 <sup>d,t</sup>	2.7 <sup>d,t</sup>	3.2 <sup>d,t</sup>	3.8 <sup>d,t</sup>	4.6 <sup>d,t</sup>		
$AgSO_4 \rightleftharpoons Ag^+ + SO_4^{2-}$	-1,500 <sup>w</sup>	11.0 <sup>w</sup>	1.30 <sup>w</sup>	1.4 <sup>t</sup>	1.4 <sup>t</sup>	1.6 <sup>t</sup>	1.9 <sup>t</sup>	2.2 <sup>t</sup>		
$CaCO_3 \rightleftharpoons Ca^{2+} + CO_3^{2-}$	-3,130 <sup>v</sup>	25.1 <sup>v</sup>	3.20 <sup>a</sup>	3.4 <sup>t,bb</sup>	3.5 <sup>t,bb</sup>	3.9 <sup>t,bb</sup>	4.5 <sup>t,bb</sup>	5.2 <sup>t,bb</sup>		
$NaCl \rightleftharpoons Na^+ + Cl^-$							0.97 <sup>aa,bb</sup>	0.42 <sup>aa,bb</sup>	0.15 <sup>aa,bb</sup>	0.82 <sup>ii,bb</sup>
$KCl \rightleftharpoons K^+ + Cl^-$								0.9 <sup>aa,cc</sup>	0.3 <sup>aa,cc</sup>	0.6 <sup>ii,cc</sup>
$HCl \rightleftharpoons H^+ + Cl^-$	-18,630 <sup>d</sup>	34.4 <sup>d</sup>	6.1 <sup>dd</sup>	5.0 <sup>dd</sup>	4.56 <sup>d,ee</sup>	2.90 <sup>d,ee</sup>	1.23 <sup>d,ee</sup>	0.06 <sup>ff</sup>	0.67 <sup>d,ee</sup>	1.24 <sup>d,ee</sup>
$Mg(OH)_2 \rightleftharpoons Mg^{2+} + OH^-$	-2,140 <sup>x</sup>	19.0 <sup>uu</sup>	2.60 <sup>aa</sup>	2.7 <sup>t</sup>	2.8 <sup>t</sup>	3.1 <sup>t</sup>	3.6 <sup>t</sup>	4.1 <sup>t,yy</sup>		
$Fe(OH)_3 \rightleftharpoons Fe^{3+} + OH^-$	2,700 <sup>x</sup>	17.0 <sup>uu</sup>	5.7 <sup>aaa</sup>	5.6 <sup>t</sup>	5.5 <sup>t</sup>	5.4 <sup>t</sup>	5.5 <sup>t</sup>	5.7 <sup>t,yy</sup>		

<sup>a</sup> All species shown in this column are aqueous, and H<sub>2</sub>O<sup>l</sup> refers to liquid water. <sup>b</sup> Hale, Izat, and Christensen (1963) and Vanderzee and Swanson (1963). <sup>c</sup> Calculated from log K(T<sub>r</sub>) and ΔH<sub>f</sub><sup>o</sup>(T<sub>r</sub>). <sup>d</sup> Helgeson (1967a). <sup>e</sup> Computed from data given in table 3. <sup>f</sup> Cobble (1964). <sup>g</sup> Ellis and Golding (1959) and Muhammad and Sundaram (1961). <sup>h</sup> Computed from data given in table 3 using equation (6). <sup>i</sup> Maronny (1959) and Muhammad and Sundaram (1961). <sup>j</sup> Criss and Cobble (1964b). <sup>k</sup> Young and Irish (1962). <sup>l</sup> Lietzke and Stoughton (1961). <sup>m</sup> Extrapolated as a dielectric constant function from supercritical log K(T,P) values published by Quist and Marshall (1965). <sup>n</sup> Pitzer (1937). <sup>o</sup> Harned and Davis (1943). <sup>p</sup> Harned and Scholes (1941). <sup>q</sup> Extrapolated as a dielectric constant function from supercritical log K(T,P) values published by Quist and Marshall (1966). <sup>r</sup> Bell and George (1953). <sup>s</sup> Estimates calculated from equation (16). <sup>t</sup> Nair and Nancollas (1958). <sup>u</sup> Nair and Nancollas (1959). <sup>v</sup> Hopkins and Wulff (1965). <sup>w</sup> Calculated from log K(T<sub>r</sub>) and ΔS<sub>f</sub><sup>o</sup>(T<sub>r</sub>). <sup>x</sup> Estimated from an entropy correlation plot by Lafon (ms). <sup>y</sup> Carrels and Thompson (1962). <sup>aa</sup> Extrapolated. <sup>bb</sup> Figure 2 and table 2. <sup>cc</sup> Figure 2. <sup>dd</sup> Robinson (1936). <sup>ee</sup> Pearson, Copeland, and Benson (1963b) and Wright, Lindsay, and Druga (1961). <sup>ff</sup> Calculated from equation (17). <sup>gg</sup> Quist and others (1963). <sup>hh</sup> The subscript (app) indicates that the species referred to is the undifferentiated sum of H<sub>2</sub>CO<sub>3(aq)}</sub> and CO<sub>2(aq)}</sub>. <sup>ii</sup> Interpolated. <sup>jj</sup> All log K values given in the table are consistent with molal units of concentration. The values given for the dissociation of water are for the activity product constant (K<sub>w</sub>). <sup>kk</sup> These values have large uncertainties owing to assumptions made regarding ΔS<sub>f</sub><sup>o</sup>(T<sub>r</sub>)—see footnote y above. <sup>ll</sup> These values were accepted instead of those reported by Marshall (1967) and Yeatts and Marshall (1969) because sulfate complexing of Na<sup>+</sup> was not taken into account in the interpretation of the solubility data from which their log K values were derived. <sup>mm</sup> These values are consistent with the experimental data reported by Ellis and Milestone (1967) from 22°-90°C. <sup>nn</sup> Computed from the thermodynamic data for the arsenic species given by Wagman and others (1968). <sup>oo</sup> Calculated from data given in table 3 and a value of 28.0 cal mole<sup>-1</sup> deg<sup>-1</sup> for S<sub>Al(OH)<sub>3</sub>}<sup>o</sup> (Wagman and others, 1968). <sup>pp</sup> Computed from the free energy of formation of crystalline gibbsite (table 12), the hydrolysis equilibrium constant for crystalline gibbsite (Al(OH)<sub>3(crystalline)</sub> + H<sub>2</sub>O<sub>(l)} ⇌ Al(OH)<sub>3(aq)}</sub> + H<sup>+</sup>; log K(T<sub>r</sub>) = -15.3, Kittrick, 1966), and the ΔG<sub>f</sub><sup>o</sup>(T<sub>r</sub>) values for Al<sup>3+</sup> and OH<sup>-</sup> given by Wagman and others (1968). <sup>qq</sup> Estimated entropy of dissociation calculated from an expression analogous to equation (25) and an entropy correlation plot for hydroxyl complexes similar to that shown in figure 1 for chloride species but including provision for charge. <sup>rr</sup> Calculated by applying correction factors to log K values computed from equation (16). The correction factors were taken to be equivalent to those for ammonium hydroxide (0.86 at 300°C, Helgeson, 1967a). <sup>ss</sup> Computed from ΔH<sub>f</sub><sup>o</sup>(T<sub>r</sub>) and ΔS<sub>f</sub><sup>o</sup>(T<sub>r</sub>). <sup>tt</sup> Computed by the method of least squares from log K(T) values reported by Truesdell and Hostetler (1968) and Quist and others (1963). <sup>uu</sup> Computed from the equilibrium constant for Al<sup>3+</sup> + H<sub>2</sub>O<sub>(l)} ⇌ Al(OH)<sup>2+</sup> + H<sup>+</sup> (10<sup>-4.52</sup>; Heim and Robertson, 1967). <sup>vv</sup> Hostetler (1963). <sup>ww</sup> Leussing and Kolthoff (1953). <sup>xx</sup> Dissociation constants for NaCO<sub>3</sub><sup>-</sup>, MgCO<sub>3</sub>, MgHCO<sub>3</sub><sup>+</sup>, CaHCO<sub>3</sub><sup>+</sup>, and NaSO<sub>3</sub><sup>-</sup>, which are not included in this table, have been computed recently by Lafon (ms) for temperatures from 0° to 100°C.</sub></sub></sub>



TABLE 5  
 Predicted dissociation constants for metal chloride complexes in aqueous solution at elevated temperatures

Dissociational Reaction	$\Delta H^\circ(T_r)^a$ (cal mole <sup>-1</sup> )	$\Delta S^\circ_r(T_r)^b$ (cal mole <sup>-1</sup> deg <sup>-1</sup> )	$\log \beta(T)^c$						
			25°C	50°C	100°C	150°C	200°C	250°C	300°C
$\text{AgCl} \rightleftharpoons \text{Ag}^+ + \text{Cl}^-$	2,540	-6.6	-3.31 <sup>d</sup>	-3.17	-2.99	-2.92	(-2.9)	(-3.0) <sup>e</sup>	(-3.4) <sup>f</sup>
$\text{AgCl}_2^- \rightleftharpoons \text{Ag}^+ + 2\text{Cl}^-$	4,230	-9.8	-5.25 <sup>d</sup>	-5.02	-4.71	-4.57	(-4.6)	(-4.7) <sup>e</sup>	(-5.2) <sup>f</sup>
$\text{AgCl}_3^{2-} \rightleftharpoons \text{Ag}^+ + 3\text{Cl}^-$	3,280	-13.2	-5.25 <sup>d</sup>	-5.08	-4.88	-4.85	(-5.0)	(-5.3) <sup>e</sup>	(-6.0) <sup>f</sup>
$\text{AgCl}_4^{3-} \rightleftharpoons \text{Ag}^+ + 4\text{Cl}^-$	2,680	-16.4	-5.51 <sup>d</sup>	-5.38	-5.26	-5.31	(-5.6)	(-6.0) <sup>e</sup>	(-6.9) <sup>f</sup>
$\text{CuCl}_2 \rightleftharpoons \text{Cu}^+ + 2\text{Cl}^-$	420	-21.2	-4.94 <sup>d</sup>	-4.94	-5.06	-5.35	(-5.8)	(-6.5) <sup>e</sup>	(-7.4) <sup>f</sup>
$\text{CuCl}_3^- \rightleftharpoons \text{Cu}^+ + 3\text{Cl}^-$	-260	-24.4	-5.14 <sup>d</sup>	-5.18	-5.39	-5.77	(-6.4)	(-7.2) <sup>e</sup>	(-8.3) <sup>f</sup>
$\text{CuCl} \rightleftharpoons \text{Cu}^{2+} + \text{Cl}^-$	-8,650	-29.1	-0.01 <sup>b</sup>	-0.53	-1.54	-2.57	(-3.7)	(-4.8) <sup>e</sup>	(-6.0) <sup>f</sup>
$\text{CuCl}_2 \rightleftharpoons \text{Cu}^{2+} + 2\text{Cl}^-$	-10,560	-32.2	0.69 <sup>g</sup>	0.06	-1.15	-2.36	(-3.7)	(-4.9) <sup>e</sup>	(-6.5) <sup>f</sup>
$\text{CuCl}_3^- \rightleftharpoons \text{Cu}^{2+} + 3\text{Cl}^-$	-13,690	-35.4	2.29 <sup>g</sup>	1.48	-0.04	-1.52	(-3.1)	(-4.6) <sup>e</sup>	(-6.5) <sup>f</sup>
$\text{CuCl}_4^{2-} \rightleftharpoons \text{Cu}^{2+} + 4\text{Cl}^-$	-17,780	-38.6	4.59 <sup>g</sup>	3.54	1.63	-0.18	(-2.0)	(-3.9) <sup>e</sup>	(-6.1) <sup>f</sup>
$\text{PbCl}_2 \rightleftharpoons \text{Pb}^{2+} + 2\text{Cl}^-$	-380	-8.6	-1.60 <sup>h</sup>	-1.63	-1.73	-1.88	(-2.1)	(-2.4) <sup>e</sup>	(-3.0) <sup>f</sup>
$\text{PbCl}_3^- \rightleftharpoons \text{Pb}^{2+} + 3\text{Cl}^-$	-1,080	-11.8	-1.78 <sup>h</sup>	-1.85	-2.04	-2.29	(-2.6)	(-3.1) <sup>e</sup>	(-3.9) <sup>f</sup>
$\text{PbCl}_4^{2-} \rightleftharpoons \text{Pb}^{2+} + 4\text{Cl}^-$	-2,170	-15.0	-1.68 <sup>h</sup>	-1.81	-2.13	-2.50	(-3.0)	(-3.6) <sup>e</sup>	(-4.6) <sup>f</sup>
$\text{PbCl}_5^{3-} \rightleftharpoons \text{Pb}^{2+} + 5\text{Cl}^-$	-3,530	-18.2	-1.38 <sup>h</sup>	-1.59	-2.05	-2.57	(-3.2)	(-4.0) <sup>e</sup>	(-5.3) <sup>f</sup>
$\text{ZnCl}_2 \rightleftharpoons \text{Zn}^{2+} + 2\text{Cl}^-$	-7,790	-28.1	-0.43 <sup>k</sup>	-0.90	-1.82	-2.78	(-3.9)	(-4.8) <sup>e</sup>	(-6.0) <sup>f</sup>
$\text{ZnCl}_3^- \rightleftharpoons \text{Zn}^{2+} + 3\text{Cl}^-$	-8,500 <sup>l</sup>	-31.3	-0.61 <sup>k</sup>	-1.12	-2.13	-3.19	(-4.4)	(-5.5) <sup>e</sup>	(-6.9) <sup>f</sup>
$\text{ZnCl}_4^{2-} \rightleftharpoons \text{Zn}^{2+} + 4\text{Cl}^-$	-9,560	-34.5	-0.53 <sup>k</sup>	-1.14	-2.23	-3.34	(-4.8)	(-6.0) <sup>e</sup>	(-7.7) <sup>f</sup>

$\text{ZnCl}_5^{3-} \rightleftharpoons \text{Zn}^{2+} + 5\text{Cl}^-$	-10,960	-37.7	-0.20 <sup>k</sup>	-0.89	-2.14	-3.35	(-5.0)	(-6.4) <sup>e</sup>	(-8.3) <sup>f</sup>
$\text{HgCl}_2 \rightleftharpoons \text{Hg}^{2+} + 2\text{Cl}^-$	4,800 <sup>m</sup>	-12.5	-6.25 <sup>n</sup>	-5.99	-5.65	-5.50	(-5.5)	(-5.8) <sup>e</sup>	(-6.4) <sup>f</sup>
$\text{HgCl}_3^- \rightleftharpoons \text{Hg}^{2+} + 3\text{Cl}^-$	13,400 <sup>p</sup>	-15.7	-13.25 <sup>n</sup>	-12.51	-11.41	-10.71	(-10.4)	(-10.3) <sup>e</sup>	(-10.8) <sup>f</sup>
$\text{HgCl}_4^{2-} \rightleftharpoons \text{Hg}^{2+} + 4\text{Cl}^-$	15,300 <sup>p</sup>	-18.9	-15.35 <sup>n</sup>	-14.50	-13.25	-12.46	(-12.1)	(-12.1) <sup>e</sup>	(-12.7) <sup>f</sup>
$\text{FeCl}_2 \rightleftharpoons \text{Fe}^{2+} + 2\text{Cl}^-$	-7,910	-33.3	-1.48 <sup>n</sup>	-1.96	-2.94	-3.98	(-5.1) <sup>e</sup>	(-6.2) <sup>e</sup>	(-7.5) <sup>f</sup>
$\text{FeCl}_3^- \rightleftharpoons \text{Fe}^{2+} + 3\text{Cl}^-$	-7,970	-36.5	-2.13 <sup>n</sup>	-2.62	-3.63	-4.72	(-5.9)	(-7.1) <sup>e</sup>	(-7.7) <sup>f</sup>
$\text{FeCl}_4^{2-} \rightleftharpoons \text{Fe}^{2+} + 4\text{Cl}^-$	-10,290	-39.7	-1.13 <sup>n</sup>	-1.76	-3.00	-4.30	(-5.7)	(-7.1) <sup>e</sup>	(-8.0) <sup>f</sup>
$\text{FeCl}_5^{3-} \rightleftharpoons \text{Fe}^{2+} + 5\text{Cl}^-$	-13,860	-42.9	0.79 <sup>r</sup>	-0.05	-1.63	-3.23	(-4.9)	(-6.6) <sup>e</sup>	(-7.8) <sup>f</sup>
$\text{AuCl}_2 \rightleftharpoons \text{Au}^+ + 2\text{Cl}^-$	10,490	-6.0	-9 <sup>v</sup>	-8.4	-7.5	-6.9	(-6.4)	(-6.2) <sup>e</sup>	(-6.2) <sup>f</sup>
$\text{AuCl}_3 \rightleftharpoons \text{Au}^{3+} + 3\text{Cl}^-$	26,460	-30.2	-26 <sup>w</sup>	-24.5	-22.4	-21.0	(-20.2)	(-20.2) <sup>e</sup>	(-21.1) <sup>f</sup>

<sup>a</sup> Except where otherwise indicated, values in this column were computed from  $\log K(T_r)$  and  $\Delta S^\circ_r(T_r)$ . <sup>b</sup> All  $\Delta S^\circ_r(T_r)$  values were calculated from equations (25) and (27) using ionic radii (table 1) and the values of  $S^\circ_{\text{Cl}^-}$  and  $S^\circ_{\text{H}_2\text{O}}$  at 25°C given in footnote b, table 1. <sup>c</sup> The values of the overall dissociation constants were computed from  $\log K(T)$  values (eq 48) predicted from equation (16) using the  $\Delta S^\circ_r(T_r)$  and  $\Delta H^\circ_r(T_r)$  values shown above. The dissociation constants are consistent with molal units of concentration—those that are more uncertain are given in parentheses. <sup>d</sup> Jonte and Martin (1952). <sup>e</sup> Leden (1952); Berne and Leden (1953). <sup>f</sup> Chalykian (1948). <sup>g</sup> Hurlen (1961). <sup>h</sup> Näsänen (1953). <sup>i</sup> Bjerrum (1946). <sup>j</sup> Nelson and Kraus (1954); Marcus (1956). <sup>k</sup> Marcus and Mayden (1963). <sup>l</sup> This value is consistent with high temperature  $\log K(T)$  values (Kraus and Ravidon, 1960)—see footnote g, table 1. <sup>m</sup> Malcolm, Parson, and Watson (1961). <sup>n</sup> Calculated from  $\Delta H^\circ_r(T_r)$  and  $\Delta S^\circ_r(T_r)$ . <sup>o</sup> Williams (1954). <sup>p</sup> Rabinowitch and Stockmayer (1942). <sup>q</sup> Marcus (1960). <sup>r</sup> Computed from the free energy of formation of  $\text{Au}^+$  (Latimer, 1952) and the oxidation potential for the reaction  $\text{AuCl}_2^- + \text{e}^- \rightleftharpoons \text{Au}_{(s)} + 2\text{Cl}^-$  (Bjerrum and Kirschner, 1918; Bjerrum, 1948). <sup>s</sup> Extrapolated. <sup>t</sup> Computed from the free energy of formation of  $\text{Au}^{3+}$  (Latimer, 1952) and the oxidation potential for  $\text{AuCl}_4^- + 3\text{e}^- \rightleftharpoons \text{Au}_{(s)} + 4\text{Cl}^-$  (Bjerrum and Kirschner, 1918; Bjerrum, 1948). <sup>v</sup> These values are actually for 18°C, but they are uncertain to the extent that a 7 degree correction to 25°C is unwarranted.



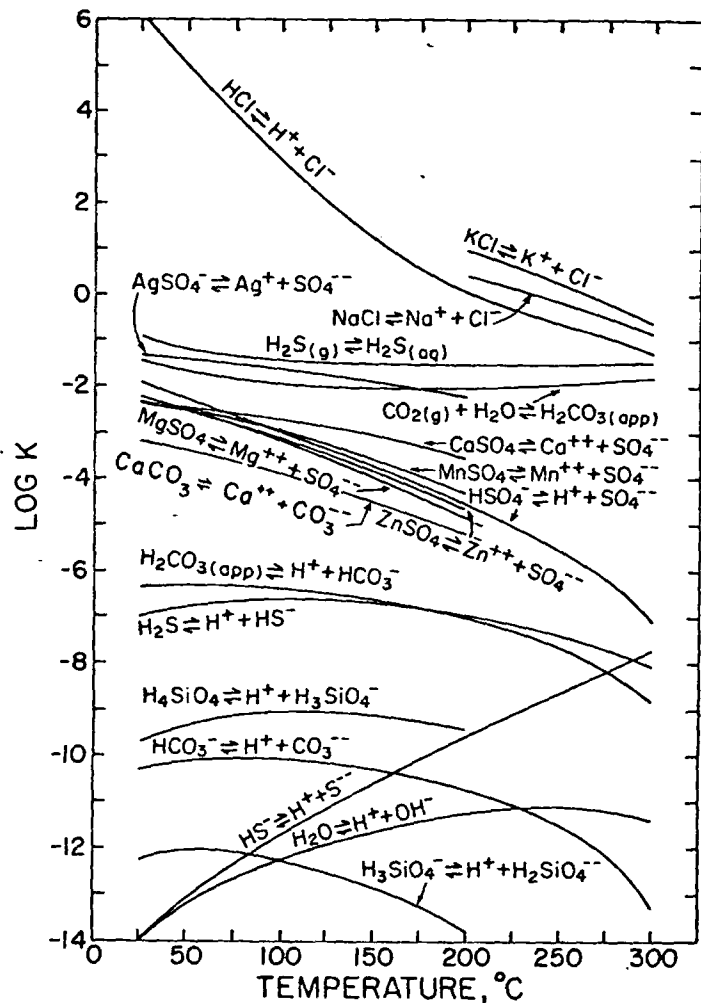


Fig. 5. Dissociation constants for complexes in hydrothermal solutions at elevated temperatures (table 4). The curves shown for the dissociation of  $\text{H}_2\text{SiO}_4$  and  $\text{H}_3\text{SiO}_4^-$  are those computed by Cobble (1964); the log K values defined by these curves are more consistent with low temperature thermodynamic data than those obtained at high temperatures by Ryzhenko (1967).

Predicted high temperature dissociation constants for chloride complexes of the ore-forming metals are shown in table 5. Log K(T) curves for these reactions are plotted in figures 6 and 7. Because the uncertainty resulting from calculation of log K(T) values with equation (16) increases substantially above 200°C (Helgeson, 1967a), and because entropy estimates (eqs 25 and 27) were used in the calculations, the numerical values for log  $\beta(T)$  given in table 5 as well as the log K(T) curves in figures 6 and 7 should be regarded as approximations.

It can be deduced from figures 5 to 7 that high temperature electrolyte solutions are highly associated. The high degree of formation attained by metal-ion chloride complexes is particularly significant with respect to the transport and deposition of the ore-forming metals in hydrothermal systems. As indicated above, calculations of sulfide solubilities in sodium chloride solutions at elevated temperatures suggest that more than adequate quantities of these metals can be carried in hydrothermal solutions to account for major ore deposits (Helgeson, 1964, 1967c; Helgeson, Garrels, and MacKenzie, 1969; Helgeson and Garrels, 1968). The results of a few such calculations involving thermodynamic values given in the tables are presented in later pages of this communication.

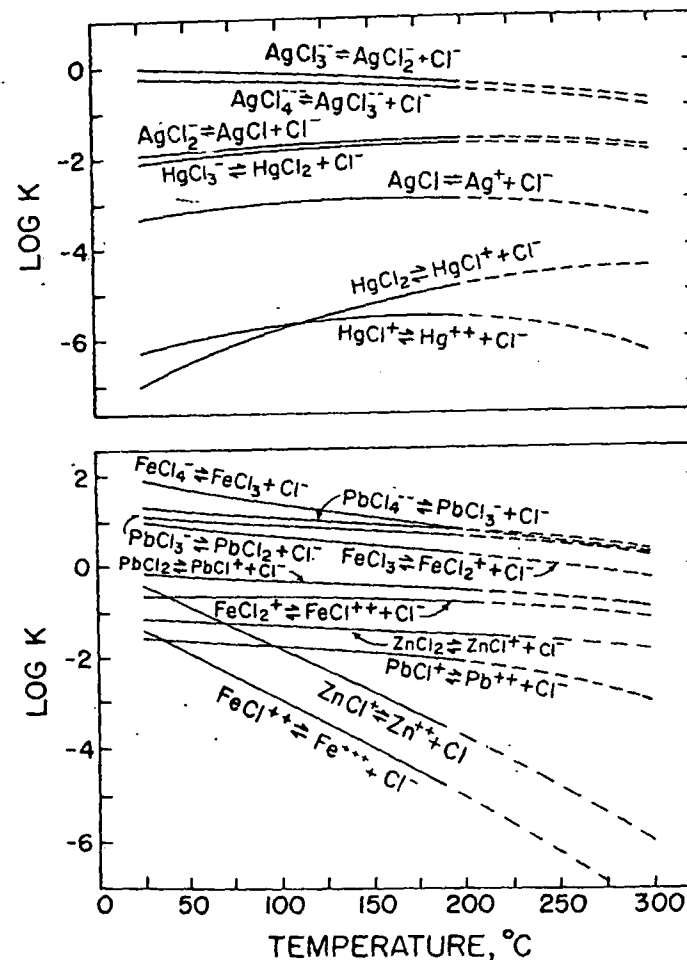


Fig. 6. Predicted dissociation constants for metal chloride complexes at elevated temperatures (table 5). The curves below 200°C were computed from equation (16) using entropy estimates from equations (25) and (27)—see text. The dashed extensions of the curves are extrapolations.

TABLE 6

Enthalpies<sup>a</sup> and entropies<sup>b</sup> of elements of interest in hydrothermal studies<sup>c</sup>

Element	Temperature, °C												
	25	50	60	100	150	200	250	300	350	400	450	500	
Au <sub>(c)</sub>	H°(T)–H°(T <sub>r</sub> )	0.0	151	212	456	763	1074	1383	1705	2025	2348	2675	3004
	S°	11.31 <sup>d</sup>	11.80	11.98	12.67	13.45	14.14	14.77	15.35	15.88	16.38	16.85	17.29
Ag <sub>(c)</sub>	H°(T)–H°(T <sub>r</sub> )	0.0	152	213	457	764	1073	1386	1702	2033	2347	2677	3011
	S°	10.20 <sup>d</sup>	10.69	10.88	11.57	12.34	13.03	13.66	14.23	14.77	15.27	15.74	16.19
Hg <sub>(liq)</sub>	H°(T)–H°(T <sub>r</sub> )	0.0	166	232	496	824	1151	1476	1802	2126	2450	2774	3098
	S°	18.2 <sup>d</sup>	18.7	18.9	19.7	20.5	21.2	21.9	22.5	23.0	23.5	24.0	24.4
Cu <sub>(c)</sub>	H°(T)–H°(T <sub>r</sub> )	0.0	147	206	443	744	1048	1356	1667	1983	2302	2625	2951
	S°	7.97 <sup>d</sup>	8.44	8.62	9.30	10.05	10.73	11.35	11.92	12.45	12.94	13.40	13.84
O <sub>(g)</sub>	H°(T)–H°(T <sub>r</sub> )	0.0	176	247	535	900	1271	1646	2024	2407	2792	3181	3573
	S°	48.996 <sup>d,e</sup>	49.56	49.78	50.60	51.51	52.34	53.09	53.79	54.43	55.02	55.58	56.10
H <sub>2</sub> (g)	H°(T)–H°(T <sub>r</sub> )	0.0	172	241	517	862	1208	1556	1906	2257	2609	2964	3320
	S°	31.21 <sup>d,e</sup>	31.76	31.97	32.76	33.62	34.40	35.10	35.73	36.32	36.87	37.37	37.85

<sup>a</sup> In cal mole<sup>-1</sup> where T<sub>r</sub> refers to 298.15°K. <sup>b</sup> In cal mole<sup>-1</sup> deg<sup>-1</sup>. <sup>c</sup> The values shown in this table are for a standard state of 1 atm and the indicated temperature. The subscripts (c), (liq), and (g) refer to crystalline, liquid, and gas respectively. All the enthalpies and entropies for temperatures of 50°C and above were computed from a statement of equation (11) written in terms of H°, and equation (12), respectively, using the coefficients shown in table 8. <sup>d</sup> Robie (1966); Robie and Waldbaum (1968). <sup>e</sup> Wagman and others (1965, 1968).

#### Standard Enthalpies, Entropies, and Heat Capacities

High temperature thermodynamic data for a variety of solids and gases of interest in hydrothermal studies are summarized in tables 6 and 7. The values shown in the tables were computed from equations (11) and (12) using the heat capacity power function coefficients for equation (10) shown in table 8. Average heat capacities of ions and several neutral species in aqueous solution are given in table 3 for temperatures from 25° to 300°C.

#### Equilibrium Constants for Oxidation-Reduction and Dissolution Reactions

Thermodynamic data for a variety of hydrothermal oxidation-reduction and solubility reactions are presented in tables 9 to 12. The log K(T) values shown in these tables were computed from equations (11) to (17) and data presented in tables 3, 6, 8, and 9 to 12. A number of the activity product constants are plotted against temperature in figure 8. Although reactions involving a large number of minerals are presented in table 12, the fact that a reaction is included in the table is not meant to imply that the mineral involved is necessarily stable in the presence of H<sub>2</sub>O at the temperatures indicated. The log K values given in table 12 are "idealized"; they can be used to describe stable or metastable

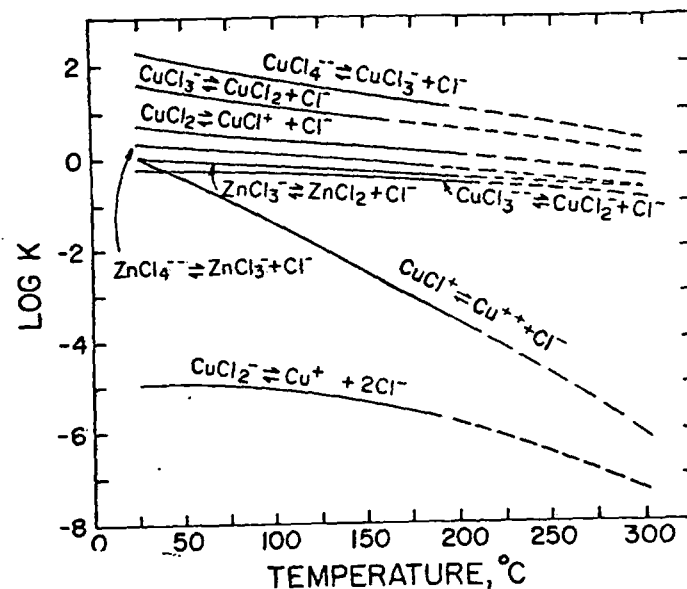


Fig. 7. Predicted dissociation constants for metal chloride complexes at elevated temperatures (table 5). The curves below 200°C were computed from equation (16) using entropy estimates from equations (25) and (27)—see text. The dashed extensions of the curves are extrapolations.

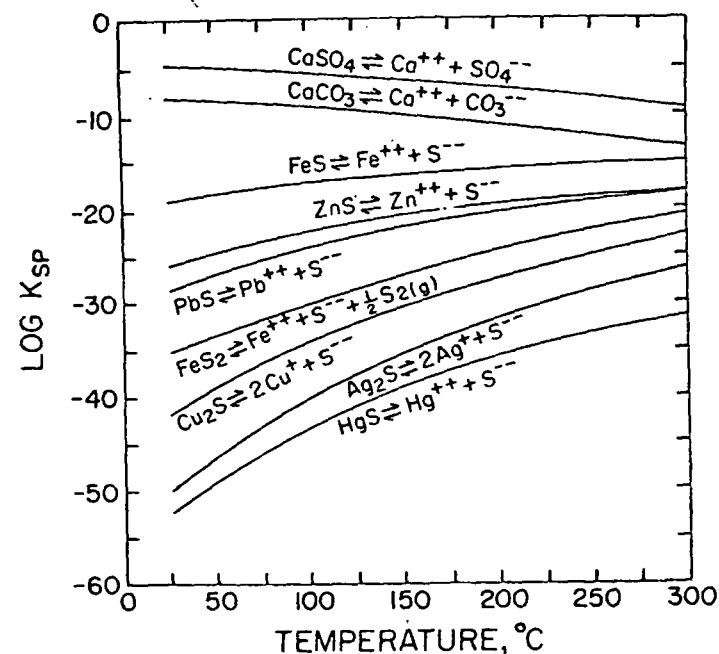


Fig. 8. Activity product constants for anhydrite, calcite, and various sulfides at elevated temperatures (table 11). HgS refers to metacinnabar.

TABLE 7

Standard entropies<sup>a</sup> and enthalpies<sup>b</sup> for various minerals and gases of interest in hydrothermal studies<sup>c</sup>

Species		Temperature, °C				
		25°	50°	60°	100°	150°
α Ag <sub>2</sub> S (acanthite)	ΔH°	-7,731 <sup>d</sup>	-7,273	-7,085	-6,307	-5,275
	S°	34.14 <sup>d</sup>	35.62	36.19	38.39	40.97
α Cu <sub>2</sub> S (chalcocite)	ΔH°	-19,143 <sup>d</sup>	-18,660	-18,465	-17,685	-16,710
	S°	28.86 <sup>d</sup>	30.43	31.02	33.23	35.69
CuS (covellite)	ΔH°	-11,610 <sup>d</sup>	-11,324	-11,210	-10,748	-10,166
	S°	15.93 <sup>d</sup>	16.85	17.20	18.51	19.97
PbS (galena)	ΔH°	-23,350 <sup>d</sup>	-23,053	-22,934	-22,452	-21,841
	S°	21.84 <sup>d</sup>	22.80	23.16	24.53	26.06
ZnS (sphalerite)	ΔH°	-49,750 <sup>d</sup>	-49,475	-49,365	-48,914	-48,337
	S°	13.77 <sup>d</sup>	14.67	14.99	16.27	17.72
HgS (metacinnabar)	ΔH°	-11,058 <sup>d</sup>	-10,869	-10,748	-10,261	-9,643
	S°	23.00 <sup>d</sup>	23.97	24.34	25.72	27.27
FeS (pyrrhotite)	ΔH°	-24,130 <sup>d</sup>	-23,795	-23,657	-23,076	-22,291
	S°	14.42 <sup>d</sup>	15.50	15.92	17.56	19.54
FeS <sub>2</sub> (pyrite)	ΔH°	-41,000 <sup>d</sup>	-40,620	-40,470	-39,830	-39,010
	S°	12.65 <sup>d</sup>	13.87	14.34	16.14	18.21
α Fe <sub>2</sub> O <sub>3</sub> (hematite)	ΔH°	-197,300 <sup>d</sup>	-196,660	-196,397	-195,309	-194,877
	S°	20.89 <sup>d</sup>	22.95	23.75	26.83	30.43
α Fe <sub>3</sub> O <sub>4</sub> (magnetite)	ΔH°	-267,400 <sup>d</sup>	-266,480	-266,100	-264,550	-262,490
	S°	36.03 <sup>d</sup>	39.00	40.14	44.55	49.71
CaCO <sub>3</sub> (calcite)	ΔH°	-288,420 <sup>b</sup>	-287,916	-287,706	-286,832	-285,676
	S°	22.15 <sup>d</sup>	23.77	24.41	26.89	29.79
CaSO <sub>4</sub> (anhydrite)	ΔH°	-343,321 <sup>d</sup>	-342,718	-342,473	-341,463	-340,160
	S°	25.5 <sup>d</sup>	27.44	28.19	31.03	34.32
α SiO <sub>2</sub> (quartz)	ΔH°	-217,650 <sup>d</sup>	-217,380	-217,260	-216,780	-216,140
	S°	9.88 <sup>d</sup>	10.76	11.11	12.46	14.07
KAlSi <sub>3</sub> O <sub>8</sub> (microcline)	ΔH°	-946,000 <sup>d, r, q</sup>	-944,720	-944,224	-942,037	-939,129
	S°	52.47 <sup>d</sup>	56.50	58.10	64.29	71.60
NaAlSi <sub>3</sub> O <sub>8</sub> (low albite)	ΔH°	-937,300 <sup>d, r, q</sup>	-936,040	-935,510	-933,330	-930,450
	S°	50.2 <sup>d</sup>	54.26	55.85	62.03	69.29
CaAl <sub>2</sub> Si <sub>2</sub> O <sub>8</sub> (anorthite)	ΔH°	-1,009,300 <sup>d</sup>	-1,008,020	-1,007,490	-1,005,260	-1,002,300
	S°	48.45 <sup>d</sup>	52.57	54.20	60.50	67.93

	Temperature, °C						
	200°	250°	300°	350°	400°	450°	500°
	-4,176	-3,012	-1,782	-486	876	2,304	3,798
	43.44	45.76	48.02	50.19	52.29	54.35	56.33
	-15,735	-14,760	-13,785	-12,810	-11,835	-10,860	-9,885
	37.86	39.82	41.60	43.23	44.74	46.14	47.44
	-9,577	-8,981	-8,379	-7,770	-7,154	-6,532	-5,903
	21.29	22.48	23.58	24.60	25.55	26.44	27.28
	-21,220	-20,589	-19,949	-19,319	-18,639	-17,969	-17,289
	27.45	28.72	29.88	30.97	31.99	32.95	33.86
	-47,749	-47,153	-46,549	-45,939	-45,323	-44,703	-44,078
	19.03	20.23	21.33	22.35	23.30	24.19	25.03
	-9,016	-8,380	-7,735	-7,081	-6,418	-5,745	-5,064
	28.67	29.95	31.13	32.22	33.24	34.21	35.12
	-21,440	-20,523	-19,540	-18,491	-17,376	-16,195	-14,948
	21.44	23.28	25.07	26.83	28.55	30.24	31.90
	-38,160	-37,295	-36,420	-35,525	-34,620	-33,720	-32,800
	20.10	21.84	23.45	24.94	26.33	27.63	28.85
	-192,374	-190,808	-189,183	-187,002	-185,767	-183,980	-182,141
	33.79	36.93	39.90	42.71	45.39	47.95	50.41
	-260,320	-258,020	-255,610	-253,070	-250,420	-247,640	-244,740
	54.57	59.18	63.58	67.82	71.92	75.90	79.77
	-284,464	-283,210	-281,920	-280,602	-279,267	-277,880	-276,499
	32.50	35.02	37.37	39.58	41.65	43.61	45.47
	-338,792	-337,365	-335,878	-334,334	-332,260	-331,068	-329,346
	37.38	40.24	42.96	45.54	48.01	50.40	52.70
	-215,470	-214,760	-214,020	-213,250	-212,450	-211,630	-210,790
	15.58	17.01	18.36	19.64	20.87	22.05	23.17
	-936,074	-932,906	-929,645	-926,306	-922,900	-919,433	-915,912
	78.42	84.79	90.74	96.82	101.58	106.55	111.25
	-927,430	-924,300	-921,080	-917,790	-914,435	-911,020	-907,550
	76.04	82.32	88.19	93.69	98.87	103.77	108.41
	-999,200	-995,980	-992,660	-989,270	-985,800	-982,280	-978,700
	74.87	81.34	87.39	93.07	98.41	103.46	108.25

TABLE 7 (continued)

Species	Temperature, °C					
	25°	50°	60°	100°	150°	
Al <sub>2</sub> Si <sub>2</sub> O <sub>5</sub> (OH) <sub>4</sub> (kaolinite)	ΔH°	-980.020 <sup>d, b, n</sup>	-978,530	-977,920	-975,370	-972,030
	S°	48.53 <sup>d</sup>	53.33	55.20	62.41	70.31
KAl <sub>3</sub> Si <sub>3</sub> O <sub>10</sub> (OH) <sub>2</sub> (muscovite)	ΔH°	-1,420,900 <sup>d, n</sup>	-1,418,920	-1,418,090	-1,414,630	-1,410,040
	S°	69.0 <sup>d</sup>	75.39	77.90	87.70	99.25
NaAlSi <sub>3</sub> O <sub>8</sub> · H <sub>2</sub> O (analcime)	ΔH°	-786,800 <sup>d, z</sup>	-785,050	-784,540	-782,540	-780,030
	S°	56.03 <sup>d</sup>	60.07	61.60	67.29	73.69
CaMg(SiO <sub>3</sub> ) <sub>2</sub> (diopside)	ΔH°	-767,400 <sup>d, s</sup>	-766,430	-766,020	-764,300	-762,000
	S°	34.20 <sup>d</sup>	37.34	38.58	43.45	49.23
MgSiO <sub>3</sub> (clinoenstatite)	ΔH°	-370,100 <sup>d, s</sup>	-369,610	-369,410	-368,560	-367,440
	S°	16.22 <sup>d</sup>	17.79	18.41	20.81	23.63
Ca <sub>2</sub> Mg <sub>5</sub> Si <sub>8</sub> O <sub>22</sub> (OH) <sub>2</sub> (tremolite)	ΔH°	-2,952,900 <sup>d, s</sup>	-2,948,980	-2,947,410	-2,941,150	-2,933,310
	S°	131.19 <sup>d, n</sup>	143.81	148.58	166.35	186.03
KAlSi <sub>3</sub> O <sub>8</sub> (leucite)	ΔH°	-721,700 <sup>d, n</sup>	-720,720	-720,230	-718,760	-716,800
	S°	44.05 <sup>d</sup>	47.21	48.40	52.85	57.80
NaAlSiO <sub>4</sub> (α nepheline)	ΔH°	-498,500 <sup>d</sup>	-497,790	-497,490	-496,230	-494,490
	S°	29.72 <sup>d</sup>	32.02	32.93	36.50	40.87
Mg <sub>3</sub> Si <sub>4</sub> O <sub>10</sub> (OH) <sub>2</sub> (talc)	ΔH°	-1,415,200 <sup>d, s</sup>	-1,413,280	-1,412,510	-1,409,430	-1,405,590
	S°	62.34 <sup>d</sup>	68.53	70.87	79.59	89.26
KMg <sub>2</sub> AlSi <sub>3</sub> O <sub>10</sub> F <sub>2</sub> (fluorophlogopite)	ΔH°	-1,498,100 <sup>d</sup>	-1,496,000	-1,495,140	-1,491,550	-1,486,850
	S°	75.90 <sup>d</sup>	82.65	85.30	95.45	107.28
Mg <sub>2</sub> SiO <sub>4</sub> (forsterite)	ΔH°	-519,000 <sup>m</sup>	-518,270	-517,970	-516,720	-515,070
	S°	22.75 <sup>d</sup>	25.08	26.00	29.54	33.69
Fe <sub>2</sub> SiO <sub>4</sub> (fayalite)	ΔH°	-353,500 <sup>d, z</sup>	-352,690	-352,350	-350,980	-349,180
	S°	35.45 <sup>d</sup>	38.06	39.08	42.98	47.51
Mg(OH) <sub>2</sub> (brucite)	ΔH°	-221,200 <sup>d</sup>	-220,750	-220,570	-219,820	-218,860
	S°	15.09 <sup>d</sup>	16.53	17.09	19.20	21.63
Mg <sub>3</sub> Si <sub>2</sub> O <sub>7</sub> (OH) <sub>4</sub> (chrysotile)	ΔH°	-1,043,050 <sup>m</sup>	-1,041,360 <sup>n</sup>	-1,040,670 <sup>n</sup>	-1,037,750 <sup>n</sup>	-1,033,890 <sup>n</sup>
	S°	52.9 <sup>m</sup>	58.32 <sup>n</sup>	60.45 <sup>n</sup>	68.71 <sup>n</sup>	78.42 <sup>n</sup>
S <sub>2(g)</sub>	ΔH°	30,680 <sup>k</sup>	30,876	30,955	31,277	31,688
	S°	54.51 <sup>k</sup>	55.14	55.38	56.29	57.33
H <sub>2</sub> S <sub>(g)</sub>	ΔH°	-4,930 <sup>k</sup>	-4,724	-4,640	-4,301	-3,866
	S°	49.16 <sup>k</sup>	49.82	50.08	51.04	52.13
H <sub>2</sub> O <sub>(g)</sub>	ΔH°	-57,796 <sup>k</sup>	-57,954	-57,513	-57,186	-56,773
	S°	45.10 <sup>k</sup>	45.75	46.00	46.93	47.97

Temperature, °C						
200°	250°	300°	350°	400°	450°	500°
-963,540	-964,950	-961,250	-957,480	-953,620	-949,690	-945,700
78.59	85.82	92.56	98.88	104.83	110.45	115.79
-1,405,200	-1,400,180	-1,395,000	-1,389,700	-1,384,260	-1,378,730	-1,373,090
110.04	120.13	129.58	138.46	146.84	154.79	162.31
-777,520	-775,010	-772,500	-769,990	-767,490	-764,980	-762,470
79.20	84.24	88.82	93.01	96.88	100.48	103.84
-759,570	-757,050	-754,450	-751,800	-749,090	-746,330	-743,540
54.65	59.71	64.45	68.90	73.08	77.03	80.77
-366,260	-365,040	-363,790	-362,510	-361,200	-359,880	-358,530
26.26	28.70	30.99	33.13	35.15	37.05	38.86
-2,925,480	-2,917,640	-2,909,810	-2,901,970	-2,894,140	-2,886,300	-2,878,470
203.56	219.30	233.50	246.71	258.80	270.03	280.50
-714,830	-712,870	-710,910	-708,950	-706,990	-705,030	-703,070
62.17	66.11	69.69	72.97	76.00	78.81	81.43
-492,580	-490,490	-488,220	-485,780	-483,160	-480,360	-477,390
45.14	49.33	53.47	57.55	61.59	65.60	69.57
-1,401,740	-1,397,900	-1,394,050	-1,390,210	-1,386,370	-1,382,520	-1,378,680
97.85	105.57	112.59	119.02	124.96	130.47	135.61
-1,481,950	-1,476,920	-1,471,760	-1,466,500	-1,461,160	-1,455,740	-1,450,250
118.20	128.30	137.70	146.50	154.80	162.50	169.90
-513,350	-511,570	-509,740	-507,870	-505,970	-504,040	-502,080
37.54	41.12	44.46	47.58	50.51	53.28	55.90
-347,310	-345,390	-343,420	-341,400	-339,360	-337,270	-335,160
51.68	55.54	59.14	62.50	65.66	68.65	71.48
-217,850	-216,810	-215,720	-214,600	-213,430	-212,230	-210,990
23.88	25.98	27.46	29.84	31.63	33.36	35.02
-1,029,830 <sup>n</sup>	-1,025,610 <sup>n</sup>	-1,021,240 <sup>n</sup>	-1,016,750 <sup>n</sup>	-1,012,150 <sup>n</sup>	-1,007,430 <sup>n</sup>	-1,002,620 <sup>n</sup>
87.50 <sup>n</sup>	95.96 <sup>n</sup>	103.93 <sup>n</sup>	111.44 <sup>n</sup>	118.55 <sup>n</sup>	125.30 <sup>n</sup>	131.74 <sup>n</sup>
32,105	32,527	32,952	33,380	33,811	34,243	34,677
58.26	59.11	59.88	60.60	61.26	61.88	62.46
-3,420	-2,966	-2,502	-2,029	-1,548	-1,059	-5,619
53.13	54.04	54.89	55.68	56.42	57.12	57.79
-56,352	-55,926	-55,494	-55,055	-54,610	-54,160	-53,702
48.91	49.76	50.55	51.28	51.97	52.62	53.23

TABLE 7 (continued)

Species	Temperature, °C.					
	25°	50°	60°	100°	150°	
CO <sub>2(g)</sub>	ΔH°	-94,050 <sup>a</sup>	-93,457	-93,233	-92,392	-91,440
	S°	51.06 <sup>a</sup>	52.97	53.66	56.04	58.44

<sup>a</sup> In cal mole<sup>-1</sup> deg<sup>-1</sup>. <sup>b</sup> The enthalpies given in the table (ΔH°) are equal to the sum of the standard enthalpy of formation from the elements of the respective compounds and gases at the reference temperature (T<sub>r</sub>) plus the enthalpy change for the compound or gas resulting from a temperature increase from T<sub>r</sub> to temperature T; the units are cal mole<sup>-1</sup>. The values shown for the silicates (and brucite) above 25°C have been rounded to the nearest 10 cal mole<sup>-1</sup>. <sup>c</sup> The values shown in this table are for a standard state of 1 atm at the indicated temperature. All the enthalpies and entropies for temperatures of 50° and above were computed from equations (11) and (12) respectively, using the heat capacity power function coefficients shown in table 8.

TABLE 8

Heat capacity power function coefficients (eq 10) for solids and gases<sup>a</sup>

Species <sup>f</sup>	a''	b'' x 10 <sup>3</sup>	c'' x 10 <sup>-5</sup>
<sup>a</sup> Ag <sub>2</sub> S (acanthite)	10.13	26.4	0.0
<sup>a</sup> Cu <sub>2</sub> S (chalcocite)	19.50	0.0	0.0
CuS (covellite)	10.60	2.64	0.0
PbS (galena)	10.66	3.92	0.0
ZnS (sphalerite)	11.77 <sup>1</sup>	1.26 <sup>1</sup>	-1.16 <sup>1</sup>
ZnS (wurtzite)	11.82 <sup>1</sup>	1.16 <sup>1</sup>	-1.04 <sup>1</sup>
HgS (metacinnabar)	10.90	3.65	0.0
HgS (cinnibar)	11.57 <sup>c,m</sup>		
FeS (pyrrhotite)	5.19	26.4	0.0
CuFeS <sub>2</sub> (chalcopyrite)	15.6 <sup>1</sup>	21.6 <sup>1</sup>	0.6 <sup>1</sup>
FeS <sub>2</sub> (pyrite)	17.88	1.32	-3.05
Cu <sub>2</sub> FeS <sub>4</sub> (bornite)	44.4 <sup>1</sup>	40.0 <sup>1</sup>	0.6 <sup>1</sup>
Ag <sub>(c)</sub> (native silver)	5.09	2.04	0.36
Au <sub>(c)</sub> (native gold)	5.66	1.24	0.0
Cu <sub>(c)</sub> (native copper)	5.41	1.50	0.0
Hg <sub>(liq)</sub> (native mercury)	6.44	0.0	0.19
<sup>a</sup> Fe <sub>2</sub> O <sub>3</sub> (hematite)	23.49	18.6	-3.55
<sup>a</sup> Fe <sub>3</sub> O <sub>4</sub> (magnetite)	21.88	48.2	0.0
<sup>a</sup> SiO <sub>2</sub> (quartz)	11.22	8.20	-2.70
CuO (tenorite)	9.27	4.80	0.0
Cu <sub>2</sub> O (cuprite)	14.90	5.70	0.0
CaCO <sub>3</sub> (calcite)	24.98	5.24	-6.20
CaMg(CO <sub>3</sub> ) <sub>2</sub> (dolomite)	37.65 <sup>c,k</sup>		
ZnCO <sub>3</sub> (smithsonite)	9.30	33.0	0.0
PbCO <sub>3</sub> (cerrusite)	12.39	28.60	0.0
FeCO <sub>3</sub> (siderite)	11.63	26.80	0.0
<sup>a</sup> CaF <sub>2</sub> (fluorite)	14.30	7.28	0.47
CaSO <sub>4</sub> (anhydrite)	16.78	23.60	0.0
BaSO <sub>4</sub> (barite)	33.80	0.0	-8.43
PbSO <sub>4</sub> (anglesite)	10.96	31.0	4.20
KAlSi <sub>3</sub> O <sub>8</sub> (microcline, orthoclase, adularia, and sanidine)	63.83	12.90	-17.05
NaAlSi <sub>3</sub> O <sub>8</sub> (low albite)	61.70	13.90	-15.01
CaAl <sub>2</sub> Si <sub>2</sub> O <sub>8</sub> (anorthite)	64.42	13.70	-16.89
Al <sub>2</sub> Si <sub>2</sub> (OH) <sub>4</sub> (kaolinite)	67.93 <sup>1,b</sup>	19.22 <sup>1,b</sup>	-13.78 <sup>1,b</sup>
KAl <sub>2</sub> Si <sub>2</sub> O <sub>10</sub> (OH) <sub>2</sub> (muscovite)	97.56 <sup>a</sup>	26.33 <sup>a</sup>	-25.44 <sup>a</sup>
K <sub>0.8</sub> Mg <sub>0.2</sub> Al <sub>2.2</sub> Si <sub>2.8</sub> O <sub>10</sub> (OH) <sub>2</sub> (illite)	87.91 <sup>a</sup>	35.01 <sup>a</sup>	-19.51 <sup>a</sup>
KFe <sub>2</sub> AlSi <sub>2</sub> O <sub>10</sub> (OH) <sub>2</sub> (annite)	100.41 <sup>a</sup>	36.41 <sup>a</sup>	-14.31 <sup>a</sup>
Mg <sub>3</sub> Al <sub>2</sub> Si <sub>2</sub> O <sub>10</sub> (OH) <sub>2</sub> (chlorite)	96.8 <sup>1</sup>	36.1 <sup>1</sup>	-23.9 <sup>1</sup>

Species	Temperature, °C						
	200°	250°	300°	350°	400°	450°	500°
CO <sub>2(g)</sub>	ΔH°	-90,563	-89,739	-88,952	-88,192	-87,451	-86,726
	S°	60.40	62.05	63.49	64.76	65.91	66.94

<sup>a</sup> Robie and Waldbaum (1968). <sup>b</sup> Computed from the enthalpy of formation from the oxides (Robie, 1966) using enthalpies of formation of the oxides from the elements reported by Robie and Waldbaum (1968). <sup>c</sup> Waldbaum (1966). <sup>d</sup> Rounded to the nearest even 50 cal mole<sup>-1</sup>. <sup>e</sup> Barany and Kelley (1961). <sup>f</sup> Barany (1964). <sup>g</sup> Weller and King (1963). <sup>h</sup> Wagman and others (1965, 1968). <sup>i</sup> Kelley and others (1959). <sup>j</sup> King and others (1967). <sup>k</sup> Computed using the heat capacity power function for antigorite (table 8). <sup>l</sup> Computed from the entropy given above for calcite and an activity product constant of 10<sup>-3.37</sup> (Berner, 1967) at 25°C and 1 atm. <sup>m</sup> Adjusted (within the uncertainty range reported in the source reference) to achieve internal consistency among equilibrium constants describing mineral assemblages at 25°C.

TABLE 8 (continued)

Heat capacity power function coefficients (eq 10) for solids and gases<sup>a</sup>

Species <sup>f</sup>	a''	b'' x 10 <sup>3</sup>	c'' x 10 <sup>-5</sup>
Na <sub>0.33</sub> Al <sub>2.33</sub> Si <sub>2.67</sub> O <sub>10</sub> (OH) <sub>2</sub> (montmorillonite)	84.9 <sup>1</sup>	34.3 <sup>1</sup>	-19.7 <sup>1</sup>
K <sub>0.33</sub> Al <sub>2.33</sub> Si <sub>2.67</sub> O <sub>10</sub> (OH) <sub>2</sub> (montmorillonite)	85.3 <sup>1,n</sup>	34.9 <sup>1,n</sup>	-19.7 <sup>1,n</sup>
Ca <sub>0.167</sub> Al <sub>2.33</sub> Si <sub>2.67</sub> O <sub>10</sub> (OH) <sub>2</sub> (montmorillonite)	84.2 <sup>1</sup>	33.6 <sup>1</sup>	-20.0 <sup>1</sup>
Mg <sub>0.167</sub> Al <sub>2.33</sub> Si <sub>2.67</sub> O <sub>10</sub> (OH) <sub>2</sub> (montmorillonite)	84.0 <sup>1</sup>	33.7 <sup>1</sup>	-19.9 <sup>1</sup>
NaAlSi <sub>3</sub> O <sub>8</sub> · H <sub>2</sub> O (analcime)	50.17 <sup>c</sup>		
CaMg(SiO <sub>3</sub> ) <sub>2</sub> (diopside)	52.87	7.84	-15.74
MgSiO <sub>3</sub> (clinoenstatite)	24.55	4.74	-6.28
Ca <sub>2</sub> Mg <sub>5</sub> Si <sub>8</sub> O <sub>22</sub> (OH) <sub>2</sub> (tremolite)	156.7 <sup>c,e</sup>		
KAlSi <sub>3</sub> O <sub>8</sub> (leucite)	39.23 <sup>c</sup>		
NaAlSiO <sub>4</sub> (α nepheline)	6.63	70.60	0.0
Mg <sub>3</sub> Si <sub>4</sub> O <sub>10</sub> (OH) <sub>2</sub> (talc)	76.89 <sup>c,e</sup>		
KMg <sub>3</sub> AlSi <sub>3</sub> O <sub>10</sub> F <sub>2</sub> (fluorphlogopite)	100.86	17.16	-21.46
Mg <sub>3</sub> Si <sub>4</sub> O <sub>10</sub> (forsterite)	35.81	6.54	-8.52
Fe <sub>2</sub> SiO <sub>4</sub> (fayalite)	36.51	9.36	-6.70
Mg(OH) <sub>2</sub> (brucite)	13.04	15.80	0.0
Al(OH) <sub>3</sub> (gibbsite)	8.65	45.6	0.0
Mg <sub>3</sub> Si <sub>2</sub> O <sub>7</sub> (OH) <sub>2</sub> (antigorite)	75.82 <sup>b</sup>	31.6 <sup>b</sup>	-17.58 <sup>b</sup>
S <sub>2(g)</sub>	8.72	0.16	-0.90
H <sub>2</sub> S <sub>(g)</sub>	7.81	2.96	-0.46
H <sub>2</sub> O <sub>(c)</sub>	7.30	2.46	0.0
O <sub>2(g)</sub>	7.16	1.0	-0.40
H <sub>2(g)</sub>	6.52	0.78	0.12
CO <sub>2(g)</sub>	10.57	2.10	-2.06

<sup>a</sup> Kelley (1960). <sup>b</sup> The estimated power-function coefficients for kaolinite give 58.16 cal mole<sup>-1</sup> deg<sup>-1</sup> for the heat capacity of kaolinite at 25°C, compared to 58.62 cal mole<sup>-1</sup> deg<sup>-1</sup> reported by King and Weller (1961). <sup>c</sup> Heat capacity at 25°C (cal mole<sup>-1</sup> deg<sup>-1</sup>). When this quantity is used as the a'' coefficient in equations (11) and (12) with b'' and c'' set to zero, the heat capacity is treated as a constant. <sup>d</sup> Pankratz (1964). <sup>e</sup> Robie and Stout (1963). <sup>f</sup> The subscripts (c), (liq), and (g) refer to crystalline, liquid, and gas, respectively. <sup>g</sup> King and others, 1967. <sup>h</sup> Estimated by summing (in appropriate proportions) the coefficients in the heat capacity power functions for the elements (Kelley, 1960) in the mineral (see text). <sup>i</sup> Estimated by summing (in mole proportions) the coefficients in the heat capacity power functions of the oxide components (Kelley, 1960) in the mineral using ice (C<sub>p</sub> = a'' = 9.0 cal mole<sup>-1</sup> deg<sup>-1</sup>) to represent H<sub>2</sub>O (see text). <sup>j</sup> Stout and Robie (1963). <sup>k</sup> Pankratz and King (1965). <sup>l</sup> King and Weller (1962). Computed using C<sub>p,K<sub>2</sub>O</sub> = 18.1 + 8.8 × 10<sup>-3</sup> T obtained by fitting the enthalpies for K<sub>2</sub>O between 400° and 1000°K reported by Robie and Waldbaum (1968).

mineral assemblages, define mineral stabilities, and predict (by controlled extrapolation) higher temperature stability regions.

Activity Coefficients and Degrees of Formation of Complexes

Stoichiometric individual ion activity coefficients for Al<sup>+++</sup>, S<sup>---</sup>, SO<sub>4</sub><sup>---</sup>, CO<sub>3</sub><sup>---</sup>, and various ore-forming metals in concentrated NaCl solutions to 300°C are shown in tables 13 and 14 and plotted in figures 9 to 14. These values, together with the activity coefficients for Na<sup>+</sup>, K<sup>+</sup>, and Ca<sup>++</sup> in tables 13 and 14, were computed from equilibrium constants given in tables 4 and 5, mass balance expressions of the kind shown in equation (49), true individual ion activity coefficients computed from equation (43) using 25°C  $\lambda$  values<sup>7</sup>, and the data in table 2. Values of  $\gamma_{CO_2}$  in NaCl solutions (table 2) were used in the calculations to

represent the activity coefficients of the neutral species. Also,  $a_{Cl-}$ ,  $\bar{I}$ , and  $B'$  in the calculations were taken to be those in pure NaCl solutions (table 2) because other constituents in hydrothermal solutions are commonly present in small concentrations compared to NaCl. The stoichiometric individual ion activity coefficients shown in table 14 are conservative values; that is, they do not include provision for divalent and trivalent complexes of the metal ions (see discussion above and footnote 3, table 14). The complexes with the higher charges were omitted to preclude any substantial errors that might be introduced by the assumption of constant  $\lambda$  values.

The degrees of formation achieved by metal chloride complexes in concentrated sodium chloride solutions at high temperatures are depicted in figure 15. The distribution of species shown in figure 15 is based on evaluation of

$$\alpha_c = \frac{a_{Cl-}^x \gamma_i}{\beta_c \gamma_c} \quad (54)$$

where  $\alpha_c$  is the degree of formation of the  $c$ th mononuclear complex containing  $y$  moles of chloride and 1 mole of the  $i$ th cation. The curves for the respective metal ions in figure 15 include provision for all of the reactions and species involving those ions shown in table 5; the  $\beta_c$ ,  $\gamma_c$ , and  $\gamma_i$  values used in the calculations were computed in the manner described above. Because 25°C  $\lambda$  values were used to compute the activity coefficients required to evaluate equation (54), appreciable error may have been incorporated into the calculations of  $\alpha_c$  for the divalent complexes at the higher temperatures. Figure 15 thus illustrates only the distribution of species in solution that occurs if the  $\lambda$  values for the ions remain essentially constant from 25°C to 300°C. If they in fact increase significantly, the diagrams in figure 15 will change substantially, but the  $\gamma_i$  values presented in tables 13 and 14 and figures 9 to 14 will be affected only slightly owing to the fact that the divalent (and higher

<sup>7</sup> The values of  $\lambda$  were assigned on the basis of Kielland's (1937)  $\lambda$  values assuming equalities for similar complexes.

TABLE 9  
Equilibrium constants for hydrothermal oxidation-reduction reactions involving aqueous species at high temperatures

Reaction*	$\Delta H_c^\circ(T)^\dagger$ (cal mole <sup>-1</sup> )	$\Delta S_c^\circ(T)^\ddagger$ (cal mole <sup>-1</sup> deg <sup>-1</sup> )	log K(T) <sup>e</sup>									
			25°C	50°C	60°C	100°C	150°C	200°C	250°C	300°C		
2H <sub>2</sub> S + O <sub>2(aq)</sub> ⇌ S <sub>2(aq)</sub> + 2H <sub>2</sub> O <sup>h</sup>	- 87,890	- 22.9	59.44	54.4*	52.57	46.27	39.99	35.05	30.6*	27.21		
H <sub>2</sub> S + 2O <sub>2(aq)</sub> ⇌ H <sup>+</sup> + HSO <sub>4</sub> <sup>-</sup>	-204,440	-102.2	127.54	115.5*	111.71	97.30	83.05	71.62	62.5*	55.61		
H <sub>2</sub> S + 2O <sub>2(aq)</sub> ⇌ 2H <sup>+</sup> + SO <sub>4</sub> <sup>---</sup>	-208,290	-124.2	129.55	113.2*	109.31	94.31	79.31	67.13	57.1*	48.55		
HS <sup>-</sup> + 2O <sub>2(aq)</sub> ⇌ H <sup>+</sup> + SO <sub>4</sub> <sup>---</sup>	-213,090	-108.4	132.53	120.0*	116.02	103.93	86.03	74.09	64.4*	56.61		
2H <sup>+</sup> + S <sup>---</sup> + 1/2 O <sub>2(aq)</sub> ⇌ 1/2 S <sub>2(aq)</sub> + H <sub>2</sub> O <sup>h</sup>	- 62,040	23.5	50.62	47.1*	45.85	41.54	37.33	34.05	31.3*	29.39		
2HS <sup>-</sup> + O <sub>2(aq)</sub> + 2H <sup>+</sup> ⇌ S <sub>2(aq)</sub> + 2H <sub>2</sub> O <sup>h</sup>	- 97,490	8.9	73.42	68.0*	66.01	59.53	53.43	48.97	45.3*	43.33		
S <sup>---</sup> + 2O <sub>2(aq)</sub> ⇌ SO <sub>4</sub> <sup>---</sup>	-226,390	- 89.4	146.43	133.9*	128.86	112.70	96.68	83.74	72.7*	64.26		
Fe <sup>+++</sup> + 1/2 H <sub>2</sub> O ⇌ Fe <sup>++</sup> + 1/4 O <sub>2(aq)</sub> + H <sup>+</sup>	24,557	46.89	- 7.75	- 6.35*	- 5.87	- 4.16	- 2.48	- 1.15	- 0.1*	0.84		
Cu <sup>++</sup> + 1/2 H <sub>2</sub> O ⇌ Cu <sup>+</sup> + 1/4 O <sub>2(aq)</sub> + H <sup>+</sup>	35,697	36.89	- 18.10	- 16.1*	- 15.35	- 12.83	- 10.34	- 8.35	- 6.64*	- 5.33		
S <sup>---</sup> + 4H <sub>2</sub> O <sup>h</sup> ⇌ SO <sub>4</sub> <sup>---</sup> + 4H <sub>2(aq)</sub>	46,870	66.80	- 19.76	- 17.15*	- 16.26	- 13.30	- 10.69	- 8.92	- 7.6*	- 6.87		
8Fe <sup>+++</sup> + 4H <sub>2</sub> O <sup>h</sup> + S <sup>---</sup> ⇌ 8Fe <sup>++</sup> + SO <sub>4</sub> <sup>---</sup> + 8H <sup>+</sup>	29,930	285.72	84.43	83.1*	81.90	79.42	76.84	74.62	71.9*	70.98		
8Cu <sup>+++</sup> + 4H <sub>2</sub> O <sup>h</sup> + S <sup>---</sup> ⇌ 8Cu <sup>++</sup> + SO <sub>4</sub> <sup>---</sup> + 8H <sup>+</sup>	59,190	205.72	1.63	5.1*	6.06	10.66	13.96	16.70	19.6*	21.62		
Cu <sup>+</sup> + Fe <sup>+++</sup> ⇌ Cu <sup>++</sup> + Fe <sup>++</sup>	- 11,140	10.00	10.35	9.7*	9.48	8.67	7.86	7.20	6.6*	6.17		

\* All reactants and products are aqueous unless otherwise indicated by the subscript (g) for gas. <sup>b</sup> Computed from thermodynamic data given in tables 3, 6, and 7. <sup>c</sup> The log K(T) values shown for 25°C were computed from the  $\Delta H_c^\circ(T)$  and  $\Delta S_c^\circ(T)$  values shown in the table; those for 60°C and above were calculated using  $\Delta H_c^\circ(T)$ ,  $S_c^\circ(T)$ , and average heat capacity values for the ions, H<sub>2</sub>S<sub>(aq)</sub>, and H<sub>2</sub>O<sub>(aq)</sub> (table 3) to first compute  $\Delta H_c^\circ(T)$  and  $S_c^\circ(T)$  for these species at elevated temperatures (eqs 13 and 14). These values were then used together with those for gases in tables 6 and 7 to evaluate equation (15). All the log K(T) values are consistent with molal units of concentration. <sup>d</sup> Liquid water. <sup>e</sup> Interpolated.

TABLE 10  
Equilibrium constants for the disproportionation of aqueous ions, oxidation-reduction of hydrothermal minerals, and dissolution of gases in aqueous solution at elevated temperatures

Reaction <sup>a</sup>	$\Delta H^{\circ}_f(T_r)^b$ (cal mole <sup>-1</sup> )	$\Delta S^{\circ}_f(T_r)^b$ (cal mole <sup>-1</sup> deg <sup>-1</sup> )	log K(T) <sup>c</sup>							
			25°C	50°C	60°C	100°C	150°C	200°C	250°C	300°C
$2\text{Cu}^+ \rightleftharpoons \text{Cu}^{2+} + \text{Cu}^0$	-18,470	-34.45	6.01	4.92 <sup>d</sup>	4.57	3.20	1.84	0.66	0.37	1.27
$3\text{Au}^+ \rightleftharpoons 2\text{Au}^{3+} + \text{Au}^0$	-33,200 <sup>e</sup>	-66.4	9.82 <sup>e</sup>	7.91 <sup>b</sup>	7.22 <sup>b</sup>	4.76 <sup>b</sup>	2.24 <sup>b</sup>	0.16 <sup>b</sup>	1.60 <sup>b</sup>	3.11
$\text{Cu}_2\text{FeS}_3 + 4\text{FeS}_2 \rightleftharpoons 5\text{CuFeS}_2 + \text{S}_{2(g)}$	56,750 <sup>f</sup>	68.91 <sup>1</sup>	-26.5	-23.2 <sup>d</sup>	-22.2	-18.2	-14.2	-11.1	-8.5	-6.4 <sup>1</sup>
$4\text{FeS}_2 + 4\text{H}_2\text{O} \rightleftharpoons 4\text{Fe}^{2+} + 7\text{S}^{2-} + \text{SO}_4^{2-} + 8\text{H}^+$	199,430	-249.04	-200.57	-189.7 <sup>d</sup>	-185.46	-171.89	-158.96	-149.17	-141.49	-136.04
$3\text{Fe}_2\text{O}_3(c) \rightleftharpoons 2\text{Fe}_3\text{O}_4(c) + \frac{1}{2}\text{O}_{2(g)}$	57,100	33.89	-34.43	-31.13 <sup>d</sup>	-30.04	-26.02	-22.07	-18.95	-16.44	-14.35
$\text{FeS}_2(c) \rightleftharpoons \text{FeS}(c) + \frac{1}{2}\text{S}_{2(g)}$	32,210	29.02	-17.26	-15.42 <sup>d</sup>	-14.78	-12.50	-10.25	-8.48	-7.03	-5.81
$\text{FeS}(c) + \text{FeS}_2(c) + \frac{3}{2}\text{O}_{2(g)} \rightleftharpoons \text{Fe}_3\text{O}_4(c) + \frac{3}{2}\text{S}_{2(g)}$	907,350	7.49	63.69	58.67 <sup>d</sup>	56.96	50.89	44.92	40.20	36.38	33.22
$\text{FeS}_2(c) + \frac{3}{2}\text{O}_{2(g)} \rightleftharpoons \text{Fe}_2\text{O}_3(c) + \frac{3}{2}\text{S}_{2(g)}$	-53,940	31.12	46.33	43.18 <sup>d</sup>	42.18	38.39	34.66	31.72	29.35	28.19
$3\text{FeS}_2(c) + 2\text{O}_{2(g)} \rightleftharpoons \text{Fe}_3\text{O}_4(c) + 3\text{S}_{2(g)}$	-52,360	63.98	52.27	49.15 <sup>d</sup>	48.24	44.57	40.95	38.11	35.81	33.93
$\text{Cu}_2\text{S}(c) + \frac{1}{2}\text{S}_{2(g)} \rightleftharpoons 2\text{CuS}(c)$	-19,412	24.20	8.92	7.71 <sup>d</sup>	7.32	6.06	4.72	3.66	2.77	2.09
$\text{Cu}^+(c) + 2\text{H}^+ + \frac{1}{2}\text{O}_{2(g)} \rightleftharpoons \text{Cu}^{2+} + \text{H}_2\text{O}(l)$	-52,925	-39.34	30.19	27.1 <sup>d</sup>	26.13	22.45	18.84	16.04	13.78	11.94
$2\text{Cu}^+(c) + \frac{1}{2}\text{S}_{2(g)} \rightleftharpoons \text{Cu}_2\text{S}(c)$	-34,488	-14.29	22.15	20.20 <sup>d</sup>	19.50	17.09	14.78	12.88	11.38	10.16
$\text{Cu}^+(c) + \text{H}^+ + \frac{1}{4}\text{O}_{2(g)} \rightleftharpoons \text{Cu}^+ + \frac{1}{2}\text{H}_2\text{O}(l)$	-17,227	-2.44	12.09	11.1 <sup>d</sup>	10.78	9.63	8.50	7.69	7.07	6.61
$\text{Cu}^+(c) + \frac{1}{2}\text{S}_{2(g)} \rightleftharpoons \text{CuS}(c)$	-26,945	-19.27	15.54	14.01 <sup>d</sup>	13.46	11.58	11.35	9.94	7.09	6.13
$\text{Ag}^+(c) + \text{H}^+ + \frac{1}{4}\text{O}_{2(g)} \rightleftharpoons \text{Ag}^+ + \frac{1}{2}\text{H}_2\text{O}(l)$	-8,847	3.60	7.27	6.74 <sup>d</sup>	6.60	6.01	5.44	5.06	4.74	4.50
$2\text{Ag}^+(c) + \frac{1}{2}\text{S}_{2(g)} \rightleftharpoons \text{Ag}_2\text{S}(c)$	-23,077	-13.51	13.96	12.65 <sup>d</sup>	12.19	10.57	9.00	7.77	6.79	5.99
$\text{Hg}^+(l) + 2\text{H}^+ + \frac{1}{2}\text{O}_{2(g)} \rightleftharpoons \text{Hg}^{2+} + \text{H}_2\text{O}(l)$	-26,725	-31.69	12.66	11.13 <sup>d</sup>	10.61	8.72	6.84	5.97	4.15	3.14

$\text{Hg}^+(l) + \frac{1}{2}\text{S}_{2(g)} \rightleftharpoons \text{HgS}(c)$ <sup>1</sup>	-26,500	-22.75	14.43	12.86 <sup>d</sup>	12.40	10.55	8.73	7.30	6.14	5.19
$\text{Au}^+(c) + \frac{3}{4}\text{O}_{2(g)} + 3\text{H}^+ \rightleftharpoons \text{Au}^{3+} + \frac{3}{2}\text{H}_2\text{O}(l)$	4,850 <sup>e</sup>	-46.0	-13.61 <sup>e</sup>	-13.34 <sup>b</sup>	-13.24 <sup>b</sup>	-12.91 <sup>b</sup>	-12.59 <sup>b</sup>	-12.35 <sup>b</sup>	-12.17 <sup>b</sup>	-12.02 <sup>b</sup>
$\text{Au}^+(c) + \frac{1}{4}\text{O}_{2(g)} + \text{H}^+ \rightleftharpoons \text{Au}^+ + \frac{1}{2}\text{H}_2\text{O}(l)$	12,680 <sup>e</sup>	6.8	-7.81 <sup>e</sup>	-7.03 <sup>b</sup>	-6.82 <sup>b</sup>	-5.89 <sup>b</sup>	-4.94 <sup>b</sup>	-4.17 <sup>b</sup>	-3.52 <sup>b</sup>	-2.97 <sup>b</sup>
$\text{CO}_{2(g)} + \text{H}_2\text{O}(l) \rightleftharpoons \text{H}_2\text{CO}_{3(aq)}$ <sup>o</sup>	-4,650	-22.3	-1.46	-1.70 <sup>d</sup>	-1.78	-1.97	-2.07	-2.06	-1.98	-1.83
$\text{H}_2\text{S}(g) \rightleftharpoons \text{H}_2\text{S}(aq)$	-4,100	-18.3	-0.99	-1.20 <sup>d</sup>	-1.26	-1.43	-1.52	-1.54	-1.52	-1.46

<sup>a</sup> All reactants and products are aqueous unless otherwise indicated by the subscripts (c) for crystalline or (g) for gas; the subscript (liq) refers to liquid. The crystalline compounds correspond to the mineral designations given in tables 7 and 8. <sup>b</sup> Except where noted otherwise, these values were computed from thermodynamic data given in tables 3, 6, and 7. <sup>c</sup> Except where noted otherwise, the log K(T) values for 25°C were computed from the values of  $\Delta H^{\circ}_f(T_r)$  and  $\Delta S^{\circ}_f(T_r)$  shown in the table; those for 60°C and above were calculated using  $\Delta H^{\circ}_f(T_r)$ ,  $S^{\circ}_f(T_r)$ , and average heat capacities for the ions,  $\text{H}_2\text{O}(l)$ , and  $\text{H}_2\text{S}(aq)$  (table 3) to first compute  $\Delta H^{\circ}_f(T)$  and  $S^{\circ}_f(T)$  for these species at elevated temperatures (eqs 13 and 14). These values were then used together with those computed from equations (11) and (12) using data given in tables 6, 7, and 8 for minerals and gases to evaluate equation (15). The enthalpies of formation and entropies of chalcopyrite used in the calculations are given in footnotes j and k below. All the log K(T) values are consistent with molal units of concentration. <sup>d</sup> Interpolated. <sup>e</sup> The subscript (app) indicates that the species referred to is the undifferentiated sum of  $\text{H}_2\text{CO}_{3(aq)}$  and  $\text{CO}_{2(aq)}$ . <sup>f</sup> Computed from  $\Delta S^{\circ}_f(T_r)$  and log K(T). <sup>g</sup> Computed from free energies of formation from the elements (Latimer, 1952). <sup>h</sup> Predicted assuming a constant  $\Delta C^{\circ}_{p,r}(T)$  equal to a mean value computed from average heat capacities for the respective ions (table 3) and the true heat capacities of the other species calculated from equation (10) using the coefficients in table 8. <sup>i</sup> Metacinnabar. <sup>j</sup> Computed from entropies given in table 7 and estimates of the entropy of chalcopyrite (31.2 cal mole<sup>-1</sup> deg<sup>-1</sup>) and bornite (91 cal mole<sup>-1</sup> deg<sup>-1</sup>) at 25°C obtained by summing (in appropriate proportions) the values tabulated by Latimer (1952) for the entropy contributions of iron, copper, and sulfide in solids—see text. <sup>k</sup> Computed from enthalpies of formation given in table 7 and those for chalcopyrite (-44,550 cal mole<sup>-1</sup>) and bornite (-84,820 cal mole<sup>-1</sup>) calculated from estimated free energies of formation for these minerals (-45,000 cal mole<sup>-1</sup> and -89,000 cal mole<sup>-1</sup>, respectively) at 25°C (Bartholomé, 1958) together with corresponding entropies of formation of the minerals from the elements calculated from the entropy estimates given in footnote j above and data for the elements taken from Robie and Waldbaum (1968). Bartholomé's values for the free energies of chalcopyrite and bornite appear to be more consistent with high temperature equilibrium data for the sulfides (Barton and Skinner, 1967) than do Young's (1967). <sup>l</sup> This value compares favorably with that (-6.9) reported by Barton and Skinner (1967), but the slope of log K(T) is more positive. Barton and Skinner assumed the heat capacity of reaction to be zero; the present calculations indicate that the heat capacity is neither zero nor constant.

TABLE 11  
Activity products for hydrothermal minerals and equilibrium constants for various silicate reactions involving an aqueous phase at high temperatures

Reaction*	$\Delta H^\circ_f(T_r)^b$ (cal mole <sup>-1</sup> )	$\Delta S^\circ_f(T_r)^b$ (cal mole <sup>-1</sup> deg <sup>-1</sup> )	log K(T) <sup>c</sup>								
			25°C	50°C	60°C	100°C	150°C	200°C	250°C	300°C	
$\text{Cu}_2\text{FeS}_{2(\text{bornite})} \rightleftharpoons 4\text{Cu}^+ + \text{Cu}^{2+} + \text{Fe}^{2+} + 4\text{S}^{--}$	183,210 <sup>d</sup>	-120,10 <sup>d</sup>	-160.5	-150.0 <sup>e</sup>	-146.4	-133.4	-120.8	-110.6	-102.3	-95.6	
$\text{CuFeS}_{2(\text{chalcopyrite})} \rightleftharpoons \text{Cu}^{2+} + \text{Fe}^{2+} + 2\text{S}^{--}$	57,080 <sup>d</sup>	-89.90 <sup>d</sup>	-61.5	-58.4 <sup>e</sup>	-57.1	-53.1	-49.2	-46.2	-43.7	-41.9	
$\text{PbS} \rightleftharpoons \text{Pb}^{2+} + \text{S}^{--}$	32,030	-23.34	-28.57	-26.67 <sup>e</sup>	-26.14	-23.96	-21.93	-20.36	-19.14	-18.31	
$\text{ZnS}_{(\text{sphalerite})} \rightleftharpoons \text{Zn}^{2+} + \text{S}^{--}$	22,040	-43.77	-25.72	-24.44 <sup>e</sup>	-24.03	-22.48	-21.01	-19.81	-18.86	-18.17	
$\text{ZnS}_{(\text{wurtzite})} \rightleftharpoons \text{Zn}^{2+} + \text{S}^{--}$	18,385 <sup>f</sup>	-46.56 <sup>f</sup>	-23.65	-22.58 <sup>e</sup>	-22.24	-20.96	-19.73	-18.73	-17.95	-17.99	
$\text{Ag}_2\text{S} \rightleftharpoons 2\text{Ag}^+ + \text{S}^{--}$	67,427	-2.76	-50.02	-46.17 <sup>e</sup>	-44.83	-40.08	-35.45	-31.71	-28.74	-26.36	
$\text{Cu}_2\text{S} \rightleftharpoons 2\text{Cu}^+ + \text{S}^{--}$	62,080	-14.06	-48.57	-45.05 <sup>e</sup>	-43.79	-39.37	-35.05	-31.54	-28.65	-26.32	
$\text{CuS} \rightleftharpoons \text{Cu}^{2+} + \text{S}^{--}$	36,070	-43.53	-35.96	-33.91 <sup>e</sup>	-33.18	-30.66	-28.21	-26.28	-24.73	-23.56	
$\text{HgS}_{(\text{metacinnabar})} \rightleftharpoons \text{Hg}^{2+} + \text{S}^{--}$	61,830	-32.40	-52.37	-48.84 <sup>e</sup>	-47.64	-43.36	-39.23	-35.98	-33.42	-31.45	
$\text{HgS}_{(\text{cinnabar})} \rightleftharpoons \text{Hg}^{2+} + \text{S}^{--}$	64,560 <sup>f</sup>	-29.12 <sup>f</sup>	-53.68	-50.02 <sup>e</sup>	-48.73	-44.25	-39.91	-36.51	-33.83	-31.72	
$\text{FeS} \rightleftharpoons \text{Fe}^{2+} + \text{S}^{--}$	12,200	-42.52	-18.89	-18.17 <sup>e</sup>	-17.96	-17.12	-16.33	-15.71	-15.22	-14.94	
$\text{FeS}_2 \rightleftharpoons \text{Fe}^{2+} + \text{S}^{--} + \frac{1}{2}\text{S}_{2(\text{g})}$	29,070	-43.75	-36.15	-33.50 <sup>e</sup>	-32.74	-30.17	-26.60	-24.19	-22.25	-20.75	
$\text{CaSO}_4 \rightleftharpoons \text{Ca}^{2+} + \text{SO}_4^{--}$	-3,755	-34.10	-4.70 <sup>n</sup>	-4.99 <sup>f,n</sup>	-5.09 <sup>f,n</sup>	-5.63 <sup>n</sup>	-6.35 <sup>n</sup>	-7.18 <sup>n</sup>	-8.12 <sup>n</sup>	-9.05 <sup>n</sup>	
$\text{BaSO}_4(\text{barite}) \rightleftharpoons \text{Ba}^{2+} + \text{SO}_4^{--}$	6,140 <sup>f</sup>	-23.80 <sup>f</sup>	-9.70	-9.42 <sup>e</sup>	-9.34	-9.22	-9.34	-9.76	-10.34	-11.05	
$\text{PbSO}_4(\text{anglesite}) \rightleftharpoons \text{Pb}^{2+} + \text{SO}_4^{--}$	220 <sup>f</sup>	-28.2 <sup>f</sup>	-7.75	-7.70 <sup>e</sup>	-7.70	-7.86	-8.26	-8.88	-9.60	-10.44	
$\text{CaCO}_3 \rightleftharpoons \text{Ca}^{2+} + \text{CO}_3^{--}$	-3,190	-49.0	-8.37	-8.62 <sup>e</sup>	-8.74	-9.39	-10.25	-11.37	-12.72	-14.10	

$\text{CaMg}(\text{CO}_3)_2(\text{dolomite}) \rightleftharpoons \text{Ca}^{2+} + \text{Mg}^{2+} + 2\text{CO}_3^{--}$	-8,290 <sup>f</sup>	-105.69 <sup>f</sup>	-17.02 <sup>e</sup>	-17.63 <sup>e</sup>	-17.92	-19.28	-21.02	-23.26	-25.83	-28.46
$\text{ZnCO}_3(\text{smithsonite}) \rightleftharpoons \text{Zn}^{2+} + \text{CO}_3^{--}$	4,420 <sup>f</sup>	-59.30 <sup>f</sup>	9.72	-10.05 <sup>e</sup>	-10.19	-10.88	-11.77	-12.90	-14.18	-15.52
$\text{PbCO}_3(\text{cerussite}) \rightleftharpoons \text{Pb}^{2+} + \text{CO}_3^{--}$	5,710 <sup>f</sup>	-42.40 <sup>f</sup>	-13.45	-13.19 <sup>e</sup>	-13.16	-13.21	-13.54	-14.30	-15.31	-16.50
$\text{FeCO}_3(\text{siderite}) \rightleftharpoons \text{Fe}^{2+} + \text{CO}_3^{--}$	5,030 <sup>f</sup>	-65.8 <sup>f</sup>	-10.69	-11.04 <sup>e</sup>	-11.21	-11.95	-12.86	-14.05	-15.32	-16.67
$\text{CaF}_2(\text{fluorite}) \rightleftharpoons \text{Ca}^{2+} + 2\text{F}^-$	1,530 <sup>f</sup>	-36.26 <sup>f</sup>	9.04	9.01 <sup>e</sup>	9.01	9.20	9.66	10.26	11.08	12.13
$\text{KAlSi}_3\text{O}_8 + \text{Na}^+ \rightleftharpoons \text{NaAlSi}_3\text{O}_8 + \text{K}^+$	5,939	7.83	-2.64	-2.29 <sup>e</sup>	-2.19	-1.80	-1.43	-1.15	-0.95	-0.79
$3\text{KAlSi}_3\text{O}_8 + 2\text{H}^+ \rightleftharpoons \text{KAl}_3\text{Si}_3\text{O}_{10}(\text{OH})_2 + 2\text{K}^+ + 6\text{SiO}_2(\text{tr})$	8,880	19.87	10.85	10.31 <sup>e</sup>	10.17	9.55	8.91	8.40	8.12	7.82
$2\text{KAl}_3\text{Si}_3\text{O}_{10}(\text{OH})_2 + 2\text{H}^+ + 3\text{H}_2\text{O} \rightleftharpoons 3\text{Al}_2\text{Si}_2\text{O}_7(\text{OH})_4 + 2\text{K}^+$	13,395	6.46	11.22	10.45 <sup>e</sup>	10.16	9.12	7.96	7.04	6.20	5.44
$4\text{CaMg}(\text{SiO}_3)_2 + \text{Mg}^{2+} + 2\text{H}^+ \rightleftharpoons \text{Ca}_3\text{Mg}_6\text{Si}_6\text{O}_{22}(\text{OH})_2 + 2\text{Ca}^{2+}$	32,430	-3.81	22.93	21.00 <sup>e</sup>	20.42	18.08	15.62	13.63	11.76	10.13
$\text{NaAlSi}_3\text{O}_8 + \text{K}^+ + \text{H}_2\text{SiO}_4 \rightleftharpoons \text{KAlSi}_3\text{O}_8 + \text{Na}^+ + 2\text{H}_2\text{O}$	9,009	-8.19	4.81	4.32 <sup>e</sup>	4.13	3.50	2.92	2.45	2.05	1.75
$2\text{Al}(\text{OH})_3 + 2\text{H}_2\text{SiO}_4 \rightleftharpoons \text{Al}_2\text{Si}_2\text{O}_7(\text{OH})_4 + 5\text{H}_2\text{O}$	9,275	6.90	8.29	7.8 <sup>e</sup>	7.59	6.97	6.44	6.02	5.70	5.54
$\text{Mg}_5\text{Al}_2\text{Si}_8\text{O}_{20}(\text{OH})_8 + 10\text{H}^+ \rightleftharpoons \text{Al}_2\text{Si}_2\text{O}_7(\text{OH})_4 + 5\text{Mg}^{2+} + \text{H}_2\text{SiO}_4 + 5\text{H}_2\text{O}$	-111,865	-75.08	65.57	59.6 <sup>e</sup>	57.15	49.81	42.86	37.95	34.18	31.26



TABLE 11 (continued)

Reaction <sup>a</sup>	$\Delta H_f^\circ(T_r)^b$ (cal mole <sup>-1</sup> )	$\Delta S_f^\circ(T_r)^b$ (cal mole <sup>-1</sup> deg <sup>-1</sup> )	log K(T) <sup>c</sup>							
			25°C	50°C	60°C	100°C	150°C	200°C	250°C	300°C
$4CaAl_2Si_2O_8 + 5Mg^{++} + 18H^+ \rightleftharpoons Ca_2Mg_5Si_8O_{22}(OH)_2 + 2Ca^{++} + 8Al^{+++} + 8H_2O^*$	-185,710	-429.53	42.25	39.1 <sup>f</sup>	28.06	15.28	2.74	-6.65	-14.48	-20.79
$Mg_3Al_2Si_2O_{10}(OH)_2 + 2Ca^{++} + 5H_2SiO_4 + 2H^+ \rightleftharpoons Ca_2Mg_3Si_8O_{22}(OH)_2 + 2Al^{+++} + 14H_2O^*$	-53,630	-103.47	16.69	13.6 <sup>f</sup>	12.68	9.96	6.32	4.22	2.84	1.97
$Mg_5Si_3O_{16}(OH)_2 + 5H_2O^* \rightleftharpoons Mg_3Si_2O_8(OH)_2 + 2H_2SiO_4$	17,605	-1.31	-13.19	-12.20 <sup>f</sup>	-11.83 <sup>g</sup>	-10.60 <sup>g</sup>	-9.43 <sup>g</sup>	-8.47 <sup>g</sup>	-7.68 <sup>g</sup>	-7.08 <sup>g</sup>

<sup>a</sup> Where no indication is given, all reactants and products except liquid water, H<sub>2</sub>SiO<sub>4</sub>, and ionic species correspond to the mineral designations given in table 7. H<sub>2</sub>SiO<sub>4</sub> and all ionic species are in the aqueous standard state. <sup>b</sup> Except where noted otherwise, the values in these columns were computed from thermodynamic data given in tables 3, 7, and 10 (footnotes j and k). <sup>c</sup> Except where noted otherwise, the log K(T) values for 25°C were computed from the values of  $\Delta H_f^\circ(T_r)$  and  $\Delta S_f^\circ(T_r)$  shown in the table; those for 60°C and above were calculated using  $\Delta H_f^\circ(T_r)$ ,  $S_f^\circ(T_r)$ , and average heat capacity values for the ions, H<sub>2</sub>O<sub>(l)</sub>, and H<sub>2</sub>SiO<sub>4</sub> (table 3) to first compute  $\Delta H_f^\circ(T)$  and  $S_f^\circ(T)$  for these species at elevated temperatures (eqs 13 and 14). These values were then used together with those computed from eq (11) and (12) using data given in tables 7, 8, and 10 (footnotes j and k) for the solids and S<sub>298</sub> to evaluate equation (15). With the exception of dolomite (see footnote l below), values of  $\Delta H_f^\circ(T_r)$  and  $S_f^\circ(T_r)$  for minerals not included in tables 7 and 10 were taken from Robie and Waldbaum (1968). All the log K(T) values are consistent with molal units of concentration. <sup>d</sup> See footnotes j and k, table 10. <sup>e</sup> Liquid water. <sup>f</sup> Interpolated. <sup>g</sup> Computed using the heat capacity power function for antigorite (table 8) to represent chrysotile. <sup>h</sup> Chrysotile. <sup>i</sup> Computed from data given in table 3 for the ionic species and, except where noted otherwise, the enthalpies of formation and entropies of the minerals at 25°C tabulated by Robie and Waldbaum (1968). <sup>j</sup> Computed using the entropy for dolomite reported by Stout and Robie (1963). <sup>k</sup> Langmuir (1964); Hsu (1967); Berner (1967). <sup>l</sup> The  $\Delta H_f^\circ(T_r)$  value for dolomite used in the calculations was computed from the activity product constant for dolomite and a calculated entropy of formation of dolomite from the elements at 25°C (see footnote j above). <sup>m</sup> See footnote p, table 7. <sup>n</sup> These values differ from those reported by Yeatts and Marshall (1969), who did not take into account explicitly the effects of calcium sulfate complexing in their calculation of the activity product for anhydrite. <sup>o</sup> Crystalline gibbsite.

TABLE 12  
Equilibrium constants for the hydrolysis of silicates and various oxide, hydroxide, and carbonate minerals at elevated temperatures<sup>a</sup>

Reaction <sup>a</sup>	$\Delta H_f^\circ(T_r)^b$ (cal mole <sup>-1</sup> )	$\Delta S_f^\circ(T_r)^b$ (cal mole <sup>-1</sup> deg <sup>-1</sup> )	log K(T) <sup>c,d</sup>						
			25°C	60°C	100°C	150°C	200°C	250°C	300°C
$SiO_2 + 2H_2O \rightleftharpoons H_2SiO_4$	6,220	2.54	-4.00	-3.52	-3.08	-2.67	-2.35	-2.11	-1.94
$KAlSi_3O_8(\text{microcline}) + 4H^+ + 4H_2O \rightleftharpoons K^+ + Al^{+++} + 3H_2SiO_4$	-11,960	-34.19 <sup>e</sup>	1.29	0.42	-0.32	-1.14	-1.57	-1.96	-2.38
$KAlSi_3O_8(\text{adularite}) + 4H^+ + 4H_2O \rightleftharpoons K^+ + Al^{+++} + 3H_2SiO_4$	-12,960 <sup>d</sup>	-37.71 <sup>d</sup>	1.26	0.30	-0.50	-1.37	-1.88	-2.31	-2.77
$KAlSi_3O_8(\text{high andalusite}) + 4H^+ + 4H_2O \rightleftharpoons K^+ + Al^{+++} + 3H_2SiO_4$	-13,580 <sup>d</sup>	-38.66 <sup>d</sup>	1.51	0.50	-0.34	-1.25	-1.80	-2.26	-2.74
$NaAlSi_3O_8(\text{low albite}) + 4H^+ + 4H_2O \rightleftharpoons Na^+ + Al^{+++} + 3H_2SiO_4$	-17,900	-42.02	3.94	2.61	1.48	0.31	-0.41	-1.01	-1.59
$NaAlSi_3O_8(\text{high albite}) + 4H^+ + 4H_2O \rightleftharpoons Na^+ + Al^{+++} + 3H_2SiO_4$	-20,690 <sup>d</sup>	-46.49 <sup>d</sup>	5.00	3.46 <sup>g</sup>	2.13 <sup>g</sup>	0.75 <sup>g</sup>	-0.17 <sup>g</sup>	-0.91 <sup>g</sup>	-1.65 <sup>g</sup>
$NaAlSi_3O_8 \cdot H_2O + 4H^+ + H_2O \rightleftharpoons Na^+ + Al^{+++} + 2H_2SiO_4$	-25,780	-43.56	9.37	7.45	5.79	4.18	3.13	2.31	1.63
$CaAl_2Si_2O_8 + 8H^+ \rightleftharpoons Ca^{++} + 2Al^{+++} + 2H_2SiO_4$	-70,590	-123.77	24.69	19.32	14.53	9.79	6.34	3.47	1.12
$Al_2Si_2O_8(OH)_{2(\text{halloysite})} + 6H^+ \rightleftharpoons 2Al^{+++} + H_2O + 2H_2SiO_4$	-38,415	-93.94	7.63	4.75	2.27	-0.12	-1.72	-2.98	-4.02
$Al_2Si_2O_8(OH)_{2(\text{dickite})} + 6H^+ \rightleftharpoons 2Al^{+++} + H_2O + 2H_2SiO_4$	-39,270 <sup>d</sup>	-92.51 <sup>d</sup>	8.56	5.63 <sup>m</sup>	3.10 <sup>m</sup>	0.69 <sup>m</sup>	-0.90 <sup>m</sup>	-2.13 <sup>m</sup>	-3.09 <sup>m</sup>
$Al_2Si_2O_8(OH)_{2(\text{halloysite})} + 6H^+ \rightleftharpoons 2Al^{+++} + H_2O + 2H_2SiO_4$	-43,440 <sup>d</sup>	-94.01 <sup>d</sup>	11.29	8.03 <sup>m</sup>	5.21 <sup>m</sup>	2.50 <sup>m</sup>	0.67 <sup>m</sup>	-0.75	-1.89 <sup>m</sup>
$KAl_2Si_2O_8(OH)_2 + 10H^+ \rightleftharpoons K^+ + 3Al^{+++} + 3H_2SiO_4$	-64,320	-137.68	17.05	12.21	7.97	3.80	0.93	-1.38	-3.31
$K_{0.6}Mg_{0.25}Al_{2.25}Si_{2.0}O_{10}(OH)_{2(\text{halloysite})} + 8H^+ + 2H_2O \rightleftharpoons 0.6K^+ + 0.25Mg^{++} + 2.3Al^{+++} + 3.5H_2SiO_4$	-46,486 <sup>f</sup>	-108.60 <sup>f</sup>	10.34	6.85	3.82	0.81	-1.23	-2.87	-4.29

TABLE 12 (continued)

Réaction <sup>a</sup>	$\Delta H_f^\circ(T_r)^b$ (cal mole <sup>-1</sup> )	$\Delta S_f^\circ(T_r)^b$ (cal mole <sup>-1</sup> deg <sup>-1</sup> )	log K(T) <sup>c</sup>						
			25°C	60°C	100°C	150°C	200°C	250°C	300°C
$KFe_3AlSi_3O_{10}(OH)_{2(montmorillonite)} + 10H^+ \rightleftharpoons K^+ + 3Fe^{++} + Al^{+++} + 3H_4SiO_4$	-60,470 <sup>f</sup>	-96.2 <sup>g</sup>	23.3	18.7	14.7	10.8	8.0	5.8	3.9
$NaAlSi_3O_8 + 4H^+ \rightleftharpoons Na^+ + Al^{+++} + H_4SiO_4$	-33,840	-46.38	14.66	12.11	9.84	7.62	6.05	4.76	3.70
$KAlSi_3O_8 + 4H^+ + 2H_2O \rightleftharpoons K^+ + Al^{+++} + 2H_4SiO_4$	-24,830	-38.19	9.85	7.98	6.34	4.70	3.60	2.71	1.95
$Mg_3Al_2Si_4O_{20}(OH)_{2(chlorite)} + 16H^+ \rightleftharpoons 5Mg^{++} + 2Al^{+++} + 3H_4SiO_4 + 6H_2O$	-150,280 <sup>f</sup>	-169.02 <sup>g</sup>	73.20	61.90	52.08	42.74	36.23	31.20	27.24
$3Na_{0.33}Al_{2.33}Si_{3.67}O_{10}(OH)_{2(montmorillonite)}^k + 22H^+ + 8H_2O \rightleftharpoons 3Na^+ + 7Al^{+++} + 11H_4SiO_4$	-127,900 <sup>f</sup>	-341.74 <sup>g</sup>	19.06	9.48	1.18	-7.03	-12.56	-17.00	-20.89
$3K_{0.33}Al_{2.33}Si_{3.67}O_{10}(OH)_{2(montmorillonite)}^k + 22H^+ + 8H_2O \rightleftharpoons 3K^+ + 7Al^{+++} + 11H_4SiO_4$	-124,420 <sup>f</sup>	-333.44 <sup>g</sup>	18.32	9.00	0.92	-7.11	-12.51	-16.87	-20.70
$6Ca_{0.167}Al_{2.33}Si_{3.67}O_{10}(OH)_{2(montmorillonite)}^k + 44H^+ + 16H_2O \rightleftharpoons 6Ca^{++} + 14Al^{+++} + 22H_4SiO_4$	-264,170 <sup>f</sup>	-715.88 <sup>g</sup>	37.10	17.34	-0.11	-17.00	-28.68	-38.13	-46.39
$6Mg_{0.167}Al_{2.33}Si_{3.67}O_{10}(OH)_{2(montmorillonite)}^k + 44H^+ + 16H_2O \rightleftharpoons 6Mg^{++} + 14Al^{+++} + 22H_4SiO_4$	-267,850 <sup>f</sup>	-730.88 <sup>g</sup>	36.60	16.49	-0.96	-18.25	-30.09	-39.53	-47.81
$MgSiO_3 + 2H^+ + H_2O \rightleftharpoons Mg^{++} + H_4SiO_4$	-20,055	-15.29	11.36	9.83	8.48	7.14	6.16	5.37	4.70
$CaMg(SiO_3)_2 + 4H^+ + 2H_2O \rightleftharpoons Ca^{++} + Mg^{++} + 2H_4SiO_4$	-32,270	-17.34	19.86	17.41	15.23	13.01	11.41	10.03	8.85
$Ca_2Mg_3Si_8O_{22}(OH)_2 + 14H^+ + 8H_2O \rightleftharpoons 2Ca^{++} + 5Mg^{++} + 8H_4SiO_4$	-96,650	-65.55	56.51	49.22	42.84	36.42	32.01	28.36	25.27
$Mg_3Si_4O_{20}(OH)_2 + 6H^+ + 4H_2O \rightleftharpoons 3Mg^{++} + 4H_4SiO_4$	-35,010	-30.42	19.01	16.40	14.17	11.96	10.53	9.42	8.45
$Mg_3Si_2O_{13}(OH)_{2(chrysotile)} + 6H^+ \rightleftharpoons 3Mg^{++} + 2H_4SiO_4 + H_2O$	-52,615	-29.11	32.20 <sup>f</sup>	28.23 <sup>g</sup>	24.77 <sup>g</sup>	21.39 <sup>g</sup>	19.00 <sup>g</sup>	17.10 <sup>g</sup>	15.53 <sup>g</sup>
$Fe_2SiO_5 + 4H^+ \rightleftharpoons 2Fe^{++} + H_4SiO_4$	-36,560	-43.81	17.22	14.43	11.96	9.50	7.67	6.25	5.05

$MgSiO_3 + 4H^+ \rightleftharpoons 2Mg^{++} + H_4SiO_4$	-49,880	-33.31	29.28	25.47	22.08	18.74	16.26	14.26	12.61
$Fe_2O_3 + 6H^+ \rightleftharpoons 2Fe^{+++} + 3H_2O$	-30,445	-110.96	-1.93	-4.24	-6.28	-8.22	-9.69	-10.86	-11.81
$Fe_3O_4 + 8H^+ \rightleftharpoons Fe^{++} + 2Fe^{+++} + 4H_2O$	-49,060	-136.49	6.57	2.79	-0.57	-3.77	-6.21	-8.13	-9.69
$CuO_{(tenorite)} + 2H^+ \rightleftharpoons Cu^{++} + H_2O$	-15,785 <sup>d</sup>	-17.08 <sup>d</sup>	7.84	6.63	5.56	4.50	3.72	3.09	2.59
$Cu_2O_{(cuprite)} + 2H^+ \rightleftharpoons 2Cu^+ + H_2O$	5,945 <sup>d</sup>	13.11 <sup>d</sup>	-1.49	-1.01	-0.48	0.05	0.62	1.16	1.70
$Mg(OH)_2 + 2H^+ \rightleftharpoons Mg^{++} + 2H_2O$	-25,820	-9.81	16.78	14.84	13.10	11.41	10.09	9.08	8.53
$Al(OH)_{3(crystalline\ gibbsite)} + 3H^+ \rightleftharpoons Al^{+++} + 3H_2O^h$	-23,845 <sup>f</sup>	-43.52 <sup>g</sup>	7.96	6.17 <sup>l</sup>	4.62 <sup>l</sup>	3.16 <sup>l</sup>	2.15 <sup>l</sup>	1.36 <sup>l</sup>	0.76 <sup>l</sup>
$Al(OH)_{3(cryptocrystalline\ gibbsite)} + 3H^+ \rightleftharpoons Al^{+++} + 3H_2O^h$	-25,560 <sup>d</sup>	-43.52 <sup>d</sup>	9.23	7.30	5.63	4.05	2.94	2.08	1.41
$CaCO_3 + 2H^+ \rightleftharpoons Ca^{++} + H_2O + CO_{2(g)}$	-4,020	32.37	9.76	9.48	9.25	9.04	8.95	8.81	8.73

<sup>a</sup> Where no indication is given, all reactants other than H<sub>2</sub>O and H<sup>+</sup> correspond to the mineral designations given in table 7. H<sub>4</sub>SiO<sub>4</sub> and all ionic species are in the aqueous standard state, and H<sub>2</sub>O refers to liquid water. The subscript (g) refers to gas. <sup>b</sup> Except where noted otherwise, the values in these columns were computed from data given in tables 3 and 7. <sup>c</sup> The log K(T) values for 25°C were computed from the values of  $\Delta H_f^\circ(T_r)$  and  $\Delta S_f^\circ(T_r)$  shown in the table; those for 60°C and above were calculated using  $\Delta H_f^\circ(T_r)$ ,  $S_f^\circ(T_r)$ , and average heat capacities for the ions, H<sub>2</sub>O(liq), and H<sub>4</sub>SiO<sub>4</sub> (table 3) to first compute  $\Delta H_f^\circ(T)$  and  $S_f^\circ(T)$  for these species at elevated temperatures (eqs 13 and 14). These values were then used together with those computed from equations (11) and (12) using data given in tables 7 and 8 for the solids to evaluate equation (15). Values of  $\Delta H_f^\circ(T_r)$  and  $S_f^\circ(T_r)$  for minerals not included in table 7 were taken from Robie and Waldbaum (1968), as were data used to compute average heat capacities for high albite. All the log K(T) values are consistent with molal units of concentration. <sup>d</sup> Computed from data given in table 3 for ionic species, H<sub>2</sub>O, and H<sub>4</sub>SiO<sub>4</sub>, and the enthalpies of formation and entropies of the minerals at 25°C tabulated by Robie and Waldbaum (1968). <sup>e</sup> Computed from data given in table 3 and an estimated third law entropy for the mineral at 25°C obtained by summing (in appropriate proportions) the entropies of the oxide components of the minerals using 9.4 cal mole<sup>-1</sup> deg<sup>-1</sup> (Laitimer, 1952) for H<sub>2</sub>O—see text and footnotes f and g below. <sup>f</sup> Computed from data given in table 3 together with the free energies of formation of the minerals obtained from solubility studies and entropies of formation

TABLE 12 (continued)

calculated from the third law entropy estimates for the minerals given below. The calculated free energies and enthalpies of formation and estimated entropies of the minerals at 25°C are (per mole of the mineral with the composition given above):

Mineral	$\Delta H_f^\circ(T_r)$ (cal mole <sup>-1</sup> )	$S^\circ(T_r)$ (cal mole <sup>-1</sup> deg <sup>-1</sup> )	$\Delta G_f^\circ(T_r)$ (cal mole <sup>-1</sup> )	Source of $\Delta G_f^\circ(T_r)$
Illite	-1,390,820	66.4	-1,300,980	Computed from the solubilities of illite and kaolinite in sea water reported by Mackenzie and Garrels (1965).
Mg-chlorite	-2,169,840	112	-1,954,800	Calculated from the solubilities of chlorite and kaolinite in sea water reported by Mackenzie and Garrels (1965).
Ca-montmorillonite	-1,367,980	61.2	-1,279,240	Computed from the composition of Sierra Nevada waters (Feil, Roberson, and Polzer, 1964) considered to be in equilibrium with calcium montmorillonite (Garrels and Mackenzie, 1967).
Na-montmorillonite	-1,366,840	62.8	-1,277,760	Calculated from the free energy of formation of calcium montmorillonite assuming $\log(a_{Na^+}/a_{Ca^{++}}) = 1.1$ for the exchange of calcium for sodium (computed by R. M. Garrels (personal commun.) from data reported by Schachtschabel, 1940).
K-montmorillonite	-1,368,920	63.4	-1,279,600	Calculated from the free energy of formation of sodium montmorillonite assuming $\log(a_{Na^+}/a_{K^+}) = 0.5$ for the exchange of sodium for potassium (computed by R. M. Garrels (personal commun.) from data reported by Schachtschabel, 1940).
Mg-montmorillonite	-1,364,140	61.2	-1,275,340	Calculated from the free energy of formation of calcium montmorillonite assuming $\log(a_{Mg^{++}}/a_{Ca^{++}}) = 0$ for the exchange of calcium for magnesium (computed by R. M. Garrels (personal commun.) for data reported by Schachtschabel, 1940).
Crystalline gibbsite	-308,100	16.75 <sup>1</sup>	-275,200	Computed from the solubility of crystalline gibbsite reported by Kittrick (1966) using data given by Wagman and others (1968)—see footnote u, table 4.

<sup>u</sup> Computed from the equilibrium constant obtained by Eugster and Wones (1962) for  $Fe_3O_4(\text{maghemite}) + KAlSi_3O_8(\text{kaolinite}) + H_2O(l) \rightleftharpoons KFe_3AlSi_3O_{10}(OH)_2(\text{annite}) + \frac{1}{2}O_2(g)$  at 500°C and 2070 bars using data taken from tables 6, 7, and 8, Anderson (1967), and Robie and Waldbaum (1968). The procedure used in the calculation is described in the text. The estimated third law entropy of annite at 25°C is

100 cal mole<sup>-1</sup> deg<sup>-1</sup> (see footnote e above), and the calculated values of  $\Delta G_f^\circ(T_r)$  and  $\Delta H_f^\circ(T_r)$  for annite are -1,150,100 and -1,233,750 cal mole<sup>-1</sup>, respectively. <sup>b</sup> It can be deduced from comparison of various equilibrium constants given above that the assemblage gibbsite + quartz is not stable with respect to kaolinite + H<sub>2</sub>O in the temperature range 25° to 300°C. However, calculations of high temperature equilibrium constants for the hydrolysis of corundum, boehmite, and diaspore using solubilities determined by Apps (ms) or thermodynamic data compiled by Robie and Waldbaum (1968) result in values that require kaolinite to be unstable with respect to each of these minerals + quartz + H<sub>2</sub>O at temperatures well below 300°C. In view of experimental evidence indicating that kaolinite is stable up to ~ 300°C (Henley and Jones, 1964) it appears that the thermodynamic data for corundum, boehmite, and diaspore at 25°C are in error. On the other hand, the crystallinities of kaolinite, gibbsite, diaspore, and boehmite produced experimentally are quite variable, and thus (see footnote r below) the substantial agreement that exists between the results of solubility studies involving kaolinite and the thermodynamic data (table 7) used to compute the log K values for kaolinite given above is not necessarily a definitive criterion for resolving the conflict. <sup>c</sup> The illite in this reaction is close to an illitic end member composition in the montmorillonite-mixed layer illite solid solution series (Hawer and Mowatt, 1966). <sup>d</sup> Computed using the heat capacity of cryptocrystalline gibbsite to represent that of crystalline gibbsite. <sup>e</sup> Idealized end members in the beidellite solid solution series. <sup>f</sup> The entropy of crystalline gibbsite at 25°C was assumed to be equivalent to that of cryptocrystalline gibbsite in the calculations. <sup>g</sup> Computed using  $C_p^\circ(T_r)$  for halloysite and dickite (58.85 and 57.24 cal mole<sup>-1</sup> deg<sup>-1</sup>, respectively, King and Weller, 1961) as constants. <sup>h</sup> Computed using the heat capacity of antigorite to represent that of chrysotile. <sup>i</sup> These values are consistent with those reported by Hostetler and Christ (1968). <sup>j</sup> Computed using average heat capacities for high albite—see footnote e above. <sup>k</sup> Owing to the significant effect of crystallinity on the thermodynamic behavior of the clay minerals, the actual hydrolysis of these minerals in geochemical processes cannot necessarily be described in terms of the log K values shown in this table; the hydrolysis constants given in the table are "idealized" values. <sup>l</sup> Hydrolysis constants are given in this table for a number of minerals that are not stable in the presence of H<sub>2</sub>O at the temperatures indicated, (for example, enstatite, forsterite, et cetera). These reactions were included to enable additive calculation of equilibrium constants for stable assemblages and to facilitate extrapolation to higher temperatures. <sup>m</sup> Constant heat capacity fits of the log K values given in the table results in the following estimates of equilibrium constants for the reactions (in the above order) at 0°C: -4.4, 2.1, 2.1, 2.4, 5.1, 6.3, 11.1, 29.4, 10.2, 11.2, 14.2, 21.4, 13.5, 26.4, 16.9, 11.5, 83.3, 27.4, 26.6, 54.5, 54.4, 12.7, 22.0, 62.8, 21.4, 35.7, 19.7, 32.6, 0.1, 9.9, 8.9, -1.9, 18.5, 9.6, 11.0, 10.0.

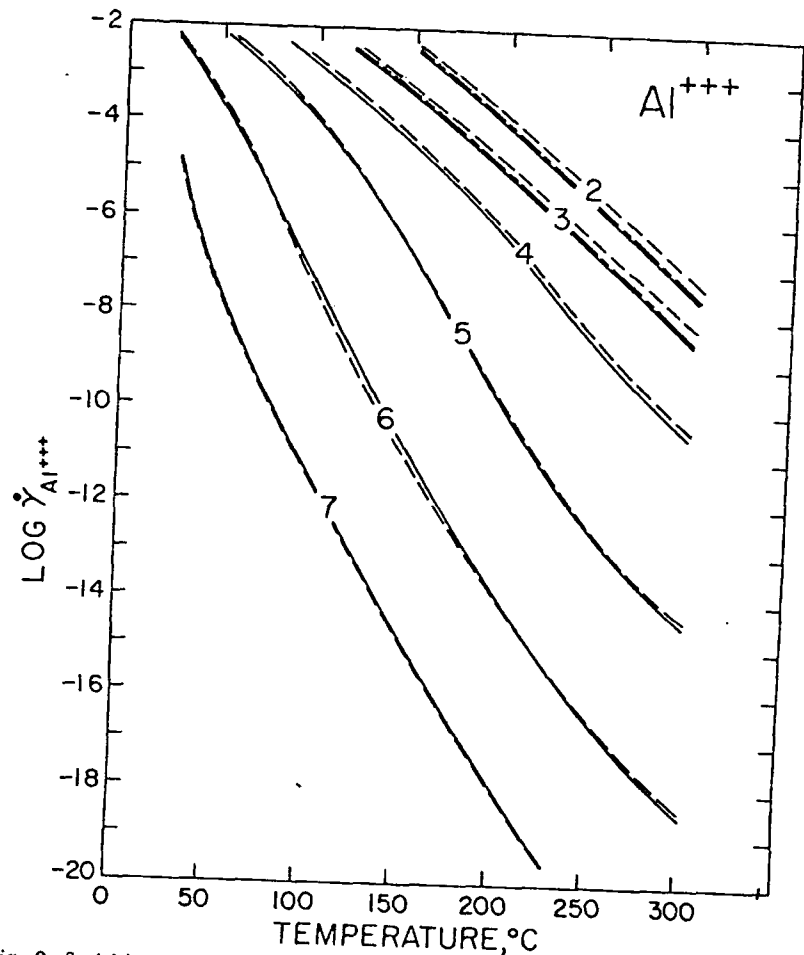


Fig. 9. Stoichiometric individual ion activity coefficients ( $\gamma_i$ ) for the aluminum ion as a function of temperature at constant pH (indicated by the numbers on the curves) in 1 (---), 2 (— — —), and 3 (—) molal NaCl solutions (see text and table 13.)

charged) complexes were omitted from the calculations represented in the tables.

Distribution diagrams are presented in figures 16 and 17 for aluminum hydroxide species and complexes involving the hydrogen ion and carbonate, sulfide, and sulfate ligands, respectively. Unlike the curves in figure 15, those in figures 16 and 17 represent the equilibrium pH at a given temperature for equal activities of the species shown on either side of the curves. Similar distribution diagrams for sulfur, copper, and iron species in terms of fugacity of oxygen and pH at two temperatures are shown in figures 18 and 19. The relation between fugacity of oxygen and the ratio of the concentration of total sulfate to that of total sulfide

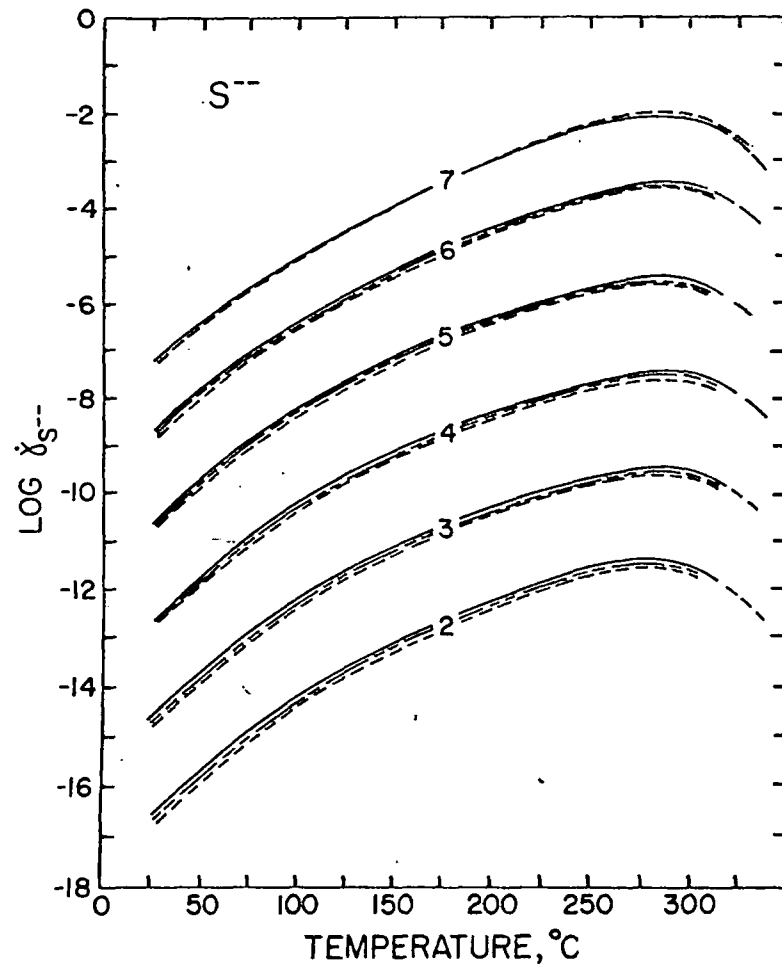


Figure 10. Stoichiometric individual ion activity coefficients ( $\gamma_i$ ) for the sulfide ion as a function of temperature at constant pH (indicated by the numbers of the curves) in 1 (---), 2 (— — —), and 3 (—) molal NaCl solutions (see text and table 13).

in a 3 molal NaCl solution with a pH of 5 at elevated temperatures is depicted in figure 20. The curves shown in figures 16 to 20 were computed from data given in tables 4, 6, and 9.

#### CONCLUDING REMARKS

Although many equilibria are considered in the preceding pages, all hydrothermal reactions of interest in hydrothermal geochemistry could not be included in this communication. On the other hand, the data and equations summarized above permit other high temperature equilibrium constants to be calculated to suit the requirements of one or another investigation. In many instances, a desired equilibrium constant can be

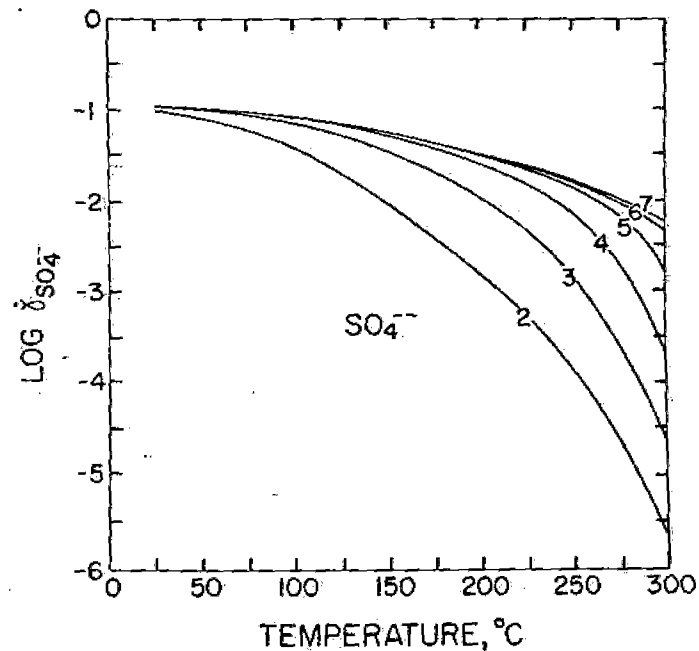


Fig. 11. Stoichiometric individual ion activity coefficients ( $\gamma_i$ ) for the sulfate ion as a function of temperature at constant pH (indicated by the numbers on the curves) in 3 molal NaCl solutions (see text and table 13).

obtained by combining various reactions for which  $\log K(T)$  values are given in the tables. Values of  $\gamma_i$  can be taken directly from the tables and graphs, and values of  $\gamma_i^*$  can be computed as needed from the data and equations given in the foregoing discussion.

The information contained in the tables permits quantitative calculations for hydrothermal systems and processes at high temperatures without the aid of a computer. As an example, calculated sulfide solubilities are plotted against temperature in figure 21. Note that with the exception of metacinnibar, the computed solubilities of the individual sulfides in a 3 molal NaCl solution with a pH of 5 are more than sufficient at high temperatures to account for hydrothermal ore deposits of the metals considered. It can also be seen in figure 21 that the solubilities of a number of the sulfides are similar at high temperatures, but change differentially with decreasing temperatures. Many other conclusions, observations, and implications of considerable geologic significance can be drawn from similar calculations involving the thermodynamics of hydrothermal reactions summarized above. Discussion of these is beyond the scope of the present paper, but in future communications the thermodynamic relations presented here will be used to define phase relations among silicates in hydrothermal systems and to evaluate polyphase equilibrium states and the mass transfer involved in hydrothermal vein for-

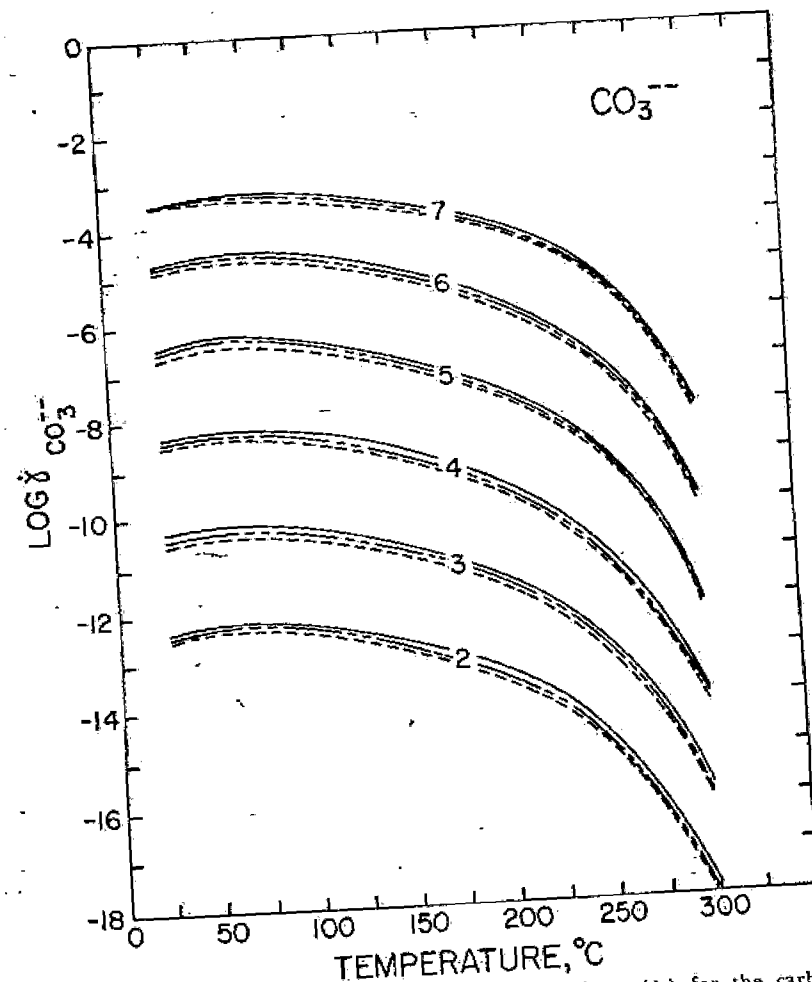


Fig. 12. Stoichiometric individual ion activity coefficients ( $\gamma_i$ ) for the carbonate ion as a function of temperature at constant pH (indicated by the numbers on the curves) in 1 (---), 2 (— — —), and 3 (—) molal NaCl solutions (see text and table 13).

Such calculations make it possible to characterize quantitatively the mutual solubilities of sulfides and silicates at high temperatures. Irreversible reactions responsible for metasomatism and the paragenesis, replacement, and zoning of hydrothermal minerals have been programmed for machine evaluation. The methods employed in the calculations and idealized models of the mass transfer involved in various geochemical processes have been presented elsewhere (Helgeson, 1968b; Helgeson, Garrels, and Mackenzie, 1969; Helgeson and Garrels, 1968).

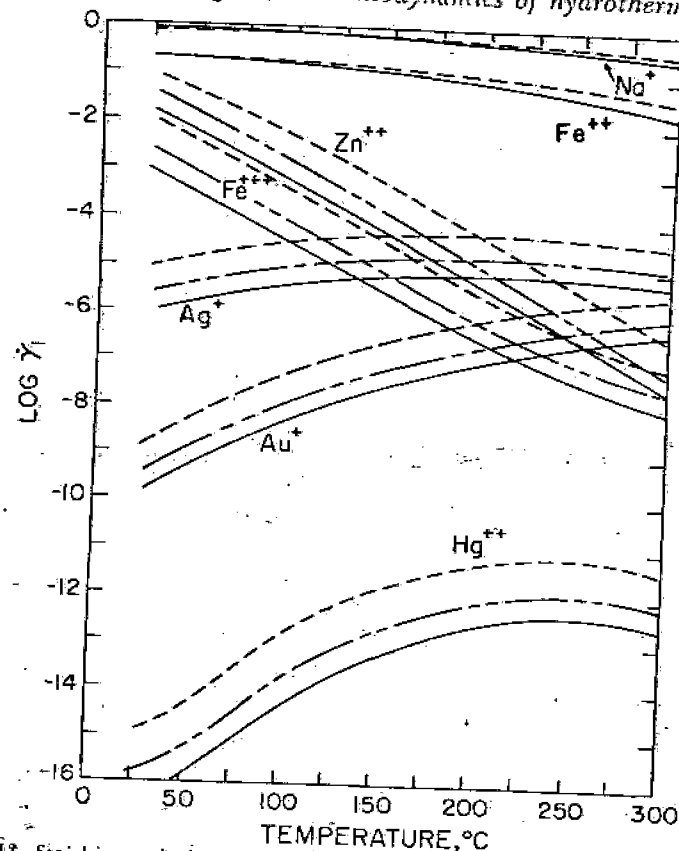


Fig. 13. Stoichiometric individual ion activity coefficients ( $\gamma_i$ ) for metal ions in 1 (---), 2 (---), and 3 (—) molal NaCl solutions at elevated temperatures (see text and table 14).

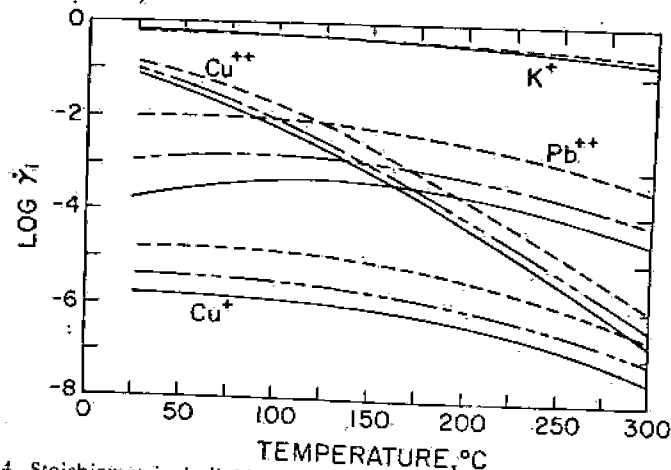


Fig. 14. Stoichiometric individual ion activity coefficients ( $\gamma_i$ ) for metal ions in 1 (---), 2 (---), and 3 (—) molal NaCl solutions at elevated temperatures (see text and table 14).

TABLE 13.

Stoichiometric individual ion activity coefficients ( $\gamma_i$ ) for aluminum, sulfide, carbonate, sulfate, and calcium ions present in relatively small concentrations in 3.0 molal sodium chloride solutions

Ion	pH	log $\gamma_i^*$						
		25°C	50°C	100°C	150°C	200°C	250°C	300°C
Al <sup>+++</sup> (assuming the presence of Al(OH) <sup>++</sup> and Al(OH) <sub>3</sub> )	2	-1.17	-1.22	-1.46	-2.49	-4.07	-5.71	-7.55
	3	-1.17	-1.25	-1.94	-3.45	-5.04	-6.71	-8.56
	4	-1.21	-1.47	-2.83	-4.45	-6.27	-8.65	-10.50
	5	-1.49	-2.18	-3.94	-6.72	-9.83	-12.60	-14.45
	6	-2.26	-3.54	-7.34	-10.70	-13.83	-16.60	-18.45
	7	-4.87	-7.33	-11.34	-14.70	-17.83	-20.60	-22.45
	8	-8.86	-11.33	-15.34	-18.70	-21.83	-24.60	-26.45
	9	-12.86	-15.33	-19.34	-22.70	-25.83	-28.60	-30.45
	10	-16.86	-19.33	-23.34	-26.70	-29.83	-32.60	-34.45
	11	-20.86	-23.33	-27.34	-30.70	-33.83	-36.60	-38.45
	12	-24.86	-27.33	-31.34	-34.70	-37.83	-40.60	-42.45
	S <sup>-</sup> (assuming the presence of HS <sup>-</sup> and H <sub>2</sub> S <sub>(aq)</sub> )	2	-16.60	-15.64	-14.17	-13.11	-12.29	-11.69
3		-14.60	-13.64	-12.17	-11.11	-10.29	-9.69	-9.42
4		-12.61	-11.65	-10.17	-9.11	-8.29	-7.69	-7.42
5		-10.62	-9.66	-8.20	-7.13	-6.30	-5.70	-5.42
6		-8.71	-7.81	-6.39	-5.30	-4.43	-3.78	-3.47
7		-7.20	-6.39	-5.04	-3.93	-2.98	-2.27	-2.11
CO <sub>3</sub> <sup>-</sup> (assuming the presence of HCO <sub>3</sub> <sup>-</sup> , H <sub>2</sub> CO <sub>3(aq)</sub> , and CO <sub>2(aq)</sub> <sup>b</sup> )		2	-12.38	-12.22	-12.37	-12.79	-13.52	-14.79
	3	-10.38	-10.22	-10.37	-10.79	-11.52	-12.79	-15.88
	4	-8.39	-8.23	-8.37	-8.79	-9.52	-10.79	-13.88
	5	-6.43	-6.28	-6.41	-6.81	-7.53	-8.79	-11.88
	6	-4.73	-4.58	-4.65	-4.97	-5.62	-6.83	-9.88
	7	-3.50	-3.35	-3.33	-3.58	-4.08	-5.10	-7.93
	SO <sub>4</sub> <sup>-</sup> (assuming the presence of HSO <sub>4</sub> <sup>-</sup> in the absence of calcium)	2	-1.01	-1.09	-1.43	-2.03	-2.77	-3.79
3		-0.96	-1.00	-1.14	-1.42	-1.92	-2.82	-4.62
4		-0.95	-0.99	-1.10	-1.26	-1.51	-2.07	-3.64
5		-0.95	-0.99	-1.10	-1.25	-1.43	-1.79	-2.77
6		-0.95	-0.99	-1.10	-1.24	-1.43	-1.75	-2.33
7		-0.95	-0.99	-1.10	-1.24	-1.43	-1.75	-2.25
$a_{Ca^{++}}$		0.001	-0.95	-1.0	-1.1	-1.3	-1.5	
	0.01	-1.04	-1.1	-1.2	-1.4	-1.7		
$a_{SO_4^{--}}$	0.001	-0.67	-0.7	-0.8	-0.9	-1.2		
	0.01	-0.75	-0.8	-1.0	-1.2	-1.5		

\* Computed from equation (49) or expressions for anions analogous to equation (49) using data given in tables 2 and 4 (see text). <sup>b</sup> If the total molality of calcium present in the solution is one or less, the computed values of  $\gamma_{CO_3^{--}}$  are not affected by the formation of CaCO<sub>3(aq)</sub>. <sup>c</sup> Where total CO<sub>2(aq)</sub> is less than 1 molal, the CaCO<sub>3(aq)</sub> species has a negligible effect on  $\gamma_{Ca^{++}}$  at pH 6 and below.

TABLE 14

Stoichiometric individual ion activity coefficients ( $\gamma_i$ ) for Na<sup>+</sup> and cations present in relatively small concentrations in 1.0, 2.0, and 3.0 molal sodium chloride solutions

Ion	$m_{i,NaCl}$	$\log \gamma_i^a$						
		25°C	50°C	100°C	150°C	200°C	250°C	300°C
Ag <sup>+</sup>	1.0	-5.07	-4.8	-4.5	-4.3	-4.3	-4.2 <sup>b</sup>	-4.5 <sup>b</sup>
	2.0	-5.68	-5.5	-5.1	-4.8	-4.8	-4.7 <sup>b</sup>	-5.0 <sup>b</sup>
	3.0	-6.06	-5.8	-5.5	-5.2	-5.1	-5.0 <sup>b</sup>	-5.3 <sup>b</sup>
Cu <sup>c</sup>	1.0	-4.75	-4.8	-4.9	-5.0	-5.4	-6.0 <sup>b</sup>	-6.6 <sup>b</sup>
	2.0	-5.36	-5.4	-5.5	-5.6	-6.0	-6.5 <sup>b</sup>	-7.1 <sup>b</sup>
	3.0	-5.75	-5.8	-5.9	-6.0	-6.3	-6.9 <sup>b</sup>	-7.5 <sup>b</sup>
Cu <sup>++</sup>	1.0	-0.91	-1.0	-1.7	-2.6	-3.7 <sup>b</sup>	-4.8 <sup>b</sup>	-6.0 <sup>b</sup>
	2.0	-1.03	-1.2	-2.0	-3.0	-4.1 <sup>b</sup>	-5.2 <sup>b</sup>	-6.4 <sup>b</sup>
	3.0	-1.10	-1.3	-2.2	-3.2	-4.3 <sup>b</sup>	-5.4 <sup>b</sup>	-6.7 <sup>b</sup>
Pb <sup>++</sup>	1.0	-2.07	-2.0	-2.2	-2.3	-2.5	-2.9 <sup>b</sup>	-3.5 <sup>b</sup>
	2.0	-2.99	-2.6	-2.8	-3.0	-3.2	-3.5 <sup>b</sup>	-4.2 <sup>b</sup>
	3.0	-3.75	-3.1	-3.3	-3.4	-3.6	-3.9 <sup>b</sup>	-4.6 <sup>b</sup>
Zn <sup>++</sup>	1.0	-1.00	-1.4	-2.3	-3.2	-4.3	-5.2 <sup>b</sup>	-6.5 <sup>b</sup>
	2.0	-1.43	-1.9	-2.9	-3.8	-5.0	-5.8 <sup>b</sup>	-7.2 <sup>b</sup>
	3.0	-1.84	-2.4	-3.4	-4.3	-5.4	-6.3 <sup>b</sup>	-7.6 <sup>b</sup>
Hg <sup>++</sup>	1.0	-14.98	-14.4	-12.8	-11.8	-11.3	-11.1 <sup>b</sup>	-11.4 <sup>b</sup>
	2.0	-15.90	-15.3	-13.7	-12.7	-12.1	-11.9 <sup>b</sup>	-12.2 <sup>b</sup>
	3.0	-16.50	-15.9	-14.3	-13.3	-12.6	-12.3 <sup>b</sup>	-12.6 <sup>b</sup>
Fe <sup>+++d</sup>	1.0	-2.02	-2.5	-3.4	-4.4	-5.5 <sup>b</sup>	-6.6 <sup>b</sup>	-7.1 <sup>b</sup>
	2.0	-2.60	-3.1	-4.1	-5.1	-6.1 <sup>b</sup>	-7.2 <sup>b</sup>	-7.6 <sup>b</sup>
	3.0	-2.98	-3.5	-4.5	-5.5	-6.5 <sup>b</sup>	-7.5 <sup>b</sup>	-8.0 <sup>b</sup>
Fe <sup>++e</sup>	1.0	-0.64	-0.67	-0.7	-0.8	-1.0	-1.2 <sup>b</sup>	-1.4 <sup>b</sup>
	2.0	-0.68	-0.71	-0.8	-0.9	-1.0	-1.2 <sup>b</sup>	-1.6 <sup>b</sup>
	3.0	-0.67	-0.70	-0.8	-0.9	-1.0	-1.3 <sup>b</sup>	-1.7 <sup>b</sup>
Au <sup>f</sup>	1.0	-8.8	-8.2	-7.3	-6.6	-6.0	-5.6 <sup>b</sup>	-5.5 <sup>b</sup>
	2.0	-9.4	-8.9	-7.9	-7.2	-6.6	-6.2 <sup>b</sup>	-6.0 <sup>b</sup>
	3.0	-9.8	-9.2	-8.3	-7.5	-6.9	-6.5 <sup>b</sup>	-6.3 <sup>b</sup>
Au <sup>+++g</sup>	1.0	-25.4	-24.0	-21.7	-20.1	-19.1	-18.7 <sup>b</sup>	-19.2 <sup>b</sup>
	2.0	-26.7	-25.2	-23.0	-21.3	-20.2	-19.8 <sup>b</sup>	-20.2 <sup>b</sup>
	3.0	-27.5	-26.0	-23.8	-22.0	-20.9	-20.4 <sup>b</sup>	-20.8 <sup>b</sup>
Na <sup>+</sup>	1.0	-0.18	-0.19	-0.21	-0.25	-0.31	-0.41 <sup>b</sup>	-0.61 <sup>b</sup>
	2.0	-0.17	-0.18	-0.20	-0.25	-0.33	-0.46 <sup>b</sup>	-0.68 <sup>b</sup>
	3.0	-0.15	-0.15	-0.17	-0.24	-0.33	-0.49 <sup>b</sup>	-0.73 <sup>b</sup>
K <sup>+</sup>	1.0	-0.22	-0.22	-0.25	-0.29	-0.35	-0.44 <sup>b</sup>	-0.62 <sup>b</sup>
	2.0	-0.22	-0.23	-0.25	-0.30	-0.37	-0.49 <sup>b</sup>	-0.71 <sup>b</sup>
	3.0	-0.20	-0.21	-0.24	-0.28	-0.37	-0.51 <sup>b</sup>	-0.76 <sup>b</sup>

<sup>a</sup> The dissociation constants for the metal chloride complexes used in calculating the values of  $\gamma_i$  in this table from equation (49) are shown in table 5. To insure minimal uncertainty and conservative values (see text), divalent and trivalent metal chloride complexes were not considered in the calculations; that is,  $q$  in equation (49) was assigned a value of  $Z_i + 1$  for each metal ion. Because all the metal ions considered above, with the exception of Fe<sup>++</sup>, associate with the chloride ion to a significant degree, the individual ion activity coefficients for the ions themselves have no significant effect, except in the case of Na<sup>+</sup>, K<sup>+</sup>, and Fe<sup>++</sup>, on the  $\gamma_i$  values shown above. <sup>b</sup> These values have a higher uncertainty than the others given in the table owing to extrapolation of equilibrium constants and activity coefficients used

in the calculations. <sup>c</sup> No log K(T) data are available for CuCl<sub>3(aq)</sub>, so this species was not considered specifically in the calculations. <sup>d</sup> The term for FeCl<sup>++</sup> was omitted from equation (49) to eliminate the influence of the divalent charge on this species, which is the most stable of the ferric chloride complexes. The degree of formation achieved by this species is represented by the magnitude of the overall dissociation constants for the higher order ferric chloride complexes considered in the calculations. <sup>e</sup> There is little indication that chloride complexes of Fe<sup>++</sup> form to significant degrees, at least at low temperatures. The values shown for Fe<sup>++</sup> are thus equivalent to individual ion activity coefficients. Because the ion is divalent and a 25°C  $\lambda$  was used in the calculations, the activity coefficients shown for this species at high temperatures are probably too small. On the other hand, there are indirect indications from solubility data that Fe<sup>++</sup> may form stable complexes with chloride in the region of 300°, and that the overall stability constant is of the order of 10<sup>2</sup> or 10<sup>3</sup>. In view of these uncertainties, the activity coefficients shown above for Fe<sup>++</sup> should be considered provisional estimates. <sup>f</sup> The values shown for these ions are based on the dissociational reactions for the gold species shown in table 5.

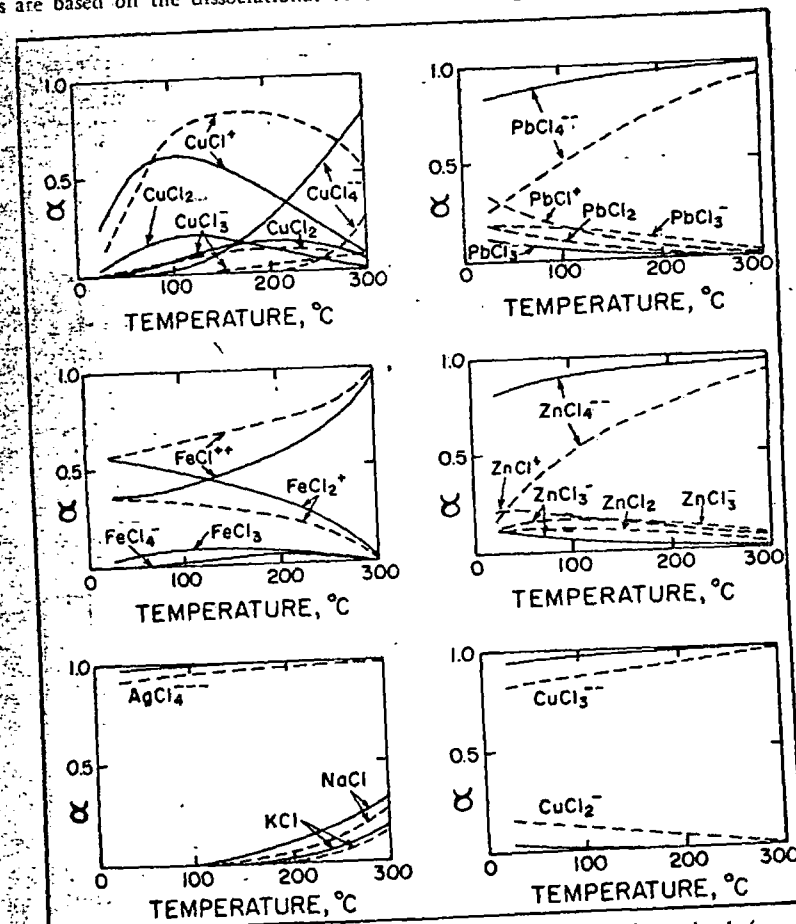


Fig. 15. Degrees of formation ( $\alpha$ ) for metal chloride complexes in 1 (---) and 3 (—) molal NaCl solutions at elevated temperatures (see text—eq 54). Mercury is not shown because the species HgCl<sub>3</sub><sup>-</sup> accounts for >98 percent of the mercury in solution. Complexes that form to less than a few percent have been omitted from the diagrams. Unlike the  $\gamma_i$  values shown in table 14 and figures 13 and 14, the  $\alpha$  values shown above were calculated (eq 54) assuming the presence of all chloride complexes (of each cation) in table 5 (see text).

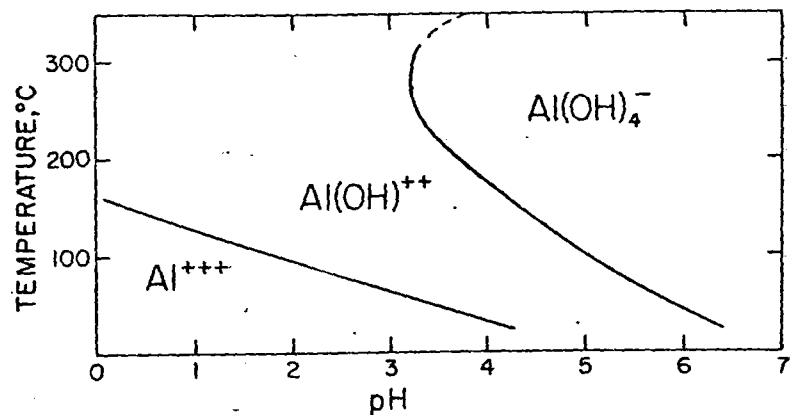


Fig. 16. Distribution of aluminum species in aqueous solution as a function of temperature and solution pH. The curves represent equal activities of the species shown in adjoining fields in the diagram. The positions of the curves are defined by dissociation constants in table 4.

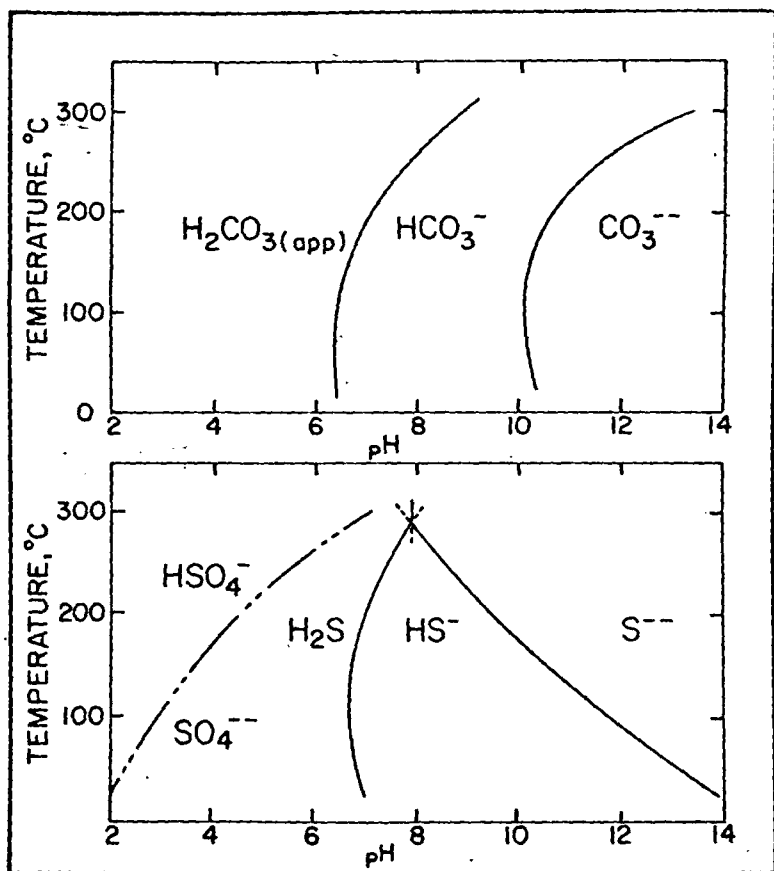


Fig. 17. Distribution of carbonate, sulfide, and sulfate species in aqueous solution as a function of temperature and solution pH. The curves represent equal activities of the species shown in adjoining fields in the diagrams. The positions of the curves are defined by dissociation constants in table 4. The subscript (app) indicates that the species referred to is the undifferentiated sum of  $H_2CO_3$  and  $CO_{2(aq)}$ .

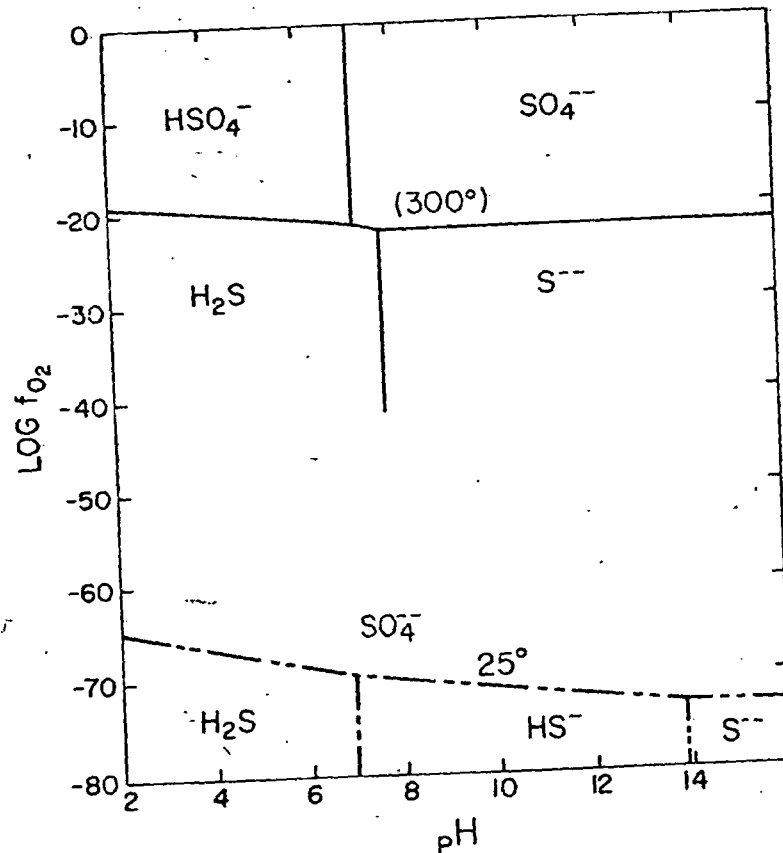


Fig. 18. Distribution of sulfur species at 25°C (---) and 300°C (—) as a function of  $f_{O_2}$  and solution pH. The curves, which define the positions of equal activities of the species in adjoining fields in the diagram, were computed from the equilibrium constants given in table 9. The field for  $HSO_4^-$  at 25°C lies to the left of the diagram.

#### ACKNOWLEDGMENTS

I am indebted to R. M. Garrels, F. T. Mackenzie, C. L. Christ, and J. J. Hemley for their encouragement, helpful suggestions, and constructive criticism during the preparation of this paper, and to C. L. Christ and John Haas for reviewing the manuscript. The impetus to undertake this task came from stimulating discussions with J. J. Hemley. Also I would like to acknowledge the invaluable assistance and suggestions I received from the following students: T. H. Brown, A. Nigrini, T. A. Jones, W. R. James, J. R. Riehle, and G. M. Lafon. The work reported here was supported in part by NSF Grants GU-1700, GA-828, GA-11285,



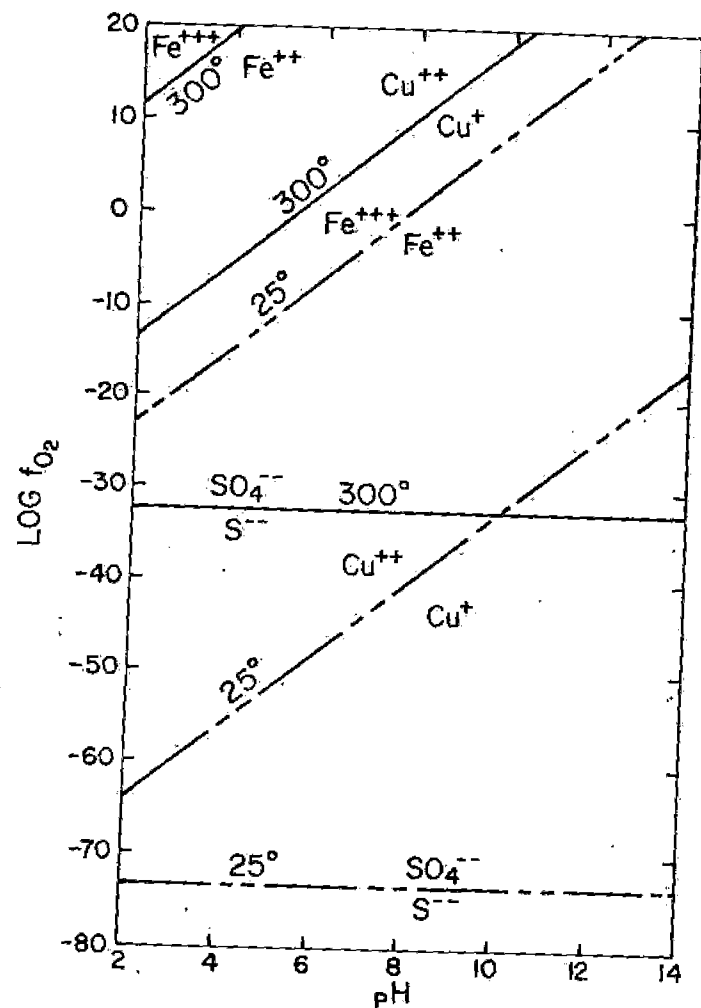


Fig. 19. Distribution of iron, copper, and sulfur species at 25°C (---) and 300°C (—) as a function of  $f_{O_2}$  and solution pH. The curves, which define the positions of equal activities of the species in adjoining fields in the diagram, were computed from the equilibria constants given in table 9.

GA-9758, and GU-2190, together with funds made available by the office of Research Coordination at Northwestern University, and the Petroleum Research Fund of the American Chemical Society. The help of J. M. Klyce, W. R. James, P. Abrams, K. Vonesh, and especially R. H. Leeper in assisting with the computer calculations is also acknowledged with thanks. Finally, I would like to express my appreciation to Mrs. E. J. Faulkner for many hours spent in typing and retyping the manuscript.

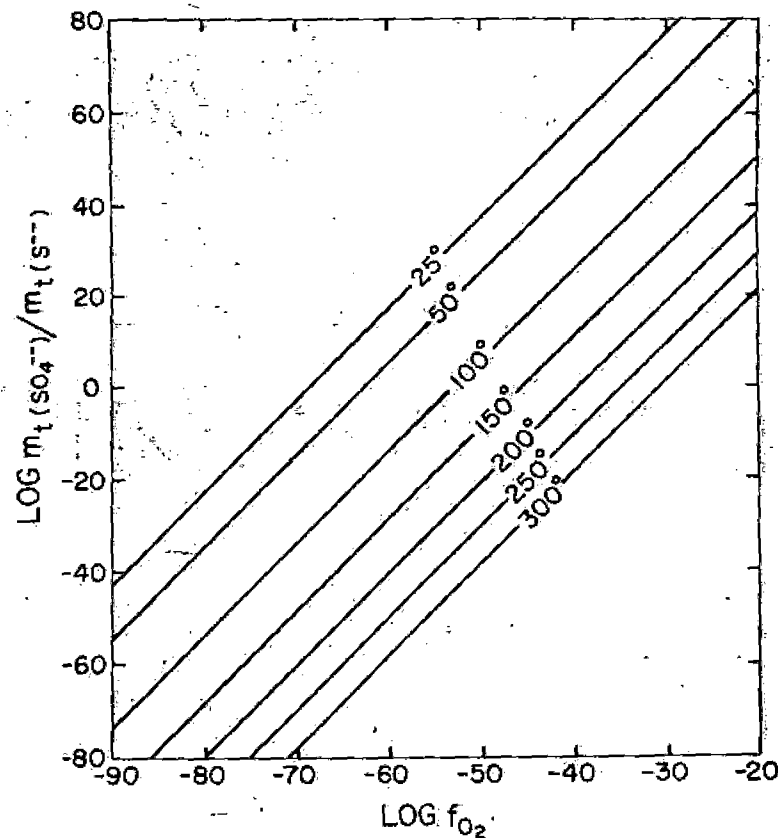


Fig. 20. Ratio of the total concentration of sulfate to sulfide in a 3.0 molal NaCl solution as a function of  $f_{O_2}$  from 25° to 300°C at a pH of 5. The positions of the isotherms were computed from the data given in tables 9 and 13.

#### REFERENCES

- Akerlof, G. C., and Oshry, H. I., 1950, The dielectric constant of water at high temperatures and in equilibrium with its vapor: *Am. Chem. Soc. Jour.*, v. 72, p. 2844-2847.
- Ahluwalia, J. C. and Cobble, J. W., 1964, The thermodynamic properties of high temperature aqueous solutions. III. The partial molal heat capacities of hydrochloric acid from 0°-100° and the Third-Law potentials of the silver chloride and calomel electrodes from 0°-100°: *Am. Chem. Soc. Jour.*, v. 86, p. 5331-5334.
- Anderson, G. M., 1967, Specific volumes and fugacities of water, in Barnes, H. L., ed., *Geochemistry of Hydrothermal Ore Deposits*: New York, Holt, Rinehart, and Winston, Inc., p. 632-635.
- Apps, J. A., ms, 1969, The system albite, analcime, and montmorillonite at 25°C and one atmosphere: Ph.D. thesis, Harvard Univ., Dept. of Geol. Sci., Cambridge, Mass.
- Austin, J. M., Matheson, R. A., and Parton, H. N., 1959, Some thermodynamic properties of solutions of salts of bivalent metals, in Hamer, W. J., ed., *Structure of electrolytic solutions*: New York, John Wiley & Sons, p. 365-379.
- Barany, R., 1964, Heat and free energy of formation of muscovite: U.S. Bur. Mines Rept. Inv. 6356, 6 p.
- Barany, R., and Kelley, K. K., 1961, Heats and free energies of formation of gibbsite, kaolinite, halloysite, and dickite: U.S. Bur. Mines Rept. Inv., no. 5825, 13 p.
- Barnard, W. M., and Christopher, P. A., 1966, Hydrothermal synthesis of chalcopyrite: *Econ. Geology*, v. 61, p. 897-902.

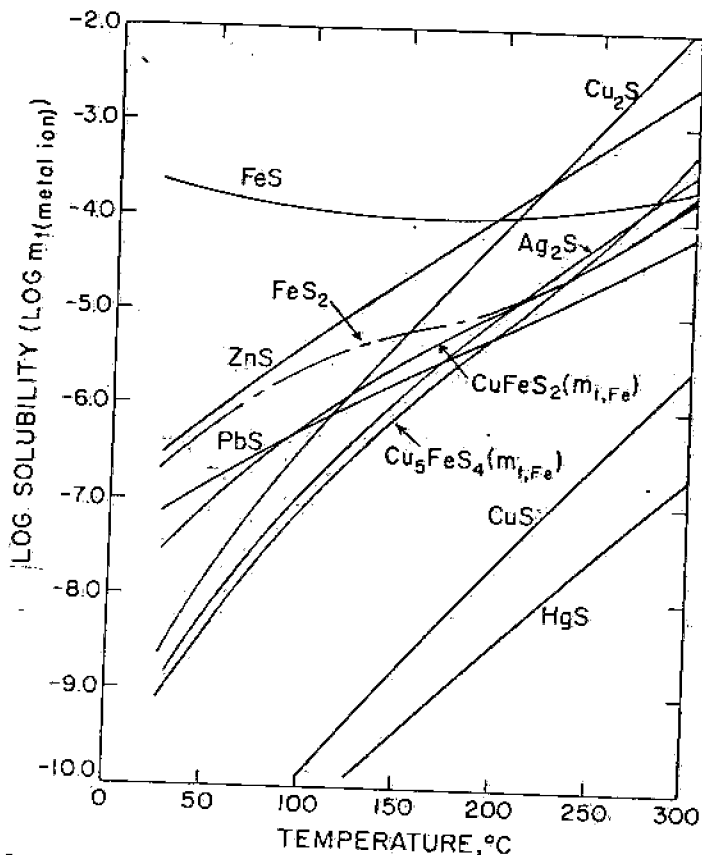


Fig. 21. Calculated stoichiometric solubilities (in terms of the total molality of the metal ion) of various individual sulfides in a 3 molal sodium chloride solution with a pH of 5 at elevated temperatures. HgS refers to meta-cinnabar. Except for pyrite, chalcopyrite, and bornite, the solubilities were computed from equation (51) and the data presented in tables 11, 13, and 14. Pyrite solubilities were calculated by evaluating  $4\text{FeS}_2 + 8\text{H}^+ + 4\text{H}_2\text{O} \rightleftharpoons 8\text{H}_2\text{S} + 4\text{Fe}^{2+} + \text{SO}_4^{2-}$  and  $4\text{FeS}_2 + 7\text{H}^+ + 4\text{H}_2\text{O} \rightleftharpoons 7\text{H}_2\text{S} + 4\text{Fe}^{2+} + \text{HSO}_4^-$  with the aid of the data in tables 10, 13, and 14. The solubilities of chalcopyrite and bornite were computed from oxidation-reduction equations analogous to those given above for pyrite, which are written in terms of the predominant species in the aqueous phase. This procedure permits the molalities of all species in the reactions to be defined in terms of the molality of  $\text{Fe}^{2+}$ , and therefore the solubilities of the minerals can be computed directly from the Law of Mass Action equations for the reactions. Owing to the limitation imposed by the computed stoichiometric individual ion activity coefficients (see footnote a, table 14), all solubilities depicted above should be regarded as minimal approximations of the true mineral solubilities.

- Bartholomé, P., 1958, On the paragenesis of copper ores: Leopoldville, Belgian Congo. *Studia Univ. Lovanium*.
- Barton, P. B., and Skinner, B. T., 1967, Sulfide mineral stabilities, in Barnes, H. L., ed., *Geochemistry of hydrothermal ore deposits*: New York, Holt, Rinehart, and Winston, Inc., p. 236-333.
- Bell, R. P., and George, J. H. B., 1953, Incomplete dissociation of some thallos and calcium salts at different temperatures: *Faraday Soc. Trans.*, v. 49, p. 619-627.
- Berne, E., and Leden, I., 1953, Solubility of silver chloride and the formation of complexes between silver and chloride ions: *Svensk. kem. tidskr.*, v. 65, p. 88-97.

- Berner, R. A., 1967, Comparative dissolution characteristics of carbonate minerals in the presence and absence of aqueous magnesium ion: *Am. Jour. Sci.*, v. 265, p. 45-70.
- Bjerrum, J., 1946, Acidic complex formation I. Optical investigations on cupric chloride in mixtures with other chlorides: *Kgl. Danske Vidensk. Selsk. Mat-fys. Medd.*, v. 22, no. 18, 45 p.
- Bjerrum, N., 1948, La stabilité des chlorures d'or: *Soc. Chimie Belge Bull.*, v. 57, p. 432-445.
- Bjerrum, N., and Kirschner, A., 1918, Die Rhodanide des Goldes und das freie Rhodan mit einem Anhang über das Goldchlorid: *Kgl. Danske Vidensk. Selsk. Skr., Naturvidensk. math. Afdel.*, v. 5, p. 1-77.
- Chalykan, O., 1948, Properties of cuprous complexes: *Zhur. obshchek Khim.*, v. 18, p. 1626-1638.
- Cloke, P. L., 1969, Solubility of ZnS, PbS, Cu<sub>2</sub>S, and MoS<sub>2</sub> in NaCl solutions: *Econ. Geology*, v. 64, in press.
- Cobble, J. W., 1953a, Empirical considerations of entropy. I. The entropies of the oxy-anions and related species: *Jour. Chem. Physics*, v. 21, p. 1443-1446.
- , 1953b, Empirical considerations of entropy. II. The entropies of inorganic complex ions: *Jour. Chem. Physics*, v. 21, p. 1446-1450.
- , 1964, The thermodynamic properties of high temperature aqueous solutions. VI. Applications of entropy correspondence to thermodynamics and kinetics: *Am. Chem. Soc. Jour.*, v. 86, p. 5394-5401.
- , 1966a, High temperature aqueous solutions: *Science*, v. 152, p. 1479-1485.
- , 1966b, Thermodynamics, in Eyring, H., ed. *Annual Review of Physical Chemistry*: Palo Alto, California, Annual Review Inc., p. 15-36.
- Couture, A. M., and Laidler, K. J., 1956, The partial molal volumes of ions in aqueous solution. I. Dependence on charge and radius: *Canadian Jour. Chemistry*, v. 34, p. 1209-1216.
- Criss, C. M., and Cobble, J. W., 1964a, The thermodynamic properties of high temperature aqueous solutions. IV. Entropies of the ions up to 200° and the correspondence principle: *Am. Chem. Soc. Jour.*, v. 86, p. 5385-5390.
- , 1964b, The thermodynamic properties of high temperature aqueous solutions. V. The calculation of ionic heat capacities up to 200°: Entropies and heat capacities above 200°: *Am. Chem. Soc. Jour.*, v. 86, p. 5390-5393.
- Ellis, A. J., 1966, Partial molal volumes of alkali chlorides in aqueous solution to 200°: *Chem. Soc. [London] Jour.*, p. 1579-1584.
- , 1967, Partial molal volumes of MgCl<sub>2</sub>, CaCl<sub>2</sub>, SiCl<sub>4</sub>, and BaCl<sub>2</sub> in aqueous solution to 200°: *Chem. Soc. [London] Jour.*, p. 660-664.
- , 1968, Partial molal volumes in high-temperature water, Pt. 3. Halide and oxoanion salts: *Chem. Soc. London Jour. A*, p. 1138-1143.
- Ellis, A. J., and Golding, R. M., 1959, Spectrophotometric determination of the acid dissociation constants of hydrogen sulfide: *Chem. Soc. [London] Jour.*, p. 127-130.
- , 1963, The solubility of carbon dioxide above 100°C in water and in sodium chloride solutions: *Am. Jour. Sci.*, v. 261, p. 47-60.
- Ellis, A. J., and Milestone, N. B., 1967, The ionization constants of hydrogen sulfide from 20° to 90°C: *Geochim. et Cosmochim. Acta*, v. 31, p. 615-620.
- Eugster, H. P., and Wones, D. R., 1962, Stability of the ferruginous biotite, annite: *Jour. Petrology*, v. 3, p. 82-125.
- Fenwick, F., 1926, The equilibrium between cupric ion, cuprous ion, and metallic copper: *Am. Chem. Soc. Jour.*, v. 48, p. 860-870.
- Feth, J. H., Roberson, C. E., and Polzer, W. L., 1964, Sources of mineral constituents in water from granitic rocks, Sierra Nevada, California and Nevada: *U. S. Geol. Survey Water-Supply Paper* 1535-I, 170 p.
- Franck, E. U., 1961, Überkritisches Wasser als electrolytisches Lösungsmittel: *Angew. Chemie*, v. 73, p. 309-322.
- Fyfe, W. S., Turner, F. J., and Verhoogen, John, 1958, Metamorphic reactions and metamorphic facies: *Geol. Soc. America Mem.* 73, 239 p.
- Gardner, E. R., Jones, P. J., and de Nordwall, H. J., 1963, Osmotic coefficients of some aqueous sodium chloride solutions at high temperatures: *Faraday Soc. Trans.*, v. 59, p. 1994-2000.
- Garrels, R. M., and Christ, C. L., 1965, *Solutions, minerals and equilibria*: New York, Harper and Row, 450 p.
- Garrels, R. M., and Mackenzie, F. T., 1967, Origin of the chemical composition of some springs and lakes, in Gould, R. F., ed., *Equilibrium concepts in natural water systems*: Washington, D. C., Am. Chem. Soc. Pubs., p. 222-242.

- Garrels, R. M., and Thompson, M. E., 1962, Chemical model for sea water at 25°C and 1 atmosphere total pressure: *Am. Jour. Sci.*, v. 260, p. 57-66.
- Giron, M., Marcus, Y., and Shiloh, M., 1963, A modified Debye theory of salting of non-electrolytes in electrolyte solutions: *Jour. Phys. Chemistry*, v. 67, p. 2495-2497.
- Hale, J. D., Izat, R. M., and Christensen, J. J., 1963, The calorimetric study of the heat of ionization of water at 25°C: *Jour. Phys. Chemistry*, v. 67, p. 2605-2608.
- Harned, H. S., 1961, Osmotic coefficients of hydrochloric acid, potassium and sodium chloride from 0° to 40° or 50°: U.S. Atomic Energy Comm., Doc. TID-12096.
- Harned, H. S., and Davis, R., 1943, The ionization constant of  $H_2CO_3$  in water and the solubility of  $CO_2$  in water and aqueous solutions from 0 to 50°: *Am. Chem. Soc. Jour.*, v. 65, p. 2030-2037.
- Harned, H. S., and Owen, B. B., 1958, The physical chemistry of electrolyte solutions, 3d ed.: New York, Reinhold, 803 p.
- Harned, H. S., and Scholes, S. R., 1941, The ionization constant of  $HCO_3^-$  from 0 to 50°: *Am. Chem. Soc. Jour.*, v. 63, p. 1706-1709.
- Helgeson, H. C., 1964, Complexing and hydrothermal ore deposition: New York, Pergamon Press, 128 p.
- 1967a, Thermodynamics of complex dissociation in aqueous solution at elevated temperatures: *Jour. Phys. Chemistry*, v. 71, p. 3121-3136.
- 1967b, Solution chemistry and metamorphism, in Abelson, P. H., ed., *Researches in Geochemistry*, v. 2: New York, John Wiley & Sons, p. 362-404.
- 1967c, Silicate metamorphism in sediments and the genesis of hydrothermal ore solutions, in Brown, J. S., ed., *Genesis of stratiform lead-zinc-barite-fluorite deposits*: *Econ. Geology*, Mon. 3, p. 333-342.
- 1968a, Geologic and thermodynamic characteristics of the Salton Sea geothermal system: *Am. Jour. Sci.*, v. 266, p. 129-166.
- 1968b, Evaluation of irreversible reactions in geochemical processes involving minerals and aqueous solutions: I. Thermodynamic relations: *Geochim. et Cosmochim. Acta*, v. 32, p. 853-877.
- Helgeson, H. C., and Garrels, R. M., 1968, Hydrothermal transport and deposition of gold: *Econ. Geology*, v. 63, p. 622-635.
- Helgeson, H. C., Garrels, R. M., and Mackenzie, F. T., 1969, Evaluation of irreversible reactions in geochemical processes involving minerals and aqueous solutions. II. Applications: *Geochim. et Cosmochim. Acta*, v. 33, p. 455-481.
- Helgeson, H. C., and James, W. R., 1968, Activity coefficients in concentrated electrolyte solutions at high temperatures: *Am. Chem. Soc.*, 155th Natl. Mtg., San Francisco, California, April 1968, Abs., p. 5-130.
- Hem, J. D., 1968, Graphical methods for studies of aqueous aluminum hydroxide, fluoride, and sulfate complexes: U. S. Geol. Survey Water-Supply Paper 1827B, 33 p.
- Hem, J. D., and Roberson, C. E., 1967, Form and stability of aluminum hydroxide complexes in dilute solution: U. S. Geol. Survey Water-Supply Paper 1827-A, 55 p.
- Hemley, J. J., 1959, Some mineralogical equilibria in the system  $K_2O-Al_2O_3-SiO_2-H_2O$ : *Am. Jour. Sci.*, v. 257, p. 241-270.
- Hemley, J. J., and Jones, W. R., 1964, Chemical aspects of hydrothermal alteration with emphasis on hydrogen metasomatism: *Econ. Geology*, v. 59, p. 538-569.
- Hemley, J. J., Meyer, Charles, Hodgson, C. J., and Thatcher, A. B., 1967, Some sulfide solubilities in alteration-controlled systems: *Science*, v. 158, p. 1580-1582.
- Hemley, J. J., Meyer, Charles, and Richter, D. H., 1961, Some alteration reactions in the system  $Na_2O-Al_2O_3-SiO_2-H_2O$ : U.S. Geol. Survey Prof. Paper 424D, p. D338-D340.
- Hepler, L. C., 1965, Entropy and volume changes on ionization of aqueous acids: *Jour. Phys. Chemistry*, v. 69, p. 965-967.
- Holser, W. T., and Kennedy, C. C., 1958, Properties of water, IV: Pressure-volume-temperature relations of water in the range 100 to 400°C. and 100 to 1400 bars: *Am. Jour. Sci.*, v. 256, p. 744-753.
- Hopkins, H. P., and Wulff, C. A., 1965, The solution thermochemistry of polyvalent electrolytes. II. Silver sulfate: *Jour. Phys. Chemistry*, v. 69, p. 9-11.
- Hostetler, P. B., 1963, The stability and surface energy of brucite in water at 25°C: *Am. Jour. Sci.*, v. 261, p. 238-258.
- Hostetler, P. B., and Christ, C. L., 1968, Studies in the system  $MgO-SiO_2-CO_2-H_2O$  (I): The activity-product constant of chrysotile: *Geochim. et Cosmochim. Acta*, v. 32, p. 485-497.
- Hower, J., and Mowatt, T. C., 1966, The mineralogy of illites and mixed-layer illite/montmorillonites: *Am. Mineralogist*, v. 51, p. 825-854.
- Hsu, K. J., 1967, Chemistry of dolomite formation, in Chilingar, G. V., Bissell, H. J., and Fairbridge, R. W., eds., *Carbonate Rocks*: New York Elsevier, p. 170-191.
- Hugus, Z.Z., 1951, The partial molal entropy of the cuprous ion: *Am. Chem. Soc. Jour.*, v. 73, p. 5459-5460.
- Hurlen, T., 1961, Electrochemical behavior of copper in acid chloride solutions: *Acta Chem. Scandinavica*, v. 15, p. 1231-1233.
- Jonte, H. H., and Martin, D. S., 1952, Solubility of silver chloride and the formation of complexes in chloride solution: *Am. Chem. Soc. Jour.*, v. 74, p. 2052-2054.
- Keenan, J. H., and Keyes, F. G., 1936, Thermodynamic properties of steam: New York, John Wiley & Sons, 90 p.
- Kelley, K. K., 1960, Contributions to the data on theoretical metallurgy. XIII. High temperature heat content, heat capacity and entropy data for the elements and inorganic compounds: U.S. Bur. Mines Bull. 584, 232 p.
- Kelley, K. K., Barany, R., King, E. G., and Christensen, A. U., 1959, Some thermodynamic properties of fluorophlogopite mica: U.S. Bur. Mines Rept. Inv. 5436, 16 p.
- Kelley, K. K., and King, E. G., 1961, Contributions to the data on theoretical metallurgy: U.S. Bur. Mines Bull. 592, 149 p.
- Kennedy, G. C., 1950, A portion of the system silica-water: *Econ. Geology*, v. 45, p. 629-653.
- Kielland, J., 1937, Individual ion activity coefficients of ions in aqueous solutions: *Am. Chem. Soc. Jour.*, v. 59, p. 1675-1678.
- King, E. G., Barany, R., Weller, W. W., and Pankratz, L. B., 1967, Thermodynamic properties of forsterite and serpentine: U.S. Bur. Mines Rept. Inv. 6962, 19 p.
- King, E. G., and Weller, W. W., 1961, Low temperature heat capacities and entropies at 298.15° K of diaspor, kaolinite, dickite, and halloysite: U.S. Bur. Mines Rept. Inv. 5810, 6 p.
- 1962, Low temperature heat capacity and entropy at 298.15°K of red mercuric sulfide: U.S. Bur. Mines Rept. Inv. 6001, 4 p.
- Kittrick, J. A., 1966, The free energy of formation of gibbsite and  $Al(OH)_3^-$  from solubility measurements: *Soil Sci. Soc. America Proc.*, v. 30, p. 595-598.
- Kozintseva, T. N., 1964, Solubility of hydrogen sulfide in water at elevated temperatures: *Geokhimiya*, v. 8, p. 758-765.
- Kraus, K. A., and Raridon, R. J., 1960, Anion exchange studies. XXXI. Adsorption of Zn (II) and Ga (III) from HCl solutions in the temperature range 25°-150°: *Am. Chem. Soc. Jour.*, v. 82, p. 3271-3276.
- Lafon, G. M., ms, 1969, Some quantitative aspects of the chemical evolution of the oceans: Ph.D. thesis, Northwestern Univ., Dept. Geol. Sci., Evanston, Ill.
- Langmuir, D., ms 1964, Stability of carbonates in the system  $CaO-MgO-CO_2-H_2O$ : Ph.D. thesis, Harvard Univ.; Cambridge, Mass.
- Latimer, W. M., 1952, The oxidation states of the elements and their potentials in aqueous solutions: Englewood Cliffs, N.J., Prentice-Hall, Inc., 392 p.
- Leden, I., 1952, The use of anion-exchange resin to prove the presence of anionic complexes in some cadmium and copper salts: *Svensk. kem. tidskr.*, v. 64, p. 145-149.
- Leussing, D. L., and Kolthoff, I. M., 1953, The solubility product of ferrous hydroxides and the ionization of the aquo-ferrous ion: *Am. Chem. Soc. Jour.*, v. 75, p. 2476-2479.
- Lietzke, M. H., Hupf, H. B., and Stoughton, R. W., 1965, Electromotive force studies in aqueous solution at elevated temperatures: VI. The thermodynamic properties of HCl-NaCl mixtures: *Jour. Phys. Chemistry*, v. 69, p. 2395-2399.
- Lietzke, M. H., and Stoughton, R. W., 1961, The calculation of activity coefficients from osmotic coefficient data: *Jour. Phys. Chemistry*, v. 65, p. 508-509.
- Lietzke, M. H., Stoughton, R. W., and Young, T. F., 1961, The bisulfate acid constant from 25 to 225° as computed from solubility data: *Jour. Phys. Chemistry*, v. 65, p. 2247-2249.
- Lindsay, W. T., Jr., and Liu, C. T., 1968, Vapor pressure lowering of aqueous solutions at elevated temperatures: Final report, Contract no. 14-01-0001-407, Division of Chemistry, Office of Saline Water, U. S. Dept. Interior, Washington, D.C., 235 p.
- Mackenzie, F. T., and Garrels, R. M., 1965, Silicates: reactivity with sea water: *Science*, v. 150, p. 57-58.
- Malcolm, G. N., Parton, H. N., and Watson, I. D., 1961, Enthalpies and entropies of formation of Hg (II) halide 1 : 1 complex ions: *Jour. Phys. Chemistry*, v. 65, p. 1900-1902.
- Marcus, Y., 1956, "personal communication," cited in Stability constants of metal-ion complexes by Sillén, L. G., and Martell, A. E., 1964: *Londón. Chem. Soc.*, 308 p.
- 1960, The anion exchange of metal complexes. IV. Iron (III) chloride system: *Jour. Inorganic Nuclear Chemistry*, v. 12, p. 287-296.

*Geoexploration*, 11 (1973) 141-149

© Elsevier Scientific Publishing Company, Amsterdam - Printed in The Netherlands

## Research Papers

# TEMPERATURE INVERSIONS IN GEOTHERMAL SYSTEMS

GUNNAR BODVARSSON

*School of Oceanography, Oregon State University, Corvallis, Oreg. (U.S.A.)*

(Accepted for publication August 11, 1972)

## ABSTRACT

Bodvarsson, G., 1973. Temperature inversions in geothermal systems. *Geoexploration*, 11: 141-149.

Temperature inversions have been observed in deep boreholes in a number of geothermal areas. An elementary investigation indicates that the observed inversions may be manifestations of temperature disequilibria around fractures or permeable horizons where the thermal or flow conditions have changed recently. In particular, the permeable structures may recently have been invaded by thermal waters. Two cases from Iceland are discussed in some detail.

## INTRODUCTION

Measurements in deep boreholes in geothermal areas frequently reveal a rather characteristic shape of the vertical temperature profile. The temperature increases quite rapidly in the uppermost few hundred meters, and may then become practically constant at greater depths. The upper section of the temperature profile is generally characteristic of formations with a relatively low fluid permeability and, hence, a more or less conductive temperature field. The constant temperature section is usually indicative of a formation with a sufficiently high permeability to allow an equalization of the temperature field by forced or free convection of interstitial waters. This section may constitute a part of the local geothermal reservoir and its temperature is often referred to as the base temperature of the thermal area. A typical temperature profile measured in a deep borehole in one of the major low-temperature thermal areas in Iceland is shown in Fig. 1 (Sigurdsson, 1967).

Deviations from this rather standard temperature profile are, however, not altogether uncommon. Perhaps the most interesting anomalies are the temperature inversions which have been observed in a number of major geothermal areas. Cases from boreholes in geothermal areas in Iceland are illustrated in Fig. 2 and 3 (Bodvarsson and Palmason, 1964). The temperature data in both figures show very clear maximums and sections where the temperature decreases with depth. No less conspicuous temperature inversions have been observed in five boreholes in the El Tatio geothermal area in Northern Chile (Healy, 1971). This condition appears to prevail throughout the entire geothermal system at El Tatio which extends over an area of several tens of square kilometers. Such temperature inversions are quite interesting, in particular, because they can be of diagnostic value as to the structural and flow characteristics of the thermal systems involved. The present paper dis-

UNIVERSITY OF UTAH  
RESEARCH INSTITUTE  
EARTH SCIENCE LAB.

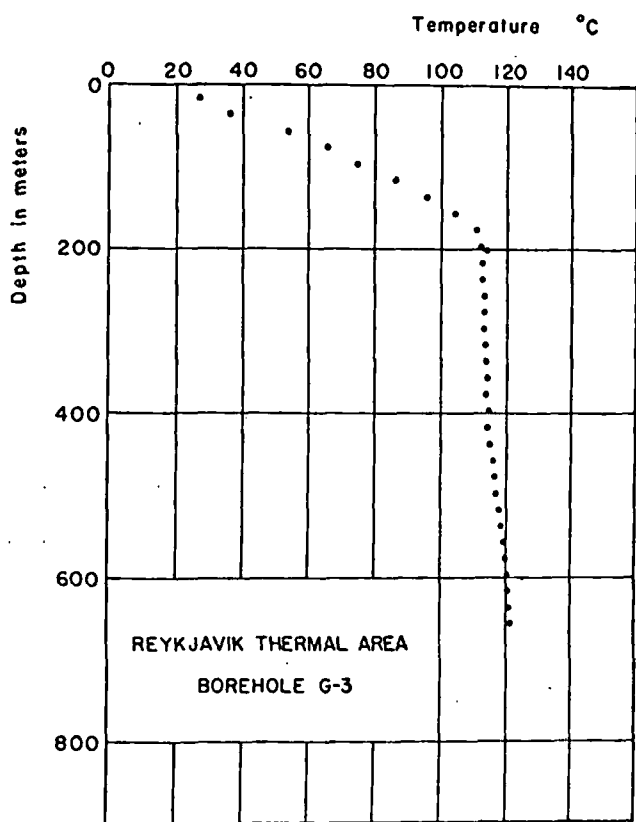


Fig.1. Temperature data from a borehole in the Reykjavik thermal area in Iceland.

cusses briefly the possible causes of temperature anomalies of this nature and calls attention to their practical implications.

POSSIBLE CAUSES OF TEMPERATURE INVERSIONS

Several situations leading to temperature inversions in boreholes can be envisioned, viz, the following models:

(1) Horizontal or quasi-horizontal sheet-like currents of thermal water flowing above currents of colder water. By constant flow over a sufficiently long time interval, the temperature field in the adjacent formations can attain steady state. This situation is sketched in Fig.4.

(2) Downward attenuation by geometric spreading of the steady-state temperature field adjacent to currents of thermal water. The measurements may have been made in a borehole located close to a concentrated current. A very simple example is given in Fig.5.

(3) Temperature disequilibria in the formations adjacent to currents of thermal waters. The thermal water has relatively recently invaded the formations, or there have been recent

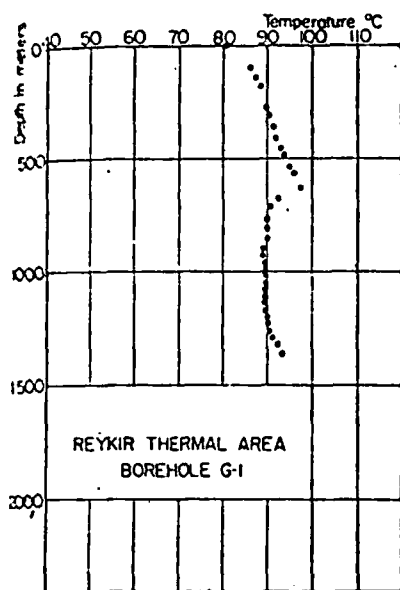


Fig.2. Temperature data from a borehole in the Reykir thermal area in Iceland.

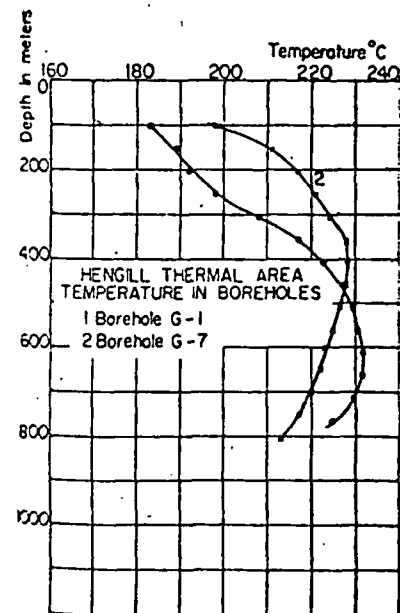


Fig.3. Temperature data from boreholes in the Hengill thermal area in Iceland.

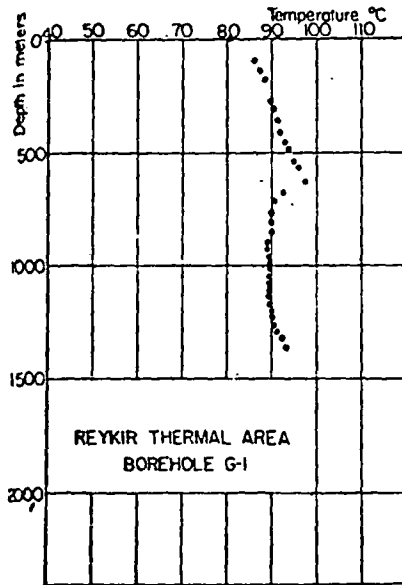


Fig.2. Temperature data from a borehole in the Reykir thermal area in Iceland.

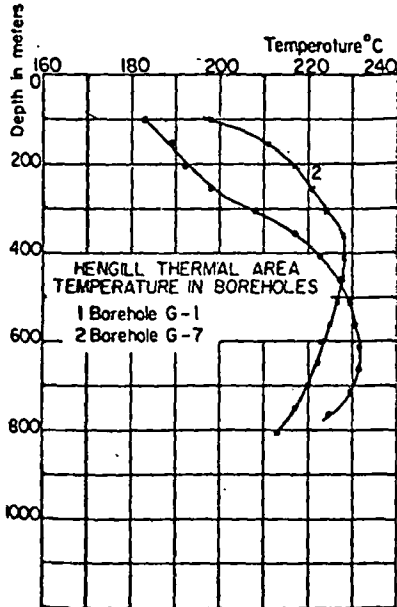


Fig.3. Temperature data from boreholes in the southern part of the Hengill thermal area in Iceland.

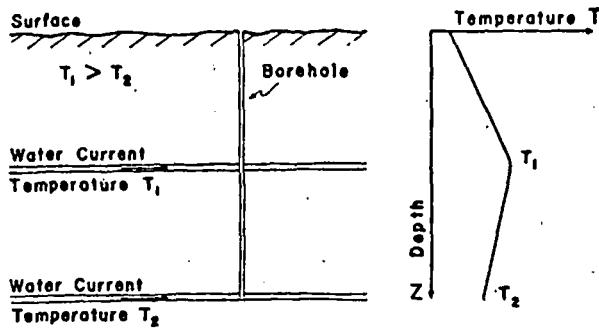


Fig. 4. Sketch of model (1), two horizontal sheet-like currents of thermal water with different temperatures.

increases in the temperature of the flowing water. An example involving a very thin extended sheet-like horizontal current is shown in Fig. 6.

(4) Local inhomogeneities in the temperature field due to convective movements of interstitial waters. The temperature inversions may result from the spreading of upward-moving plumes of thermal water. A hypothetical example is shown in Fig. 7. The possibilities of the occurrence of phenomena of this nature in convective flows in porous formations have been discussed by Donaldson (1971).

(5) The observed inversions may be artifacts caused by local thermal disequilibria in the boreholes from which the data were obtained and do not therefore reflect the true formation temperature.

Model (1) is based on the concept of a stationary conductive temperature field between two or more current sheets of different temperatures and at different levels. In general, one will assume that the temperature between the sheets is a linear function of the depth. This model has been suggested by Healy (1971) as a possible explanation for the temperature inversions which have been observed in the geothermal area at El Tatio in Northern Chile.

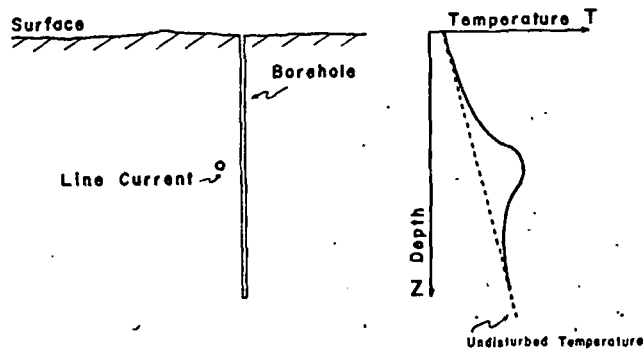


Fig. 5. A simple example of model (2), the temperature field adjacent to a concentrated line current of thermal water.

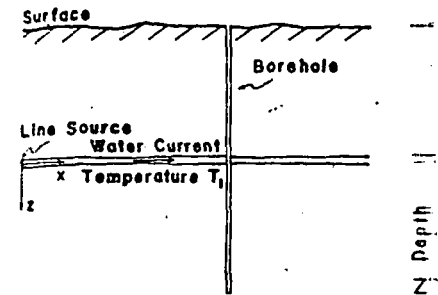


Fig. 6. A simple example of model (3), temperature of thermal water of recent origin.

Models (2), (4), and (5) can generally served consistently over substantial sections are based on phenomena of a local character non-local pattern.

The attention will therefore focus on temperature inversions are non-local in character. In distinguishing between these two models it is clear that inversions have a distinctly non-linear shape. Model (1) would not appear to offer a promising discussion in the next section will indicate that areas are likely to be transient in nature. Attention to model (3) which is essential.

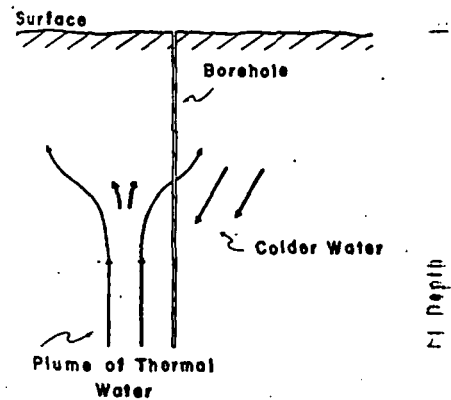


Fig. 7. Model (4), temperature field at an upward-moving plume of thermal water.

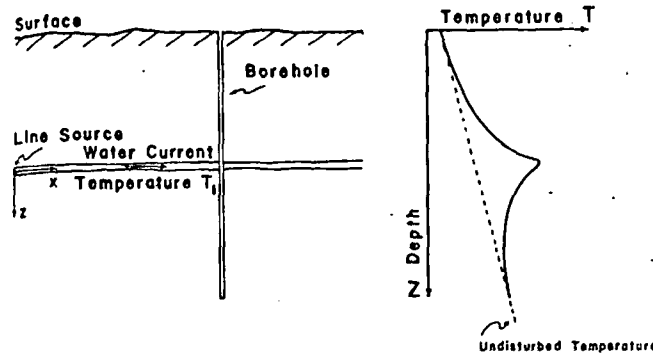


Fig. 6. A simple example of model (3), temperature disequilibrium adjacent to a sheet-like horizontal current of thermal water of recent origin.

Models (2), (4), and (5) can generally be ruled out if the temperature inversions are observed consistently over substantial sections of geothermal systems. These three models are based on phenomena of a local character which are unlikely to exhibit a consistent non-local pattern.

The attention will therefore focus on models (1) and (3) when the observed temperature inversions are non-local in character. In order to establish crude criteria for distinguishing between these two models it is of interest to note that many observed temperature inversions have a distinctly non-linear shape as, for example, the case shown in Fig. 2. Model (1) would not appear to offer a plausible explanation in this case. Moreover, the discussion in the next section will indicate that subsurface temperature fields in geothermal areas are likely to be transient in nature. There are, therefore, reasons to turn our main attention to model (3) which is essentially based on the assumption of thermal disequilibria.

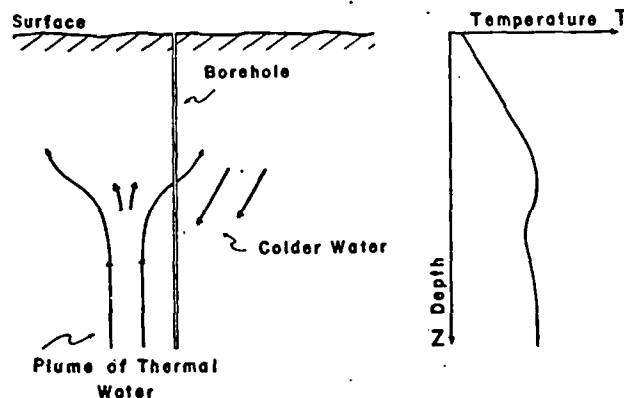


Fig. 7. Model (4), temperature field at an upward moving plume of thermal water.

A. J. BODVARSSON, PH.D., GEOTHERMAL ENGINEER, UNIVERSITY OF UPPSALA, SWEDEN



## THERMAL INERTIA AND FLOW TRANSIENTS

Rock formations have a very low thermal diffusivity and consequently a considerable thermal inertia. Consider an infinite homogeneous space of thermal diffusivity  $a$  and having at time  $t = 0$  an initial temperature equal to zero everywhere except within an infinite slab of thickness  $2b$  where the initial temperature is unity. Assuming pure heat conduction, an elementary result in heat conduction theory (see Carslaw and Jaeger, 1959, p. 54) gives the temperature at the center plane of the slab  $T_c = \text{erf}(b/2\sqrt{at})$ . Since for most common rock  $a = 10^{-6} \text{ m}^2/\text{sec}$  (Clark, 1966), the time required for  $T_c$  to fall, for example, to 1/2 of its initial value is  $t_r = 1.11b^2 \cdot 10^6 \text{ sec}$ . For a thickness  $2b = 1 \text{ km}$  we find that approximately  $t_r = 10^4 \text{ years}$ . Since the relaxation time increases with the square of the characteristic dimensions, it is consequently unlikely that a steady state can be attained by large-scale temperature fields in geologically very active areas.

Moreover, fractures of very small widths can carry substantial mass flows of water. Consider a hypothetical plane fracture of a uniform width  $h$  and carrying a uniform flow in the direction of the  $x$ -axis which is placed in the fracture. Let the kinematic viscosity of the fluid be  $\nu$ . Assuming laminar or quasi-laminar flow, the mass flow per unit length across the flow is given approximately by (see Lamb, 1932, p. 582):

$$q = -(h^3/12\nu)dp/dx \quad (1)$$

where  $dp/dx$  is the pressure gradient in the direction of the flow. To take a specific case, let the fracture have a width of  $h = 1 \text{ mm}$  and carry water at a temperature of  $200^\circ\text{C}$ . Moreover, let the pressure gradient be of a convective origin such that, for example,  $dp/dx = -10^3 \text{ N/m}^3$ . Since  $\nu = 0.16 \cdot 10^{-6} \text{ m}^2/\text{sec}$  eq. 1 gives  $q = 0.5 \text{ kg m}^{-1} \text{ sec}^{-1}$ , that is, a fracture 1 km long will carry a total mass flow of 500 kg/sec. This is of the same order as the total discharge of water in many thermal areas. The third power of  $h$  in eq. 1 indicates that  $q$  is very sensitive to  $h$ . Hence, common fractures are very likely to undergo frequent substantial changes in their fluid conductance due to both the precipitation of minerals and tectonic movements.

Both factors, viz. the sensitivity of the fluid conductance and the inertia of the temperature field, underline the high probability of frequent changes in the flow pattern and temperature disequilibria in active geothermal areas. This fact is quite strongly in favor of the disequilibrium model (3).

## THE DISEQUILIBRIUM MODEL

To give the most important elementary example to model (3) above, consider a uniform extensive sheet-like current of thermal water originating from a line-source and flowing through a plane fracture of practically infinitesimal width in an infinite homogeneous solid. As above, place the  $x$ -axis in the fracture in the direction of the flow such that  $x = 0$  at the origin, and the  $z$ -axis perpendicular to the plane of the fracture. Let the flow from the line-source be initiated at time  $t = 0$ , the initial temperature of the rock be zero and the

## TEMPERATURE INVERSIONS IN GE

temperature of the water at the source flow per unit length of the fracture in the direction of the  $x$ -axis can be neglected in the  $z$ -axis. This implies that the temperature field is treated as a one-dimensional field in the  $x$ -direction.

Assuming pure heat conduction, the temperature field in the fracture can be derived on the basis of the heat conduction in semi-infinite solids. Since the boundary at  $z = 0$  is approximately at the surface, see Carslaw and Jaeger (1959, p. 63), viz:

$$T = T_0 \text{erfc}(z/2\sqrt{at})$$

and hence the temperature gradient

$$g_0 = \left(\frac{\partial T}{\partial z}\right)_{z=0} = -T_0/\sqrt{\pi at}$$

which can be rewritten in terms of  $\tau$

$$\tau = T_0^2/\pi a g_0^2$$

Hence,  $\tau$  can be determined if  $T_0$  and  $g_0$  are known. In the present case,  $T_0$  and  $g_0$  fields have been disregarded on the basis of eq. 1 for such fields.

## DISCUSSION OF THE PRESENT DATA

The temperature profiles shown in Figure 1 and no particular attention has been given to the data are therefore somewhat incomplete. Both thermal areas to furnish convincing evidence of local phenomena. Nevertheless, we can see that the simple sheet-like disequilibrium model requires a duration of flow required to establish the temperature field.

In the case of the deep Reykir borehole, the average temperature gradient is found to be  $0.112^\circ\text{C/m}$ . According to Palmason (1966) the average temperature gradient in Iceland is  $0.112 + 0.065 = 0.177^\circ\text{C/m}$ . Moreover, the average temperature gradient at a depth of 630 m, and the average temperature gradient is found that  $T_0 = 97 - (630 \cdot 0.065 + 5) = 57.5^\circ\text{C}$ . This is a surprisingly low but it is in agreement with the evidence through the permeable horizon at the base of the cal evidence of very recent disturbances.

consequently a considerable normal diffusivity  $a$  and having except within an infinite slab being pure heat conduction, an (Jaeger, 1959, p. 54) gives  $(\sqrt{at})$ . Since for most common to fall, for example, to  $1/2 = 1$  km we find that approximately the square of the characteristic can be attained by large-

ential mass flows of water. Consider carrying a uniform flow in at the kinematic viscosity of mass flow per unit length (p. 582):

(1)

flow. To take a specific case, at a temperature of  $200^\circ\text{C}$ . Moreover that, for example,  $dp/dx = 5 \text{ kg m}^{-1} \text{ sec}^{-1}$ , that is, a fracture is of the same order as the power of  $h$  in eq. 1 indicates very likely to undergo frequent the precipitation of minerals

and the inertia of the temperature changes in the flow pattern and fact is quite strongly in favor of

el (3) above, consider a uniform flow from a line-source and flowing in an infinite homogeneous solid. Let the flow from the fracture. Let the flow from the surface of the rock be zero and the

temperature of the water at the source be  $T_0$ . Moreover, for convenience, let the specific flow per unit length of the fracture be large enough that the temperature gradient in the direction of the  $x$ -axis can be neglected as compared with the gradient in the direction of the  $z$ -axis. This implies that the temperature field on both sides of the fracture can be treated as a one-dimensional field in a semi-infinite solid. The model is illustrated in Fig. 6.

Assuming pure heat conduction, the temperature field in the formations adjacent to the fracture can be derived on the basis of elementary results for one-dimensional heat conduction in semi-infinite solids. Since the initial temperature is zero and the temperature at the boundary  $z = 0$  is approximately  $T_0$ , the relevant result for  $T(z)$  is given by Carslaw and Jaeger (1959, p. 63), viz:

$$T = T_0 \operatorname{erfc}(z/2\sqrt{at}) \quad (2)$$

and hence the temperature gradient with respect to  $z$  at  $z = 0$  is:

$$g_0 = \left( \frac{\partial T}{\partial z} \right)_{z=0} = -T_0/\sqrt{\pi at} \quad (3)$$

which can be rewritten in terms of the duration of the flow:

$$t = T_0^2/\pi a g_0^2 \quad (4)$$

Hence,  $t$  can be determined if  $T_0$  and  $g_0$  are known. Since stationary regional temperature fields have been disregarded on the above model, borehole data will have to be corrected for such fields.

#### DISCUSSION OF THE PRESENT DATA

The temperature profiles shown in Fig. 2 and 3 are the result of routine measurements and no particular attention has been given to the inversions occurring in the profiles. The data are therefore somewhat incomplete. Moreover, there are too few deep boreholes in both thermal areas to furnish convincing evidence that the temperature inversions are non-local phenomena. Nevertheless, we can tentatively interpret the results on the basis of the simple sheet-like disequilibrium model discussed in the previous section and estimate the duration of flow required to establish the observed inversions.

In the case of the deep Reykir borehole in Fig. 2 the observed inversion gradient is found to be  $0.112^\circ\text{C/m}$ . According to Palmason (1967), recent results on the undisturbed regional temperature gradient in Iceland indicate a value of  $0.065^\circ\text{C/m}$ . This is probably a reasonable value for the Reykir area and, hence, the total inversion gradient is estimated at  $g_0 = 0.112 + 0.065 = 0.177^\circ\text{C/m}$ . Moreover, since the temperature maximum of  $97^\circ$  is obtained at a depth of 630 m, and the average surface temperature in the Reykir area is  $5^\circ\text{C}$ , we find that  $T_0 = 97 - (630 \cdot 0.065 + 5) = 51^\circ\text{C}$ . Inserting these values into eq. 4 gives  $t = 830$  years. This is a surprisingly low but by no means unreasonable value for the age of the flow through the permeable horizon at the depth of 630 m. Unfortunately, there is no geological evidence of very recent disturbances in the thermal area which would allow an indepen-

dent testing of this result. It should be remarked that there is a small leak of thermal water from the horizon at 630 m into the borehole causing the elevated temperatures in the upper section of the hole. The borehole, which is drilled into Tertiary flood basalts, has a surface casing of only 100 m.

There is greater uncertainty with regard to the temperature data measured in boreholes G-1 and G-7 in the Hengill area given in Fig.3. The inverted section of the profile from G-1 is too short to furnish meaningful values. Moreover, the slight convexity of the inverted section in G-7 throws some doubts on the disequilibrium model. However, this detail is too uncertain to be regarded as a serious objection to the model. In G-7 the temperature maximum is 228°C at a depth of 400 m and the inversion gradient is approximately 0.03°C/m. Since the Hengill area is quite active, it appears reasonable to estimate the undisturbed regional temperature gradient at 0.1°C/m. Hence,  $g_0 = 0.03 + 0.1\Omega = 0.13^\circ\text{C/m}$  and  $T_0 = 228 - 40 = 188^\circ\text{C}$ . Inserting these two values in eq. 4 gives  $t = 21,000$  years.

It is evident that because of the low temperatures and steep inversion gradient, the ratio  $T_0/g_0$  is quite small in the case of the Reykir borehole. The calculated values of the flow time  $t$  will therefore be unusually low in this case. The data from G-7, on the other hand, give a high ratio and, hence, a relatively long flow time. Inversions observed in other cases will tend to give flow time values falling between these two rather extreme values.

Judging on the basis of the relatively frequently observed changes in the flow pattern in geothermal areas, the time values obtained above do not appear physically unreasonable. The results, therefore, lend some support to the disequilibrium model. Nevertheless, since there is at this juncture no possibility of verifying the above estimates independently by other means, further research is needed before the disequilibrium theory can be confirmed. On the other hand, it is quite clear that the possibility of being able to estimate ages of flow transients is quite important for the exploration of geothermal areas. The age is an important geological parameter.

#### ACKNOWLEDGEMENT

This work was supported by National Science Foundation grant GA-25896.

#### REFERENCES

- Bodvarsson, G. and Palmason, G., 1964. Exploration of subsurface temperature in Iceland. In: *Proc. U.N. Conf. New Sources of Energy, Rome, 1961*. United Nations, New York, N.Y., 2: 91-98.
- Carlsaw, H.S. and Jaeger, J.C., 1959. *Conduction of Heat in Solids*. Oxford University Press, Oxford, 2nd ed., 496 pp.
- Clark, Jr., S.P. (Editor), 1966. *Handbook of Physical Constants. Memoir 97*, Geol. Soc. Am., New York, N.Y., 587 pp.
- Donaldson, I.G., 1971. The simulation of geothermal systems with a simple convection model. In: *Proc. U.N. Symp. Development and Utilization of Geothermal Resources, Pisa, 1970*. International Institute for Geothermal Research, Pisa, pp. 649-654.
- Healy, J., 1971. Geological report on wells 1-5, El Tatio, Internal Report. In: *Survey for Geothermal Development in Northern Chile*. UNDP Geothermal Project in Chile, Santiago, 34 pp.

Lamb, H., 1932. *Hydrodynamics*. Dover.

Palmason, G., 1967. On heat flow in Iceland. In: *Geothermal Energy in Iceland* (Editor), Iceland and Mid-Ocean Research Institute, Reykjavik, 12 pp.

Sigurdsson, S., 1967. *Temperature Inversions in Geothermal Areas*. Energy Authority, Reykjavik, 12 pp.

is a small leak of thermal water  
 elevated temperatures in the up-  
 Tertiary flood basalts, has a  
 temperature data measured in boreholes  
 and section of the profile from  
 the slight convexity of the inverted  
 model. However, this detail is  
 model. In G-7 the temperature maxi-  
 mum is approximately  $0.03^{\circ}\text{C}/\text{m}$ .  
 to estimate the undisturbed  
 $0.03 + 0.10 = 0.13^{\circ}\text{C}/\text{m}$  and  $T_0 =$   
 $t = 21,000$  years.  
 steep inversion gradient, the ratio  
 the calculated values of the flow  
 from G-7, on the other hand,  
 inversions observed in other cases  
 rather extreme values.  
 and changes in the flow pattern  
 appear physically unreasonable.  
 convection model. Nevertheless, since  
 the estimates independently by  
 equilibrium theory can be confirmed.  
 being able to estimate ages of  
 geothermal areas. The age is an

tion grant GA-25896.

temperature in Iceland. In: *Proc.*  
*Conf. on Geothermal Energy*, New York, N.Y., 2: 91-98.  
 Oxford University Press, Oxford.

*Memoir 97*, Geol. Soc. Am., New

in a simple convection model. In:  
*Geothermal Resources, Pisa, 1970*. International

Report. In: *Survey for Geothermal*  
*Resources, Chile*, Santiago, 34 pp.

Lamb, H., 1932. *Hydrodynamics*. Dover Publications, New York, N.Y., 6th ed. 738 pp.

Palmason, G., 1967. On heat flow in Iceland in relation to the mid-Atlantic ridge. In: S. Bjornsson  
 (Editor), *Iceland and Mid-Ocean Ridges*. Soc. Sci. Islandica, Reykjavik, 38: 111-127.

Sigurdsson, S., 1967. *Temperature Measurements in Boreholes 1966*, Internal Report. National  
 Energy Authority, Reykjavik, 12 pp.

UNIVERSITY OF UTAH LIBRARY

SUBJ  
GTHM  
TMS

# Tapping the Main Stream of Geothermal Energy

A Reprint  
May 1980

UNIVERSITY OF UTAH  
RESEARCH INSTITUTE  
EARTH SCIENCE LAB.

ELECTRIC POWER RESEARCH INSTITUTE

# EPRI JOURNAL

**O**pening the frontier of U.S. geothermal energy can be visualized as a continental migration. But instead of beginning at St. Augustine, Jamestown, or Plymouth Rock, it begins at The Geysers, some 90 miles north of San Francisco, California.

This technological quest began in 1960, when Pacific Gas and Electric Co. (PG&E) put 11 MW of capacity on-line and generated the nation's first commercial geothermal electricity. Its fuel was natural dry steam drawn from wells drilled among the vents, or fumaroles, that mark a relatively shallow zone of seismically fractured hot rock. Today the field supports 14 PG&E units totaling 800 MW, and at least 7 more units are under construction or planned by PG&E and others for operation between now and 1983. Most of the newer units carry 110-MW ratings.

Many routes of geothermal development now lead eastward from The Geysers. They radiate up into Idaho, across to Utah, over to New Mexico, and down to California's border with Mexico. Their goal is the economic use of underground steam and hot water at commercial scale, mostly for conversion to electricity. One long beckoning path curves along the Gulf Coast of Texas and Louisiana, where geologic processes trapped huge amounts of energy, in the form of natural gas dissolved in hot water, in deep sediments at great pressure.

The U.S. Geological Survey has mapped geothermal water resources (those above 90°C, or 194°F, to a depth of 3 km, or 2 mi) beneath 24 of the continental states. This wide distribution is attractive because it puts geothermal energy potentially within reach for process and space heating—the 35% of our nationwide requirements that can use lower temperatures. Only last July an exploratory well in Maryland established the presence of 60°C (140°F) water beneath the Atlantic Coastal Plain. Thus the first trails of geothermal energy development have spanned the continent.

#### Temperature-based technology

Our continental map suggests the broad extent of a resource that takes many forms. But the sites that hold early power generation potential for electric utilities are more limited. For example, natural dry steam occurs in very few places, notably The Geysers and Lassen Volcanic and Yellowstone national parks (the parks are precluded from development). Geothermal water, however, underlies most states, and such hydrothermal resources total some 2400 quadrillion ( $2.4 \times 10^{18}$ ) Btu of recoverable energy.

Vasel Roberts, manager of the Geothermal Power Systems Program at EPRI, is quick to qualify this figure in two ways. "First, only about 900 quadrillion [ $900 \times 10^{15}$ ] Btu is what we call electricity grade—that is, 150°C [300°F] or hotter. And all of that is in the western states.

"In addition," Roberts goes on, "the estimate of 900 quadrillion Btu includes resources so far only inferred, or assumed to exist, on the basis of geophysical data. When we narrow it down to the identified portion, we're talking about perhaps 220 quadrillion Btu."

Is this a meaningful figure? "Yes, indeed," Roberts affirms, "because it readily translates to a generating capacity of about 24 GW with a useful life of at least 30 years, clearly a feasible target for utility development in the next 20 years."

Hydrothermal temperatures and pressures (dry steam included) are well below those at the turbine inlet of a fossil-fueled power plant. At The Geysers, for instance, steam conditions are about 180°C (356°F) and 110 psi (760 kPa); in a modern coal-fired plant, 540°C (1000°F) and 2400 psi (16.6 MPa). Accordingly, the respective energy conversion efficiencies are about 15% and 33%, but the geothermal steam plant competes because its steam is ready-made and inexpensive and the plant availability is higher, often more than 80%.

If the hydrothermal fluid is above 210°C (410°F), its wellhead pressure can be reduced so that part of the water vaporizes (flashes) into steam. Conversion efficiency is about 15%, and what is important, this method uses the same kind of turbine as a geothermal steam plant. Such technology is well established, used for generating power not only at The Geysers but at many hydrothermal sites around the world: Italy (400 MW), New Zealand (190 MW), Mexico (150 MW), as well as the Philippines, El Salvador, Iceland, and Japan.

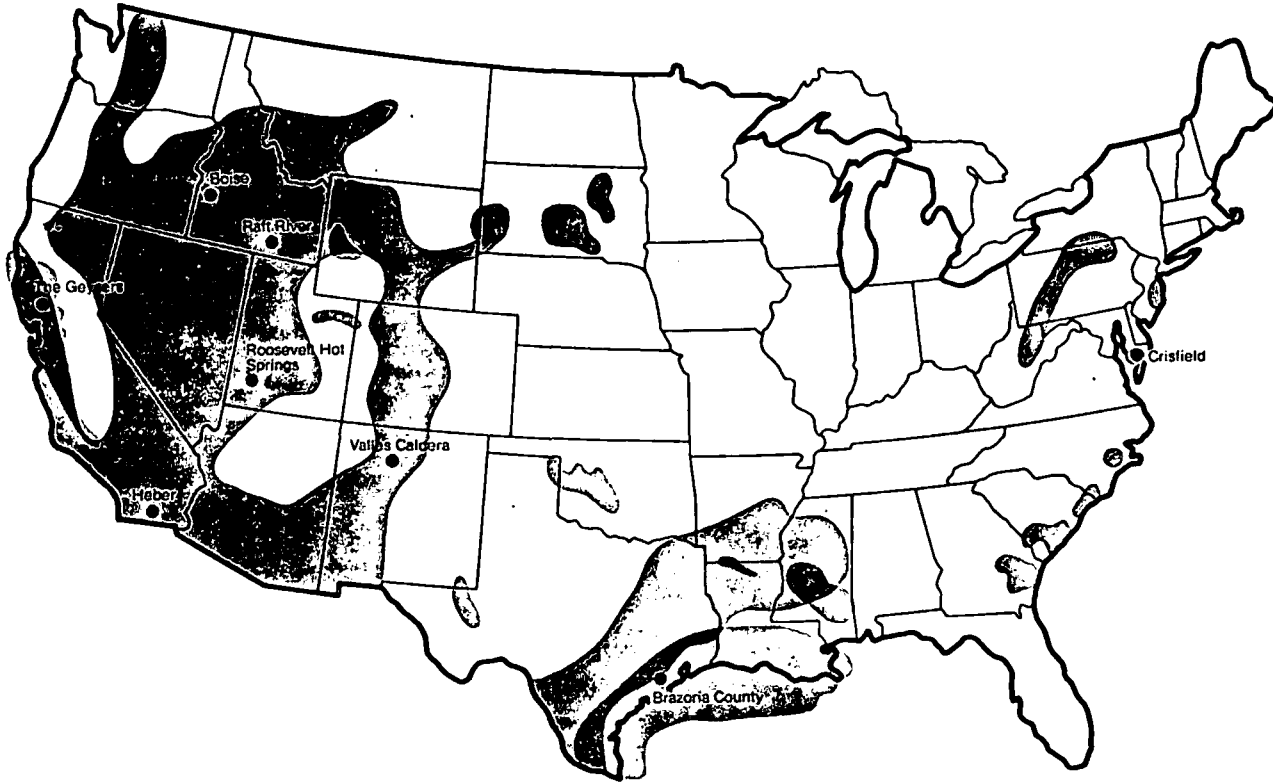
About half the electricity-grade hydrothermal energy in the United States is in this high-temperature range of 210°C (410°F) and above. The other half is in the moderate-temperature range of 150–210°C (300–410°F), for which the direct-flash technology is not assuredly economic. Inlet and exhaust steam conditions define the energy that can be extracted by a turbine, but operation of the condenser imposes its own lower limit on the cycle. If the flash temperature of the steam is too low, the available differential represents too little energy for economic operation.

A different technological approach is necessary for moderate temperatures, the binary cycle. It is this cycle that EPRI believes will afford the greatest reliability and lowest busbar electricity cost for utilities. Just this year cooperative negotiations have begun for DOE and EPRI to join with San Diego Gas & Electric Co. (SDG&E) and several other organizations to build a binary-cycle demonstration plant at commercial scale. The site is a 180° (356°F) reservoir of low-salinity geothermal brine at Heber in California's Imperial County, south of the Salton Sea and only four miles from the border communities of Calexico and Mexicali.

#### Demonstrating the binary cycle

The binary cycle is a way to make vapor that will run an expansion turbine when the available water temperature and

Electric power generation success at The Geysers in California has motivated nationwide identification and assessment of hydrothermal resources, as well as several research and pilot projects for energy conversion. Green areas indicate regions with known and inferred hydrothermal reservoirs. In the eastern and midwestern states, the temperature of the resource is less than 150°C; in the western states, some reservoirs contain water and steam of electricity-grade temperatures. Gray areas indicate known and inferred geopressured zones; the best known are those that extend along the Gulf Coast.



#### REPRESENTATIVE U.S. GEOTHERMAL PROJECTS

Location	Purpose	Technology	Capacity (MW)	Starting Date	Sponsors
The Geysers, California	Electricity, commercial	Natural steam cycle	800	1960-1980	Pacific Gas and Electric Co.; Union Oil Co. of California
Heber, California	Electricity, demonstration	Binary cycle	45	1984	DOE; EPRI; San Diego Gas & Electric Co.; Chevron Resources Co.
East Mesa, California	Electricity, pilot	Binary cycle	11	1979	Magma Power Co.
Raft River, Idaho	Electricity, experiment	Binary cycle	5	1980	DOE
Valles Caldera, New Mexico	Electricity, demonstration	Direct-flash steam cycle	50	1982	DOE; Public Service Co. of New Mexico; Union Oil Co. of California
Northern Nevada (site to be selected)	Electricity, commercial	Direct-flash steam cycle	50	1984	Sierra Pacific Power Co. and other utilities
Heber, California	Electricity, commercial	Direct-flash steam cycle	41	1982	Southern California Edison Co.; Chevron Resources Co.
Roosevelt Hot Springs, Utah	Electricity, commercial	Direct-flash steam cycle	20	(pending)	Utah Power & Light Co.; Phillips Petroleum Co.
Brawley, California	Electricity, pilot	Direct-flash steam cycle	10	1980	Southern California Edison Co.; Union Oil Co. of California
Boise, Idaho	District heat, commercial	NA	NA	1981	DOE; State of Idaho; City of Boise
Crisfield, Maryland	Hydrothermal, exploration	NA	NA	1979 (reached 60°C water)	DOE
Brazoria County, Texas	Geopressure, exploration	NA	NA	1979 (well complete)	DOE

pressure (geothermal or any other kind) are too low for the direct-flash approach. It involves a second fluid (hence the term *binary*) that vaporizes at a much lower temperature than water and a way to transfer the thermal energy from one to the other. Usually this is a surface heat exchanger in which many thin-walled tubes carry geothermal water through a cylindrical shell containing the second fluid. Thus heated and vaporized, the second fluid is piped into a turbine; it is the working fluid.

Both systems are closed loops. Geothermal water from production wells passes through the heat exchanger and returns to the reservoir through injection wells. Significantly, a binary cycle requires only about two-thirds the water volume (at 180°C; 356°F) needed by a direct-flash cycle to produce the same amount of electric power. For any given water cost, this fact materially contributes to the binary cycle's lower busbar power cost.

Heber is a \$130 million project, entailing about \$84 million in capital cost and about \$46 million for fuel and operation over a demonstration period of at least two years (1985 and 1986). These figures represent totals of current dollars for the years in which costs are incurred. To some extent, operating costs will be offset by electricity revenue.

Recommended since early 1977 by Vasek Roberts and his EPRI colleagues and advisers, Heber is now ready for detailed engineering design. Preliminary work, including environmental reports and vital permits, is in hand from earlier R&D sponsored by EPRI and SDG&E. At least four other participants will be involved: DOE, Imperial Irrigation District, Southern California Edison Co., and California's Department of Water Resources. Two vital suppliers and customers are ready: Chevron Resources Co., part owner of the hydrothermal field and producer of its brine; and Imperial Irrigation District, supplier of cooling water and buyer of electricity.

The turbine generator for Heber could be on order a year from now, followed by plant construction beginning in August 1982 and ending two years later. On this basis, Heber will be through its startup phase in the fall of 1984, ready for demonstration operation and power generation at 65 MW—pumping brine and running the plant with 20 MW and delivering 45 MW of baseload electricity—four times the capacity of the first geothermal steam plant at The Geysers in 1960.

The foremost feature of the Heber project is its size, which is representative of commercial binary-cycle hydrothermal plants to follow. Its demonstration is vital for data and experience in all aspects of equipment design, manufacture, operation, reliability, and overall economics.

#### Heber project features

Scale-up of the turbine is the biggest question mark of the Heber plant. Similar but much smaller turbines (by a factor of 3) have precedent in the petrochemical industry, where hydrocarbon fluids at conveniently compatible temperature and pressure are vaporized and used in turbines to generate shaft horsepower for pumps and compressors.

Heber's single hydrocarbon turbine will generate 65 MW. In contrast, the 11.2-MW Magma Power Co. pilot plant at East Mesa, California, is using two 5-MW and one 1.2-MW turbines. That plant uses two hydrocarbon fluids (propane and isobutane) separately in a pair of binary cycles that power the turbines. Elsewhere, Freon is the working fluid of a 100-kW experimental binary cycle to be tested by Arkansas Power & Light Co. for generating auxiliary power in conjunction with a geothermal minerals recovery operation.

The Heber project will also help resolve key questions about sustained hydrothermal reservoir production, but it shares this purpose with another venture, the 50-MW demonstration of

direct-flash technology using high-temperature geothermal fluids at Valles Caldera, New Mexico. DOE is also the major sponsor there, with cofunding and participation by Public Service Co. of New Mexico and Union Oil Co. of California.

At Heber, brine will be pumped from about 12 production wells at the center of the reservoir (the hottest part) and delivered to the heat exchangers at about 182°C (360°F). It will be returned to the reservoir periphery down six injection wells at about 71°C (160°F). The planned extraction rate is some 880 kg/s (7 million lb/h), but the more important measure is its equivalent heat content, initially seen as 470 Btu/kg (214 Btu/lb). Brine production will draw down the natural well level at the center of the field, encouraging inflow from surrounding strata. Because about 80% of the reservoir heat is actually contained in the solid material, the reinjected brine will continuously sweep the reservoir of heat as it flows toward the drawn-down center, to be pumped again for another heat extraction cycle.

Sustaining reservoir production flow over a plant's life is central to the use of hydrothermal resources, but the possibility of declining temperature and heat content is very real. How can this be hedged? Short of extensive turbine modifications, the answer is to alter the properties of the working fluid. For Heber, the initial design is a mixture of isobutane (90%) and isopentane (10%), to be delivered to the turbine inlet under supercritical conditions of about 150°C (300°F) and 575 psi (4 MPa).

By changing the proportions of the two hydrocarbons, molecular weight of the fluid can be increased, enhancing its kinetics so that reduced heat input has the least adverse effect on turbine performance and power output. As defined by inlet vapor conditions, the peak of the turbine efficiency curve is thus moved to compensate for declining brine temperature.



## Handling heat and minerals

Heat exchange ahead of a binary-cycle turbine and heat rejection beyond any thermal expansion turbine (to condense the vapor for recirculation) are two more geothermal research areas. Both have inherent problems of minerals control. Even though most hydrothermal resources are no more saline than seawater (34,000 ppm), they often carry significant amounts of calcium carbonate, silica, and metal sulfides and sulfates. These and other minerals precipitate at the reduced temperature in a binary-cycle heat exchanger or elsewhere in a direct-flash system. The scale problem is pervasive, reducing both fluid flow and heat transfer and requiring periodic removal.

EPRI concludes that corrosion is also a problem but probably not a serious one for moderate-temperature systems. Roberts observes that hydrothermal fluids tend to be slightly acid and contain little or no free oxygen. "Therefore, if we keep oxygen out of the water cycle during startup and shutdown and during cleaning, corrosion should be minimal."

Mineral-scale control has called for extensive research in anticipation of the development of many hydrothermal systems having different fluid mineral compositions. Notable in this regard are EPRI-sponsored computer programs that can simulate various water chemical compositions and the point-by-point scaling rates they produce throughout a given power plant under different temperature, pressure, and flow conditions.

Four related programs enable design parameters to be optimized for given geothermal fluid conditions, including those in the reinjection wells. The latter point is important. Although the binary-cycle water loop is closed (and many environmental problems thereby avoided), fluids may well cause additional scaling in the reinjection wells and silting when they are returned to the reservoir at reduced temperature.

Heat-exchange equipment must be considered in light of these problems. At the very least, its design must acknowledge the need for expeditious and economic cleaning at intervals of from months to years. There may be an alternative to the surface heat exchanger and its scaling problems. In direct-contact exchange, the fluids are mixed in a single vessel, the working fluid vaporizes and thus is separated for use, while the cooled water is pumped away for reinjection in the reservoir. This avenue is only experimental so far, but is being followed by DOE on the premise that it could be more economic.

The evident saving is avoidance of mechanical complexity. The technical problems, and possible further costs, derive from the possibility of incomplete fluid separation. Hydrocarbon fluid might need to be retrieved from the spent water, or makeup quantities might have to be constantly added. Similarly, the presence of residual water or water vapor in the working fluid might alter the efficiency and economy of its function in the turbine expansion cycle.

## Environmental effects

When geothermal water or steam is used in direct-flash cycles, noncondensable gases are a direct influence on thermal efficiency because of their effect on overall vapor kinetics, and some of them may be environmental problems as well. Ammonia, boron, and hydrogen sulfide are examples. Hydrogen sulfide is present in some 20–25% of all hydrothermal resource systems, emitting a disagreeable odor at a concentration of only 30 ppb and considered toxic at 10 ppm. The 200-ppm concentration in steam at The Geysers is not necessarily typical, but it emphasizes that this effluent must be controlled.

Any method of gas removal represents a parasitic energy load on the geothermal power plant; the objective is to minimize that load while eliminating pollutants. Scrubbing geothermal steam

is one approach being tested by PG&E and DOE. This entails introducing copper sulfate to react with the hydrogen sulfide and permit its removal in an altered form.

Condensation and reevaporation of the steam is another approach, being investigated by EPRI. The noncondensable hydrogen sulfide is mechanically separated after the first step. Then, recirculated through a shell-and-tube heat exchanger, the water is again evaporated by heat that is extracted from the incoming steam that follows it through the unit.

Tests of the second technology at The Geysers have successfully removed 90–97% of the hydrogen sulfide, which can later be disposed of by chemical treatment. Furthermore, the vent gas retains enough energy to drive vacuum pumps on the power plant steam condensers, thereby reducing the parasitic load otherwise imposed on the turbine steam supply.

Heat rejection is the final practical problem of any thermal power cycle, especially for geothermal technologies because of their already low thermal efficiency and consequent need for extensive cooling capacity.

PG&E's plants at The Geysers get all their cooling water from the steam itself: turbine condensate passes through evaporative cooling towers and is recirculated for condenser cooling. Direct-flash power plants derive their cooling water in the same way. Binary-cycle power plants could use extra reservoir fluid in a cooling cycle, but purifying it for this purpose would add considerable cost.

"We're fortunate at Heber," Vassel Roberts acknowledges, "because we'll have fresh water from the irrigation district for five years. After that we plan to use agricultural drain water." Beyond these examples, he adds, geothermal power applications and their economics will depend on the results of concurrent R&D in water-conserving combinations of wet and dry cooling.

## CLASSIFYING GEOTHERMAL RESOURCES

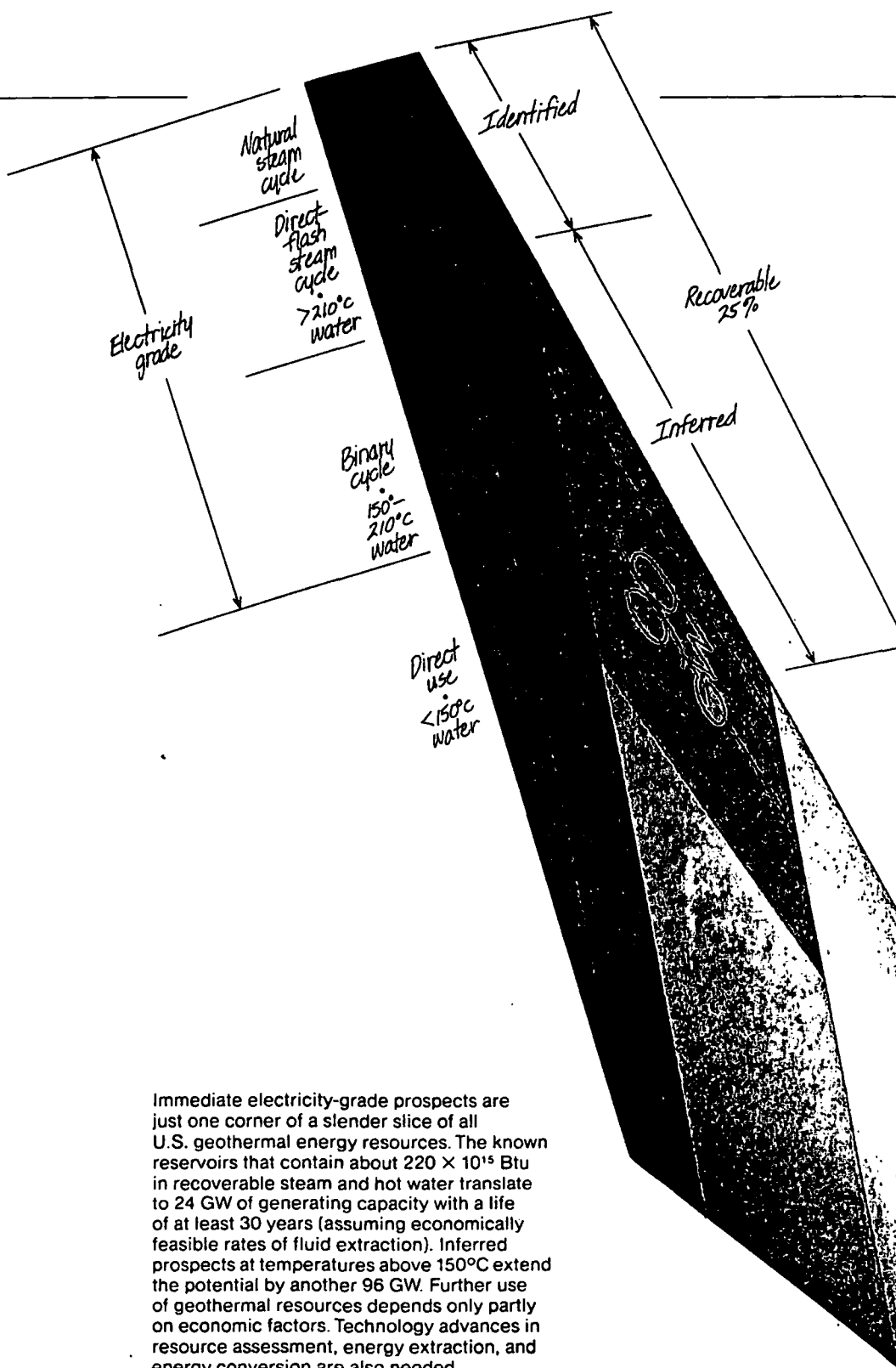
The earth's high internal temperature means that heat underlies every square foot of its surface. But no discernible path yet exists for developing most of it.

Where the earth's crust is structurally consistent, its temperature increases about 25°C (77°F) with each kilometer of depth, the result of heat conduction from the earth's mantle. Attractive quantities of this normal-gradient heat are at least 3 km (2 mi) down, but more like 5-7 km (3-4 mi) if the criterion is a temperature suitable for generating electricity (at least 150°C; 300°F).

Excluding normal-gradient heat, the accessible U.S. geothermal energy in place falls into three very broad categories, petrothermal, geopressed, and hydrothermal, which total about 1.2 million quadrillion ( $1.2 \times 10^{21}$ ) Btu. This estimate covers resources at temperatures greater than 15°C (59°F) as both identified and inferred by the U.S. Geological Survey to a depth of 10 km (6.2 mi).

Petrothermal energy accounts for some 85% of the total. This is in molten igneous material (magma) that has been intruded relatively close to the earth's surface by volcanic activity and faulting and in crystalline rock that has cooled from magma. Even though the resulting temperature gradients are steeper (depths therefore less than those for equivalent normal-gradient heat) and U.S. petrothermal regions are well charted, this energy form cannot now be counted as recoverable for electric power production.

Methods and materials for drilling into magma do not exist. In hot rock alone, the best foreseen method of energy extraction calls for injecting water that would be heated and then pumped back up; but the energy and monetary costs involved may not be



Immediate electricity-grade prospects are just one corner of a slender slice of all U.S. geothermal energy resources. The known reservoirs that contain about  $220 \times 10^{15}$  Btu in recoverable steam and hot water translate to 24 GW of generating capacity with a life of at least 30 years (assuming economically feasible rates of fluid extraction). Inferred prospects at temperatures above 150°C extend the potential by another 96 GW. Further use of geothermal resources depends only partly on economic factors. Technology advances in resource assessment, energy extraction, and energy conversion are also needed.

economic. Furthermore, the complexity of underground strata, especially their varying porosity and permeability, poses practical problems in retrieving the injected water. And water itself is becoming a scarce resource for energy processes.

Continued research may overcome these problems. The technology focus now is on mechanisms of reservoir development: how to drill into dry hot rock, how to induce its fracturing, and how to circulate water in and out of a system of wells for efficient and reliable heat extraction. DOE is funding a \$14 million program in petrothermal energy, with Los Alamos Scientific Laboratory doing much of the research.

Geopressured resources make up the next largest class, perhaps 165,000 quadrillion ( $165 \times 10^{18}$ ) Btu, or 14% of the accessible geothermal energy in place. Geopressured zones lie beneath the Gulf Coast, formed by southerly drainage and deposition from the rivers of past geologic times. Impermeable shale caps were deposited above sediments that contained water and organic material, and the latter decomposed to form natural gas. As a result of subsequent settlement and compression, the sediments now exhibit pressures well above the natural hydrostatic values for their depth—as much as 10,000–15,000 psi (70–100 MPa) at 2–6 km (1–4 mi). Those pressures will be the key mechanism for bringing up the hot water (100–180°C; 220–356°F) and the natural gas now dissolved in it.

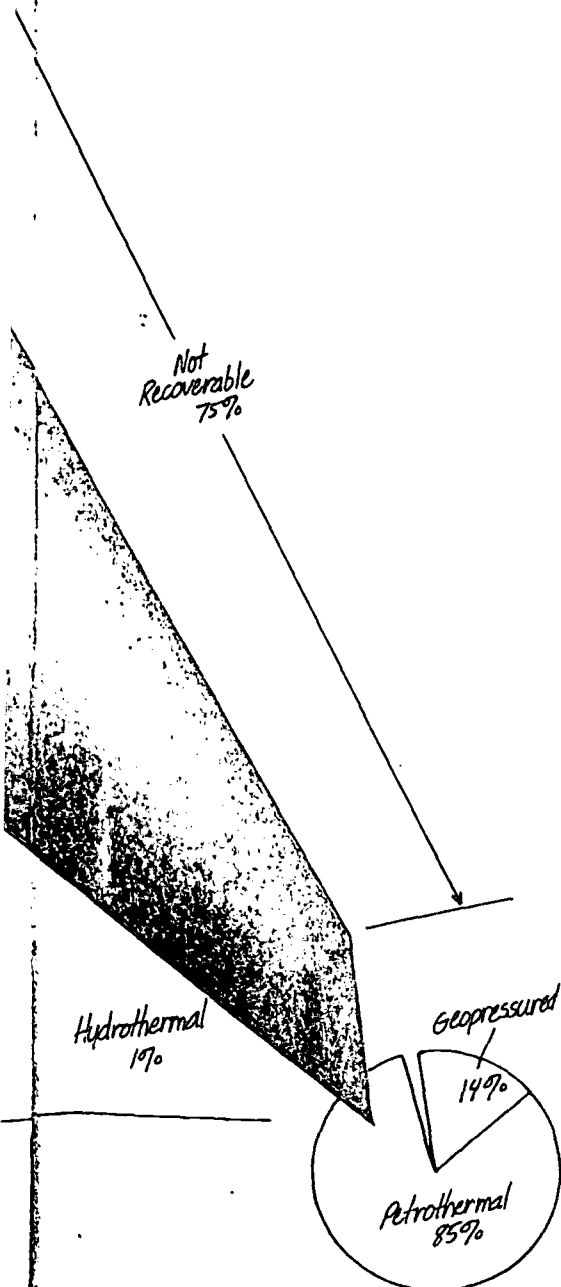
As with any underground resource, the recoverable energy is only a fraction of the accessible total in place. In the case of geopressured resources, the concern today is whether they are sufficiently concentrated to be economically attractive.

Hydrothermal systems of steam and water are the smallest geothermal resource class, about 9600 quadrillion ( $9.6 \times 10^{18}$ ) Btu, or barely 1% of the total; and most of it is in the West. The anticipated recoverable portion, however, is about 2400 quadrillion ( $2.4 \times 10^{18}$ ) Btu, a far higher proportion than for geopressured energy.

Dry steam occurs where geologically recent volcanic activity is combined with paths for water to percolate deeply and flow into contact with very hot rock. The spectacular eruption of Washington's Mount St. Helens has so far been driven largely by steam, but this is a special circumstance. The percolation of the past 123 years has produced tremendous steam volume and pressure directly beneath an acutely weakened and vulnerable rock mass, the volcano's plug. This is one of nature's relief valves at work.

Natural steam systems, although obvious, are the rarest geothermal resource, perhaps only 40 quadrillion ( $40 \times 10^{15}$ ) Btu, and a quarter of that is represented by the 2000 MW of capacity already in place or planned at The Geysers in northern California. Closely akin to dry steam systems are hot water systems. Deep geologic heat warms water-bearing strata, creating vast, slow-moving thermal convection patterns that rise, blossom, and spread into overlying sediments.

Such hydrothermal reservoirs make up most of the recoverable hydrothermal resource base, and about 900 quadrillion ( $900 \times 10^{15}$ ) Btu of their energy content may be above the 150°C (300°F) threshold useful for electricity production with today's technology. Such hydrothermal systems require thorough definition and economic justification; they are the major focus of today's electric power R&D by EPRI, DOE, and others.



### Future technologies and resources

Even direct-flash and binary cycles are not the full spectrum of generation possibilities, according to Roberts. "There is the total-flow concept—how to use both flashed steam and the residual water to improve energy efficiency. We've field-tested a 20-kW rotary separator-turbine at Roosevelt Hot Springs in Utah. It could get an extra 15–20% efficiency from a direct-flash generation unit."

The rotary separator is a disc with a flanged rim. When flashed steam is directed against the disc, the water droplets are caught by the inner surface of the rim; that is, the flange acts as a single large bucket and delivers the droplets into the cups of a hydraulic turbine. Steam in the separator chamber is piped into a conventional steam turbine, and the hydraulic turbine output is essentially a bonus.

This approach to total flow is distinctive because it employs the liquid and vapor phases of the geothermal fluid separately. It perhaps represents EPRI's

longest reach toward advanced technology for flashed-steam power cycles. Lawrence Livermore Laboratory and Jet Propulsion Laboratory (California Institute of Technology) have studied and tested other approaches, notably a turbine designed for two-phase fluids (liquid and vapor in a single stream) and a positive-displacement mechanism. In one such configuration, fluid is admitted to the cavity between two meshing helical screws. Fluid flow and expansion against the surfaces of the screws causes their shafts to rotate.

Roberts also acknowledges the possible combination of combustion and steam or binary cycles in geothermal energy technology, perhaps to exploit the methane and thermal content of some geopressured resources.

In general, geopressured resources are not yet a large prospect for electric power generation. On the basis of work by Southwest Research Institute, EPRI acknowledges perhaps 1100 MW of capacity that might be developed and

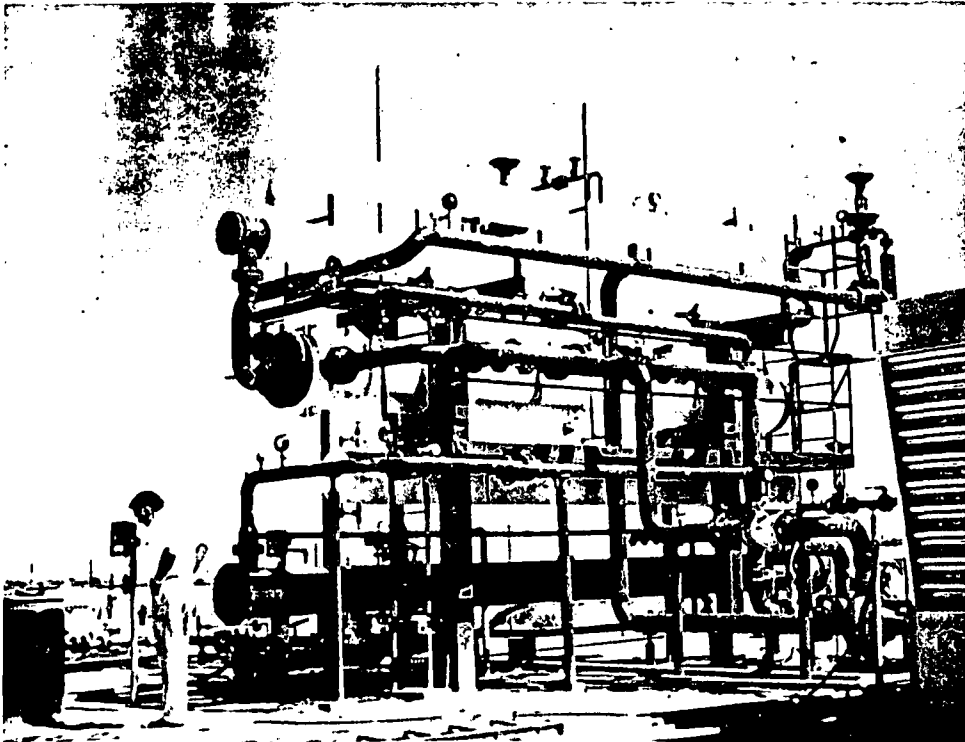
installed by the year 2000. This estimate comes from a study of 20 specific prospects in Texas and Louisiana. All together, Southwest Research concludes that the potential exists for extracting  $7 \times 10^{12}$  ft<sup>3</sup> ( $200 \times 10^6$  km<sup>3</sup>) of methane containing 7 quadrillion ( $7 \times 10^{15}$ ) Btu, plus hot water containing 13 quadrillion ( $13 \times 10^{15}$ ) Btu, for a total that is equivalent to about 5300 MW over 30 years. Economic feasibility would depend, for one thing, on a methane price of at least \$5/1000 ft<sup>3</sup> (\$17.75/m<sup>3</sup>).

The biggest shadows hanging over this resource, however, are the methane content of the geopressured fluid, the cost of production, and reservoir life. For example, early indications are that methane content runs about 20–25 ft<sup>3</sup>/bbl of fluid and that reservoirs are small because of their geologic structure. Data for full evaluation of the resource potential are being developed in a \$39 million DOE program.

### Free energy at least cost

When all is said and done, geothermal heat itself is indeed free in the sense that any natural resource in place is free. More important, it is renewable and essentially inexhaustible if not withdrawn at excessive rates. But the fluids that contain and convey that heat are quite evidently a spectrum of resource forms and temperatures, site-specific in their energy and mineral content, their ease of access, and their reliability of production. Familiar thermal power cycles are being carefully adapted to deal with these characteristics. The cost of adaptations and the cost of the fluids must meet the competitive market set by other fuels and technologies.

The bottom line is still a combination of reliability and busbar electricity cost. As fossil fuels escalate in price, the trend favors geothermal energy in general; and it especially favors the 24 GW of capacity that can be developed from known hydrothermal resources with the direct-flash and binary-cycle technologies soon to be demonstrated.



After throttling, the fluid is condensed and cooled in successive stages to 49°C (120°F) for recycling. Portions of the cooling tower appear at the right. The condenser is insulated for safety and for precise measurements of its performance.

Subj  
(200) GTHM  
TLGS  
8290  
82-926

UNITED STATES DEPARTMENT OF INTERIOR  
(GEOLOGICAL SURVEY (U.S.))

THE LASSEN GEOTHERMAL SYSTEM

by

L. J. Patrick Muffler, Nancy L. Nehring, Alfred H. Truesdell,  
Cathy J. Janik, Michael A. Clynne, and J. Michael Thompson  
U. S. Geological Survey

Open-File Report  
82-926  
1982



This report will be published in the proceedings of the  
Pacific Geothermal Conference,  
Auckland, New Zealand, November 1982.

UNIVERSITY OF UTAH  
RESEARCH INSTITUTE  
EARTH SCIENCE LAB.

## THE LASSEN GEOTHERMAL SYSTEM

L. J. Patrick Muffler, Nancy L. Nehring, Alfred H. Truesdell,  
Cathy J. Janik, Michael A. Clyne, and J. Michael Thompson

U.S. Geological Survey, Menlo Park, California, U.S.A

**Abstract** The Lassen geothermal system consists of a central vapor-dominated reservoir underlain by hot water that discharges peripherally at lower elevations. The major thermal upflow at Bumpass Hell (elevation 2,500 m) displays numerous superheated fumaroles, one of which in 1976 was 159°C. Gas geothermometers from the fumarole areas and water geothermometers from boiling Cl-bearing waters at Morgan Hot Springs (elevation 1,530 m; 8 km south of Bumpass Hell) and from 176°C waters in a well 12 km southeast of Bumpass Hell both indicate 230-240°C for the deep thermal water. With increasing distance from Bumpass Hell, gases are progressively depleted in H<sub>2</sub>S relative to CO<sub>2</sub> and N<sub>2</sub>, owing to oxidation of H<sub>2</sub>S to pyrite, sulfur, and sulfates and to dilution with atmospheric N<sub>2</sub>. H<sub>2</sub>O/gas ratios and degree of superheat of fumaroles can be explained by mixing of steam of maximum enthalpy (2,804 J g<sup>-1</sup>) with near-surface water and with the condensate layer overlying the vapor-dominated reservoir.

**Introduction** The Lassen geothermal system is located in the southernmost part of the Cascade Range, a linear belt of Quaternary volcanoes that extends from southern British Columbia to northern California (Muffler, Bacon, and Duffield, 1982, figure 1). The Lassen geothermal system has by far the most conspicuous surface hydrothermal manifestations of any geothermal system in the Cascades. However, most of the system is located in Lassen Volcanic National Park (LVNP) and is therefore not available for commercial development except perhaps in peripheral, hot-water zones outside LVNP.

**Geologic setting** The Cascade Range in the Lassen region is a broad ridge of late Pliocene and Quaternary volcanic rocks consisting primarily of pyroxene andesite flows and pyroclastic rocks with subordinate basalt flows, silicic flows, and silicic pyroclastic rocks. The regional basement probably consists of Mesozoic granitic and metamorphic rocks overlain by a thin sequence of late Cretaceous marine sedimentary rocks which are in turn overlain by the Pliocene Tuscan Formation (Anderson, 1933; Lydon, 1968), a broad apron of andesitic debris flows with minor interbedded lava flows, ash-flow tuffs, and alluvial material deposited 3.5-2 m.y. ago (Lydon, 1961; Gilbert, 1969).

Late Pliocene and Holocene volcanic rocks overlying the Tuscan Formation were extruded primarily from long-lived major volcanic centers, at least three of which have been recognized in the Lassen region (figure 1):

- Dittmar volcanic center, active from perhaps 1.2 to 2.5 m.y.;
- Maidu volcanic center, active between 1.8 and 1.0 m.y. (Wilson, 1961);
- Lassen volcanic center, active from 0.6 m.y. to the present.

Each volcanic center evolved in three stages: (1) an initial cone-building period of andesite lava flows and pyroclastic rocks, (2) a later cone-building period of thick siliceous andesite lava flows, and (3) eruption of dacite to rhyolite domes and flows flanking the main composite cone. Silicic magma chambers related to the late domes and flows provided potent heat sources for hydrothermal convection systems within the cores of each of the main cones. However, the silicic magma chambers of the Dittmar and Maidu volcanic centers have cooled, and their hydrothermal systems are extinct. The present hydrothermal system at Lassen is associated with the active silicic volcanism of the Lassen volcanic center.

Flows and pyroclastic rocks of Stages 1 and 2 of the Lassen volcanic center were extruded primarily from a composite cone centered near Sulphur Works (Williams, 1932) during the period 0.6 to 0.35 m.y. (G. B. Dalrymple, personal commun., 1977-82). After a hiatus of approximately 0.1 m.y., at least 15 vents in a broad zone on the northeastern flank of this composite cone extruded flows and domes of dacite and rhyodacite, forming a dome field of approximately 130 km<sup>2</sup>. The most recent events were the emplacement of the dacite dome of Lassen Peak approximately 11,000 years ago (Crandell, 1972), the eruption of rhyodacite pyroclastic flows and domes at Chaos Crags approximately 1,050 years ago (Crandell and others, 1974; D. A. Trimble, USGS, personal commun., 1982), and the relatively small eruption at the summit of Lassen Peak in 1914-1917 (Day and Allen, 1925; Loomis, 1926). Concurrent with this silicic volcanism, basalt and mafic andesite shield volcanoes grew to the north and east of the Lassen volcanic center, and mixing of silicic and basaltic magmas

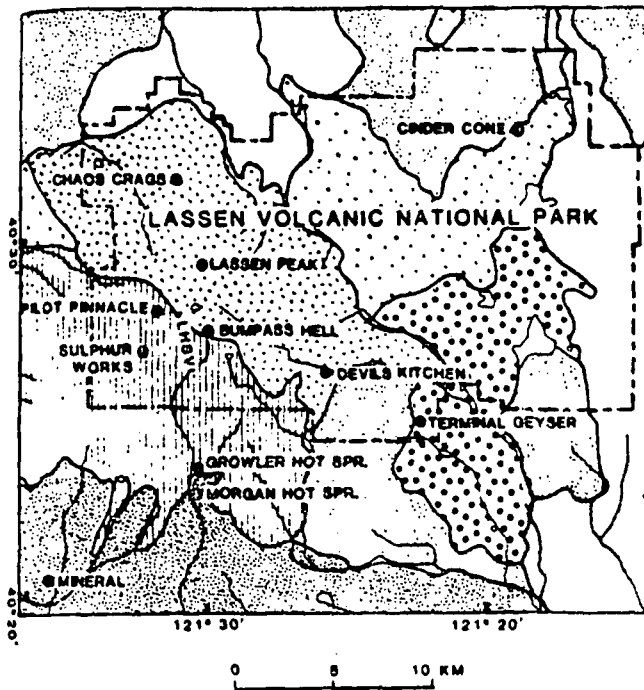


Figure 1.--Generalized geologic map of the Lassen region (adapted from Muffler, Clynne, and Cook, 1982). LHSV = Little Hot Springs Valley

produced intermediate lava flows on the east flank of the Lassen dome field (Eichelberger, 1975). The most recent eruption in this area was at Cinder Cone in 1850-51 (Finch and Anderson, 1930).

The long history of pyroclastic and dome-building eruptions in the Lassen dome field, the historical production of magma at two separate vents, and the existence of a major gravity low suggest that a partially molten silicic magma body still underlies the dome field (Heiken and Eichelberger, 1980).

The Lassen Geothermal System Geological and geochemical observations in the Lassen region all

fit a model originally suggested by D. E. White (written commun., 1971) of a single large geothermal system with a central vapor-dominated reservoir (or reservoirs) underlain by a reservoir of hot water discharging at lower elevations (figure 2). The focus and major thermal upflow of the Lassen geothermal system is at Bumpass Hell along the contact between the andesitic composite cone and the dacite dome field of the Lassen volcanic center. Some of the outflow of hot water reaches the surface at Morgan and Growler Hot Springs to the south of LVNP and has been produced from the geothermal well Walker "O" No. 1 at Terminal Geyser in the southeast corner of LVNP.

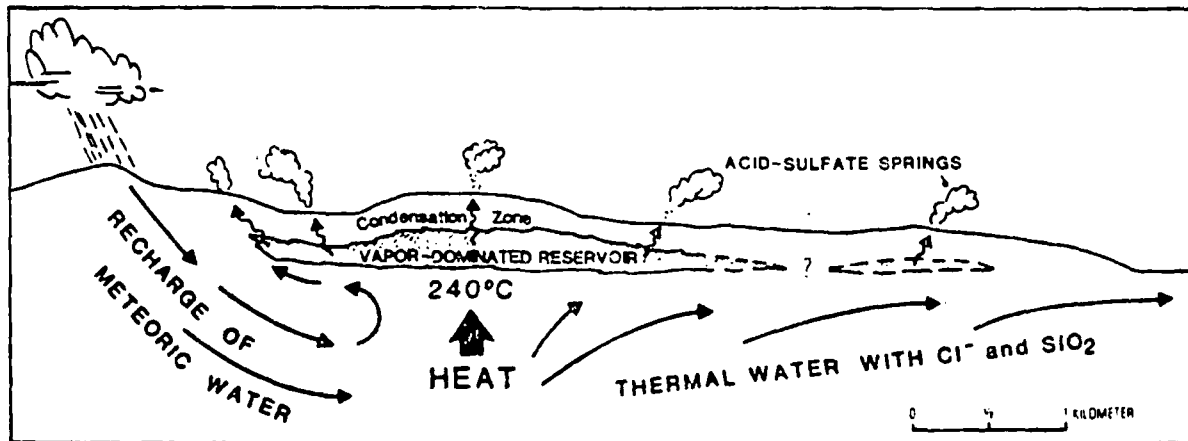


Figure 2.--Schematic cross-section of the Lassen geothermal system (adapted from Muffler, Clynne, and Cook, 1982)

Bumpass Hell (elevation 2,500 m) contains numerous superheated fumaroles, one of which in 1976 had a temperature of 159°C. Approximately 75 major fumaroles, acid-sulfate hot springs, and mudpots occur in Bumpass Hell (Muffler, Jordan, and Cook, 1982), plus a myriad of similar features too small to map. An area of approximately 0.13 km<sup>2</sup> is intensely altered to a white aggregate of opal and kaolinite + alunite; the surface of the active part of Bumpass Hell is commonly covered with orange and yellow sulfates. Pyrite is common in many of the hot springs as linings of the vents and discharge channels, as scum floating on the surface of pools, and as dispersions in brown or black mudpots. Significant sinter does not occur, although a few springs show a weak deposit of silica around their rims and in the first few centimeters of their discharge channels. Silica is also found as bright-red mixtures with iron oxides in some drainages in the forest below acid-altered bare ground. Neither of these occurrences is indicative of a hot-water geothermal system. The acid-sulfate water from Bumpass Hell (table 1) is typical of hot springs related to a vapor-dominated reservoir in having low pH, high sulfate, and no significant Cl.

Table 1.--Chemical analyses of waters from thermal springs in and near LVNP. Constituents in mg L<sup>-1</sup>; flow in L min<sup>-1</sup>; n.d. = not determined. BH, Bumpass Hell; DK, Devil's Kitchen; SW, Sulfur Works; LHSV, Little Hot Springs Valley; TG, Terminal Geyser; GHS, Growler Hot Spring; MHS, Morgan Hot Springs.

	BH	DK	SW	LHSV	TG	GHS	MHS
Date	8/79	9/76	7/75	8/79	8/76	8/79	8/79
Flow	20	8	seep	4	4	20	8
T(°C)	55	68	86	93	92	95	95
pH	2.2	2.5	1.9	5.55	4.5	7.45	7.25
SiO <sub>2</sub>	215	171	213	123	46	272	225
Al	16.2	nd	nd	.4	nd	.4	.2
Fe	10	6.1	nd	.33	nd	.04	.01
Mn	0.12	0.08	nd	.15	nd	.01	.03
As	nd	nd	nd	nd	nd	11	10.6
Ca	19.5	10.5	8.8	26	5.2	81	94
Mg	6.05	6.4	9.8	4.1	1.9	.07	.47
Sr	nd	nd	nd	nd	nd	.9	1.1
Ba	nd	nd	nd	nd	nd	2.5	3.0
Na	22.1	2.0	11	87	8	1340	1260
K	6.6	7.2	8.3	12	3	173	162
Li	0.5	0.015	0.01	.05	.01	6.3	6.1
Rb	nd	nd	nd	nd	nd	1.4	1.2
Cs	nd	nd	nd	nd	nd	.6	.4
NH <sub>4</sub>	nd	nd	30	3.5	nd	9.5	13
HCO <sub>3</sub>	0	0	0	19	33	55	68
SO <sub>4</sub>	364	226	938	301	48	110	123
Cl	5.7	0.5	0.5	5.2	3	2370	2210
F	0.33	0.17	0.35	.84	0.1	2.3	3.0
Br	nd	nd	nd	nd	nd	10	14.5
I	1.1	0.3	4.4	4.2	1.6	84	nd
H <sub>2</sub> S	nd	nd	0.2	.03	nd	.02	.03
Calculated Geothermometer Temperatures							
Quartz Alunite <sup>a</sup>				158		187	176
Quartz Conductive <sup>a</sup>				166		202	188
Na-K-Ca <sup>b</sup>				95		223	219

<sup>a</sup> Equation from Truesdell, 1976

<sup>b</sup> Equation from Fournier and Truesdell, 1973

Fumaroles, acid-sulfate springs, and mudpots also are abundant in Little Hot Springs Valley just to the west and 230-400 m lower than Bumpass Hell. Several fumaroles in Little Hot Springs Valley are superheated, with a highest temperature of 125°C measured in 1976.

Devil's Kitchen (1,835 m) is an area of intense fumaroles, acid-sulfate springs, and mudpots (Muffler, Jordan, and Cook, 1982). Although a temperature of 106.6°C was measured in 1947 by D. E. White (written commun., 1982), at present the hottest fumaroles are superheated only by a degree or two. Several centimeters of sinter at two spots along the stream flowing through Devil's Kitchen indicate discharge of hot thermal water in the recent past.

Several other geothermal areas in LVNP also are characterized by fumaroles, mudpots, and acid-sulfate hot springs (see chemical analyses in table 1). Conspicuous among these are Sulphur Works (elevation 2,124-70 m), Pilot Pinnacle (2,516 m), Boiling Springs Lake (1,798 m), and Terminal Geyser (1,792 m). Steam discharging currently from these areas is either saturated or only slightly superheated.

Several springs near Sulphur Works and in Little Hot Springs Valley are relatively rich in HCO<sub>3</sub> and deposit travertine (CaCO<sub>3</sub>). These springs are interpreted to be surface discharge from the zone of steam condensate that overlies the vapor-dominated reservoir.

Natural discharge from the hot-water part of the Lassen geothermal system occurs only at Morgan Hot Springs and Growler Hot Spring, both located in the canyon of Mill Creek at elevations of 1,530 and 1,570 m, respectively. These springs discharge moderate amounts of near-neutral water with significant Cl (table 1) and deposit conspicuous sinter. Na-K-Ca, sulfate-water isotope, and mixing model geothermometers indicate that the deep thermal water feeding these springs has a temperature of 220-240°C. Both Cl and SiO<sub>2</sub> concentrations decrease systematically south-southwest from Growler Hot Spring through Morgan Hot Springs (Thompson, 1982).

High-Cl hot water from the Lassen geothermal system has also been found in the Walker "O" No. 1 well (Beall, 1981) at Terminal Geyser. Samples taken during flow of the well on 10-11 October 1978 show Na, K, and Cl increasing with time to maximum values of 1,300, 180, and 2,200 mg L<sup>-1</sup>, respectively; flow tests were terminated before the chemical constituents reached constant values. Measured pH ranged from 8.1 to 8.6. Temperatures taken in the plugged liner 10 months after the well was flowed reach a maximum of 176°C between 603 and 640 m and then decrease gradually to 124°C at the well bottom (1,222 m).

The Cl-bearing water found in Walker "O" No. 1 does not discharge in Terminal Geyser. This vent is not a true geyser but is a fumarole



discharging into a small surface stream. Water discharged by Terminal Geyser (table 1) appears to be local precipitation heated by steam.

Thermodynamic evidence for steam sources High-temperature superheated geothermal fumaroles are uncommon, but during the California drought of 1976-77 high degrees of superheat were observed in three areas of LVNP. In late 1976 Big Boiler fumarole in Bumpass Hell reached 159°C, to our knowledge the highest temperature ever recorded from a geothermal (non-volcanic) fumarole. This temperature is close to the temperature (163°C) of steam decompressed adiabatically to Lassen surface pressure (0.75 bar abs) from saturated steam of maximum enthalpy (2,804 J g<sup>-1</sup> at 235°C and 31 bar abs; figure 3). Steam of higher temperature and enthalpy (up to 260°C and 2,980 J g<sup>-1</sup> at 5 bars abs; Truesdell and White, 1973) has been produced from wells at Larderello, Italy, by the isothermal decompression of saturated steam in the reservoir (flow in the wells is adiabatic). This isothermal decompression, however, is a result of drastically reduced pressures caused by rapid withdrawal of steam through wells. Isothermal decompression is unlikely to occur in a natural system because cooler rocks between the reservoir and the surface can be heated only to the temperature of the steam. Thus the limiting

process in nature is adiabatic (isoenthalpic) decompression.

The range of superheat in the Lassen steam samples could have resulted from two processes: (1) adiabatic decompression of saturated steam with different temperatures, or (2) mixing of highly superheated steam with liquid water or with saturated steam of lower temperature. After mixing, the resulting steam would undergo further decompression to reach surface conditions. This second process is the simpler explanation and is in accord with the observed H<sub>2</sub>O/gas ratios.

On a plot of H<sub>2</sub>O/gas ratio vs. enthalpy (figure 4), the Lassen data fall on two trend lines that intersect at the point of maximum steam enthalpy (2,804 J g<sup>-1</sup>). Line A consists of Big Boiler (Bumpass Hell) samples and trends toward a relatively high H<sub>2</sub>O/gas end member; line B (from Bumpass Hell and other areas) trends toward a relatively low H<sub>2</sub>O/gas end member. These two trends are also distinguished on a plot of percent H<sub>2</sub> vs. H<sub>2</sub>O/gas ratio (figure 5). In this plot, one trend has a slope of 1, suggesting that H<sub>2</sub> was in equilibrium with H<sub>2</sub>O (at constant temperature and P<sub>CO<sub>2</sub></sub>), and the other has a slope of infinity, suggesting lack of equilibrium due to short reaction times or low

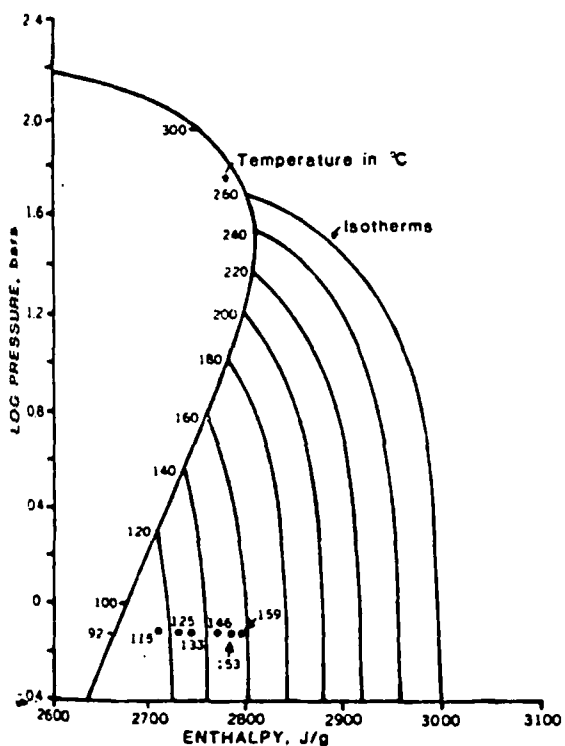


Figure 3.--Diagram showing the relations between saturated steam, the isothermal decompression paths of superheated steam, and the surface enthalpy, temperature, and pressure of superheated fumarolic steam from LVNP. Numbers give temperatures in °C.

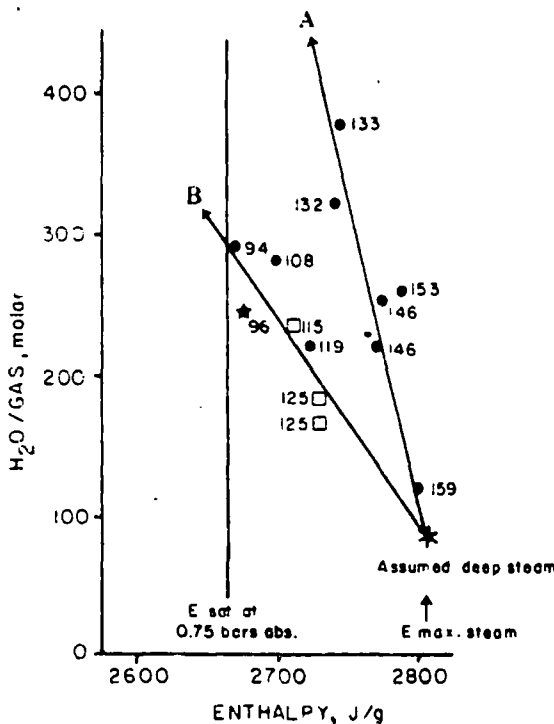


Figure 4.--Diagram showing the relations between H<sub>2</sub>O/gas and enthalpy of steam samples from LVNP. Numbers give temperatures in °C. See figure 6 for explanation of symbols. Line A trends towards 235°C liquid water with 0.7 bar P<sub>CO<sub>2</sub></sub> and 7,900 H<sub>2</sub>O/gas. Line B trends towards 90°C liquid water with 1.1 bar P<sub>CO<sub>2</sub></sub> and 3,900 H<sub>2</sub>O/gas.

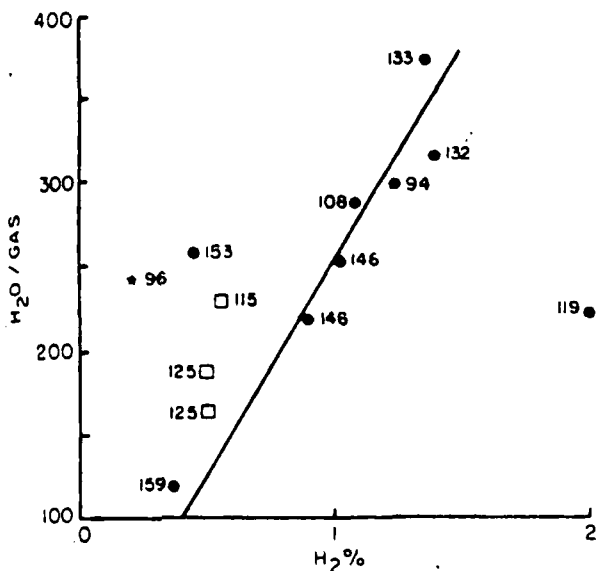


Figure 5.--Diagram showing relations between  $H_2O/gas$  and  $H_2$  content of gas samples from fumarole areas in LVNP. Numbers give temperature in  $^{\circ}C$ . See figure 6 for explanation of symbols. Hydrogen in geothermal systems appears to be generated by the dissociation of water ( $H_2O = H_2 + 1/2 O_2$ ) with the pressure (fugacity) of oxygen controlled by mineral reactions.

temperature. Although the correspondence is not complete, 5 of the 7 points on the line with a slope of 1 lie on line A of figure 4, and 4 of the 5 points with a slope of infinity lie on line B.

This behavior of  $H_2$  strongly suggests that steam samples falling along line B resulted from mixture of superheated steam and liquid water near the surface, where residence times were too short for  $H_2-H_2O$  equilibration. A possible low-temperature end-member would be  $90^{\circ}C$  water in equilibrium with  $CO_2$  at 1.1 atm pressure and with a  $H_2O/gas$  ratio of 3,600. This heated, gas-charged water might reasonably saturate the near-surface zones of the fumarolic areas and be entrained into superheated steam as it flowed upward. The total pressure (water vapor +  $CO_2$ ) of this liquid water would be 1.8 bars, which would allow the mixing to occur within 8 m of the surface by boiling-point-to-depth relations.

Steam samples along line A (figure 4) must mix at greater depths, where  $H_2$  and  $H_2O$  can equilibrate after mixing. If this mixing occurs in the upper part of the deep reservoir near  $235^{\circ}C$ , the  $H_2O/gas$  ratio of the liquid water mixing with steam would have been 7,900 and the  $PCO_2$  about 0.7 bar. The  $H_2O/gas$  ratio of reservoir steam with  $PCO_2 = 0.7$  bar would be 50, close to the ratio of the hypothetical deep steam ( $H_2O/gas = 85$ ).

Using these end members, we find that the steam samples along trend A are mixtures of superheated

steam ( $2,804 J g^{-1}$  and  $85 H_2O/gas$ ) with 0.5-4.0 percent liquid water at  $235^{\circ}C$ ,  $1,014 J g^{-1}$  and  $7,900 H_2O/gas$ . Those samples along trend B are mixtures of superheated steam with 2-6 percent liquid water at  $90^{\circ}C$ ,  $377 J g^{-1}$ , and  $3,600 H_2O/gas$ . These fractions of liquid are so small they might not be detected by isotopic methods, but owing to the high gas content of the deep steam are readily distinguished by  $H_2O/gas$  ratios.

Stable isotopes of hydrogen and oxygen Isotopic analyses of samples collected from 1977 to 1981 provide extensive data supporting interpretations made by Truesdell and Hulston (1980) on limited data. The isotopic compositions of D and  $^{18}O$  of meteoric waters in the Lassen region fall along a line defined by  $\delta D = 8 \delta^{18}O + 12$  (figure 6). This pattern largely reflects the prevailing south-southeast to north-northwest regional storm direction and is only locally affected by depletion of D and  $^{18}O$  with increasing elevation. Cold waters southwest of the LVNP near Mineral are significantly heavier than spring waters north of the thermal features.

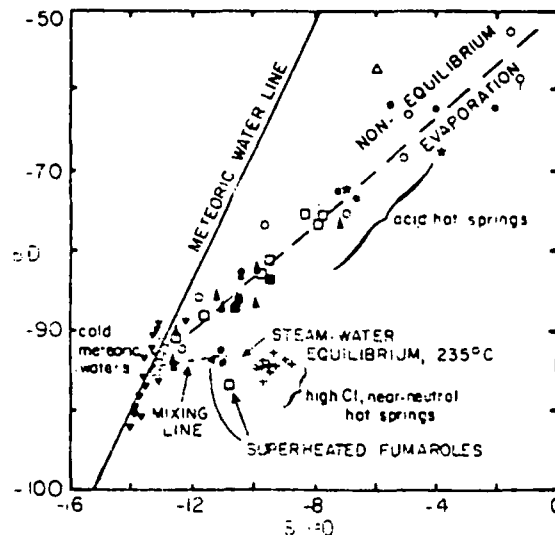


Figure 6.--Diagram showing relations between deuterium and  $^{18}O$  for water and steam samples from LVNP and vicinity. ●, Bumpass Hell; □, lower Little Hot Springs Valley; ☆, Pilot Pinnacle and upper Little Hot Springs Valley; ○, Sulphur Works; △, Cold Boiling Lake; ▲, Devil's Kitchen; ★, Boiling Springs Lake; ⊠, Terminal Geyser; +, Growler and Morgan Hot Springs; ▼, meteoric water.

The thermal waters issuing from Morgan and Growler Hot Springs have  $\delta D$  values similar to meteoric waters on the andesitic composite cone, suggesting that recharge to the Lassen geothermal system occurs on the composite cone. These thermal waters exhibit an oxygen isotope shift of up to  $+4\text{‰}$  due to water-rock isotopic exchange at high temperature.

If, as shown above, the most superheated steam from Bumpass Hell is derived directly from a 235°C vapor-dominated reservoir by adiabatic expansion, steam in the reservoir would have the same isotopic composition as the highest-temperature samples (average  $\delta D = -93.4$  and  $\delta^{18}O = -10.93$ ). The calculated composition of water in equilibrium with this steam at 235°C is  $\delta D = -95.0$  and  $\delta^{18}O = -9.09$  (data in Truesdell et al., 1977). These calculated values are very similar to those measured for Growler Hot Spring waters (average  $\delta D = -94.6$  and  $\delta^{18}O = -9.27$ ), indicating that the water of Growler Hot Spring is deep reservoir water mixed with only a minor amount of local meteoric water. A balance calculation based on the  $^{18}O$  data indicates that the thermal component is about 95%. Morgan Hot Springs have  $\delta^{18}O = -9.7$ , which corresponds to 84% thermal water.

Waters from the acid-sulfate hot springs and drowned fumaroles define a line of nonequilibrium surface evaporation of steam at temperatures of 70-90°C (figure 6; Craig, 1963; Truesdell and Hulston, 1980).

**Gas Geochemistry** Analyses of major gases from fumarole areas of LVNP are depicted on figure 7. The gas compositions can all be derived by two major near-surface processes that remove  $H_2S$  from a reservoir gas composition very near to the composition of gas from Big Boiler in Bumpass Hell. The first process is oxidation of  $H_2S$  either to pyrite ( $FeS_2$ ) or to elemental sulfur without involving oxygen from air (either directly or dissolved in water). The second

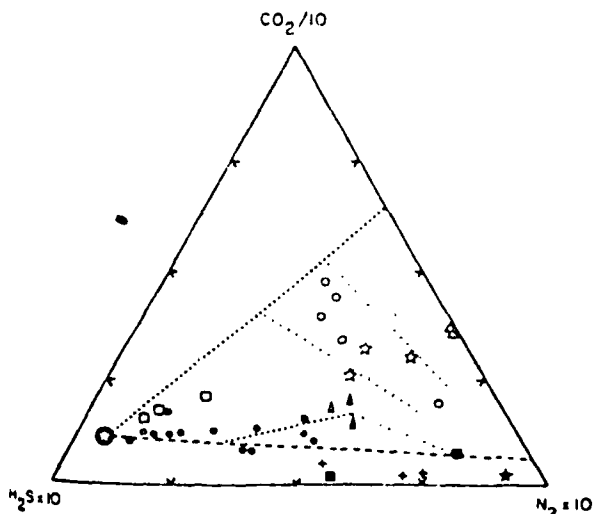


Figure 7.--Triangular plot of  $CO_2$ - $H_2S$ - $N_2$  in gas samples from LVNP and vicinity.  $\odot$ , reservoir gas composition;  $\dots\dots$ , oxidation of  $H_2S$  to pyrite or elemental sulfur;  $-\cdot-\cdot-$ , oxidation with air or air dissolved in water to produce sulfates;  $\dots\dots$ , near-surface addition of air without reaction with  $H_2S$ . See figure 6 for explanation of other symbols.

process involves oxidation with air or air dissolved in water to produce sulfates; this reaction is accompanied by admixture of  $N_2$ . The intersection of the lines representing these processes gives an estimate of the ratio of  $CO_2$ - $H_2S$ - $N_2$  in the reservoir. The three samples plotting nearest the reservoir composition are from the hottest fumaroles in Bumpass Hell and Little Hot Springs Valley; all are over 125°C. The reconstructed composition of the gas in the vapor-dominated reservoir (from figures 5 and 7) is (in mol percent)  $CO_2$ , 92.7;  $H_2S$ , 6.6;  $H_2$ , 0.01;  $NH_3$ , 0.075;  $N_2$ , 0.6; Ar, 0.013;  $O_2$ , 0.0; and  $CH_4$ , 0.05, with a  $H_2O$ /gas ratio of 85 (figure 4).

Gases from Boiling Springs Lake, Terminal Geyser, Growler Hot Spring, and Morgan Hot Springs appear to originate from the hot-water reservoir rather than the vapor-dominated reservoir. High  $H_2O$ /gas ratios (2,000-4,000) and high  $H_2S/CO_2$  ratios indicate that the water has previously been degassed by formation of a vapor phase at high temperature (235°C). When this degassed water approaches the surface and boils a second time, the steam that is formed is depleted in total gas and in  $CO_2$  relative to  $H_2S$  (the latter because  $H_2S$  is more soluble in water than is  $CO_2$ ).

Temperatures calculated using the gas geothermometer of D'Amore and Panichi (1980) are given in table 2. Within the uncertainties in the calculation ( $\pm 15^\circ C$ ), the temperature determined from the calculated reservoir gas composition is compatible with the 220-240°C calculated from Na-K, Na-K-Ca, and sulfate isotope relations for Growler Hot Spring waters. The temperatures from Little Hot Springs Valley and Bumpass Hell appear somewhat high, probably due to near-surface loss of  $CH_4$ . Temperatures from Sulphur Works and Pilot Pinnacle are somewhat low, apparently due to the great loss of  $H_2S$  (see figure 7).

Table 2.--Temperatures in °C calculated by the geothermometer of D'Amore and Panichi (1980) for gases from fumaroles and hot springs in LVNP and vicinity. Temperature for the reservoir is calculated from the reservoir gas composition given in the text.

Reservoir	Bumpass Hell	Little Hot Springs Valley	Sulphur Works
244	248	265	201
Pilot Pinnacle	Devil's Kitchen	Terminal Geyser	Growler Hot Spg
212	237	233	242

A physical model for the Lassen geothermal system New geologic, chemical, and isotopic data combined with thermodynamic and physical constraints on the production of superheated steam allow us to add considerable detail to the previously suggested model of the Lassen geothermal system as a central vapor-dominated reservoir underlain by hot water that discharges

peripherally at lower elevations. The critical observations are:

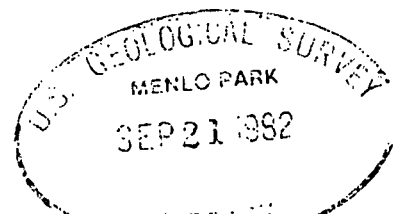
1. Oxygen isotopic data suggest that recharge to the Lassen geothermal system is local and probably on the composite cone of Lassen volcanic center.
2. These data further suggest that the Morgan-Growler water and the Bumpass Hell superheated steam separated at about 235°C and have undergone little alteration in isotopic composition during passage to the surface.
3. Considerations of the H<sub>2</sub>O/gas and H<sub>2</sub>O/H<sub>2</sub> ratios and the temperatures of the superheated steam suggest that the highest temperature samples (mostly from Big Boiler at Bumpass Hell) consist of adiabatically decompressed samples of saturated 235°C reservoir steam with small (= 0.5%) additions of condensate from the top of the reservoir.
4. Gas chemistry suggests that this highest-temperature steam is the least altered sample of deep steam; gas equilibration temperatures are near 235°C.
5. Hot water compositions at Morgan and Growler Hot Springs give geothermometer temperatures of 220-240°C and show progressive dilution away from LVNP.

These observations support a model in which cold meteoric water from the composite cone of the Lassen volcanic center in LVNP flows underground and is heated by a cooling intrusion related to the silicic volcanic activity of the past 0.25 m.y. Geothermal liquid at approximately 235°C at depth boils to form an overlying vapor-dominated reservoir, steam from which leaks upward to feed the fumaroles in LVNP. Part of the geothermal water flows laterally to the south to feed the Morgan and Growler Hot Springs and to the southeast where it is encountered in the Walker "O" No. 1 well at Terminal Geyser. Most of the steam that flows to the thermal areas of LVNP mixes with local ground water to form acid hot springs, but some steam in relatively large conduits undergoes adiabatic decompression with small addition of deep or surface waters to form superheated fumaroles. Assuming boiling point-depth relations in the condensate layer, the top of the 235°C vapor-dominated reservoir is probably near 2,100 m elevation. The bottom of the vapor-dominated reservoir is roughly constrained by the elevation of the springs at Growler Hot Spring (1,570 m). This gives a thickness of the two-phase vapor-dominated zone at Lassen of only 500-600 m, comparable to parts of Larderello, Italy, but much thinner than the two-phase reservoir at The Geysers, California.

#### References cited

Anderson, C. A., 1933, The Tuscan formation of northern California, with a discussion concerning the origin of volcanic breccias: University of California, Department of Geological Sciences Bulletin, v. 23, n. 7, p. 215-276.

- Beall, J. J., 1981, A hydrologic model based on deep test data from the Walker "O" No. 1 well, Terminal Geyser, California: Geothermal Resources Council Transactions, v. 5, p. 153-156.
- Craig, Harmon, 1963, The isotopic geochemistry of water and carbon in geothermal areas, in Tongiorgi, E. (ed.), Nuclear Geology on Geothermal Areas: Pisa, Italy, Consiglio Nazionale delle Ricerche, Laboratorio de Geologia Nucleare, p. 17-53.
- Crandell, D. R., 1972, Glaciation near Lassen Peak, northern California: U.S. Geological Survey Professional Paper 800-C, p. C179-C188.
- Crandell, D. R., Mullineaux, D. R., Sigafos, R. S., and Rubin, Meyer, 1974, Chaos Crags eruptions and rockfall-avalanches, Lassen Volcanic National Park, California: U. S. Geological Survey Journal of Research, v. 2, no. 1, p. 49-59.
- D'Amore, Franco, and Panichi, Costanzo, 1980, Evaluation of deep temperatures of hydrothermal systems by a new gas geothermometer: Geochimica et Cosmochimica Acta, v. 44, p. 549-556.
- Day, A. L., and Allen, E. T., 1925, The volcanic activity and hot springs of Lassen Peak: Carnegie Institution of Washington, 190 p.
- Eichelberger, J. C., 1975, Origin of andesite and dacite; evidence of mixing at Glass Mountain in California and at other circum-Pacific volcanoes: Geological Society of America Bulletin, v. 86, p. 1381-1391.
- Finch, R. H., and Anderson, C. A., 1930, The quartz basalt eruptions of Cinder Cone, Lassen Volcanic National Park, California: University of California, Department of Geological Sciences Bulletin, v. 19, p. 245-273.
- Fournier, R. O., and Truesdell, A. H., 1973, An empirical Na-K-Ca geothermometer for natural waters: Geochimica et Cosmochimica Acta, v. 37, p. 1255-1275.
- Gilbert, N. J., 1969, Chronology of post-Tuscan volcanism in the Manton area, California: M.S. thesis, University of California at Berkeley, Department of Geological Sciences, 79 p.
- Heiken, G., and Eichelberger, J. C., 1980, Eruptions at Chaos Crags, Lassen Volcanic National Park, California: Journal of Volcanology and Geothermal Research, v. 7, no. 3/4, p. 443-481.
- Loomis, B. F., 1926, Pictorial history of the Lassen volcano: Loomis Museum Association, Lassen Volcanic National Park, Mineral, California, 96 p.
- Lydon, P. A., 1961, Sources of the Tuscan Formation in northern California: Geological Society of America, Abstracts for 1961, p. 50.
- Lydon, P. A., 1968, Geology and lahars of the Tuscan Formation, northern California: Geological Society of America Memoir 116, p. 441-475.



- Muffler, L. J. P., Bacon, C. R., and Duffield, W. A., 1982, Geothermal systems of the Cascade Range: Pacific Geothermal Conference, Auckland, N. Z., Nov. 1982 (in press).
- Muffler, L. J. P., Clynne, M. A., and Cook, A. L., 1982, Mineral and geothermal resource potential of the Wild Cattle Mountain and Heart Lake Roadless Areas, Plumas, Shasta, and Tehama Counties, California: U.S. Geological Survey Open-File Report (in press).
- Muffler, L. J. P., Jordan, Raymond, and Cook, A. L., 1982, Thermal features and topography of Bumpass Hell and Devils Kitchen, Lassen Volcanic National Park, California: U.S. Geological Survey Miscellaneous Field Studies Map (in press).
- Thompson, J. M., 1982, Preliminary chemical studies from Lassen Volcanic National Park and vicinity: Geothermal Resources Council Transactions, v. 6 (in press).
- Truesdell, A. H., 1976, Summary of section III-geochemical techniques in exploration: Second United National Symposium on the Development and Use of Geothermal Resources, San Francisco, May 1975, U.S. Government Printing Office, p. liii-lxiii.
- Truesdell, A. H., and Hulston, J. R., 1980, Isotopic evidence on environments of geothermal systems, in Fritz, P., and Fontes, J.-C., eds., Handbook of Environmental Isotopes: Amsterdam, Elsevier, p. 179-225.
- Truesdell, A. H., Nathenson, Manuel, and Rye, R. O., 1977, The effects of subsurface boiling and dilution on the isotopic compositions of Yellowstone thermal waters: Journal of Geophysical Research, v. 82, p. 3694-3704.
- Truesdell, A. H., and White, D. E., 1973, Production of superheated steam from vapor-dominated geothermal reservoirs: Geothermics, v. 2, no. 3-4, p. 145-164.
- Williams, Howel, 1932, Geology of the Lassen Volcanic National Park, California: University of California, Department of Geological Sciences Bulletin, v. 21, no. 8, p. 195-385
- Wilson, T. A., 1961, The geology near Mineral, California: M.S. Thesis, University of California at Berkeley, Department of Geological Sciences, 92 p.

SUBJ  
GTHM  
TSH

# A Theoretical Study of Heat Extraction From Aquifers With Uniform Regional Flow

A. C. GRINGARTEN AND J. P. SAUTY

*Bureau de Recherches Géologiques et Minières, Service Géologique National, Orléans, France*

A mathematical model is presented for investigating the non-steady state temperature behavior of a pumped aquifer during reinjection of a fluid at a temperature different from that of the native water. Results are presented in terms of dimensionless parameters and should be helpful in the design of geothermal space-heating projects. Applications to practical cases are also included.

UNIVERSITY OF UTAH  
RESEARCH INSTITUTE  
EARTH SCIENCE LAB.

## INTRODUCTION

The use of geothermal energy for space heating and the production of electricity is currently limited to a small number of regions around the world with exceptionally high geothermal gradients [Kruger and Otte, 1973]. Geothermal space heating or air conditioning can also be used, however, in regions with normal temperature gradients if it is possible and economically feasible to drill a well deep enough to reach an aquifer with adequate water temperature. Aquifers at depths of the order of 2000 m have already been used for space heating [Maugis, 1971] and were found suitable with the current space-heating technology. Other heating processes should permit the use of much shallower formations. Free surface aquifers can also be used for air cooling, or even for space heating, by means of heat pumps. With the energy crisis and increasing fuel prices, aquifers may thus become a very important source of heat energy.

Disposal of the heat-depleted water, however, may often be a problem because of the mineral contents, the temperature, or the volumes involved, all of which would prevent the water from being wasted into sewage lines. One solution consists of reinjecting the water back into the aquifer. This procedure maintains the reservoir pressure, prevents subsidence, and insures an indefinite supply of water. It also permits the recovery of the heat contained in the rock, but as a result it creates a zone of injected water around each injection well at a different temperature from that of the native water. These zones will grow with time and will eventually reach the production wells. After breakthrough occurs, the water temperature is no longer constant at the production wells, and this may reduce drastically the efficiency of the whole operation.

It is thus important to design such a system in order to prevent injected water breakthrough before a specified time and to maintain the temperature variations at the production wells after breakthrough within reasonable limits. Although a few authors have considered a similar problem for a single recharging-discharging well pair [Houpeurt et al., 1965; Lagarde and Maugis, 1966], no general theory has been published to date.

It is the purpose of this paper to develop a mathematical model for investigating the non-steady state temperature behavior of production wells during the reinjection of heat-depleted water into aquifers with uniform regional flow. Results are presented in terms of dimensionless parameters and should be helpful for the design of such systems.

## MATHEMATICAL MODEL

Our discussion will be based on an analytical model.

A rectilinear system is placed such that the  $x, y$  plane coincides with the midplane of the aquifer. A few simplifying assumptions that are usual in this type of problem are made. These are listed below and will be discussed later.

1. The aquifer is assumed to be horizontal and of uniform thickness  $h$ . The cap rock and the bedrock, above and below the aquifer, are impermeable to flow and of infinite extent in the vertical direction. The system is thus symmetrical with respect to the midplane of the aquifer.

2. Flow is assumed to be steady, since the duration of the transient flow period is short in comparison with the length of time required to reach thermal equilibrium. The total injection rate  $Q$  is constant and equal to the total production rate. All wells fully penetrate the aquifer. The flow field due to the recharging and discharging wells is superimposed on a natural system of areal parallel flow of Darcy velocity  $V_0$ , whose orientation is at an angle  $\alpha$  with the  $x$  axis, as measured counter-clockwise from that axis.

3. Initially, the water and rock in the aquifer and the cap rock and bedrock are at the same temperature  $T_0$ . (Actually, the cap rock and bedrock temperatures are neither identical nor uniform initially, because of the geothermal gradient, but this fact can be neglected, since we only consider temperature perturbations.) At time  $t = 0$  the temperature of the injected water is set equal to  $T_1$  and is maintained constant thereafter. Thermal equilibrium is supposed to take place instantaneously between the water and the rock in the aquifer, so that anywhere in the aquifer the rock has the same temperature as the surrounding fluid.

4. In the aquifer the effect of the thermal conductivity is neglected in the horizontal direction (high Peclet number). Furthermore, the aquifer is assumed to be thin enough that the temperature is always uniform in the vertical direction (infinite vertical thermal conductivity).

5. In the cap rock and the bedrock the effect of the horizontal thermal conductivity is also neglected, and the vertical thermal conductivity is finite. The temperature remains constant and equal to the initial temperature at infinity in the vertical direction.

6. There is no heat transfer coefficient between the aquifer and the cap rock and bedrock, and the aquifer temperature is assumed to be equal to the cap rock temperature at the contact between the cap rock and the aquifer ( $z = h/2$ ).

7. The product of the density and the heat capacity for both the water and the rock, and the cap rock vertical thermal conductivity, are constant. Differences in viscosity between

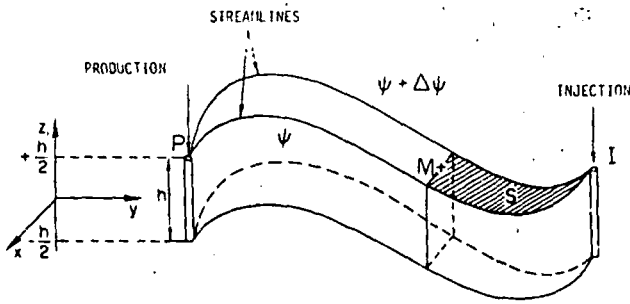


Fig. 1. Visualization of a stream channel.

injected water and native water are neglected. A 'no-mixing' condition and pistonlike displacement are assumed in the aquifer.

The above assumptions allow each stream channel leaving a particular injection well to be treated independently. The temperature corresponding to a given stream channel, bounded by two streamlines  $\psi$  and  $\psi + d\psi$ , can be described by a one-dimensional function  $T_w^\psi(S, t)$  in the aquifer and by a two-dimensional function  $T_R^\psi(S, z, t)$  in the cap rock or the bedrock,  $S$  being the stream channel area from the corresponding injection well (Figure 1).

The differential equation governing the water temperature  $T_w^\psi$  within a stream channel is obtained by writing a heat balance on an element of stream channel between the areas  $S$  and  $S + dS$  from the injection well (Figure 2). The derivation is similar to that published by *Lauwerier* [1955] and *Carslaw and Jaeger* [1959] for one-dimensional mass flow. The result is

$$\frac{h}{2} \rho_A C_A \frac{\partial T_w^\psi(S, t)}{\partial t} + \frac{q}{2} \rho_w C_w \frac{\partial T_w^\psi(S, t)}{\partial S} = K_R \frac{\partial T_R^\psi(S, z, t)}{\partial z} \Big|_{z=h/2} \quad (1)$$

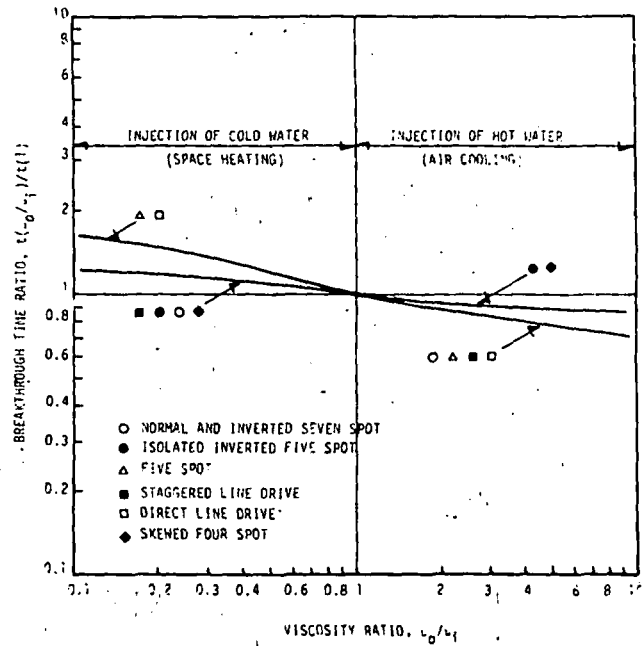


Fig. 3. Effect of viscosity ratio on breakthrough time for various well patterns (after data reported by *Craig* [1971]).

where  $q$  is the rate of flow within the stream channel,  $\rho_w C_w$  is the water heat capacity,  $\rho_A C_A = \phi \rho_w C_w + (1 - \phi) \rho_m C_m$  is the aquifer heat capacity ( $\rho_m C_m$  being that of the matrix and  $\phi$  being the aquifer porosity), and  $K_R$  is the cap rock thermal conductivity.

The cap rock temperature is governed by the heat conduction equation

$$\frac{\partial^2 T_R^\psi(S, z, t)}{\partial z^2} = \frac{\rho_R C_R}{K_R} \frac{\partial T_R^\psi(S, z, t)}{\partial t} \quad z \geq \frac{h}{2} \quad (2)$$

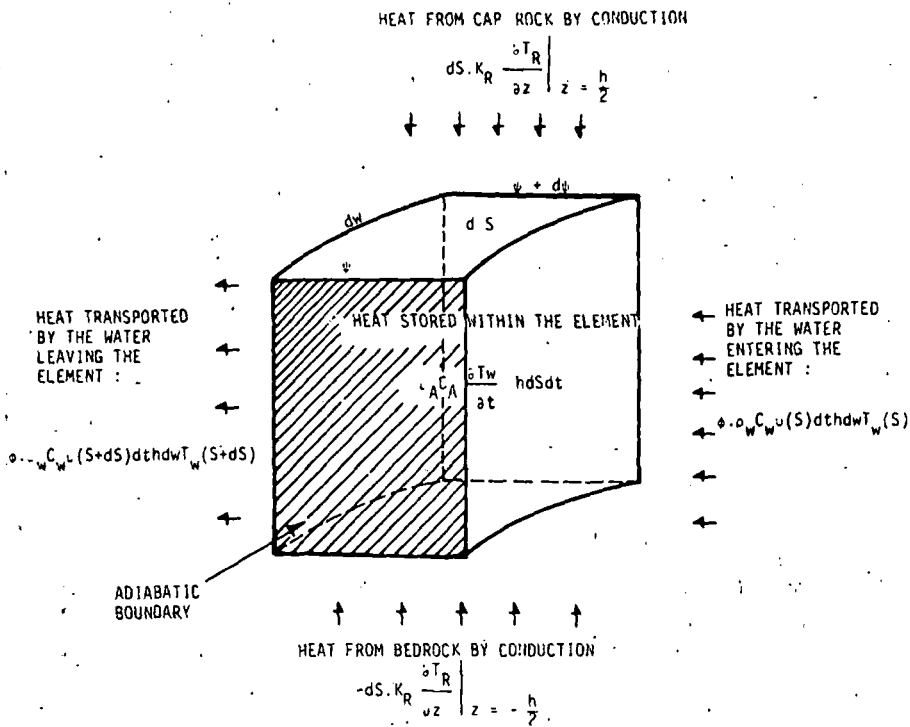


Fig. 2. Heat balance on a stream channel element.

where  $\rho_R C_R$  is the cap rock heat capacity. The temperatures must also satisfy the following conditions:

$$T_R^\psi(S, z, t) = T_w^\psi(S, t) = T_0 \quad t < \phi h S / q \quad (3)$$

ahead of the hydrodynamic front,

$$T_w^\psi(0, t) = T_0 \quad t \leq 0 \quad (4)$$

$$T_w^\psi(0, t) = T_i \quad t > 0$$

$$T_w^\psi(S, t) = T_w^\psi(S, h/2, t) \quad \forall t \text{ and } S \quad (5)$$

$$\lim_{z \rightarrow 0} T_R^\psi(S, z, t) = T_0 \quad (6)$$

The simultaneous solution of (1) and (2), subject to conditions (3)-(6), is easily obtained from Lauwerier's one-dimensional solution. The result for the water temperature within the stream channel is obtained as

$$\frac{T_0 - T_w^\psi(S, t)}{T_0 - T_i} = \operatorname{erfc} \left[ \frac{(\rho_w C_w)^2}{K_R \rho_R C_R} \left( \frac{q}{S} \right)^2 \left( t - \frac{\rho_A C_A}{\rho_w C_w} \frac{h S}{q} \right) \right]^{-1/2} \quad (7)$$

In the case in which there is no heat exchange by conduction between the aquifer and the cap rock and bedrock ( $K_R = 0$ ), (7) reduces to a step function:

$$\frac{T_0 - T_w^\psi(S, t)}{T_0 - T_i} = u \left( t - \frac{\rho_A C_A}{\rho_w C_w} \frac{h S}{q} \right) = 0 \quad t < (\rho_A C_A / \rho_w C_w)(h S / q)$$

$$\frac{T_0 - T_w^\psi(S, t)}{T_0 - T_i} = u \left( t - \frac{\rho_A C_A}{\rho_w C_w} \frac{h S}{q} \right) = 1 \quad t > (\rho_A C_A / \rho_w C_w)(h S / q) \quad (8)$$

which corresponds to a pistonlike thermal front displacement with a velocity equal to  $\rho_w C_w \phi / \rho_A C_A$  times that of the hydrodynamic front. The water temperature is  $T_0$  ahead of the thermal front and  $T_i$  behind it. On the other hand, if  $K_R$  is different from zero, there is a transition zone behind the thermal front in which the temperature varies from  $T_0$  to  $T_i$ .

If the streamlines leaving a recharge well reach a discharge well, the water temperature at that discharge well within an elementary stream channel is obtained by substituting the total stream channel area between the two wells,  $S_{max}$ , for  $S$  in (7). (Except in a few simple cases,  $S_{max}$  must be computed numerically.)

The result can be written in terms of dimensionless parameters as

$$\frac{T_0 - T_w^\psi(t)}{T_0 - T_i} = \operatorname{erfc} \left\{ \frac{d(S_{max}/D^2)}{d(\psi/Q)} \left[ \lambda \left( t_D - \frac{d(S_{max}/D^2)}{d(\psi/Q)} \right) \right]^{-1/2} \right\} \quad (9)$$

where

$$\lambda = (\rho_w C_w \rho_A C_A / K_R \rho_R C_R)(Qh/D^2) \quad (10)$$

$$t_D = (\rho_w C_w / \rho_A C_A)(Qt/D^2h) \quad (11)$$

$D$  is some characteristic length, and  $d(S_{max}/D^2)/d(\psi/Q)$  is the dimensionless derivative of the total stream channel area with respect to the stream function. Heat transfer between the aquifer and the cap rock or bedrock is negligible for  $\lambda \geq 10^4$ .

The water temperature at the recharge well at a given time  $t_D$  is then obtained by integrating the right-hand side of (9) with respect to  $\psi$  for all stream channels that have reached the discharge well at  $t_D$ :

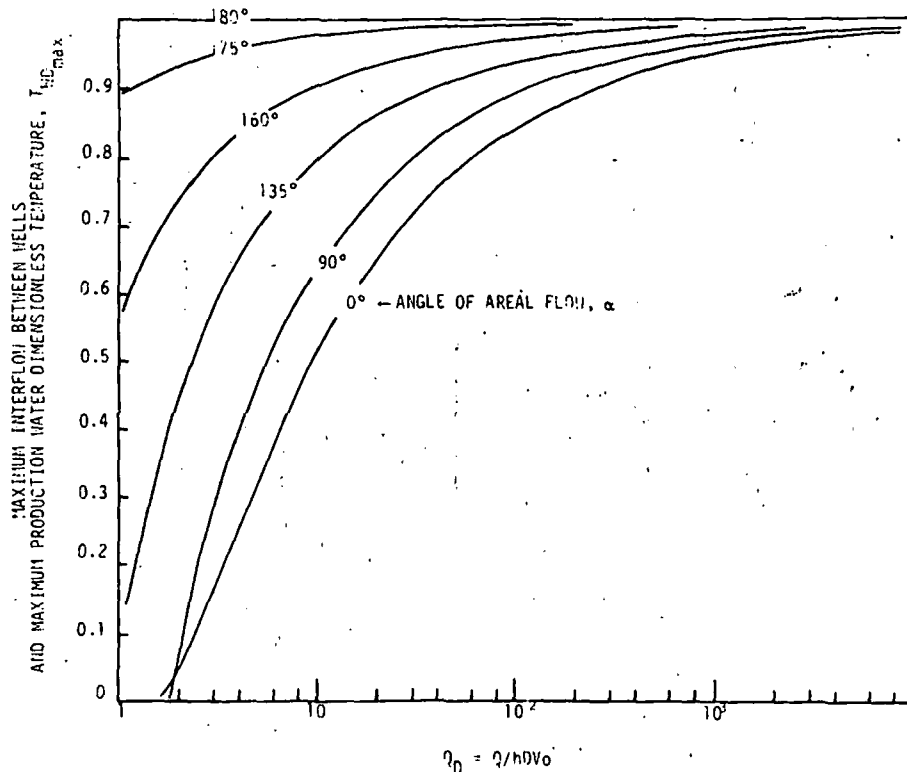


Fig. 4. Maximum water temperature at the production well of a doublet as a function of  $Q/hDV_0$  and the angle of area flow.



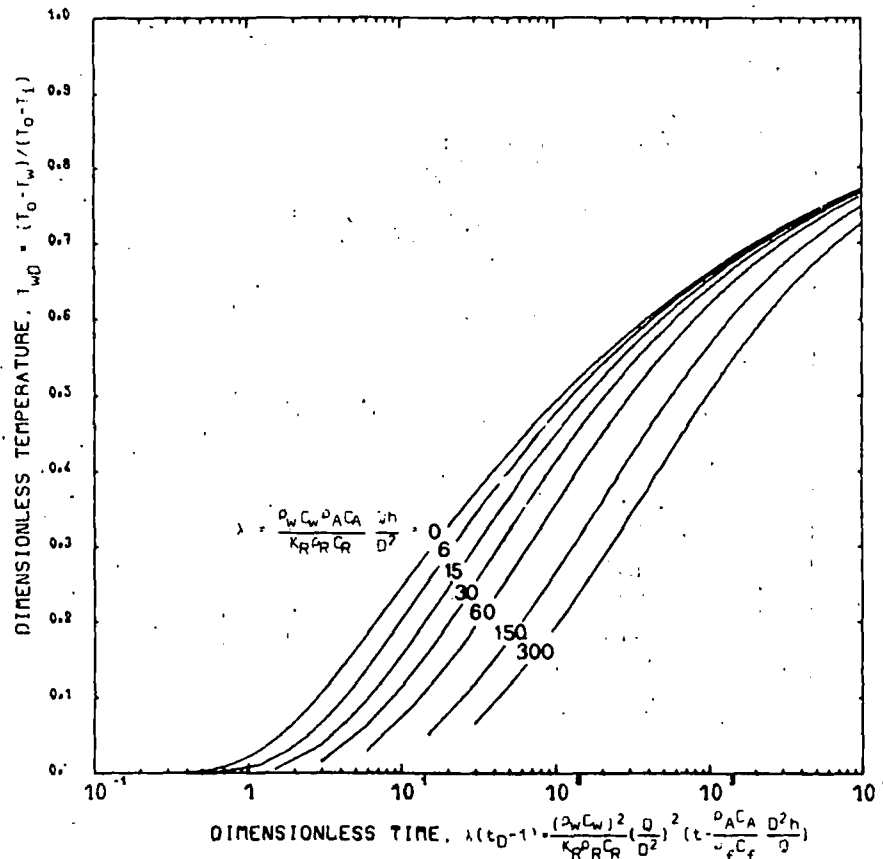


Fig. 5. Dimensionless temperature versus dimensionless time at the production well of a doublet in a deep confined aquifer ( $Q_D > 10^4$ ) for various values of  $\lambda$  from 0 to 300.

$$\frac{T_0 - T_w(t)}{T_0 - T_i} = \int \operatorname{erfc} \left\{ \frac{d(S_{\max}/D^2)}{d(\psi/Q)} \right. \\ \left. \left[ \lambda \left( t_D - \frac{d(S_{\max}/D^2)}{d(\psi/Q)} \right) \right]^{-1/2} \right\} d\left(\frac{\psi}{Q}\right) \\ = T_{wD}[f(\psi), \lambda, t_D] \quad (12)$$

where  $f(\psi)$  depends on the stream function.

This result is perfectly general.  $T_w$  can then be evaluated if the flow field is known.

#### DISCUSSION

Equation (12) will also yield satisfactory results if not all of the rather restrictive assumptions of the mathematical model are satisfied.

The total injection rate may change if the duration of the change is short in comparison with the total time length of interest and if the change does not modify drastically the stream channel: the injection rate to be used in (10) and (11) is then equal to the total volume of injected water divided by the total injection time.

On the other hand, a variable injection temperature can be taken into account exactly by superposition. If, for instance, the injection temperature is  $T_{i1}$  for time 0 to time  $t_1$ ,  $T_{i2}$  for  $t_1$  to  $t_2$ , etc., the temperature of the water at the production well at time  $t$  is given by

$$T_0 - T_w(t) = (T_0 - T_{i1})T_{wD}[f(\psi), \lambda, t_D] \\ + (T_{i1} - T_{i2})T_{wD}[f(\psi), \lambda, t_D - t_{D1}] \\ + (T_{i2} - T_{i3})T_{wD}[f(\psi), \lambda, t_D - t_{D2}] + \dots \quad (13)$$

and for a continuous injection temperature function  $T_i(t)$ ,

$$T_w(t) = T_0 + \int_0^t \frac{dT_i(\tau)}{d\tau} T_{wD}[f(\psi), \lambda, t_D - \tau_D] d\tau \quad (14)$$

The effect of the contrast of viscosity between in-place water and injected water is more difficult to evaluate. Information, however, may be obtained from studies on water flooding in the oil industry. Water flooding is a secondary recovery process in which oil is displaced by injected water. Calculations for viscosity ratios of unity were compared with laboratory experiments at viscosity ratios other than unity for a variety of well arrangements. Results were usually given in terms of pattern areal sweep efficiency or fraction of pattern area contacted by water at breakthrough. These values can be transformed to yield the  $t_D$  value (from (11)) at which breakthrough of the thermal front occurs for each well pattern in the case in which there is no heat exchange with the cap rock or the bedrock ( $\lambda = \infty$ ).

In order to evaluate the influence of the viscosity ratio on the advancement of the thermal front for various well patterns the ratio of the breakthrough  $t_D$  value at a viscosity ratio of unity to that at a viscosity ratio of other than unity has been plotted in Figure 3 versus the ratio of the viscosity of native water to that of injected water. The data used are those published by Craig [1971]. It is apparent from Figure 3 that breakthrough occurs later for viscosity ratios less than unity and earlier for viscosity ratios greater than unity. In other words, if cold water is injected into a warm aquifer (as occurs in geothermal space heating), the temperature will remain constant at the production wells for a period longer than that computed with our method. On the other hand, if the reinjected water is

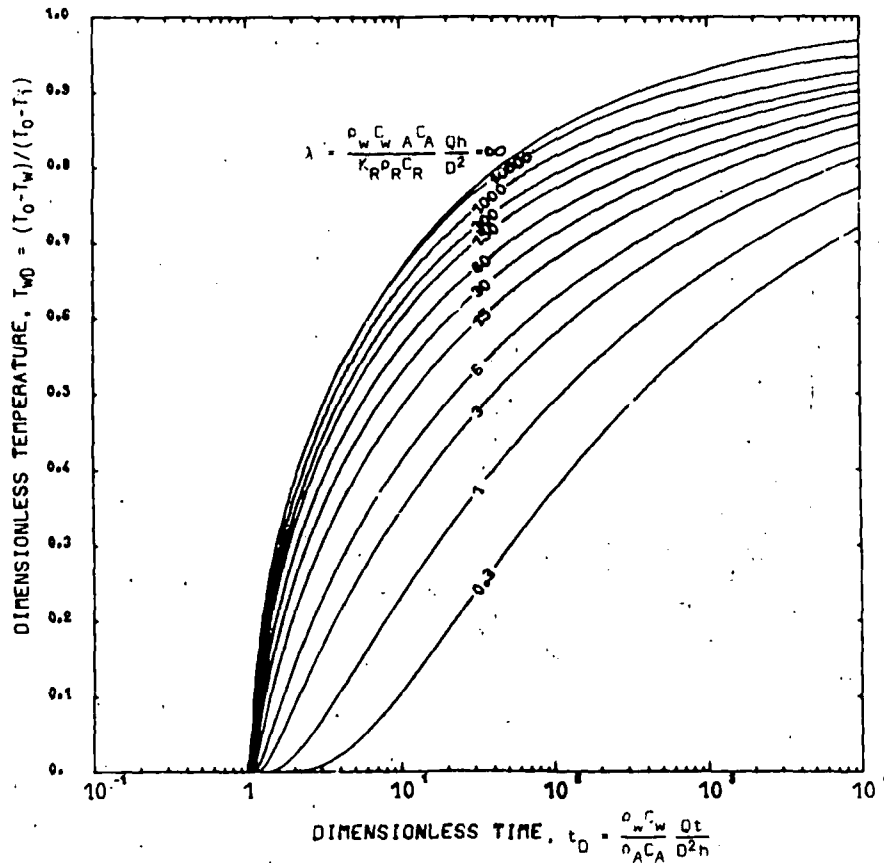


Fig. 6. Dimensionless temperature at the production well of a doublet in a deep confined aquifer ( $Q_D > 10^4$ ) for various values of  $\lambda$  from 0.3 to infinity.

warmer than the aquifer, as occurs in air cooling, the temperature at the production wells will rise earlier than would be predicted.

RECHARGING-DISCHARGING WELL PAIR

The previous results have been applied to the case of a single recharging-discharging well pair (called a 'doublet' hereafter) in uniform flow. The recharge well is on the  $x$  axis at a point with coordinates  $(+a, 0)$ , and the discharge well on the  $x$  axis at a point with coordinates  $(-a, 0)$ . (The recharge well is downstream when  $\alpha = 0$ .) The characteristic length  $D$  in (10) and (11) is now the distance between the two wells ( $D = 2a$ ).

Information on the flow field created by a recharging-discharging well pair in a homogeneous and isotropic aquifer with uniform flow is available in the literature [Da Costa and Bennett, 1960; Grove et al., 1970]. The stream function can be expressed in terms of two parameters only: the angle of areal flow  $\alpha$  and a dimensionless parameter

$$Q_D = Q/hDV_0 \tag{15}$$

which characterizes the importance of the well recharge-discharge rate compared to that of the areal flow.

The dimensionless water temperature at the production well can thus be expressed from (12) as a function of four dimensionless parameters only:

$$\frac{T_0 - T_w(t)}{T_0 - T_i} = T_{wD}(\alpha, Q_D, \lambda, t_D) \tag{16}$$

Equation (16) has been evaluated by computer as a function of  $t_D$  for various values of  $\alpha$ ,  $Q_D$ , and  $\lambda$ . As was mentioned

before,  $\lambda$  accounts for the heat transfer by conduction with the cap rock and the bedrock, whereas  $\alpha$  and  $Q_D$  set the maximum interflow between wells, i.e., the total amount of injected water in the water produced at the production well after an infinite time ( $t_D = \infty$ ). The maximum interflow is independent of  $\lambda$  and is also equal to the maximum temperature change  $T_{wD_{max}}$

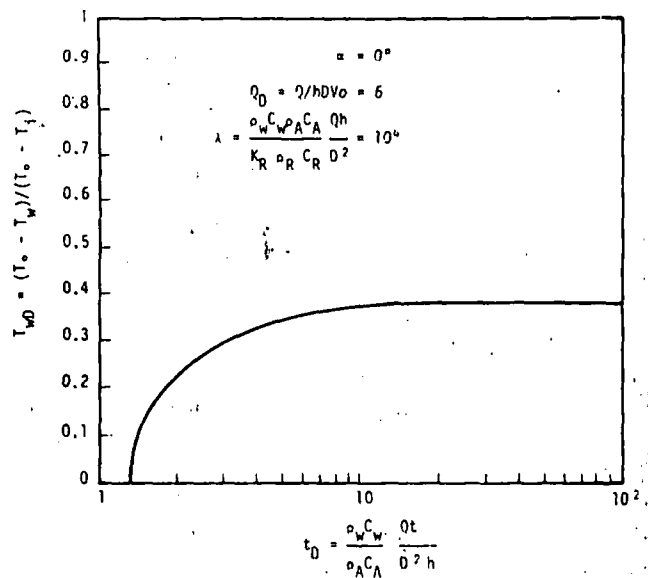


Fig. 7. Dimensionless temperature at the production well versus dimensionless time for  $\alpha = 0^\circ$ ,  $Q_D = 6$ , and  $\lambda = 10^4$ .

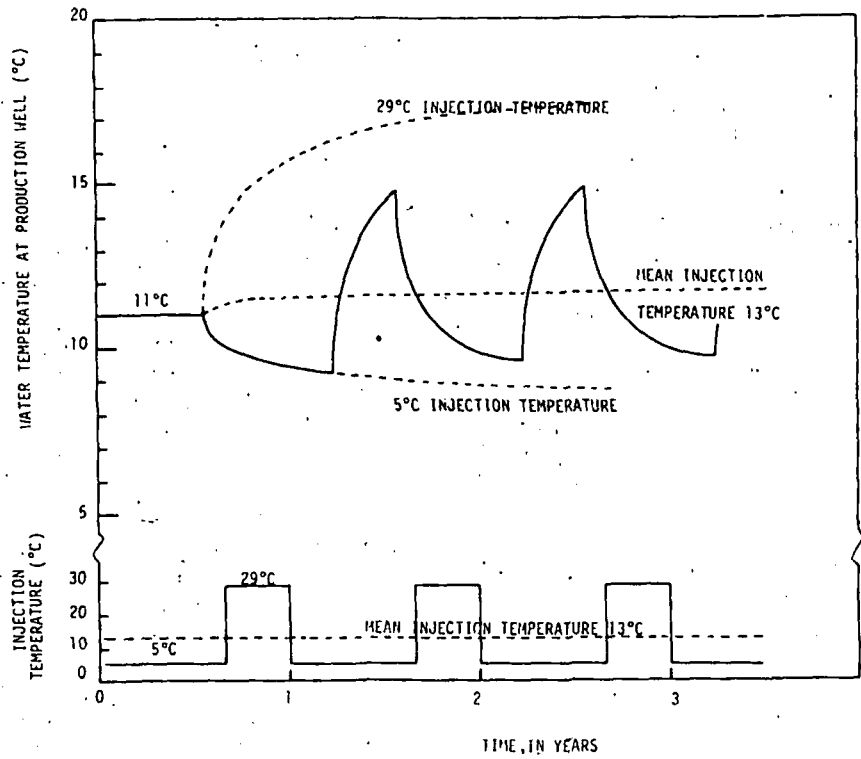


Fig. 8. Temperature of water at the production well under periodic change in injection temperature.

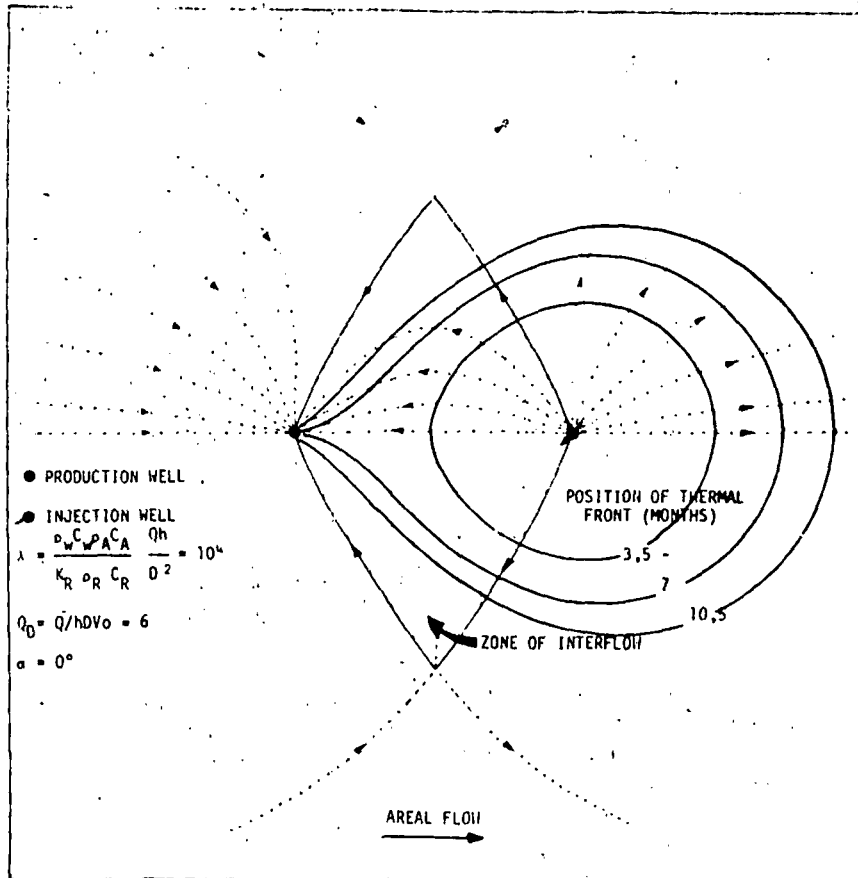


Fig. 9. Propagation of thermal front.

of the water at the production well.  $T_{wD, \max}$  is plotted versus  $Q_D$  in Figure 4 for various values of  $\alpha$  from  $0^\circ$  to  $180^\circ$ . Two limiting cases are of interest. (1) At  $Q_D$  values greater than  $10^4$ , interflow is maximum and independent of  $\alpha$ :  $T_{wD, \max} = 1$ , and  $T_{wD}$  is only a function of  $\lambda$  and  $t_D$ . This is the case in most deep confined aquifers. (2) On the other hand, at low  $Q_D$  values, when areal flow dominates (as in most free surface aquifers), it is possible to have no interflow between wells, except if  $\alpha = 180^\circ$ .

It is not practical to present in this paper a set of curves that will cover all practical cases. These are provided only for deep aquifers ( $Q_D \geq 10^4$ ).  $T_{wD}$  is plotted in Figure 5 versus  $t_D$  for various values of  $\lambda$  from 0.3 to infinity and in Figure 6 versus  $\lambda$  ( $t_D - 1$ ) for  $\lambda$  values ranging from 0 to 300. Figures 5 and 6 can be used to calculate (1) the spacing between the two wells in order not to have any change in temperature at the production well during a specified period and (2) the temperature change at the production well after breakthrough.

#### EXAMPLE OF CALCULATION

Thermal front breakthrough occurs at  $t_D = 1.04$  if  $\lambda > 10$  (Figure 5) and at  $\lambda(t_D - 1) = 0.5$  if  $0 < \lambda < 10$  (Figure 6). Actually, this last formula can be used with a good approximation for all  $\lambda$  values. Hence if there must be no change in the produced water temperature for a period of length  $\Delta t$  (that is, if  $\Delta t$  is the useful life of the doublet), the spacing, in cgs units, must at least be equal to

$$D = \left\{ 2 \cdot Q \cdot \Delta t / \left[ \left( \phi + (1 - \phi) \frac{\rho_R C_R}{\rho_w C_w} \right) h + \left( \left( \phi + (1 - \phi) \frac{\rho_R C_R}{\rho_w C_w} \right)^2 h^2 + 2 \frac{K_R \rho_R C_R}{(\rho_w C_w)^2} \Delta t \right)^{1/2} \right] \right\}^{1/2} \quad (17)$$

Equation (17) has been used to evaluate the spacing between wells of isolated doublets that will be drilled for space heating in the 1800-m-deep Dögger aquifer near Paris, France. For  $h = 50$  m,  $Q = 100$  m<sup>3</sup>/h,  $\Delta t = 30$  years,  $\rho_w C_w = 1$  cal/cm<sup>3</sup>/s,  $\rho_R C_R = 0.5$  cal/cm<sup>3</sup>/°C, and  $K_R = 6 \times 10^{-3}$  cal/cm/s/°C, equation (17) yields  $D = 863$  m. This value includes a safety factor, since cold water is injected into a warm aquifer. The results from (17) would be  $D = 917$  m if  $K_R$  were taken as zero. One such scheme has been operating in Melun, France, since 1969.

In free surface aquifers, where areal flow is usually important, it is theoretically possible to locate the wells so that there will be no interflow at all. In that case the temperature will always remain constant at the production well. Unfortunately, this may not always be practical, as is illustrated by the following example. A 70-m-thick free surface aquifer is to be used for space heating for 8 months and for air cooling for 4 months, by means of heat pumps. The water temperature in the aquifer has been found to be constant and equal to  $11^\circ\text{C}$  all year around, a finding which indicates that there is no heat exchange through the 3-m-thick unsaturated zone. The rate of water to be withdrawn and injected is 900 m<sup>3</sup>/h, and the injection temperature is  $5^\circ\text{C}$  during the space-heating stage and  $29^\circ\text{C}$  during the air-cooling period. Aquifer porosity is 10%, and the areal flow has a real velocity magnitude of 1.7 m/d. How should the doublet be designed in order to keep the temperature at the production well as constant as possible?

Figure 4 indicates that no interflow will take place between the wells if  $Q_D$  is less than 1.8.  $D$  must therefore be greater than  $Q/(1.8h \cdot V_0)$ , or  $D \geq 965$  m. However, in this particular situation the two wells must be drilled on a property within a heavily built area, and the maximum practical spacing between the wells is only 300 m in the direction of areal flow.  $Q_D$  is thus equal to 6. Figure 4 then indicates that interflow will be the least and that it will be equal to 38% if the recharge well is placed directly downgrade of the discharge well ( $\alpha = 0$ ).

The time variation of the water temperature at the production well due to the seasonal change in injection temperature is obtained by first computing the  $T_{wD}$  function from (16) for the appropriate values of  $\alpha$ ,  $Q_D$ , and  $\lambda$  and then substituting it into (13). The calculations were made on the assumption that the aquifer is bounded above and below by two adiabatic boundaries ( $\lambda = \infty$ ), in order to obtain an upper limit for the produced water temperature.  $T_{wD}(0, 6, \infty, t_D)$  is plotted in Figure 7 versus  $t_D$ , and the temperature variation in time at the production well obtained from (13) is shown in Figure 8. Propagation of the thermal front is presented in Figure 9.

With a 300-m spacing, the temperature at the production well will thus be a periodic function of time having the same period as the injection temperature function and oscillating between  $10^\circ\text{C}$  and  $15^\circ\text{C}$ . This was found to be inadequate, and it was decided to use wells with partial penetration to take advantage of the high anisotropy between the horizontal and the vertical directions. Water is pumped out from the top of the aquifer and reinjected at the bottom. The system has been operating for about 1 year and has been found to be satisfactory so far.

*Acknowledgments.* The investigations reported herein have been carried out at the Bureau de Recherches Géologiques et Minières (BRGM) in Orléans, France. The authors wish to express their appreciation to the management of BRGM for permission to publish this paper. Thanks are extended to J. Goguel, BRGM vice-president, for many stimulating discussions on the paper topic. The assistance of P. A. Landel in setting up the computer program is gratefully acknowledged.

#### REFERENCES

- Carslaw, H. S., and J. C. Jaeger, *Conduction of Heat in Solids*, 2nd ed., p. 396, Clarendon, Oxford, 1959.
- Craig, F. F., *The Reservoir Engineering Aspects of Waterflooding*, Monogr. Ser., vol. 3, Society of Petroleum Engineers, Dallas, Tex., 1971.
- Da Costa, J. A., and R. R. Bennett, The pattern of flow in the vicinity of a recharging and discharging pair of wells in an aquifer having areal parallel flow, *Int. Ass. Sci. Hydrol. Publ.* 52, 524-536, 1960.
- Grove, D. B., W. A. Beetem, and F. B. Sower, Fluid travel time between a recharging and discharging well pair in an aquifer having a uniform regional flow field, *Water Resour. Res.* 6(5), 1404, 1970.
- Houpeurt, A., J. DeLouvrier, and R. Ifly, Fonctionnement d'un doublet hydraulique de refroidissement, *Houille Blanche*, no. 3, 239-246, 1965.
- Kruger, P., and C. Otte, *Geothermal Energy*, Stanford University Press, Palo Alto, Calif., 1973.
- Lagarde, A., and P. Maugis, Méthodes d'étude des possibilités d'exploitation des nappes d'eau souterraines pour le chauffage urbain, *Réf. 14072*, Inst. Fr. du Pétrole, Rueil-Malmaison, France, Dec. 1966.
- Lauverier, H. A., The transport of heat in an oil layer caused by the injection of hot fluid, *Appl. Sci. Res., Sect. A*, 5, 145, 1955.
- Maugis, P., Exploitation d'une nappe d'eau chaude souterraine pour le chauffage urbain dans la région parisienne, *Ann. Mines*, no. 5, 135-142, 1971.

(Received January 27, 1975;  
revised August 18, 1975;  
accepted August 18, 1975.)

SUBJ  
GTHM  
TSOB

UNIVERSITY OF UTAH  
RESEARCH INSTITUTE  
EARTH SCIENCE LAB.

## The temperature stabilization of a borehole

Y. Leblanc\*, L. J. Pascoe\*, and F. W. Jones\*

### ABSTRACT

Analytic solutions for the temperature stabilization of both square and circular boreholes are considered. It is found that a previously published solution for a square borehole is incorrect in that it does not reproduce the initially assumed conditions. The correct analytic solution for a square well, as well as that for a circular well, indicates a much more rapid approach to the formation temperature. The temperature stabilization curves for a range of thermal diffusivity values are given.

### INTRODUCTION

A technique for estimating the true formation temperature by curve-matching analytic solutions to time-sequential bottom hole temperatures was recently developed and applied to the Cooper basin of South Australia by Middleton (1979). Middleton (1979) derived a set of thermal stabilization curves based on an assumed thermal diffusivity, and he was able to superimpose his derived curves on actual data to estimate a formation temperature.

However, we have found that the solution used by Middleton (1979) to derive the stabilization curves is not consistent with the initial conditions imposed on the model.

### THE SQUARE WELL

The square well model is shown in Figure 1, with initial conditions illustrated. At time  $t = 0$ , the drilling mud within the well is at temperature  $T_m$ , and the surrounding formation temperature is  $T_f$ . After circulation ceases, heat flows radially into the well as shown, and we are concerned with the rate of increase of temperature at the center of the well (origin  $O$ ) and at some distance above the bottom of the well. The thermal diffusivity ( $k$ ) is taken as the same both within and outside the well.

The solution presented by Middleton (1979) for the bottom hole temperature (BHT) in the center of the well is

$$BHT(t) = T_m + (T_f - T_m) \left[ \operatorname{erfc} \left( \frac{a}{2\sqrt{kt}} \right) \right]^2 \quad (1)$$

where

- $T_m$  = the temperature of the mud inside the well,
- $T_f$  = the true formation temperature ( $T_f > T_m$ ),
- $a$  = one-half the length of the side of the square cylinder, and
- $k$  = the diffusivity constant.

Relation (1) is derived from

$$BHT(x, y, t) = T_m + \frac{(T_f - T_m)}{4} \left[ \operatorname{erfc} \left( \frac{a-x}{2\sqrt{kt}} \right) + \operatorname{erfc} \left( \frac{a+x}{2\sqrt{kt}} \right) \right] \left[ \operatorname{erfc} \left( \frac{a-y}{2\sqrt{kt}} \right) + \operatorname{erfc} \left( \frac{a+y}{2\sqrt{kt}} \right) \right] \quad (2)$$

where  $x = y = 0$ .

Equation (2) is an extension in two dimensions of equation (4) of Carslaw and Jaeger (1959, p. 54). However, equation (2) is inconsistent with the initial conditions, and it does not produce the true behavior of the BHT inside the well.

The initial temperature distribution given by equation (2) is shown in Figure 2a. The proper initial temperature distribution is shown in Figure 2b. The corresponding analytic solution was

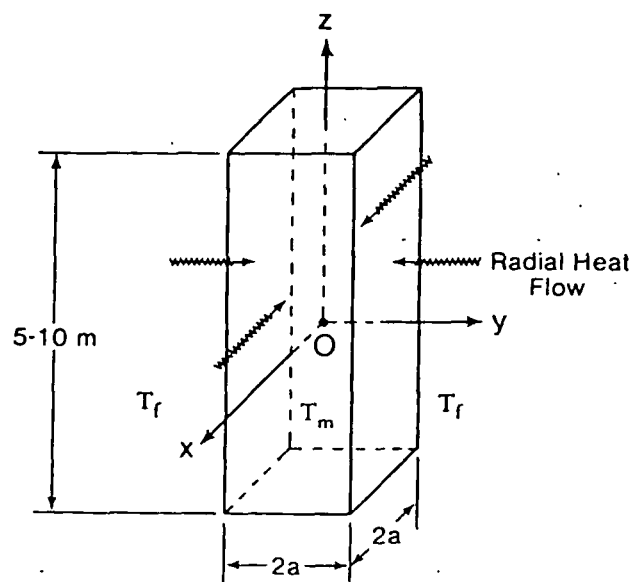


FIG. 1. The basal portion of the square well ( $t = 0$ ).

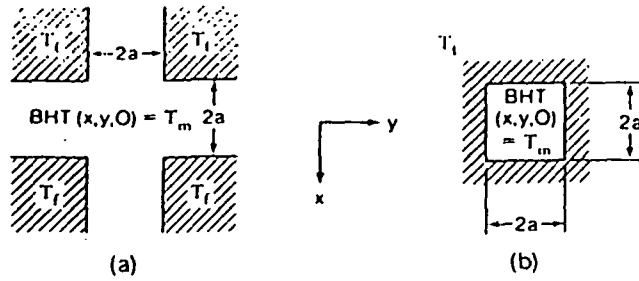


FIG. 2. (a) Initial temperature distribution from equation (2). (b) Initial temperature distribution from equation (3).

given by Carslaw and Jaeger [1959, p. 56, equation (9)]

$$\begin{aligned}
 \text{BHT}(x, y, t) = T_f - \frac{(T_f - T_m)}{4} & \left[ \text{erf} \left( \frac{a-x}{2\sqrt{kt}} \right) \right. \\
 & + \text{erf} \left( \frac{a+x}{2\sqrt{kt}} \right) \left. \right] \left[ \text{erf} \left( \frac{a-y}{2\sqrt{kt}} \right) \right. \\
 & \left. + \text{erf} \left( \frac{a+y}{2\sqrt{kt}} \right) \right]. \tag{3}
 \end{aligned}$$

At the center of the well ( $x = y = 0$ ), this becomes

$$\text{BHT}(t) = T_f - (T_f - T_m) \left[ \text{erf} \left( \frac{a}{2\sqrt{kt}} \right) \right]^2. \tag{4}$$

or

$$\text{BHT}(t) = T_m + \Delta T \left\{ 1 - \left[ \text{erf} \left( \frac{a}{2\sqrt{kt}} \right) \right]^2 \right\}.$$

where  $\Delta T = T_f - T_m$ .

The behavior of this function is like that of equation (1), but it approaches the asymptotic value  $T_f$  much more rapidly.

THE CIRCULAR WELL

The initial conditions for the circular well are similar to those for the square well. Assuming circular symmetry and assuming that heat flow is radial (no  $z$  dependence), the heat flow equation in cylindrical coordinates may be written

$$\frac{1}{k} \frac{\partial T(r, t)}{\partial t} = \frac{\partial^2 T(r, t)}{\partial r^2} + \frac{1}{r} \frac{\partial T(r, t)}{\partial r}, \quad 0 < r < \infty. \tag{5}$$

A particular solution of equation (5) is [Luikov, 1968, p. 134, equation (4.5.8)]

$$T(r, t) = C J_0(\lambda r) \exp[-\lambda^2 kt], \tag{6}$$

where  $C$  is a constant.

The general solution is

$$T(r, t) = \int_0^\infty C(\lambda) J_0(\lambda r) \exp[-\lambda^2 kt] \lambda d\lambda. \tag{7}$$

Solving this equation for the initial distribution,

$$T(r, 0) = \begin{cases} T_0, & 0 < r < a \\ 0, & r > a, \end{cases} \tag{8}$$

where  $a$  is the radius of the hole, we obtain

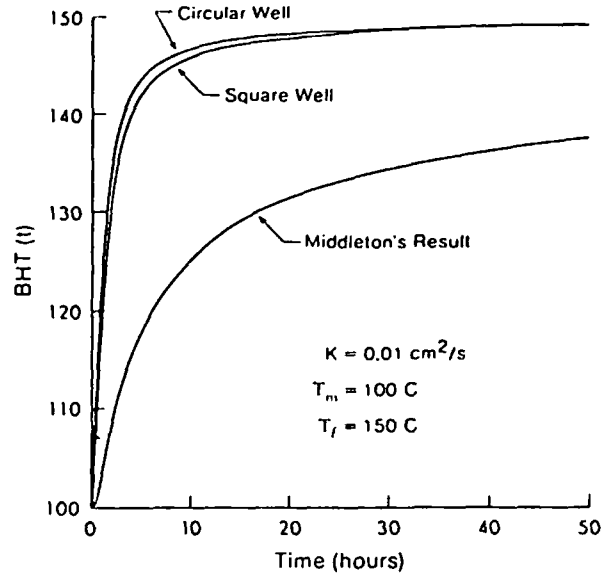


FIG. 3. A comparison of the circular and square well stabilization curves with that of Middleton (1979).

$$\begin{aligned}
 T(r, t) = \frac{a^2 T_0}{4kt} \sum_{m=0}^\infty & \left[ \frac{1}{(m+1)!} \left( \frac{-a^2}{4kt} \right)^m \right. \\
 & \left. \cdot F \left( -m, -1-m; 1; \frac{r^2}{a^2} \right) \right], \tag{9}
 \end{aligned}$$

where  $F(a, b; c; z)$  is the Gaussian hypergeometric series. If  $T_0 = T_f - T_m$ , then we can write

$$\text{BHT}(r, t) = T_f - T(r, t), \tag{10}$$

which is the solution for the temperature behavior of a circular well.

Equation (9) corresponds to the integral given by Carslaw and Jaeger [1959, p. 260, equation (12)]. Either form of the solution must be evaluated numerically. At the center of the hole this becomes

$$T(0, t) = T_0 (1 - e^{-a^2/4kt}) \tag{11}$$

as in Carslaw and Jaeger [1959, p. 260, equation (13)]. The expression for the temperature within the hole is then

$$\text{BHT}(0, t) = T_f - (T_f - T_m) [1 - e^{-a^2/4kt}]. \tag{12}$$

or

$$\text{BHT}(0, t) = T_m + \Delta T [e^{-a^2/4kt}],$$

where  $\Delta T = T_f - T_m$ . The behavior of this function is approximately the same as equation (4), and it approaches the asymptotic value  $T_f$  at approximately the same rate.

Results for the circular and square wells are compared in Figure 3 with Middleton's square well result, for  $k = 0.01 \text{ cm}^2 \text{ sec}^{-1}$ ,  $t_m = 100^\circ \text{C}$ , and  $T_f = 150^\circ \text{C}$ .

The effect of diffusivity

One of the assumptions in the foregoing is that the thermal diffusivity of the mud in the well is equal to the thermal diffusivity of the surrounding region. Middleton takes a value  $0.01 \text{ cm}^2 \text{ sec}^{-1}$  for the average thermal diffusivity of the sedi-

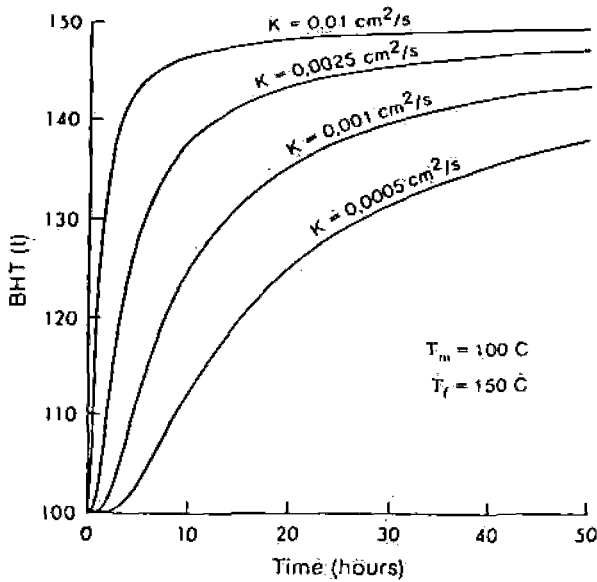


FIG. 4. Temperature stabilization curves from various values of thermal diffusivity for a circular well.

ments. However, we may assume that the fluids in the borehole are a mixture of water and sediments. From Carslaw and Jaeger (1959, p. 497), the thermal diffusivity of water is approximately  $0.00144 \text{ cm}^2 \text{ sec}^{-1}$ . This is about one-tenth that of sediments. According to Tye (1969, p. 319), the effective thermal conductivity  $\lambda$  for granular materials may be estimated from the empirical formula

$$\lambda = \lambda_m^{(1-f)} \lambda_s^f \quad (13)$$

where:

$\lambda_s$  = the conductivity of the solid component,

$\lambda_m$  = the conductivity of the fluid component, and

$f$  = the volume fraction of the solid component.

The thermal diffusivity

$$k = \frac{\lambda}{C\rho} \quad (14)$$

where

$C$  = specific heat, and  
 $\rho$  = density.

Also, we can estimate  $\rho$  and  $C$  from

$$\rho = (1-f)\rho_m + f\rho_s$$

and

$$C = (1-f)C_m + fC_s \quad (15)$$

If we assume that the volume fraction of the solid component of the mixture is about one-half, then we can estimate from values furnished by Carslaw and Jaeger (1959, p. 497) a value of approximately  $0.0027 \text{ cm}^2 \text{ sec}^{-1}$  for  $k$ . This value is approximately one-quarter that of the surrounding region.

By decreasing  $k$  (taking into account the diffusivity of the drilling mud), the stabilization takes place much more slowly. We have calculated stabilization curves for a range of  $k$ . Such curves are shown for a circular well in Figure 4.

The initial boundary conditions have been assumed ideal and as such may only be approximate at some distance from the bottom of the hole. The stabilization rate will be affected by variations from the ideal initial distribution.

#### ACKNOWLEDGMENTS

The authors wish to acknowledge initial numerical work by B. Prager which originally pointed to a discrepancy in the previous published results. Also, the authors are indebted to P. Weichman who assisted in gaining the analytical solution for a circular well.

One author (Y. L.) wishes to thank the Natural Sciences and Engineering Research Council of Canada for assistance in the form of a summer scholarship. The work was supported by the Natural Sciences and Engineering Research Council of Canada and the Imperial Oil Co. of Canada.

#### REFERENCES

- Carslaw, H. S., and Jaeger, J. C., 1959, *Conduction of heat in solids*: Oxford, Oxford Univ. Press.  
 Luikov, A. V., 1968, *Analytical heat diffusion theory*: New York, Academic Press.  
 Middleton, M. F., 1979, A model for bottom-hole temperature stabilization: *Geophysics*, v. 44, p. 1458-1462.  
 Tye, R. P., 1969, *Thermal conductivity*, v. 1: London, Academic Press.

SUBJ  
GTHM  
TTD

*Geoexploration*, 15 (1977) 1-9

© Elsevier Scientific Publishing Company, Amsterdam - Printed in The Netherlands

1

## TRUE-TEMPERATURE DETERMINATION OF GEOTHERMAL RESERVOIRS

DOO JUNG JIN

*Texas Instruments Inc., Dallas, Texas (U.S.A.)*

(Received November 6, 1974; revision accepted November 3, 1975)

### ABSTRACT

Jin, D.J., 1976. True-temperature determination of geothermal reservoirs. *Geoexploration*, 15: 1-9.

Parameters governing the resistivity in geothermal areas are analyzed. A method for the calculation of the true temperature of geothermal reservoirs is explained, and the effectiveness of the method is evidenced.

### INTRODUCTION

Recently geothermal energy as a major potential energy source has drawn considerable attention due to the realization of the limited amount of hydrocarbon energy resources, of the advantages of the terrestrial heat over other forms of energy sources, and of the fact that economically accessible geothermal energy is more widespread than was believed only a few years ago (Armstead et al., 1974).

The utilization of geothermal energy is relatively free from danger of human life and environmental pollution, and requires neither advanced technology, as in the case of nuclear energy, nor massive construction, as in the case of hydroelectric power. From a study of the economics of geothermal power in Italy, New Zealand, and the United States, Facca and Ten Dam (McNitt, 1965) concluded that geothermal power is the cheapest among various sources of energy available at the time of McNitt's report. Cost analyses reported by Kaufman (1970), using the standard evaluation procedures suggested by the U.S. Federal Power Commission, reveal that of various energy sources geothermal energy will be least in total cost for the generation of electricity under favorable conditions, still inexpensive and competitive with others under less favorable conditions. His cost comparison was made with assumption of a base-load plant with a capacity of 1500 MW, privately financed, having either variable load factors for the various fuels or a constant 90% load factor for all fuels over the plant life of 30 years except for hydropower which was estimated at 50 years. In the case of geothermal energy, well life was estimated at 20 years.



The principal use of geothermal fluid is for the generation of electric power. The power is generated by tapping the natural thermal fluid underground and guiding it to drive a turbine of the generator system. The geothermal fluid is also utilized for space heating, agriculture, industries, hydrotherapy, extraction of chemicals which it may contain, and for fresh water.

For the exploration of geothermal resources, geophysical techniques such as electrical resistivity, gravity, magnetic, seismic, and heat flow methods as well as geological and geochemical methods have been employed in Italy, New Zealand, Iceland, the United States, Japan, Mexico, and the Soviet Union among others.

Of the various geophysical methods, the electrical resistivity method is considered to be and has been one of the most effective tools for geothermal energy prospecting. Keller (1970) has reported more effective aspects of electromagnetic induction methods over direct current methods in measuring resistivity in geothermal areas. Readers who are interested in the induction methods are referred to his well presented paper. The resistivity method has advantages of easy operation, low expenses, and wide range of applicability. One of its unique aspects may be that it is very useful in estimating both the quantity and quality of the ground water in geothermal provinces.

In the following, parameters which are essential in the resistivity method are analyzed and a method, with evidences for its effectiveness, of calculation of the true temperature of geothermal reservoirs is presented. Although the nature of, and the relationship between, those parameters are known to a limited number of people, the fact that the true temperature of geothermal reservoirs can be determined, has not yet, to this author's knowledge, been pointed out clearly to broad readers by using an explicit formula.

#### THEORY

In the following, physical and chemical theories which govern the electrical resistivity of earth materials are explained concisely. For most earth materials near the surface of the earth, the conduction of electricity is almost entirely through the water contained in the pores of the materials. In this paper, consideration is given to geothermal reservoirs whose rock possesses appreciable porosity and does not contain a high percentage of electricity conducting minerals such as graphite, pyrite, magnetite, specular hematite, chalcopyrite and pyrrhotite. Therefore in geothermal reservoirs considered in this paper, the electric conduction is assumed to be liquid-electrolytic, with the adjective "liquid" meaning the phase of the electrolyte contained in the pores of the solid rock at moderate temperatures rather than the phase of the rock itself in fused state at very high temperatures.

The resistivity of water-bearing rocks largely depends on the amount of water they contain, the chemical and physical, including thermal, properties of the water, and on the manner in which the water is distributed in them.

#### Porosity — quantity

The resistivity content. In a water porosity, while the (Archie, 1942) method

$$\rho_{100} = a \rho_w \phi^{-m}$$

where  $\rho_{100}$  is the resistivity of the water and  $a$  and  $m$  are constants of one type of formation discussion. Although sedimentary rocks on this subject in common has been observed (1970).

From eq. 1, the amount of water from the equation

$$V_w = V \left( a \frac{\rho_w}{\rho_{100}} \right)^{-1/m}$$

In eq. 2,  $V$  and  $\rho_w$  can be measured

#### Salinity — quality

The electrical the same terms of an electrolyte the salinity or concentration

$$\frac{1}{\rho} = F \sum_{i=1}^n c_i m_i \nu_i$$

where  $\rho$  is the resistivity (96,490 C/mole (moles/cm<sup>3</sup>),  $m_i$  (cm<sup>2</sup>/V sec),  $\nu_i$  is the number of kind resistivity of a ion in the solution in turn the viscosity below.

### Porosity — quantity of water

The resistivity of a water-bearing rock decreases with increasing water content. In a water-saturated rock, the amount of water may be equated with porosity, while the porosity is related to the resistivity by the Archie's law (Archie, 1942) modified by Winsauer and others (Winsauer et al., 1952):

$$\rho_{100} = a \rho_w \phi^{-m} \quad (1)$$

where  $\rho_{100}$  is the bulk resistivity of the water-saturated rock,  $\rho_w$  is the resistivity of the water contained in the pore structure,  $\phi$  is the porosity of the rock, and  $a$  and  $m$  are empirical constants. It is noted here that, for simplicity, only one type of formation water is assumed to exist in the pores of the rock under discussion. Although the amount of data on igneous rocks is much less than on sedimentary rocks, chiefly due to the historic development of the research on this subject in connection with petroleum exploration, the above relationship has been observed for measurements made on various igneous rocks, too (Keller, 1970).

From eq. 1, the amount of water stored in a reservoir can be determined. With  $a$  and  $m$  for a particular aquifer or formation already established, the amount of water,  $V_w$ , which an aquifer of volume  $V$  contains can be calculated from the equation:

$$V_w = V \left( \frac{\rho_w}{a \rho_{100}} \right)^{1/m} \quad (2)$$

In eq. 2,  $V$  and  $\rho_{100}$  can be calculated from geophysical field survey data and  $\rho_w$  can be measured in the laboratory with water sample taken from the field.

### Salinity — quality of water

The electrical properties of a water-bearing rock should be describable in the same terms as the electrical properties of an electrolyte. The conductivity of an electrolyte contained in a rock can be expressed as a linear function of the salinity or concentration of the electrolyte (Milazzo, 1963):

$$\frac{1}{\rho} = F \sum_{i=1}^n c_i m_i v_i \quad (3)$$

where  $\rho$  is the resistivity of the electrolyte ( $\Omega$  cm),  $F$  is Faraday's number (96,490 C/mole),  $c$  is the concentration of each species of ion in solution (moles/cm<sup>3</sup>),  $m$  is the electrical mobility of each species of ion in solution (cm<sup>2</sup>/V sec),  $v$  is the ionic valence of the individual ionic species, and  $n$  is the number of kinds of ions present in the solution. Eq. 3 tells us that the resistivity of a rock is inversely proportional to the salinity and mobility of ions in the solution. The mobility of ions increases with decrease in viscosity, in turn the viscosity decreases with increase in temperature which is considered below.

### Temperature

Contrary to metal, in water-bearing earth materials, resistivity decreases with increase in temperature. In either an electrolyte or a rock saturated with an electrolyte, increased temperature lowers the viscosity of the electrolyte and the decreased viscosity helps the ions move freely.

At moderate temperatures, the dependence of resistivity on temperature for a rock saturated with an electrolyte is defined by the equation (Glasstone, 1937):

$$\rho_t = \frac{\rho_{15}}{1 + \alpha_t (t-15)} \quad (4)$$

where  $\rho_t$  is the resistivity at the ambient temperature  $t^\circ\text{C}$ ,  $\rho_{15}$  is the resistivity measured at a reference temperature of  $15^\circ\text{C}$  (any other reference temperature may be used), and  $\alpha_t$  is the temperature coefficient of resistivity.

### Degree of saturation

The pore space of a rock may or may not be filled with an electrolyte; above the water table, part of the pore space is filled with air. The amount of water in the zone of aeration changes with time as meteorological and hydrological processes such as precipitation, drainage, evaporation on the soil surface and transpiration through plants take place.

A quantitative relationship between resistivity and the degree of saturation in a rock has been observed to hold (Keller, 1953):

$$\rho = \begin{cases} \rho_{100} S^{-n_1}, & S > S_c, \\ b\rho_{100} S^{-n_2}, & S < S_c \end{cases}$$

where  $\rho$  is the bulk resistivity of a partially saturated rock,  $\rho_{100}$  is, as defined previously, the resistivity of the same rock when it is completely saturated with the same electrolyte,  $S$  is the degree of saturation which is expressed as the ratio of pore volume filled with electrolyte to the total pore volume,  $S_c$  is the critical water saturation, which is the least saturation for which there is a continuous film of water over all the surfaces in the rock, and  $b$ ,  $n_1$ , and  $n_2$  are experimental parameters.

### Texture

The textural factors such as the particle-size distribution of the constituent particles, the shape of the particles, the orientation of the particles in space and with respect to each other, and the forces tending to bind the particles together, play a significant role in the resistivity of the rock. Pore space must be interconnected and filled with water in order that a rock may conduct electricity. Pores may be classified as interconnected and isolated ones,

depending  
pores may  
the storage  
expected f  
to storage  
stones and

A math  
rock in its  
follows (W

$\rho = F\rho_w$   
and:

$$F = \frac{L_w}{L} \left( \right.$$

where  $\rho$  an  
efficient (  
which act  
of the dim  
cross-secti  
to that of

Both th  
and shape  
interconn  
 $a\phi^{-m}$ , wh  
author be  
better. It  
the porosi  
small pore  
due to liq  
discussion  
to format  
duction is

Interactio

It is kn  
always th  
the rock.  
independ  
formatio  
when it is  
concept c  
negatively  
cations a  
under an

depending on the connection of pore space with others. The interconnected pores may consist of two parts; the larger voids, which are major space for the storage of water, and the finer connecting channels. A high resistivity is expected from a rock which has very small volume ratio of connecting pores to storage pores even when it possesses great porosity as in some shales, limestones and volcanic rocks.

A mathematical expression which accounts for the role of the texture of a rock in its resistivity may be shown by use of the formation factor,  $F$ , as follows (Ward and Fraser, 1967):

$$\rho = F\rho_w \quad (5a)$$

and:

$$F = \frac{L_w}{L} \left( \frac{A}{A_w} \right) \quad (5b)$$

where  $\rho$  and  $\rho_w$  are the same as defined previously;  $L_w/L$ , the tortuosity coefficient (Pirson, 1958), is the ratio of the length of the electrolyte path via which actual electric current flows, to that of the rock;  $A/A_w$ , the reciprocal of the diminution coefficient (Ward and Fraser, 1967), is the ratio of the cross-sectional area of the rock perpendicular to the direction of electric current, to that of the electrolyte path, which is in an arbitrary direction.

Both the tortuosity and diminution coefficients are controlled by the size and shape of the rock pores and the manner in which they are disposed and interconnected. For the formation factor, the expression in eq. 5b, instead of  $a\phi^{-m}$ , which can be derived from eq. 1, has been employed here, since the author believes that eq. 5b explains the characteristics of the formation factor better. It is noted from both the expressions for the formation factor that as the porosity decreases the formation factor increases. For a rock of extremely small porosity, the formation factor becomes so great that the ionic conduction due to liquid electrolyte in the rock becomes insignificant. Therefore the above discussions which were based on electrolytic conduction of rocks apply only to formations with large enough porosities in which liquid electrolytic conduction is predominant.

#### *Interaction between rock and electrolyte*

It is known that the conductivity of the water extracted from a rock is not always the same as that which the water would have before it is removed from the rock. According to eq. 1 or 5a, the formation factor,  $\rho/\rho_w$ , should be independent of  $\rho_w$  for a given rock. However, it is usually found that the formation factor of a rock is less when it is saturated with a dilute solution than when it is with a highly saline solution. This phenomenon is explained by the concept of surface conduction. The surface conduction is attributed to the negatively charged surface of clay materials, which is balanced by adsorbed cations and systematically oriented water molecules, which are free to move under an applied electric field.

UNIVERSITY OF UTAH LIBRARIES

Rock-forming minerals usually fracture in such a way that one species of ion in the crystal is commonly closer to the surface than others. In the silica—alumina units, which are the most abundant constituents of the crust, the oxygen ions are usually closest to the surface, resulting in the negatively charged surface of the clay materials (Keller and Frischknecht, 1966). Substitution within the lattice structure of clay materials of cations of lower valence for those of higher valence would also result in a negatively charged surface (Grim, 1968). This negative charge of the surface would be balanced by adsorption of cations in the electrolyte. The adsorbed cations are free to move under an applied electric field, therefore increase the electric conductivity. Since, in a high salinity solution, the increased ionic pressure in the adsorbed layers increases the viscosity of the electrolyte and decreases the mobility of ions (Keller and Frischknecht, 1966), the effect of this added conductivity is greater in a rock saturated with a dilute solution than one with a high salinity solution.

A similar effect takes place with water molecules, which are polar. When an electrolyte is in contact with a negatively charged rock surface, the water molecules will become adsorbed to the surface in such a way that the positive hydrogen atom side is closer to the surface than the negative oxygen atom side. The conductivity of water in this systematically oriented phase is higher than that of free water (Keller and Frischknecht, 1966). The thickness of the oriented adsorbed water molecule layer will be greater in a rock saturated with a dilute solution than one with highly saline solution, since the abundant cations, in a high salinity solution, adsorbed to the surface earlier than the water molecules due to their charges being stronger than those of water molecules, will neutralize the rock surface to some extent.

#### APPLICATION

The resistivity of a rock formation decreases with increase of temperature so that it is possible to map a geothermal area by resistivity observations. Moreover, it is very interesting and important to note that the actual temperature of the thermally anomalous underground can be determined by the resistivity values measured at the surface.

Utilizing eq. 4, the following formula which explicitly gives the temperature of the geothermal reservoir is easily deduced:

$$t_h = t_c + \frac{1}{\alpha} \left( \frac{\rho_c}{\rho_h} - 1 \right) \quad (6)$$

where  $t_h$  and  $\rho_h$  are, respectively, the temperature and resistivity of the hot portion of the earth, that is, geothermal reservoir;  $t_c$  and  $\rho_c$  are, respectively, the temperature, which is around 15°C, and the resistivity of the cold portion of the earth; and  $\alpha$  is the temperature coefficient of resistivity of the ground water in the area under question.  $\rho_c$  and  $\rho_h$  are calculated from resistivity field survey data and  $\alpha$  is determined by laboratory measurements. In applying

eq. 6 to the

Eq. 4 from  
temperatu  
than boili  
in order to  
is the high  
eq. 6 is fou  
formulated  
at high ten  
from 17°C  
from 17°C  
calculation  
observation  
which are i  
calculation  
ture coeffi  
The use of  
study area  
Whenever c  
for individ  
of the outc  
the pertine

The effe  
corroborat  
reported a  
"Electrical  
results of h  
country is  
the mean v  
A value of  
and cold w

Another  
McNitt (19  
have been v  
electrically  
voirs, are o  
is successfu  
fault block,  
well as the  
reservoir."

A word c  
in either lat  
to anomalo  
provinces a  
different te

eq. 6 to the geothermal problems, however, the following should be considered.

Eq. 4 from which eq. 6 was derived has been established only for the temperatures ranging from slightly higher than freezing point to slightly lower than boiling point of the water. Therefore laboratory examination is necessary in order to determine whether eq. 6 is valid at temperatures up to 388°C, which is the highest reported reservoir temperature (Mercado, 1969), or higher. If eq. 6 is found to be invalid at higher temperatures, a new function should be formulated. However, eq. 6 agrees reasonably well with the observations made at high temperatures. Breusse (McNitt, 1965) has reported that ground heated from 17°C to 150°C decreased in resistivity by a factor of 5, and if heated from 17°C to 280°C, its resistivity decreased by a factor of 9. Meanwhile, the calculations by eq. 6 for the same temperature increments as those in Breusse's observations yield resistivity decrements of 4.33 and 7.58 times, respectively, which are in rather good agreement with those measured by Breusse. In this calculation, 0.025/°C was used for  $\alpha$ . This is the average value of the temperature coefficient of resistivity of ground water (Keller and Frischknecht, 1966). The use of the particular value of  $\alpha$  measured of the samples from the Breusse's study area could bring the resistivity changes closer to Breusse's observations. Whenever desired, the exact value of the temperature coefficient of resistivity for individual geothermal areas may be obtained by laboratory measurements of the outcrop of the water, that is, hot spring or body of water derived from the pertinent geothermal area.

The effectiveness of the resistivity method in geothermal areas is also corroborated by the results of other successful workers. Studt (1958) has reported a successful resistivity survey in Kawerau, New Zealand. He wrote: "Electrical surveying extended the hot water zone", and further described the results of his observation: "The best contrast between hot and cold water country is recorded with an electrode separation of 100 feet; at this spacing, the mean values in hot and cold country were 60 and 600  $\Omega$ m respectively. A value of 150  $\Omega$ m may be taken as an approximate dividing line between hot and cold water."

Another example of a successful resistivity survey has been described by McNitt (1965): "Electric resistivity surveys, in conjunction with gravity surveys, have been very helpful in locating major faults in the Italian steam fields. The electrically resistant anhydrite and carbonate rocks, which are the steam reservoirs, are overlain by an impermeable, conductive shale. The resistivity method is successful because the thickness of the shale cover is characteristic of earth fault block, so that the resistivity survey shows the position of the faults as well as the comparative thickness of the shale, and therefore the depth to the reservoir."

A word of warning is appropriate at this point. Lower resistivity of an area, in either lateral or vertical sense, than in the surroundings, can be attributed to anomalously high temperature only where both the high and low resistivity provinces are geologically or geoelectrically the same or similar except for their different temperatures. The problem of differentiation between various causes

UNIVERSITY OF UTAH LIBRARIES

of the low resistivity should be solvable by incorporating the resistivity data with geologic, geochemical and other geophysical findings of the area. An excellent example of non-thermal province with lower resistivity than the adjacent geothermal reservoir is provided in the report by Zohdy and others (1973), where geothermal reservoir of about 30  $\Omega$ m is bounded by non-thermal lacustrine deposits with resistivity of 10–12  $\Omega$ m.

It should also be admitted here that the above examples are only some of successful results of reported investigations carried out under somewhat favorable conditions. However, it is, in the main, the aim of this paper to present the theoretical capability of the determination of the true temperature of the geothermal reservoirs. It is only a matter of improving our technique in order for us to be able to utilize the theory not only under favorable conditions but also under many unfavorable conditions as well. We have witnessed that only theoretically possible things turned out to be reality, as our techniques advance, in other disciplines of geophysics in our time.

#### CONCLUSION

The electrical resistivity method has been very useful in exploration of geothermal fields. The resistivity method is effective not only for estimating the amount of geothermal fluid but also for determining the true temperature of the thermal fluid reservoirs and in that point this method is unique.

#### ACKNOWLEDGEMENTS

This study was initiated as a term project in a course at Southern Methodist University, taught by Dr. David D. Blackwell. I wish to thank the reviewers of this manuscript, whose names are unknown to me, for their constructive criticisms and very valuable suggestions. I also would like to thank Mr. Francis J. (Buck) Buckmeier and Dr. Donald F. Saunders of Texas Instruments Inc., who kindly made available many informative materials during the revision stage of this paper.

#### REFERENCES

- Archie, G.E., 1942. The electrical resistivity log as an aid in determining some reservoir characteristics. AIME Tech. Publ., 1422: 1–8.
- Armstead, H.C.H., Gorhan, H.L. and Müller, H., 1974. Systematic approach to geothermal development. *Geothermics*, 3: 41–52.
- Glasstone, S., 1937. *The Electrochemistry of Solutions*. Methuen, London, 2nd ed., 551 pp.
- Grim, R.E., 1968. *Clay Mineralogy*. McGraw-Hill, New York, N.Y., 2nd ed., 596 pp.
- Kaufman, A., 1970. The economics of geothermal power in the United States. *Geothermics*, Spec. Issue 2, 2(1): 967–973.
- Keller, G.V., 1953. Effect of wettability on the electrical resistivity of sand. *Oil and Gas J.*, 51: 62–65.
- Keller, G.V., 1970. Induction methods in prospecting for hot water. *Geothermics*, Spec. Issue 2, 2(1): 318–332.

Keller, G.V. a  
Pergamon,  
McNitt, J.R.,  
Heat Flow  
Mercado, S.,  
Soc. Am. I  
Milazzo, G., 1  
Pirson, S.J., 1  
pp.  
Studt, F.E., 1  
Geophys.,  
Ward, S.H., an  
Mining Ge  
Winsauer, W.C  
saturat(d) s  
Zohdy, A.A. I  
induce(d)-p  
1130-114

- Miller, G.V. and Frischknecht, F.C., 1966. *Electrical Methods in Geophysical Prospecting*. Pergamon, London, 517 pp.
- Nitt, J.R., 1965. Review of geothermal resources. In: W.H.K. Lee (Editor), *Terrestrial Heat Flow*. AGU, Geophys., Monogr., 8: 240-266.
- Mercado, S., 1969. Chemical changes in geothermal well M-20, Cerro Prieto, Mexico. *Geol. Soc. Am. Bull.*, 80: 2623-2629.
- Mazzo, G., 1963. *Electrochemistry*. Elsevier, Amsterdam, 708 pp.
- Masson, S.J., 1958. *Oil Reservoir Engineering*. McGraw-Hill, New York, N.Y., 2nd ed., 735 pp.
- Studdt, F.E., 1958. Geophysical reconnaissance in Kawerau, New Zealand. *N.Z.J. Geol. Geophys.*, 1: 219-246.
- Ward, S.H. and Fraser, D.C., 1967. Conduction of electricity in rocks. *Soc. Explor. Geophys. Mining Geophys.*, 2: 197-223.
- Winsauer, W.O., Shearin, H.M., Masson, P.H. and Williams, M., 1952. Resistivity of brine-saturated sands in relation to pore geometry. *Am. Assoc. Pet. Geol. Bull.*, 36: 253-257.
- Labdy, A.A.R., Anderson, L.A. and Muffler, L.J.P., 1973. Resistivity, self-potential, and induced-polarization surveys of a vapor-dominated geothermal system. *Geophysics*, 38: 1130-1144.



SUBJ  
GTHM  
TTG

in *Bulletin Volcanologique*  
Vol XXVII, 1964  
Napoli, Italy

## Theory and Technology of a Geothermal Field

GIANCARLO FACCA and FRANCO TONANI

### Introduction

The problems related with the development of a geothermal field from a theoretical as well as a practical point of view have only been studied on limited scale. In this paper we have the intention to study one point of particular importance: the rules, which control the evaporation of water in the formation, due to the difference between the formation pressure and the pressure in the well. Some of the results of this theoretic study can immediately find useful application in the exploitation technique and in the choice of well locations: other considerations will on the contrary require to be controlled by measurements and observations in wells and fields, observations, which have hitherto not yet been carried out and which could be of great importance for the development of geothermal fields.

### Relation between temperature, depth and pressure Definition of a field

#### 1. *Example of a Geothermal Field producing Overheated Steam.*

In previous papers (Lit. 7, 8) we have exposed, among other things, the geological conditions of a geothermal field producing overheated steam. In summary an example of a geothermal field (fig. 1) is composed of:

a) A deep sequence of layers, heated by an underlying magmatic stock and which in its turn heats the overlying porous strata. This is called the *heat-source*.

For example, the heat-source in a geothermal field is the complex of rocks of limited permeability, through which the heat, generated by the magmatic stock, is transmitted to the producing strata.

J. Geophys. Research 57,  
m. Monthly notices Roy.  
geol. Mijnbouw. Genoot.  
Bull. Seism. Soc. Am. 30,  
Bull. Seismol. Soc. Am.  
er core. Monthly Notices  
hypothesis. ibid. 6, 50-59  
l, New York, 1940.  
y. J. Geophys. Research  
e. Trans. Am. Geophys  
Am. 48, 301-314 (1958 b).  
k (1959).  
3, 183-240 (1956).  
56).  
s, Teil I, 17, (1939-1946).  
high pressures and the  
34 (1954).  
z und seine Entstehung  
56 (1941).  
0, 689-696 (1942).  
kosität und Relaxations  
itung von Longitudinal  
Phys. Chem. 202, 124-160  
inem homogenen Erdin  
340 (B. Gutenberg Ed.)  
Union, 18, 123-124 (1937).  
D. FERRY, *Viscoelastic*  
otices Roy. Astron Soc.  
lag Stuttgart (1960).  
n of the C-layer within  
30 (1958).

The fundamental factor, which determines the industrial value of a geothermal field is the heat-flux coming from the heat-source, as defined above.

b) A strongly permeable layer with thickness, porosity and permeability of such an order as to allow the formation and the permanence of a system of convection currents in the water filling the pores of the rock. This layer is called the *reservoir*.

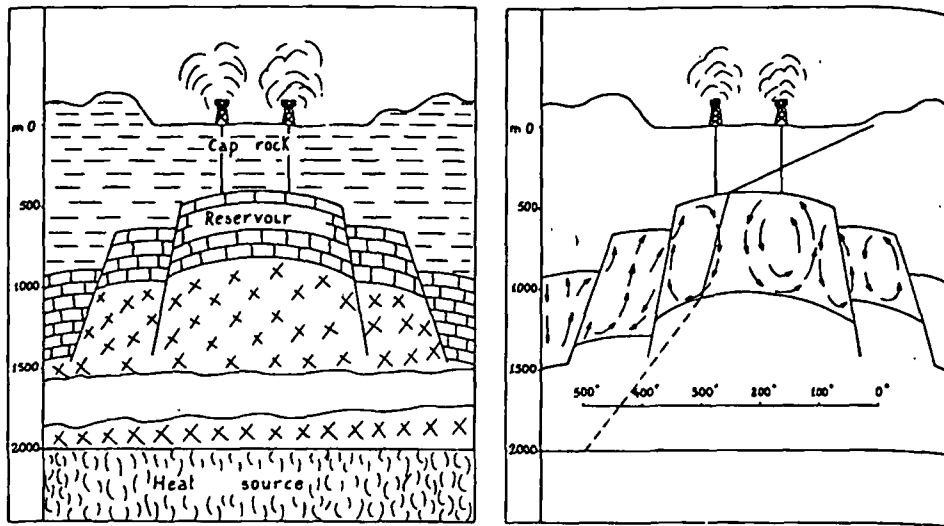


Fig. 1 - Scheme of a geothermal field.

c) An impermeable stratum, the *caprock*, overlying the reservoir. The permeability of this layer has to be low in order to prevent the escape of the hot water out of the reservoir, as a consequence of the currents, which bring the hot water as high as possible.

In the example, briefly sketched above, we recognize easily the fundamental relations, which exist between the three basic conditions for a geothermal field and the conditions required for a field of economic interest.

The heat, transmitted by the heat-source, can only be exploited if it is contained in a fluid, which can be produced at the surface in sufficient quantity to generate energy: the quantity of fluid produced has therefore always to be considered in relation with the energy

contained in t  
lutely necessa  
we will see be  
when we consi  
phase, i.e. the  
from the pro  
commercial va  
temperature. I  
wells has the  
the heat produ  
transformed in  
the difference  
chines.

## 2. Thermal F

We have to  
regulate the ter  
there is a therm

The heat-fl  
by the differenc  
of the stratum.  
heat, the lower

In an imp  
which applies th

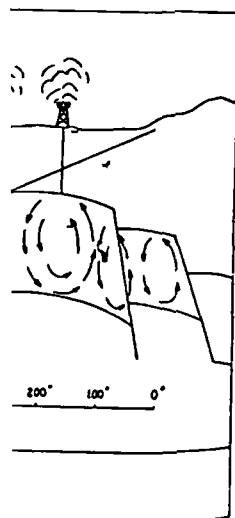
in which  $Q$  is th  
and upper surfac  
the material, the

In a produci  
already more con  
in two ways: by  
the formation wa  
conduction is low  
is high in beds  
amounts of steam

When conduc

the industrial value  
of the heat-source,

porosity and permeability  
and the permeability  
filling the pores



ing the reservoir.  
to prevent the  
consequence of  
ossible.

gnize easily the  
basic conditions  
for a field of

ly be exploited  
the surface in  
fluid produced  
with the energy

contained in the fluid and is always considerable. It is therefore absolutely necessary that the producing horizon has great permeability: we will see below that this condition becomes even more imperative, when we consider the phenomena which occur during the exploitation phase, i.e. the process which takes place when the hot fluid enters from the producing formation into a well. It is obvious that the commercial value of the fluid encountered in wells increases with the temperature. It is therefore important that the fluid produced in these wells has the highest possible temperature. In fact, the fraction of the heat produced, which can be utilized, i.e. which can be effectively transformed into energy, for example in a turbine, is proportional to the difference in temperature at the inlet and the outlet of such machines.

## 2. Thermal Flux and Temperature of Formation Water.

We have to study at this point what the conditions are, which regulate the temperature of the fluid in a permeable medium, where there is a thermal flux, due to heating from below.

The heat-flow through a layer of rocks is very generally defined by the difference in temperature between the lower and upper surfaces of the stratum. The better a stratum transmits a given amount of heat, the lower is this difference in temperature at top and bottom.

In an impermeable medium there is thermal conduction, to which applies the law of FOURIER:

$$Q = K (T_2 - T_1)$$

in which  $Q$  is the heat-flow,  $T_2$  and  $T_1$  the temperatures of the lower and upper surfaces of the stratum and  $K$  the characteristic factor of the material, the so-called thermal conductivity factor.

In a producing horizon, which is therefore permeable, things are already more complicated, as the heat is transmitted simultaneously in two ways: by conduction through the rocks and by convection in the formation water. The capacity of the rocks to transmit heat by conduction is low, whereas the capacity to transmit heat by convection is high in beds with sufficient permeability to furnish commercial amounts of steam.

When conduction prevails, as occurs in impermeable strata, the

temperature distribution is very simple, i.e. proportional with the depth (fig. 2).

When on the contrary convection prevails, things are more complicated. This problem has been treated satisfactorily by GOGUEL (Lit. 10), at least from a geological point of view. This author has studied the movements provoked in formation waters by heat, and

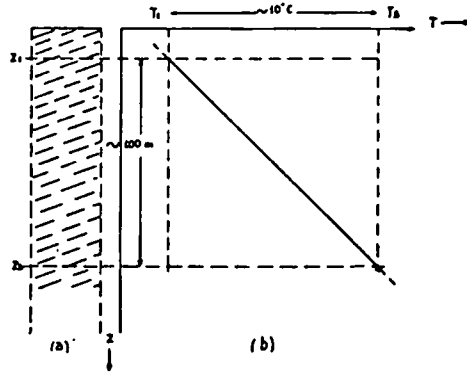


Fig. 2 - Temperature distribution in an impermeable layer heated from below. The law of FOURIER gives the simplest temperature distribution. In the interval under consideration the temperature is conditioned by the depth. It shows an ideal example in which these conditions are present: an impermeable layer (a) through which passes a heat-flow and in which there is a temperature distribution as indicated in the diagram (b). The numerical data of this example are:

thermal conductivity (clay)	= 0.0025 cal × sec <sup>-1</sup> ×
	× cm <sup>-1</sup> × degree <sup>-1</sup>
thermal gradient 1° C each 10 m	= 0.001 degree × cm <sup>-1</sup>
heat flow	= 0.0000025 cal × sec <sup>-1</sup> ×
	× cm <sup>-2</sup>

the conditions required for the formation of convection currents. We will not enter into the details of this process as we accept as a whole the results of GOGUEL. We will limit ourselves to the important consequences of these principles in the distribution of temperature in a permeable stratum.

We therefore include above all in our fig. 3 a) some elements of GOGUEL's work, and particularly the flow lines for the sections of an indefinite cylindrical convection cell. The straight lines  $T_1$  and  $T_2$  represent two isotherms of the static regime, not perturbed by convection.

In fig. 3  
figured as th

T<sub>1</sub>

T<sub>2</sub>

Fig.

the movemen  
general the r

Fig.

The mos  
not to requi  
 $T_1$  and  $T_2$ , a

In fig. 3b) the isotherms corresponding with fig. 3a) have been figured as they result in this particular case from the equation of

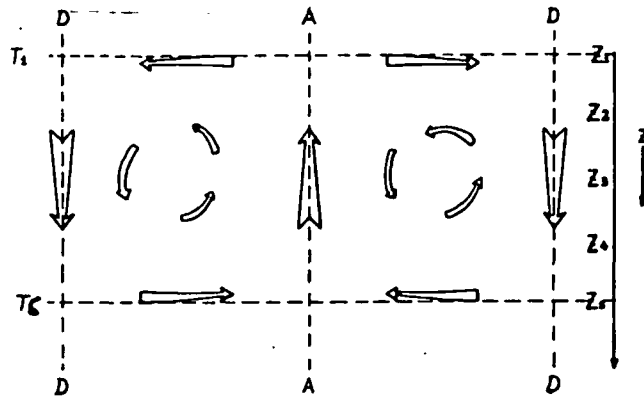


Fig. 3 a - Convection currents lines in section of an indefinite cylindrical convection cell.  
A - Area of upward currents. D - Area of downward currents.  $Z_1, Z_2, \dots$ : depth.  $T_1, \dots, T_5$ : temperature.

the movement and the distribution of the temperature anomalies. In general the non-perturbed isothermal surfaces can be not planes.

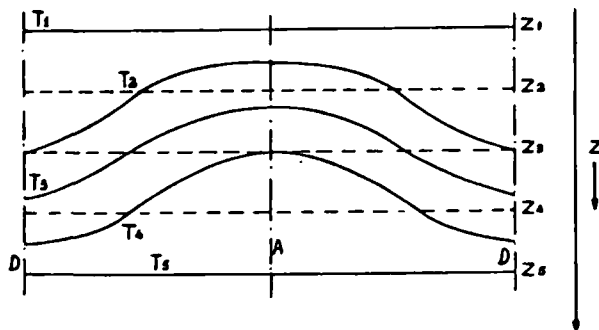


Fig. 3 b - Isotherms corresponding with the conditions in A), for a particular case ( $\Delta t = a \sin x$ )  
 $\Delta t$  = the thermal anomaly of a static regime.  
 $T_1, T_2, \dots$  = isotherms corresponding with depth.  
 $Z_1, Z_2, \dots$  = in the here considered static regime.

The most important consequence for us is sufficiently evident not to require more explanation. We can define two temperatures,  $T_1$  and  $T_2$ , at the base and at the top of the permeable stratum (in

proportional with the things are more com- isatisfactorily by GOGUEL view. This author has waters by heat, and

le layer heated simplest tem- r consideration eph. It shows is are present: passes a heat- re distribution ical data of

al  $\times \text{sec}^{-1} \times$   $\times \text{degree}^{-1}$   $\text{gree} \times \text{cm}^{-1}$   $\text{cal} \times \text{sec}^{-1} \times$

onvection currents. ss as we accept as ves to the important ion of temperature

3 a) some elements es for the sections raight lines  $T_1$  and not perturbed by

the worst case: two average temperatures) and we can therefore refer to a temperature gradient (average) in the permeable stratum, affected by convection currents.

In reality no indefinite cylindrical convection cells are formed. For our purpose we can approximately accept the validity of the sections in fig. 3. For a homogeneous medium, heated from below,

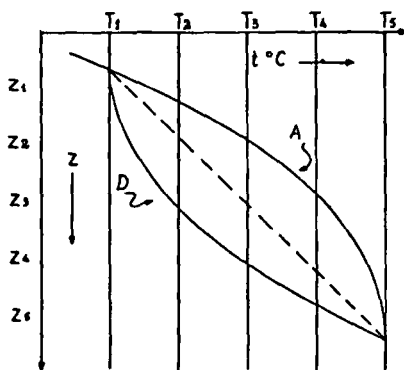


Fig. 3 c - Temperature-depth diagram for areas affected by the convection currents of Fig. 3 a. A = the curve for an area with upward currents. D = the curve for an area with downward currents. Dotted line indicates the average corresponding with the equivalent law of FOURIER.

the convection cells present themselves as in fig. 4. In real geologic cases, the horizontal thermal gradients and the distribution of permeability will have a decisive influence on the geometry of the convection phenomena and the result is qualitatively indicated in fig. 5 and 6.

Convection is a very efficient mechanism for the transport of heat, as, due to the convection, the hottest part of the fluid is brought into contact with the coolest surface of the stratum and the coolest part of the formation fluid is brought in contact with the hottest surface of the reservoir. Furthermore this movement is continuous, so that the formation fluid is continuously renewed, the difference in temperature maintained and the transmission coefficient of the heat at the contact of the fluid and the solid rock is better as the fluid is in movement. The difference in average temperature of the hot and the cool sides of the stratum changes little when the heat-flow from below increases, once convection currents are established. This system as a whole behaves as if it had a much greater thermal con-

ductivity, si  
but the res  
more intens



Fig. 4 - Disposit  
cells, w  
2 = do



Fig. 5 - Dispositi  
onal fiss

we can therefore refer to the permeable stratum, affected

convection cells are formed. Not the validity of the law, heated from below,



is affected by the shape of the curve for an area. The curve for an area indicates the average law of FOURIER.

fig. 4. In real geologic conditions the distribution of permeability and the geometry of the convection cells are as indicated in fig. 5

For the transport of heat, the fluid is brought up from the stratum and the coolest fluid is in contact with the hottest part of the stratum. This contact is continuous, so that the difference in temperature is reduced. As a result, the coefficient of the heat conduction is better as the fluid temperature of the hot part is higher when the heat-flow is established. This leads to a greater thermal con-

ductivity, since this greater apparent thermal conductivity is nothing but the result of fluid circulation, a stronger heat-flow will cause a more intense circulation.

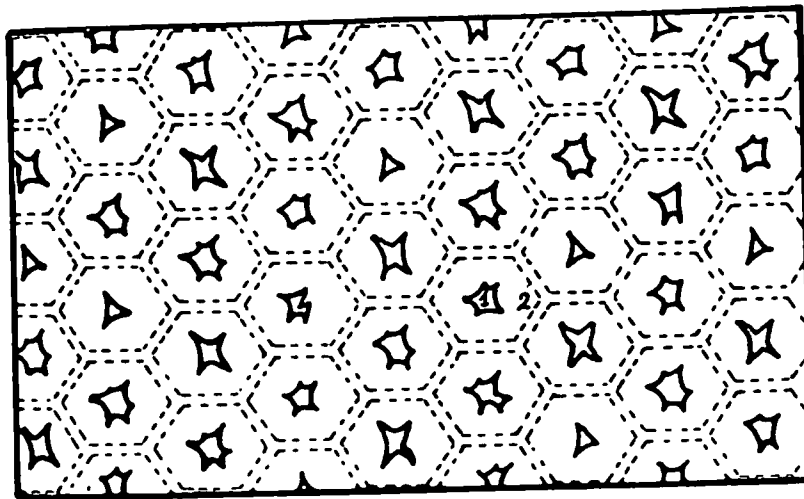


Fig. 4 - Disposition of the convection cells in planimetric projection. Subhexagonal cells, which are established in a homogeneous medium. 1 = upward current; 2 = downward currents.

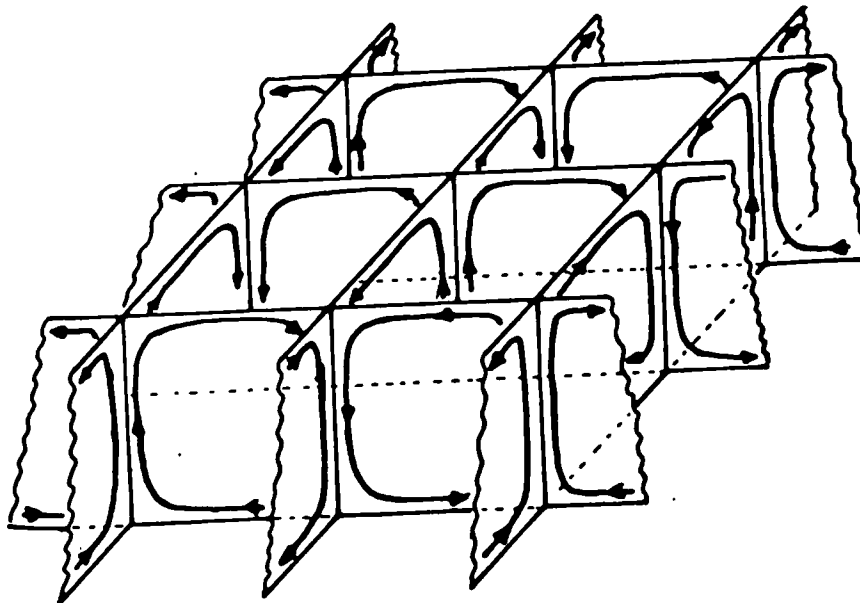


Fig. 5 - Disposition of convection cells in perspective in the case of a system of orthogonal fissures.

But GOGUEL has demonstrated that the higher the permeability is, the lower the thermal gradient; sufficient to pass from a static regime to convection currents and the higher the flow in these currents. It seems evident, therefore, that the smaller the average thermal gradient, the higher is the permeability, all other conditions being equal and especially under the influence of a given heat-flow.

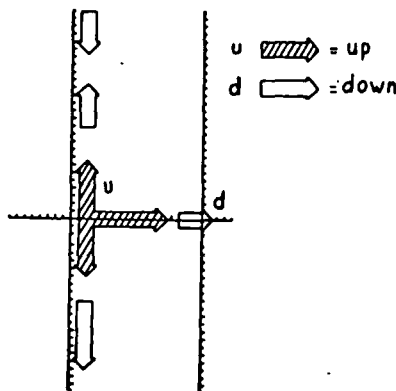


Fig. 6 - Convection cells in a layer with non-uniform permeability. The rock is fractured and the permeability is larger along the fault planes. Convection currents are established in the zones with higher permeability.

It is possible that the permeable layer as a whole is poorly pervious to heat, due to the thermal resistance between the circulating fluid and the rocks.

The result, however, is identical to the one produced by the presence of poorly heat-conductive rocks at the top of the reservoir. The average thermal gradient remains low in the permeable beds, whereas the average formation fluid temperature increases.

We can take as an example a heavily fractured and cavernous formation; practically a true « boiler », in which the resistance to movement is reduced to the resistance due to the internal friction of the fluid. The average thermal gradient is negligible. To make the example more evident we will consider an initial, non-permanent state (fig. 7), i.e. during the long process that ended with the formation of the convection currents. The heat-flow from the heat-source to the reservoir increases the temperature of the fluids in the reservoir, and therefore the difference in temperature between the reservoir and

the caprock. A  
from the heat-  
ervoir to the ca  
remains small,  
convection cur

Fig. 7 -

Figure 8 is in  
place in a molt

The air car  
also with mode  
convection diss  
transmits the h

This is a ve  
conduction or c  
tribution.

In summary  
and therefore th  
heat transmissi  
the average the



permeability from a static flow in these or the average other conditions given heat-flow.

the caprock. A stationary situation is attained when the heat-flow from the heat-source to the reservoir equals the flow from the reservoir to the caprock. The thermal gradient in the reservoir, however, remains small, because the efficiency of the heat transmission by convection currents in the formation fluid does not diminish.

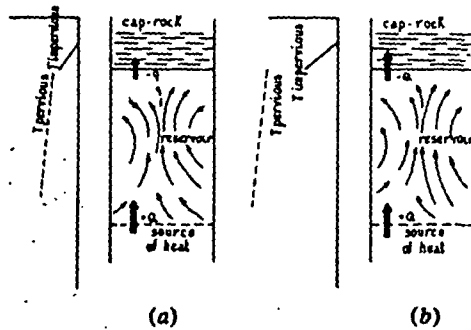


Fig. 7 - Effect of the convection. The heat-flow from below, i.e. from the heat-source, provokes convection currents in the water contained in the permeable layer (reservoir). Temperature differences in the reservoir are small. The caprock is impermeable and therefore cannot be affected by convection currents: the temperature gradient is much more inclined. In (a), initial, non-permanent stage ( $-q$  is the outgoing heat-flow, much less than  $Q$ , the incoming flow). In (b), stationary stage: the heat-flow from the heat-source to the reservoir is equal to the flow from the reservoir to the caprock ( $-Q$ , the outgoing heat-flow is equal to  $+Q$ , the incoming heat flow) because the average difference between the temperature of the fluid and the temperature of the rock is increased.

Figure 8 indicates schematically how heat transmission takes place in a molten lava lake covered by a solidified lava crust.

The air can dissipate large quantities of heat from one surface, also with moderate temperature differences. The air in movement by convection dissipates the heat rapidly, whereas the solidified lava crust transmits the heat in a much less efficient way by conduction.

This is a very clear example of the role which layers, where heat conduction or convection prevail, play in determining temperature distribution.

In summary, if the local temperature anomalies are not considered and therefore things are considered on a large scale, also in case of heat transmission by convection the thermal flow is proportional to the average thermal gradient, when all other conditions are equal.

Very generally one can say that a law of the type of FOURIER's law will be roughly applicable. The transmission coefficient of heat in this case should be approximately constant. In reality it depends from the temperature and furthermore changes abruptly passing from one regime to the other. In regions where a regime of convection currents is established, the heat transmission coefficient is higher and therefore for a given heat-flow there is a lower thermal gradient; and vice-versa for a given thermal gradient there is a higher heat-flow.

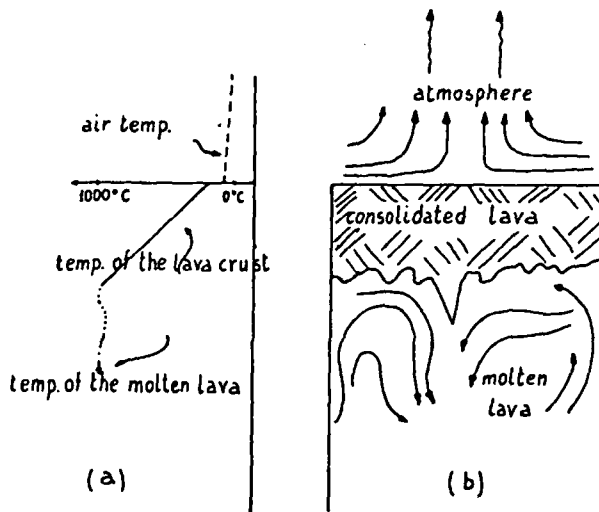


Fig. 8 - Heat transport in a lake of molten lava on which floats a crust of solid lava. In (a), a temperature diagram: in (b), geological section. The air can dissipate large amounts of heat on one side, even with a small temperature difference. Therefore the surface of the lava is cold with few meters of solidified lava. The moving air has a convection coefficient many times larger than the convection coefficient of solid lava and its average temperature is practically uniform (it is understood that the adiabatic gradient is neglected).

### 3. The Concept of Trap for Convection Currents.

In a geothermal field of the type taken by us for example, the caprock reduces the dispersion of heat at the surface and therefore is an essential condition for the increase in temperature of the water in the reservoir. In fact, if the water, affected by convection currents, can reach the surface, where it is exposed only to the atmospheric pressure, it cannot pass the temperature corresponding with the boiling point at atmospheric pressure, i.e. around 100° C. The system reservoir-caprock therefore constitutes a trap for convection currents. One

easily remain  
the caprock  
mulation un  
poorly perme  
energy by d  
(fig. 9-10).

Fig. 9 - Two  
the  
of the  
vect  
is ch  
whe  
impe  
uous  
thol

Let us  
of the ty  
steam bu  
slow con  
highest p  
different  
temperat

We  
permeabi  
reach the  
condition  
replenis  
the press  
wells wo  
Ther

of FOURIER's law is of heat in this case depends from the temperature gradient. Convection currents are higher and therefore the temperature gradient is lower; and vice-versa for conduction.



ts a crust of solid lava. The air can dissipate the temperature difference. Layers of solidified lava are larger than the convection currents (which are neglected).

s for example, the surface and therefore the temperature of the water. Convection currents on the atmospheric side are higher and therefore the temperature gradient is lower; and vice-versa for conduction.

... easily remarks the analogy with what happens in an oil-trap, where the caprock stops the upward movement of the oil and causes accumulation under pressure. In a similar way, in a geothermal field the poorly permeable caprock interrupts the transmission of the thermal energy by convection, a process much more efficient than conduction (fig. 9-10).

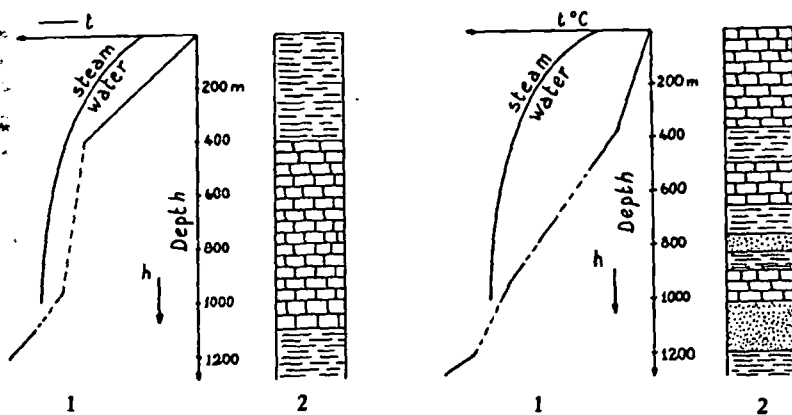


Fig. 9 - Two hypothetical examples of temperature-depth diagrams. This goes out from the hypothesis that the gradient is essentially controlled by the permeability of the rocks and that in porous rocks there are conditions which provoke convection currents in the water contained in the permeable and porous beds. It is clear that the temperature gradient in the permeable producing horizon, where there are convection currents (dotted lines) is low, whereas in the impermeable caprock, where the heat is transmitted by conduction (continuous lines), the gradient is higher. 1 = Temperature-depth diagram; 2 = Lithology.

Let us consider now the thermal conditions of a geothermal field of the type of our example (fig. 1). The reservoir does not contain steam but water of meteoric origin in liquid phase. This water is in slow conventional movement. The temperatures of the water at the highest point of the reservoir and at the bottom are only slightly different because of the convection currents, which lower the average temperature gradient.

We will presume that the reservoir has a lateral continuity of permeability and porosity and that the rocks forming the reservoir reach the surface at a point outside the geothermal field. If this latter conditions would not be fulfilled, the hydraulic pressure and the replenishing of the water could not be maintained and therefore the pressure in the producing horizon would rapidly decline and the wells would be depleted in short time.

Therefore there is the necessity for a closure of the reservoir,

similar to the closure of a structure of an oilfield. As shown in fig. 11, the closure of a structure is the difference in elevation between the highest and the lowest point of the contact between reservoir and caprock.

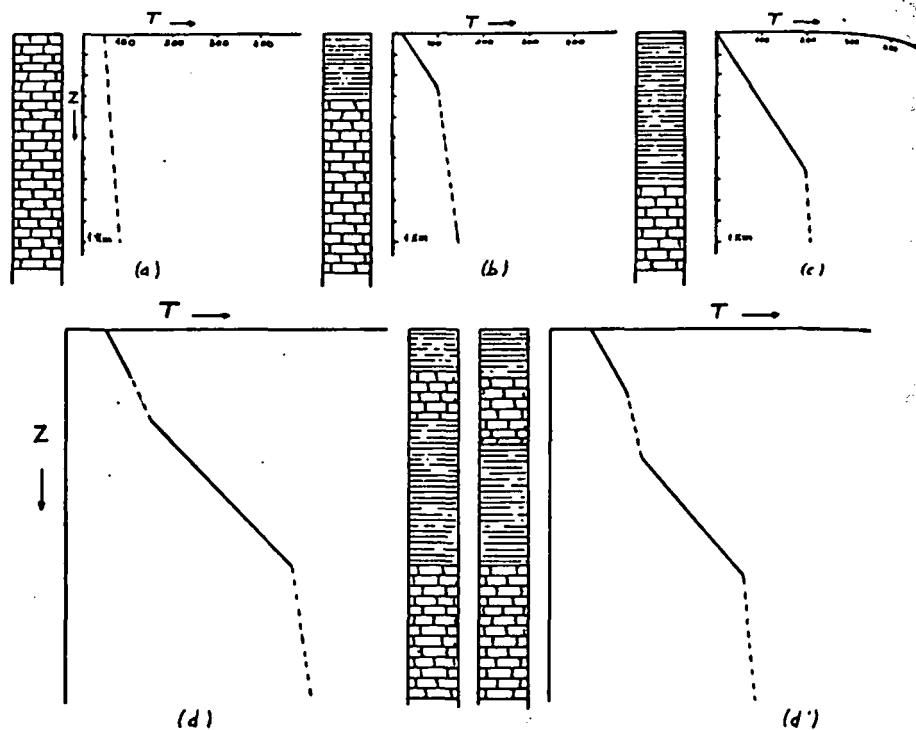


Fig. 10 - Temperature distribution in a permeable layer in relation to the caprock (schematic).

a) There is no caprock and the permeable layer is on the surface: the average temperature has a tendency to approach 100° C or anyway the boiling temperature of the water on the surface.

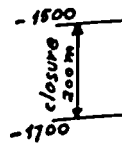
b) and c) The gradient in the caprock is a function of the geothermal flow. For a given flow and a given gradient in the caprock, the temperature in the reservoir is higher if the thickness of the caprock is greater.

d) The caprock contains an intercalation of permeable rocks of a thickness not sufficient to form convection currents: the variation of the gradient in this layer is minimal.

d') The caprock contains an intercalation of permeable rocks sufficiently thick for the formation of convection currents: the temperature-depth curve straightens in the permeable intercalation.

We have already pointed out that the similarity of oil-traps and traps for geothermal convection currents—should not let us forget the evident differences which exist between these two cases. We

limit course  
for a trap



(A)



(B)

Fig. 11 - The  
betw

A) T  
flank

B) T  
thro  
beds

horizontal  
it is necess  
the top an

limit ourselves to remind for example that the geological conditions for a trap for convection currents can also be realized when there is a reservoir and

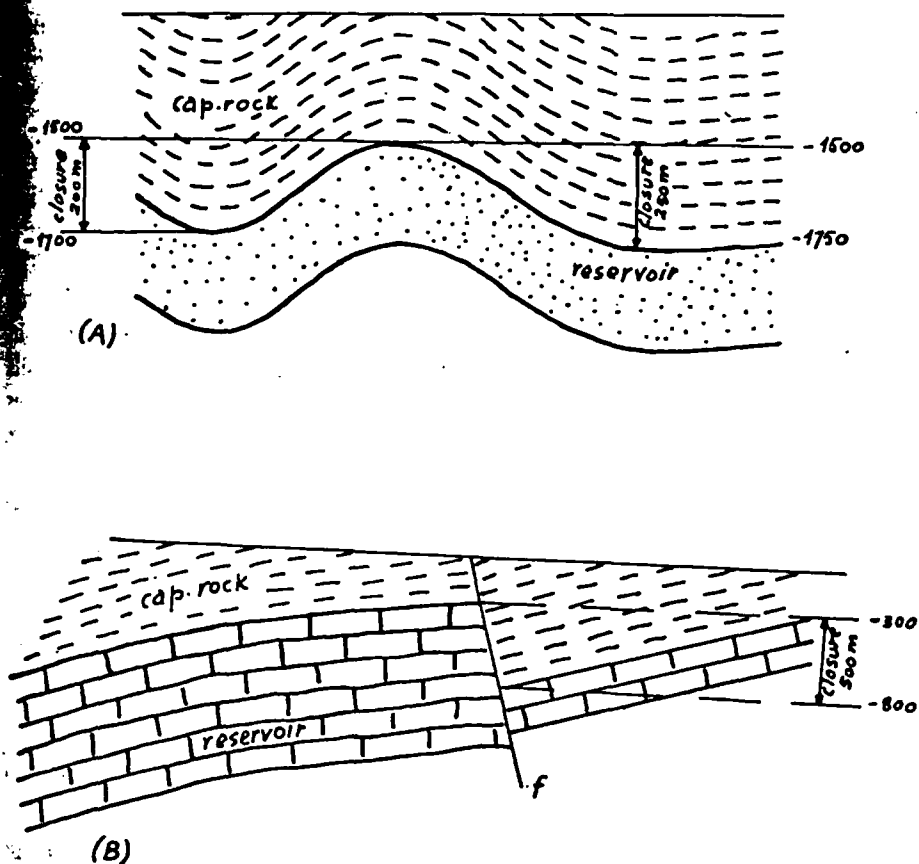


Fig. 11 - The concept « closure » in an oiltrap. Closure is the difference in elevation between the top and the lowest point of the reservoir.

A) The trap is formed by an anticline: the closure is different on the two flanks.

B) The trap is conditioned by a fault. The effective closure is given by the throw of the fault, measured by the difference in elevation of the limestone beds at both sides of the fault.

oil-traps and let us forget two cases. We horizontal caprock, which is not the case for oil-traps. In other words, it is necessary that the reservoir has a porosity high, limited towards the top and laterally by the caprock.

#### 4. *The Temperature of the Formation Fluid and the Depth. The Factors BTD and BPD.*

We have admitted that the water in the reservoir is in liquid phase and that the convection currents have the tendency to equalize the temperature in the reservoir; we can conclude that the water in the reservoir can not pass the boiling point corresponding to the hydraulic pressure at the highest point of the reservoir. For example, if the highest point of the reservoir is at 500 m depth and if the hydrostatic head has to be taken from the surface, the formation pressure at the highest point of the reservoir is 50 kg/cm<sup>2</sup>. For such a pressure and for distilled water the boiling point is 263° C. The water temperature cannot pass this figure, which can be considered practically the maximum temperature at every point of the reservoir. The formation water is generally fairly rich in mineral salts and boils at slightly higher temperatures. These minor differences can however be neglected, as they are smaller than the thermal gradient we have neglected in this way.

From this it is clear that this temperature is approximately the temperature of the entire reservoir, also at the base or on the flanks of the structure.

Hence, in the zones of the trap, where the reservoir-caprock contact is at greater depth, we have higher pressure, whereas the temperature will only be slightly higher—always under geometric conditions of the porosity of the type indicated in our example.

Previously we had considered the top of the geothermal trap, assuming a depth of 500 m. Let us now consider another point of the same trap, but on its flanks, for example where the reservoir-caprock contact is at a 1000 m depth. There the pressure is of the order of 100 kg/cm<sup>2</sup>, corresponding with a boiling point of 310° C. The water temperature, however, is the same or nearly the same on the flanks as well as on the top. While therefore at the top of the trap the water is near to its boiling point, it is considerably below the boiling point on the flanks. If in our example at the top, at 500 m depth, the water temperature reaches the limit of 263° C and is at its boiling point, at 1000 m the water temperature is 47° C under the boiling point.

We define as « *boiling temperature distance* » (BTD) at a given point in the reservoir, the difference between the temperature of the formation fluid and the boiling point, corresponding with the for-

mation press  
example, as 1

In the fo  
as it princip  
duction. This  
face from th  
occurs the f  
which the st

Fig.

A simila  
back to our  
a temperatur  
at 1000 m de  
cm<sup>2</sup>, the BP  
water at 263

The two  
and iso-BPD  
productive a

In orde

and the Depth. The

formation pressure at the point under consideration. In our previous example, as mentioned before, the BTD at 100 m depth is 47° C.

In the following we will see that this factor is of great importance, as it principally conditions the possibility of overheated steam production. This factor also controls the distance of the evaporation surface from the well and therefore the extension of the zone in which occurs the precipitation of salts, resulting in incrustations, and in which the steam may separate from the water.

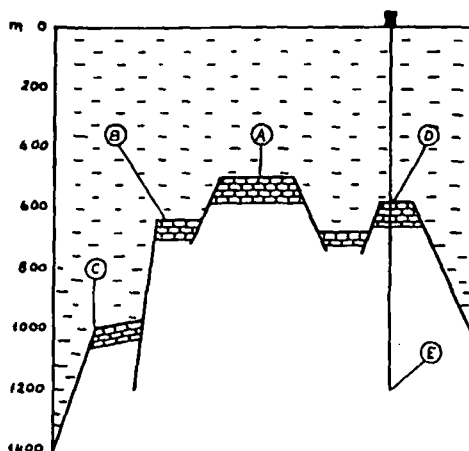


Fig. 12 - The factors BTD and BPD. A geothermal field is defined by the temperature of the hot water producible by a permeable reservoir; the water temperature is nearly equal in all points of the reservoir of the same pool. In the highest point of a reservoir the temperature and pressure conditions are the most favorable, because they are nearest the boiling point. The remainder is explained in the text where the conditions in the points A, B, C, D and E are indicated.

A similar factor is the « boiling pressure distance » (BPD). Going back to our example, at 500 m depth at the top of the reservoir with a temperature of 263° C (i.e. at boiling point), the BPD is zero, whereas at 1000 m depth, with the same temperature and a pressure of 100 kg/cm<sup>2</sup>, the BPD is 100 — 50 = 50 kg/cm<sup>2</sup>, as the boiling pressure of water at 263° C is 50 kg/cm<sup>2</sup>.

The two factors allow us to build maps figuring curves of iso-BTD and iso-BPD, which are very useful in delimiting the commercially productive area of a field, as will be shown more in detail below.

In order to clarify these concepts let us study in fig. 12 the

reservoir is in liquid  
e tendency to equalize  
clude that the water in  
corresponding to the  
reservoir. For example,  
0 m depth and if the  
surface, the formation  
is 50 kg/cm<sup>2</sup>. For such  
g point is 263° C. The  
hich can be considered  
point of the reservoir:  
mineral salts and boils  
differences can however  
ermal gradient we have

re is approximately the  
e base or on the flanks

e the reservoir-caprock  
pressure, whereas the  
ys under geometric con-  
in our example.

of the geothermal trap,  
nsider another point of  
le where the reservoir-  
e the pressure is of the  
boiling point of 310° C.

e or nearly the same on  
efore at the top of the  
it is considerably below  
mple at the top, at 500 m  
it of 263° C and is at its  
ture is 47° C under the

ance » (BTD) at a given  
n the temperature of the  
esponding with the for

conditions of the water at various points of one and the same pool, i.e. of a productive reservoir without impermeability barriers and therefore containing water of approximately the same temperature in all its points.

For simplicity we accept that the hydrostatic head corresponds with the depth.

The water temperature is approximately the same throughout but the pressure varies with depth. Let us consider the conditions in points A, B, C, D and E; the first four are on the reservoir-caprock contact, whereas E is at greater depth in the producing horizon.

We can assume a water temperature of 250° C, i.e. slightly below the boiling temperature corresponding with the pressure at the highest point of the reservoir (A in our figure). Being at a depth of 500 m it has a hydrostatic head of 50 kg/cm<sup>2</sup>.

The following table indicates the factors **BTD** and **BPD** at the various points under consideration:

	A	B	C	D	E
Depth in m	500	640	1000	580	1200
Pressure in kg/cm <sup>2</sup>	50	64	100	58	120
Temperature in °C	250	250	250	250	250
Boiling temperature in °C	262,7	278,5	309,5	272	323,1
BTD in °C	12,7	28,5	59,5	22	73,1
BPD in kg/cm <sup>2</sup>	10	24	60	18	80

As we will see more clearly below, the best production conditions for steam from hot water by means of wells are present when the two factors are smallest, i.e. when the water is near its boiling point.

Confronting the conditions at D and E, it is clear that there is no advantage whatsoever to put a well on production at a depth far below the reservoir-caprock contact.

Given the practical importance of these factors for the exploitation of a geothermal field, the maps allowing the understanding of a geothermal field and therefore its rational production are:

- a) Contour map of the reservoir-caprock contact;
- b) Isotherm maps at various depths in the caprock.
- c) Iso-BTD and iso-BPD maps at the top of the reservoir.

5. Defini

After  
with conti  
concept of  
system of  
temperatur  
equal for

It see  
top of the  
water at th  
ature of t  
when the

There  
the heat-fl  
ature is v  
mation pr

Follow  
erations, v  
ature, in  
well, this  
and we h  
horizons

We re  
able to b  
the Larde  
correspon

The r  
the reserv  
which co  
and the A  
water, wh  
Flysch, n  
hot water  
springs d  
wells. It  
tap the s

The  
with tem



### 3. Definition of a Field.

After what has been said about the temperature in a reservoir with continuity of porosity and permeability, we can now define the concept of a geothermal field. A geothermal field is constituted by a system of convection cells and its temperature is given by the average temperature of the formation water, a temperature which is essentially equal for all points of the reservoir.

It seems important to repeat here that the temperature at the top of the reservoir cannot be higher than the boiling point of the water at the corresponding pressure, and therefore the average temperature of the water in a reservoir is never far from this value, also when the wells produce dry steam.

Therefore a field is defined by the formation temperature. If the heat-flow from the source of heat is sufficiently high, this temperature is very near to the boiling point, corresponding with the formation pressure at the top of the reservoir.

Following the preceding definition based on our previous considerations, when there are substantial differences in formation temperature, in various wells or in various porous horizons in the same well, this means that there are several producing horizons or pools and we have to suppose that in general each of these producing horizons is separated from the other by an impermeable barrier.

We refer here schematically to an example, which we have been able to build up from data furnished to us by the technical staff of the Larderello Company. Figure 13 is purely schematic and does not correspond with the actual situation, but facilitates the understanding.

The rocks of the Anhydritic series, which at Larderello constitute the reservoir, are outcropping on a hill and are surrounded by Flysch, which constitutes the caprock. At the contact between the Flysch and the Anhydritic series, there were at a time springs with boiling water, which have formed a considerable deposit of travertine. In the Flysch, near the contact, some wells were drilled, which have yielded hot water of the same temperature as the hot springs. The hot springs dried up with the starting production of hot water in the wells. It is evident that these wells (indicated with A in our figure) tap the same pool as the hot springs.

The C wells of our figure are large producers of overheated steam with temperatures around 230° C. Also the B well has given a similar

and the same pool, stability barriers and same temperature in

head corresponds

same throughout, or the conditions in the reservoir-caprock producing horizon.

, i.e. slightly below pressure at the highest a depth of 500 m

D and BPD at the

	D	E
	580	1200
	58	120
	250	250
,5	272	323,1
,5	22	73,1
	18	80

duction conditions present when the its boiling point. clear that there is on at a depth far

s for the exploit- understanding of ction are:

tact; .  
aprock.  
ie reservoir.

result: evidently the C and B wells produce from the same pool and between B and A there is a permeability barrier (indicated by x), probably due to a deposition of silica or limestone, precipitated on the fissures from the hot water of the superficial manifestations.

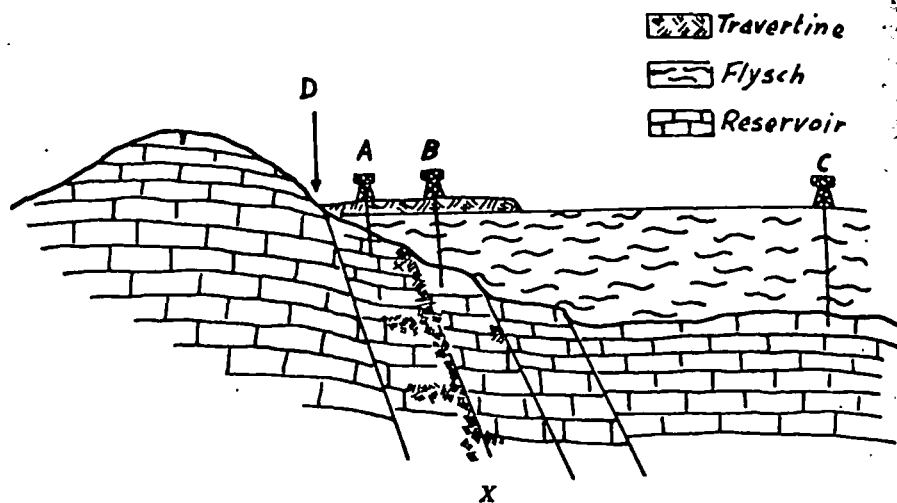


Fig. 13 - Two different pools separated by an impermeable barrier due to incrustations. Explanation in the text. A - Wells with hot water. D - Hot water spring. B, C - Wells which produce superheated steam. X-X - Impermeability barrier. Dotted: travertine.

## 6. Consequences for Exploration.

The previously exposed theories allow us to give a rational basis to geothermal exploration, in particular they allow us to establish the stratigraphic and structural objectives. In fact the existence of a geothermal field is conditioned by a reservoir with good permeability protected by a caprock; the geometry of the reservoir-caprock contact has to be such as to constitute a trap for convection currents. It has to be added here that also the depth of the reservoir is an important element, as the formation pressure is depending of it, which in its turn controls the thermal characteristics of the formation water. It is in particular of great importance to know the depth of the highest point of the reservoir, as from this depth we can calculate the pressure at this point and thus the maximum possible temperature of the water in the reservoir.

This way we can outline the various phases of geothermal explo

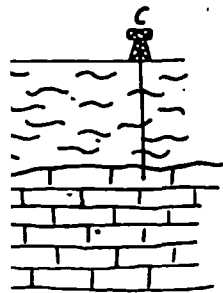
ration: re  
definite s  
rents.  
Let u

a) I

In  
with Qu  
indicate  
actual s  
shallow  
necessa  
geologic

the same pool and indicated by x), precipitated on the manifestations.

- Travertine
- Flysch
- Reservoir



rier due to incrusta  
Hot water springs  
permeability barrier.

a rational basis  
us to establish  
the existence of a  
good permeability  
caprock contact  
currents. It has  
is an important  
it, which in its  
formation water. It  
th of the highest  
calculate the pres-  
temperature of  
geothermal explo

ation: reconnaissance of a hyperthermal area, individualization of a definite stratigraphic objective, search for a trap for convection currents.

Let us examine briefly each of these phases.

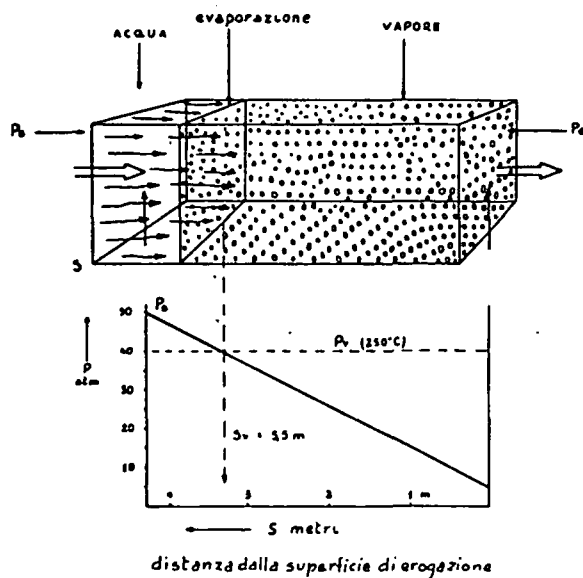


Fig. 14 - Evaporation in a stream tube. Steady state. The movement of the fluid is indicated by arrows and takes place from the water carrier at formation pressure towards the well.

$P_s$  = pressure of formation water.

$P_v$  = boiling pressure of water at 250° C.

$S_v$  = diameter of the evaporation sphere in meters from the well.

$S$  = distance of the well in meters.

#### a) Reconnaissance of Hyperthermal Areas.

In general the areas with active or recent volcanism and those with Quaternary or Pliocene volcanic activity are most appropriately indicated for the exploration of hyperthermal zones. In fact in the actual stage of our knowledge it seems fairly sure that only a relatively shallow magmatic stock can furnish the impressive quantity of heat, necessary for the existence of a commercial geothermal field. Other geological phenomena which could have generated some heat, as

friction on faults, radioactivity and certain chemical reactions taking place in the subsurface, do not give a sufficiently important flow of heat.

It should however be emphasized that the geothermal science and even volcanology are still in their childhood and that our knowledge is still very limited. Although we must today dedicate most of our attention to the volcanic areas, we can not prejudicate the future and exclude that there are geothermal possibilities outside the volcanic zones.

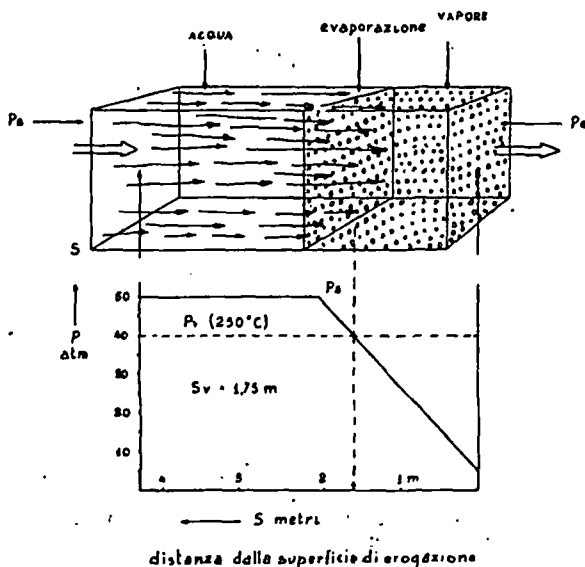


Fig. 15 - As Fig. 14 but with a smaller diameter of the well.

It is nearly superfluous to say that with volcanic regions we do not mean the zones where volcanoes actually rise above the surface; volcanic activity is a normal geological event and generally affects wide zones with multiple manifestations, only a part of which can be observed by us.

Many submarine or subsurface volcanic phenomena entirely escape our attention and in general we can not predict the birth of a new volcano.

We also remain unaware of the rise in the upper part of the earth's crust of certain magmatic stocks, which have not sufficient

energy t  
necessar  
As d  
can exist  
The near  
age and  
however  
Campani  
As v

consider  
petrolet  
tentially  
It s  
or recei  
have to  
regions  
expecte  
limited  
tant pr  
Ge

chemical reactions taking  
 an important flow of

geothermal science and  
 that our knowledge  
 dedicate most of our  
 to indicate the future and  
 outside the volcanic



energy to generate a volcano, whereas they can furnish the heat  
 necessary for a geothermal field.

As demonstrated by the example of Larderello, a geothermal field  
 can exist at a considerable distance of active or extinct volcanoes.  
 The nearest volcano to Larderello is the Monte Amiata, of Pliocene  
 age and at a distance of approximately 70 km. The zone of Larderello  
 however falls in the large volcanic zone of Tuscany, Latium and  
 Campania.

As we have pointed out elsewhere, geothermal exploration has to

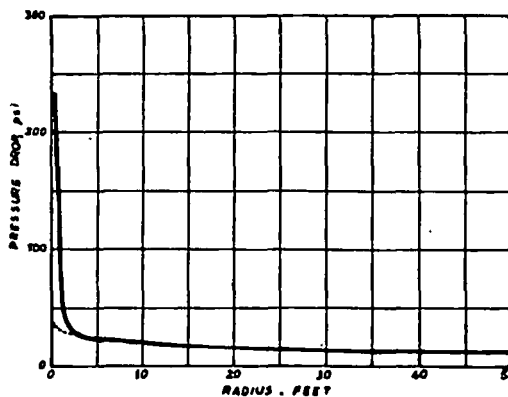


Fig. 16 - Distribution of pressure around an oilwell. Production  
 10,000 BOPD.  
 Full line : pressure drop in a fissure of 1 mm diameter.  
 Dotted line: producing horizon with a permeability of  
 1 darcy, thickness 87 m, holesize 6 inches (after W. J.  
 BAKER).

of the well.

volcanic regions we do  
 above the surface;  
 and generally affects  
 a part of which can  
 phenomena entirely escape  
 the birth of a new  
 upper part of the  
 have not sufficient

consider the volcanic zones as specially indicated. In a similar way  
 petroleum exploration considers the large sedimentary basins as po-  
 tentially most favorable.

It should be mentioned here, that besides the regions with active  
 or recent volcanism and at least including the Pliocene volcanism, we  
 have to think also about the potentially volcanic zones, i.e. those  
 regions, where in a geologically near future volcanic activity can be  
 expected. As mentioned above, our knowledge in this field is rather  
 limited but we may hope that the volcanology will accomplish impor-  
 tant progress in this direction.

Generally speaking, hyperthermal areas present more or less nu-

merous surface manifestations of heat, as e.g. hot springs, travertine deposits, silicified zones and hydrothermal mineral deposits.

The importance of these manifestations is obvious and it is not necessary to emphasize them. It should be mentioned however, that these indications have to be interpreted to their right value. Their value should not be underestimated nor exaggerated.

In fact, surface indications of heat-flow are not a sufficient reason for locating a test-well: they merely give indications of regional hyperthermality.

They are evidently connected with a more than normal heat-flow, but they do not as such prove the existence of a geothermal field of commercial interest.

Surface indications are frequently located at the contact of an impermeable series and a permeable sequence. The potential reservoir reaches the surface or is at shallow depth and thus cannot contain water at high temperature, because it is only under low pressure.

A geochemical and isotopic investigation of the surface indications of heat-flow appears more and more important. Without these data a correct interpretation of a surface manifestation is not possible. In many cases the geochemical history of the deeper waters can be pieced together from the surface indications; also the thermal history of the water can be outlined. Valuable data can also be collected for the exploitation, as a chemical study of the waters allows us to have a first idea of their incrustating properties.

This is not the place to discuss this important argument. We will merely emphasize that a geochemical study of the fluids contained in the surface manifestations of heat-flow constitutes a necessary part of any geothermal exploration program.

During the last few years the importance of « geothermal wells » has come clearly to the foreground. With this expression, not too well chosen and which we would prefer to substitute by « gradient wells », are meant shallow holes drilled with the purpose of measuring the thermal gradient of an area.

The depth recommended by us is 80 meters; others retain that 30 meters are sufficient.

We will not enter into the details as the present paper has another aim. The utility of the survey of the thermal gradient is quite evident; if it is possible to determine a zone with an interesting gradient, as e.g. 2°-5° C each 10 meters, one is certain to be in front of a zone with good geothermal possibilities. Also in this case, however, this

indication  
ularly nec  
depth and  
act as a g  
The g  
for a rati  
delimiting  
with seism  
method of

b) The

After I  
to define a  
in the loca  
bility and  
the establi  
this forma  
to be adequ  
mation wa  
reservoir n  
can howeve

High j  
reservoir:  
high in ord  
that the p  
order that  
see below.

The pe  
permeabili  
excellent r

In the  
tance, whe

c) The

Once 1  
the structu  
currents. A  
contact bet

indication is not sufficient. Other data have to be added: it is particularly necessary to have data concerning the stratigraphic series, the depth and the structure of the strata of the local series, which could act as a good reservoir.

The gradient wells, as the surface indications, are not sufficient for a rational test-well location. They are however very useful in delimiting the area to be investigated by other methods and specially with seismic methods. The low cost of these gradient wells makes this method of investigation apt to wide-spread application.

#### b) *The Stratigraphic Objective.*

After having detected a hyperthermal zone it becomes necessary to define a stratigraphic objective. It is therefore necessary to indicate in the local stratigraphic series a formation with sufficient permeability and thickness for commercial geothermal production and for the establishment of convection currents in the water contained in this formation. The reservoir must furthermore offer the possibility to be adequately refurnished in meteoric water, in order that the formation water will not be exhausted by production in short time. The reservoir must finally be protected by an impermeable layer, which can however be of limited thickness, as *e.g.* at Wairakei.

High permeability is the most important characteristic of the reservoir: not only in fact it is important that the permeability is high in order that convection currents can occur. It is also necessary that the pressure drop around the bottom of the well is great, in order that the evaporation space is as large as possible, as we will see below.

The permeability due to fracture is in general higher than primary permeability; any dense rock, also with poor porosity, can become an excellent reservoir rock if it has a high fracture permeability.

In the geothermal field, in fact, porosity is not of great importance, whereas a high permeability is essential.

#### c) *The Structural Objective.*

Once the stratigraphic objective is defined we must determine the structural conditions which can constitute a trap for convection currents. As we have already seen, such a trap is present when the contact between the reservoir and the caprock is disposed in such a

way as to prevent the convection currents to reach the topographic surface. This condition is most effectively realized, when the reservoir-caprock contact is concave towards the base as in horsts, anticlines and other positive structures (faulted monoclines, buried hills etc). The geometric similarity with oil-traps is evident as at the other hand the dissimilarities: e.g. a commercial geothermal field cannot exist where the reservoir is represented by lenses of sand surrounded entirely by shale.

Let us also remember that in contrast with oil-traps, even the horizontal disposition of the reservoir-caprock contact can constitute an efficient trap for convection currents.

The important conclusion is that, to determine traps for convection currents, geothermal exploration has to call on the same methods as in petroleum exploration: in the first place a surface geological and a seismic survey. Anyway a rational exploration program has to be accurately studied for each particular case, in order to adapt the means of exploration to the stratigraphic series and the structure of the zone.

The exploration methods to be taken into consideration are geological and photogeological surveys, gravity surveys, magnetic, radioactivity, radio-sonde, seismic, electric, geochemical and gradient surveys, etc.

Whatever method is used, the purpose of these surveys is the individualization of a trap for convection currents and the determination of the depth of the top of the reservoir rock: in other words one of the most important purposes of these surveys is the compilation of a contour map of the reservoir in a zone, recognized as being hyperthermal.

#### d) *Faults in Geothermal Exploration.*

For a long time a quite different concept as guide for geothermal exploration prevailed. It was accepted then that the only sources of heat for a geothermal field were the juvenile waters, i.e. steam of magmatic origin, which was presumably separated from a cooling magmatic stock and which, as the name indicates, reached the surface of the earth for the first time. The formulation of this idea is due to LOTTI, who studied the Larderello field.

Consequently it was thought that a large system of open faults was needed, which would constitute a passage for the steam from the

magmatic reservoir  
nating in its  
first place a  
steam, produce

The hypothesis  
explanation of  
long time consi  
from hot water

Elsewhere  
the overheating  
secondary thermody  
erated by the  
to discuss this  
elsewhere and  
this problem.

We prefer  
explanation is  
important diff  
pressure. If the  
at formation te  
well flows stea

During pro  
sure to zones  
pressure at ea  
by one kg stea  
up-hole equals  
same kg of stea  
each section of  
not change dur  
the well-head.

This circula  
of overheating.  
the maximum  
enthalpy is suc  
we described  
overheating.

Furthermore  
the steam reac  
culated a veloc  
the rock aroun



magmatic reservoir to the productive horizon. This theory, so fascinating in its simplicity and so genial in its formulation gave in the first place a simple and direct explanation of the overheating of the steam, produced by the Larderello wells.

The hypothesis of LOTTI gave in fact a satisfactory geological explanation of this apparently mysterious fact and which was for a long time considered as incompatible with a direct origin of the steam from hot water in the sub-surface.

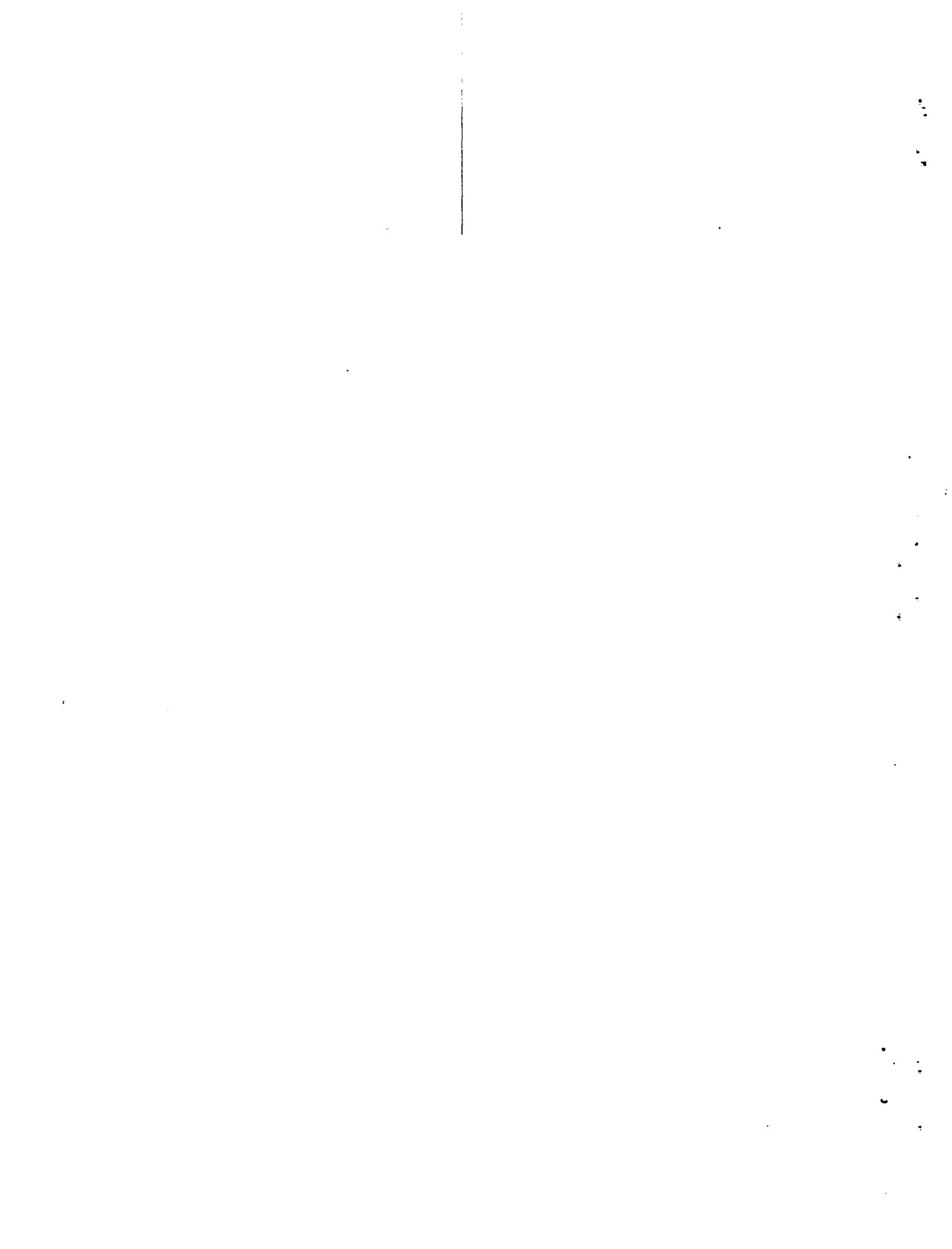
Elsewhere (Lit: 7,8) we have demonstrated that on the contrary the overheating of the geothermal steam is better justified on elementary thermodynamic considerations, admitting that the steam is generated by the boiling of hot subterranean waters. We do not want to discuss this point in detail here, because we have dealt with it elsewhere and also because we intend to dedicate a special study to this problem.

We prefer to illustrate the elementary principle on which the explanation is based. When a well is put on production there is an important difference in the formation pressure and the well-head pressure. If the latter is lower than the boiling pressure of the water at formation temperature the formation water starts boiling and the well flows steam.

During production the steam flows from a zone with high pressure to zones with lower pressures and thus expands. But if the pressure at each point does not change with time, the work spent by one kg steam in expansion against the steam at lower pressure up-hole equals the work which other steam down-hole spends to the same kg of steam, pushing it upward. As this condition is present in each section of the borehole, the enthalpy of one kg of steam does not change during its flow and its expansion from the reservoir to the well-head.

This circumstance alone is sufficient to explain a certain degree of overheating. In fact, the saturated steam at around 24 kg/cm has the maximum possible enthalpy for saturated steam and precisely its enthalpy is such that, if separated from the water, expanding the way we described it will give overheated steam in the right order of overheating.

Furthermore the steam acquires a high velocity: at Larderello the steam reaches supersonic velocities and already NASINI had calculated a velocity up to 500 m/sec at the well-head. The velocity in the rock around the well can be greater. If the steam is separated



from the water in these conditions, a simple slowing down in the borehole provokes overheating; but also if these conditions are not realized, there remains the fact that in the well the conditions for the passage of laminar movement to turbulent movement (REYNOLDS' number) are surpassed and therefore part of the kinetic energy is transformed into thermal energy and the steam is ultimately overheated.

If, in addition, the flow in the subsurface is sonic, many aspects of the problem change, but in each case there is overheating of the steam down-stream of the narrowest point.

Each of these phenomena, occurring after the separation of steam from water, produces such an increase in enthalpy per kg, sufficient to explain the production of overheated steam with the qualities of the Larderello and The Geysers steam.

The hypothesis outlined by us has two advantages over the one put forward by LOTTI and over other more or less similar ones. In the first place the hypothesis of formation water as geothermal fluid is geologically much simpler. Secondly it explains easily the moderate overheating which is observed in geothermal fields, whereas with the previous theories it remained unexplained how the observed enthalpy never surpasses a limit rather near the value of the maximum enthalpy of saturated steam and rather similar for the various known fields.

The theory of LOTTI was carried to its extreme consequences, when it came to establish the limit of the production possibilities of a field in relation to the dimensions of the area of open faults, carrying the steam. The reasoning was as follows: the channels feeding the steam have a certain section; if the wells altogether have tapped this section, one has reached the maximum limit of production, as the wells tap all the steam that can be furnished by the magmatic stock through the faults.

In 1955 for example the hasty conclusion was reached that the field, which then produced 1,9 billion kwh per year, could not have increased its production and that even probably there was going to be a slow decline.

This conclusion was justified by studying what was actually the mean production curve of the individual wells: in fact many wells showed a high initial production, followed at first by a rather rapid decline, after which the curve shows a rather flat line of a very slow decline. The validity of this curve of decline of a single well was extend-

ed over the fatal decline

Fortuna as in reality 1,9 billion k agree that t

This wa the first pla but meteoric ly. Secondly

crustation, therefore th the whole f

In the t Larderello f a general co the notion the bounda

In fact, from delimit the any serious theless a de

When discovered of Lardarel duction po ing zone.

Return that the s the steam horizon of as feeders faults can opment v the fact t therefore vection c strictly c porosity and perm

since ~~since~~ coming down in the  
so ~~in~~ conditions are not  
n the ~~well~~ conditions for  
rbu~~ment~~ (REYNOLDS'  
part ~~of~~ kinetic energy is  
the ~~heat~~ ultimately over-

urface ~~is~~ basic, many aspects  
e there ~~is~~ overheating of the  
oint.

after ~~the~~ separation of steam  
in ~~energy~~ per kg, sufficient  
steam ~~with~~ the qualities of

two ~~knowles~~ over the one  
ore. ~~It~~ similar ones. In  
on ~~with~~ geothermal fluid  
it ~~explains~~ easily the mod-  
geothermal fields, whereas  
explained ~~from~~ the observed  
at the ~~value~~ of the maximum  
mils ~~for~~ the various known

its ~~serious~~ consequences,  
production possibilities of  
the area of open faults, car-  
llows: ~~the~~ channels feeding  
wells ~~altogether~~ have tapped  
im ~~limit~~ of production, as  
urnished ~~by~~ the magmatic

sion was ~~reached~~ that the  
1 per year, could not have  
obably ~~there~~ was going to

ing what ~~was~~ actually the  
wells: in ~~fact~~ many wells  
at first by a rather rapid  
er flat ~~line~~ of a very slow  
of a single well was extend-

ed over the entire production of the field and the conclusion was its  
tial decline.

Fortunately the facts have very clearly disproved these arguments  
as in reality the production of the Larderello field has passed from  
19 billion kwh to 2,3 billion kwh (year 1961); today all technicians  
agree that the production of Larderello can easily be increased.

This way of thinking was erroneous from all points of view: in  
the first place the steam produced in the wells is not juvenile steam,  
but meteoric water at least for the greatest part and probably entire-  
ly. Secondly, the decline in production of a single well is due to in-  
crustation, which necessarily takes place at the bottom of a hole and  
therefore the curve of decline of a well cannot be extrapolated to  
the whole field.

In the third place finally, one had entirely forgotten to define the  
Larderello field as a concept nor from a practical point of view. As  
a general concept in fact, one had confused, though purely implicitly,  
the notion of geothermal field with producing area, forgetting that  
the boundaries of the producing area had not yet been determined.  
In fact, from the practical point of view no steps had been taken to  
delimit the field with dry holes and it was therefore impossible to have  
any serious idea concerning the extension of the production. Never-  
theless a decline of production was anticipated.

When wells were drilled outside the producing area, steam was  
discovered and continues to be found. Still today the geothermal field  
of Lardarello is not delimited and it is certain that the area with pro-  
duction possibilities extends considerably beyond the actually produc-  
ing zone.

Returning to the guiding concepts for exploration, we know now  
that the supposed deep faults are not the channels through which  
the steam is fed from the magmatic reservoir into the producing  
horizon of the wells. Therefore the criterium of the search for faults  
as feeders of the steam becomes obsolete; the individualization of the  
faults can however be of help for the location of testwells or devel-  
opment wells for entirely other motives and essentially because of  
the fact that in the fault zone the fracture permeability is higher and  
therefore there are better possibilities for the establishment of con-  
vection currents or for a more abundant production, as both are  
strictly connected with the permeability. Finally near the faults the  
porosity and permeability are higher as there is secondary porosity  
and permeability by fracturing. Consequently the choking of the wells

by incrustation is slower, under similar conditions, in the faulted zones.

*e) Depth of the Reservoir.*

In both the exploration and exploitation stages it is of the utmost importance to know the depth of the reservoir. We have in fact seen that the formation water cannot exceed the temperature of its boiling point at the pressure, corresponding with the highest point of the reservoir. For example, if the top of the trap is at 100 m depth and if at this point there is a normal hydrostatic pressure of 10 kg/cm<sup>2</sup> the temperature of the water cannot exceed 179° C and so on.

Therefore, if in a hyperthermal zone we have the contours of two different traps, of which one has its top at 100 m depth, and thus with formation water at a temperature not exceeding 179° C and the other with the top at 300 m depth, where the temperature of the formation water can reach 232,8° C, the second prospect will be preferred over the first.

In the second part of this paper we will deal with the conditions which rule the production of steam in geothermal fields; we will thus have the occasion to return more in detail to the relations between depth, temperature, pressure and type of production, also in respect to the incrustations, provoked by the passage of hot water from the liquid phase into steam. We will see that the depth of the payzone and the diameter of the well are important factors for the production of steam.

For these reasons, the most exact possible knowledge of the depth of the reservoir-caprock contact is of primary importance in geothermal exploration.

Naturally these data have also definite economic and technical importance; if for instance the geophysical surveys allow us to build a contour map of the reservoir-caprock contact it is possible to avoid drilling wells, where the reservoir is at too great a depth.

**Production of steam in wells**

We have on several occasions emphasized that the formation fluid of a geothermal field, producing overheated steam, is water near the boiling point corresponding with the pressure at the highest point of the reservoir.

We will now have to demonstrate and explain the rules according to which the hot water in the formation passes into dry, overheated steam at the well-head.

In the first place we are giving an analysis of the fluids collected at the well-head, followed by an attempt to discuss the geochemical meaning of these analyses.

### 1. Well-head Fluids.

The composition of the fluids produced by wells in the various geothermal fields varies largely from field to field, whereas it is constant for the wells, which produce from the same pool.

For the Larderello field there are the following analyses, furnished by the Larderello Company in a work by A. MAZZONI (1951).

steam	955,0 gr
CO <sub>2</sub>	42,5 gr
hydrocarbons and hydrogen	0,19 gr
H <sub>2</sub> S	0,88 gr
N <sub>2</sub>	0,16 gr
H <sub>3</sub> BO <sub>3</sub>	0,30 gr
NH <sub>3</sub>	0,30 gr
He, Ar, Ne	1 cubic cm

This analysis concerns a 1 kilo sample of fluid. The analysis of one cubic meter of fluid, without steam is as follows:

CO <sub>2</sub>	1 942,20
CH <sub>4</sub>	1 9,40
H <sub>2</sub>	1 17,90
H <sub>2</sub> S	1 25,00
N <sub>2</sub>	1 5,50
He, Ar, Ne	25 cub. cm.

These analytic data, which have been now repeated since many years, are not sufficient to give a clear picture of the steam of Larderello and of its variation. It seems that these analyses are averages;

anyway the samples were taken at well-head and not at bottom-hole and therefore give incomplete information.

It is said, although not supported by published analysis, that the percentage of  $H_3BO_3$  in the fluid is decreasing. A special study of this feature, based on a sufficient number of observations, could be of great interest and lead to important conclusions.

Also many thermal waters of Tuscany are boric. Nearly all these waters are sulphatic-calcic water, as many waters condensed by steam-jets.

A. J. ELLIS (6) has published numerous analyses of the waters in the geothermal wells at Wairakei and of the other New Zealand fields.

These analyses differ considerably from each other and ELLIS has separated three groups of water characterized by the following Na/K index: 1st group: below 9,6; 2nd group: between 9,6 and 10,0 and 3rd group: between 10,0 and 11,5.

Analyses of Wairakei waters in parts per million (ppm) (ELLIS 1961):

	1st group (well 26)	2nd group (well 27)	3rd group (well 28)
pH	8,2	8,5	8,4
Li	14,8	13,5	13,4
Na	1340	1300	1320
K	245	215	220
Rb	3,3	3,3	2,9
Cs	3,1	2,9	2,7
Ca	10	10	10
Mg	3	4	3
F	7,7	8,3	8,0
Cl	23,00	22,10	22,40
Br	5,8	6,1	5,2
I	—	0,6	0,6
SO <sub>4</sub>	—	31	34
HBO <sub>3</sub> total	122	112	115
SiO <sub>2</sub> total	—	690	660
As	4,5	4,8	4,7
NH <sub>3</sub> total	0,25	0,15	0,15
CO <sub>2</sub> total	15	23	31
H <sub>2</sub> S total	2	—	2

It is serves fu concentratio feeding c tion is n The 0,008 and gases gav

In th is mixed tion of tl

2. Geoc

Amo: gas is wi gaseous l of Monte but there was dow

It is not easy to understand these differences and the problem deserves further investigations. ELLIS believes that the differences in concentration are related to the distance between the well and the steam-feeding channels, identified as the faults in ignimbrite. But this assumption is not satisfactorily proved.

The Wairakei steam is mixed with a little gas varying between 0,008 and 0,07 (mole/100 mole of H<sub>2</sub>O). The analysis of the well-head gases gave by rounding off figures:

	%	range
CO <sub>2</sub> average	93	89-97
H <sub>2</sub> S	4	1-6
Hydrocarbons sat.	1	0,4-2
H <sub>2</sub>	1	0,1-2
N <sub>2</sub>	1	0,3-3

In the Geysers field (California) the steam produced by the wells is mixed with a small amount of gas (average 0,75%). The composition of the non-condensable gases at the Geysers is:

		% weight
CO <sub>2</sub>	88,73	
Hydrocarbons	5,49	
H <sub>2</sub>	0,74	
N <sub>2</sub>	1,29	
H <sub>2</sub> S	2,96	
NH <sub>4</sub>	0,79	
	<hr/>	
	100,00	

*Geochemical Significance of the Analysis.*

Among the non-condensable gases prevails carbon dioxide. This gas is wide-spread in nature and is found currently associated with gaseous gas hydrocarbons in natural gas fields. In the geothermal field of Monte Amiata the first wells gave large amounts of CO<sub>2</sub> and H<sub>2</sub>S, but thereafter the percentage of gas has rapidly decreased and in 1961 was down to 30%, according to oral communications.



In general the carbon dioxide found mixed with natural gas and steam can have a biologic, a metamorphic or a magmatic origin.

Carbon dioxide of biologic origin is formed in metabolic processes, which provide the necessary energy with the respiration and in other aerobic processes: the combustion of organic substances normally takes place at the cost of the oxygen of the atmosphere: in anaerobic processes the oxygen is derived from certain salts, e.g. the sulfates.

The carbon dioxide, thus formed, whether it enters directly into the atmosphere or, as occurs mostly, when it is formed in the subsurface, is dissolved in water in the form of carbonic acid and mainly as bicarbonates of sodium and calcium. The latter can precipitate as carbonate and thus liberate half of its carbon dioxide. It should be emphasized that the formation of carbon dioxide is generally accompanied by the formation of hydrocarbons and hydrogen at one side and of ammonia and H<sub>2</sub>S at the other side.

During these various processes carbon dioxide (and not only of biologic origin; but also the CO<sub>2</sub> coming directly from the atmosphere and dissolved in the hydrosphere) becomes fixed in the lithosphere, principally in the form of limestone. In the lithosphere the rock can be submitted to metamorphic processes, which liberate the carbon dioxide from the carbonates; this principally occurs as consequence of an increase in temperature.

The main chemical reactions produced by a rise in temperature are: 1) the formation of calcium silicates at the expense of the limestones; 2) the decomposition of the bicarbonates, dissolved in the waters and 3) the destruction of organic substances due to the effect of the heat.

It should be pointed out that the quantity of carbon dioxide, which can be formed, depends on the rise in temperature and not on the absolute value, when all other factors remain constant. It is thus clear that this is a process which can also take place at low temperature.

Magma contains dissolved carbon dioxide; in fact carbon dioxide has been found in gases which issue from lavas and it has experimentally been proved that carbon dioxide is soluble in silicate melts of which it lowers the viscosity. Furthermore carbon dioxide is found in the various stages of magmatic crystallization.— — —

As far as concerns the presence of carbon dioxide in natural

steam, this could be natural steam. But they will derive from the gaseous carbon dioxide which can be enriched in hydrogen.

Hydrogen manifestations during their cooling in hydrogen sulfide. The percentage of the water in hydrogen sulfide.

In the volcanic region (Kilauea) to 2% magmatic rocks are easily formed: water action



Furthermore, with sulphur, aerobic fermentation. At the other end or be oxidized.

From the magma in a natural gas during its magmatic

Hydrogen liberation with the

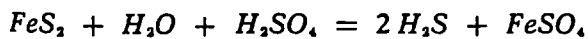
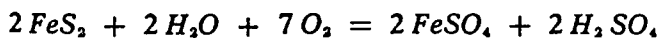
or with equivalent

It is well known that there are hydrogen in the contact with the rocks. At the

steam, this could be invoked to confirm the magmatic origin of natural steam. But in reality, as we have seen, carbon dioxide can very well derive from sedimentary series: this is particularly probable as the gaseous constituents are in general very mobile and therefore can be enriched in certain points and can mix with each other intimately.

**Hydrogen sulphide:** Hydrogen sulphide is common in thermal manifestations. In the volatiles of the magmas, which deposit during their cooling the metal sulphides and specially pyrite, the content of hydrogen sulphide must for this simple reason reach at least one percent of the water (19). This percentage is 20 times as much as the hydrogen sulphide percentage of the Larderello steam-jets.

In the volcanic gases, the available analyses gave from 12½ % (Kilauea) to 2% and 0,4% of  $H_2S$  in the gas dissolved in water of magmatic rocks due to heating. From the various sulphides  $H_2S$  is easily formed: for example during the alteration of sulphides due to water action there are formed hot sulphurous waters:

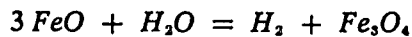


Furthermore, as already pointed out, the gaseous products of fermentation and generally of the decomposition of organic substance with sulphur contain  $H_2S$ ; the latter can be formed during the anaerobic fermentation by reduction of the sulphates.

At the other hand  $H_2S$  can be used in its turn to form sulphides or be oxydized to sulphuric acid and sulphur.

From these facts it is clear that the presence or absence of  $H_2S$  in a natural gas does not constitute a substantial indication concerning its magmatic or metamorphic origin.

**Hydrogen.** Hydrogen must be present in magmatic gases, in relation with the equilibrium:



with equivalent ones.

It is well understood how in magmatic gases issuing from lavas there are hydrogen, carbon oxide and methane capable to burn at the contact with the atmosphere. In fact iron oxide is always present in rocks. At the other hand, at temperatures, higher than those, which

favor the life of methane fermentation bacteria, sulphur bacteria etc. (i. e. over 50° C), there is the development of bacteria capable of producing hydrogen.

It is superfluous to point out that hydrogen is formed by distillation of organic material. Also the hydrogen of natural steam can therefore come from magmatic volatiles as well as from the sedimentary series; this way another argument supporting the magmatic origin of natural steam loses much of its value.

*Gaseous hydrocarbons.* It is known that small quantities of gaseous hydrocarbons have been observed in volcanic volatiles. Methane can be in equilibrium with hydrogen and carbon dioxide and thus be present in magmatic volatiles.

It is known however, that practically all hydrocarbons have an organic origin and are found in nearly all sedimentary series. There is therefore no difficulty whatsoever to explain the presence of methane in natural steam, as product of a magmatic process or rather as result of the decomposition of organic material during metamorphic modification, at low temperature, or finally as product of biological activity. We point out here that methane enters for 1/10.000 to 1/1000 in the non-condensable gas-fraction at Wairakei, whereas at Larderello it varies between 1/100 and 1/1000 and this would correspond with the difference in the sedimentary series in both areas.

*Nitrogen and ammonia.* The presence of nitrogen and its composites in the magmatic gas as such is doubtful and also little probable. It is however well known that nitrogen and its composites are a normal constituent of natural gas of biologic origin; furthermore nitrogen is the fundamental constituent of the atmosphere and is dissolved in surface waters. Ammonia is a normal product of the decomposition of organic material.

*Inert gases.* The emanation of radium, helium and argon 40 is formed as product of the radio-active decay of uranium and potassium. For this reason they are present in practically all natural gases. However, argon 40 as well as argon 36 in proportion 250 to 1 are among the most abundant constituents of the atmosphere (circa 1 %).

Argon dissolves in water approximately two times better than nitrogen. In fact, in water there is one part argon on every 35 parts of nitrogen, whereas in the air there is one part argon on every 78 parts of nitrogen. In Larderello, the proportion of argon in comparison with nitrogen varies between 1:50 in the oldest analyses and 1:300 in the more recent analyses.

In the old the same order the quantity of to a biological

We have accompany ge the presence o termine the or ture of gases a these constitue

We may p helium/radon tive chemical i can be derived their quantitati

*The isotop* Deuterium and cording to the i clear Studies of

We have ar lyses by Prof. C We know furtho tigation in the Pisa. We can ac his conviction

theoric origin and Tritium, as generated in the dioactivity tritium At present the d produced during

The half-life from recent pre tritium concentr

The waters c tent of less than this means that in view of the r period of over 40

In the older analyses the proportions of the two elements is of the same order as in the surface waters; in the more recent analyses the quantity of argon decreases in respect to nitrogen. This fact points to a biological origin of nitrogen.

We have considered one for one the non-condensable gases which accompany geothermal steam on the surface and we have seen that the presence of these gases does not offer a decisive argument to determine the origin of these constituents. The composition of the mixture of gases as a whole and specially the relation between some of these constituents, allow a more elaborate discussion.

We may point out that particularly the argon/nitrogen and the helium/radon ratios merit more attention also because of the relative chemical inertia of these gases. Even more important arguments can be derived from the presence of helium of certain isotopes and their quantitative ratios.

The isotopes, which can render useful information are Tritium, Deuterium and Oxygen 18 in the waters and Carbon 13 in the CO<sub>2</sub>, according to the investigations of S. KAUFMANN and W. B. LIBBY for Nuclear Studies of Chicago (1953).

We have analyses of Prof. LIBBY and interpretations of these analyses by Prof. G. BOATO (Lit. 16), who has communicated them to us. We know furthermore that Prof. TONGIORGI is continuing these investigations in the Laboratory of Nuclear Geology of the University of Pisa. We can add here that Prof. TONGIORGI has repeatedly expressed his conviction that the formation waters of Larderello are of meteoric origin and not juvenile.

Tritium, as an isotope of hydrogen with a mass 3, is continuously generated in the atmosphere by cosmic radiation. Because of its radioactivity tritium can be traced even in extremely small quantities. At present the distribution of Tritium has been altered by the Tritium produced during the nuclear tests.

The half-life of Tritium is around 12 years: the water coming from recent precipitation, as had been demonstrated by LIBBY had a Tritium concentration nearly constant all over the earth.

The waters of Larderello have experimentally given a tritium content of less than 0,4 U. T. which is the limit of measuring sensitivity; this means that the waters of Larderello are older than 40 years. But in view of the rather slow movement of water in the subsurface, a period of over 40 years can be easily required for the meteoric water

to penetrate from the outcrop zone of the productive series to the depth where it is reached by wells.

In the Wairakei wells, according to O'BRIEN and BAINBRIGGE (1961) tritium has been encountered and shows an activity of 0,5 T. U. against 2 to 3 T. U. for average surface water samples of the same area. These measurements indicate an age of less than 40 years for the formation water at Wairakei, i.e. of the order of 24 to 30 years.

Also oxygen 18 can give indications concerning the juvenile or meteoric origin of water and steam. For instance, the steam in a fumarole of the volcano Paracutin has shown considerable increase in oxygen 18 content.

The analyses of thermal waters of Lassen Park, The Geysers and Yellowstone have shown that they are of meteoric origin: the water of Larderello take in an intermediate position, according to BOATO and therefore it is not possible to come to a definite conclusion at the actual state of our knowledge. It seems however according to BOATO, that a completely juvenile origin of the steam is to be excluded. He concludes prudently that a larger number of analyses of steam of volcanic origin and of Larderello is required.

CRAIG, BOATO and WHITE (4) have studied the percentages of isotopes in many thermal waters, including those of the hot springs of New Zealand; Y. B. HULSTON (1961) has confirmed their conclusion for New Zealand, that less than 5 % of the formation water can be of magmatic origin.

We have tried to study the geochemical and geological significance of the helium/radon, of the nitrogen/argon/oxygen and helium/argon ratios; we do not repeat here the results of these studies as they would require too long a discussion. We are planning to publish these results and will limit ourselves here as to confirm that these do not furnish any proof for the juvenile origin of the steam.

### 3. *Non-Gaseous Constituents of Natural Steam.*

Natural steam also contains various constituents besides the non-condensable gases, hydrogen sulphide and carbon dioxide. The presence of non-gaseous constituents of the steam should be considered with much prudence. In practice it is not easy to distinguish between condense water and water mechanically carried up with the steam.

Up to the present there is no lack of examples which show that often the water which accompanies the steam is carried upward from

the payzone as such can case with the boric waters

$CaSO_4$  is culation in caozoic. Also the condense water of the sulphate. The fluorine has probably

It is there fluorine content temperature fluorides, fluoramaroles.

Also the salts contained field are an inc. It is symptomatic conditions, as e.g. abundant in t.

This is in not a proof the payzone or wises of the steam at Wairakei, steam. The pH acid and silica

Possibly t in reality not geochemical b and the rather steam, prevent the fumarolic

The same tially present tially of marine boric acid.

the payzone by the steam. Consequently the chemistry of the steam as such can be mis-interpreted. Certainly, for instance, this is the case with the  $\text{CaSO}_4$  contained in so-called condense water and in the boric waters of certain wells of the Larderello zone.

$\text{CaSO}_4$  is a usual constituent of the waters in Tuscany due to circulation in calcareo-dolomitic and anhydritic formations of the Mesozoic. Also the fluorine encountered in some analyses of these so-called condense waters, has to be attributed to the typical fluorine content of the sulphatic-calcitic waters, in view of its ratios and the  $\text{pH}$  value. The fluorine measured in the « fumaroles » of Larderello by GAUTIER has probably the same meaning.

It is therefore evident that the geochemical significance of such a fluorine content is entirely different from the fluorine content of high-temperature fumaroles, which is in the form of hydrofluoric acid, fluorides, fluoborates and fluosilicates in the sublimates of these fumaroles.

Also the sodium chloride, sodium hydrocarbonate and the other salts contained in this water carried by the wells of the Wairakei field are an indication of waters carried up mechanically by the steam. It is symptomatic that even constituents, volatile under certain conditions, as e.g. boric acid and silica, are nevertheless relatively more abundant in the waters than in the real steam.

This is in accordance with the  $\text{pH}$  of the solution but it is as such not a proof that we have to do with a solution carried up from the payzone or with a real condensation product. In the published analyses of the steam of test-wells and the water of the producing wells at Wairakei, fluorine seems relatively much more abundant in the steam. The  $\text{pH}$  of the water and the above described behaviour of boric acid and silica make us consider these data with perplexity.

Possibly the steam and water analyses which we considered are in reality not directly comparable. In consideration of the general geochemical behaviour of fluorine, the absence of hydrochloric acid and the rather amazing presence of hydrofluoric acid in the Wairakei steam, prevent us to consider the latter data as definite indication for the fumarolic or juvenile character of the Wairakei steam-jets.

The same applies, even more so, to boric acid, which is essentially present in the chlorinated waters. These are very probably essentially of marine origin and contain already an appreciable amount of boric acid.

It is not difficult to explain a 50 time increase in the  $H_2BO_3$  content in respect to  $NaCl$ , considering that the steam can have volatilized much of the boric acid and carried up a little water and that this mixture is collected in the separator at lower temperature, so that the liquid phase of the water has a much larger boric acid content.

#### 4. *Conclusion as to the Origin of the Steam.*

All chemical products, the presence of which in geothermal steam has been often indicated as a proof for its juvenile origin, are found in appreciable amounts in sedimentary formations.

Such chemical compounds have a high geochemical mobility at high temperatures. This explains the possibility of a high concentration due to a strong flux of heat, such as encountered in hyperthermal zones.

In conclusion there is no proof whatsoever for the direct magmatic origin of the fluids produced by geothermal wells. In some cases, as *e.g.* for Wairakei, we have proof that the steam and water produced by the wells are at least for 95 % of meteoric origin. For other cases, and in particular for Larderello, there is no geochemical proof whatsoever for a juvenile origin of the fluids, whereas there are many indications, though no definite proof, for an atmospheric origin of the water, which, penetrating from the surface into the reservoir rock at depth, is enriched by various chemical products, due to the high temperature.

It is however indicated to make a distinction between the various problems: the problem of the origin of the waters is different from the problem in what phase the water is present in the producing horizon: in liquid or gaseous phase.

Even when considering the water of a geothermal field as juvenile, there remains the fact that it is in liquid phase in the reservoir.

This is certain for the Wairakei field. We believe that we have demonstrated that this is true for the Geysers field, in a previous paper (Lit. 8). Many of the considerations, brought forward in this paper and in other published papers, apply to the Larderello field. It is therefore sufficient to add here that the only important argument, which has made other authors believe that the payzone contains water in gaseous phase, is the fact that the steam produced in wells is overheated over the maximum value of any saturated steam.

We  
explaine  
It is  
ed steam  
is not in  
The  
sions, ve  
work as

#### 5. *Prod*

We h  
not have  
with the  
water is  
When  
cises a pr  
horizon h  
till there  
pressure  
contrary,

In bo  
The drillin  
duction a  
point of tl  
exhaust fr  
column di  
well. In tl  
can enter

Natur  
creasing th  
ods simila  
production

The hc  
ily decreas  
than the b

When  
pressure is  
steam, whi  
The la

We believe to have demonstrated that the overheating can be explained in another way (Lit. 7).

It is on the other hand rather difficult to imagine that overheated steam could exist in an extensive porous horizon, i.e. steam, which is not in contact, not even laterally, with water in liquid phase.

The fundamental work by J. GOGUEL (Lit. 10) comes to conclusions, very similar to ours, following another way. We consider this work as the basis of the modern geothermal science.

### *5. Production of a Well and Flow in Stationary State.*

We have seen that the hot water of the producing horizon does not have a temperature higher than the boiling point, corresponding with the pressure at the highest point of the payzone, i.e. that the water is in liquid phase.

When a well reaches the payzone, the drilling mud normally exercises a pressure in excess of the formation pressure; if the producing horizon has large open fissures there can occur a loss of circulation till there is established a pressure equilibrium between drilling mud pressure and formation pressure. With normal permeability, on the contrary, there is formed an impermeable wall cake.

In both cases the well does not enter in production immediately. The drilling mud at the bottom of the hole however, is heated by conduction and gradually the entire mud column is heated till in some point of the mud column boiling can start; therefore, if the steam can exhaust from the well-head, the height and the density of the mud column diminish and at the end the formation water penetrates in the well. In this way, after a more or less prolonged period, the well can enter on production.

Naturally, this period can be abbreviated or eliminated by decreasing the weight of the mud, or by extracting the mud, with methods similar to those employed in the petroleum industry to put on production an oil or gaswell.

The hot formation water, rising in the well, is submitted to a steady decreasing pressure: at a certain point its pressure becomes lower than the boiling pressure and the water starts boiling.

When all the water in the well has evaporated, the bottomhole pressure is the same as the well-head pressure plus the weight of the steam, which fills the borehole.

The latter is negligible: for steam at 200° C at a depth of 1000



meters it is around  $0.5 \text{ kg/cm}^2$  for saturated steam at 10 atmospheres wellhead pressure.

When a well starts producing, evaporation takes place in a tumultuous way and there is a real eruption of steam and hot water; rather large rock fragments can also be thrown out with violence by the well, as reported by drillers at Larderello and Wairakei.

We should remember that evaporation is the more tumultuous and violent, the smaller is the BPD (=boiling pressure distance) of the water and the larger the difference between formation pressure and well-head pressure; this is valid as long as the fluid does not reach sound velocity at any point; beyond sound velocity the flow depends on the geometry of the well.

As, furthermore, one cannot modify the temperature of the formation water, it is indicated to open the well-head as much as possible in order to obtain steam eruption and to create at the bottom of the hole a maximum drop in pressure. In this way the best conditions are realized, as boiling takes place in the formation, as far as possible from the well.

In a previous paper (Lit. 7) we have introduced the concepts « evaporation space » and « evaporation surface » for production at a stationary state.

We intend now to come back to these concepts, whereas we will at a later stage return to the initial transition period, i.e. the putting on production of a well. In this phase, the process is like an adiabatic expansion, whereas the normal production flow is iso-enthalpic.

The « evaporation space » is the portion of the reservoir, where the water evaporates or is in steam-phase. The « boiling front » is that portion of the evaporation space where evaporation starts. We can imagine its form more or less as a hollow sphere, at the outside of which there is 100% water, whereas on the inside there is up to 100% volume steam.

The evaporation space can be roughly indicated as a sphere; it would be very similar to a sphere if the payzone would have an isotropic permeability and porosity, which will be rather difficult to realize. In reality the evaporation space will be more extensive, where the permeability is larger as along an open fissure. Other deformations can be in relation with the length of the producing interval in the well, with the form of the producing part of the well and with the operations carried out in the well in order to increase the productivity (hydrafrac, acidification etc.).

For  
selves to  
space, i.e.  
meability

It is  
many rea  
in the fo  
Some of  
productio  
the reason  
all spaces  
ceases, be

The  
first appr

where:

- $r_e$  = the
- $r_o$  = the
- $P_i$  = the
- $P_o$  = the
- tom
- flow
- $P_i$  = the
- wat

It is c  
sure distar

We wi  
12. If the c  
E is 300 m  
meter of t  
450 mm, 7

One r  
and E, situ  
radius as l  
the radius

For the moment, therefore, we will forget all this and limit ourselves to consider the much simpler case of a spherical evaporation space, i.e. we will consider the case of a payzone with constant permeability.

It is important to know the diameter of the evaporation space for many reasons and first of all because the chemical products dissolved in the formation water are separated starting from the boiling front. Some of these are precipitates, causing incrustations, which limit the production of a well or which make it cease. The incrustations are the reason of the production decline: obviously, when these have filled the spaces not occupied by the rocks of the boiling front, production ceases, because there is no more permeability.

The radius of the evaporation surface is ruled by a formula of first approximation:

$$r_e = r_o \frac{P_t - P_o}{P_i - P_s}$$

where:

- $r_o$  = the distance from the well to the evaporation surface.
- $r_e$  = the diameter of the well in mm.
- $P_t$  = the formation pressure in kg/cm<sup>2</sup>.
- $P_o$  = the bottom-hole pressure during flow, assuming that the bottom-hole pressure is the same as the well-head pressure of a flowing well.
- $P_i$  = the boiling pressure of the water at the temperature of the water in the formation.

It is clear that  $P_t - P_s$  corresponds with the BPD, i.e. boiling pressure distance.

We will apply this formula to several examples, referring to Fig. 12. If the diameter of the wells at the various locations A, B, C, D and E is 300 mm and the bottomhole flow pressure is 10 kg/cm<sup>2</sup>, the diameter of the evaporation sphere is respectively at 1200 mm, 657 mm; 450 mm; 798 mm and 336 mm from the axis of the well.

One remarks in particular the difference between the points D and E, situated in the same well. At D the evaporation surface has a radius as long as twice that of the well, whereas at E it barely reaches the radius of the well.

At greater depth than E, for example at 1300 m, the BPD is around 90 km/cm<sup>2</sup> and the evaporation takes place in the well.

With a well diameter of 150 mm, the other conditions remaining the same, the diameter of the evaporation sphere is reduced to half. already at C evaporation takes place in the well itself.

The hot water, containing salts at saturation, deposits these when evaporates. This takes place on the boiling front; if evaporation takes place in the well itself, the well will be completely incrustated in a short time. With all other conditions being the same, furthermore, the deeper well of two wells in the same field will incrustate the first.

Also the diameter of the well has a strong influence.

The above formula shows that the evaporation area increases greatly, when BPD is near to 0. The difference between the points D and E of our example is very near to 0, whereas the BPD of E is finite.

We can make an attempt to form an idea of the order of time necessary for the complete obstruction of the evaporation space with incrustations.

If the radius of the evaporation sphere is one meter, the volume of the sphere is  $4 \times 10^6$  cm<sup>3</sup>; with a porosity of 20 % the space to be filled is  $8 \times 10^5$  cm<sup>3</sup>. Accepting a water of a sulphatic calcareous type, saturated and containing 2 % CaSO<sub>4</sub> with a density of 2, each liter of evaporated water deposits 10 cm<sup>3</sup> of salt. Therefore  $8 \times 10^4$  liters of water, i.e. 80 tons, are needed for complete obstruction: here we should point out that good producing wells in Larderello give up to 300 tons of steam per hour.

This calculation therefore cannot be strictly applied in actual cases where the calculated evaporation sphere is of small diameter. It should be mentioned that not all the water reaching the outer surface of the evaporation sphere is really evaporated: one part evaporates and the greater part circulates. This latter part can redissolve the incrustations.

But there are other reasons for some caution in the application of numerical calculations of the above mentioned type. If the payzone has mainly a fracture porosity, as in Larderello, the Geysers and Wairakei, the rules of the pressure variations near the well are much different as W. J. BAKER (Lit. 1) has demonstrated also experimentally. This author has even calculated the distance in the well where turbulent movement starts.

It is nearly not necessary to remind that the analogy between an oilwell and a steam-well should be treated with extreme caution. In

fact in a steam in phase from tail the behavior many processes thalpy due to the section in the w flow, from lami before, il BAKER if it is reached.

It is indicat inestimable part movement in the be saturated.

Il evaporati tion can be ex in a few minutes diameter and fo salinity of 2 gr/ well completely: needed.

There are st few minutes and water nor steam several wildcats (near Naples) he periods from a f tion subsequent.

In these cas and that incrust duction. It seem meter and we h lated to the dia

It would b wells in the Ph acidification, the result in widen overheated stea

What we tl sures and abou the transition f

In a steam-well the pressure drop is in relation with the change of phase from liquid water to the steam. We have not studied in detail the behaviour of the biphasic fluid. After separation of the steam, many processes contribute to the overheating: 1) increase of the entropy due to the decrease in velocity in relation with the greater flow section in the well; 2) increase of the enthalpy due to the change in flow from laminar to turbulent, when the steam enters the well or before, if BAKER's data can be applied; and 3), supersonic flow effect, if it is reached.

It is indicated to take into account other facts. For example, an important part of the salts can be expelled from the fluids in rapid movement in the evaporation sphere. Furthermore the water may not be saturated.

All evaporation takes place inside the well, obstruction by incrustation can be extremely rapid and the opening can be in fact closed in a few minutes, when the water is rich in salts. For a well of 300 mm diameter and for a length of 1 meter the volume is 707 cm<sup>3</sup>. With a salinity of 2 gr/liter 800 liters of water are sufficient to obstruct the well completely: i.e. a few minutes of evaporation are all that is needed.

There are suspicions that some wildcats, which gave steam for a few minutes and which afterwards did not give any production of water nor steam, were in the above described conditions. Specially several wildcats on the island of Ischia and in the Phlegraean Fields (near Naples) have given steam and water for more or less expanded periods from a few hours to a few days or weeks, ceasing all production subsequently, as reported by F. PENTA (Lit. 15).

In these cases it seems to us that boiling took place in the well and that incrustation is the only reason for the cessation of the production. It seems that these wells entered the payzone in small diameter and we have seen that the size of the evaporation zone is related to the diameter of the well.

It would be interesting to reexamine the data concerning the wells in the Phlegraean Fields and Ischia; it could very well be that acidification, the application of abrajat or hydrafrac treatments would result in widening the evaporation surface of the wells and perhaps overheated steam could be obtained.

What we thus far have said about the movement of fluids in fissures and about the importance of the slowing down, possibly also of the transition from linear flow to turbulent flow, for the overheating,

gives a rational basis to the empiric observations which had already indicated the importance of fractures for the production of overheated steam.

The wells which produce overheated steam in larger amounts are those which have the payzone fractured to a larger extent. Larderello and The Geysers are classical examples. But also at Wairakei the best production is obtained in wells, where the Wairora formation, which forms the payzone, is fractured.

### Conclusions

In a geothermal field with wells which produce overheated steam we can distinguish three elements: the heat-source, the permeable payzone and the impermeable caprock.

The permeable payzone contains water in liquid phase at hydrostatic pressure; when the heat-flow is sufficient, the temperature of the water is near the boiling temperature corresponding to the hydrostatic pressure at the highest point of the reservoir.

The water in the payzone is affected by convection currents; therefore the temperature of the water differs little from one point to the other in the reservoir. A pool is therefore defined by its average temperature.

Geologically a geothermal field is a trap for convection currents.

The depth has a great influence on the behaviour of the water which is to produce overheated steam: the best conditions are in the highest point of the reservoir, because at that point the hydrostatic pressure of the water is the lowest and its temperature nearest to the boiling point. In any other point of the reservoir the distance between boiling temperature and boiling pressure is larger. The BTD (= boiling temperature distance) and BPD (= boiling pressure distance) factors allow to build rather useful maps for the exploitation of a field. These maps together with contour maps of the caprock-reservoir contact are the basic documents for the location of the wells and for the choice of the right size of hole.

The evaporation volume is the space around the well where the transition of the water in liquid phase to its gaseous steam phase takes place and therefore where the incrustations occur. The production decline of steam with time in a well is due to incrustations.

It is therefore important that the evaporation volume is as big

as possible. The  
and BTD and the

Both the sph  
pressure drop near  
to the turbulent f  
cause the transfor  
overheating of the

Treatments of  
which improve or  
the initial yeld of  
of incrustation. Pe  
allow to obtain ov

1. - BAKER, W. J. - *Flow* II) 1961.
2. - BOZZA, G. - *Sull'orig* rello S.p.A.) 1961.
3. - BURGASSI, R. - *Pros* (U. N. Conference o
4. - CRAIG, H.; BOATO, G. (Proc. of 2nd Confe Science, Nat. Res. C
5. - ELLIS, A. J. and ANI *New Zealand Therma*
6. - ELLIS, A. J. - *Geother* Sources of Energy, p
7. - FACCA, G. and TONANI *rence on New Source*
8. - FACCA, G. and TONANI *fisica Teorica ed App*
9. - FACCA, G. and TONANI, *Mineraria, Anno XIII*
10. - GOGUEL, J. - *Le régime* 1953.
11. - HULSTON, J. R. - *Isot* N. Conference on New
12. - MARINELLI, G. - *L'éner* gique de Belgique, t. 1
13. - McNITT, J. R. - *Geol* rence on New Source
14. - NASINI, R. - *I soffioni*

possible. The most important factors are permeability, the BPD and BTM and the size of the hole.

Both the spheric flow and the fissure permeability allow a rapid pressure drop near the bore-hole. The velocity decreases, the transition to the turbulent flow and the processes related with the sonic flow cause the transformation of kinetic energy into thermal energy. The overheating of the steam is due to these phenomena.

Treatments of the type of hydrafrac, acidification and abrajet, which improve or create fracture permeability, cause an increase in the initial yield of the wells and are useful in eliminating the effects of incrustation. Perhaps hydrafrac treatment might in certain cases allow to obtain overheated steam instead of saturated steam.

#### BIBLIOGRAPHY

- BAKER, W. J. - *Flow in fissured formation* (IV World Petroleum Congress. Section II) 1961.
- BOZZA, G. - *Sull'origine della termalità nelle acque e nel vapore endogeno* (Larderello S.p.A.) 1961.
- BURGASSI, R. - *Prospecting of Geothermal Fields... in various Regions of Italy.* (U. N. Conference on New Sources of Energy) 1961.
- CRAIG, H.; BOATO, G. and WHITE, D. E. - *Isotopic Geochemistry of Thermal Waters.* (Proc. of 2nd Conference on Nuclear Processes in Geological Setting. Nat. Acad. Science. Nat. Res. Council. Pub. 400) (1956).
- ELLIS, A. J. and ANDERSON, D. W. - *The Geochemistry of Bromine and Iodine in New Zealand Thermal Waters.* (N.Z.Y. Science) 1961.
- ELLIS, A. J. - *Geothermal drillholes. - Chemical investigations* (U. N. Conf. on New Sources of Energy, paper G/42) 1961.
- FACCA, G. and TONANI F. - *Natural Steam Geology and Geochemistry* (U. N. Conference on New Sources of Energy, Rome 1961, G/67) 1961.
- FACCA, G. and TONANI F. - *Natural Steam Exploration in U.S.A.* (Bollettino di Geofisica Teorica ed Applicata, vol. IV, n. 14) 1962.
- FACCA, G. and TONANI, F. - *Geologia e Geochimica del vapore naturale.* (L'Industria Mineraria, Anno XIII, Marzo 1962) 1962.
- GOGUEL, J. - *Le régime termique de l'eau souterraine.* (Annales des Mines, X, p. 3-32) 1953.
- HULSTON, J. R. - *Isotope Geology in the Hydrothermal Areas of New Zealand.* (U. N. Conference on New Sources of Energy, paper G/31) 1961
- MARINELLI, G. - *L'énergie géothermique en Toscane.* (Annales de la Société Géologique de Belgique, t. 85, 1961-1962, Bull. No. 10, pp. B 417-438) 1963.
- McNITT, J. R. - *Geology of The Geysers Thermal Area, California.* (U. N. Conference on New Sources of Energy) 1961.
- NASINI, R. - *I soffioni ed i lagoni della Toscana e l'industria boracifera.* Roma 1930.

15. - PENTA, F. - *Ricerche e studi sui fenomeni esalativo-idrotermali ed il problema delle forze endogene.* (Annali di Geofisica; vol. VIII, No. 3, Roma) 1954.
16. - BOATO, G. - *Discussione di alcune misure di abbondanza isotopiche nei gas e nelle acque di Larderello e di altre aree termali.* (unpublished) 1961.
17. - UNITED NATIONS - Conference on New Sources of Energy. 77 papers. Rome 1961.
18. - WILSON, S. H. - *Chemical prospecting of hot springs areas for utilization of geothermal steam.* (U. N. Conference on New Sources of Energy, paper G/35) 1961.
19. - KRAUSKOPF - *Researches in Geochemistry*, 1959, P. 264.

### Discussion

G. GOGUEL: M. Facca a justement insisté sur le fait que la majorité des gisements géothermaux contiennent de l'eau sous forme liquide, à une température plus ou moins proche de la saturation. Cependant, si il existe une couverture imperméable avec une fermeture suffisante, il peut y avoir des poches de vapeur, dans lesquelles le gradient vertical de pression est très faible, à cause de la densité de la vapeur. Si celle-ci est en équilibre à sa base avec l'eau phréatique, sa pression au point haut peut être très supérieure à la pression hydrostatique. Si une baisse de pression produit la vaporisation, et si on cherche comment la zone de vaporisation peut pénétrer dans le terrain, on trouve que la forte viscosité de la vapeur, entraîne un gradient de pression beaucoup plus fort du côté vapeur que du côté eau. Ceci peut entraîner la rupture du terrain, et sa pulvérisation à mesure que la vaporisation progresse.

C. J. BANWELL: In the Wairakei field lapping large fissures do not cause separation of steam in the feeding formation (? *not clearly legible*, N. of the E.). In these holes, the curve of main (? *not clearly legible*, N. of the E.) output versus pressure has a characteristic form which agrees well with that calculated from two phase flow theory. In other holes lapping a smaller feeding fissure or less permeable zone there is a discontinuity in the output pressure curve and the main output rises little above a limiting value as wellhead pressure is reduced.

G. C. FACCA: Geothermal steam is quite often overheated steam, i.e. in Larderello, The Geysers. However, the range of the enthalpy values is narrow. Enthalpy never overcomes about 700 kcal/kg, being mostly about 670 kcal/kg: and of course also less than that, down to moist steam. This is just the maximum enthalpy for saturated steam (just the steam which will become overheated during adiabatic isoenthalpic flow); or, at most, the same enthalpy value plus some tens of kcal. These latter tens of kcal correspond strictly with the excess kinetic energy of steam having sonic velocity at the hole-bottom (p, T) conditions.

Such an overall energy of the gas phase will be attained in the region of the narrowest section when approaching maximum output conditions. It is just the expected enthalpy of the geothermal fluid, when the water formed in the narrowing sections has the possibility to separate from the gas phase.

On the contrary, we are able to observe practically any temperature, i.e. enthalpy value, where some independent source feeds heat to geothermal fluids. For instance, in most fumaroles and fumarole fields of volcanic regions all the

condition  
eral hund  
acteristic  
sers, seen  
reason ag  
for accep  
fields. It  
not know  
However,  
phase flow  
in the nar

A. R.

through p  
in the ren  
measurement  
5 feet of  
could occur

G. C.

fact, the s  
At the sur  
the section  
hole-bottom

On the  
wells, it se  
Thus, in g  
in the feed  
in general  
mum press  
roughly hor  
for natural

J. HEAL

finer depos  
place. When  
permeability  
many wells  
data on this

conditions are observed, going from saturated steam to water-rich gases several hundred degrees hot. The agreement between some thermodynamical characteristics of water, and the overheating observed at Larderello and The Geysers, seems to us hardly a fortuitous coincidence. We report it as a general reason against the *a priori* rejection of the process of separation of water, and for accepting some two phases process as a basis for a theory of geothermal fields. It was not our aim in this work to develop such a theory. Thus, we do not know *how* steam separates, nor claim detailed arguments about well output. However, we could recall that a limiting value of the output is expected for one-phase flow, by decreasing pressure down-hole, when sound velocity is attained in the narrowest section.

A. R. MCBIRNEY: It is a characteristic of the flow of compressible fluids through pipes that the pressure gradient is much greater near the outlet than in the remaining length of the pipe. I believe that this has been shown by measurements in New Zealand, where most of the pressure drops occurs within 5 feet of the surface. It therefore seems unlikely that a large pressure drop could occur near the walls of the well at any significant depth.

G. C. FACCA: We did not treat the problem of the flow through pipes. In fact, the strata feeding the wells are, generally speaking, a porous medium. At the surface of a cavity in a porous medium, or in the region limiting it, the section of the flow rises more or less abruptly. This will be the case at the hole-bottom, or at the border region of cavities feeding it.

On the other hand, when considering the flow of fluids from strata to the wells, it seems evident that stream tubes in the porous medium are narrowing. Thus, in general we have a minimal section effective for the flow somewhere in the feeding porous formation. This section is not very far from the well, — in general — and different conditions may be realized but are less usual. Maximum pressure drop will occur where stream tubes are the narrowest in the roughly homogeneous porous medium, as laboratory and field evidence indicates for natural gas and oil.

J. HEALY: In New Zealand the largest producing wells tap water. This confines deposition of calcite and silica to the wells at levels where boiling takes place. Where this occurs in the country deposition of minerals may reduce permeability. However, water levels are still falling in the Wairakei field, and many wells will change in character, so we will be able to collect additional data on this.



USER COUPLED CONFIRMATION DRILLING PROGRAM

PUBLIC INFORMATION MEETING

REGISTRATION

NAME \_\_\_\_\_

AFFILIATION \_\_\_\_\_

ADDRESS \_\_\_\_\_

\_\_\_\_\_

\_\_\_\_\_

TELEPHONE \_\_\_\_\_

I am a

- Prospective User
- Prospective Developer
- Prospective Financier
- Contractor/Consultant
- State or Local Government Employee
- Regulatory Agency Employee
- DOE Contractor
- Other: \_\_\_\_\_

Area(s) of Expertise

- Exploration
- Drilling
- Reservoir Testing
- Architecture/Engineering
- Equipment Manufacturing
- Application
- Financing
- Institutional
- Environmental
- Other: \_\_\_\_\_

YES NO

I want to be on the mailing list for the User Coupled Confirmation Drilling Program

CONSULTANTS AND CONTRACTORS QUESTIONNAIRE

Place an "X" in each box that identifies one of your activities:

By filling out and returning this questionnaire, you will be added to our list of consultants and contractors. This list will be furnished to those interested in using or developing geothermal energy.

	<u>Consulting</u>	<u>Contracting</u>
Geophysical Studies	<input type="checkbox"/>	<input type="checkbox"/>
Geochemical Studies	<input type="checkbox"/>	<input type="checkbox"/>
Geological Studies	<input type="checkbox"/>	<input type="checkbox"/>
Hydrological Studies	<input type="checkbox"/>	<input type="checkbox"/>
Reservoir Engineering	<input type="checkbox"/>	<input type="checkbox"/>
Well Logging	<input type="checkbox"/>	<input type="checkbox"/>
Well Stimulation	<input type="checkbox"/>	<input type="checkbox"/>
Subsidence	<input type="checkbox"/>	<input type="checkbox"/>
Induced Seismicity	<input type="checkbox"/>	<input type="checkbox"/>
Thermal Gradient Drilling	<input type="checkbox"/>	<input type="checkbox"/>
Deep Drilling (over 5000 ft.)	<input type="checkbox"/>	<input type="checkbox"/>
Shallow Drilling (under 5000 ft.)	<input type="checkbox"/>	<input type="checkbox"/>
Environmental Studies	<input type="checkbox"/>	<input type="checkbox"/>
	<u>Yes</u>	<u>No</u>
Geothermal Experience	<input type="checkbox"/>	<input type="checkbox"/>
Oil & Gas Experience	<input type="checkbox"/>	<input type="checkbox"/>
Mining Experience	<input type="checkbox"/>	<input type="checkbox"/>
Geotechnical Experience	<input type="checkbox"/>	<input type="checkbox"/>

Name \_\_\_\_\_

Company \_\_\_\_\_

Address \_\_\_\_\_  
\_\_\_\_\_

Telephone ( ) \_\_\_\_\_

Return to:

Earth Science Laboratory  
University of Utah Research Institute  
420 Chipeta Way, Suite 120  
Salt Lake City, UT 84108  
Attn: Sue Moore

**U. S. DEPARTMENT OF ENERGY  
DIVISION OF GEOTHERMAL ENERGY**



**USER COUPLED  
CONFIRMATION  
DRILLING PROGRAM**

**a new program to provide  
FEDERAL COST-SHARING  
for  
EXPLORATION, DRILLING AND TESTING  
to confirm  
HYDROTHERMAL RESERVOIRS  
for  
DIRECT HEAT APPLICATIONS**

## THE ENERGY SITUATION TODAY

This country is embroiled in an energy crisis. The United States produces only about three-quarters of the energy that it consumes. Approximately 48% of our energy consumption is in the form of petroleum products. Petroleum products are also important in the manufacture of many consumer goods such as plastics. Approximately one-half of the total petroleum consumed in the U.S. comes from foreign countries. The \$80 billion the U.S. spends yearly in foreign markets for petroleum has a highly detrimental effect on the U.S. economy. Alternative sources of energy that can be used to decrease our dependence on foreign petroleum are needed. Energy use forecasts for the year 2000 and beyond indicate that all feasible alternative energy sources will be needed and that conservation measures will have to be practiced as well if our standard of living is to be maintained. The energy crisis is real!

### HYDROTHERMAL ENERGY -- A VIABLE ENERGY ALTERNATIVE

Of the undeveloped alternative sources of energy, hydrothermal energy is probably closest to being economically feasible. Hydrothermal energy is geothermal energy in the form of hot water and steam that occurs naturally at many locations beneath the earth's surface. Studies by the U.S. Geological Survey indicate that hydrothermal energy forms a very large energy reserve in the United States. The potential for development of hydrothermal energy in the U.S. is estimated to be 2400 Quads ( $2400 \times 10^{15}$  BTU), compared to today's yearly total energy use of about 80 Quads. Little of this large resource has been developed in the past due to the availability of relatively inexpensive energy in other forms. But today, energy costs are increasing worldwide and hydrothermal energy is becoming cost competitive with more traditional sources. Hydrothermal energy is truly a viable energy alternative.

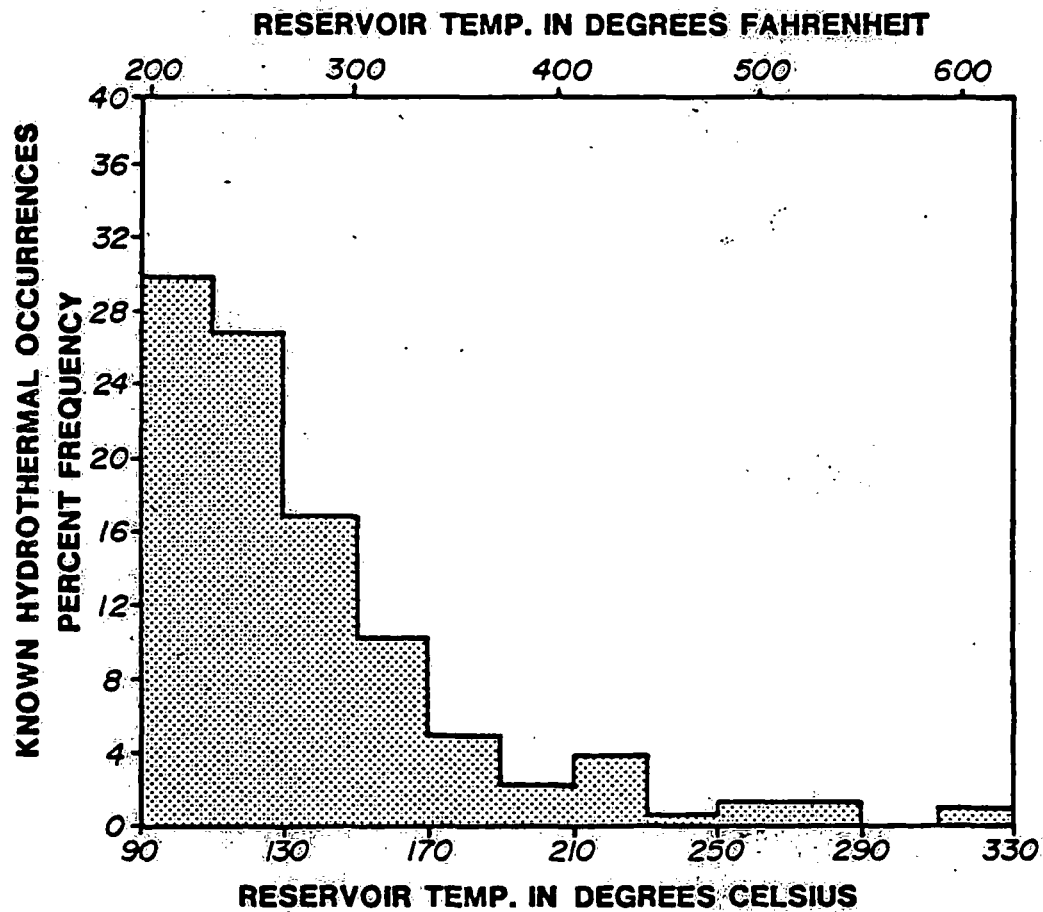
## NATURE OF HYDROTHERMAL ENERGY

Hydrothermal energy can be used either for generation of electricity or by direct application of the heat in industrial processing, space heating, and other uses. High energy, high temperature geothermal steam is currently being used to generate electricity at The Geysers steam field in northern California, which provides enough electrical power to supply a city the size of San Francisco. Hydrothermal electrical power is also generated in other countries, including Italy, Mexico, El Salvador, New Zealand, Japan, and the Philippines. Direct geothermal uses are also important in the United States. Since before the turn of the century, Klamath Falls, Oregon and Boise, Idaho have had district heating systems to heat houses and public buildings with hydrothermal energy. In Iceland, a volcanically active island that is part of the mid-Atlantic ridge, much of the space and industrial process heat is geothermal. Extensive use of direct applications is also being made in France, where many of the homes and other buildings in the Paris basin are geothermally heated; in New Zealand, where industrial uses of direct heat are on line; in Japan, where geothermal fluids find many uses including raising poultry and fish; and in Hungary, where large greenhouse complexes are geothermally heated.

The temperature of geothermal fluids ranges from over 300°C (572°F) down to shallow groundwater temperature, which averages about 15°C (59°F). High temperature hydrothermal resources (>150°C = 302°F) are relatively rare--much more common are low- and moderate-temperature resources. Figure 1, taken from U.S. Geological Survey Circular 790, "Assessment of Geothermal Resources in the United States--1978"<sup>1</sup>, shows the relationship between number of known occurrences and resource temperature down to 90°C. Little at all is known about resources with temperatures lower than 90°C.

---

<sup>1</sup> Available free by written request to Branch of Distribution, U. S. Geological Survey, 1200 South Eads Street, Arlington, VA 22202.



Geothermal resources are comprised of three main geological components: 1) a source of heat, 2) a fluid (water or steam) to carry the heat to a drill hole from which it flows or can be pumped to the surface, and 3) a permeable system of pores or fractures in the rock through which the fluids can circulate. The heat source is sometimes a shallow body of molten or recently solidified hot rock. Alternatively, the shallow heat may result simply from very deep circulation of groundwater to hotter regions two to three miles down where the water is heated and rises buoyantly to the surface.

Hydrothermal resources occur throughout the United States, although the West has the largest share of presently known resources. Such hydrothermal surface manifestations as hot springs and hot wells are abundant in the West. Figure 2 shows the location of many of the known hot springs and wells in the United States. Although many occurrences and areas favorable for occurrence of hydrothermal resources are shown on Figure 2, little is known in detail about individual areas. This is because little exploration and drilling of geothermal areas has been done to date. Thus, although the large number of occurrences indicates a widespread and substantial resource base, there are few confirmed reservoirs. Drilling and flow testing of resource areas to determine temperature and productivity will be required for reservoir confirmation before development can take place.

#### DEVELOPMENT OF HYDROTHERMAL ENERGY

Hydrothermal energy is not widely recognized by the public as an energy resource. The past common use of hot springs has been for spas, and little thought has been given to other application of the heat energy. Therefore, there has been virtually no industry built up around direct hydrothermal uses. We lack good exploration and drilling techniques and experience, and, as mentioned before, there is little detailed knowledge of the resource base, few confirmed reservoirs. Few states have adequate geothermal use laws at present. There is little economic data on direct geothermal uses, and this makes economic feasibility studies uncertain and financing difficult to obtain. In short, there is no private sector infrastructure adequate to develop direct geothermal uses at the rate that the relatively large resource base indicates as possible and that this country's needs indicate as being desirable.

Exploration for hydrothermal reservoirs is a high risk enterprise. To insure that a suspected reservoir will be economic, the developer must drill into the resource at depth, measure the temperature and flow rate, and use sophisticated analysis techniques to estimate the productivity and longevity of the resource. The present high risk level for reservoir confirmation stems

partly from the lack of resource knowledge stated above and partly from the fact that present surface surveying techniques are not well enough developed to ensure a high level of probability that a drill hole will intercept a resource. Hydrothermal reservoirs are never uniform or continuous, and unproductive holes are sometimes drilled in the middle of the best of resources. Better techniques for and more experience in siting wells are needed to decrease the risk of drilling an unproductive well.

Present developers of electrical power generation from high-temperature reservoirs are generally large resource companies that can finance reservoir confirmation by spreading the high risk and cost over many projects. However, these large companies are usually not interested in development or utilization of lower-temperature reservoirs because of the relatively small scale of such projects. Smaller developers, the ones most likely to be interested in low- and moderate-temperature geothermal resources, are often unable to spread risk and cost in the same way that a large company can. A single unproductive well can mean financial disaster for them. In addition, many prospective developers and users of direct heat hydrothermal energy are not resource companies and therefore are not accustomed to the techniques and risks of resource development. In some companies risk money for geothermal development can not be obtained from management. For these reasons, it is not expected that the direct heat user in the private sector will be able to perform needed reservoir confirmation of significant magnitude for direct heat hydrothermal resources by himself in the near future. Without federal assistance there will continue to be very little use of the large hydrothermal resource base that exists in the United States.

The User Coupled Confirmation Drilling Program will speed hydrothermal industrialization by absorbing some of the high risk and cost while at the same time developing an experienced industry in the private sector that will reduce future risk and that can carry on without federal aid in the future.



## USER COUPLED CONFIRMATION DRILLING PROGRAM

### Summary Program Description

The U.S. Department of Energy, Division of Geothermal Energy is sponsoring a new program that absorbs a portion of the high front-end risk and cost of development by providing cost-sharing of hydrothermal reservoir confirmation for direct heat applications. The User Coupled Confirmation Drilling Program will cost-share expenses for exploration to site drill holes, drilling, flow testing, reservoir engineering, and injection well drilling (if required). Cost-sharing or financing for the utilization system to be installed once the reservoir is confirmed are not covered under this program. The federal percentage of cost-share will be determined by a negotiated formula based upon usability of the thermal fluids intersected by the drilling. For a completely successful project, the DOE cost-share will be 20 percent, whereas for a completely unsuccessful project the DOE cost-share will be 90 percent. The degree of success and the corresponding DOE cost-share are expected to range between these extremes for individual projects.

The new program will be initiated by a DOE Solicitation for Cooperative Agreement (SCA), to be issued in May 1980. A 90-day period will be available thereafter for preparation and submission of proposals. It will be required that proposals detail, among other things, 1) the geologic evidence that a resource exists at the site of interest, 2) the direct heat use to be made of geothermal fluids if discovered and confirmed, 3) an adequate exploration, drilling, flow testing and data analysis program, and 4) an acceptable cost-share plan based on degree of success of the project. Proposals will be reviewed and awards made in accordance with applicable federal regulations. Successful proposers will negotiate a contract with DOE. The contractor's funds can be used to perform the project, or alternatively a loan can be obtained from a commercial financial institution, using the DOE contract as evidence that project risk has been substantially reduced. The project will then proceed under contractor management. After flow testing, the degree of success will be determined through analysis of flow testing results and by application of provisions for this purpose that have been negotiated in the

contract. The DOE cost-share is then determined, and DOE pays this amount to the contractor, completing the agreement.

### Program Objectives

The objective of the User Coupled Confirmation Drilling Program is to foster economically viable use of direct heat hydrothermal energy in the United States by the industrial and private sectors by:

- 1) getting direct heat utilization started by absorbing a portion of the risk associated with confirmation of hydrothermal reservoirs while at the same time;
- 2) developing an experienced infrastructure of exploration, confirmation and utilization engineering consultants, contractors and equipment manufacturers who will reduce reservoir confirmation risks in the future.

This federal program is scheduled to phase out as private industry begins to grow on its own.

We must anticipate that some unproductive wells will be drilled. The extent to which successful reservoir confirmation will occur will depend upon 1) probability of occurrence of the resource, 2) probability that a well will be sited properly to intercept the resource, and 3) probability that the well will be drilled and tested properly. Petroleum and minerals resource developers understand and accept these probabilities and do not become discouraged when unproductive holes are drilled. This same attitude must be adopted by the new direct heat geothermal industry and by others associated with this program.

### Proposals to DOE

A 90-day period will be available for development of a proposal after DOE issues the Solicitation for Cooperative Agreement in late May 1980. Those who write proposals can be users or developers of direct heat hydrothermal energy. Proposals must contain evidence that:

- 1) there is a user who intends to use the resource if discovered;
- 2) the user or developer has or can obtain rights to required land and geothermal fluid and/or heat;
- 3) other required permits can be obtained, and
- 4) environmental considerations can be handled.

The proposal must detail a project that the proposer intends to carry out to confirm a hydrothermal reservoir for direct heat application. Reservoir confirmation requires flow testing of a hydrothermal well and analysis of the results in terms of temperature, producibility and longevity of the resource. The proposal can be to test an existing well or to drill a new well for testing. The original contract will generally be for the drilling of a single reservoir test or confirmation well, although contract modification to allow more drilling is feasible depending on initial drilling results.

The proposal must document the geologic evidence that a reservoir exists at the site proposed. Proposals with good geologic evidence for existence of a reservoir will be favored over those with poor evidence. The best geologic evidence would be direct evidence consisting of known thermal springs or wells or of thermal spring deposits. All geological, geophysical, geochemical, and hydrological evidence should be given that bears upon existence of the suspected reservoir, and negative evidence should be given as well.

The end use(s) to be made of geothermal fluids should be given along with an analysis of the engineering and economic feasibility of the project. The end use(s) will specify the temperature and quantity of geothermal fluid required, and this will bear on determination of degree of project success. Engineering items to be discussed include process energy requirements

(temperature, flow, load factor) and system design. Economic data to be furnished include capital requirements, replacement costs, annual costs and taxes for the follow-on utilization system as well as detailed costs for the cost-shared portion of the project.

If a well is to be drilled, the proposal must justify the well site selection and must show the data and analysis used in siting the well, or alternatively the proposal must specify an exploration program to develop data for use in well siting. Geological, geophysical, geochemical, hydrological and other data generation and analysis are encouraged. Shallow drilling for thermal gradient determination may also be a useful tool to help select a test well site and will be cost-shared. The proposal should also contain a drilling prognosis that briefly describes preliminary drilling plans. Later in the project, before actual drilling begins, a more detailed plan will be required.

A preliminary plan for reservoir testing and analysis of the results must be presented. This plan can be modified later depending upon drill results. The plan must be grounded in modern-day hydrology and reservoir engineering and must basically determine usability of the geothermal resource for the purpose intended. Items to be specified include testing methods, duration, flow rate, measurements to be made and accuracy and techniques to analyze test data.

A method must be proposed for determining degree of success of the project. This method should depend upon results of the flow testing and upon the intended or other possible end use(s). It is recognized that even though the quantity or temperature of fluids discovered may not support the entire primary intended end use, these hydrothermal fluids are likely to be usable at some level or to be worth something in a sale. This should be accounted for in determining degree of success. The degree to which each project is successful will vary from site to site and it is not possible for DOE to specify a certain formula for determining degree of success. Rather it will be up to each proposer to specify degree of success for his particular project as a function of properties of the fluids intersected. The proposed method

for determining DOE's cost-share should be addressed in the proposal and should be based upon and tied to the proposed method for determining degree of success.

The proposal should give evidence that the proposer has a method of financing and carrying through the project if an award is made. Financing can be either internal or external (bank loan, stock, bonding, limited partnerships, etc). There is the possibility that up to 20 percent of the DOE cost-share could be invoiced as expenses occur, but the major portion of financing must be arranged by the proposer. At the time of the proposal, it will not be necessary to have these financial arrangements complete, but evidence should be given that financing can be arranged.

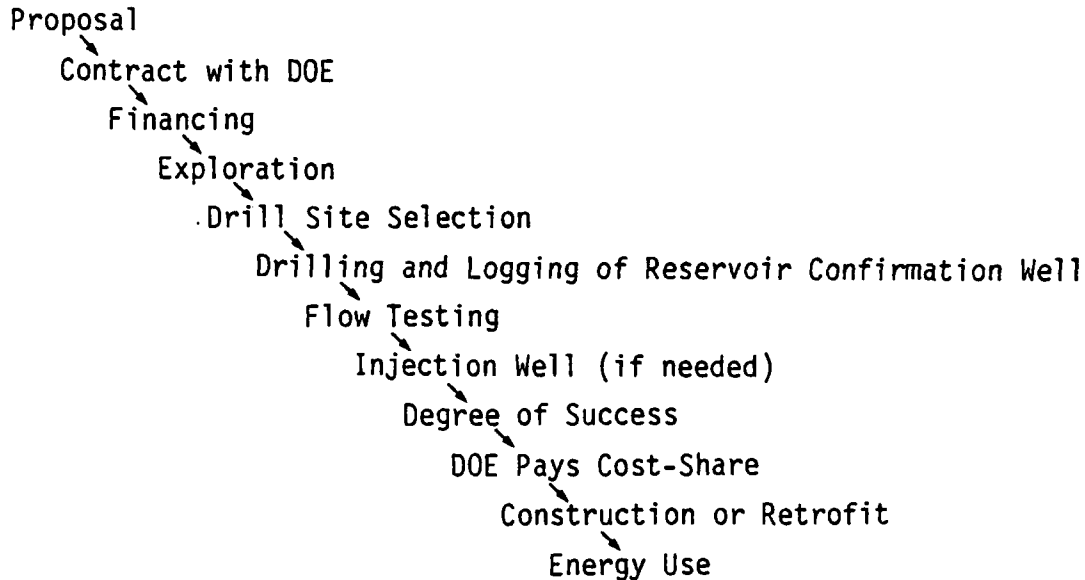
Proposals that address projects to develop a large amount of hydrothermal direct heat use and therefore to displace a relatively large amount of conventional energy, will be favored over those that address only a small amount of direct heat development.

Proposers are advised and encouraged to obtain the services of reliable and competent consultants and contractors for exploration, drilling, reservoir testing, utilization, financing, legal, and other aspects of their proposed project for which they lack specific expertise. Projects that are to be carried out by a competent staff will be favored.

Once proposals are evaluated, notification will be made to those proposers that are successful. A contract between the proposer and DOE will then be negotiated, and the project can begin.

## The Project

The basic project work flow is visualized as follows:



Once a contract is negotiated, the successful proposer will finance his project either internally or with a loan, as discussed previously. This proposed method of funding has advantages over full federal funding in that it develops contacts between users and bankers that will continue once the federal government has stepped out of the program. It also decreases substantially the total cost to DOE, which means that more projects can be funded for the same program budget. Once financing is obtained, exploration will begin, followed by drill site selection, drilling and logging, flow testing, and if needed an injection well. At each step, data will be sent to DOE, and from analyses of those data a joint decision will be made by DOE and the proposer as to how to proceed. When the well is tested, the degree of success will be determined as agreed in the initial contract, and DOE will pay its share, concluding the project. Follow-on installation of equipment to use the geothermal fluids will be the responsibility of the user or developer. Financial assistance for this may be available through the Geothermal Loan Guaranty Program.

At several stages in the program, more detailed plans will be required than were submitted during the proposal and contract negotiation stages. Before test well drilling, a detailed drilling plan describing procedures, anticipated problems and methods to abide by regulations will be needed. A detailed plan for well testing will be required before this testing begins. Similarly, more detailed, DOE-approved environmental plans will be needed before test drilling, before flow testing and for site restoration. The most sensitive environmental issue will probably be fluid disposal during flow testing and during subsequent operation. DOE will assist in the environmental reporting process by issuing a generic environmental document that will be useful to some users who can simply attach environmental considerations for their individual projects and the report will meet regulatory requirements.

#### Who is Eligible

Private individuals or companies and state and local government agencies can offer proposals under this program. The proposer will be required to demonstrate that he has included adequate geological, drilling, engineering, and other expertise in the proposed project. Consultants and contractors can be used to provide this expertise as needed.

#### Schedule

The first SCA will be issued in the last part of May, 1980. Response period will be 90 days. Successful proposers will be notified about September 1980 and then contract negotiations will begin. It is anticipated that some projects can begin in November 1980. Present plans call for follow-on solicitations on about a 6-month cycle. A prospective proposer who misses the first solicitation period would thus have later opportunity to propose a project.

## Management

The User Coupled Confirmation Drilling Program will be managed for DOE Headquarters by the Idaho Operations Office of DOE with assistance from the Earth Science Laboratory of the University of Utah Research Institute and from EG&G, Idaho, Inc.

## Technology Transfer

In order quickly to develop a knowledge and experience base in the private sector, much of the resource and exploration data for the project will be publicly available on open-file. In addition, selected case studies will be published. Although it is very important to make data, techniques and results widely available, it is also important to protect proprietary processes and techniques. Propriety of information can be protected, if desired and provision to do so will be negotiated in the contract.

## Interface With Other DOE Programs

The User Coupled Confirmation Drilling Program has important interfaces with other DOE programs. Among the most important of these is with the Geothermal Loan Guaranty Program (GLGP). Assistance with financing for installation and operation of utilization equipment will not be part of the User Coupled Confirmation Drilling Program. The resources of the GLGP, however, will be available for this purpose. Details are still being worked out with the intention of making it as easy as possible to move into the GLGP once the reservoir has been confirmed.

Two other important DOE programs exist that can offer help to proposers to the User Coupled Confirmation Drilling Program. These are the State Coupled Resource Assessment Program and the State Commercialization Planning Program. Figure 3 shows states in which there are teams working to assess geothermal resources and to facilitate all aspects of industrialization of



geothermal energy. Prospective users and developers of hydrothermal energy in these states are encouraged to contact state teams for assistance. More information on these programs can be obtained from DOE-Idaho Operations Office in Idaho Falls, Idaho.

### Anticipated Program Results

It is anticipated that this program will result in an increased utilization of direct heat hydrothermal energy that will decrease our dependence on foreign petroleum and aid in mitigating the energy crisis. The extent to which this will be possible will depend critically on the amount of funding that Congress authorizes for this program. It is estimated that for a federal expenditure of \$250 million in 1980 dollars that direct heat uses as a result of this program would result in an annual petroleum savings of about 28 million barrels per year by the year 1987. For an oil price of \$26/bbl, this represents an annual savings in payments for foreign petroleum of over \$700 million per year.

# GEOHERMAL RESOURCES

modified from U.S.G.S Circular 790



FIGURE - 2



## THE STATE COUPLED TEAM

DOE-HEADQUARTERS (Washington) - Gerald P. Brophy (202-633-9491)  
Program planning, guidance, priorities.

DOE-IDAHO FALLS OPERATIONS - Leland L. Mink (208-526-0638)  
Program implementation, contracting, management.

STATE CONTRACTORS  
Performance of state project.

UNIVERSITY OF UTAH RESEARCH INSTITUTE (UURI) - Duncan Foley (801-581-5283)  
LOS ALAMOS SCIENTIFIC LABORATORY (LASL) - A. William Laughlin (505-667-6711)

GRUY FEDERAL - Joel L. Renner (703-892-2700)

VIRGINIA POLYTECHNIC INSTITUTE AND STATE UNIVERSITY (VPI) - John K. Costain (703-961-5096)  
Management assistance to DOE, exploration, and technology development.

NATIONAL OCEANIC AND ATMOSPHERIC ADMINISTRATION (NOAA) - Paul J. Grim (303-499-1000)  
Publishing state resource maps.

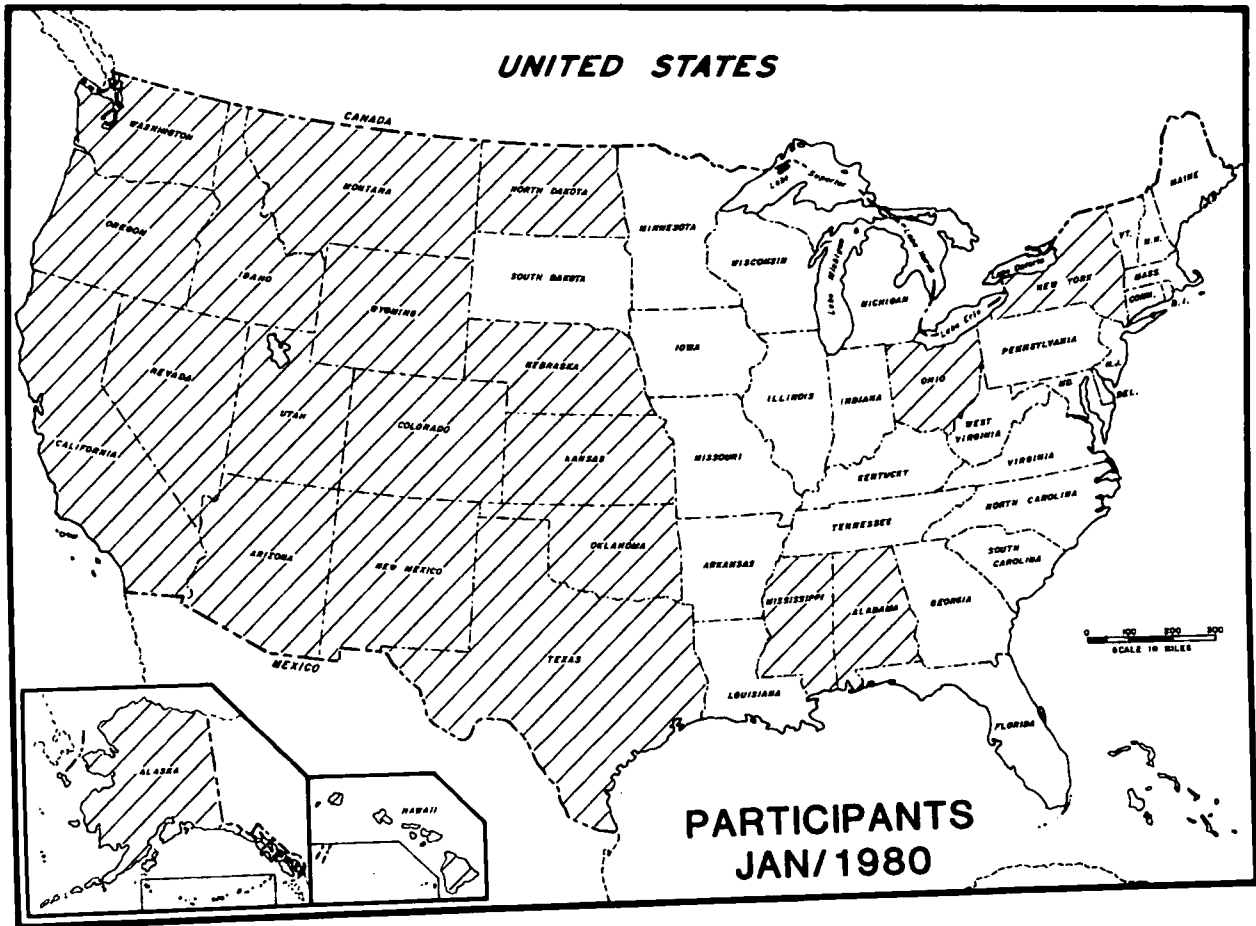
U. S. GEOLOGICAL SURVEY (USGS) - Marshall J. Reed, James R. Swanson (415-323-8111)  
Assessment of U. S. Geothermal resources and computer storage of geothermal data.

## PARTICIPATING STATES

Alabama	Gary V. Wilson	205-349-2852
Alaska	Donald L. Turner	907-479-7198
	Ross G. Schaff	907-277-6615
Arizona	W. Richard Hahman, Sr.	602-884-2733
California	Roger C. Martin	916-323-0967
Colorado	Richard H. Pearl	303-839-2611
Hawaii	Charles E. Helsley	808-948-8760
Idaho	John C. Mitchell	208-334-4477
Kansas	Don W. Steeples	913-864-3965
Mississippi	Alvin R. Bicker	601-354-6228
Montana	John Sonderegger	406-792-8321
Nebraska	William D. Gosnold	402-554-2457
	Duane A. Eversoll	402-472-3471
Nevada	Dennis T. Trexler	702-784-6691
New Mexico	Chandler A. Swanberg	505-646-1920
New York	Burton Krakow	518-465-6251
	James R. Dunn	518-783-8102
North Dakota	Kenneth L. Harris	701-777-2231
Ohio	Frank L. Majchszak	614-466-5344
Oklahoma	William E. Harrison	405-325-3032
Oregon	Donald A. Hull	503-229-5580
Texas	Charles M. Woodruff	512-474-5994
	David M. White	512-475-5588
Utah	Robert F. Roy	915-747-5501
Washington	J. Wallace Gwynn	801-581-6831
Wyoming	J. Eric Schuster	206-753-5327
	Edward R. Decker	307-766-3278

# THE STATE COUPLED PROGRAM

## LOW-AND MODERATE-TEMPERATURE GEOTHERMAL RESOURCES



U.S DEPARTMENT OF ENERGY  
DIVISION OF GEOTHERMAL ENERGY



J.R. McNitt, Technical Adviser, United Nations

1979

Abstract

Although the emphasis of United Nations' assisted geothermal projects has been on demonstrating the feasibility of producing modest amounts of geothermal fluids, the potential capacity of individual fields has been estimated by the energy in place methods developed by Bodvarsson, and tested by the decline curve method.

The energy in place method, including single fracture flow, intergranular flow and intergranular vaporization models, has been applied to three geothermal fields resulting in total resource estimates ranging from 380 to 16,800 MW-yrs. The results of these studies must be considered highly tentative, however, due to inadequate reservoir data and a poor knowledge of producing mechanisms.

The decline curve method has not given quantitative results concerning ultimate field potential because of the relatively short duration of well tests (several weeks to a maximum of 11 months). In all cases, however, the decline of flowing wellhead pressure, field pressure, and flow rate has continued to decrease with time, which is interpreted to indicate pressure maintenance by the mechanism of steam separation in the reservoir.

A regional assessment of geothermal potential is in progress for Central America. The method adopted requires the estimation of the probable number of geothermal fields in the region, as inferred from geologic and geochemical information, and the estimation of the probable productivity of the potential fields as inferred from a statistical analysis of fields already under development throughout the world. The statistical study, based on data from 42 fields, has been completed with the following results:

UNIVERSITY OF UTAH  
RESEARCH INSTITUTE  
EARTH SCIENCE LAB.

- a) The probable average power capacity of reservoirs contained in volcanic rock is 360 MW, and there is a 68 per cent probability that the capacities of such reservoirs will be in the range of 90 to 1380 MW.
- b) The probable average power capacity of reservoirs in sedimentary rock is 1560 MW, and there is a 68 per cent probability that the capacities of such reservoirs will be in the range of 480 to 5200 MW.

elds

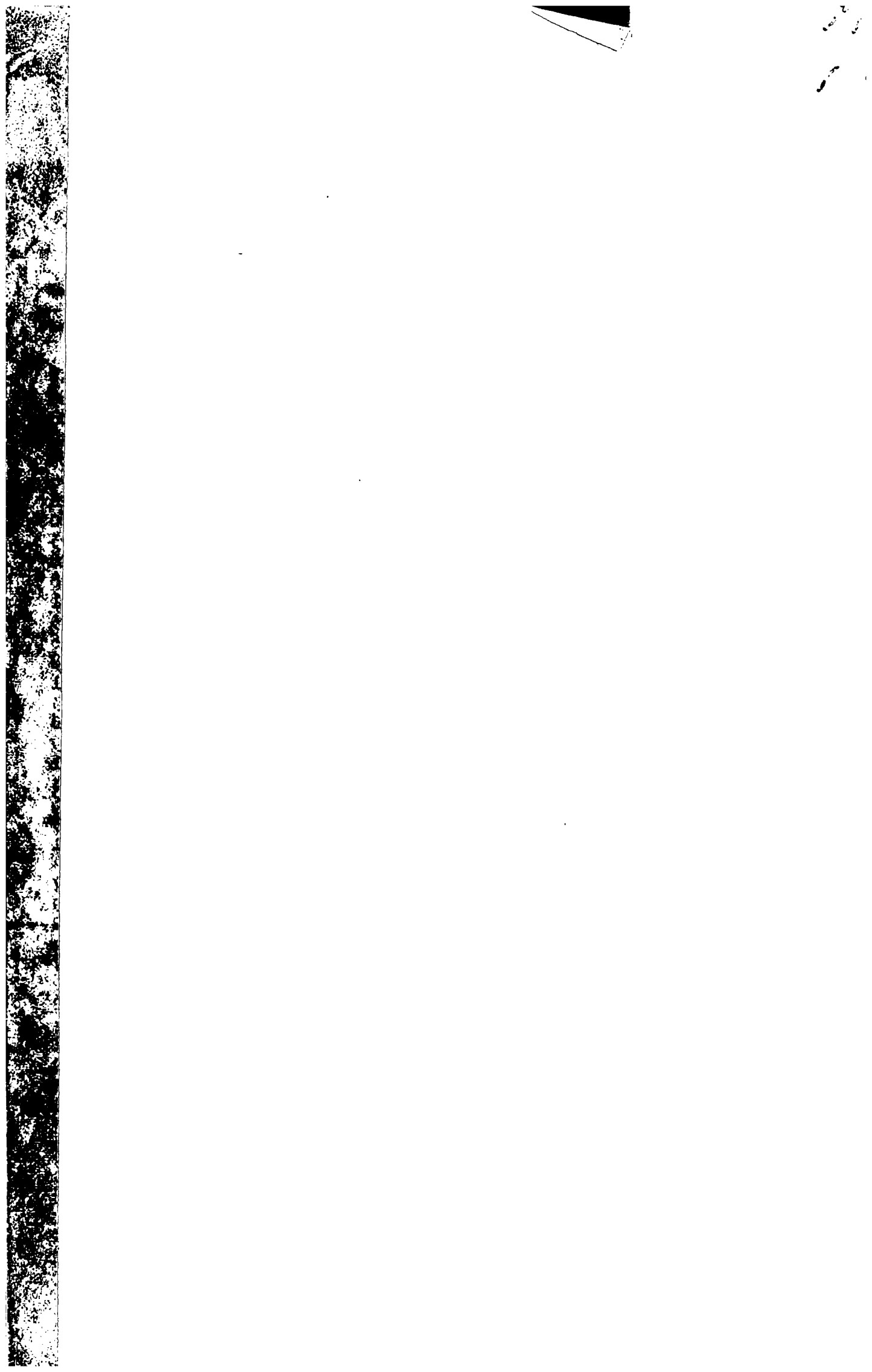
oned Cum. % Sedimentary rock reservoirs	Area of Productive Wells Km <sup>2</sup>	Proven Power Capacity MW	Unit Power Capacity MW/km <sup>2</sup>	Ref. No.*
				14
				16
				14
				6
				32
				45
	0.35	20	57	38
	0.35	20	57	7
	0.4	25	62	38, 44
	0.3	5	17	17, 41, 42
				33
7.14	2	7	3.5	9, 13
				18
	0.6	70	117	15, 16, 25
	0.03	11	367	31, 45
				45
14.3	0.15	12.5	83	32, 34
				10
				35
	0.3	13	43	37
21.4	1.5	44	29	2, 40
				43
	0.13	8	62	30
	1.5	148	99	21, 22
	2.6	165	63	8, 29
	0.25	16	64	28
				23
28.6	7	15	2.1	9, 13
35.7				43
42.9				11
				43
				21
50.0				36, 39
				3
57.1				43
				11
64.3				33, 43
				24, 27
				4
71.4				1, 19
78.6	1.5	75	50	12, 7
85.7	80	264	3.3	20,
92.9	26.3	900	34	



TABLE 1 Area and Power Capacity

Field	Area of field or area of associated anomaly Km <sup>2</sup>	Area, Log <sub>10</sub>	Cum. %
1. Tahuangtusi	0.5	-0.301	2.33
2. Bouillante	0.8	-0.097	4.65
3. Matsao	0.8	-0.097	6.98
4. Reykjanes	1	0.000	9.30
5. Krafla	2	0.301	11.63
6. Takenoyu	2	0.301	13.95
7. Matsukawa	2.1	0.322	16.28
8. Momotombo	3	0.477	18.60
9. Onikobe	3	0.477	20.93
10. Paujetskaya	3.5	0.544	23.26
11. Svartsengi	4	0.602	25.58
12. Bagnore	5	0.699	27.91
13. Hawaii	6	0.778	30.23
14. Ahuachapan	6	0.778	32.56
15. Otake	6	0.778	34.88
16. Hatchobaru	6	0.778	37.21
17. Namafjall	7	0.845	39.53
18. Travale	7	0.845	41.86
19. N. Hachimantai	7	0.845	44.19
20. Kawerau	9	0.954	46.51
21. Kizildere	12	1.079	48.84
22. Brady	12	1.079	51.16
23. Olkaria	12	1.079	53.49
24. Wairakei	12	1.079	55.81
25. Broadlands	13	1.114	58.14
26. El Tatio	14	1.146	60.47
27. Kawah Kamajang	14	1.146	62.79
28. Piancastagnaio	15	1.176	65.12
29. Brawley	18	1.255	67.44
30. Alfina	18	1.255	69.77
31. Beowawe	21	1.322	72.09
32. Waiotapu	28	1.447	74.42
33. E. Mesa	40	1.602	76.74
34. Krisuvik	40	1.602	79.07
35. Heber	50	1.699	81.40
36. Hengill	50	1.699	83.72
37. Salton Sea	54	1.732	86.05
38. Long Valley	60	1.778	88.37
39. Cesano	65	1.813	90.70
40. Cerro Prieto	70	1.845	93.02
41. Larderello	80	1.903	95.35
42. Geysers	100	2.000	97.67

\* References for Table 1 can be found in Appendix A



SUBJ  
GTHM  
USGI

# U.S. GEOTHERMAL INDUSTRY IN 1978

By Robert Rex  
Republic Geothermal, Inc.

UNIVERSITY OF UTAH  
RESEARCH INSTITUTE  
EARTH SCIENCE LAB.

## INTRODUCTION

The geothermal industry in the United States has been growing rapidly and undergoing significant change from its early orientation focus on The Geysers dry steam field in California. As can be expected, the first commercial field in the United States has set the pace for the geothermal industry. Technology and environmental problems, economics and operating practices, have all been shaped by The Geysers field which has grown steadily in capacity over the past twenty five years. It should exceed the 1,000 Mw production figure by about 1980 or 1981 (Figure 1).

The growth of this capacity appears to be sustainable for at least another 1,000 Mw and geophysical exploration suggests that several thousand Mw of capacity are possible. Significant step-cut drilling in the central and northern parts of The Geysers KGRA should be done in the next three years, and then we will be able to better evaluate the contribution of the probably extensive hot water resources in the area, and more clearly define the real extent of the dry steam field.

## INDUSTRY CAPACITY

One measure of geothermal production

## GENERATING CAPACITY AT THE GEYSERS KGRA

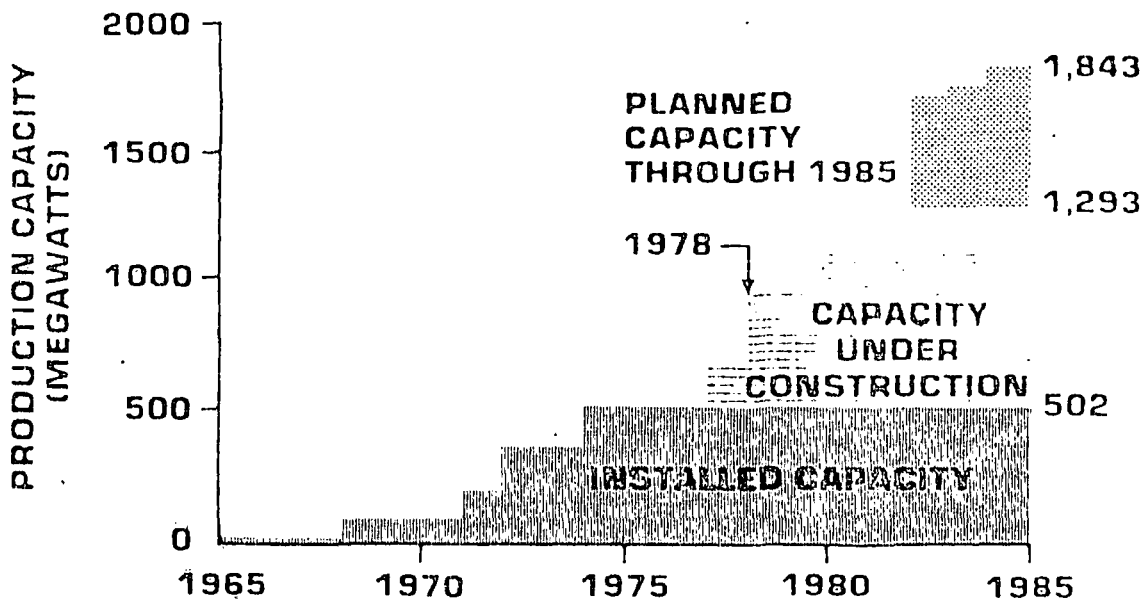


Figure 1.

capacity is the amount of steam production currently being sold and contracted to be sold. The principal operator in The Geysers field is the Union Oil Company, which operates for the joint venture that includes Magma Power and Thermal Power (Natomas). Union has a 50% working interest in the project, with Magma and Thermal each having a 25% working interest.

The Union-Magma-Thermal group is presently the only supplier of steam that is being sold, and the Pacific Gas & Electric Company (PG&E) is using that steam to supply their 502 Mw of installed capacity. Aminoil USA, Inc., successor to the Burmah Oil Company and Signal Oil interests, is scheduled to have 135 Mw of capacity on line with sales to Pacific Gas & Electric Company starting in approximately another year (Figure 2). Hughes Aircraft Company's Thermogenics, Inc. should have 55 Mw on line in approximately another year and a half, also selling steam to the Pacific Gas & Electric Company.

The Shell Oil Company expects to have sales in the early 1980s to the Northern California Power Association, and the

McCulloch Oil Corporation intends to have significant capacity on line for sale to the California Department of Water Resources in the mid 1980s. Several other operators are actively drilling for steam and hot water in The Geysers. These companies include Occidental Petroleum, Standard Oil Company of California (Chevron), Phillips Petroleum Company, Republic Geothermal, Inc., and AMAX Exploration, Inc., with the probable addition of several others. Other than The Geysers, there is no commercial production of geothermal resources under way in the United States. However, several other commercial projects are now under construction. Probably the first of these to go into production, at a commercial level, will be the 48 Mw hot water/wet steam facility that is located on Federal leases in the East Mesa field in the Imperial Valley. This particular project, which Republic Geothermal has under construction, utilizes a nearly fresh water resource that has no corrosion, scaling or hydrogen sulfide problems. The power cycle for this plant will use conventional dual flash steam technology.

### PROJECTION OF INSTALLED GEOTHERMAL POWER CAPACITY IN MEGAWATTS

	1977	1978	1979	1980	1981	1982	1983	TOTAL
UNION MAGMA THERMAL	502	106	110		220		440	1378
AMINOIL			135					135
THERMOGENICS				55				55
SHELL						110		110
McCULLOCH						55		55
REPUBLIC			10	48				58
UNION			10	10				20
MAGMA			10					10
CHEVRON							50	50
PHILLIPS						50		50
<b>TOTAL</b>	<b>502</b>	<b>106</b>	<b>275</b>	<b>113</b>	<b>220</b>	<b>50</b>	<b>655</b>	<b>1921</b>

Figure 2.

The second commercial project will probably be a 50 Mw dual flash steam power plant on the Federal leases in the Roosevelt KGRA in Utah, near the town of Milford. Here, the Phillips Petroleum Company, in a joint venture with Rogers International, will be producing wet steam and converting it into electricity for sale to the Utah Power and Light Company. This project will utilize a low salinity water that also is relatively free of corrosion and hydrogen sulfide problems. Roosevelt has one of the hottest geothermal resources yet discovered in the U. S., and other than its distance from markets, it could be one of the more economically attractive geothermal fields in the country. Unfortunately, it is distant from major markets and it will have to compete with old, low cost, coal-fired facilities, making it economically somewhat handicapped compared to projects closer to rapidly growing load centers such as Southern California.

Several other commercial wet steam/hot water power projects are now under way in

the Imperial Valley, some with initial 10 Mw facilities, to be followed by full-scale 50 Mw plants. These include a Magma Power Company 10 Mw experimental binary fluid facility at East Mesa, which should be in operation by 1979, and a 10 Mw facility supported by the Union Oil Company at the North Brawley field. Standard Oil Company of California and the Southern California Edison Company have announced a 50 Mw project at Heber in the Imperial Valley which would probably come on line in the 1982 to 1984 time frame. The Union Oil Company, Southern Pacific Land Company and the Southern California Edison Company have announced a project to develop the hypersaline corrosive brine at the Salton Sea for power. They have announced that they will first build a 10 Mw facility to be followed by a commercial 50 Mw power plant. The demonstrated success of the existing DOE/SDG&E test facility at Niland makes it probable that the Union project will be successful (Figure 3).

### PROJECTION OF INSTALLED GEOTHERMAL POWER CAPACITY THROUGH 1983 IN MEGAWATTS

<b>GEYSERS</b>	<b>1733</b>
UNION, MAGMA, THERMAL, THERMOGENICS, AMINOIL & SHELL	
<b>IMPERIAL VALLEY</b>	<b>138</b>
REPUBLIC GEOTHERMAL UNION, MAGMA & CHEVRON	
<b>UTAH</b>	<b>50</b>
PHILLIPS	

*Figure 3.*

In Nevada there appears to have been several discoveries made by Phillips, the Union Oil Company and the Standard Oil Company of California, of hot water/wet steam resources in temperature ranges appropriate for commercial development of power. It now appears that Nevada may contribute significant amounts of electricity from geothermal resources starting in the mid-1980's.

Union Oil Company has projected 400 Mw of potential from their discovery in the Valles Caldera within the Jemez Volcano in New Mexico. The aggregate contribution from the California, Nevada, Utah and New Mexico discoveries could easily amount to 1,000 megawatt centuries of proven reserves by the late 1980s. Further expansion of this figure could be accelerated by a lightening of the heavy tax burden which geothermal energy carries.

**DRILLING ACTIVITY**

The relative activities of geothermal operators in the U.S. can be characterized by considering the amount of drilling that they have done in the past three years. An

index of this drilling is the actual footage drilled, which is available from public records (Figure 4). The leader has been the Union Oil Company with over 435,000' of drilling, acting for itself and as operator for Magma and Thermal. The number two company is Aminoil with over 180,000' drilled over the past three years, all of it in The Geysers.

The number three company is Republic Geothermal with nearly 128,000' drilled in California, Utah and Nevada. The number four company is the Shell Oil Company with nearly 100,000' drilled, all of it in The Geysers. The number five company is Phillips with over 65,000' drilled, primarily in Utah but also with some activities in Nevada and California. The number six company is Chevron (Standard of California) with nearly 52,000' drilled in Nevada and California. The number seven is McCulloch with nearly 47,000' drilled primarily in California, and the number eight company is Magma with nearly 42,000' drilled in their own name in Nevada and California. However, it should be remembered that Magma has a one quarter

**SUMMARY OF GEOTHERMAL DRILLING IN THE U.S.**

FOOTAGE DRILLED IN 1975 - 1976 - 1977

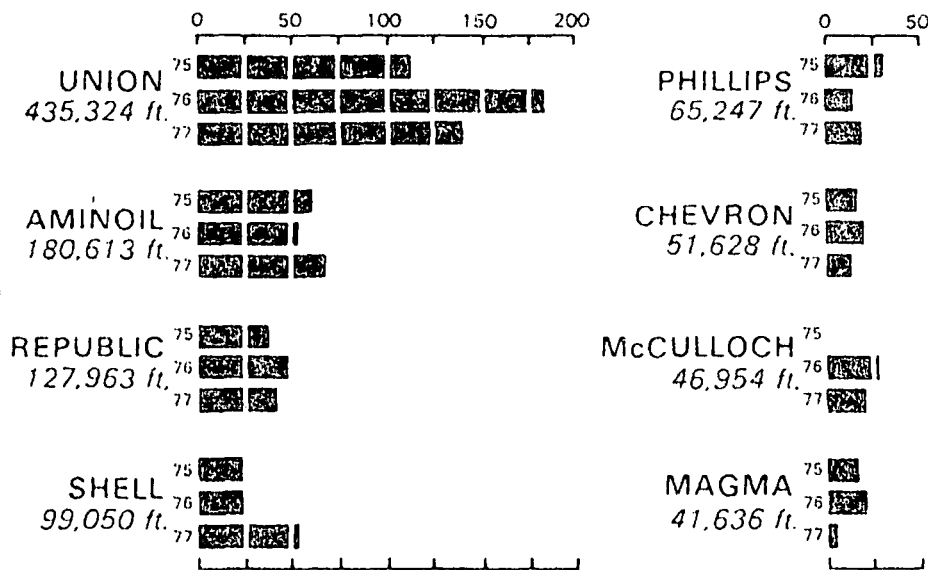


Figure 4.

participation in Union's activities at The Geysers and although not an operator there, it does have a quarter working interest and that, therefore, the position as an operator does not truly reflect Magma's actual position in the industry. Several other companies, while not all comparably active over the past three years, still have been significant in the past and can be expected to become important again in the future. These include Hughes Aircraft Company (Thermogenics), Occidental Petroleum, Natomas, Geothermal Kinetics, Hunt Energy, Getty Oil Company and others.

**INDUSTRY ROSTER**

In addition to the operators, a broad spectrum of support services, hardware suppliers and financial enterprises have become active in the area of geothermal energy. Some indication of this activity can be gained from the roster of members of the Geothermal Resources Council (Figure 5). The current participants include a large number of corporate and organizational enterprises. There are 122 operators among the members, whereas support services are

represented by 413 organizations. These include everything from well logging firms to environmental contractors.

There are 80 hardware and supply company members, 38 that can be considered financial organizations, and some 21 individuals or groups involved in direct applications of geothermal energy, primarily in its use for space heat. In addition there are some 34 members affiliated with utilities. In total, we have seen an explosive growth of commercial and industrial activity in the geothermal area with the preponderance of the operators coming from the oil, gas and mining industries. There are only a handful of independents, but several of these have become significant factors in the industry and appear able to hold their own in competition with the larger oil companies.

All the signs are that the industry is healthy and growing, but that it is very sensitive to the tax climate and to the prices of alternative fuels. The extensive ongoing program of the Department of Energy to encourage the development of geothermal technology, support environmental assessments, and assist in the development

**GEOHERMAL INDUSTRY  
PARTICIPANTS IN 1978  
FROM GEOHERMAL RESOURCES COUNCIL ROSTER**

OPERATORS	122
SUPPORT SERVICES	413
HARDWARE/SUPPLY	80
FINANCIAL	38
DIRECT APPLICATIONS	21
UTILITY	34

*Figure 5.*

of financially independent small companies by the use of the loan guaranty program, appears to be developing successfully. The development of geothermal energy in the United States is currently comparable to a young plant shortly after sprouting - it is vigorous, growing rapidly but very sensitive to adverse treatment. It would only take a short period of thoughtlessness with respect to tax treatment of geothermal drilling to completely devastate the industry at this stage of its development.

Currently, uranium and coal have significant tax advantages compared to geothermal energy in spite of the fact that they are environmentally much more polluting. It seems as though some of our legislators are so concerned about the broad philosophy of taxation as a tool of social reorganization that they are willing to risk destroying the geothermal industry in its earliest period of growth before it really has the staying power needed to permit it to carry a heavy tax burden.

One of the most important geothermal developments in the last three years has been the high incidence of discovery of

commercial geothermal resources on Federal leases. I can speak from personal experience that Federal leases offer the largest potential for new geothermal discoveries for the next ten years. Consequently, the Federal government will not only obtain a tax return from geothermal development but also will obtain royalty income of at least 10% of the gross revenues.

Our economic studies show that the tax benefits, combined with the royalty income, will produce somewhere between \$1 to \$2 billion of revenue to the Federal Treasury over the next 30 years from each 1,000 Mw of geothermal power capacity.

When one compares this to the small size of the Federal investment in this energy resource, it is readily evident that the Federal government is getting an extremely high rate of return on its so-called tax expenditures and industry assistance programs.

\* 11823 East Slauson Avenue, Suite 1, Santa Fe Springs, CA 90670

## ESTIMATED GOVERNMENT REVENUES FROM FIELD DEVELOPMENT PROGRAM

### EAST MESA 48 MW PROJECT

10% FEDERAL ROYALTY PAYMENTS	\$70,200,000
FEDERAL INCOME TAXES	67,110,000
STATE INCOME TAXES	16,590,000
AD VALOREM TAXES	59,700,000
	\$213,600,000

**ASSUMES:  
25 MILS/KWH  
30 YEAR PROJECT LIFE  
6% ANNUAL INFLATION RATE**

*Figure 6.*



## ESTIMATED GOVERNMENT REVENUES FROM FIELD DEVELOPMENT PROGRAM 1000 MW PROJECT

10% FEDERAL ROYALTY PAYMENTS	\$1,462,500,000
FEDERAL INCOME TAXES	1,243,750,000
STATE INCOME TAXES	1,398,125,000
AD VALOREM TAXES	345,625,000
	<hr/>
	\$4,450,000,000

**ASSUMES:  
25 MILS/KWH  
30 YEAR PROJECT LIFE  
6% ANNUAL INFLATION RATE**

*Figure 7.*

---

## Pumps for Geothermal Applications

The special nature of geothermal pumping creates unique problems. We have been actively pumping geothermal fluids for geothermal power and exploration projects since 1960. We can help you. Write to Peerless Pump or phone (213) 726-1232. Ask for George Crabtree, Darrell Payne, Harold Samford or Ray West.

Deep Well (Down Hole)  
Pumps  
Injection Pumps  
Circulators

Boosters  
Brines  
Condensates  
Heat Transfer Fluids



**Peerless Pump**

An Indian Head Company

1200 Sycamore Street  
Montebello, California 90640

# Vapor-Dominated Hydrothermal Systems Compared with Hot-Water Systems<sup>1</sup>

D. E. WHITE, L. J. P. MUFFLER, AND A. H. TRUESDELL

## Abstract

Vapor-dominated ("dry-steam") geothermal systems are uncommon and poorly understood compared with hot-water systems. Critical physical data on both types were obtained from U. S. Geological Survey research in Yellowstone Park. Vapor-dominated systems require relatively potent heat supplies and low initial permeability. After an early hot-water stage, a system becomes vapor dominated when net discharge starts to exceed recharge. Steam then boils from a declining water table; some steam escapes to the atmosphere, but most condenses below the surface, where its heat of vaporization can be conducted upward. The main vapor-dominated reservoir actually is a two-phase heat-transfer system. Vapor boiled from the deep (brine?) water table flows upward; most liquid condensate flows down to the water table, but some may be swept out with steam in channels of principal upflow. Liquid water favors small pores and channels because of its high surface tension relative to that of steam. Steam is largely excluded from smaller spaces but greatly dominates the larger channels and discharge from wells. With time, permeability of water-recharge channels, initially low, becomes still lower because of deposition of carbonates and  $\text{CaSO}_4$ , which decrease in solubility with temperature. The "lid" on the system consists in part of argillized rocks and  $\text{CO}_2$ -saturated condensate.

Our model of vapor-dominated systems and the thermodynamic properties of steam provide the keys for understanding why the major reservoirs of The Geysers, California, and Larderello, Italy, have rather uniform reservoir temperatures near  $240^\circ\text{C}$  and pressures near  $34\text{ kg/cm}^2$  (absolute; gases other than  $\text{H}_2\text{O}$  increase the pressures). Local supply of pore liquid and great stored heat of solid phases account for the physical characteristics and the high productivity of steam wells.

We suggest that vapor-dominated systems provide a good mechanism for separating volatile mercury from all other metals of lower volatility. Mercury is likely to be enriched in the vapor of these systems; the zone of condensation that surrounds the uniform reservoir is attractive for precipitating HgS.

A more speculative suggestion is that porphyry copper deposits form below the deep water tables hypothesized for the vapor-dominated systems. Some enigmatic characteristics of these copper deposits are consistent with such a relationship, and warrant consideration and testing.

## Introduction

ALTHOUGH hot springs throughout the world have been studied for centuries, direct knowledge of their subsurface relationships was lacking until commercial and research drilling was initiated in the 20th Century. With a few notable exceptions (Allen and Day, 1927; Fenner, 1936) little significant scientific data were available prior to 1950.

Efforts to produce electricity from natural steam were first successful in the Larderello region of Italy, starting about 1904. Drilling from 1920 to 1925 showed that large quantities of natural steam could also be obtained at The Geysers in California, but economic development was not feasible until 1955. At both The Geysers and Larderello, wells deeper

than a hundred meters or so<sup>2</sup> and near centers of surface activity were found to yield slightly superheated steam (Burgassi, 1964). Some wells on the borders of the active systems<sup>3</sup> produced hot water

<sup>2</sup>The metric system is used throughout this paper. Some readers may find useful the following conversion factors:

Length: 1 m = 3.281 ft; 1 km = 3,281 ft = 0.6214 mi.

Temperature:  $(^\circ\text{C} \times 9/5) + 32 = ^\circ\text{F}$ .

Pressure: 1  $\text{kg/cm}^2$  = 0.9678 atm = 0.9807 bars = 14.22 psi. All pressures absolute, with 0.78  $\text{kg/cm}^2$  added to gage pressure for Yellowstone Park, and 1.03  $\text{kg/cm}^2$  added to gage pressure at sea level and geothermal areas at low altitudes.

Heat: 1 cal =  $3.9685 \times 10^{-8}$  BTU; 1 cal/gm = 1.80 BTU/lb.

<sup>3</sup>A geothermal system includes a source of heat within the earth's crust (regional heat flow or local igneous intrusion) and the rocks and water affected by that heat. When geothermal systems involve circulating waters, they are also

<sup>1</sup>Publication authorized by the Director, U. S. Geological Survey.

UNIVERSITY OF UTAH  
RESEARCH INSTITUTE  
EARTH SCIENCE LAB.

SUBJ  
GTHM  
VDH

MARKS  
345  
ILY VN.  
TRACE CU  
30  
LY VN.  
TER PY  
05  
EINLET  
CP AFTER  
TN  
90  
BN  
NOR CP.  
AND DG  
MINOR TN  
BN AFTER  
FACE EM  
17  
Y WITH  
TER PY.  
IN  
5 E25965  
ME CP AFTER  
ND TN  
CP. MINOR  
45 E27070  
OF MAIN  
PLACING PY.  
CC AND  
ER CP  
5355  
ND TN AFTER  
ER BN  
1793  
WALL  
MINOR CC  
1 BN RE-  
TR CP AND  
REPLACING  
1 CC  
340 E35140  
MINNIE  
COLO VN.  
CING PY  
760  
QUARTZ  
MINNIE  
CC AND BN  
ACE CP  
N  
LL. TRACE  
N  
STEWARD VN.  
ING PY  
000 E28000  
3R CP

and steam in noncommercial quantities and pressures (Allen and Day, 1927, p. 82); the characteristics of such wells have not yet been adequately described.

From 1946 to 1970 approximately 100 geothermal systems throughout the world were explored at depth by drilling. Initially, the objective of this search was to discover areas yielding dry steam, as at Larderello and The Geysers. This effort, however, soon revealed that most hot-spring systems yield fluids that are dominated by hot water rather than by steam.

New Zealand first demonstrated that a source of dry steam was not essential for the generation of geothermal power. At Wairakei, subsurface hot water at temperatures up to 260° C is erupted through wells to the surface; some of the water flashes to steam as temperature and pressure decrease to the operating pressure, commonly from 3 to 6 kg/cm<sup>2</sup>. This steam, generally 10 to 20 percent of the total mass flow, is separated from the residual water and directed through turbines to generate electricity. The high energy potential of subsurface water has also been demonstrated in Mexico, Iceland, Japan, USSR, El Salvador, the Philippines, and the United States.

A few systems, other than Larderello and The Geysers, yield vapor with little or no associated liquid water. These include the Bagnore and Piancastagnaio fields near Monte Amiata southeast of Larderello (Burgassi, 1964; Cataldi, 1967), and probably the Matsukawa area of northern Honshu, Japan, (Saito, 1964; Hayakawa, 1969; Baba, 1968), the Silica Pit area of Steamboat Springs, Nevada (White, 1968b), and the Mud Volcano area of Yellowstone National Park, considered in this report.

Hot-water systems have attracted nearly all of the research drilling in natural hydrothermal areas. The first two research holes in the world were drilled by the Geophysical Laboratory of the Carnegie Institution of Washington in the hot water systems of Yellowstone Park in 1929-30 (Fenner, 1936), and seven of the eight research holes drilled at Steamboat Springs, Nevada, in 1950-51 (White, 1968b) were in a hot-water system. The eighth was in the small vapor-dominated Silica Pit system, subsidiary to the larger water-dominated area.

Although research drilling by the U. S. Geological Survey in Yellowstone National Park during 1967 and 1968 was aimed mainly at a better understanding of the hot-water systems of the major geyser basins, a specific effort was made to find and drill a vapor-

called hydrothermal systems. The hot part of each hydrothermal system is commonly emphasized, but in its broader meaning the marginal parts involve convective downflow of cold water, and are also included. A hot spring area is the surface expression of a geothermal system and contains hot springs, fumaroles, and other obvious hydrothermal phenomena.

dominated system. The Mud Volcano area was found to be such a system and is described here.

In spite of long and extensive commercial development at Larderello and The Geysers, the origin and nature of the systems that yield dry or superheated steam, and why they differ from the abundant hot-water systems, are not nearly so well understood. Facca and Tonani (1964), for example, seem to deny that Larderello and The Geysers differ significantly from Wairakei, New Zealand, and the other water-dominated areas. Marinelli (1969) states that Larderello is a hot-water area. James (1968) and in less detail Elder (1965) and Craig (1966) have instead proposed that the reservoirs are filled with steam maintained by boiling from a deep water table.

We submit, in agreement with James (1968), that fundamental differences do exist between two main types of natural hydrothermal systems; each type is recognizable by geologic, physical, and geochemical criteria. However, in contrast with James (1968) and others, we consider that steam and water must coexist in the reservoirs of these systems that yield dry steam at the surface.

#### Acknowledgments

We are much indebted to our associates, R. O. Fournier, John Haas, Warren Nokleberg, and J. T. Nash, for their helpful suggestions and review of this manuscript. Gunnar Bodvarsson has been especially helpful in clarifying the properties of coexisting liquid and vapor and in pointing out important differences in specific resistance to flow of liquid water and steam.

#### Summary of Characteristics of Hot-water Systems

Hot-water systems are usually found in permeable sedimentary or volcanic rocks and in competent rocks such as granite that can maintain open channels along faults or fractures. Total discharge from typical systems ranges from several hundred to several thousand liters per minute (lpm), with individual springs commonly discharging a few lpm to several hundreds of lpm. Where near-surface rocks are permeable and the surrounding water table is relatively low, much or all of the circulating hot water escapes below the ground surface, and little or none is discharged from local surface springs. For example, nearly 95 percent of the water at Steamboat Springs, Nevada, escapes in such a way (White, 1968b). On the other hand, where spring outlets are at or below the level of the surrounding water table, all hot water of the system is likely to be discharged in local visible springs.

The spring systems that discharge at low to moderate temperatures are commonly similar chemically

to nearby ground waters, but the near-boiling hot waters of moderate to high discharge are nearly always characterized by relatively high contents of alkali chlorides,  $\text{SiO}_2$ , B, and As (table 1, anal. 4, 8, and 10; White and others, 1963, Tables 17 and 18). In confusing contrast, some gassy springs of low discharge may differ greatly from these chloride-rich waters in physical and chemical characteristics. Surrounding ground is commonly bleached and hydrothermally altered to a porous siliceous residue that may be mistaken for hot-spring sinter. The bleached ground may contain native sulfur, white, yellow, and orange sulfate minerals, and clay minerals, especially kaolinite; vegetation is generally sparse or absent. Chemical analyses of such springs (table 1, anal. 9; White and others, 1963, table 20) contrast strikingly with those of higher discharge; chloride is generally less than 20 ppm, sulfate is the dominant anion, pH is usually between 2.5 and 5, and Fe, Al, Ca, and Mg are abundant relative to Na and K.

Where these two contrasting types of springs coexist in the same general area, topographic relationships and results of shallow drilling and augering indicate that the nearly neutral to alkaline chloride springs are from the main water body, occurring where the water table intersects the ground surface. Where the water table is low, acid springs may result from boiling at this water table. Some steam condenses in cooler ground and in pools of rain water, perched ground, and previously condensed steam.

$\text{H}_2\text{S}$  that evolves with the steam reacts near the surface with atmospheric oxygen to form sulfuric acid, thus accounting for the high sulfate contents and the low pH's characteristic of these waters. Bacterial oxidation of intermediate forms of sulfur may be involved (Schoen and Ehrlich, 1968). The acid dissolves available cations from the surrounding rocks, which are adequate sources for the reported constituents (White and others, 1963, table 20).

The geochemistry of chloride is critical in understanding the differences between the coexisting neutral-chloride and acid-sulfate waters, as well as the differences between vapor-dominated systems and hot-water systems. Most metal chlorides are highly soluble in liquid water, and the low content of Cl in most rocks can be selectively dissolved in water at high temperatures (Ellis and Mahon, 1964, 1967). The common metal chlorides, however, have negligible volatility and solubility in low-pressure steam (Sourirajan and Kennedy, 1962; Krauskopf, 1964). The only chlorides with sufficient volatility to account for significant transfer of Cl in steam at low temperatures and pressures are HCl and  $\text{NH}_4\text{Cl}$ , both of which are minor constituents of most hot-spring systems. The very low Cl content of the perched acid

springs associated with some hot-water systems is thus consistent with near-surface attainment of acidity from oxidation of  $\text{H}_2\text{S}$ , rather than by vapor transfer of HCl from initially acid sources.

The temperatures of many explored hot-water systems increase with depth to a "base" temperature (Bodvarsson, 1964a, 1970) that differs with each system that has been drilled deep enough. Temperatures at Wairakei, New Zealand, rise to a maximum of  $260^\circ\text{C}$  near 450 m of depth but increase little if any more at further explored depths (Banwell and others, 1957, p. 52-56), and at Steamboat Springs, Nevada, the temperatures in six drill holes were near  $170^\circ\text{C}$  at depths close to 100 m, but deeper drilling found no higher temperatures even though major channels were intersected below 150 m (White, 1968b). In such an area, meteoric water (Craig, 1963; White, 1968b) evidently penetrates to considerable depths along permeable channels of a huge convection system; the water is heated to its base temperature by rock conduction, perhaps augmented slightly by magmatic steam. It then rises in the core of the spring system, losing only a little heat because of its relatively high rate of upflow through wallrocks of low thermal conductivity. As the hot water rises the hydrostatic pressure decreases, and eventually a level is attained where pressure is low enough for boiling to begin.

Of about one hundred hot-water systems throughout the world that have now been explored by drilling, fewer than 30 are known to exceed  $200^\circ\text{C}$  in temperature and only about 10 demonstrably exceed  $250^\circ\text{C}$ . The liquid of the two reservoirs known to exceed  $300^\circ\text{C}$  is brine rather than relatively dilute water. The Salton Sea system has about 250,000 ppm of dissolved salts and a maximum temperature of about  $360^\circ\text{C}$  (Helgeson, 1968). The Cerro Prieto system, about 90 km to the south in Baja California, Mexico, has a salinity of about 17,000 ppm and temperatures as high as  $388^\circ\text{C}$  (Mercado, 1969).

Hot-water systems have a high potential for self-sealing (Bodvarsson, 1964b; Facca and Tonani, 1967) by means of deposition of minerals in outlet channels.  $\text{SiO}_2$  is the most important constituent for the self-sealing of high-temperature systems because quartz is so abundant and its solubility increases so much with temperature (Fournier and Rowe, 1966). Quartz dissolves rather rapidly at high temperatures; when quartz-saturated waters are cooled, quartz precipitates rather readily down to about  $180^\circ\text{C}$  but with increasing sluggishness at lower temperatures. The  $\text{SiO}_2$  content of many waters, after cooling, greatly exceeds the solubility of quartz and may even exceed the solubility of amorphous  $\text{SiO}_2$ . Near the surface where temperatures are near or below

Table 1.--Chemical analyses of waters associated with vapor-dominated and hot-water geothermal systems

Name	1/ The Geysers	2/ The Geysers	3/ GS-7	4/ Spring 8	5/ Mud Volcano	6/ Mud Volcano	7/ Y-11, Mud Volcano
Location	Calif.	Calif.	Steamboat, Nev.	Steamboat, Nev.	Yellowstone, Wyo.	Yellowstone, Wyo.	Yellowstone, Wyo.
Water type	HCO <sub>3</sub> -SO <sub>4</sub>	Acid-sulfate	HCO <sub>3</sub> -SO <sub>4</sub>	Cl-HCO <sub>3</sub>	Acid-sulfate	HCO <sub>3</sub> -SO <sub>4</sub>	HCO <sub>3</sub> -SO <sub>4</sub>
System type	Vapor-dom.	Vapor-dom.	Vapor-dom.	Hot water	Vapor-dom.	Vapor-dom.	Vapor-dom.
SiO <sub>2</sub>	66	225	14	293	540	215	
Al		14		0.5	146		
Fe		63		0.05	17		
Mn		1.4		0.05			
As				2.7			
Ca	58	47	6.3	5.0	14	28.7	28
Mg	108	281	0	0.8	11	16.4	0.47
Na	18	12	9.3	653	16	74.3	105
K	6	5	4.5	71	17	47.5	12.6
Li			0	7.6		.20	.18
NH <sub>4</sub>	111	1,400		<1	26	.18	3.2
H		9.5			43		
HCO <sub>3</sub>	176	0	21	305		298	258
CO <sub>3</sub>	--	--	--	--	--	--	--
SO <sub>4</sub>	766	5,710	24	100	3,149	65.3	74
Cl	1.5	0.5	0.5	865	Tr.	13.5	9.6
F			0	1.8	1	2.0	
Br				0.2			
NO <sub>3</sub>			Tr.	--			0.2
B	15	3.1	1.3	49		.6	0.1
H <sub>2</sub> S	0	--	2.4	4.7	0		
Total reported	1,330	7,770	83	2,360	3,980	761.7	491.4
pH	neutral	1.8*	6.5	7.9	Strong acid	7	8.5(?)
Temperature °C	100	Boiling?	161	89.2	65	58.5	131.7

1/ Witches Cauldron, White and others, 1963, p. F47, modified from Allen and Day, 1927.

2/ Devils Kitchen, White and others, 1963, p. F46, modified from Allen and Day, 1927.

3/ White and others, 1963, p. F47. Condensate inapor-filled hole.

4/ . . . Do . . . . . p. F40.

5/ Allen and Day, 1935, p. 427; described as "Big Sulphur Pool" 0.3 km N. of Mud Volcano; location indicates Old Sulphur Cauldron of fig. 4, 60 m SSW of Y-11 drill hole.

6/ Spring discharging from sinter, E. bank of Yellowstone River 0.5 km SE of Y-11 drill hole; has deposited sinter in recent past, if not now. Analyzed by Mrs. Roberta Barnes.

7/ Erupted from Y-11 drill hole Sept. 22, 1969 after hole had caved to 28 m depth (table 1); collected by R. O. Fournier, analysis by Mrs. Roberta Barnes. pH not representative of in-hole environment because of CO<sub>2</sub> loss, storage in plastic with clays.

Note: The wordapor should read vapor in footnote 3.  
Reference to Table 1 in footnote 7 should read Table 4.

100° C, the excess silica in such waters may precipitate as chalcedony, opal, and cristobalite (White and others, 1956). Self-sealing by silica minerals is likely to be slight in hot-water systems that do not

exceed 150° C, but as maximum temperatures increase above this value, the potential for self-sealing increases greatly.

Calcite, zeolites, and some other hydrothermal

VAPOR-DOMINATED HYDROTHERMAL SYSTEMS

Table 1.--Chemical analyses of waters associated with vapor-dominated and hot-water geothermal systems (continued)

Name	8/ Norris Basin	9/ Norris Basin	10/ Well 4	11/ Well 5	12/ Carboli A,	13/ Well MR-1
Location	Yellowstone, Wyo.	Yellowstone, Wyo.	Wairakei, N.Z.	Wairakei, N.Z.	Italy	Matsukawa, Japan
Water type	Cl(HCO <sub>3</sub> )	Acid sulfate	Cl	HCO <sub>3</sub> SO <sub>4</sub>	SO <sub>4</sub> HCO <sub>3</sub> (Cl)	SO <sub>4</sub> (HCO <sub>3</sub> )
System type	Hot water	Hot water	Hot water	Vapor-dom.(?)	Hot water	Vapor-dom.(?)
SiO <sub>2</sub>	529	109	386	191		635
Al		2.4			Trace	29
Fe		0.8			Trace	508
Mn						
As	3.1					
Ca	5.8	2.2	26	12		
Mg	0.2	0	<0.1	1.7	5.0	8.7
Na	439	2.0	1,130	230	56.6	264
K	74	3.0	146	17	32.0	144
Li	8.4		12	1.2		
NH <sub>4</sub>	0.1	30	0.9	0.2	19.0	
H		14				
HCO <sub>3</sub>	27	--	35	670	89.7	37
CO <sub>3</sub>	--	--	0(?)			
SO <sub>4</sub>	38	758	35	11	137.4	1,780
Cl	744	15	1,930	2.7	42.6	.12
F	4.9		6.2	3.7		
Br	0.1					
NO <sub>3</sub>	--					
B	12	6.9	26	0.5	13.9	61.2
H <sub>2</sub> S	.0		1.1	0		Trace
Total reported	1,890	943	3,750	1,140	396.2	1,478.9
pH	7.5	1.97	8.6	6.7		4.9
Temperature °C	84.5	90	228+	High	~300	~240

8/ Dr. Morey's Porkchop, 60 m southwest of Pearl Gevser (White and others, 1963, p. F40).

9/ Locomotive Spring, 55 m WSW of Norris Basin drill hole of Fenner (1936); seeping discharge (White and others, 1963, p. F46).

10/ Typical of shallow Wairakei system; 375 m deep with maximum temperature of 245°C (Banwell and others, 1957). Analysis by Wilson; also contains 11 ppm free CO<sub>2</sub> (Wilson, 1955; quoted in White and others, 1963, p. F40).

11/ Western part of Wairakei field (Wilson, 1955, quoted in White and others, 1963, p. F47). Similar to some waters of vapor-dominated systems; 467 m deep, maximum 217°C at 271 m.

12/ Deepest well of hot-water field on So. border Larderello steam fields (Cataldi and others, 1969). Orig. anal. in nom, supplied by R. Cataldi, 1970.

13/ Well 945 m deep, produced steam, some water for 1 year before drying; this anal. while still wet; condensate of steam 50 ppm H<sub>2</sub>S and 6.2 ppm S (Nakamura and Sumi, 1967; Hayakawa, 1969).

minerals are also effective in producing self-sealed margins of some hot-water systems, but generally less so than the silica minerals. Self-sealing is likely to

be most extensive where temperatures decrease most rapidly. These marginal parts are of secondary interest for production drilling, and they have not been

Table 2.--Analyses of gases associated with vapor-dominated and hot-water geothermal systems, in volume percent

	Total vapor, including H <sub>2</sub> O		Gases, excluding H <sub>2</sub> O					
	1/ The Geysers, California	2/ Larderello, Italy	3/ The Geysers, California (1), recal.	4/ Larderello Italy (2), recal.	5/ Y-11 Mud Volcano, Yellowstone	6/ Mud Volcano Yellowstone	7/ Y-9, Norris, Yellowstone	8/ Spring Norris Yellowstone
H <sub>2</sub> O	98.045	98.08						
CO <sub>2</sub>	1.242	1.786	63.5	93.02	98.4	98.90	91.5	97.40
H <sub>2</sub>	0.287	-0.037	14.7	} 1.92	<0.01	0.00	0.9	0.00
CH <sub>4</sub>	0.299		15.3		Tr.	0.10	0.1	0.20
C <sub>2</sub> H <sub>2</sub>					0.0		0.0	
N <sub>2</sub>	} 0.069	0.0105	} 3.5	0.54	0.8	} 1.00	5.1	} 1.60
A					0.013		0.08	
H <sub>2</sub> S	0.033	0.049	1.7	2.55	0	0.10	1.4	0.75
NH <sub>3</sub>	0.025	0.033	1.3	1.72				
H <sub>3</sub> BO <sub>3</sub>	0.0018	0.0075	0.09	0.39				
O <sub>2</sub>					0.2	0.00	1.0	0.05?
Total	100.002	100.003	100.09	100.14	99.42	100.10	100.08	100.00

1/ Well 1, The Geysers (Allen and Day, 1927, p. 76).

2/ Average vapor from producing wells (Burgassi, 1964), recalculated from analysis in gm per kgm; 2,850,000 kg produced per hour; also contains 1 cm<sup>3</sup> total rare gases per kg.

3/ Recalculated from 1/, without H<sub>2</sub>O.

4/ Recalculated from 2/, without H<sub>2</sub>O.

5/ Collected July 10, 1968, by R. O. Fournier, when hole was still open to 316 ft (table 3).

6/ Gas from same spring as anal. 5 of table 1 (Allen and Day, 1935, p. 86).

7/ Collected by R. O. Fournier, Sept. 18, 1969, and analyzed by D. Byrd, U.S. Geol. Survey; gas separated from water; nearest drill hole to springs of anal. 8 and 9, table 1.

8/ Gas from unnamed acid-sulfate spring "near Congress Pool," perhaps Locomotive (table 1, anal. 9). Allen and Day, 1935, p. 86, 469.

Note: Reference to Table 3 in footnote 5 should read Table 4.

cored and studied in much detail except in research drilling in Yellowstone Park (unpublished data).

For similar geochemical reasons, most hot-water systems with subsurface temperatures of 180° C or higher (White, 1967a) have hot springs or geysers that deposit sinter (amorphous silica precipitated on the ground surface by flowing hot water). Waters that deposit sinter nearly always have SiO<sub>2</sub> contents of at least 240 ppm, equivalent to a quartz-equilibration temperature of 180° C. Because the solubility of amorphous SiO<sub>2</sub> is so much higher than that of quartz, a quartz-saturated water at 180° C must cool to about 70° C in order to precipitate amorphous silica. If the water becomes sufficiently concentrated in SiO<sub>2</sub> by evaporation, as on the borders of pools and in erupted geyser water, precipitation can occur at somewhat higher temperatures.

The existence of sinter, as distinct from travertine

(CaCO<sub>3</sub>) and siliceous residues from acid leaching, is evidence for a hot-water system with present or past subsurface temperatures of more than 180° C.

#### Summary of Characteristics of Vapor-dominated ("Dry-steam") Systems

The near-surface rocks of Larderello, Italy, and The Geysers, California, are relatively tight and incompetent, and evidently do not permit large quantities of meteoric water to penetrate deep into their systems (White, 1964). Even in these areas, however, isotopic data indicate that most of the water is of surface origin (Craig and others, 1956; Craig, 1963).

Surface springs at The Geysers<sup>4</sup> typically have

<sup>4</sup>"The Geysers" is an unfortunate misnomer. The area has never had true geysers, which are restricted to the hot-water systems (White, 1967a).

COPY TO METEOS (100 scale)

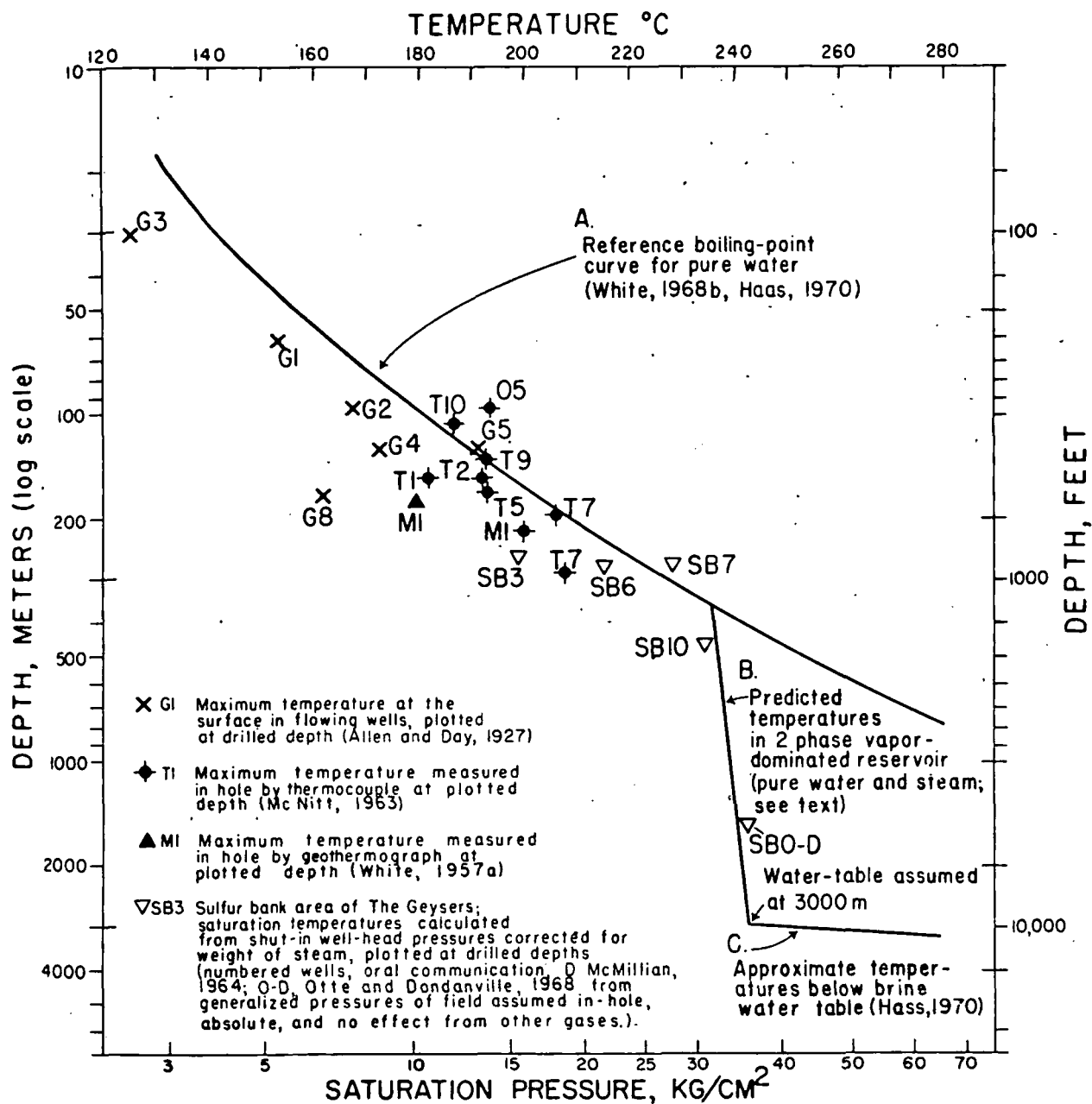


Fig. 1. Measured and calculated temperatures from The Geysers, Calif., with some theoretical curves. The reference boiling-point curve for pure water, curve A, differs in shape from its usual representation because of the logarithmic scale for depth. Note that curves B and C are temperature-deficient and pressure-deficient relative to curve A.

very low discharge, totaling little more than 100 lpm (Allen and Day, 1927). Most of the springs are strongly acidic (pH from 2 to 3). The few neutral springs (Table 1, anal. 1) have chloride contents of less than 2 ppm, similar to local rain water. A careful search of the creek that flows through the area was made on the chance that undetected chloride springs might be seeping into the creek (White, 1957a, p. 1651). However, throughout an area of at least 30 square miles surrounding The Geysers, the

surface and ground waters are no higher in chloride than normal cold streams.

Chloride contents have not been included in reports on natural springs associated with the original vapor-dominated Larderello fields, but available descriptions of spring activity, dominated by mud pots and fumaroles, suggest the presence of sulfate waters low in chloride. However, present springs are not low in pH (R. Cataldi, written commun., 1970), perhaps because of the neutralizing action of abun-



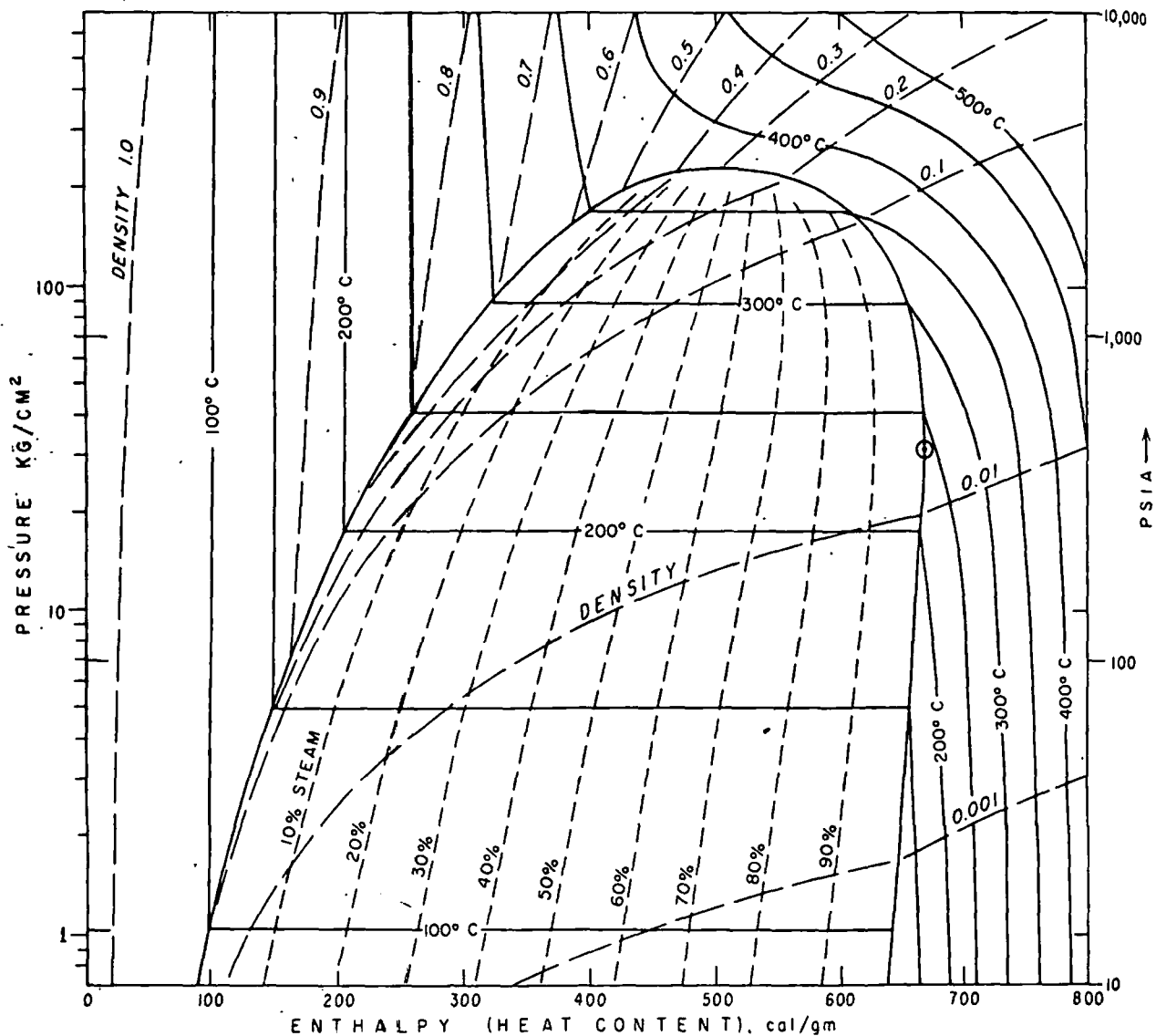


FIG. 2. Pressure-enthalpy diagram for pure water and vapor, showing contours of equal temperature, density, and mass proportions of steam to water (computed from Keenan and Keyes, 1936). Open circle indicates maximum enthalpy of saturated steam, 670 cal/gm at 236° C and 31.8 kg/cm<sup>2</sup>.

dant  $\text{NH}_3$  absorbed from the gases. Some springs and wells of the Carboli area just south of the vapor-dominated fields (Cataldi and others, 1969) contain some chloride (42.6 ppm, Table 1). Although this Cl content is not notably high, it is consistent with the abundant water and old travertine which suggest that Carboli is a hot-water system.

In general where surface springs are all low in chloride and subsurface thermal waters are similarly low (< 20 ppm) a vapor-dominated system is indicated. The Cl content of steam is normally less than 1 ppm, but near-surface waters involved in condensation of the steam commonly contain a few ppm of Cl because, with little or no discharge, Cl can be selectively concentrated.

Typical wells at Larderello (Burgassi, 1964) produce dry or slightly superheated steam with 1 to 5 percent of  $\text{CO}_2$  and other gases (Table 2, anal. 2). Liquid water evidently occurs in some noncommercial wells on the borders of the fields. Shut-in well-head pressures in typical steam wells tend to increase with depth up to a maximum of about 32 kg/cm<sup>2</sup> (Penta, 1959; Burgassi, 1964). Increased productivity reported at greater depths evidently is not due to significantly higher initial pressures. Ferrara and others (1963) list the temperatures of two Larderello wells as 251° C, but all other cited wells are 240° C or lower (depths not given).

Typical wells at The Geysers also produce dry or superheated steam containing gases similar to those

in the I  
up to a  
wells  
whethe  
and ga  
Fig  
sured  
The C  
point  
identi  
plote  
low w  
tionsf  
for hy  
plot  
hydro  
All  
drille  
ther  
surfr  
gest  
liqui  
of th  
maje  
sure  
(19  
zon  
con  
den  
A  
at  
pro  
cur  
ner  
tio  
fig  
ar  
ab  
w  
de  
(  
cr  
st  
h  
p  
c

in the Larderello field (Table 2, anal. 1). Pressures up to about 35 kg/cm<sup>2</sup> were measured in the deeper wells (500 psi, Otte and Dondanville, 1968), but whether pressures were at the well-head or in-hole, and gage or absolute were not specified.

Figure 1 shows the maximum temperatures measured or calculated for individual shallow wells in The Geysers field. For a variety of reasons each point is individually unreliable and is probably not identical with the original ground temperature at its plotted depth. Nevertheless, temperatures of shallow wells (< 350 m) do show a rather close relationship to curve A, the reference boiling-point curve for hydrostatic pressure of pure water. A few points plot above this curve, indicating pressures above hydrostatic but below lithostatic.

All of the early shallow wells at The Geysers were drilled in or near fumaroles, hot springs, and hydrothermally altered ground that provided evidence of surface discharge of thermal fluids. Figure 1 suggests, and our model (to be discussed) assumes, that liquid water condensed from rising steam fills much of the pore spaces; this condensed water provides a major buffering control over temperatures and pressures in the zone of upflowing fluids. McNitt (1963) concluded from other data that a near-surface zone is water saturated; we support his general conclusions but disagree on the nature of the evidence.

Although available data are scanty, temperatures at The Geysers increase irregularly with depth, probably along or near the hydrostatic boiling-point curve, until temperatures near 236° C (and pressures near 32 kg/cm<sup>2</sup>) are attained, with only slight additional increases approximately along curve B of figure 1 to explored depths. In the Sulphur Bank area of The Geysers (Otte and Dondanville, 1968), about 1½ km west-northwest of the original field, wells range from 450 m to more than 2,000 m in depth and are remarkably uniform in temperature (close to 240° C) and in pressure (about 35 kg/cm<sup>2</sup>), as shown in Figure 1. Otte and Dondanville state that "the fluid exists in the reservoir as superheated steam," but the reported temperatures and pressures indicate approximate saturation. No specific data for individual wells are available.

No data have been published to indicate that wells in the central parts of any vapor-dominated field have penetrated a deep water-saturated zone or a water table. In such a penetration, in-hole pressures should increase downward through the water-filled parts of shut-in wells instead of remaining near 32 kg/cm<sup>2</sup>. This evidently does occur in parts of the Italian fields (R. Cataldi, written commun., 1970), but detailed relationships are not yet available. The expected temperature-depth relationships below the

Table 3.--Pressures and temperatures in a two-phase reservoir in which steam is the continuous phase. Top of reservoir assumed to be 236°C 31.8 kg/cm<sup>2</sup>, and 360 m deep (from hydrostatic boiling-point curve).

Depth meters	Pressure, kg/cm <sup>2</sup> (bottom hole)	Temperature °C
360	31.8	236.0
500	32.0	236.1
1,000	33.5	239.0
1,500	34.3	240.3
2,000	35.1	241.6

Note: Second line of column 3 should read 236.3.

deep water table are shown in Figure 1, curve C. This curve has an increasing slope with depth and all points on it are also deficient in pressure with respect to external water pressures, probably to depths of 2,000 m or more below the water table.

James (1968) noted that initial temperatures and pressures of the Larderello steam fields were close to the temperature (236° C) and pressure (31.8 kg/cm<sup>2</sup>) of saturated steam of maximum enthalpy (670 cal/gm; indicated on Fig. 2). James reasoned that enthalpies up to this maximum can be obtained in undisturbed steam reservoirs by evaporation at a subsurface water table. Higher temperatures (and pressures) can exist below but not at the water table. He reasoned that if saturated steam at 350° C and 68.7 kg/cm<sup>2</sup>, for example, with an enthalpy of only 612 cal/gm (Fig. 2), formed deep in a system and rose up to levels of lower hydrostatic pressure, part of the steam would increase in enthalpy as it continued to rise while the rest would condense to liquid water and remain behind. For a pure water system, this separation of liquid from vapor continues until the pressure at maximum enthalpy is attained.

The enthalpy of saturated steam near its maximum, however, is not very sensitive to changes in temperature and pressure (Fig. 2). James suggested that the top of a natural vapor-dominated reservoir is likely to have a temperature near 236° C and a pressure near 31.8 kg/cm<sup>2</sup> but that, because of the weight of steam in a deep reservoir, the temperature near a boiling water table may be as much as 240° C at a pressure near 34 kg/cm<sup>2</sup>. Table 3 shows expected depth-related variations in temperature and pressure of a pure water system in a homogeneous, vapor-dominated reservoir.

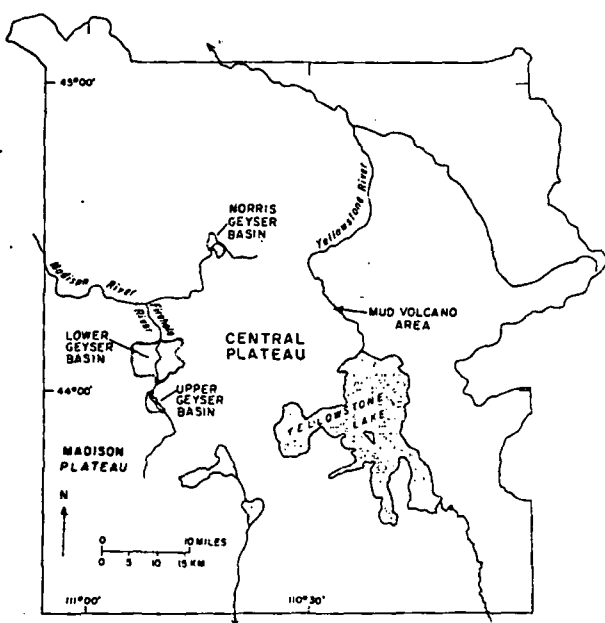


FIG. 3. Index map of Yellowstone National Park, Wyoming, showing location of Mud Volcano area and the major geysers basins.

The scanty available data suggest that temperatures and pressures may exceed the limits suggested by James because of the effects of dissolved salts and the partial pressures of other gases. In addition, although the maximum enthalpy of steam does seem to buffer these systems at temperatures near 236° to 240° C and pressures near 32 to 34 kg/cm<sup>2</sup>, we see no fundamental reason why the available heat supply may not form somewhat more steam than can escape at these pressures through available channels. In this paper we shall assume James' suggested range in temperatures and pressures as the most probable, but we emphasize that more precise data are essential in understanding the detailed characteristics of these systems.

Recorded temperatures of the vapor-dominated reservoirs are significantly lower than in some hot-water fields, which range up to 388° C (Mercado, 1969). The Carboli field on the southern edge of the Larderello steam fields is notable in being the only described field in the Larderello region that produces more water than steam by mass and thus is a hot-water system. Its maximum temperature is about 300° C (Cataldi and others, 1969), which clearly exceeds all temperatures reported from the vapor-dominated areas.

#### The Mud Volcano Area, Yellowstone Park

*General Setting.*—The Mud Volcano area is located along the Yellowstone River about 8 km north of Yellowstone Lake (Fig. 3). Bedrock of the area

is rhyolitic ash-flow tuffs erupted approximately 600,000 years ago (R. L. Christiansen and J. D. Obradovich, 1969, written commun.). Glacial gravels and sands of Pinedale age (about 25,000 to 12,000 years B.P.) mantle the bedrock except near the center of the area.

Thermal activity in the Mud Volcano area consists almost entirely of vigorously bubbling mud pots, acid-sulfate springs, and steam vents concentrated on north-northeast lineaments. Total discharge is only about 80 lpm (Allen and Day, 1935, p. 58) from an area of 2½ km<sup>2</sup>. There are no chloride-rich springs like those of the major geysers basins, even along the Yellowstone River, which is the local base level for the water table of the area. Instead, acid-sulfate and nearly neutral bicarbonate-sulfate springs occur along the river (anals. 5 and 6, Table 1). A little silica is being deposited by evaporation from algal mats at two of these nearly neutral springs, and opal-cemented Holocene alluvium is common along the riverbanks. Although none of the present springs has enough silica to deposit hard sinter from flowing water on the surface (generally requiring at least 240 ppm SiO<sub>2</sub>), three small areas of old sinter occur as much as 3 m above river level. This indicates that sometime in the past 12,000 years silica-rich water, presumably also rich in chloride, discharged at the surface in the Mud Volcano area.

Acid-sulfate springs similar in discharge and chemistry to the Mud Volcano springs occur locally where H<sub>2</sub>S is abundant in high ground of the major Yellowstone geysers areas (anal. 9, Table 1). However, in contrast to drill hole Y-11 in the Mud Volcano area (anal. 7, Table 1), all drill holes in the geysers basins tapped water rich in chloride and similar to waters from the geysers and the principal flowing springs (anal. 8, Table 1).

Y-11 was drilled by the U. S. Geological Survey at the north end of the Mud Volcano area, 75 m north-northeast of Old Sulphur Cauldron. Figure 4 shows the locations of the hole and the "tree line" inside of which trees do not grow because temperatures are too high. Also shown are two heat-flow contours mapped by snowfall calorimetry (White, 1969). The 900 µcal/cm<sup>2</sup> sec (microcalories per sq cm per second) contour is probably within 20 percent of the existing total conductive and convective heat flow. This heat flow is about 600 times the world-wide average conductive heat flow of the earth (Lee and Uyeda, 1965). The 5,000 µcal contour is less precisely located, but total heat flow obviously increases rapidly southeast from Y-11 drill hole.

*Near-surface Ground Temperatures.*—Relationships between heat flow, depth, and temperature determined in shallow auger holes near Y-11 clarify some principles of major significance to the vapor-

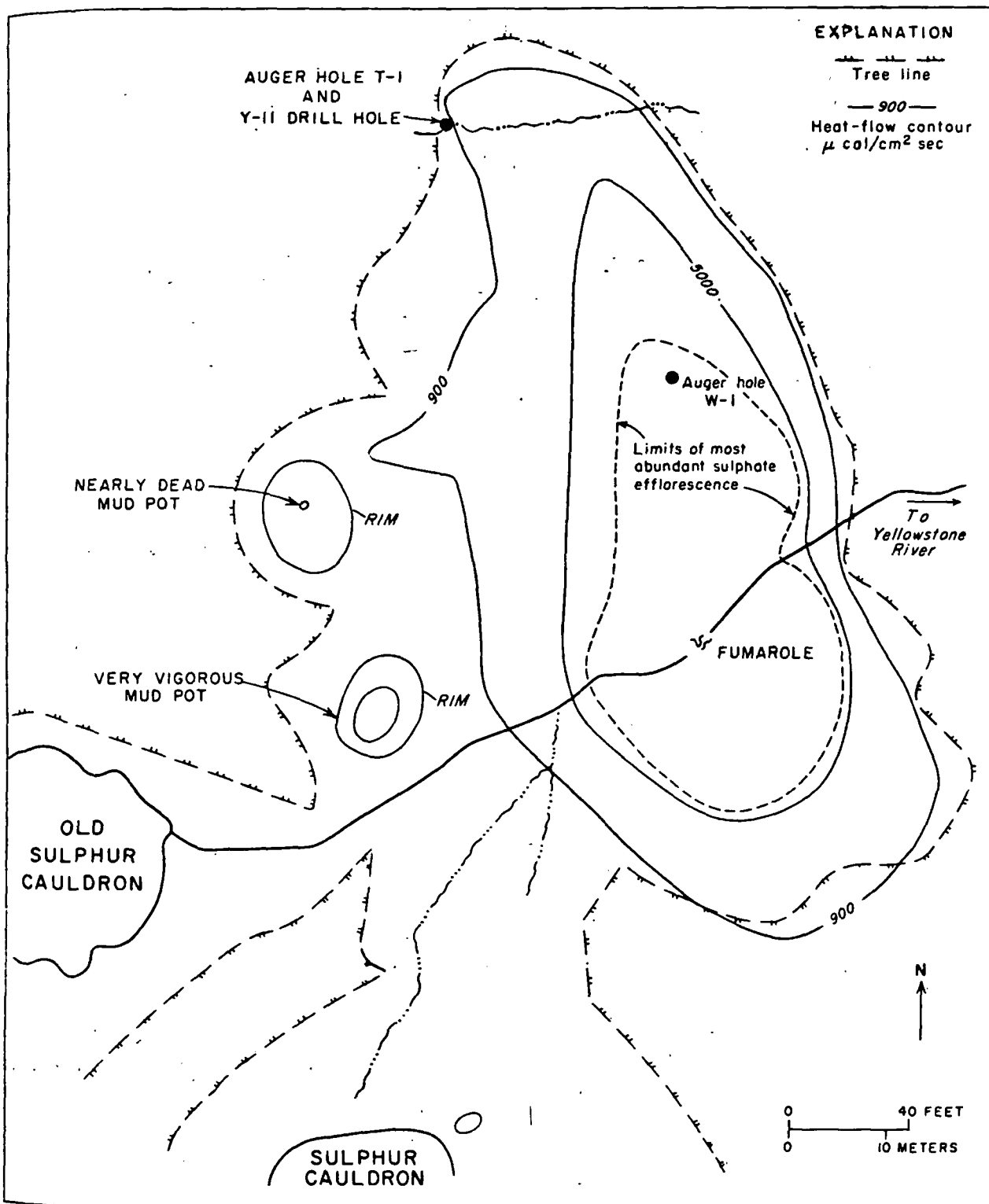


Fig. 4. Sulphur Cauldron area, north end of Mud Volcano area, showing location of Y-11 drill hole relative to heat flow and other features.

oximately  
nd J. D.  
cial grav-  
15,000 to  
cept near

a consists  
ud pots,  
trated on  
e is only  
from an  
h springs  
along the  
level for  
ilfate and  
cur along  
tle silica  
l mats at  
nd opal-  
along the  
t springs  
n flowing  
least 240  
occur as  
cates that  
ch water,  
ed at the

nd chem-  
ir locally  
he major  
) How-  
Mud Vol-  
es in the  
and simi-  
principal

al Survey  
ea, 75 m  
Figure  
ree line,"  
tempera-  
heat-flow  
(White,  
ories per  
within 20  
d convec-  
times the  
the earth  
contour is  
obviously  
l hole.

Relation-  
emperature  
11 clarify  
ne vapor-

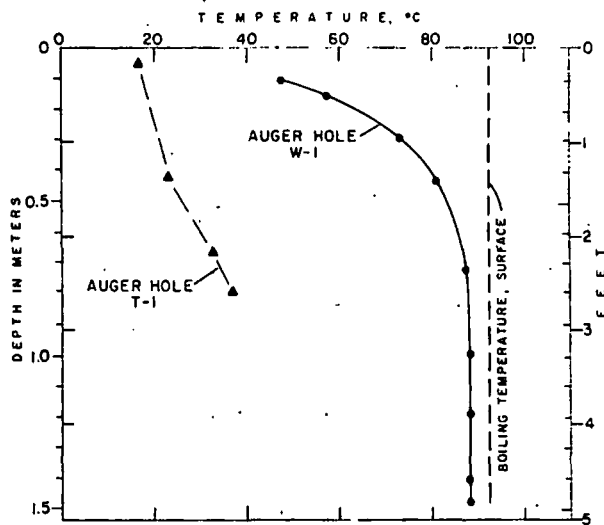


FIG. 5. Temperature-depth curves in shallow auger holes in ground with dispersed upflow of steam and other gases.

dominated systems. Hole T-1 (Fig. 5) was augered on the Y-11 site just prior to drilling, and hole W-1 was augered 35 m to the southeast (Fig. 4). The near-surface temperature at any given depth increases abruptly to the southeast, correlating with increasing heat flow.

Temperatures in W-1 increased rapidly with depth to about  $\frac{3}{4}$  m, where they leveled off at 88.2° C. From 1.0 to 1.55 m there was no temperature change. Consequently, heat cannot be transferred by conduction through this interval, and all heat that flows out

at the surface must be transferred in steam and other gases through the no-gradient zone. Total heat flow at the surface of W-1 auger hole has not been measured by snowfall calorimetry, but extrapolation of data on Figure 4 suggests a heat flow of perhaps 10,000  $\mu\text{cal}/\text{cm}^2 \text{ sec}$ .

The leveling off of temperatures in W-1 at 4.1° C below the boiling temperature of pure water (92.3° C at this altitude) is due to the high content of CO<sub>2</sub>, H<sub>2</sub>S, and other gases in the rising vapor. The vapor pressure of water at 88.2° C is 491 mm of Hg, but the atmospheric pressure averages about 572 mm of Hg. Thus 14 percent of the total vapor pressure results from the partial pressures of other gases. At a depth where the temperature is 85° C, 25 percent of the total pressure is due to residual gases (143 mm of 572 mm of total Hg pressure); similarly, 50 percent consists of other gases at 75° C, 90 percent at 40° C, and 97.7 percent at 15° C.

The depth at which the temperatures level off is dependent on the heat flux from below, the thermal conductivity of the soil, the air-ground interface temperature, and the amount and nature of precipitation of the preceding few days or weeks. If the rate of upflow of steam increases sufficiently, a surface fumarole is produced. If, in contrast, the rate of upflow decreases, complete condensation occurs at a greater depth appropriate to the thermal conductivity heat flow, and surface temperature.

In the steam-gas mixture in W-1 auger hole, no steam condenses between a depth of 1.0 m and the bottom of the hole because of the absence of a tem-

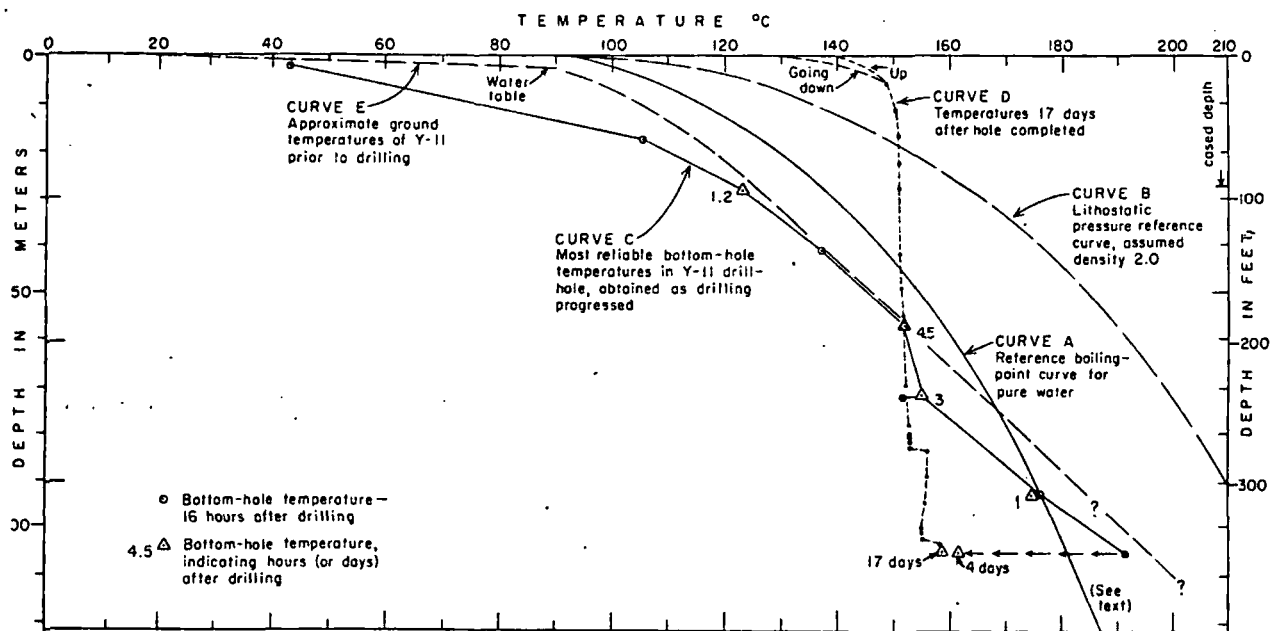


FIG. 6. Temperatures in Y-11 (Sulphur Cauldron) drill hole, Mud Volcano area, Yellowstone Park, Wyoming.

Table 4.--Temperatures, pressures, and other data from Y-11 (Sulphur Cauldron) drill hole, Mud Volcano area, Yellowstone National Park, Wyoming

Underlined data considered most reliable

Date and time 1968	Observation depth, m	Temperature, °C	Depth to water, m	Total pressure, kg/cm <sup>2</sup>	Comments
13 8:35A	2.0	<u>43.0</u> ?			Drilled to 6.1 m, set 4 in. casing, and cemented on May 14; on cement at 2.0 m, temp. probably minimum.
12:10	8.3	(36.0)	2.3		80 min. after circulation ceased; good water level 1 hr. after circulation ceased.
3:25	18.1	87.0		0.85	Drilled 18.3 m; pressure all gas.
16 8:15A		104.4		1.17	Do.
4:23	<u>17.3</u>	106.4	2.3	1.08	Gas only; 91°C at water level.
1:25P	27.7	<u>123.3</u>		2.05	1.2 hrs. since circulation; could have erupted; drilled, set 27.4 m 3 in. casing and cemented.
17 8:00A	13.7	73.0			On cement; temperature probably minimum.
4:45P	(41.8)	(116.1)	5.2		Drilled 41.8 m; lost circulation 37.2-41.8 m.
18 7:50A		137.0	4.9		Gas pressure from outside rods, 1.56 kg/cm <sup>2</sup> ; temperature at water level inside rods 73°C.
8:08A	41.4	137.2		<u>137.1</u>	
1:00 P	(57.0)	(120.3)	4.7		Low circulation 41.8-57.0 m; temp. 1-1/2 hrs. after circulation.
19 10:50A		152.4			
11:00	56.9	151.4	4.6		23 hrs. after circulation.
20 7:54A	57.0	151.4			45 hrs. after circulation.
8:05	57.0	153.4			
8:12		150.9		<u>151.9</u>	
8:22		131.9	0.3		Water level fluctuating.
2:00P	72.2	<u>154.5</u>		0.8	3 hrs. after circulation, pressure fluctuating; water discharged outside of rods; drilled 72.3 m.
21 7:45A		151.1		3.5-3.6	Gas pressure; note temp. decrease since May 20. Drilled to 93.6 m; erupted after pulling core; nearly all steam after much initial water.
7:57	72.2	152.0		<u>151.6</u>	
12:20P		<u>174.3</u>		5.8 then to 4.1	Temp. 40 min. after eruption; some water with steam at 4.1 kg/cm <sup>2</sup> .
3:45P	93.4	174.7		7.8 down to 5.9	Leaking steam at 7.8 kg/cm <sup>2</sup> , then down to 5.9 kg/cm <sup>2</sup> , some water.
3:50				4.4	Pressure on side valve, outside drill rods.
22 8:00A		175.7		10.1 down to 8.0	Leaking vapor only.
8:12	<u>93.4</u>	176.1		<u>175.9</u>	Vapor and a little water; drilling increasingly difficult >100 m. Violent eruption at 105.7 m, initially much water (drill water?), then mostly steam.
23 8:15A		191.6		12.7 to 11.2	Leaking vapor only. Drill rods in hole a few feet off bottom; exact depth not noted.
8:30A	105.7	191.1		<u>191.4</u>	
-11:00A				5.0	Rods pulled, pumping cold water down outside rods throughout; pressure with open hole >27.4 m. Hang up at about 33.6 m, erupted to clear--powerful steam eruption but little water.
27 Not noted	105.5	161.1		5.3	Note major permanent changes in temperature and pressure after rods out of hole.
		161.4		<u>161.3</u>	
Sept. 19 10:00A	-105	<u>158.6</u>		5.3 to 5.4	Thermistor temperature series plotted on fig. 6. Temperature generally steady and reproducible down to 84.1 m, fluctuating somewhat at greater depths, up to 4°C at bottom (maximum is plotted).
10	96.3			5.0	R. O. Fournier attempted to sample; filled with vapor to existing bottom.
28	39.0			4.6	Blocked; no access to greater depths; no water to 39.0 m.
Sept. 1969 21	28.0	<u>131.7</u>		3.2 to 3.5	Attempting thermistor series; initial temperature at top 75°C, increasing to 107°C with leakage of gas. Hole filled with gas to cave at 28.0 m just below casing; thermistor wedged and lost. Erupted gas, mud, and water, and collected water sample.
					Pumped in 5 sacks of cement at pressures up to 11.3 kg/cm <sup>2</sup> .

and other  
eat flow  
en mea-  
ation of  
perhaps  
4.1°C  
(92.3'  
of CO<sub>2</sub>  
e vapor  
-lg. hu-  
num of  
ressure  
gases.  
25 per-  
l gases  
; simi-  
75° C.  
off is  
hermal  
urface  
cipita-  
re rate  
urface  
ate of  
s at a  
ctivity  
le, no  
nd the  
tem-



perature gradient. As steam rises above a depth of 1 m, however, a little starts to condense as a temperature gradient first becomes evident. The gra-

dient increases upward as the surface is approached, so more water vapor can condense. The residual gases are progressively concentrated upward as H<sub>2</sub>O

is condensed, the velocity of upflow consequently decreases, and a correspondingly smaller proportion of the total heat is transported by water vapor. Convective transport of heat at the air-ground interface must be largely in the residual gases, but water vapor, even though a minor constituent, is still a significant transporter of heat because of its high heat of vaporization (588 cal/gm at 15° C), relative to heat content of other gases.

The water vapor that condenses between 1.0 m and the surface at W-1 percolates downward against the flow of steam. The ground is unsaturated with liquid at the bottom of the auger hole and probably to the local water table (2.3 m in Y-11 drill hole). Below the water table at W-1, pressures must exceed atmospheric, and temperatures probably rise along or near the hydrostatic boiling point curve of Figure 6.

The near-surface temperature gradient in auger hole W-1 of Figure 5 is much higher than in T-1, as we should expect from the heat-flow contours of Figure 4. Projection of the T-1 gradient downward to the water table at 2.3 m suggests that temperatures were slightly below boiling at this depth. It appears that only a little water vapor and other gases were rising at the Y-11 site prior to drilling, and most heat was being transferred from the water table to the ground surface by conduction.

*Physical Measurements Made During Drilling of Y-11.*—Data from Y-11 are summarized in Table 4, and bottom-hole temperatures are plotted in Figure 6. The bottom-hole temperatures considered to be most reliable are connected by a solid line. Much effort was made to obtain reliable data from Y-11 as drilling progressed, in part because of the paucity of such data from the large commercial vapor-dominated systems. Because of the high cost of drilling and other factors, available data from the commercial systems are entirely restricted to completed wells, and almost no data are obtained at shallow and intermediate depths as drilling progresses.

In the recent holes drilled in Yellowstone National Park, temperatures measured at each temporary bottom, just before resumption of drilling (generally after overnight shut-down of about 16 hours), provided reasonable approximations of pre-drilling ground temperatures; they are far superior to temperature profiles measured in completed holes (White, Fournier, Muffler, and Truesdell, unpublished data). Measured bottom-hole temperatures in Y-11, however, are less reliable than in the other holes but are considered to be within a few degrees of original ground temperature. At depths less than 27.4 m, rapid drilling plus the setting of two strings of casing prevented acquisition of reliable data. From 37.2 to 79.3 m, all drill water was lost into the

ground, and at greater depths only about 50 percent returned to the surface. Despite the apparent high permeability and loss of drill water, however, the temperature of 151.9° C at 57.0 m depth is probably reliable because it was repeated on successive days with no disturbance by drilling.

A temperature profile made in the open hole 17 days after completion is shown on Figure 6 (curve D). It differs greatly from the temperature profile obtained as drilling progressed. The temperatures from 12.2 to 83.5 m were almost constant, rising only 2° or so, to 153° C at 83.5 m. At greater depths, rapid fluctuations of 1° to 5° were observed. These fluctuations were not due to instrumental defects and were far too large and too rapid to be caused by only a vapor phase; coexistence of steam and water is thus indicated from 83.5 to 103.7 m. The pressure of saturated steam at 153° C is 5.3 kg/cm<sup>2</sup>, which is very close to the measured well-head pressure, 5.4 kg/cm<sup>2</sup>. The temperature of 158.2° C at 103.7 m, however, is not consistent with the well-head pressure, unless liquid water was present near the bottom of the hole. From drill records, we conclude that water was probably entering the hole from depths as shallow as 58 m or less, while an upward flow of steam dominated the central part of the casing. Detailed relationships that existed during the thermistor measurements between 83.5 and 103.7 m cannot be deciphered completely. Evidently some steam was flowing in near 84.2 and 103.7 m. Water seeping down from higher levels did not accumulate extensively but was either forced out into permeable walls or was evaporated by the higher temperature steam. At shallow depths in the hole, horizontal and vertical temperature gradients were so high that most water vapor condensed and residual gases were concentrated, as in auger hole W-1. The condensed water trickled down the walls of the casing.

On several occasions during the drilling of Y-11, we were unable to prevent the hole from erupting for short intervals. The eruptions differed notably, however, from those in holes in the hot-water systems of the geyser basins. In drill holes in permeable rocks, with adequate water supply, and a temperature of 160° C, for example, only 11 percent of the total liquid water vaporizes to steam when erupted (at constant enthalpy) to atmospheric pressure (Fig. 2). The remaining 89 percent of the erupted mass is liquid; the large content of liquid water produces effects that are similar to those of the early stages of geyser eruptions. During an eruption of Y-11, however, the local supply of liquid water was soon nearly exhausted and steam became completely dominant. We estimated that the steam was associated with less than 10 percent of liquid water

by weight  
charge d  
lent that  
eruption  
hole had  
uncased  
tures in  
m pore  
and E,

The p  
rods on  
sents th  
assumin  
to 4½ m  
and neg  
bottom  
below t  
was ab  
about  
bottom  
water  
kg/cm<sup>2</sup>  
static v  
that to  
those c  
must  
model

Liqu  
the S  
ground  
2.3 m  
the be  
drillin  
dropp  
to the  
down  
been  
temp  
depth  
E);  
temp

TI  
at a  
erup  
dant  
stea  
char  
tigh  
avai  
beh  
from  
(W  
high  
no  
me  
tive

by weight. Although at no time did the hole discharge dry steam free of liquid water, we are confident that a dry discharge would have occurred if the eruption had been permitted to continue or if the hole had been cased a little deeper. (The hole was uncased below 27.4 m, and the bottom-hole temperatures indicate an original dominance of liquid water in pore spaces to depths of about 73 m; curves C and E, Fig. 6.)

The pressure of 12.7 kg/cm<sup>2</sup> measured in the drill rods on May 23 at the greatest drilled depth represents the approximate total pressure at the drill bit, assuming vapor-filled drill rods raised the usual 3 to 4½ m above bottom (1 to 1½ lengths of drill rods), and neglecting the weight of the vapor. If 3.7 m off bottom is assumed, with liquid water filling the hole below the rods, the calculated bottom-hole pressure was about 13.1 kg/cm<sup>2</sup> (with a possible range from about 12.8 to 13.6 kg/cm<sup>2</sup>). The pressure at the bottom of an open hole 105.8 m deep and filled with water everywhere just at boiling should be 10.5 kg/cm<sup>2</sup>. Thus, the excess pressure above hydrostatic was about 2.6 kg/cm<sup>2</sup> or 25 percent. The fact that temperatures and pressures are higher than those of a simple hydrostatic control is important and must be consistent with any satisfactory general model of the vapor-dominated systems.

*Liquid-dominated and Vapor-dominated Parts of the System.*—In Y-11 drill hole, water-saturated ground evidently extended from the water table at 2.3 m down to a depth of about 73 m. At 72.2 m, the bottom-hole temperature measured 3 hours after drilling ceased was 154.5° C; 18 hours later it had dropped 3° C. We believe that this change was due to the cooling effect of drill water continuing to drain down the hole and into channels that had formerly been dominated by vapor. The pre-drilling ground temperature probably was not attained at this drilled depth and was probably about 165° C (Fig. 6, curve E); flow of water down the hole prevented a normal temperature recovery.

The hole was definitely in vapor-dominated ground at a depth of 93.4 m. At this depth an unanticipated eruption through the drill rods first discharged abundant drill water and then changed rapidly to wet steam with only traces of liquid water. Such a change in behavior is not particularly significant in tight rocks of a hot-water system when the water available for immediate eruption is exhausted; the behavior is similar to that of a geyser as it changes from its main eruptive phase to a steam phase (White, 1967a). However, permeability was so high at all depths below 37 m in Y-11 that little or no drill water returned to the surface. Lack of permeability clearly does not explain the observed eruptive behavior; a limited supply of available liquid

water provides the only reasonable alternative. If all lost drill water had remained in nearby permeable ground, the eruption likewise could not have been so nearly dry. The drill water must have percolated down former vapor-filled channels to become unavailable in supporting the eruption.

Forty-six days after completion of the hole, measurements made by an in-hole sampling device (Fournier and Truesdell, 1970) demonstrated that the hole was filled with vapor to 96.4 m, where caving had occurred. Presumably all drill water was then exhausted and all inflowing pore water from higher levels either evaporated completely or escaped downward through former vapor-filled channels.

From these data we can conclude that vapor pressure in the hot core of the system below about 76 m is now significantly above hydrostatic pressure (Fig. 6). Some vapor is being forced upward and outward into the cooler walls. The excess driving pressure above hydrostatic presumably is dispersed in overcoming the frictional resistance to flow of vapor along narrow channelways, which become increasingly clogged upward and outward with liquid water condensed from steam; some of the gases other than steam dissolve in this liquid condensate. If many large free-flowing channels vented to the surface as fumaroles and mud volcanoes, the high vapor pressures in excess of hydrostatic obviously could not be maintained.

Another factor that may be of major importance in impeding the escape of vapor is the formation of montmorillonite and kaolinite, which are the dominant alteration products in rocks and fracture fillings of Y-11 drill core from about 15 to 58 m. Montmorillonite and kaolinite also occur sporadically at greater depths but are generally less abundant than other hydrothermal minerals and unaltered rock silicates. The condensed steam is saturated with CO<sub>2</sub> and other gases from the rising vapor. This carbonated water, represented by analyses 6 and 7 of Table 1, is highly effective in altering feldspars and other silicates to clay minerals, and in leaching cations from the rocks. Pyrite is also relatively abundant through the same general interval, from 18 to 61 m, but is sporadic at greater depths. Much sulfide from the rising H<sub>2</sub>S evidently dissolves in the condensate and becomes fixed, combining with Fe of the rocks.

The hot vapor-dominated core of the system evidently is not sharply separated by a single fluid interface from the cooler liquid-dominated walls. We conclude that, in the core of the system, the largest fractures and open spaces are mostly or entirely filled with vapor but open spaces of similar dimensions in the margins of the system are largely filled with liquid water, except for dispersed clays



and vapor bubbles that sporadically rise through the water.

**General Model of Vapor-dominated Geothermal Systems**

A vapor-dominated geothermal system must normally develop from water-saturated rocks. This statement may be unconvincing for young volcanic rocks (how do we know that such rocks were ever water-saturated?) but is irrefutable for old marine sediments that are now far below the regional water table, as in Tuscany and The Geysers. A new regime is initiated with the introduction of a local potent source of heat at depth (probably a body of magma). Much heat is transferred via conduction and circulating water into surrounding rocks that

have some permeability. Because of thermal expansion and resulting decrease in density of the heated water, a hot-water convection system is then initiated. Most rocks seem to be sufficiently permeable to persist as hosts for hot-water systems; the rate of flow of water remains high enough and the supply of conducted heat below the circulation system remains low enough for most of the water flowing through the system to remain liquid. Near-surface temperatures in the hotter systems, however, are high enough for some boiling to occur as the water rises to intersect the boiling point curve (A of Fig. 6). The depth where boiling first occurs in the rising water depends mainly on the temperature of the water.

Many hot-water systems are to a major extent self-regulating. With more heat flow, the upflowing

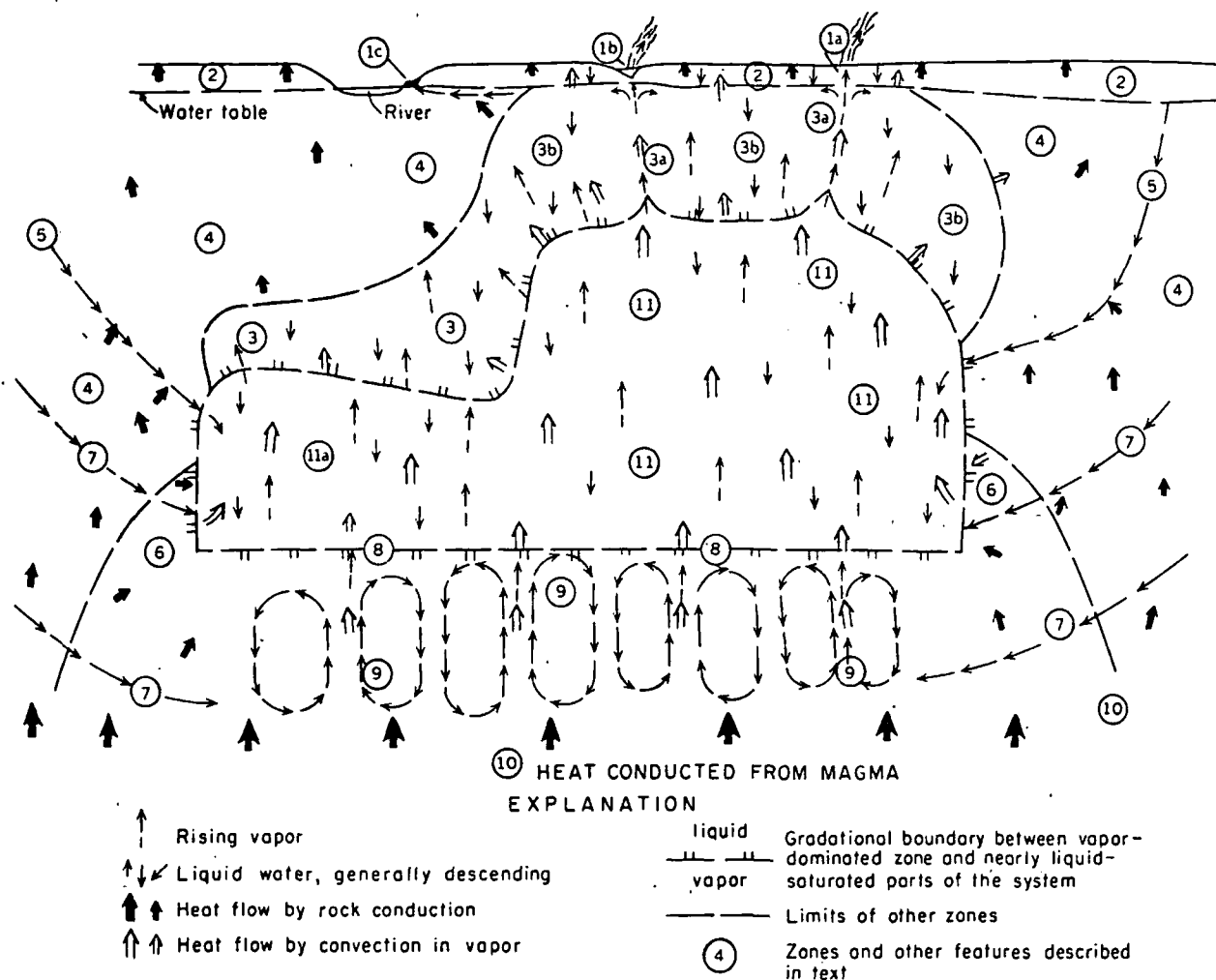


FIG. 7. Model of dynamic vapor-dominated geothermal reservoir surrounded by water-saturated ground. The most significant parts of the model, inward and downward by number, are: 4) zone of conductive heat flow; 3) zone of condensation of steam (conductive and convective heat flow equally important); 11) main vapor-dominated reservoir, with convective upflow of heat in larger channels, and downflow of condensate in small pores and fractures (surface tension effects); 9) deep zone of convective heat transfer, probably in brine; 10) deep zone of conductive heat flow (too hot for open fractures to be maintained). Other features are discussed in text.

water  
osity  
the in  
the ac  
may l  
Wil  
reason  
water  
boil o  
A rap  
rect  
liquid  
system  
evid  
system  
hot v  
little  
early  
flow  
and  
be d  
Fi  
deve  
disc  
(1  
muc  
Fur  
surf  
sprin  
muc  
in d  
5,  
Sur  
veg  
by  
abs  
are  
mu  
Tai  
(  
the  
gas  
W  
is  
die  
ne  
Ti  
ri  
M  
In  
sh  
as  
cl  
d

water becomes hotter and lower in density and viscosity; the pressure drive for recharge increases, and the increased rate of through-flow removes most of the additional heat. This self-regulation, however, may be limited by insufficient permeability.

With sufficiently potent heat supply or, for any reason, a decreasing rate of recharge of water, a hot-water system of limited permeability may start to boil off more water than can be replaced by inflow. A *vapor-dominated system* then starts to form. Direct evidence for the assumed initial dominance of liquid water is lacking for the major vapor-dominated systems. Hot-spring sinter constitutes the clearest evidence, and is so interpreted for the Mud Volcano system. However, sinter is deposited only from very hot water that flows so rapidly to the surface that little  $\text{SiO}_2$  precipitates en route. In addition, the early hot-water stage of these systems of high heat flow and low permeability is likely to have been brief and their thin sinter deposits (if any) are likely to be destroyed by erosion.

Figure 7 is our tentative general model of a well-developed vapor-dominated system. Different parts, discussed below, are keyed by number on the figure.

(1) Fluids that discharge at the surface provide much of the evidence for a vapor-dominated system. Fumaroles (1a) are generally at temperatures near surface boiling or somewhat lower. High-chloride springs are completely absent; associated springs and mud pots are generally acid, high in sulfate, and low in discharge (such as 1b of Fig. 7, and anal. 2 and 5, Table 1), and they deposit little if any sinter. Surrounding ground may be bleached and lacking in vegetation. Some springs not so strongly influenced by oxidation of  $\text{H}_2\text{S}$  (or containing enough  $\text{NH}_3$  absorbed from gases) are nearly neutral in pH and are dominated by bicarbonate and sulfate without much chloride (1c, Fig. 7, and anal. 1 and 6, Table 1).

(2) Zone 2 lies between the ground surface and the water table.<sup>5</sup> Where hot enough, steam and other gases rise above the water table, as in auger hole W-1 of Figure 5. At the water table heat transfer is nearly all convective, but as the temperature gradient increases upward and water vapor condenses, near-surface heat transfer becomes largely conductive.

(3) Zone 3 inhibits the free escape of rising vapor. The zone is nearly saturated with liquid water derived largely from condensing steam rich in  $\text{CO}_2$ . Montmorillonite and kaolinite form by reaction of this

<sup>5</sup> In sands and gravels the water table is easily recognized. In clays, however, the water table is poorly defined, but we consider it to be the level at which water is maintained in a shallow open hole. The zone of saturation can rise as much as 10 m above this level, owing to surface tension in the clays. Hydrostatic pressure increases downward only below the water table as defined in the open hole.

$\text{CO}_2$ -saturated condensate with rock silicates. Clay minerals and condensed water clog most pore spaces and channels, impeding but in many places not prohibiting the escape of residual uncondensed gases. Temperatures in this zone may be similar to those along the hydrostatic reference curve A of Figure 6. Near major channels of upflowing steam (3a, Fig. 7), temperatures and pressures are somewhat above hydrostatic, and conductive heat flow and condensation of steam are consequently high; at least part of the condensate is swept upward to the water table or to surface springs, mud pots, and mud volcanoes. A crude steady-state rate of upflow is determined by pressure gradients, dimensions of the channels, strength of wallrocks, and impedance provided by condensate and suspended clays. Other parts of zone 3 (3b, Fig. 7) are dominated by downflowing condensate and some surface water, with temperatures that are likely to be somewhat lower than those along reference curve A of Figure 6. As temperature gradients in general increase outward and upward through zone 3, more of the heat of vaporization in the rising steam can be transferred by conduction, so water vapor is continuously condensing and the rate of mass flow of vapor therefore decreases upward. A part of the heat in rising vapor is transferred through local horizontal gradients to heat the downward-percolating condensate, which must absorb heat as it descends into hotter ground. The dashed line bounding the outer part of zone 3 marks the gradation in mode of heat transfer from dominantly convective to dominantly conductive.

The lower limit or "pinch-out" of zone 3 is at a depth where the hydrostatic pressure of water in the reservoir margins exceeds the total vapor pressure of steam and gases in the reservoir. Below this depth, vapor can no longer effectively penetrate the reservoir margin.

Wells drilled into parts of zone 3 may produce liquid dominantly, but if drilled and cased into deeper parts they probably yield wet steam and some water when first produced (as in Y-11 drill hole). If an uncased section of hole intercepts channels of upflowing steam and zones of cooler downflowing condensate, the temperature and pressure of the steam will commonly dominate the hole. This occurred in Y-11 below 72 m.

(4) Zone 4 is characterized mainly by conductive heat flow, with heat being supplied from condensing steam within zone 3. Wells bottomed in zone 4 may fill with water, and may erupt hot water and some steam, but discharge rates are likely to be low and the wells noncommercial.

(5) Representative channels of intermediate-level recharge are deep enough at points of entry for hydrostatic pressure to exceed the vapor pressure of

expan-  
heated  
tiated.  
o per-  
if flow  
of cons-  
ns low  
gh the  
atures  
gh for  
tersect  
depth  
depends

extent  
lowing

4

4

4

4

4

4

most sig-  
of con-  
oir, with  
(surface  
eat flow

about 31 to 35 kg/cm<sup>2</sup> in the main reservoir (zone 11).

Channels of inflow tend to be enlarged by solution of SiO<sub>2</sub> as the inflowing water is heated by conduction (indicated by heat-flow arrows in Fig. 7). Channels are diminished, however, by deposition of CaCO<sub>3</sub> and CaSO<sub>4</sub>, which are rather unusual in decreasing in solubility with increasing temperature (see, for example, Holland, 1967). In all rocks with recharge waters relatively high in CaCO<sub>3</sub> and CaSO<sub>4</sub>, channel permeabilities are especially likely to decrease rather than increase with time. These considerations may be important in understanding Larderello, which involves anhydrite-bearing limestone and shales, and The Geysers, where mafic lavas and serpentine are associated with graywacke and shale.

(6) Zone 6 consists of reservoir margins where temperatures decrease toward the reservoir. The depth of the top of zone 6 is not easily predicted. If there were no convective heat flow, the depth would be near that of the 240° C isotherm of the original conductive gradient from the surface to the magma chamber. If 600° C is assumed at 4 km, for example, and the rocks are homogeneous, 240° C would be at 1.6 km depth. The development and downward penetration of the main vapor-dominated reservoir as excess pore water is vaporized result in extensive convective modifications of temperature that greatly change the relationships. Convective cooling from downflowing meteoric water increases this depth, and a shallower intrusion at higher temperature decreases it. These reservoir margins contain channels of inflowing water at pressures that are close to hydrostatic and much greater than ~33 kg/cm<sup>2</sup> of the reservoir. Sharp pressure and temperature gradients decreasing toward the reservoir must therefore exist in zone 6. In contrast to zone 3, heat is transmitted through zone 6 by conduction (and inflowing H<sub>2</sub>O) to the reservoir. The temperatures of zone 6 grade downward into, and are maintained by conduction from zone 10.

(7) Channels of inflowing water are narrowed by precipitation of calcite and anhydrite as zone 6 is approached; clogging of channels by these minerals of decreasing solubility may be offset entirely or in part by solution of quartz, which increases in solubility as long as the liquid water continues to rise in temperature. At the outer edge of zone 6, however, pressures and temperatures in the recharge channels attain their maxima; with further flow toward the reservoir, boiling commences and temperature declines as the pressure drops to that of the reservoir. The fluid in these channels is now a two-phase mixture of steam and water. Specific resistance to flow (resistance per unit of mass) of steam is much

greater than that of liquid water, and specific flow resistance of a two-phase mixture is greater than a linear combination would indicate (I. G. Donaldson and Gunnar Bodvarsson, oral commun., 1970). Because of evaporative concentration by boiling and because of decreasing temperature, quartz and other minerals are now deposited, further impeding the flow of the two-phase mixture. The result of all of these processes is to decrease the rate of recharge through the deeper channels.

(8) The deep subsurface water table recedes as long as the heat supply is sufficient for net loss of liquid water and vapor from the system to exceed net inflow (water table shown in Fig. 7 is horizontal, but it may be very irregular in detail). As mentioned above, recharge tends to decrease with time as resistance to flow of H<sub>2</sub>O through individual channels increases. As the water table recedes and liquid water in the reservoir is largely replaced by vapor at nearly constant pressure throughout the reservoir, the driving pressure on the deeper channels of inflow increases, offsetting in part the increasing impedances. A crude steady state may be attained in some systems, especially as rate of heat flow eventually starts to decline.

(9) With time, if not initially, the water boiling below the deep water table becomes a brine as recharging water boils off and as dissolved substances of low volatility are residually concentrated. Vapor from brine is superheated with respect to pure water at the same pressure. Steam boiling from 25 percent NaCl brine at 35 kg/cm<sup>2</sup>, for example, is superheated by about 12° C with respect to saturated steam and pure water (254° vs 242° C, Haas, 1970). The critical temperature of a salt solution increases above that of pure water (374° C) as salinity increases; that of a 1 percent NaCl solution is about 384° C (Sourirajan and Kennedy, 1962, p. 134); that of a 10 percent solution is about 480° C; and that of a 25 percent solution is about 675° C. Thus, brine can be a very effective agent for convective transfer of heat and dissolved matter at temperatures much above 374° C. Note that Figure 7 has no vertical scale; the depth of zone 9 may be 1,000 m or more, and through all or most of this depth, pressures are lower than hydrostatic pressures outside the system (Fig. 1, curve C, increases downward in slope).

(10) Conductive heat flow from the magma predominates deep under the reservoir where rock plasticity due to increasing temperature prevents the maintenance of open channels. On the outer margins of zone 10 where convective disturbance is not so severe, conductive heat flow predominates to higher levels than under zone 9, grading upward without distinct boundaries into zones 6 and 4. The amount of convective circulation may eventually de-

crease by  
decreased  
and poss  
establishe

11) The  
liquid wa  
in major  
above the  
rise in th  
is lowest  
borders c  
from all  
tures dec  
cent for co  
oi steam.  
down int  
and pore  
surface to  
flow of 1

Edwin  
suggested  
tems is s  
oped rem  
pipes" (C  
"several  
porting h  
consist of  
by a capi  
a volatile  
the hotter  
denses.

action to  
ents in th  
may be th  
some lim  
natural  
tems, and  
gravity a  
of conden

Parts c  
Figure 7  
vapor and  
Larderello  
apparent  
throughou  
the total  
modified l  
of vapor  
top of the  
riched in  
flushed ou  
of the m  
condenses  
nated rese  
part of the  
ents exist

crease beneath the vapor-dominated reservoir by decreased permeability from deposition of minerals, and possibly as a stable salinity gradient becomes established.

11) The main vapor-dominated reservoir contains *liquid water and vapor coexisting*, except possibly in major channels of steam discharge and locally just above the brine water table. Steam and other gases rise in the largest channels where resistance to flow is lowest. Steam starts to condense on the outer borders of the reservoir and continues to condense from all vapor escaping into zone 3, where temperatures decrease outward and provide a thermal gradient for conductive transfer of the heat of vaporization of steam. The condensate from zone 3 percolates down into the reservoir, favoring narrow channels and pore spaces between mineral grains because of surface tension and the lower specific resistance to flow of liquid water relative to steam.

Edwin Roedder (personal commun., 1970) has suggested that our model for vapor-dominated systems is similar in many respects to recently-developed remarkable devices that have been called "heat pipes" (Eastman, 1968). These devices may be "several thousands of times more efficient in transporting heat than the best metallic conductors." They consist of a closed chamber with inside walls lined by a capillary structure or wick, and saturated with a volatile fluid. Heat is transferred by vapor from the hotter to the cooler end, where the vapor condenses. The liquid condensate returns by capillary action to the evaporator section; temperature gradients in the pipe may be extremely low. The top end may be the hotter, with capillary return of liquid (to some limited height) being opposed by gravity. Our natural "heat pipes" are not completely closed systems, and their depth has no theoretical limit because gravity assists rather than opposes the return flow of condensate.

Parts of the subsurface reservoir such as 11a of Figure 7 may be isolated from direct outflow of vapor and may be representative of parts of the Larderello and The Geysers systems that have no apparent direct discharge in fumaroles. Pressures throughout the reservoir are controlled primarily by the total vapor pressure at the boiling water table, modified by frictional resistance to the upward flow of vapor and by the weight of the vapor. Near the top of the reservoir the vapor may be greatly enriched in  $\text{CO}_2$ ,  $\text{H}_2\text{S}$ , and other gases that are not flushed out of the system as actively as near the top of the main reservoir (11). Much water vapor condenses below the boundary of the vapor-dominated reservoir near 11a. In contrast to the flushed part of the main reservoir, significant thermal gradients exist in the poorly flushed parts. Consequently,

Table 5.--Saturation temperatures of water calculated for ideal steam-gas mixtures at constant vapor pressure, 31.8 kg/cm<sup>2</sup>.

Percent steam	Percent other gases	Pressure, kg/cm <sup>2</sup>	Saturation temp., °C
100	0	31.8	236
99	1	31.5	235.5
98	2	31.2	234.9
95	5	30.2	233.1
90	10	28.6	230.1
80	20	25.4	223.7
70	30	22.3	216.9
50	50	15.9	200.1
30	70	9.5	176.8
10	90	3.2	134.7
5	95	1.6	113.0
1	99	0.3	68.0

some steam can condense and other gases are residually concentrated. Pressure of the remaining water vapor requires lower saturation temperatures, as shown in Table 5. This table suggests that temperatures in isolated parts of the reservoir differ little from 236° C until the residual gases are enriched above 5 percent. With higher residual gas contents, temperature gradients and conductive heat flow increase.

The above-described relationships may explain the relatively high pressures and low temperatures of the vapor-dominated fields of Bagnore and Piancastagnaio near Monte Amiata (Burgassi and others, 1965; Cataldi, 1967). Initial pressures were 22 to 40 kg/cm<sup>2</sup> and gas contents of the vapor were as high as 96 percent, but reported temperatures did not exceed about 150° C (Burgassi, 1964; Burgassi and others, 1965; Cataldi, 1967). Pressures and gas contents of the vapor decreased rapidly with production.

Similar reasoning indicates that high contents of gas in vapor coexisting with liquid water at a temperature near that of the maximum enthalpy of steam can result in total vapor pressure significantly above 31.8 kg/cm<sup>2</sup> at 236° C (Table 6). These data indicate that, as contents of other gases increase in the vapor phase at constant temperature of liquid and vapor, total pressures must increase. The least



We do not claim that *all* mercury deposits form in this way. The Sulphur Bank and Abbott mines east of The Geysers, for example, are associated with discharging thermal chloride waters that may be, respectively, metamorphic and connate waters being forced out of their source rocks by lithostatic pressure (White, 1957b, 1967b). During peak mineralization at high temperatures, similar water was almost certainly being discharged, perhaps with more abundant vapor than now.

*Porphyry Copper Deposits.*—The possibility that porphyry copper deposits may be forming in the zone of boiling brine below vapor-dominated systems (zone 9 of Fig. 7) should be tested in these systems by looking for copper minerals in core and cuttings from the deepest drill holes. The model provides attractive possibilities for explaining many aspects of these deposits:

1. Recent isotope studies (Sheppard, Nielsen, and Taylor, 1969) demonstrate that water of meteoric origin probably is dominant over water of other origins during mineralization stages.

2. Temperatures of filling of fluid inclusions are most commonly above 250° C and exceptionally range up to 725° C (Edwin Roedder, oral and written commun.). The salinities of many inclusions are exceedingly high, probably ranging up to 60 percent of total fluid by weight. However, many inclusions are largely vapor, probably indicating boiling of the saline fluid at the time of entrapment.

3. Fluid relationships and the geologic setting of Copper Canyon, Nevada, are considered to be generally similar to porphyry copper deposits (J. T. Nash, written commun., 1970). Extensive fluid-inclusions studies by Nash and Theodore (1970) demonstrate that a) temperatures are most commonly in the range of 315° to 375° C; b) salinities of the ore fluids are commonly in the order of 40 percent (or higher, if CaCl<sub>2</sub> is abundant), with highest salinities in and near the porphyry intrusion and with lower salinities (2 to 15 percent) in peripheral gold-bearing deposits; c) vapor bubbles were trapped in many inclusions, demonstrating the prevalence of boiling or near-boiling conditions. The copper deposits are largely dispersed in the intruded rocks adjacent to the porphyry, and thus are within the spectrum of deposits that have been called porphyry copper deposits (Lowell and Guilbert, 1970).

4. High-salinity brines can develop from residual concentration of dilute (or saline) recharge water, providing a satisfactory system for transferring heat, metals, sulfur and CO<sub>2</sub> from the large magma body that presumably underlies the small multiple porphyry intrusions of most deposits. The critical temperature of water increases with salinity; with sufficient con-

tents of alkali and calcium chlorides, water can remain liquid at temperatures as high as those of the magma body. Copper and other metals could be derived from the local porphyries, a larger underlying magma chamber, and from surrounding rocks.

5. The return flow of condensate through the vapor-dominated reservoir is relatively dilute, but is normally saturated in SiO<sub>2</sub> (with respect to quartz, 440 ppm at 240° C, Fournier and Rowe, 1966). Reevaporation of this water may account for much of the abundant hydrothermal quartz of porphyry copper deposits.

6. Condensate from the discharge areas of vapor-dominated systems is high in sulfate. Some and perhaps much of this condensate may drain downward to the deep water table and account for the abundant anhydrite of many porphyry copper deposits.

7. The most commonly quoted range in depth for the tops of porphyry copper deposits is from 1,000 to 3,000 meters (Lowell and Guilbert, 1970). The shallower depths seem too low for attaining the indicated temperatures and salinities, but may be possible in a brine below a shallow vapor-dominated reservoir (Fig. 1, curve C, can be at shallower as well as greater than plotted depth).

8. If porphyry copper deposits were indeed formed at depths of 1,000 to 3,000 meters, if most of the water of the ore fluids is of surface origin, as indicated by isotopes, and if near-magmatic temperatures and excess heat flow were maintained close to the surface for thousands of years, some type of hydrothermal activity *must* have characterized the then-existing ground surface. Hot-water systems are numerically far more abundant than vapor-dominated systems, and may be the surface expression of some kinds of ore generation (White, 1967b, 1968a), but dissolved salts are *dispersed* by discharging water, and extreme salinities are not ordinarily attained. The highest salinity yet known in active hot-water systems is about 25 percent, characterizing both the Salton Sea, and the Red Sea geothermal brines (White, 1968a). Chemical evidence indicates strongly that the high salinities of these two systems result from the solution of NaCl-rich evaporites. We doubt that evaporites are also involved in the generation of all porphyry copper deposits; some other mechanism for attaining extreme salinity is indicated. Our proposed mechanism for residual concentration of salts by boiling below vapor-dominated systems is a feasible and attractive possibility.

9. The postulated water below a vapor-dominated reservoir may be characterized by high positive temperature and salinity gradients extending downward from the deep water table (Fig. 1), thereby providing a favorable environment for upward transport and

deposition of copper sulfides and pyrite. Temperatures in the water-dominated zone must increase toward the source of heat, presumably an igneous intrusion; actual gradients are highly dependent on the extent of convection in this zone. Formation of vapor bubbles probably occurs largely near the base of penetration of water of the system, where temperatures are highest relative to pressure. Salinity is thereby increased by residual concentration near the base, where permeability is low enough to inhibit convection. On the other hand at higher levels near the deep water table, dissolved salts are being diluted by three processes: (a) *condensation* of dilute water from steam bubbles rising in the brine, as pressures decrease to about 34 kg/cm<sup>2</sup>, as discussed above; (b) downward percolation of *condensate* of steam from the upper margins of the vapor-dominated reservoir; and (c) entry of *new water* recharging the system; this water is likely to be considerably more dilute than the average deep water.

Porphyry copper deposits should be reexamined with consideration of these speculations on temperatures and salinities. If temperatures and salinities do increase sharply downward, our model may provide a new understanding of mode of transport and deposition of the ore minerals. Both decreasing temperature and decreasing salinity upward should favor precipitation of copper sulfides because of the decreasing stability of copper chloride complexes. Introduction of the ore metals may normally occur during a late stage in the total activity after very high salinities have been attained from residual concentration by boiling, and perhaps after the deepest permeable fractures (zone 9 of Fig. 7) have extended downward into a partly cooled major magma chamber.

Porphyry copper deposits should also be examined to determine whether the primary deposits were limited in upward development by a subsurface water table (8 of Fig. 7). Copper and other base metals have low volatilities and could not be transferred into the vapor-dominated reservoir. Pyrite and cinnabar are likely to be characteristic of the zone of condensation (zone 3), and pyrite can also form within the reservoir (zone 11) by reactions involving H<sub>2</sub>S and Fe of the rocks. However, pyrite is likely to be much more abundant below the brine water table. Thus, where the original upper limit of copper mineralization and the level of the former brine water table are exposed in the present topography, the water table may be indicated by an anomalous upward *decrease* in supergene oxidation, where pyrite was initially so scarce.

U. S. GEOLOGICAL SURVEY,  
MENLO PARK, CALIFORNIA,  
July 15; Aug. 22, 1970

## REFERENCES

- Allen, E. T., and Day, A. L., 1927, Steam wells and other thermal activity at "The Geysers," California: Carnegie Inst. Washington Pub. 378, 106 p.
- , 1935, Hot springs of the Yellowstone National Park: Carnegie Inst. Washington Pub. 466, 525 p.
- Baba, Kenzo, 1968, On the temperature and pressure measurements of the geothermal well Matsukawa No. 4: Japan Geol. Survey Bull., v. 19, no. 11, p. 725-728.
- Banwell, C. J., Cooper, E. R., Thompson, G. E. K., and McCree, K. J., 1957, Physics of the New Zealand thermal area: New Zealand Dept. Sci. and Indus. Research Bull. 123, 109 p.
- Barnes, H. L., and Czamanske, G. K., 1967, Solubilities and transport of ore minerals, in Barnes, H. L., Editor, *Geochemistry of Hydrothermal Ore Deposits*: New York, Holt, Rinehart, and Winston, Inc., p. 334-381.
- Bodvarsson, Gunnar, 1964a, Physical characteristics of natural heat resources in Iceland, in *Geothermal Energy I: United Nations Conf. New Sources Energy, Rome, 1961, Proc.*, v. 2, p. 82-90.
- , 1964b, Utilization of geothermal energy for heating purposes and combined schemes involving power generation, heating, and/or by-products, in *Geothermal Energy II: United Nations Conf. New Sources Energy, Rome, 1961, Proc.*, v. 3, p. 429-436.
- , 1970, Evaluation of geothermal prospects and the objectives of geothermal exploration: *Geoexploration*, v. 8, p. 7-17.
- Burgassi, Renato, 1964, Prospecting of geothermal fields and exploration necessary for their adequate exploitation performed in the various regions of Italy, in *Geothermal Energy I: United Nations Conf. New Sources Energy, Rome, 1961, Proc.*, v. 2, p. 117-133.
- , Cataldi, R., Mouton, J., and Scandellari, F., 1965, Prospezione delle anomalie geotermiche e sua applicazione alla regione Amiatina: *l'Industria Mineraria*, v. 16, p. 1-15.
- Cataldi, R., 1967, Remarks on the geothermal research in the region of Monte Amiata (Tuscany-Italy): *Bull. Vulcanol.*, v. 30, p. 243-270.
- , Ferrara, G. C., Stefani, G., and Tongiorgi, E., 1969, Contribution to the knowledge of the geothermal field of Larderello (Tuscany, Italy). Remarks on the Carboli area: *Bull. Vulcanol.*, v. 33, no. 1, p. 1-27.
- Craig, H., 1963, The isotopic geochemistry of water and carbon in geothermal areas, in *Nuclear geology on geothermal areas*. Spoleto: Consiglio Nazionale delle Ricerche, Laboratorio di geologia nucleare, Pisa, p. 17-53.
- , 1966, Superheated steam and mineral-water interactions in geothermal areas: *Am. Geophys. Union Trans.*, v. 47, p. 204-205.
- , Boato, Giovanni, and White, D. E., 1956, Isotopic geochemistry of thermal waters: *Natl. Acad. Sci.*, no. 400, p. 29-38.
- Dall'Aglio, M., DaRoit, R., Orlandi, C., and Tonani, F., 1966, Prospezione geochemical del mercurio—distribuzione del mercurio nelle alluvioni della Toscana: *Industria Mineraria*, v. 17, p. 391-398.
- Dickson, F. W., and Tunell, George, 1968, Mercury and antimony deposits associated with active hot springs in the western United States, in Ridge, J. D., Editor, *Ore deposits of the United States 1933-1967* (Graton-Sales volume), v. 2: New York, Am. Inst. Mining Metall. Petroleum Engineers, Inc., p. 1673-1701.
- Eastman, G. Yale, 1968, The heat pipe: *Scientific American*, v. 218, p. 38-46.
- Elder, J. W., 1965, Physical processes in geothermal areas, in W. H. K. Lee, Editor, *Terrestrial heat flow: Am. Geophys. Union Mon.*, ser. 8, p. 211-239.
- Ellis, A. J., and Mahon, W. A. J., 1964, Natural hydrothermal systems and experimental hot-water/rock interactions: *Geochim. et Cosmochim. Acta*, v. 28, p. 1323-1357.
- , 1967, Natural hydrothermal systems and experimental hot water/rock interactions (Pt. II): *Geochim. et Cosmochim. Acta*, v. 31, no. 4, p. 519-538.



- Facca, Giancarlo, and Tonani, Franco, 1964, Theory and technology of a geothermal field: *Bull. Volcanol.*, v. 27, p. 143-189.
- , 1967, The self-sealing geothermal field: *Bull. Volcanol.*, v. 30, p. 271-273.
- Fenner, C. N., 1936, Bore-hole investigations in Yellowstone Park: *Jour. Geol.*, v. 44, no. 2, pt. 2, p. 225-315.
- Ferrara, G. C., Ferrara, G., and Gonfiantini, R., 1963, Carbon isotopic composition of carbon dioxide and methane from steam jets of Tuscany, in Tongiorgi, Editor, *Nuclear geology on geothermal areas, Spoleto 1963*: Pisa, Consiglio Nazionale Delle Ricerche, Laboratorio di Geologia Nucleare, p. 277-284.
- Fournier, R. O., and Rowe, J. J., 1966, Estimation of underground temperatures from the silica content of water from hot springs and wet-steam wells: *Am. Jour. Sci.*, v. 264, no. 9, p. 685-697.
- , and Truesdell, A. H., 1970, A device for measuring down-hole pressures and sampling fluids from geothermal wells: *Jour. Sci. Instruments* [in press].
- Haas, J. L., Jr., 1970, The effect of salinity on the maximum thermal gradient of a hydrothermal system of hydrostatic pressure and near boiling: *ECON. GEOL.*, in press.
- Hayakawa, M., 1969, Anomalous heat flow in Japan: *Bull. Volcanol.*, v. 33, no. 1, p. 57-68.
- Helgeson, H. C., 1968, Geologic and thermodynamic characteristics of the Salton Sea geothermal system: *Am. Jour. Sci.*, v. 266, p. 129-166.
- Holland, H. D., 1967, Gangue minerals in hydrothermal deposits, in H. L. Barnes, Editor, *Geochemistry of Hydrothermal Ore Deposits*: New York, Holt, Rinehart, and Winston, Inc., p. 382-436.
- James, Russell, 1968, Wairakei and Larderello; geothermal power systems compared: *New Zealand Jour. Sci. and Technology*, v. 11, p. 706-719.
- Keenan, J. H., and Keyes, F. G., 1936, *Thermodynamic Properties of Steam*: New York, John Wiley and Sons, 89 p.
- Krauskopf, K. B., 1964, The possible role of volatile metal compounds in ore genesis: *ECON. GEOL.*, v. 59, p. 22-45.
- Lee, W. H. K., and Uyeda, S., 1965, Review of heat flow data, in W. H. K. Lee, Editor, *Terrestrial heat flow*: *Am. Geophys. Union, Geophys. Mon.* 8, p. 87-190.
- Lowell, J. D., and Guilbert, J. M., 1970, Lateral and vertical alteration-mineralization zoning in porphyry ore deposits: *ECON. GEOL.*, v. 65, p. 373-408.
- Marinelli, G., 1969, Some geological data on the geothermal areas of Tuscany: *Bull. Volcanol.*, v. 33, no. 1, p. 319-334.
- McNitt, J. R., 1963, Exploration and development of geothermal power in California: *Calif. Div. Mines and Geology Spec. Rept.* 75, 45 p.
- Mercado, Sergio, 1969, Chemical changes in geothermal well M-20, Cerro Prieto, Mexico: *Geol. Soc. America Bull.*, v. 80, p. 2623-2629.
- Muffler, L. J. P., White, D. E., and Truesdell, A. H., 1971, Hydrothermal explosion craters in Yellowstone National Park: *Geol. Soc. America Bull.* [in press].
- Nakamura, Hisayoshi, and Sumi, Kiyoshi, 1967, Geological study of Matsukawa geothermal area, northeast Japan: *Japan Geol. Survey Bull.*, v. 18, no. 2, p. 58-72.
- Otte, Carel, and Dondanville, R. F., 1968, Geothermal developments in The Geysers area, California [abs.]: *Am. Assoc. Petroleum Geologists Bull.*, v. 52, p. 575.
- Penta, Francesco, 1959, *Sulle Origini del Vapore Acqueo Naturale e Sull' attuale Stato delle Relative Ricerche (Ricerche per "forze Endogene")*: *La Ricerca Scientifica*, v. 29, num. 12, p. 2521-2536.
- Saito, Masatsugu, 1964, Known geothermal fields in Japan, in *Geothermal Energy I: United Nations Conf. New Sources Energy, Rome, 1961, Proc.*, v. 2, p. 367-373.
- Schoen, Robert, and Ehrlich, G. G., 1968, Bacterial origin of sulfuric acid in sulfurous hot springs: *Internat. Geol. Cong.*, 23d, Prague, v. 17, p. 171-178.
- Sheppard, S. M. F., Nielsen, R. L., and Taylor, H. P., Jr., 1969, Oxygen and hydrogen isotope ratios of clay minerals from porphyry copper deposits: *ECON. GEOL.*, v. 64, p. 755-777.
- Sourirajan, S., and Kennedy, G. C., 1962, The system H<sub>2</sub>O-NaCl at elevated temperatures and pressures: *Am. Jour. Sci.*, v. 260, p. 115-141.
- White, D. E., 1957a, Thermal waters of volcanic origin: *Geol. Soc. America Bull.*, v. 68, no. 12, p. 1637-1658.
- , 1957b, Magmatic, connate, and metamorphic waters: *Geol. Soc. America Bull.*, v. 68, p. 1659-1682.
- , 1964, Preliminary evaluation of geothermal area by geochemistry, geology, and shallow drilling, in *Geothermal Energy I: United Nations Conf. New Sources Energy, Rome, 1961, Proc.*, v. 2, p. 402-408.
- , 1967a, Some principles of geyser activity, mainly from Steamboat Springs, Nevada: *Am. Jour. Sci.*, v. 265, p. 641-648.
- , 1967b, Mercury and base-metal deposits with associated thermal and mineral waters, in Barnes, H. L., Editor, *Geochemistry of Hydrothermal Ore Deposits*: New York, Holt, Rinehart, and Winston, Inc., p. 575-631.
- , 1968a, Environments of generation of base-metal ore deposits: *ECON. GEOL.*, v. 63, no. 4, p. 301-335.
- , 1968b, Hydrology, activity, and heat flow of the Steamboat Springs thermal system, Washoe County, Nevada: *U. S. Geol. Survey Prof. Paper* 458-C, p. C1-C109.
- , 1969, Rapid heat-flow surveying of geothermal areas, utilizing individual snowfalls as calorimeters: *Jour. Geophys. Research*, v. 74, no. 22, p. 5191-5201.
- , Brannock, W. W., and Murata, K. J., 1956, Silica in hot-spring waters: *Geochim. et Cosmochim. Acta*, v. 10, p. 27-59.
- , Hem, J. D., and Waring, G. A., 1963, Chemical compositions of subsurface waters, in *Data of geochemistry*: *U. S. Geol. Survey Prof. Paper* 440-F, 67 p.
- Wilson, S. H., 1955, Chemical investigations, in Grange, L. I., Editor, *Geothermal steam for power in New Zealand*, chap. 4: *New Zealand Dept. Sci. and Indus. Research Bull.* 117, p. 27-42.



## VARIATION OF FRACTURING PRESSURES WITH DEPTH NEAR THE VALLES CALDERA

Zora Dash and Hugh Murphy

Los Alamos National Laboratory, MS J981  
Los Alamos, New Mexico 87545

## ABSTRACT

Hydraulic Fracturing at the Fenton Hill Hot Dry Rock Geothermal site near the Valles Caldera has yielded fracturing pressures from 14 to 81 MPa (2030 to 11750 psi) at depths ranging from 0.7 to 4.4 km (2250 to 14400 ft). This data can be fit to a fracture gradient of 19 MPa/km (0.84 psi/ft), except for an anomalous region between 2.6 to 3.2 km where fracturing pressures are about 20 MPa lower than estimated using the above gradient. This anomaly coincides with a biotite granodiorite intrusive emplaced into a heterogeneous jointed metamorphic complex comprised of gneisses, schists and metavolcanic rocks. Microseismic events detected with sensitive downhole geophones suggest that shear failure is an important process during hydraulic fracturing of such jointed rock. Consequently the usual relation between minimum earth stress and fracture opening pressure, based upon classic tensile failure, cannot be used a priori; fracture opening pressure is instead a complex function of joint orientation and all three components of principal earth stress.

FRACTURING EXPERIMENTS

The Los Alamos National Laboratory, with financial support from the U.S. D.O.E., West Germany's Ministry for Science and Technology, and Japan's New Energy Development Organization, has drilled five wells into Precambrian crystalline basement rock as part of the Hot Dry Rock geothermal energy program. The experimental site, Fenton Hill, is located in the western flank of the Valles Caldera, a dormant volcano in the Jemez Mountains of northern New Mexico. The first well, GT-1, was drilled to 0.75 km for exploratory purposes. The second and third wells, GT-2 and EE-1, were drilled to approximately 3 km, and were used for numerous HDR heat extraction experiments.<sup>1</sup> These wells were connected by hydraulic fractures, one of which extended vertically 300 m from initiation point in EE-1 to intersection with GT-2. The fourth and fifth wells, EE-2 and EE-3, were drilled to 4.4 and 4.0 km respectively. The temperature at 4.4 km was 325°C. The bottom sections of these wells were directionally drilled, at an angle of 35° from vertical, with horizontal

deviation in the ENE direction, parallel to the estimated direction of the minimum principal earth stress. These wells are to be connected by fractures which must be about 370 m high, because the wells are separated vertically by this distance.

In all fracturing experiments conducted to date, the fracturing fluid has been water, to which friction reducer and fine silica have been added occasionally to reduce wellbore friction and to increase fracturing efficiency by blocking permeability of the rock faces contiguous to the fracture. Other than the addition of friction reducer the water was not viscosified, and no proppants were injected. Injection rates have ranged from 1 to 76 l/s, and injection volumes from 1 to 5000 m<sup>3</sup>. The great depths and temperatures have so far precluded the successful use of impression packers or televiwers to determine fracture orientation, but monitoring of microseismic acoustic emissions during fracturing with 3 axis geophones installed to depths of 2.9 km in neighboring wells indicate that the fracture planes generally strike NS, nearly as expected. All fractures are vertical, or nearly so, except in the lower zone of EE-2, (below 4.3 km) where acoustic emission patterns suggest a fracture zone with a dip of 45°.

Table I summarizes total downhole fracture pressures,  $P_f$ , determined in all fracture experiments conducted in the Fenton Hill geothermal wells to date. Later we discuss the relationship of  $P_f$  and minimum horizontal earth stress. The designation ISIP indicates that a reasonably constant pressure was observed after shut-in, but extrapolated ISIP indicates that the "Muskat analysis" was required, in which a straight line fit of logarithm of pressure versus time is extrapolated back to actual time of shut-in.<sup>2</sup> "Fracture extension" indicates that re-injection provided such a clear arrest in the pressure-time curve, and at reasonably low flow rates, that this arrest could be taken as  $P_f$ . The designation "P from PTA" indicates the fracture extension pressure derived from noting the pressure required to change hydrological characteristics of the existing fracture, e.g. enlargement. The last two methods of  $P_f$  determination, termed  $P$  vs  $Q^{0.25}$

Table I. Fenton Hill Fracture Pressures			
Well / Expt	Depth (km)	Fracture Opening Pressure (MPa)	Method Of Determination
<u>GI-1</u>	0.745	13.7-14.8	ISIP
<u>GI-2</u>	2.0	33.5-34.9	Extrapolated ISIP
	2.53	36.6-37.3	Fracture Extension
<u>EE-1</u>	1.96	30.6-31.5	Fracture Extension
	2.93	37.5	Fracture extension pressure from PIA
<u>EE-2</u> 2018(82/07/19)	3.46-3.59	51.0(6)*	P vs Q <sup>0.25</sup> Extrapolation
		67.5(6)	P vs Q <sup>0.5</sup> Extrapolation
2020(82/10/06)	3.46-3.59	62.7	ISIP
		75.0	Extrapolated ISIP
		63.0(5)	P vs Q <sup>0.25</sup> Extrapolation
		68.5(5)	P vs Q <sup>0.5</sup> Extrapolation
2011(82/05/30)	4.25-4.36	67.7-73.9	ISIP (4 measurements)
		70.0-74.2	Extrapolated ISIP (3)
		59.2(2)	P vs Q <sup>0.25</sup> Extrapolation
		69.9(2)	P vs Q <sup>0.5</sup> Extrapolation
2012(82/06/04)	4.25-4.36	80.2	ISIP
		80.3	Extrapolated ISIP
		74.5(7)	P vs Q <sup>0.25</sup> Extrapolation
		78.7(7)	P vs Q <sup>0.5</sup> Extrapolation
2016(82/06/19)	4.25-4.36	80.2	ISIP
		80.3	Extrapolated ISIP
		71.7(9)	P vs Q <sup>0.25</sup> Extrapolation
		77.0(9)	P vs Q <sup>0.5</sup> Extrapolation
<u>EE-3</u> 2006(82/01/19)	3.09-3.15	81.2	ISIP
		81.3	Extrapolated ISIP
		38.1	Extrapolated ISIP
2007(82/02/17)	3.09-3.15	33.6(3)	P vs Q <sup>0.25</sup> Extrapolation
		35.9(3)	P vs Q <sup>0.5</sup> Extrapolation
		38.4	Extrapolated ISIP
2023(82/11/08)	3.09-3.15	33.9(6)	P vs Q <sup>0.25</sup> Extrapolation
		37.3(6)	P vs Q <sup>0.5</sup> Extrapolation
		38.6	ISIP
		42.5	Extrapolated ISIP
2025(82/12/14)	3.35-3.44	45.4(14)	P vs Q <sup>0.25</sup> Extrapolation
		56.6(14)	P vs Q <sup>0.5</sup> Extrapolation

\* Number in Parentheses is Number of P - Q Data Points in Curve Fit.

(laminar flow) and  $P$  vs  $Q^{0.5}$  (turbulent flow) are scaling laws for refracturing pressure variation with flow rate, using a simple fracture aperture (opening) and pressure relation<sup>3</sup>. Figure 1 presents the variation of the fracture extension pressure with  $Q$  for Experiment 2012. As can be seen, reasonable fits to the data can be obtained with either  $Q^{0.25}$  or  $Q^{0.5}$  scaling, a typical value of the discrepancy between data and curve fit being only about 1%. The values of  $P_f$  obtained by extrapolation are 74.5 MPa for  $Q^{0.25}$  scaling and 78.7 MPa for  $Q^{0.5}$  scaling, but below we show that this difference, though small, is significant and we will argue that  $Q^{0.5}$  scaling is more appropriate.

The single value of  $P_f$  derived from PTA was based upon 15 injection tests.<sup>4</sup> The range of ISIPs provided for Experiment 2020 represents four separate determinations<sup>5</sup> during the course of injecting 3300 m<sup>3</sup> (860,000 gallons) over 15 hours.

Table I demonstrates the excellent repeatability of all the methods of estimating  $P_f$ . For example, three separate fracturing experiments were conducted in EE-2 in the depth interval 4.25 to 4.36 km. The six separate  $P_f$  measurements by ISIP and extrapolated ISIP vary by a maximum of 1.4% from minimum to maximum.

For Experiment 2011, only two data points were available for  $P - Q$  curve fitting and, as can be seen, the value of  $P_f$  so derived is significantly different from the other estimates. For the other two experiments at 4.25 to 4.36 km, the number of data points was greater and the agreement is much better. In fact, if the  $P_f$  estimates based upon two point  $P$  vs  $Q$  extrapolation are excluded, the agreement of the remaining  $P_f$  estimates is excellent, ranging only from 71.7 to 81.3 MPa, or a variation of 6% about the mean. Similar observations pertain for the 8 measurements of  $P_f$  at 3.46 to 3.59 km in EE-2 and the 8 measurements at about 3.1 km in EE-3.

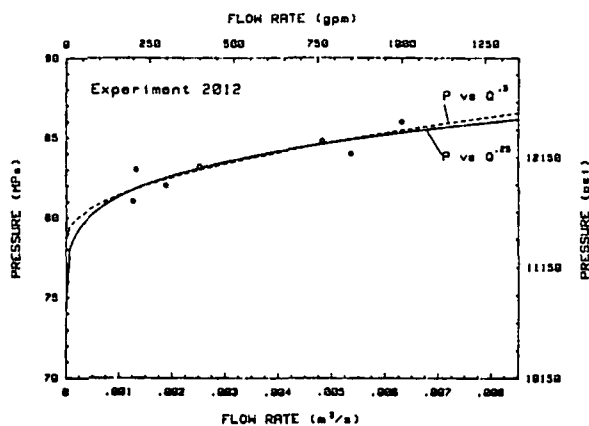


Figure 1. Variation of fracture extension pressure with injection rate.

With the possible exception of Experiment 2018, the  $P_f$  determined from  $Q^{0.25}$  extrapolation is always significantly lower than the other determinations. This argues that a laminar flow rule is inappropriate, an entirely reasonable finding considering the high injection rates used in these experiments. If  $Q^{0.25}$  extrapolation is excluded from consideration, the agreement of  $P_f$  determinations would be  $\pm 3\%$  at 4.3 km,  $\pm 8\%$  at 3.5 km, and  $\pm 8\%$  at 3.1 km.

Figure 2 presents the variation of fracture pressure with depth. All measurements, with the exception of those from  $P - Q^{0.25}$  extrapolation and the two-point  $Q^{0.25}$  extrapolation are plotted. Also shown is the vertical overburden stress computed from the density of the overlying formations. Except for the biotite granodiorite intrusive located at 2.6 to 3.2 km,  $P_f$  can be represented as a linear function of depth, with a fracture pressure gradient of 19 MPa/km (0.84 psi/foot).

#### RELATIONSHIP OF FRACTURE PRESSURE AND EARTH STRESSES

According to conventional theory, the fracture pressure derived from shut-in or from fracture extension pressure is equivalent to the minimum principal earth stress,  $S_{min}$ . However, before this equivalence can be drawn for the present measurements it must be shown that the mode of fracturing is tensile in nature, not due to shear. In addition, because

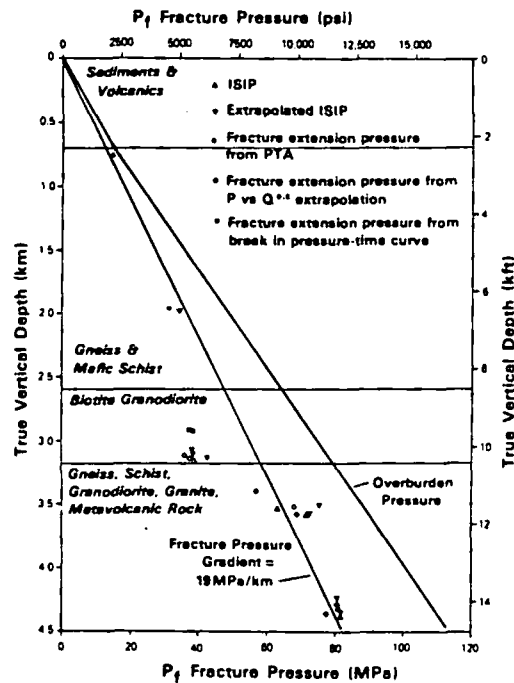


Figure 2. Variation of fracture pressure with depth.

fracturing in these crystalline rock formations undoubtedly opens up pre-existing fractures, or joints, rather than creating virgin rock failures, it must also be shown that the joints preferentially stimulated are perpendicular, or nearly so, to  $S_{min}$ , or else that the principal earth stresses are sufficiently close in magnitude that joint orientation makes little difference. Let us first consider the possibility of shear fracturing. For joints without strength or cohesion, it can be shown that as the fluid pressure is increased, eventually the effective normal stress on the joint will be reduced to the point where the joint can slip; theoretically shear slippage occurs before the effective stress is reduced to zero, and the joint completely opens ("jacking" is the descriptive term used in reference 6). Adopting Amonton's friction law, it can be shown that if  $\beta$  is the angle between a joint plane and the direction of the maximum principal stress,  $S_{max}$ , and  $\phi$  is the friction angle, (the coefficient of friction is  $\tan\phi$ ) then

$$\frac{S_{min}}{P_f} = \frac{2 + (\lambda - 1) S_{max}/P_f}{\lambda + 1} \quad (1)$$

where  $\lambda = \cos 2\beta + (\sin 2\beta)/\tan\phi$ .

Thus  $S_{min}$  can be estimated from the measured  $P_f$  if independent estimates of  $S_{max}$ ,  $\beta$  and  $\phi$  are available. Usually  $S_{max}$  is the readily estimated overburden stress, but in tectonically active regions such as the Valles Caldera this must be established, and the means of doing so was derived from differential strain analysis (DSA) of core specimens<sup>8</sup> as well as fault plane solutions<sup>9</sup> of microseismic acoustic emissions. DSA earth stress measurements are based upon the stress required to close microcracks in the core, the assumption being that all such cracks are closed *in situ*. This method is consequently qualitative in nature, subject to considerable uncertainties, and with a tendency to overestimate actual earth stress. Figure 3 presents the results: the solid lines indicate the estimated minimum horizontal stresses, and the dashed lines represent the maximum horizontal stresses. The four core specimens were unoriented, so the direction of the DSA principal horizontal stresses are unknown. While considerable uncertainty is noted it appears that the maximum horizontal stress is less than, or approximately equal to, the vertical stress.

Microseismic acoustic emissions during hydraulic fracturing experiments were detected with a downhole, three-axis geophone (or occasionally an accelerometer) as well as a surface network of 13 stations located within 5 km of the geothermal wells. Full details are provided in reference 9, but can be summarized as follows: the fault plane solution for fracturing at the 4.3 km interval

in EE-2 indicates strike slip faulting on a N-S vertical plane. The solution at 3.5 km indicates dip slip on a N-S vertical plane. These two solutions indicate that over a short depth interval, only 800 m, the maximum earth stress changes from nearly vertical to nearly horizontal, which strongly implies that the maximum horizontal stress is nearly equal to the overburden stress over this depth interval, being slightly greater at 3.5 km, and slightly less at 4.3 km. This result is entirely consistent with the DSA stress ranges shown in Figure 3. Consequently the magnitude of the maximum stress can be taken as that of the overburden stress. At 3.5 km the ratio  $S_{max}/P_f$  is then 1.30 while at 4.3 km the ratio is 1.37; both intervals can be characterized, on average, as  $S_{max}/P_f = 1.34$ . Substitution in equation (1) yields, in Table II, the ratios of  $S_{min}/P_f$  provided by the shearing criterion for various values of fracture orientation and friction angle. Friction angles of  $30^\circ$  to  $60^\circ$  encompass the range of reasonable values for crystalline granitic rock.

For the 3.5 km interval the fault plane was not well constrained, and the plane could dip from  $50^\circ$  to  $90^\circ$  ( $\beta = 0^\circ$  to  $40^\circ$ ). The fracture orientation provided by mapping the microseismic hypocenters is also poorly constrained, but the general pattern appears to be a vertical fracture striking roughly N-S. The fault plane solution for the 4.3 km interval is more tightly constrained, with dip of  $85^\circ$  and strike  $N10^\circ E$ . Usual fault plane convention places the P axis direction at  $45^\circ$  to the fault, so  $\beta = 45^\circ$ . However, hypocenter maps suggest a fracture dipping  $45^\circ$  and striking roughly N-S. This could be construed as a single fracture, with a dip at variance with that given by the fault plane solution (but still with  $\beta \leq 45^\circ$ ), or as a series of en echelon fractures, each with vertical fault plane, but joined to adjacent fractures by off-vertical natural joints.

In every case discussed,  $\beta < 45^\circ$ , so that the minimum earth stresses in Table II are remarkably well constrained:  $S_{min}/P_f = 1.08 \pm 8\%$ , for  $30^\circ < \phi < 60^\circ$ . Thus the use of either the conventional interpretation or one

Table II  
Ratios of Minimum Earth Stress To Fracture Pressure According to Shear Fracturing Criterion With  $S_{max}/P_f = 1.34$ .

$\beta$	$\phi = 30^\circ$	$\phi = 45^\circ$	$\phi = 60^\circ$
$0^\circ$	1.00	1.00	1.00
$15^\circ$	1.09	1.05	1.02
$30^\circ$	1.17	1.05	1.00
$45^\circ$	1.07	1.00	0.91
$60^\circ$	1.00	0.84	0.64
$75^\circ$	0.66	0.27	-0.26

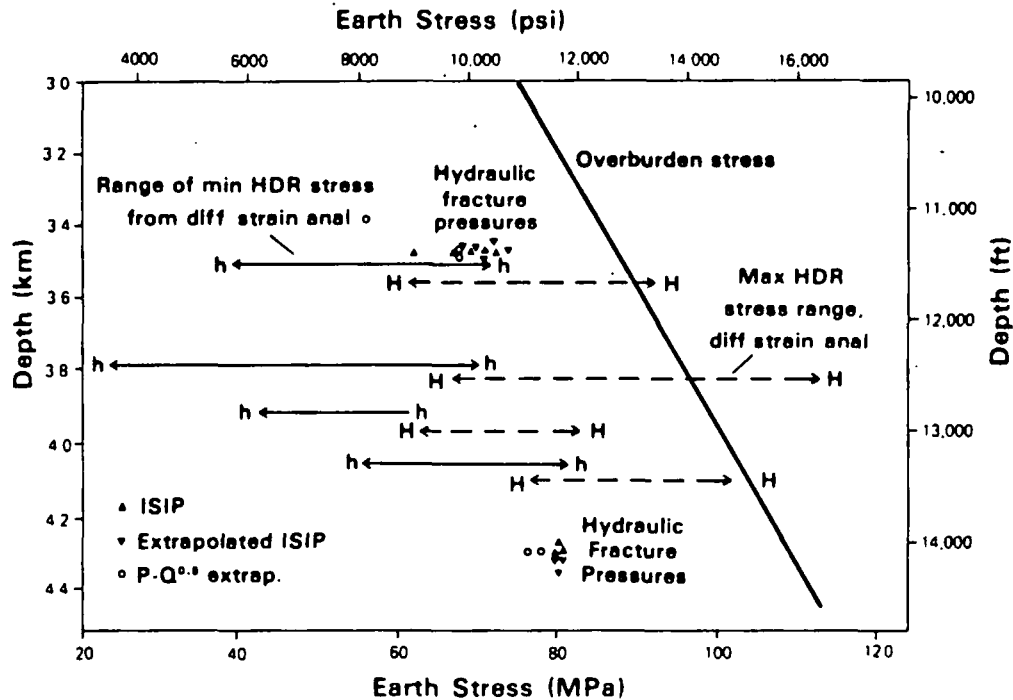


Figure 3. Comparison of DSA Earth Stresses and Fracture Pressures.

based upon shear fracturing results in essentially the same result,  $S_{min} = P_f$ , or  $S_{min} = 1.08 (\pm 0.08) P_f$ .

The final check is to consider the possibility of joint "jacking" on planes non-perpendicular to  $S_{min}$ . In this case the normal stress must be equal to  $P_f$ , and rotational stress transformation yields:

$$\frac{S_{min}}{P_f} = \frac{2 - (1 - \cos 2\beta) S_{max}/P_f}{1 + \cos 2\beta} \quad (2)$$

Table III indicates that unlike shear fracturing, it requires a fracture pressure greater than  $S_{min}$  to jack open joints inclined significantly to the  $S_{max}$  direction. It may be concluded that static considerations alone preclude the opening of such off angle joints by jacking, because these would shear first.

Table III  
Ratio of Minimum Earth Stress To Fracture Pressure For "Jacking";  $S_{max}/P_f = 1.34$

$\beta$	$S_{min}/P_f$
0°	1
15°	0.97
30°	0.89
45°	0.66

However dynamic factors must also be considered.<sup>10</sup> The injected fluid must be accommodated by fracture and formation porosity. Depending upon injection rate, fluid viscosity, fracture size, and formation permeability and compressibility some fluid permeates the rock adjacent to the fracture and is thus stored in existing porosity. The remaining fluid is stored in the dilated fracture. In principle, jacking requires higher pressures, which leads to greater dilation than shearing, but rough estimates<sup>11</sup> suggest that formation permeation accommodated 90% of the water injected in these fracturing experiments. Consequently little fracture dilation was required, and despite the vast differences in physical scale this fracturing was probably similar to the shear fracturing observed by Lockner and Byerlee<sup>12</sup> when core specimens were fractured at low injection rates. Thus, it is likely that jacking in the present experiments, if it occurred at all, was confined to low  $\beta$  joints, for which  $S_{min}/P_f \approx 1$ .

To briefly summarize estimated earth stresses at other depths, it is noted that the maximum ratio of  $S_{max}/P_f$  occurs for the biotite granodiorite intrusive, where the ratio is 2, resulting in  $S_{min}/P_f = 1.25 \pm 0.25$  based upon the shear criterion for joints with  $\beta < 45^\circ$ . However in this interval a completed reservoir was developed and simple geometrical relations between fracture initiation zones and intersection zones in the opposite well indicate

nearly vertical fractures,  $\beta < 10^\circ$ , so  $S_{min}/P_f$  is constrained to less than 1.10. The jacking criterion for  $\beta < 10^\circ$  likewise results in  $S_{min}/P_f = 0.95$ . In summary  $S_{min} \approx P_f$  closely for this interval. For depth intervals not yet discussed no similar geometrical constraints are available, but in these intervals  $S_{max}/P_f = 1.5$ ; and the shear criterion results in  $S_{min}/P_f = 1.12 \pm 0.12$ .

#### CONCLUSIONS

Fracture pressures were estimated from direct ISIPs, extrapolated ISIPs, observed changes in hydrological characteristics, and extrapolations of fracture extension pressure versus injection rate. Excluding "laminar" flow scaling, and "turbulent" flow scaling where only a very few data sets (P vs Q) are available, excellent agreement is found for all five methods. Because of the nearly lithostatic state of stress at this site, in which the ratio of  $S_{max}/S_{min}$  was typically 1.5 (2.0 in the worst case), it was possible to show that  $S_{min} \approx P_f$  even if the mode of fracturing is shear, or if off-vertical joints were "jacked" open. Except for the Biotite Granodiorite intrusive, where  $S_{min}$  appears to be 20 MPa lower than expected, the minimum principal earth stress is linear with depth, with a gradient of 19 MPa/km (0.84 psi/ft) and is horizontally oriented in approximately the EW direction. The maximum horizontal stress is nearly equal to the overburden stress.

#### REFERENCES

1. Dash, Z., et al, "Hot Dry Rock Geothermal Reservoir Testing: 1978 to 1980", J. Volcan. Geotherm. Res., 15, 59-99, 1983.
2. Aamodt, R. L., and Kuriyagawa, M., "Measurement of Instantaneous Shut-In Pressure in Crystalline Rock", appears in Hydraulic Fracturing Stress Measurements Nat'l Acad. Press Washington, DC. 1983.
3. Perkins, T. K. and Kern, L. R., "Widths of Hydraulic Fractures", J. Petr. Tech., 13, 937-946, September, 1966.
4. Murphy, H. D., Lawton, R. G., Tester, J. W., Potter, R. M., Brown, D. W., and Aamodt, R. L., "Preliminary Assessment of a Geothermal Energy Reservoir Formed by Hydraulic Fracturing", Soc. Petr. Engr. J., 317-326, August 1977.
5. Brown, D. W., "Recent Results - Los Alamos Hot Dry Rock Project", Proc. 8th Workshop Geothermal Reservoir Engineering, Stanford, Univ., December 1982.
6. Pine, R. J. and Batchelor, A. S., "Downward Growth of Hydraulic Stimulation by Shearing in Jointed Rock", submitted to Int. J. Rock Mech. Min. Sci. Geomech. Abstr., 1983.
7. Bombolakis, E. G., "Some Constraints and Aids for Interpretation of Fracture and Fault Development", Proc. 2nd Int. Conf. Basement Tectonics, Denver, 1979.
8. Anon. "Differential Strain Curve Analysis and Differential Wave Velocity Analysis of Fenton Hill EE-2 Cores", Dowell Rock Mechanics Laboratory, Tulsa, Oklahoma, November 1983.
9. Cash, D., Homuth, E. F., Keppler, H., Pearson, C., and Sasaki, S., "Fault Plane Solutions for Micro Earthquakes Induced at Fenton Hill Hot Dry Rock Geothermal Site: Implications for the State of Stress Near a Quaternary Volcanic Center", to appear in Geophys. Rev. Lett., 1984.
10. Murphy, H. D., Pine, R. J., "Dendritic Hydraulic Fracturing in Geothermal Energy Reservoirs", Proc. Energy Tech. Conf. and Exhibit, New Orleans, Feb. 12-16, 1984.
11. Murphy, H. D. Keppler, H. and Dash, Z., "Does Hydraulic Fracturing Theory Work in Jointed Rock Masses?", Trans. Geotherm. Res. Council 7, 461-466, 1983.
12. Lockner, D. and Byerlee, J. D., "Hydrofracture in Weber Sandstone at High Confining Pressure and Differential Stress", J. Geophys. Res., 82, 2018-2026, 1977.

*Edward*

## 2. Worldwide Status of Geothermal Resources Development

JAMES. B. KOENIG

SUBJ  
GTHM  
WSG

UNIVERSITY OF UTAH  
RESEARCH INSTITUTE  
EARTH SCIENCE LAB.

The Earth is a great reservoir of heat energy, but most of its heat is buried too deeply or spread too diffusely to be felt tangibly at the surface, especially as it is masked by incoming solar radiation. We become aware that the Earth is a great heat engine during episodes of volcanic eruption, when material at temperatures upwards of 800°C is emitted at the surface. Hot springs, geysers, and fumaroles are other surface manifestations of the Earth's heat content.

When recoverable, the heat of the Earth can be made to do useful work. The uses depend upon the enthalpy (heat content), physical state, and chemistry of the transporting medium. Despite very high enthalpy, molten lava has found no direct use. Similarly, hot, dry rock has found only the most limited and local uses. High-enthalpy aqueous fluids (above about 200 cal/g) are of proved use in the generation of electricity and in industrial processes, and may find application in desalination. Fluids of lower enthalpy have many uses as process heat in industry, and perhaps can be used also in desalination. Low-enthalpy fluids (above about 100 cal/g) are used widely in space heating and in agriculture. Additionally, certain mineralized waters may yield industrially valuable chemicals as a by-product of heat extraction or desalination. Developments in the technology of heat-exchanging and desalination may extend the range of uses of low-enthalpy fluids significantly in the next few decades.

High-enthalpy geothermal systems are known only in regions of youthful volcanism, crustal rifting, and recent mountain building. The

---

James B. Koenig is with the California Division of Mines and Geology, Sacramento, California.

Reprinted from **GEOTHERMAL ENERGY: RESOURCES, PRODUCTION, STIMULATION**, edited by Paul Kruger and Carel Otte. Stanford University Press, Stanford, California. © 1973 by the Board of Trustees of the Leland Stanford Junior University.

major geothermal and volcanic belts are the circum-Pacific margin; island groups of the mid-Atlantic rift; the rift zones of east Africa and the adjacent Middle East; and the irregular belt of mountains and basins extending from the Mediterranean basin of Europe and north Africa across Asia to the Pacific (see Fig. 1).

Lower-enthalpy fluids are far more abundant in volcanic zones and elsewhere, and may represent a greater reserve of useful energy by an order of magnitude or more. Significant areas of lower-enthalpy geothermal fluids include the Gulf Coast of the United States, an extensive region in western Siberia, and portions of central Europe just north of the Alps and the Carpathian Mountains. Geologically, these are subsiding sedimentary basins at the margins of folded mountain ranges. Water encountered during exploration for oil in sedimentary basins has usually been considered a nuisance. But in the future these hot waters of relatively low enthalpy may represent an energy source as valuable as oil, and perhaps as widespread. Other low-enthalpy waters have been encountered in wells and mines or as occasional warm springs in older folded mountains, but rarely in the ancient stable platforms and shields of continental interiors.

This paper summarizes the distribution of geothermal resources on a

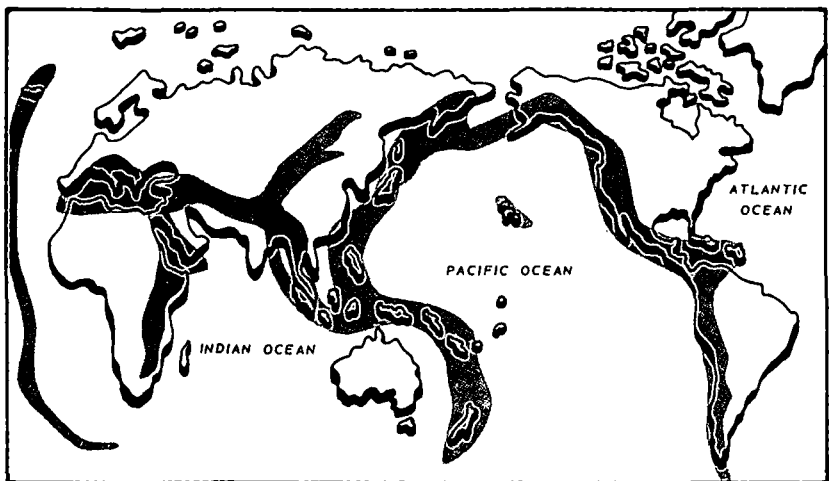


Fig. 1. Regions of intense geothermal manifestations; the distribution accords generally with recent volcanism and youthful mountain-building, and in part outlines boundaries of mobile crustal plates.



worldwide scale, reviews development and exploration activities, and evaluates the potential for development over the next decade.

### *The Framework for Utilization of Geothermal Energy*

Because heat dissipates rapidly, geothermal fluids cannot be transported far from their point of recovery without suffering diminished quality. The maximum transport distance depends upon the initial enthalpy (heat content) of the fluid and the use for which the fluid is intended. For steam used in electric-power generation, the probable maximum distance is on the order of 2 to 3 km. Hot water for agricultural use or space heating can be transported farther, the greatest reported distance being 20 km for municipal hot water in Iceland.

Where heat energy is converted to electric power, the energy can then be distributed throughout the power-transmission grid. Conversion to electric power represents a practical means of transferring heat energy from what are often remote geothermal fields to population centers. However, the price of conversion is a substantial loss of energy, and further losses occur in transmission and in the subsequent use of electricity to do mechanical or thermal work. Additionally, electricity cannot be stored easily or efficiently, which means that a power system must be built to meet peak demand, almost without regard for base load. In terms of capital investment, this can be expensive and wasteful. Because of these unfavorable factors, direct utilization (i.e. without conversion) is likely to increase in such applications as space heating, agriculture, industrial processing, and perhaps desalination, especially as costs rise for other fuels. Energy for all of these processes can, of course, be supplied by electricity; but the conversion and reconversion are wasteful, especially with reconversion to heat. If energy costs rise sufficiently over the decades, new communities may develop near the geothermal-energy source, much as cities were once established to take advantage of running water to power mills. This concept is under active consideration in Hungary.

The countries that have successfully developed geothermal electricity to date are among the wealthiest and most industrially developed in the world. These include the United States, Italy, Japan, the Soviet Union, New Zealand, and Iceland. Even Mexico, where a plant is to begin operation in early 1973, is among the relatively more developed nations. This pattern appears to indicate the need for an adequate economic

and technological infrastructure. However, the majority of countries in which exploration is under way, and where opportunities for future development are greatest, are generally among the least developed of nations, lacking the economic and technological base. But even within most highly developed countries there are regions that are lacking in energy resources, low in population, or remote from the industrialized heartland, where costs of electric power often are higher. Examples are Hokkaido, the northern island of Japan, the Kamchatka Peninsula of the Soviet Union, and parts of the Great Basin of the United States, all of which exhibit geothermal potential.

Many of the industrialized nations are poor in reserves of fossil fuels, and some are chronically short of foreign exchange. The United States now typifies the latter. Fuel-short countries include Italy, Japan, and, until very recently, New Zealand. In Japan, 75 percent of all energy is imported, and this figure is expected to increase over the next 10 years to over 85 percent. Even a wealthy nation like Japan cannot afford to import four-fifths of its energy indefinitely. Finally, environmental considerations have begun to limit other modes of energy conversion in the industrialized nations. Nuclear power, although technologically feasible, has not developed as predicted—for economic and environmental reasons, and because of a deep-rooted public resistance.

Conversely, in New Zealand, where geothermal exploration has been under way since the end of World War II, recent discoveries of sizable reserves of natural gas have brought the development of geothermal-electric plants to a halt. However, the Government of New Zealand will continue to encourage the direct utilization of geothermal energy in industry, agriculture, and municipal heating. If the demand for electricity continues to increase, or if foreign markets are obtained for New Zealand natural gas, this decision may be reversed. Geothermal-energy development thus rests in an uneasy relationship with local political, economic, and technological conditions.

In summary, we can expect increased use of geothermal energy, certainly in direct utilization. Despite certain disadvantages, such as inability to sustain transport over long distances, restriction to base-load power applications, relatively low efficiency, and transmission losses, the doubling of demand for electricity every 7 to 12 years and the accelerating demand for other forms of energy throughout the world will require us to develop our geothermal-energy resources. Especially

in countries plagued by a shortage of fossil-fuel reserves or an unfavorable balance of payments, there is an incentive to develop indigenous energy sources.

*Costs*

The production costs of various modes of energy generation are difficult to compare. Available data (see Table 1) are not always accurate, and may reflect different interest and taxation rates, amortization periods, special allowances, or other hidden costs. In any case, it has been shown—in Hungary, Iceland, New Zealand, and the Soviet Union—that direct utilization of geothermal energy in industry, agriculture, and space heating is appreciably less expensive than the use of crude oil, gasoline, or diesel fuel for the same purposes. Natural gas, where obtainable, and coal are more nearly competitive, though still more expensive than hot water for heating purposes.

In the generation of electricity, only hydroelectric power has been found to be cheaper, and only in certain situations. In Iceland, for example, hydroelectricity has been shown to be less expensive than geothermal power in most circumstances. But once the more ideal hydroelectric sites were developed, geothermally generated electricity became economically competitive. Moreover, in Iceland the direct utilization of hot water for municipal heating is far cheaper than heating via hydroelectricity. At The Geysers in the United States, geothermal-

TABLE 1  
*Selected Comparative Cost Data for Geothermal Energy*

Geothermal field	Geothermal production	Local average, other fuel
Electricity, U.S. mills/kwh		
Namafjall, Iceland	2.5 - 3.5	—
Larderello, Italy	4.8 - 6.0	~ 7.5
Matsukawa, Japan	4.6	~ 6.0
Cerro Prieto, Mexico	4.1 - 4.9	~ 8.0
Pauzhetsk, U.S.S.R.	7.2	~10.0
The Geysers, United States	5.0	7.0
Space heating, U.S.\$/Gcal energy		
Reykjavik, Iceland	4.0	6.7
Szeged, Hungary	3.0	11.0
Refrigeration, U.S.\$/Gcal energy		
Rotorua, New Zealand	0.12	2.40
Drying diatomite, U.S.\$/ton		
Namafjall, Iceland	~2	~12

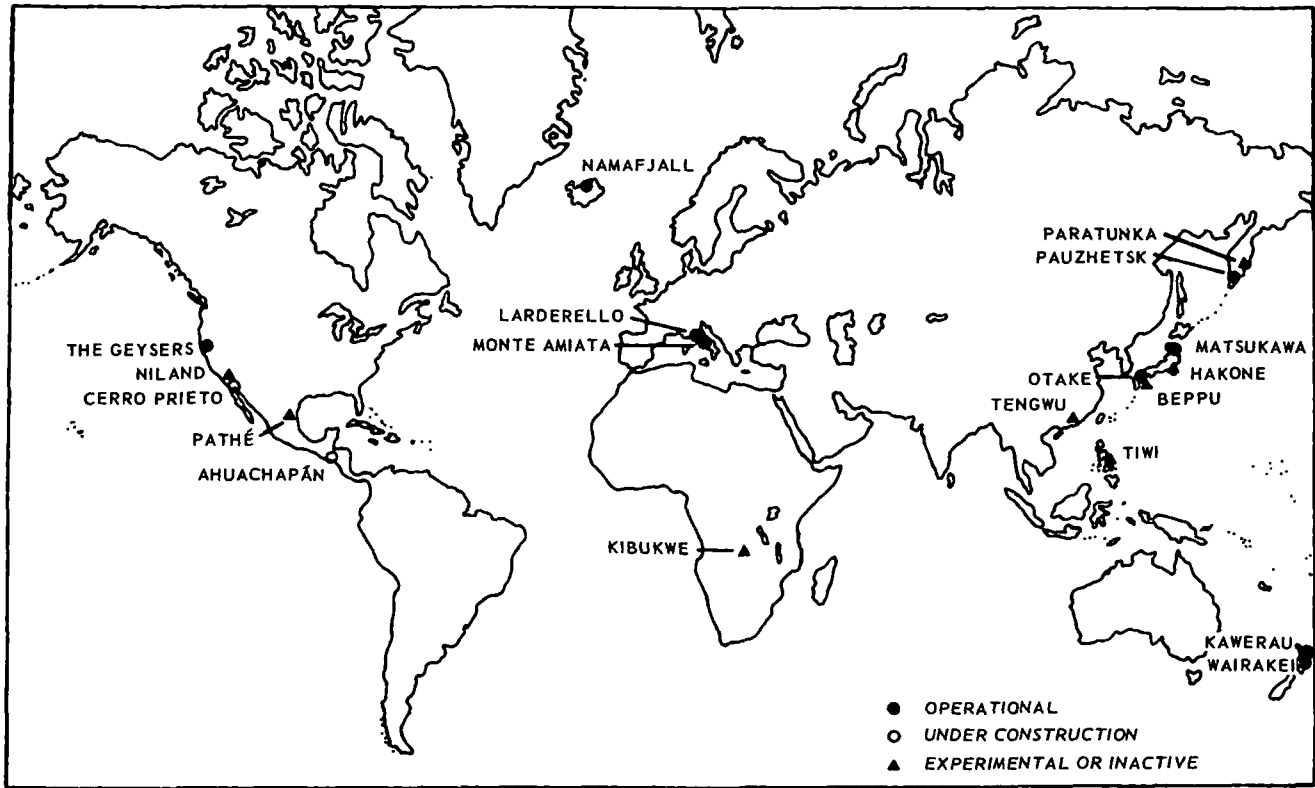


Fig. 2. Geothermal electric power stations.

electric power has proved to be cheaper than power from other fuel sources, regardless of plant size. Even in developed countries, then, geothermal power compares favorably with power from very large generating stations that have the advantage of economy of scale. And indeed, the ability of geothermal-generating systems to be developed economically in relatively small power-unit increments—say, 25 to 50 Mw—is a major consideration for underdeveloped countries, where the load and the load growth are commonly small. But the New Zealand decision must remind us that wherever it is politically or economically more advantageous to develop other energy sources, geothermal-power development may be retarded.

### *History of Development and Exploration*

The early history of geothermal development saw the utilization of thermal springs as baths and health resorts, and the occasional use of thermal waters to heat buildings. Primitive peoples had already used the heat of fumaroles for cooking food and, in arid lands, steam condensate for drinking water. Sulfur deposited from the steam of fumaroles, kaolinitic clays formed by the decomposition of rocks in fumarole zones, and to a lesser extent fumarolic mercury and alum were utilized for centuries. But it was the recovery of boric acid from the fumaroles of Larderello, Italy, that marked the beginning of modern geothermal development. Starting in 1812, mineralized hot-spring waters were boiled to dryness in cauldrons heated by wood fires, and boric acid recovered from the residue. In 1827, fumarolic steam was substituted for wood as a fuel for this operation. Shortly thereafter, the first borings were made for steam at Larderello, both as fuel and to increase the flow of borate source material.

The first experimental generation of electricity from natural steam was undertaken at Larderello in 1904. In 1913 a 250-kw generating station came into service, marking the beginning of continuous generation of geothermal electricity (see Fig. 2).

After World War I, the concept of geothermal energy was carried to the ends of the world. Experimental borings at Beppu, Japan, began in 1919, and in 1924 a 1-kw generator was installed and operated experimentally. In the United States, test borings were drilled at The Geysers and Niland, California, in the 1920s. Although low-pressure steam was found in abundance, the projects were abandoned for lack

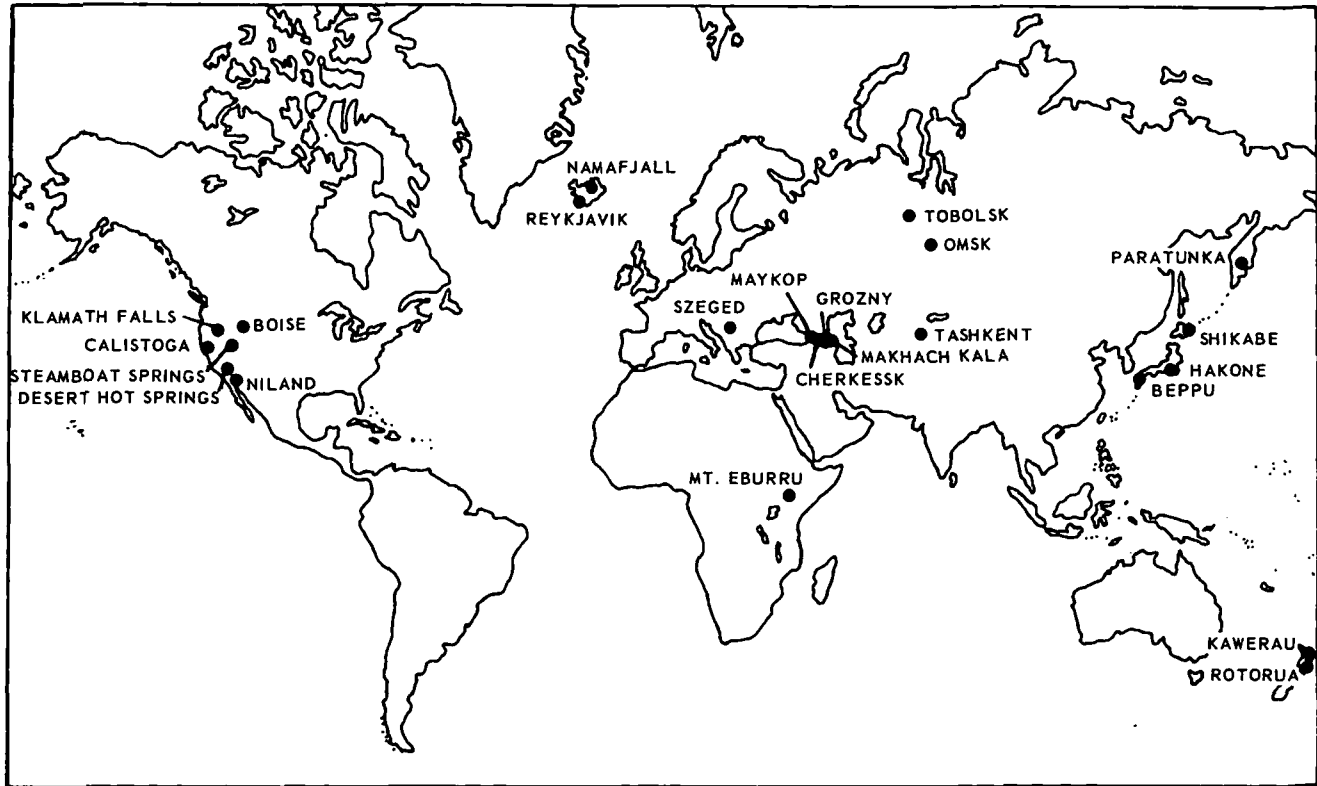


Fig. 3. Areas of significant use of geothermal energy for purposes other than generation of electric power.

of a market for electricity. Holes were drilled at other fumarole areas in the United States in the 20s and early 30s, most notably in Yellowstone National Park. A test hole was drilled in Java in 1928, but no development followed.

In Iceland, the exploration of hot-water aquifers by drilling began in 1928 at Reykjavik and in 1933 at Reykir, a few kilometers to the east (see Fig. 3). Hot water from these systems was distributed to consumers by the Reykjavik Municipal District Heating Service. Before 1940, hot-water wells had been drilled for heating purposes at Rotorua, New Zealand. In that year a great many wells were drilled for domestic use in Rotorua and in towns south of Lake Taupo.

World War II disrupted traditional patterns of living; in the reconstruction of war-devastated economies, attention focused anew on geothermal energy. This was especially true in Italy, Japan, and New Zealand: all three were short of fossil fuels for power generation, and generation and transmission facilities had been largely destroyed in Italy and Japan.

The remainder of this paper undertakes to recount, country by country, the history of geothermal-energy exploration and exploitation, for electricity generation and for industrial-process heating, space heating, chemical extraction, or the like. Table 2 gives pertinent data on thirteen important geothermal fields in eight countries; Table 3 indicates the current status of geothermal exploration and development in some fifty countries.

### *Italy*

From the simple 250-kw generator of 1913, the Italian geothermal-generating complex has grown to over 390,000-kw capacity, and is currently the world's largest. (The original boric acid recovery works, established in 1812, was shut down in 1969 because of inability to compete economically with other sources of borax.) Over 365 Mw of the electrical capacity is produced from the thirteen plants comprising the Larderello field. Some 25 Mw are supplied by the four plants at Monte Amiata, 75 km to the southeast. Individual turbine size is small, ranging from the 900-kw noncondensing unit at San Ippolito to the 26,000-kw plants at Castelnovo and Larderello. Approximately 43,000 kw are generated from a series of noncondensing turbines at the Larderello and Monte Amiata fields. Noncondensing turbines were chosen

TABLE 2  
*Characteristics of Selected Geothermal Fields*

Field	Reservoir temperature, °C	Reservoir fluid	Enthalpy, cal/g	Average well depth, meters	Fluid salinity, ppm	Mass flow per well, kg/hr	Non-condensable gases, %
Larderello	245	Steam	690	1,000	<1,000	23,000	5
The Geysers	245	Steam	670	2,500	<1,000	70,000	1
Matsukawa	230	Mostly steam	550	1,100	<1,000	50,000	<1
Otake	200+	Water	~400	500	~4,000	100,000	<1
Wairakei	270	Water	280	1,000	12,000	—	<1
Broadlands	280	Water	400+	1,300	—	150,000	~6
Pauzhetsk	200	Water	195	600	3,000	60,000	—
Cerro Prieto	300+	Water	265	1,500	~15,000	230,000	~1
Niland	300+	Brine	240	1,300	260,000	~200,000	<1
Ahuachapán	230	Water	235	1,000	10,000	320,000	~1
Hveragerdi	260	Water	220	800	~1,000	250,000	~1
Reykjanes	280	Brine	275	1,750	~40,000	~400,000	~1
Namafjall	280	Water	260	900	~4,000	400,000	6



TABLE 3  
*Status of Geothermal Exploration and Development, 1972*

Nation	Electric-power generation/construction	Experimental power stations	Significant direct utilization	Other geothermal-field discoveries	Additional exploration under way <sup>o</sup>
Chile				x	
China		x			
Ethiopia					x
Guadeloupe (Fr. W. Indies)				x	
Hungary			x		
Iceland	x		x	x	
Indonesia					x
Italy	x				x
Japan	x	x <sup>b</sup>	x	x	x
Kenya			x		x
Mexico	x <sup>a</sup>	x	x	x	x
New Zealand	x		x	x	
Nicaragua				x	
Philippines		x		x	
El Salvador	x <sup>a</sup>			x	
Taiwan				x	
Turkey				x	
U.S.S.R.	x	x	x	x	x
United States	x	x <sup>b</sup>	x	x	x
Zaire		x <sup>b</sup>			

<sup>a</sup> Under construction.

<sup>b</sup> Inactive.

<sup>o</sup> Other geothermal exploration/interest: Algeria, Argentina, Bulgaria, Burundi, Colombia, Costa Rica, Czechoslovakia, Ecuador, Fiji Islands, Greece, Guatemala, India, Israel, Malawi, Mali, Morocco, New Britain, New Hebrides, Peru, Poland, Portugal (Azores Is.), Rwanda, Spain (Canary Is.), Tanzania, Tunisia, TFAI (French Somaliland), Uganda, Venezuela, Yugoslavia, Zambia.

originally because of their simplicity, lower capital cost, and ease of construction. However, they consume approximately twice as much steam per kwh as condensing turbines, 20 kg vs. 10 kg. In a situation where steam is abundant, capital scarce, and time short, noncondensing turbines appear to be most favorable. But with the expansion of the Larderello complex to the point where many geologists believe that field capacity has been reached, or nearly so, effective utilization of steam becomes the more critical variable. For this reason, conversion to condensing turbogenerators is planned. This could add upwards of 40,000 kw of generating capacity at Monte Amiata and Larderello without any increase in steam production.

Producing pools of the Larderello field are at Capriola, Castelnuovo, Gabbro, Lago, Lagoni Rossi, Larderello, Montecerboli, Monterotondo,

San Ippolito, Sasso Pisano, and Serrazzano. From Monterotondo on the south to the northern end of the field at Gabbro is a distance of some 20 km. Total field area is probably in excess of 250 km<sup>2</sup>. In addition, steam has been discovered at Travale, Boccheggiano, and Roccastrada, east and southeast of the main Larderello field. Roccastrada is nearly halfway between the center of the Larderello field and the Bagnore and Piancastagnaio pools of the Monte Amiata field. Radicofani may represent an eastern extension of the Monte Amiata field.

Approximately 500 wells have been drilled across the Larderello and Monte Amiata fields, of which nearly 200 were in production in 1971. The reservoir fluid is steam, with a variable content of noncondensable gases, averaging (see Table 2) about 5 percent, although the initial gas content of each well is much higher; e.g., the gas content at Piancastagnaio had decreased from almost 90 percent initially to 20 percent by 1970, and was still decreasing. Reservoir temperatures reach a maximum of about 250°C.

Average well yield is about 23,000 kg/hr of steam at Larderello and perhaps 36,000 at Monte Amiata. The greater average yield at Monte Amiata reflects the shorter production history, as both mass and pressure declines are reported with time. Individual wells may deviate greatly from these averages: mass flows as large as 270,000 kg/hr have been reported. Average well depth at Larderello is slightly over 1,000 m. Wells are completed with 34-cm-diameter casing, which is the largest production diameter at any active geothermal development in the world.

There is evidence of interference between wells in certain pools, and it is reported that maximum sustainable mass flow has been attained for several parts of the field. This is reflected in the low average yield per well, which in turn reflects declines in yield per well with time. Many geologists have thus been led to state that field capacity has been reached. However, successful exploration and development is continuing at the previous margins of the field, most notably at Travale, where, beginning in 1951 with the drilling of five successful steam wells, a geothermal field was developed at the site of an old boric acid works. Two 3,500-kw turbines were installed in 1952 and operated until 1962, when decreases in well yield required the plant be dismantled. In February 1972 it was reported that several new wells had been completed, and that they were capable of producing at least 100,000 kg/hr each of dry steam. This may significantly extend field capacity.

The Larderello–Monte Amiata region is being explored by various methods, including infrared imaging, to determine if significant data have been overlooked in past work. Drilling is continuing in several pools of the Larderello field and at Travale. The volcanic centers at Roccastrada and Radicofani are also under study. Work includes geochemistry, temperature-gradient drilling, geologic mapping, and drilling of exploratory holes. As a result of this continued exploration and development effort, costs of steam have stayed constant, instead of declining as originally predicted by the operating company. Also because of the capital cost of conversion from noncondensing to condensing turbines, net costs per kwh have increased slightly over the decade.

As more condensing turbines are installed, more water effluent will require disposal. Since the cessation of boric acid recovery in 1969, borated waters have been discharged to the natural river drainage. No adverse effects upon agriculture are reported.

Steam at Larderello is produced from permeable to cavernous limestone, dolomite, and anhydrite of Upper Triassic to Upper Jurassic age. Field depth is controlled by a decrease in permeability with penetration into the carbonate sequence and underlying crystalline basement. The reservoir is capped by a thrust sheet comprising impermeable carbonates, argillites, and ophiolites of Jurassic to Eocene age. Surface leakage of steam occurs along faults extending to the carbonate-anhydrite reservoir beneath the thrust plate. There is no obvious source of heat in the immediate vicinity, although the presence of a deep pluton has been suggested. Tertiary granitic rocks are exposed on the island of Elba, some 80 km to the southwest. The closest Late Tertiary volcanic rocks are exposed at Roccastrada.

Monte Amiata consists of Pliocene and Pleistocene acidic and alkaline volcanic rocks extruded through a sequence of shales, marls, limestones, and sandstones similar to those at Larderello. The steam reservoir is also beneath an impermeable thrust sheet. Post-volcanic collapse is believed to have occurred, fragmenting the reservoir and controlling mercury mineralization and weak hot-springs activity. More basic volcanic rocks occur at Radicofani and at Monte Volsini to the south. The relationship between acidic and alkaline volcanism, post-volcanic collapse, mercury mineralization, and hot-springs activity is observed at many geothermal fields throughout the world.

A series of seven target areas has been chosen for further geothermal

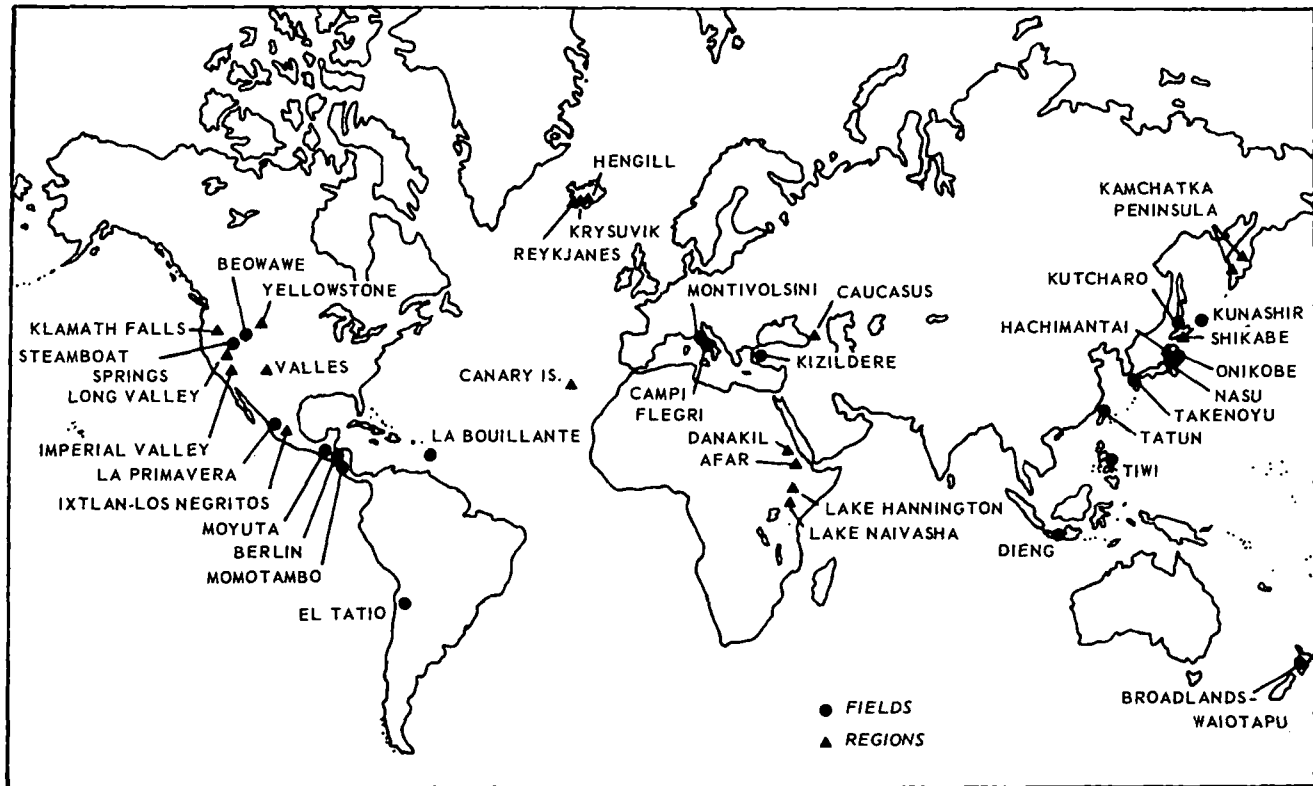


Fig. 4. Major undeveloped geothermal fields and regions under exploration.

exploration in the Apennine mountain chain (see Fig. 4). South from Monte Amiata these are: Monte Volsini; Monte Cimino, including the Viterbo area; Monte Sabatini; Colli Albani, to the southeast of Rome; the region about Naples, including Pozzuoli and the Campi Flegri solfatar fields of classical fame; and Monte Vulture, in south-central Italy. Other areas in northern Italy have been investigated and rejected. These include Monte Berici, near Padua, where there are Late Tertiary silicic volcanic rocks, and Montecatini, between Larderello and Pisa. Drilling has also been done at La Tolfa, a volcanic center southwest of Viterbo.

In the 1920s and 30s, drilling was carried out on the island of Ischia and in the vicinity of the city of Pozzuoli. Low-pressure steam was reported from certain of these tests. A project to study the feasibility of using a freon-based heat exchanger to generate electricity at the Campi Flegri was never carried through.

### *New Zealand*

The development of geothermal energy in New Zealand has been confined largely to the Taupo volcanic depression of the North Island. Utilization has centered at Wairakei, where a 160-Mw power station operates; at Kawerau, where some 180,000 kg/hr of steam are used to produce newsprint and sawn lumber and to generate 10 Mw of electricity; and at Rotorua, where steam and hot water are used extensively for heating purposes. Natural hot water is used on a small scale at Ngawha, also on North Island, and elsewhere in the Taupo depression.

The Taupo volcanic depression extends for over 200 km in a north-northeasterly direction, parallel to the main structural grain, and culminates in the north at the active volcano White Island, in the Bay of Plenty. The zone is some 25 to 30 km broad at its widest. Fumaroles and hot springs are abundant in the central 100-km-long portion of the depression. At least a dozen areas have been explored by drilling.

As a result of drilling, hot-water reservoirs of sodium-chloride composition have been found, at temperatures commonly as high as 270°C, the highest being the 306° at Rotokawa. Steam is formed during the upward flow of water in wells, giving a mixture of steam and water at the wellhead. The fraction of steam varies, averaging 20 percent at Wairakei. Only rarely is dry steam produced in wells, and this is believed to reflect a flashing effect in the producing formation brought on by lowered fluid pressure near the wellbore. Gas content varies with the

area. At Rotorua, hydrogen sulfide gas evolves from the superheated waters and is a nuisance and potential health hazard.

Declines in mass flow and pressure are observed commonly in wells of the Wairakei and Kawerau fields, necessitating redrilling and deepening of individual wells. These declines have also made it necessary to set intake pressures for turbines lower than was originally planned. Ground subsidence also has occurred at Wairakei. Deposition of calcite and silica, and corrosion at the points of oxidation of reservoir fluid, have created further problems in handling of the fluid. Saline effluent, representing about 80 percent of the original geothermal fluid, is disposed of to rivers, apparently without harmful effect.

Despite these problems, there was a rapid growth of interest in geothermal development through the late 1940s, culminating in the completion of a 160-kw generating station at Wairakei. The first experimental plant had to be abandoned in 1964, after a year of operation, because of insufficient yield from wells. Subsequent construction was centralized at one facility, with extensive steam-collection lines, to utilize a local river for cooling purposes. Increases in capacity were planned to 250 Mw at Wairakei and to between 90 and 120 Mw at the Broadlands field, just to the northeast, by 1976. But the discovery of natural gas in New Zealand changed these plans, and no geothermal power development is planned for the 1970s. However, the government is encouraging direct municipal and industrial utilization of these hot-water resources.

The most significant examples of direct utilization are at Kawerau and Rotorua. The New Zealand Department of Scientific and Industrial Research and the Ministry of Works, in conjunction with the Tasman Pulp and Paper Company, began exploration at Kawerau in 1952. Over a dozen wells have since been drilled or redrilled at Kawerau, and steam from these wells is used for heat exchanging with boiler-quality water for the generation of high-quality steam for mill processes. Additional natural steam is used for timber drying, to operate log-handling equipment, and for generation of 10,000 kw of electricity. At Rotorua, a city of some 30,000 people, over 1,000 hot-water wells supply thermal energy to individual houses, schools, hospitals, hotels, and commercial and industrial establishments. A geothermal air-conditioning scheme is in operation at a 100-room hotel at Rotorua. The construction costs were said to be as low as those of conventional cooling systems, and

the operating costs are perhaps only 5 percent as high. At Rotorua, the average well depth is 100 to 150 m, with a few as deep as 250 m. Temperatures commonly are above 120°C, and reach as high as 175° at these shallow depths. When allowed to flow, these wells produce a mixture of steam, hot water above 100°, and noncondensable gases. Because of corrosion and pollution problems associated with this fluid, heat exchanging often is accomplished with municipal water, which is circulated to consumers. Unlike the geothermal-heating systems in Iceland, which are operated by the municipality, space heating in New Zealand is not operated by government agencies. It is, however, sharply regulated, especially concerning corrosion, hydrogen-sulfide emissions, disposal, contamination of other water supplies, and effects of production upon neighboring wells.

Many hot-water wells in the Lake Taupo area supply heat to farms. Examples of agricultural applications include steaming of raw garbage as swill for hogs, heating of stock pens, cleaning of runs, and sterilization of various equipment. Also, an experimental forestry station uses steam to dry seeds and lumber, as well as to heat seed beds and buildings.

Total heat consumed for direct applications of geothermal fluid in New Zealand is probably greater than that used to generate electricity at Wairakei.

### *United States*

Development of electric power has proceeded rapidly at The Geysers, California, since the first turbine of 12,500 kw was installed in 1960. Pacific Gas and Electric Company purchases steam from producing companies and converts it to electricity through condensing turbines at a rate of 9 kg/kwh. Late in 1972, some 2.75 million kg of dry steam were consumed hourly to produce 302,000 kw of electricity. Another 110,000-kw plant is nearing completion, and is due for testing late in 1973. And construction has begun on still another plant of the same size, scheduled for completion in 1974. It is estimated that 110 Mw will be installed annually through the 1970s, which by 1980 will result in approximately 1,180,000 kw of generating capacity. This would be the largest producing geothermal complex in the world at that time.

The capacity of The Geysers field is a matter of speculation. On the basis of different estimates of field extent, well yield, well spacing, and

total fluid in storage in the reservoir, estimates of maximum sustainable production range upward from 1,200 Mw to 4,800 Mw and even more. To date, some 110 wells have been drilled across a 12-km zone with maximum width of about 3 km. Some 85 of these were completed as producers of dry steam. Field boundaries still are known only approximately, and exploration is continuing at distances of many kilometers from produceable wells.

A shallow and a deeper reservoir have been encountered, the former apparently fed from the latter along faults. Average well yield from the deeper (greater than 500 m) reservoir is on the order of 70,000 kg/hr. The production declines that have been documented for wells in the shallow reservoir have recently been demonstrated to occur also in the deeper reservoir (Budd, this volume).

The reservoir consists of highly fractured, slightly metamorphosed, sedimentary and igneous rocks of Cretaceous and Upper Jurassic age. The deepest wells have surpassed 2,500 m in depth without notable reduction in fracture permeability. Recharge is unknown, and the subject of study. Low-grade metamorphic reactions, including the deposition of silica and calcite, may have contributed to a lateral decrease in permeability, but this is not clearly documented. Reservoir temperatures reach about 250°C. The heat source is apparently an igneous mass at a depth of perhaps 5 to 8 km, which has yielded a series of alkaline and acidic volcanic rocks at the surface. The age of these rocks is probably Pleistocene, and they cover an area of perhaps 300 to 400 km<sup>2</sup>.

Of the few unproductive deep boreholes, almost all encountered high temperatures. Permeability remains the critical variable; and it is still a question whether this is controlled by local or regional fracture patterns or by mineral solution and deposition activity. If The Geysers represents a water-deficient system, as has been postulated, continued production may result in increasing fluid enthalpy over time.

Potentially countering this is the limited reinjection of condensate from the condensing turbines. After evaporative losses in cooling, only about 20 percent of the fluid remains for disposal. The high content of boron and ammonia in the condensate have precluded disposal to local streams, whose volume of flow varies sharply with the season. Injection of cooled condensate in the rock reservoir at approximately 2,000 m depth may serve as recharge allowing secondary recovery of heat from the reservoir. But it may also locally decrease enthalpy, per-



mitting a water phase to predominate. Some calculations of enthalpy from deep wells have suggested that steam and liquid water do coexist in the reservoir. Therefore, indications of long-term trends in enthalpy, mass flow, and field pressure are eagerly awaited.

Significant discoveries have been made in about half a dozen localities elsewhere in the western United States. Most attention is given currently to the Imperial Valley of California, where several companies and Government agencies are active. The U.S. Bureau of Reclamation and the Office of Saline Water are sponsoring an exploration program aimed at joint production of electricity and desalination of waters for agricultural use. Magma Energy Company and its associates are also drilling in the Imperial Valley, searching for geothermal brine suitable for use in generating electricity by heat-exchanging. A completely closed system is envisaged, with heat-depleted fluid reinjected back into the reservoir rocks. An agreement has been signed with San Diego Gas and Electric Company to construct and operate a pilot plant of this type at Niland in the Imperial Valley, with the first plant to operate in 1974.

In 1963, Standard Oil Company of California drilled a 4,000-m oil-exploration hole west of Brawley. It encountered sodium-chloride brine at a temperature of about 260°C. This brine is somewhat similar to the reservoir fluid at Cerro Prieto, Mexico, and is presumably what is sought elsewhere in the Imperial Valley.

Exploration at Niland revealed an extremely hot (to 370°C), highly saline (to 260,000 ppm total dissolved solids) brine. Niland appears to be the northernmost and most saline field of a 150-km-long geothermal province extending northward from the Gulf of California, Mexico. Data from electrical-resistivity surveys support the concept of a salinity gradient across the Valley, increasing to the northwest. An experimental generator installed at Niland in the early 1960s was never operated at its rated 3,000-kw capacity. It is now inactive. At Niland, recovery of various chlorides was attempted, most notably KCl. Market conditions and problems of corrosion, scaling, and waste disposal prevented commercial development of either electricity or a major chemical-recovery works. However, on an intermittent basis, calcium-chloride solution was marketed for a few years in the late 1960s. Also, for over 30 years carbon dioxide gas was produced from shallow wells at the northeast end of the Niland field. Over 65 wells were drilled, and approximately 100 million m<sup>3</sup> of gas were produced between 1933 and 1954. Average

well life was about 2 years. Well depth averaged 150 m. Temperatures of the CO<sub>2</sub> gas ranged between 50° and 75°. The entire gas production was converted to dry ice for use in refrigeration or railroad cars.

Space heating with geothermal fluids has succeeded most effectively in south-central Oregon. At Klamath Falls some 350 wells supply heat to buildings via heat-exchanging with pure municipal water. Elsewhere in Oregon, greenhouses, resorts, baths, farm buildings, and schools are heated by geothermal waters. Similar projects have been undertaken in California (Calistoga and Desert Hot Springs) and Idaho (Boise), and in farms and villages across the western states. Several state and national parks, such as Yellowstone, Lassen, and Mount Katmai, have been established around major geothermal fields. In a few desert locations, fumarolic steam is condensed for livestock. An unusual application at Steamboat Springs, Nevada, is the use of hot well-water as the energy source in the preparation of plastic explosive.

At Yellowstone National Park, the U.S. Geological Survey drilled thirteen shallow test holes between 1967 and 1969, the deepest being slightly over 300 m. Maximum temperature was about 240°C. One hole produced essentially dry steam, whereas the others yielded a variable ratio of steam and hot water. Because this famous area of geysers, fumaroles, and hot springs is a National Park, no development is anticipated.

Union Oil Company is the latest to undertake exploration of the Valles Caldera of north-central New Mexico. Five exploration holes have been drilled, to depths of at least 1,600 m. Temperatures to 250° are reported. Essentially dry steam is said to have been produced from a hole drilled in 1970. The others have yielded hot water with variable percentages of steam flashover.

Rock temperatures above 200° are reported from holes at Brady's Hot Springs and Beowawe, Nevada. Temperatures of at least 175° have been measured in wells at Clear Lake, California; Steamboat Springs, Nevada; Casa Diablo (Long Valley), California; and Surprise Valley, California.

Along the Gulf Coast, high-temperature and high-pressure waters have been encountered in the search for oil: a maximum temperature of 273° was measured at 5,859 m. The great depth to productive reservoirs (a minimum of 2,500 m to the 120°C isotherm), as well as problems of production, utilization, and disposal, have forestalled any attempts at commercial development.

Altogether, over 35 areas have been explored by drilling. In many of these, however, results are inconclusive because of insufficient or misdirected efforts. Exploration activity continues in California, Nevada, and Oregon, as in earlier years, but the emphasis has shifted to include Idaho, Utah, New Mexico, Arizona, and adjacent areas.

### *Iceland*

Iceland pioneered in the use of hot water for municipal heating in the 1930s. Approximately 50 percent of the 200,000 population receives geothermal heating, and this is to rise to over 60 percent in this decade. Nine out of ten homes in Reykjavik, the nation's capital, receive geothermal water for home heating, distributed by the Reykjavik Municipal District Heating Service. Low-enthalpy hot-water fields at Reykir and within Reykjavik (Laugarnes field) supply this energy from reservoirs at base temperatures of 98° and 146°C. Over 100 wells have been drilled into these fields, the deepest being 2,200 m, at Reykjavik. Another low-enthalpy field is under development at Ellidaar, 3 km from Reykjavik. It is expected that this field will supply energy for expansion of geothermal heating in the Reykjavik area. A concrete conduit with twin 35-cm steel pipelines carries hot water for distances up to 18 km and with temperature losses on the order of 5°. Distribution to users is at about 80°. Because the mineral content of the water is remarkably low for geothermal fields (less than 400 ppm average), no processing other than separation of contained gases is needed.

Space-heating systems in operation or under construction elsewhere in Iceland will serve the needs of an additional 25,000 persons, mostly in small towns and villages on the southwest coast and in the north-central part of the island. Geothermal greenhouse operations in southwestern Iceland supply much of the fresh vegetables for the Reykjavik market. Additionally, heated baths and pools are found all across the western and northern parts of the country.

At Namafjall, near Lake Myvatn in northern Iceland, rich sublacustrine deposits of diatomite are dried with geothermal steam. Nearby is a 3,000-kw geothermal power station, opened in 1969. Exploration began at Namafjall around 1947, in connection with attempts to mine sulfur from the fumarole field. Drilling revealed a high-enthalpy, hot-water reservoir with a base temperature above 260°C and a maximum measured temperature of 286°. Seven wells were drilled to an average

depth of 700 m, the deepest in excess of 1,380 m. Four of these wells are operated, yielding 1.8 million kg/hr of superheated water. Some 240,000 kg/hr of steam separates from the water and is used to operate the power plant and diatomite plant. The water, which contains mostly sodium bicarbonate and silica, is not strongly mineralized. Gas content is similar to that at Larderello. Some shallow wells have produced almost-dry steam.

In 1967, the Johns Manville Corporation, in conjunction with the Icelandic firm Kisilidjan h/f, began mining diatomite at Namafjall and purchasing steam from the government of Iceland. The initial production rate for refined diatomite was doubled to 24,000 tons per year by 1970. Simultaneously, the Laxa Power Works, which produces 22 Mw mostly by hydroelectric power, arranged for the construction of a non-condensing 2.5-Mw turbine. This turbine soon is to be reconditioned to produce 3.4 Mw. A district heating system is under design to utilize the residual hot water.

Other uses for geothermal fluids are under consideration in Iceland. An experimental salt-recovery scheme was discontinued for economic reasons. There is a pilot operation under way to dry seaweed with natural heat (water at 100°C) for recovery for alginates. A geothermal brine with the approximate composition of seawater is under study for the recovery of various chemicals, including magnesia, table salt, and bromine. Freeze drying of fish, Iceland's main export, is also being evaluated. In the 1950s, when the present generation of nuclear reactors was under design, the potential for recovery of heavy water, D<sub>2</sub>O, from geothermal fluids was evaluated. The process appeared economic but the market for D<sub>2</sub>O did not materialize.

The conditions for using noncondensing turbines in Iceland appear favorable: heat energy is cheap and abundant, and no advantage accrues from large plant size, since a small population is distributed in villages and on farms across a large area. Multiple, small-capacity plants appear to be the most effective scheme. This suggests a bright future for low-cost geothermal electric power. The savings in fuel oil for heating purposes in the Reykjavik district amounts to some 200,000 tons per year. An additional 20,000 tons of fuel oil would be required for existing greenhouse operations. This is an appreciable savings for a small nation; if this heating were done entirely by electricity, which is not the cheapest alternative and therefore not an ideal comparison, some 200,000 kw of generating capacity would be required for peak demand.

Four high-temperature regions are known, three in the southwest and one in the north-central part of the country. Myvatn thermal region, in the north-central part, has a base temperature of approximately 280°C and constitutes an area of 50 km<sup>2</sup>. It includes the Namafjall field.

In southwest Iceland, aligned from southwest to northwest at intervals of 30 km, Reykjanes, Krysuvik, and Hengill have base temperatures of 280°, 220°, and 260°, respectively. Hengill, the largest, has an area of 70 km<sup>2</sup> and includes the important field of Hveragerdi at its southern end. At least eight deep and a great many shallow holes have been drilled in this area. The deepest hole at Hveragerdi is about 1,200 m, and produces dilute superheated water. Up to 25 percent flashes to steam, and between 13 and 32 Mw of electric power are planned. Reykjanes has had seven holes drilled, to a maximum depth of 1,750 m. These wells yield brine with chloride concentration up to 29,000 ppm. This brine is considered to derive from seawater by steam separation in a thermal regime of 270°. A system for recovery of various salts from the fluid, with concurrent generation of electricity, is under evaluation. At Krysuvik, about 30 km south of Reykjavik, plans have been made to transport superheated water to the capital for space heating in the event that growth of the system exceeds the capacity of the Reykir and Reykjavik (Lau-garnes) fields. Here, too, large flows of dilute superheated waters are obtained from more than a dozen wells as deep as 1,200 m.

These and other high-temperature fields occupy the zones of crustal rifting and active volcanism in Iceland. Outward east and west from this zone are extensive sheets of Late Tertiary basalts through which abundant warm and hot springs issue. The high-temperature reservoirs, however, are associated with the main Quaternary rift. Further, many are closely associated with Late Quaternary centers of dacitic and rhyolitic volcanism rather than with plateau basalts. Significant associations of high-enthalpy reservoirs and acidic volcanism occur at Myvatn, Askja, Geysir, Hengill, and at least half a dozen other areas. Only in the zone from Reykjanes to Krysuvik, some 30 km long, is silicic volcanism absent. Permeability within a reservoir may be controlled by lithology or by fractures. Thermal emissions to the surface are generally fracture-controlled.

Low-temperature systems have been explored at several parts of the southwest, west, and northwest coasts of Iceland. At Hlidardalur, 35 km southeast of Reykjavik, a hole drilled 1,500 m deep into an area of high temperature gradient failed to yield water. Temperature measure-

ments of 150°C at 700 to 800 m indicated a potential reservoir formation. This formation was fractured artificially and induced to flow, representing perhaps the world's first geothermal-fracturing experiment. At more than a dozen localities in western and northern Iceland, hot water is produced from wells at temperatures between 90° and 180°. These, where not already in use, have potential for use in agriculture and space heating. In most cases, water quality is high; however, one or two instances of geothermally heated seawater are reported, less saline than that at Reykjanes and thus representing lower-temperature systems. These lower-enthalpy fields are almost exclusively associated with centers of basaltic volcanism.

### *Japan*

Geothermal exploration began in 1919 at Beppu, on Kyushu Island, where 1 kw of electricity was generated in 1924. Somewhat earlier, the first geothermal heating of greenhouses began. However, it was not until the years immediately after World War II, with Japan's industrial base in ruins, that serious development began. The Agency of Industrial Science and Technology, which includes the Geological Survey, and several private electric utilities, drilling companies, mining companies, and prefectural governments, independently and jointly began exploration of Japan's geothermal resources.

At Beppu, experimentation resulted in the generation of 30 kw of electricity in 1951. Even earlier, the Tone Boring Company had begun a drilling program in several areas. At Yunosawa, on the south-central coast of Honshu, geothermal steam was used in a demonstration plant to generate 8 kw in 1948. At Hakone, also on the south coast of central Honshu, 30 kw of electricity has been generated since 1960 from steam produced in a shallow well, for use at a hotel. Other experimental generation of electricity has taken place on Hokkaido Island (Atagawa) and in northern Honshu (Narugo).

Japan's hot springs have been used for therapy and recreation for centuries. Japan probably leads the world in the use of natural hot water in baths, therapeutic spas, and resorts, there being literally thousands of these. More recently, volcanic parks such as Hachimantai have been established for the preservation of the geothermal phenomena. However, space-heating systems have not developed as widely as in Iceland or the Soviet Union. Four district heating systems were in operation in 1969,

using hot water (not greater than 70°C) equivalent to about 5,000 tons of fuel oil per year.

Greenhouse heating with geothermal waters is common in farms and experimental agricultural stations, chiefly in south-central Honshu. Some are near Beppu, and a few are in the Shikabe geothermal area of Hokkaido Island. Commonly, garden vegetables, tropical fruits, and other plants are cultivated. At least two farms raise chickens. At one pond, eels and carp are raised for consumption, and at another, alligators.

There are several more specialized industrial applications. One, on Kyushu Island, involves the recovery of sulfur from deposits at fumaroles. At Beppu, 98° water is used to process about 30 tons of rice annually for use by a bakery. In the Shikabe area of Hokkaido, salt is recovered from seawater by evaporation, using geothermal hot water and steam from a 70-m well. Though the operation produces only 150 tons of salt per year, a combined geothermal power plant and salt-recovery works planned at Shikabe could produce 7,000 kw of electricity, up to 100,000 tons of salt annually, and some amount of fresh water. The proposed plant would use multi-stage vacuum distillation.

Exploration began in 1952 at Matsukawa, in northern Honshu, with the drilling of wells for steam to supply bathhouses. Japan Metals and Chemicals Company became active in exploration there in 1956, and was joined in 1958 by the Geological Survey and later by other organizations. At least nineteen wells have been drilled since 1952. Of these, six are classed as production wells, having an average depth of about 1,200 m. Five wells used for power generation yield an average of 110,000 kg/hr of dry steam. Two wells yield both steam and water in the ratio of about 4:1. Reservoir temperature, about 240° to 250°C, is much like that at The Geysers, California. The reservoir formation is a fractured series of welded dacite tuffs and lavas of probable Pliocene age. These overlie Miocene sands and shales, Lower Tertiary "green tuffs," and Paleozoic slate and chert. Above the reservoir rocks are Quaternary andesites and constructional debris of very youthful volcanoes. The area about Marumori volcano comprises a caldera of perhaps 10 km<sup>2</sup>.

Construction of the Matsukawa power plant began in 1961. Initial operation was at 9,000 kw. The facility has been expanded to 20,000 kw, and plans call for expansion to 27,000 kw in the 1970s, with future expansion to at least 60 Mw. Noncondensable gases, which average about 0.5 percent, are expelled to the air. Condensate from the condens-

ing turbine is discharged to the natural drainage, without known harmful effect.

Exploration begun in 1953 at Otake, on Kyushu Island, culminated in 1967 with the completion of a 13,000-kw power station by a group headed by Kyushu Electric Power, Inc. Ten wells were drilled at Otake, and two at Hachobaru to the south; five are connected to the condensing turbine. One well produces about 37,000 kg/hr of dry steam; the others produce larger amounts (up to 540,000 kg/hr) of steam and water, with steam making up 10 to 25 percent of flow. Noncondensable gases total less than 0.5 percent of the steam by weight. The reservoir fluid is of sodium-chloride composition, but relatively dilute, averaging about 4,000 ppm. Maximum reservoir temperature is about 200°C. Maximum well depth at Otake is 900 m; at Hachobaru, one well is 785 m deep.

The geology consists of Pleistocene andesite lava and tuff-breccia, and occasional pumice beds, overlaid by Holocene sediments and volcanic ash. Structure is largely obscured by the constructional features of Quaternary volcanoes. However, faulting is believed to be significant, forming down-dropped blocks. Hydrothermal alteration and thermal emissions are intense and widespread, suggesting fracture permeability to the surface. The wide range of flow rate and steam percentage from well to well suggests that permeability and stored fluid are limited in portions of the field. But no deep wells have been drilled, and the main reservoir may not yet have been encountered.

The Otake field is located in Aso National Park, thus requiring special permission for construction of plant facilities. To avoid pollution of natural streams, water discharges are pumped to a nearby hydroelectric reservoir. Limited life is predicted for the present wells because of scaling and fluctuations in pressure. Silica deposition in the discharge pipeline caused a restriction of power production in 1968 and 1969. Studies are still under way to control scaling. Calcium-carbonate scale, requiring acidizing, has been found in at least one well. Despite these problems, additional wells are planned and production is to increase to perhaps 180,000 kw over the next decade or so.

At least 23 areas have been explored by drilling in Japan. Several are being evaluated for development, the most significant being at Shikabe, on Hokkaido Island; at several places near Matsukawa; at Onikobe, south of Matsukawa; and at Takenoyu and Hachobaru, near Otake.



In the Hachimantai volcanic area, northwest of Matsukawa, extensive geophysical work culminated in the drilling of at least nine holes to average depths of about 750 m. Temperatures reached 200°C at the south end of the drilled area, where hot water was encountered with up to 30 percent steam fraction. Exploration is continuing there, and the construction of a 10,000-kw power plant is being considered. The geology at Takinokami, southwest of Matsukawa, is similar. Temperature surveys to 50 m (maximum temperature, about 200°) were followed by a 400-m well, which produced a steam and water mixture.

Onikobe has been the scene of exploration since 1962. It is a structural basin of about 60 km<sup>2</sup>, in which there are numerous fumaroles and hot springs. Exploration has included geologic mapping, geophysical surveys, and test drilling. On the basis of ten holes, with maximum depth over 700 m, and temperatures to 190°, drilling of production wells is under way. One hole is reported to produce nearly 30,000 kg/hr of superheated steam.

Takenoyu has been investigated since the early 1950s. Two wells were drilled to about 250 m in 1962. Bottom-hole temperatures were approximately 200°. One well ceased to produce after a short period, indicating limited permeability in the reservoir. The other, however, continues to yield 3,000 kg/hr of saturated steam. This well has been studied extensively; additional drilling was in progress in 1970.

Geothermal exploration has been carried out also at Kucharo and Showa-shinzan volcanic centers on Hokkaido Island; Nasu in central Honshu; Hakone and Atagawa, on the south coast of Honshu; Oshirakawa, in west-central Honshu; and several places in the south of Kyushu Island. Many of the drill holes were to shallow depths, and exploration cannot be considered conclusive at most locations. High-temperature reservoirs were located at Nasu (194°) and on southern Kyushu Island (over 170°).

A relationship has been noted between high-temperature reservoirs and dacitic or dacitic-rhyolitic-andesitic volcanism in Japan. This observation is similar to findings in Iceland, New Zealand, the United States, and elsewhere. The Japanese fields, however, have not been marked by the high temperatures encountered at centers of silicic volcanism in New Zealand or Iceland. Well flow has varied widely, and probably reflects fracture rather than intergranular permeability in most Japanese fields. Indeed, restricted permeability may represent a con-

straint upon development. But in power-short Japan, exploration is being pursued vigorously on all fronts.

### *Soviet Union*

Eleven geothermal developments were reported in the Soviet Union in 1969. Most significant among these were the generation of electricity at Pauzhetsk; the experimental, freon-based heat exchanger at Paratunka; and the space-heating operations at Makhach Kala. There were other space-heating projects at places in the Caucasus, in western Siberia, in central Asia, and in northeastern Siberia.

Pauzhetsk is at the southern tip of the Kamchatka Peninsula, an area of active volcanism. At Pauzhetsk there are several large, boiling springs, fumaroles, and geysers; the fumarolic volcano Koshelev is nearby to the southwest. Drilling began in 1957; by 1964, 21 holes had been drilled. Eighteen of these were considered to be production wells, ranging in depth from 200 to 1,200 m. They revealed a succession of nearly horizontal, Quaternary dacitic and andesitic tuffs and agglomerates, overlying Tertiary tuffaceous sediments, the whole cut by faults into horsts and grabens. This structure had collapsed into a caldera. Heat emissions are localized on the caldera rim and along pre-caldera faults.

Reservoir fluid is hot water, containing abundant sodium and potassium chloride. It is not as saline as fluids produced at Ahuachapán, El Salvador, or Cerro Prieto, Mexico, but is similar in composition. Maximum field temperature is about 200°C, and enthalpy, even in deeper wells, is probably less than 195 cal/g. Steam flashover is about 15 to 20 percent.

Construction of a 5,000-kw power plant began in 1964, and full operation was achieved in 1967, utilizing flashed steam from three to seven wells. Plans have been laid to increase electricity production in two stages. The first involves reconstructing the two original turbines, the second installing additional low-pressure turbines, to make total installed capacity 22 to 25 Mw by 1980. Electricity from Pauzhetsk is transported 27 km to consumers at costs 30 percent less than that of electricity generated using fuel oil.

The most significant experiment to date in heat-exchanging with geothermal fluids has been undertaken at Paratunka, near the city of Petropavlovsk, on the east coast of Kamchatka. A 680-kw freon-based generating plant was installed in 1967, and after extensive testing began rou-

tine operation in 1970, supplying power to the Paratunka State Farms. The plant comprises two 340-kw turbines and utilizes water from shallow wells at 81°C. Excess heat is used to heat greenhouses and seedbeds, and warm water is used for irrigating crops. Other space-heating projects in the vicinity use water at under 80° to heat homes, baths, and swimming pools.

There has been extensive development of geothermal-heating systems at several points across a 500-km zone on the north slope of the Caucasus. Beginning in 1947 at Makhach Kala, on the Caspian Sea, after the accidental discovery of 60° to 70° waters in the course of prospecting for oil, space heating has developed rapidly. At Makhach Kala, 15,000 people receive home heat and hot water from a municipal geothermal system; and geothermal water is used as boiler feed in an oil refinery and as heating for greenhouses, seedbeds, and baths. Trending northwest, there are similar activities at Grozny; in the Kabardin-Balkaria district; at Cherkessk, where 18,000 people are served; and in the vicinity of Maykop. In the Kabardin-Balkaria district alone, site of one of the more modest projects, an annual saving of 2,500 tons of fuel oil results. Water temperatures are between 47°, near Cherkessk, and 86°, near Maykop, though the reservoirs supplying these wells may be at temperatures of 100° to 150°C. Many of these waters are but lightly mineralized, allowing direct utilization. In some cases, however, mineralization is strong, and heat is exchanged to fresh, cool water.

Other geothermal-heating projects are near the Black Sea coast of Georgia; on the Caspian Sea near the border with Iran; in several places in northeast Siberia; in the cities of Omsk and Tobolsk in western Siberia; at several points near Tashkent in central Asia; and on the shore of Lake Baikal. Figures for the total consumption of geothermal energy in the U.S.S.R. are fragmentary and contradictory. However, the total energy consumed in these several space-heating systems is believed to be the equivalent of 1 million tons of fuel oil per year.

Exploration of high-temperature reservoirs has continued on Kamchatka Peninsula and on the island of Kunashir' in the Kurile chain. In addition to the developed fields of Paratunka and Pauzhetsk, there is geological, geophysical, and geochemical exploration under way at Bolshe-Banny, Uzon Geyzerny, Nalychersky, and six other areas on Kamchatka. At Bolshe-Banny, located about 30 km west of Paratunka, a maximum temperature of 171° was measured in drill holes.

The search for low-enthalpy waters for use in heating and in agriculture is accelerating in Georgia, the west Siberian lowlands, and areas on the northern slopes of the Pamir, Tien Shan, and Altai ranges in central Asia. Vast basins containing waters at temperatures up to 120° have been outlined in western Siberia and along the northern foothills of the Caucasus. Temperature-gradient drill holes, geochemistry, and seismic-refraction surveys are commonly used in these studies.

### *Hungary*

Extensive hot-water aquifers have been found to underlie the southwestern part of the Hungarian basin, near the Yugoslav border. Although reservoir temperatures are not high enough for the generation of electricity with present-day technology, the hot-water resource has been extensively developed for space heating. Eighty wells had been completed by early 1970, to depths of 1,800 to 2,000 m. Water temperatures from these depths are 85° to 110°C. Temperature gradients of 35° to 55° per km occur, which is not unusual for deep sedimentary basins. Like other high-gradient basins, such as the Gulf Coast of the United States, the Hungarian basin is devoid of Quaternary volcanic rocks or high-temperature surface waters. Basin fill comprises several thousand meters of Tertiary and Quaternary sediments. Reservoir formations in the Hungarian basin are highly permeable lower Pliocene sands. Average well yield is 80 to 90 m<sup>3</sup>/hr. Since the water contains calcium carbonate it must be allowed to stand, and thus to precipitate within tanks rather than within the heating system. Wells are reconditioned periodically.

The Hungarian government is developing an extensive geothermal-heating system in the province of Csongrad. Ironically, plans to heat the entire city of Szeged with natural hot water were abandoned when oil—ultimately the largest oil and gas field in Hungary—was discovered during the drilling of a hot-water well. Even so, some 1,200 housing units and associated municipal and commercial buildings are heated by hot water in Szeged. Geothermal fluids are used also to heat greenhouses, animal pens, runs, and other farm buildings, and to dry crops. In all, well over 1 million m<sup>3</sup> of space is heated geothermally, at costs well below those of conventional fuels (see Table 2). Data are incomplete and perhaps inconsistent, but the heating done by hot water in Hungary would require about 80,000 tons of fuel oil annually.

Geothermal development is expected to increase at about 15 percent per year through the decade, mainly in agricultural application.

### *Mexico*

A 75-Mw power plant is to begin operation at Cerro Prieto, Baja California, early in 1973. This will not be the first Mexican geothermal station—an experimental facility has operated at Pathé, Hidalgo, since 1960. At Pathé at least fourteen wells have been drilled, and 500 kw of electricity is produced from a generator rated at 3,500 kw and now supplied by a single well. Pathé is located in the extensive east-west volcanic belt that traverses central Mexico from the Pacific to the Gulf coastal plain. Exploration at Pathé began in 1955. The reservoir comprises a thick sequence of altered and fractured Tertiary andesites and basalts. These overlie Cretaceous carbonates and are in turn overlaid by Quaternary and Late Tertiary tuffs and sediments. Wells produce steam or steam and water, although only four can sustain flow. Production is from variable depths, since permeability is believed to be controlled by fractures. The low productivity per well and the tendency of wells to produce dry steam indicate a low permeability and limited fluid content in the reservoir. The presence of a deeper reservoir in the Cretaceous carbonate rocks has been postulated, but has not been explored by drilling.

Cerro Prieto, 30 km south of Mexicali on the Mexican-United States border, is the southernmost explored portion of the structural rift extending from north of the Salton Sea in the United States into the Gulf of California, a total distance of several hundred kilometers. Exploration is occurring in several portions of this rift in the United States. At Cerro Prieto, fumaroles and mud volcanoes in the vicinity of a Quaternary dacite-basalt volcano, aligned along a probable extension of the San Jacinto fault, attracted exploration in the late 1950s. Twenty-three deep holes have been drilled, of which fifteen have been completed as production wells. Average yield is about 230,000 kg/hr of superheated brine. Approximately 20 percent flashes to steam, giving an average electric-power yield of some 5 Mw per well, although the steam percentage varies from 13 to 25 percent in individual wells. The strongest well of the field yields nearly 700,000 kg/hr of brine, which is equivalent to 15 Mw of electricity. Though average well depth is about 1,500 m, one deep well reached 2,600 m, penetrating crystalline basement. Permeable sands are encountered between 600 to 1,200 m and at depths below

2,400 m. Only the shallower reservoirs are to be used for production. Reservoir temperatures are over 300°C, with a maximum recorded temperature of 388°C.

As elsewhere in this structural rift, several thousand meters of Late Tertiary and Quaternary sediments have filled the opening trench caused by the separation of Baja California and adjacent California from the continental mainland. Volcanism is exhibited only locally, and the heat source is believed to be molten rock of the upper mantle, which is here at depths of only 15 to 20 km. Water in these sediments may be derived from the ancestral Colorado River system.

The reservoir fluid contains between 13,000 and 25,000 ppm total dissolved solids, mostly chlorides of sodium and calcium. The feasibility of commercial extraction has been studied for such substances as potassium chloride, lithium, and boron, but no recovery operations are planned for the first plant. Disposal will be via ditches to the Rio Hardy, a distributary of the Colorado River, and thence to the Gulf of California. Some concern has been expressed over long-term consequences, and the alternatives of reinjection and ponding are under consideration. Other problems include brine corrosivity and the possibility of induced ground subsidence.

However, a second set of wells is to be drilled beginning in 1972, to supply steam for a second 75-Mw station. This would go on line in about 1980. A steam-powered drilling rig has been brought to Cerro Prieto, to operate on natural steam. This should have the effect of reducing drilling costs slightly. Water condensed from steam is used in construction and maintenance operations in this extremely arid region. Only a small portion of the Cerro Prieto geothermal zone has been drilled, and it is considered likely that total potential is many times that due for production in this decade. Exploration and development are carried out by an arm of the Comisión Federal de Electricidad, the Mexican national electricity agency.

Several high-temperature fumarole and hot-springs systems have been under exploration in the east-west volcanic belt of Mexico. This zone contains many active volcanoes and extensive evidence of Quaternary volcanism. Five systems have been explored in some detail and at a sixth, San Marcos, exploration is just under way. The five are, from west to east, La Primavera, in Jalisco; Los Negritos, Ixtlán, and Los Azufres, in Michoacán; and Los Humeros, in Puebla. This zone of volcanoes and

interspersed heat emissions is over 700 km long. La Primavera occupies the margins of a graben down-dropped within a Quaternary caldera. Superheated steam flows from fumaroles in altered rhyolites at temperatures to 100°C. Geophysical and geochemical work was in progress in 1970. Los Negritos is perhaps the best known of these fields, occupying part of a caldera whose walls show acidic tuffs, basalt flows, and lacustrine sediments. Fumarole temperatures reach 95°. Extensive geological, geophysical, and geochemical work suggests an extensive high-temperature reservoir. Ixtlán, only 27 km to the northeast, occupies an east-west structural valley, and exhibits mud volcanoes and fumaroles to 100°. Drilling of deep exploration holes was in progress in 1970. Preliminary temperature-gradient drilling had encountered temperatures to 150°. Los Azufres also occupies part of a caldera formed in basaltic and rhyolitic flows and pyroclastics. Here, superheated steam at temperatures to 110° is emitted from powerful fumaroles. Geological and geophysical work is in progress. Los Humeros, the easternmost of these fields, exhibits fumaroles to 90°, in a Quaternary caldera containing rhyolite and basalt flows and pyroclastics. Here, too, geophysical and geochemical work is continuing.

### *El Salvador*

In 1971 the national electricity agency (CEL) of El Salvador chose LC-Electroconsult of Milan, Italy, to design a 30-Mw geothermal plant for construction at Ahuachapán. This marked the successful completion of a geothermal exploration program jointly sponsored by the government and the United Nations. Even before this program began in 1965, the National Geologic Service of El Salvador had explored the Ahuachapán fumarole area and drilled two shallow wells. Over \$4 million has been spent to date on this project. In 1972 CEL is expected to call for bids for construction of the plant, and it is anticipated that electricity will flow in 1975. Production capacity will be increased through additional drilling and plant construction by 1980.

The Ahuachapán region occupies some 30 km<sup>2</sup> on the northern slopes of a range of Quaternary andesitic volcanoes, and contains over a dozen areas of fumaroles, warm ground, and hot springs. The easternmost peak of the range, Izalco, is active. Geologic mapping and subsequent drilling suggest the presence of a caldera, largely buried by late- and post-volcanic debris. Fumaroles and other heat emissions at Ahuachapán are

controlled by annular fractures forming the caldera wall and by northerly trending transverse fractures. The highest fumarole temperatures occur at the southern (uphill) end of the structure, and reach 125°C. No wells have been drilled in that area. Average well temperatures are about 225° to 230°, the maximum 235°, at depths of 600 to 900 m. However, geochemical indexes suggest a reservoir-equilibrium temperature approximately 10° to 20° higher. Several workers have thus speculated that the higher-temperature fumaroles to the south may more closely correspond to the reservoir source.

Reservoir fluid is a sodium-chloride brine of about 10,000 ppm concentration. Some 15 percent flashes to steam in the wellbore. Because average mass flow is about 320,000 kg/hr, it is expected that seven production wells will be needed for a 30-Mw plant. No pressure declines have been noted in production tests. The disposal of saline reservoir fluid presents a problem, since boron, chloride, and arsenic are present in amounts potentially harmful to agriculture. In reinjection tests, a production well has been used for disposal into a deep, hot aquifer. These tests have continued for a year and a half without definite effects upon the adjacent production wells. The question of possible silica deposition in reinjection wells remains unanswered. The alternative to reinjection is disposal to the sea via holding ponds and the natural river-drainage system.

A conservative estimate of developable potential at Ahuachapán is 100 Mw for a 50-year period. Drilling to date has explored only 2 km<sup>3</sup> of an estimated 40 km<sup>3</sup> field volume. Exploratory drilling has also been carried out at Berlin, in the eastern part of the country. A well drilled in 1968 to nearly 1,500 m encountered temperatures of at least 225°. Flow of hot water was not sustainable, indicating restricted permeability. Another hole drilled to 600 m, 10 km to the northwest, flowed strongly and continuously at about 100°. Both wells exhibited moderate chloride salinity. Further exploration is warranted.

### *Kenya*

Kenya, Uganda, and Tanzania share a common electric-power system, operated in Kenya by the nationalized East African Power and Lighting Company (EAPL). In 1957 and 1958, EAPL drilled two test holes southwest of Lake Naivasha, in the Kenyan rift. These holes could not be brought into sustained flow, despite temperatures exceeding 200°C.



In 1970, exploration began again, jointly sponsored by the United Nations and the Government of Kenya, in the rift zone. Two broad target areas were chosen, Lake Hannington, where fumaroles and boiling springs issue at the edge of the tilted fault blocks, and near Lake Naivasha. Acid igneous domes and ejecta form an arc around the lake from northwest to south, and a few miles south of the lake an east-west fracture transects the rift. There are two fumarole complexes within the volcanic field around Naivasha. The northern complex, on the slopes of Mount Eburru, has been drilled to about 150 m. Low-pressure steam is produced and condensed for use in watering livestock, and pyrethrum leaves are dried in live steam for use as insect-repellant. The southerly field, Olkaria, was the site of the earlier drill holes by EAPL. One of these holes, about 900 m deep with temperatures to 230°, has been induced to flow, and tests are continuing. Extensive geological, geochemical, and geophysical surveys have been made, and three deep exploration holes are scheduled for the summer of 1973.

### *Ethiopia*

A survey in 1970 and 1971 sponsored by the United Nations and the Government of Ethiopia catalogued the surface thermal phenomena of the Ethiopian rift zone. Over 500 separate hot spring and fumarole localities were reported. A second-stage exploration is planned to begin sometime in 1973. Three areas of greatest interest were noted: Dallol, in the Danakil depression of the northern rift; the Tendaho graben of the Afar region; and the Aluto caldera in the lakes district of the southern rift.

The Danakil depression is a north-south trench, mostly below sea level. At the north are the Dallol salt flats, an evaporite sequence over 1,000 m thick, producing salt-saturated springs at temperatures above 110°C. Immediately south is a chain of active volcanoes, with fumaroles to 220° on the flanks. At Tendaho, there are extensive boiling springs, fumaroles, Holocene cinder cones, and lava flows, in a situation of tilted and rotated fault blocks. In the lakes district several volcanic centers and calderas are characterized by hot springs and fumaroles.

Even at Addis Ababa, a city of 600,000 persons at 2,500 m elevation on the Ethiopian plateau, there is an extensive hot-water aquifer that might prove useful in space heating. Government-sponsored geothermal exploration is investigating the extensive potash reserves at Dallol and

the need for electricity for pumped irrigation in the Tendaho area. Fresh water might be a by-product of either scheme, but currently hot water and steam condensate are used only locally for bathing and stock-watering.

### *The Philippines*

At Tiwi, on Luzon in the Philippines, a 10-kw geothermal generator has operated since 1969 as a demonstration of the economic potential of the region. The area had been explored by the Philippine National Science Board and the Commission of Volcanology since 1966, when seven shallow, exploratory wells were drilled. The well that later drove the generator produced about 10,000 kg/hr of steam at 154° from 220 m depth.

In 1971 Philippine Geothermal Inc., a subsidiary of the Union Oil Company, contracted with the National Power Corporation of the Philippines to explore the 150 km<sup>2</sup> of geothermal resources in southeastern Luzon. Tests on a 1,500-m well drilled in 1972 indicated potential as a commercial power source by the mid-1970s. Two additional wells are scheduled to be drilled. Geologically, the region consists of Quaternary andesites and subsidiary dacites.

### *Indonesia*

The island nation of Indonesia is among the most volcanically active regions of the world. On Java, where over 40 million people live, active volcanoes dot the island; and there are others on Sumatra, Bali, Flores, and the Celebes. As early as 1918, reports suggested that the volcanic heat of these islands could be harnessed. In 1928, the first geothermal test holes were drilled at Kawah Kamodjang on western Java. The deepest of these three holes was 128 m. The highest temperature was 140°C, and abundant low-pressure steam was encountered. Data from these wells were recorded continuously until World War II.

After the visit of a scientific team from UNESCO, in 1966, Indonesian geologists began compiling data from Java and the southern Celebes. In 1969, the U.S. Geological Survey began a program of assistance, which is still under way, concentrating on the Dieng area of central Java. The Dieng region comprises a series of constructional volcanic forms and their explosive and extrusive products, aligned roughly northwest and extending about 20 km. Surface temperatures to 95° are recorded

within the Miocene sandstone. Electric-power potential at Tatun has been estimated at 80 to 200 Mw, and construction of a 10-Mw pilot plant at Matsao is being considered.

### *Turkey*

In 1961 the Turkish government began detailed studies of a series of geothermal manifestations in western Anatolia. The United Nations entered into a cooperative exploration venture in 1967, and the following year, after geological, geophysical, and geochemical surveys, the first well was drilled at Kizildere, in the Menderes (Meander) River valley. Hot springs are widespread through this region, with temperatures to 100°C. Mercury mineralization is also present locally.

At least seven deep holes have been drilled at Kizildere, another at Tekke Hamman, 10 km to the southwest. In the process, a hot-water reservoir has been discovered, with two horizons, at depths of about 350 to 400 m and below 600 m. Exploration has revealed a highly fragmented horst and graben terrain, primarily with east-west trend, step-faulted down to the south. A crystalline basement of schist, gneiss, marble, and quartzite is overlaid by Miocene and Pliocene fluvial and lacustrine sediments. A highly fractured Miocene limestone in this sequence constitutes the upper reservoir; fracture permeability in the crystalline rocks provides the lower reservoir. Quaternary alluvium caps the Tertiary sequence. No youthful volcanic rocks are present. Rather, the heat source is postulated to be a cooling granitic mass at depths of several kilometers. Its upward movement is believed to have generated the horst and graben structure.

Average well depth is about 450 m, and reservoir temperatures are between 180° and 200°. Yield per well is between 25,000 and 300,000 kg/hr, averaging about 150,000 kg/hr, with about 10 percent flashing to steam. It is reported that the deeper wells, into the crystalline basement, have higher flow rates. The reservoir fluid is highly carbonated, and a major problem of calcite deposition must be solved before development can proceed. The well at Tekke Hamman, in fact, is inoperable because of calcite incrustation. Installation of a 10- to 20-Mw generator, utilizing a closed-system heat-exchanger, is being considered—reservoir fluid would be produced, utilized, and reinjected into the reservoir under pressure, thus avoiding the separation of calcium carbonate from the fluid.

### *Exploration in Other Areas*

A pioneering geothermal development was begun in the 1950s at Kibukwe, in Katanga province of Zaire (Congo), where a 220-kw geothermal generating plant was installed at a metal mine. This plant, which used wet steam at about  $95^{\circ}$ , was costly and inefficient, but served satisfactorily for many years in a remote area far from cheap alternative power supplies. The plant and mine are now shut down.

In February 1972 it was reported that a small, experimental power station had operated successfully at Tengwu, in Kwangtung Province of the People's Republic of China. The station is reported to use steam flashed from hot water to turn turbines, but no details are available on plant size, water temperature, or operating characteristics.

In 1967 the United States undertook a project of geothermal exploration for the Government of Nicaragua, utilizing private U.S. concerns as contractors. Detailed geophysical surveys and geochemical and geologic evaluations were made, and a series of temperature-gradient holes was drilled in fumarolic terrain near Momotambo volcano in west-central Nicaragua. A deeper drill-hole encountered temperatures to  $230^{\circ}$ , but the project was allowed to lapse. In 1972 the United Nations entered into an agreement with the Government of Nicaragua for a second phase of exploration, which is now under way.

At Melun, France, about 50 km southeast of Paris, two holes drilled to depths of 1,800 m intersect an artesian aquifer with water at approximately  $70^{\circ}$ . This corresponds to a gradient of about  $3^{\circ}/100$  m, and is not remarkable (see Table 2). Nonetheless, a district-heating scheme is being evaluated in which one well would be used for production and the other for reinjection of heat-depleted water. Heat energy produced from this scheme would be offered at prices competitive with other fuels. The artesian basin is believed to be quite vast.

Many other countries of southern and eastern Europe, Latin America, north Africa, and Asia have begun the collection of data for geothermal exploration. Prominent among them are Algeria, Colombia, Greece, Guatemala, India, Israel, Spain (Canary Islands), Venezuela, and Yugoslavia. A listing of some 50 countries active or interested in geothermal exploration is given in Table 3.

Temperature-gradient drilling in northeastern Algeria has outlined a region of anomalous gradient near the Tunisian border. Detailed geo-

logical and geochemical studies suggest a buried batholithic mass as the source of heat for the numerous hot springs of the region.

The Government of Guatemala has chosen a geothermal area near Moyuta volcano, near the border with El Salvador, for detailed exploration. Consideration is being given to contracting in 1972 for a deep exploration hole, and several engineering firms have been asked to submit proposals for a drilling and development program.

The Spanish government is supporting geothermal exploration in the Canary Islands, a Spanish territory off the coast of Morocco. Very-high-temperature fumaroles are reported at Lanzarote Island.

In Yugoslavia and Czechoslovakia, temperature-gradient and heat-flow studies are currently in progress, with an eye to locating sizable reserves of low-enthalpy fluids for use in space heating, agriculture, and industry.

In six underdeveloped nations (El Salvador, Chile, Turkey, Kenya, Ethiopia, and Nicaragua) the United Nations has sponsored geothermal exploration jointly with the national governments. United Nations missions have also been made to India, Greece, Peru, and Guatemala in the past year to evaluate potentials for exploration; cooperative exploration projects have been proposed in several cases. The United States has supported exploration in Nicaragua and Indonesia through the Agency for International Development. Colonial administrations have carried out exploration in such underdeveloped places as the Territory of Afars and Issas (French Somaliland), the Fiji Islands, and New Britain. In the United States and Japan, private and government organizations have engaged in exploration, either jointly or separately. Private concerns have assisted in geothermal exploration in the Philippines, Algeria, Guadeloupe, and elsewhere. Usually, the initial stages of data collection and the preparation of geologic-reconnaissance reports, power-demand projections, and transmission-grid maps, are undertaken by the local geological survey or electricity agency. Shallow borings are often made at this stage, too. Much of the exploration to date has been financed and carried out by agencies of the countries involved, for in many cases the geothermal resources are owned nationally and are thus not at the disposal of private landowners. But because many nations lack a sophisticated geological infrastructure, detailed exploration is likely to require cooperative ventures with the United Nations, with more developed nations, or with private concerns.

*The Potential for Geothermal Energy Development to 1980*

At Larderello and Monte Amiata (see Table 4), increases in power generation are likely to depend upon conversion from noncondensing to condensing turbines. This may increase capacity by 15 percent over the decade. But only if significant discoveries of steam are made at Travale, Roccastrada, or Radicofani is there likely to be new construction in the steam fields of Tuscany. If exploration elsewhere in Italy is successful, new generating facilities could be on line by 1980.

There are no plans to construct additional geothermal power plants in New Zealand in this decade. Industrial and municipal applications will be encouraged, however, and some generation of electricity may result incidentally to direct utilization of heat for industrial processes.

Plans have been made to increase generating capacity at The Geysers by 110,000 kw per year through 1975, at which time 630,000 kw will

TABLE 4  
*Expected Development of Electric-Power Capacity at  
Selected Geothermal Fields to 1980*

Nation	Field	Installed capacity, late 1972, Mw	Expected development, Mw
El Salvador	Ahuachapán	—	30 by 1975; 60 by 1980
Iceland	Hengill (Hveragerdi)	—	Up to 32 by 1980
	Namafjall	3	None known
Italy	Larderello	365	15-percent increase possible
	Monte Amiata	25	
Japan	Hachimantai	—	Perhaps 10 by mid-1970s
	Matsukawa/Takinokami	20	Perhaps 60 by 1980
	Onikobe	—	Perhaps 10 by 1980
	Shikabe	—	7; salt-recovery works planned for 1970s
	Otake/Hachobaru	13	Perhaps 60 by 1980
Mexico	Cerro Prieto	75	150 by 1980
New Zealand	Kawerau	10	None planned
	Wairakei	160	None planned
U.S.S.R.	Pauzhetsk	6	Up to 25 by 1980
	Kunashir'	—	Up to 13 by 1980
United States	The Geysers	302	110 per year through 1980, to 1,180
	Imperial Valley	—	Demonstration, for desalination; power station by 1980

have been installed, making this the largest developed field in the world. By 1980, it is thought, installed generating capacity might be about 1,180,000 kw, if development continues to be successful. In the Imperial Valley it is likely that pilot electric-generation and desalination plants will be operating by 1980. Capacity is likely to be 10 to 20 Mw for demonstration plants. By then also, one or more small-scale, closed-system, heat-exchanging electric generators may be installed in that region. Conceivably, a few other pilot stations may be operating, or full-scale plants may be under construction, elsewhere in the western United States by 1980.

Several Japanese fields are likely to be developed in this decade. Matsukawa and Otake are scheduled for enlargement to perhaps 60 Mw each. This would include some development at Takinokami near Matsukawa and some at Hachobaru near Otake. Questions of scaling, well life, and water disposal may delay development somewhat. Onikobe, Hachimantai, and Nasu, on Honshu, and Shikabe, on Hokkaido, are also potential candidates for power-generation development; total installed capacity at these fields is not likely to exceed 30 Mw by 1980.

The plant at Pauzhetsk, in Kamchatka, may be expanded to as much as 25 Mw by 1980. Other fields in the Kurile Islands or on Kamchatka may be put into production, probably in the range of 10 to 20 Mw each. Space heating can be expected to increase greatly in the Caucasus and in regions of western and southern Siberia through the decade, so that by 1980 the consumption of hot water may surpass two million tons per year of fuel oil.

Similar increases in consumption of hot water can be expected in Iceland, with an equivalent of over one-third million tons of fuel oil used annually. Electric-power generation may increase slightly at Namafjall, and may begin at Hveragerdi in the Hengill area. Perhaps 15 to 35 Mw capacity will be installed by 1980.

In Hungary the consumption of hot water for space heating may more than double through the rest of this decade. Hot-water heating schemes may become operational in Yugoslavia, Czechoslovakia, France, and elsewhere in Europe by then.

A second 75-Mw plant may be installed at Cerro Prieto by 1980. And construction of generating facilities may be under way elsewhere in the central part of Mexico by then. Similarly, at Ahuachapán, El Salvador, a second 30-Mw facility may be operational at that time.

Small plants are likely to be operating or under construction in the Philippines, Kenya, Chile, Turkey, and Taiwan by 1980, and perhaps in Guadeloupe, Nicaragua, and elsewhere. Their aggregate output is likely to be between 70 and 150 Mw. But because of the 4- or 5-year minimum lead time required for exploration and construction, it is unlikely that extensive plant construction will have been undertaken elsewhere by 1980; conceivably, another 50 Mw of generating facilities will be erected in, for example, Indonesia, Ethiopia, or China.

Thus, a conservative projection of worldwide geothermal generating capacity by 1980 is on the order of 2,500 Mw, or three times present-day capacity. Because world consumption of electricity during this 8-year period is likely to double, the geothermal-power component of world output will remain at less than 1 percent of total generating capacity. Direct utilization of geothermal energy is likely to increase at a faster rate, especially in eastern Europe.

More rapid development is foreseen in the 1980s. It will depend in part upon improvements in geothermal drilling and utilization technology, increased knowledge of geothermal systems, and greater availability of funds for geothermal exploration and development.

#### SOURCE MATERIAL

Because of the great volume of source material from which this paper was drawn, citations are not given for individual references. Rather, the reader is directed to two massive proceedings that serve both as sources for data in this report and as bibliographies for continued research:

Proceedings of the United Nations Conference on New Sources of Energy, Solar Energy, Wind Power and Geothermal Energy, Rome, August 21-31, 1961; v. 2, 3, Geothermal energy. New York: United Nations, 1964.

Proceedings of the United Nations Symposium on the Development and Utilization of Geothermal Resources, Pisa, Italy, September 22-October 1, 1970; Geothermics, Special Issue 2, 2 volumes, 1971.

The former contains 77 individual papers and three summary articles by rapporteurs, and summarizes information to 1960. The latter contains 198 individual papers plus summary reports by rapporteurs of the eleven symposium sessions, and presents data for exploration and development through 1969.

Data more recent than these sources come largely from personal correspondence and discussion with informed professionals, especially L. J. P. Muffler, U.S. Geological Survey; Carel Otte, Union Oil Company of California; David N. Anderson, California Division of Oil and Gas; Gunnar Bodvarsson, Oregon State University; David Kear, New Zealand Geological Survey; G. V. Subba Rao, United Nations; and Giancarlo Facca, Lafayette, California.